MC-370

~~SECRET~~ AD 5149392
#196

UNCLASSIFIED

Technical Report

distributed by

THIS DOCUMENT HAS BEEN DOWNGRADED

TO UNCLASSIFIED

Per Director DARPA SCEO/TIO

APR 29 1993

DEFENSE TECHNICAL INFORMATION CENTER

EXCISED UNDER THE PROVISIONS OF THE FREEDOM OF INFORMATION ACT 5USC552

(b) (1)

DTIC Acquiring Information – Imparting Knowledge

Defense Logistics Agency
Defense Technical Information Center
Cameron Station
Alexandria, Virginia 22304-6145

UNCLASSIFIED

~~SECRET~~

DO NOT REMOVE

> *ZDAAAAAB0925093*

> *ZDAAAAAB02128838*

MC-310

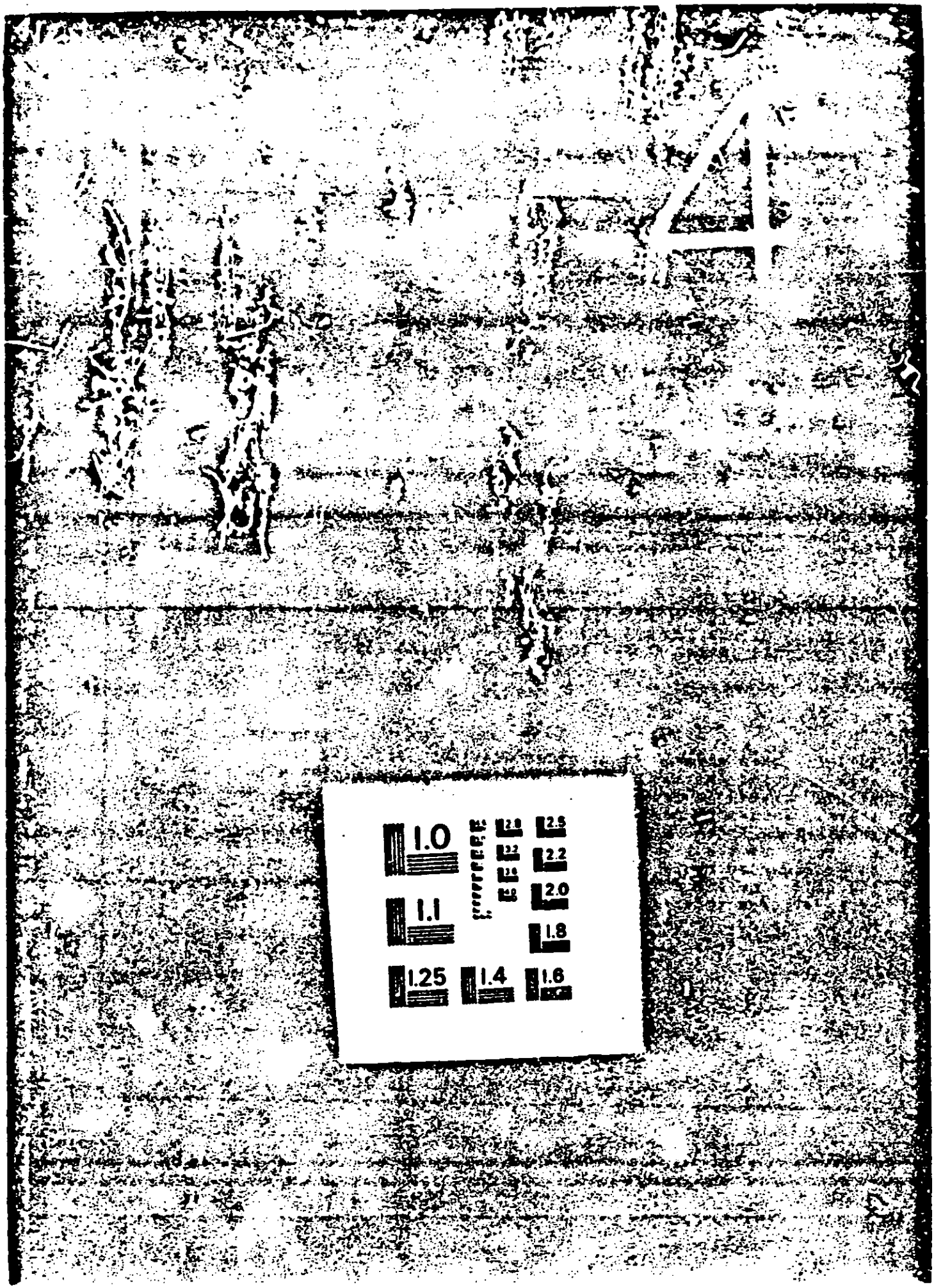

SECURITY MARKING

The classified or limited status of this report applies to each page, unless otherwise marked.
Separate page printouts MUST be marked accordingly.

THIS DOCUMENT CONTAINS INFORMATION AFFECTING THE NATIONAL DEFENSE OF THE UNITED STATES WITHIN THE MEANING OF THE ESPIONAGE LAWS, TITLE 18, U.S.C., SECTIONS 793 AND 794. THE TRANSMISSION OR THE REVELATION OF ITS CONTENTS IN ANY MANNER TO AN UNAUTHORIZED PERSON IS PROHIBITED BY LAW.

NOTICE: When government or other drawings, specifications or other data are used for any purpose other than in connection with a definitely related government procurement operation, the U.S. Government thereby incurs no responsibility, nor any obligation whatsoever; and the fact that the Government may have formulated, furnished, or in any way supplied the said drawings, specifications, or other data is not to be regarded by implication or otherwise as in any manner licensing the holder or any other person or corporation, or conveying any rights or permission to manufacture, use or sell any patented invention that may in any way be related thereto.

UNCLASSIFIED

[redacted]

THIS DOCUMENT HAS BEEN DOWNGRADED
TO UNCLASSIFIED
Per Director ARPA SEID/TIO

APR 29 1993

No 4 of 8 copies
This document consists of 254 pages
Printed 26 May 1970
(11)

(12) 235 p.

6

Proceedings of the

MAY BELL TECHNICAL WORKSHOP OF 18-22 MAY 1970

(8)

Held at RAYTHEON COMPANY LABORATORY, BURLINGTON, MASSACHUSETTS [U.]

DDC

MAY 4 1971

Prepared for:
OFFICE OF NAVAL RESEARCH
CONTRACT NOO014-69-C-0466
UNDER ARPA ORDER 1459

(15)

Prepared by:
RAYTHEON COMPANY
OHD ADVANCED DEVELOPMENT DEPARTMENT
BURLINGTON, MASSACHUSETTS

N00014-69-C-0466
ARPA Order-1459

406574

[redacted]

UNCLASSIFIED

406574

[redacted]

11200

THIS PAGE INTENTIONALLY LEFT BLANK

UNCLASSIFIED

DDC
[redacted]
DATE 7-29-70
ACCESSION NO. 63-263
COPY NO. 1

(1)

MAY BELL TECHNICAL WORKSHOP OF 19-23 MAY 1970 (U)

p

RAYTHEON COMPANY SPENCER LABORATORY
BURLINGTON, MASSACHUSETTS

DDC FILE COPY
AD 514932L

DDC
RECEIVED
MAY 4 1971
A

CONTROLLED ITEM
S70P4733
63-263

UNCLASSIFIED

DDC CONTROL
NO. 11200

UNCLASSIFIED

[redacted]

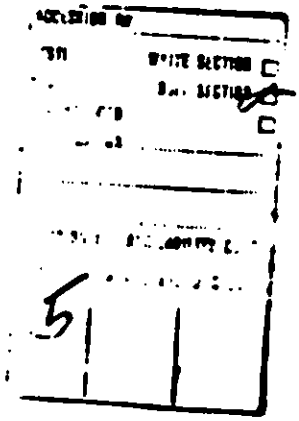

UNCLASSIFIED

CONTENTS (U)

PROJECT MAY BELL WORKSHOP PARTICIPANTS (U)

PROJECT MAY BELL WORKSHOP COMMITTEES (U)

PROJECT MAY BELL WORKSHOP DISTRIBUTION LIST (U)

INTRODUCTION (U) ([redacted])

SECTION 1. EXECUTIVE SUMMARY (U) ([redacted]) 1

SECTION 2. SUMMARY OF PAPERS (U)

PROGRAM OBJECTIVES (U) 11

Detailed Program Objectives and Key Issues (U)
Dr. J. W. Follin, Jr. ([redacted]) 13

THEORY AND MEASUREMENTS (U) 17

Theory of Attenuation and Clutter (U)
Donald E. Barrick (UNCLASSIFIED) ..... 19 ✓

Bomex Sea Scatter Observations (U)
D. D. Crombie ([redacted]) 27

Measurements of Path Loss (U)
H. Hoogasian (UNCLASSIFIED) ..... 35 ✓

Sea Clutter - Predictions and Measurements (U)
Jerald A. Grimes ([redacted]) 43

Theoretical Attenuation for Terrain - Sea Paths (U)
Dr. R. H. Ott (UNCLASSIFIED) ..... 57 ✓

SLBM Radar Cross Sections at HF (U)
G. N. Oetzel ([redacted]) 65

Measured Ship Cross Sections (U)
J. M. Headrick ([redacted]) 73

HF Back Scatter from a Ship's Wake (U)
D. D. Crombie ([redacted]) 83

FLEET AIR DEFENSE (U) 89

Fleet Air Defense Requirements (U)
Paul T. Stine ([redacted]) 91

Fleet Air Defense Requirements for Early Warning (U)
Richard J. Hunt ([redacted]) 105

FAD History (U)
J. M. Headrick ([redacted]) 117

NPL Data Analysis (U)
J. M. Hudnall ([redacted]) 122

FAD Experiment of February, 1970 (U)
Thomas D. Scott ([redacted]) 129

FAD Radar System Study (U)
Wesley N. Mollard ([redacted]) 133

Ship Detections (U)
J. L. Ahearn ([redacted]) 139

High Resolution Sea Backscatter (U)
J. R. Barnum ([redacted]) 145

BTEW Concepts (U)
Allen M. Peterson ([redacted]) 151

BTEW-1 Feasibility Tests (U)
Bruce B. Whitehead ([redacted]) 153

SLBM Observations (U)
Henry M. Baker ([redacted]) 165

Project Aquarius (BTEW-2) (U)
K. D. Snow ([redacted]) 175

Buoy Considerations (U)
Daniel M. Brown (UNCLASSIFIED) 187

MAY BELL Platform Problems (U)
Dr. Frank Bader ([redacted]) 191

BTEW Systems Analysis: Clutter (U)
Donald E. Barrick ([redacted]) 197

The Buoy Tactical Early Warning System Concept, BTEW-1 (S)
L. Edwards (SECRET) 207

Comparison of Several BTEW System Configurations (U)
J. W. Follin, Jr. ([redacted]) 215

SECTION 3. PANEL REPORTS (U) ([redacted]) 221

SECTION 4. TASK ABSTRACTS (U) ([redacted]) 227

PROJECT MAY BELL WORKSHOP PARTICIPANTS (U)

Advanced Research Projects Agency

Alvin Van Every

Army Missile Command

Samuel Uptain

Naval Research Laboratory

Jack Ahearn
James Headrick
James Hudall
Richard Sheil
Paul Stine
Dennis Trizna
Dr. Lew Wetzel

Office of Naval Research

Stan Curley
Jack Kane
Dr. William Kielhorn
Frank Mullen
Thomas Quinn

Applied Physics Laboratory (JHU)

Dr. Frank Bader
Dr. James Follin, Jr.
Richard Hunt
Mace Miyasaki
Dr. Edwin Shotland
Albert Stone

Battelle Memorial Institute

Dr. Donald Barrick

Environmental Science Services Administration

Douglas Crombie
Dr. Randolph Ott
Dr. William Utlaut

Scripps

Daniel Brown

Stanford Research Institute

Dr. George Oetzel
Dr. Allen Peterson

Astrophysics Research Corporation

Howard Grizzle
Dr. Hans von Roos

ITT Electro-Physics Laboratories, Inc.

Dr. Roy Basler
Dr. John Kelso
Wesley Mollard
Thomas Scott
William Whelan

Raytheon Spencer Laboratory

Dr. Henry Alexander
Henry Baker
Richard Close
Robert Desmond
Leonard Edwards
Jerald Grimes
Harry Hoogasian
Frank Roberts
Bruce Whitehead

Sylvania Electronic Systems West

Robert Krulee
Kenneth Snow
John White, Jr.

PROJECT MAY BELL WORKSHOP COMMITTEES (U)

Executive
A. Van Every, Chairman
D. Barrick
R. Bealer
L. Edwards
J. Follin

Path Loss
H. Hoogasian, Chairman
S. Curley
R. Ott
T. Quinn
T. Scott
I. Shotland
K. Snow
R. Trizna
L. Wetzel

Clutter
J. Grimes, Chairman
J. Ahern
H. Alexander
D. Crombie
J. Headrick
E. Shoiland
L. Wetzel

Sea State
H. Baker, Co-chairman
B. Whitehead, Co-chairman
F. Boder
W. Kielhorn
M. Miyasaki
R. Sheil

PROJECT MAY BELL WORKSHOP DISTRIBUTION LIST (U)

Copies 2, 3, 4
Director
Advanced Research Projects Agency
The Pentagon
Washington, D.C. 20301
Attn: Mr. Alvin Van Every, STO

Copy 5
Headquarters
U.S. Army Missile Command
Redstone Arsenal
Huntsville, Alabama 35809
Attn: Mr. Samuel T Upham, AMSMI-RNS

Copy 6
U.S. Department of Commerce
Environmental Science Services Administration
Boulder, Colorado 80302
Attn: Mr. Doug D. Crombie

Copy 7
U.S. Department of Commerce
Environmental Science Services Administration
Boulder, Colorado 80302
Attn: Dr. Randolph Ott

Copy 8
U.S. Department of Commerce
Environmental Science Services Administration
Boulder, Colorado 80302
Attn: Dr. William F. Utlaut

Copy 9
Director
Naval Research Laboratory
Washington, D.C. 20390
Attn: Mr. Jim Headrick, Code 5323

Copy 10
Director
Naval Research Laboratory
Washington, D.C. 20390
Attn: Dr. Lew Wetzel, Code 5400

Copies 11, 12
Chief
Office of Naval Research
Washington, D.C. 20360
Attn: Mr. Jack Kane, Code 418

Copy 13
Mr. Charles S. Lerch, Jr.
Institute for Defense Analyses
400 Army-Navy Drive
Arlington, Virginia 22202

Copy 14
Commander
Rome Air Development Center
Griffiss Air Force Base
Rome, New York 13442
Attn: Mr. R.A. Ackley, EMATS

Copy 15
Commander
Rome Air Development Center
Griffiss Air Force Base
Rome, New York 13442
Attn: Mr. Salvador DiGennaro, EMASO

Copy 16
Headquarters
Electronic Systems Division
Air Force Systems Command
L. G. Hanscom Field
Bedford, Massachusetts 01731
Attn: Lt. Col. D.F. Connors, ESSLG

Copy 17
Headquarters
Foreign Technology Division
Air Force Systems Command
Wright-Patterson AFB, Ohio 45433
Attn: Mr. S.G. Zahetakis, TDDEP

Copy 18
Office of Naval Research
495 Summer Street
Boston, Massachusetts 02210
Attn: Mr. Stanley R. Curley

Copy 19
Headquarters
Electronic Systems Division
Air Force Systems Command
L.G. Hanscom Field
Bedford, Massachusetts 01731
Attn: Major Joe Dixon, ESSLG

Copy 20
Headquarters
National Security Agency
Fort George Meade, Maryland 20755
Attn: Mr. Jerry Fuller, Code N-2

Copies 21, 22
The Johns Hopkins University
Applied Physics Laboratory
8621 Georgia Avenue
Silver Spring, Maryland 20910
Attn: Dr. James W. Follin, Jr.

Copy 23
The John Hopkins University
Applied Physics Laboratory
8621 Georgia Avenue
Silver Spring, Maryland 20910
Attn: Dr. Edwin Shotland

Copy 24
Dr. Allen Peterson
Stanford Research Institute
Menlo Park, California 94025

Copy 25
Mr. James Barnum
Stanford Electronics Laboratories
Stanford University
Stanford, California 94305

Copy 26
Dr. O.G. Villard, Jr.
Stanford Electronics Laboratories
Stanford University
Stanford, California 94305

Copy 27
Dr. Walter H. Munk
University of California, San Diego Institute of
Geophysics and Planetary Physics
La Jolla Laboratories
La Jolla, California 92037

Copy 28
Dr. Henry Booker
University of California, San Diego
La Jolla, California 92037

Copy 29
Mr. Sam Hunt
The Mitre Corporation
Post Office Box 208
Bedford, Massachusetts 01730

Copy 30
Battelle Memorial Institute
Columbus Laboratories
505 King Avenue
Columbus, Ohio 43201
Attn: Dr. Donald E. Barrick

Copy 31
Mr. Robert Schulz
Stanford Research Institute
Menlo Park, California 94025

Copy 32
Mr. L.C. Edwards
Raytheon Company
Spencer Laboratory, Dept. 8822
Wayside Road
Burlington, Massachusetts 01803

Copy 33
Mr. Harry Hoogasian
Raytheon Company
Spencer Laboratory, Dept. 8822
Wayside Road
Burlington, Massachusetts 01803

Copy 34
Dr. Roy P. Basler
ITT Electro-Physics Laboratories, Inc.
3355 52nd Avenue
Hyattsville, Maryland 20781

Copy 35
Dr. John Kelso
ITT Electro-Physics Laboratories, Inc.
3355 52nd Avenue
Hyattsville, Maryland 20781

Copy 36
Mr. Ken Snow
Sylvania Electronic Systems
Western Operation
Post Office Box 205
Mountain View, California 94042

Copy 37
Dr. Hans vonRoos
Astrophysics Research Corporation
Tishman Airport Center
Suite 1130, 9841 Airport Boulevard
Los Angeles, California 90045

Copies 1, 38-60
Mr. Henry M. Baker
Raytheon Company
Spencer Laboratory, Dept. 8822
Wayside Road
Burlington, Massachusetts 01803

THIS PAGE INTENTIONALLY LEFT BLANK

INTRODUCTION (U)

THIS PAGE INTENTIONALLY LEFT BLANK

INTRODUCTION (U)

(U)

(S) A five-day meeting was held on 18-22 May 1970 at the Raytheon Company Spencer Laboratory, Burlington, Mass., under the sponsorship of the Advanced Research Projects Agency and the US Navy. Mr. A. Van Every of ARPA was chairman. The papers are published in four sections, divided into the following subject areas:

Section 1.	Executive Summary
Section 2.	Summary of Papers
	Program Objectives
	Theory and Measurements
	Fleet Air Defense
	Buoy Tactical Early Warning
Section 3.	Panel Reports
Section 4.	Task Abstracts

(U)

(C) These meetings are regularly held to allow contractors and government agencies active in surface wave radar research to exchange information and report their findings.

(U) A list of attendees is given at the end of Section 1.

(U) Copies of these Proceedings may be requested through the Office of Naval Research, Department of the Navy, Washington, D.C. 20360, Attn: Code 418.

THIS PAGE INTENTIONALLY LEFT BLANK

SECTION 1

EXECUTIVE SUMMARY (U)

[redacted]

UNCLASSIFIED

EXECUTIVE SUMMARY (U)

I PROJECT MAY BELL OVERVIEW (U)

(U) (U) Project MAY BELL is directed towards ocean surveillance and tactical early warning and is investigating the feasibility of detecting and tracking aircraft, missiles, ships and submarines at over-the-horizon distances using HF monostatic and bistatic radar.

(U) Concepts using the basic geometric configurations shown in Figure 1 are being explored.

(U) In support of these concepts various theoretical predictions, propagation measurements, cross-section studies and feasibility detection demonstrations have been made.

(U) (U) The program emphasis during the past eighteen months has been specifically directed towards determining the attenuation and clutter propagation aspects that apply to the concepts that use the surface wave, and investigating the basic feasibility of detecting and tracking aircraft using Mode III, Fleet Air Defense (FAD), and Mode IV (a) and (b), Buoy Tactical Early Warning (B-TEW).

(U) The various efforts and their relation and importance to the basic geometric configurations are shown in Figure 2.

II SUMMARY OF RESULTS (U)

A. Theory and Measurements (U)

1. Path Loss (U)

(U) (C) Measurements of received signal strength were made over a 300-km path extending from Carter Cay in the Bahamas to the receiving site at Cape Kennedy, Florida. Detailed measurements extended from January through March, 1970.

(U) (C) The mean signal strength measurements agree well with predicted[1] received signal strengths in absolute level. The spread of points about the mean conforms to loss predictions versus sea state at 5 and and 10 MHz. Insufficient data were available at 15 and 20 MHz to permit comparisons. Day-to-day correlation of measured signal level with sea state was not reliable because only crude hindcast date was available on sea state. System drifts are concluded to be less than 2 dB. Effects of ducting on measured signal strengths are unknown. Possible spectral broadening of the direct signal by the moving sea during high sea states appears on some records.

[redacted]

UNCLASSIFIED

MODE I
SKY WAVE - SKY WAVE

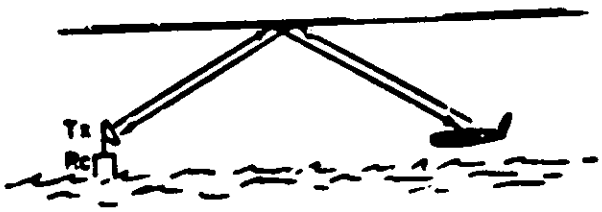

MODE II
SURFACE WAVE - SURFACE WAVE

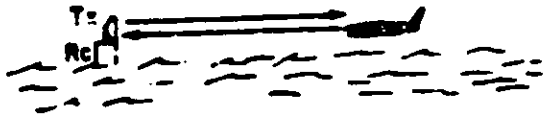

MODE III
SKY WAVE - SURFACE WAVE
FAD

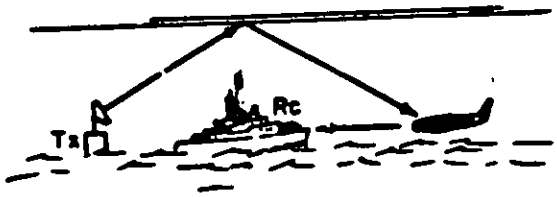

MODE III-A
DIRECT OR SURFACE WAVE -
SURFACE WAVE
BTEW-1

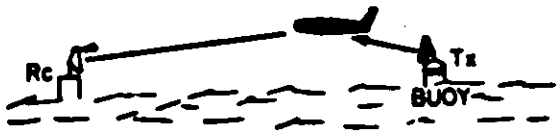

MODE III-B
DIRECT OR SURFACE WAVE -
SKY WAVE
BTEW-2

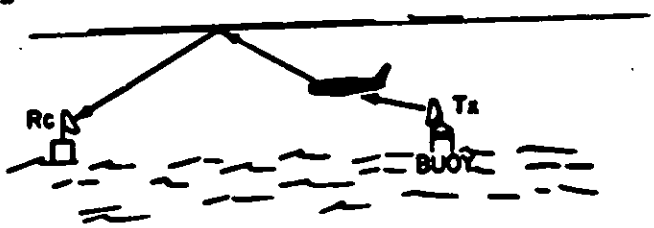

(U) (S) Figure 1. Basic Geometric Configurations (U)

[redacted]

(U)

TASK	ORGANIZATION	OBJECTIVE
A. Theory & Measurements		
1. Attenuation & Clutter Calculations	BMI	Determine surface wave attenuation and clutter as a function of sea state, frequency, and range
2. Clutter measurements	ESSA	Obtain simultaneous multifrequency backscatter sea clutter measurements
3. Attenuation & Clutter Measurements	Raytheon/ APL	Obtain bistatic clutter and path loss measurements as a function of distance and frequency
4. Attenuation Over Irregular Inhomogenous Terrain	ESSA	Calculate the extra path loss for surface waves over irregular inhomogenous terrain
5. Cross Section Studies	SRI	Compile and evaluate known cross-section information on SLBM
6. Ship Model Measurements	SU	Calculation and model measurements of two typical ship's cross-section as a function of aspect, and frequency and polarization
7. Ship Cross Section	NRL	Measurement of the actual ship cross-section with the MADRE radar
8. Wake Study	ESSA	Theoretical investigation of the HF radar cross-sections of ship and submarine wakes as a function of frequency and aspect angle
B. Fleet Air Defense		
1. Feasibility Demonstration Test	ITT/NRL/APL	Initial feasibility demonstration of fleet air defense concept using skywave illumination with a distant transmitter and bistatic reception with close in receiver
2. Ship Detection	NRL	Investigation of detecting ships on a Doppler basis using the MADRE radar.
3. Ship Detection	SU	Investigating the detection of ships on a power basis using FM/CW high resolution technique.

(U) Figure 2. Participating Organizations, Tasks and Objectives (U)

[redacted]

TASK	ORGANIZATION	OBJECTIVES
C. Buoy Tactical Early Warning (BTEW)		
1. BTEW Feasibility Demonstration No. 1	Raytheon/APL	Investigating the feasibility of detecting and tracking aircraft at short ranges using a buoy-based transmitter and land-based receiver using surface wave mode
2. BTEW Feasibility Demonstration No. 2	Sylvania	Investigating the feasibility of detecting and tracking at long range using a buoy-based transmitter and a land-based receiver using skywave
D. Planning and Coordination	APL	Technical assistance to ARPA in the overall planning, and coordination of program

Figure 2. Participating Organizations, Tasks and Objectives (cont) (U)

2. Sea Clutter (U)

Sea-scattered energy was observed at 5 and 10 MHz, with transmissions both from a buoy moored 120 km from the shore and from Carter Cay. The observations were made both with CW signals and phase-coded signals, the latter with effective pulse lengths of 25 and 200 μs.

The transmissions from the buoy proved considerably more important because the scatter area near the buoy is deep ocean water, rather than land or shoals, as in the case of the Carter Cay transmissions. The signal spectrum showed that the sea scatter was confined to two bands, or "pedestals", tenths of a hertz wide and located symmetrically within ½ hertz of the carrier; these observations agree with theory and predictions relating the Doppler shifts to the velocities of the Bragg resonant ocean waves responsible for scatter. The observed intensity for the sea clutter signal corresponds to an average scattering cross-section per unit area, σ^o, of between -24 and -30 dB; this agrees with a predicted upper limit of -23 dB.

B. Fleet Air Defense and Ship Detection (U)

1. Fleet Air Defense (FAD) (U)

(U) (S) Detection of low-flying threats to surface vessels at a range sufficient to give useful warning time and tracking information is a problem which must be solved if the surface navy is to survive. Because of the advantage of denying the enemy the opportunity of using simple direction finding techniques to locate fleet units, it is desirable that the solution not require radiation from the fleet.

(U) (S) The feasibility of using a hybrid (sky-wave/surface wave) system to solve this problem has been demonstrated during FY 70 as part of the MAY BELL Program. In this concept, the target is illuminated by sky-waves from transmitters (either shipborne or land-based) located over-the-horizon at ranges of perhaps 1000-2000 km. Surface waves which propagate from the target to a receiving system aboard a ship permit detections to be made even when the target is below the line of sight radar horizon.

(U) (S) An experiment was performed at Cape Kennedy, Florida, where a shore-based receiving station was used to simulate the shipboard environment. A Navy P3V aircraft served as a target by flying off-shore in a series of controlled flight plans, and illumination was provided by the MADRE and CHAPEL BELL transmitters located respectively in Maryland and Virginia. For most of these flights the target altitude was 200 feet, and detections were made at ranges as great as 100 km. It was shown to be possible to track the target in both range and azimuth with accuracies of about 5 nmi and one degree (depending on SNR). These results were obtained using a receiving/processing system which was assembled using existing equipment, and this equipment was in many ways not well matched to the experimental requirements, therefore, these results should not be taken as representing the capabilities or the limitations of a properly designed system.

(U) (S) The dynamic range requirements imposed by the necessity of receiving small target echoes in the presence of the incident sky-wave and of clutter were found to be well within the capability of existing technology. Cross-polarized, bistatic target cross sections were also found to be of sufficient magnitude (up to 100 m^2 for the P3V) to permit detection. Clutter was found to be composed primarily of the resonant spectral lines which are generally well understood in terms of existing theory.

2. Ship Detection (U)

(U) (S) The following is a summary of the various HF propagation techniques considered for ship detection.

(U) (S) Monostatic Groundwave Radar has demonstrated a capability for the detection of surface vessels. On the ocean (away from land), it is predicted that very modest systems (two element antennas and a few hundred watts average power) can provide detections beyond 50 nmi. The limits of location accuracy, particularly in azimuth, have not been studied.

(U) (S) Monostatic Skywave Radar has demonstrated a capability for detecting ships at one hop refraction ranges out to more than 1000 nmi. This has been done with coarse spatial resolution (60 nmi by 12-degree cell) and fine Doppler (0.1 Hz and smaller) resolution. If higher spectral resolution is employed, it is predicted that good ocean traffic surveys can be made on a daily basis. Optimum balance between the several forms of resolution has not been studied.

(U) (S) Hybrid tests using skywave illumination to the target and groundwave propagation from target to receiver have been conducted. Examination of reference targets on the surface and of returns from the sea permit some predictions. It appears that a hybrid bistatic system can (in addition to its primary function of detecting A/C, SSM, and ASM) provide a surface vessel detection capability. That is, a "quiet" fleet unit equipped with the bistatic system could have many of the sensing abilities ordinarily provided by conventional active radar plus additional capabilities.

(U) (S) It is recommended that the propagation of monostatic skywave radar illumination of the area around a fleet unit be further tested. In particular, determinations of the possibilities of ship unit observation of any attacking missiles or missile boat detections should be made. These tests should study contributions gained from the various forms of high resolution techniques and the requirements for real-time ionosphere assessment for optimum illumination.

(U) (S) The bistatic hybrid surface wave concept should be tested in the ship-mounted environment; such tests could be concurrent with the monostatic tests. The potential of slow target detection should be confirmed and thoroughly described.

[redacted]

UNCLASSIFIED

C. Buoy Tactical Early Warning (BTEW) (S) (U)

1. BTEW-1 (U)

(U) (S) The BTEW-1 concept involves detection of low flying aircraft at OTH distances by illuminating the target with a transmitter located on an off-shore buoy and reception of the target echo signal at a shore based receiver site via a ground wave propagation mode. Feasibility tests were conducted off the Florida coast using a transmitter located on Carter Cay (just north of Grand Bahama Island) and a receiving station at Cape Kennedy. The path length was 300 km and the target was a Navy P3V Aircraft.

(U) (S) The feasibility tests were successful and demonstrated that standard radar calculation techniques, with application of Barricks' loss model could be used with reasonable confidence, to describe the coverage afforded by the BTEW-1 concept. The tests, then, established and validated a model for calculating coverage.

(U) (S) Several variations of the original concept were examined, using the model, in a first attempt to assess potential capabilities in application to the defense of the CONUS, of special strategic areas, and of the fleet. The results of these analyses indicate that surveillance can be maintained out to ranges of 300 to 400 km from a shore station with systems of practical dimensions. For example, the east coast of the U.S. from Nova Scotia to the Straits of Florida, could be covered by about 10 shore stations and a fence of 30 buoys.

(U) (S) Although the primary objective of the Florida tests was to detect low flying aircraft there was also the opportunity to observe the launch of a Poseidon missile from sea. Excellent detection results were obtained. No analysis has been attempted to describe the early warning potential of this kind of system against SLBM's; however, it seems apparent that significant coverage of this threat can be achieved with a very small number of terminals.

(U) (C) The program has reached the point where basic feasibility has been demonstrated. Some refinement to the understanding of fundamental limitations is required but more emphasis now should be placed upon the definition of performance and interface requirements, of detailed concept definition, and upon examination of some of the more obvious engineering problems.

2. BTEW-2 (U)

(U) (S) The BTEW-2 concept involves target detection at long OTH ranges by illuminating the target with a buoy mounted transmitter and reception of the target signal at a remote receiver site via sky-wave. Tests of this concept were successful but indicated that coverage would be very limited for any presently practical level of buoy transmitter power.

[redacted]

UNCLASSIFIED

[redacted]

III RECOMMENDATIONS (U)

A. Additional Measurements (U)

(U) The committee recommends that additional measurements be undertaken over a 5 to 6 month period. The primary purpose of such measurements would be to obtain needed information about daily path loss fluctuations with sea state and atmospheric refractivity. Data presently available are insufficient to study these effects or establish trends and conclusions. In addition, the water along the previous path is not typical of the deep ocean. An ideal path, for example, would be the 300 - 400 km over-water stretch from Cape Cod to Northern Maine. Daily signal strength measurements should be made on 5, 10, 15, and 20 MHz and with phase-coded signals so as to eliminate sky-wave contamination.

B. Reduction of Existing Data (U)

(U) As much as possible of the existing path loss measurements on 5, 15, and 20 MHz should be processed by Raytheon. Means, variances, and confidence levels of the path loss data should then be computed. NRL personnel should complete the reduction of aerial profilometer wave-height data taken on several days during the radio measurements. These should provide some positive basis for comparison and correlation with sea state. Where possible, brief analyses should be undertaken to permit rough estimates of the effects of atmospheric ducting on the received signal.

C. Fleet Air Defense (FAD) (U)

(U) Now that the feasibility of the hybrid (sky-wave/surface wave) system concept for Fleet Air Defense has been demonstrated beyond any reasonable doubt, it is recommended that during the coming year (FY 71) the following efforts should be carried out as the next step toward the goal of developing an operational system:

- Provide a receiving/processing system which is mobile and suitable for installation aboard a ship such as a destroyer, which can eventually be integrated into a fully automated system.
- Investigate the shipboard antenna problem, select elements best suited to the FAD requirements, and provide an antenna system for shipboard use.
- Test the performance of this receiving/processing and antenna system in a land-based experiment using available illuminators (MADRE and CHAPEL BELL).
- Repeat these tests in a shipboard experiment.

[redacted]

(U) (S)

- Pursue Fleet Air Defense System studies to further define the performance requirements, the interaction with other systems, and the operational utility.
- Make model measurements of the cross sections of representative aircraft and missile targets for various frequencies, polarizations, and bistatic geometries.

D. Buoy Tactical Early Warning (BTEW)

(U) (S) It is recommended that systems analysis be continued with emphasis in the following areas:

- To provide a more complete description of coverage capabilities for various deployment concepts.
- To establish the mission and provide a definition of performance and interface requirements.
- To perform a preliminary cost trade-off analysis of the various deployment concepts.
- To investigate the antenna gain and land-sea interface problems.
- To recommend techniques for target location and tracking.
- To assess the magnitude of the dynamic range problem and to recommend solutions.
- To obtain bistatic cross-section information on representative aircraft and missile targets.

REFERENCE

1. D.E. Barrick, "Theory of Ground-Wave Propagation Across a Rough Sea at Dekameter Wavelengths (U), "Research Report, Battelle Memorial Institute. Columbus, Ohio, January 1970, UNCLASSIFIED

SECTION 2

SUMMARY OF PAPERS (U)

PROGRAM OBJECTIVES (U)

THIS PAGE INTENTIONALLY LEFT BLANK

[redacted]

UNCLASSIFIED

DETAILED PROGRAM OBJECTIVES AND KEY ISSUES (U)

Dr. J. W. Follin, Jr.

The Johns Hopkins University
Applied Physics Laboratory
8621 Georgia Avenue
Silver Spring, Md. 20910

I INTRODUCTION (U)

(U) (S) The [redacted] BELL program is aimed at obtaining solutions to the sea surveillance problem both for tactical early warning of missiles and aircraft attacking the continental United States and for fleet air defense; that is, over-the-horizon surveillance of attacking missiles, aircraft and ships. (See Figures 1 and 2.) A large number of system configurations can be used to solve parts of these problems. At this workshop we wish to determine the best combinations of systems to do the job and to estimate the effectiveness of these combinations.

(U) (S) For tactical early warning it is possible to use land-based monostatic skywave or surface wave radars or a ship-based surface wave radar. Various bistatic systems involve buoys providing line-of-sight or surface wave target illumination with either surface wave, or skywave, transmission to a land-based receiver. One interesting possibility would be transmission in the opposite direction since much higher power can be achieved, leading to a 40 dB improvement in system performance. In some geometries it appears that a buoy-to-buoy bistatic system would be effective. Finally, the use of an aircraft to generate a synthetic receiving aperture in conjunction with a skywave illuminator may provide the surveillance desired.

(U) (S) For the fleet air defense system, choices are limited if it is desired to maintain radar silence aboard ship. A monostatic land-based skywave radar can monitor the ocean around the fleet and transmit the information through appropriate communication links. Bistatic systems include the skywave target illumination and surface wave propagation to the ship, buoy line-of-sight or surface wave target illumination, and surface wave propagation to ship, and airborne synthetic aperture as above.

[redacted]

UNCLASSIFIED

(U) (S)

TACTICAL EARLY WARNING

TARGETS

SLBM
SLCM
A/C

SYSTEMS

MONOSTATIC
SURFACE WAVE RADAR
SKYWAVE RADAR

BISTATIC
BUOY LOS TARGET SURFACE WAVE TO LAND OR REVERSE
BUOY LOS TARGET SKYWAVE TO LAND OR REVERSE
BUOY-BUOY
SKYWAVE ILLUMINATE – A/C SYNTHETIC APERTURE RECEIVE

FLEET AIR DEFENSE

TARGETS

SLCM
A/C
SHIPS

SYSTEMS

MONOSTATIC

LAND-BASED SKYWAVE RADAR

BISTATIC
LAND-BASED SKYWAVE ILLUMINATE SURFACE WAVE TO SHIP
BUOY LOS ILLUMINATE – SURFACE WAVE TO SHIP
SKYWAVE ILLUMINATE – A/C SYNTHETIC APERTURE RECEIVE

(U) (S) Figure 1. MAY BELL Program Objectives, Sea Surveillance (C) (U)

(U)
(S)

SURFACE WAVES

- CLUTTER
- PROPAGATION
- CROSS SECTIONS

SKYWAVES

- COHERENCE OF PROPAGATION IN NEARBY PATHS
  - FADING
  - DOPPLER SHIFT
  - FARADAY ROTATION
  - MULTIPATH

SHIPS

- ANTENNAS
- RFI (LOCAL)

BUOYS

- ANTENNA
- POWER
- SECURITY

SYSTEMS

- ECM
- NUCLEAR ENVIRONMENT
- GIVE AWAY OF INFORMATION TO ENEMY

(U)
(S) Figure 2. Key Problems (U)

UNCLASSIFIED
UNCLASSIFIED

[redacted]

(U) (S) Before the effectiveness of these systems can be determined, the following key technical problems that must be answered: for surface waves, the effects of sea state on clutter and propagation; for sky-waves, the coherence of the ionosphere on nearby paths. For ships one problem is effective antenna aperture and beam steering in the presence of resonant superstructure, and second, the problem of RFI from intermodulation products from other transmitters aboard ship. For buoy platforms, the problems are adequate antennas, power and security and to some extent survivability of the buoy. Key system problems, in addition to accuracy, coverage, and effectiveness, are ECM, a nuclear environment, and finally possible give-away of information to the enemy as a result of our transmissions.

(U) These key problems are the basis of the questions prepared for the discussion groups and it is hoped that most of them can be answered at this workshop.

II REQUIREMENTS FOR EARLY WARNING (U)

(U) (S) The usefulness of an OTH early warning system depends on the probability of detection, the probability of false detections, and the accuracy of location and identification. These parameters are interrelated and depend on the amount of additional warning time achieved.

(U) (S) For Fleet Air Defense (see [redacted] and [redacted], a minimum of five minutes (until the threat comes over-the-horizon) is required to get the ship to general quarters, and fifteen minutes if fighters have to be scrambled. The required accuracy is ±5° since the target must be designated within the 15 - 20° acquisition sector scan of the fire control radars. It is especially important to note that attempts to defeat a cruise missile by ECM or chaff are much more effective before a missile locks on a ship.

(U) (S) For buoy tactical early warning aircraft detections should allow interceptors to be scrambled for intercept outside ASM range. Typically this requires ranges of 200 - 300 nmi and an accuracy of 5 nmi.

[redacted]

THEORY AND MEASUREMENTS (U)

THIS PAGE INTENTIONALLY LEFT BLANK

THEORY OF ATTENUATION AND CLUTTER (U)

Donald E. Barrick

Battelle Memorial Institute
505 King Avenue
Columbus, Ohio 43201

I INTRODUCTION (U)

(U) Over the past year and a half, work has been underway on the problem of the interaction of an HF radio wave with the rough sea. Two main phenomena were of concern in the study: 1) attenuation suffered by a ground wave propagating across the ocean under varying sea state conditions; and 2) the scatter (or clutter) returned to the receiver from the ocean and its relationship to sea state. Both phenomena could conceivably be limiting factors in radar performance, and a knowledge of their magnitude is of importance in the design and development of such a system.

(U) On the question of increased attenuation versus sea state, no measurements made before the MAY BELL Program were complete enough to either confirm or deny any dependence on sea state. Nor was any theoretical prediction available as to the expected magnitude of such an effect. With regard to clutter or sea scatter, measurements have been available for nearly 15 years which have satisfactorily explained the nature and mechanism of the interaction. From observed Doppler shifts it was surmised that ocean waves scatter according to the Bragg mechanism, in the same manner as a simple diffraction grating. Measurements of the magnitude of the sea scatter echo and its relationship to sea state at HF have been considerably less complete; only recently have more thorough measurements along these lines been undertaken by Crombie of ESSA, Headrick and others at NRL, and Barnum of Stanford, as well as the work on data reduction presently underway at Raytheon. These efforts, all reported under the MAY BELL Program, should provide valuable data on observed sea clutter strength. As to the theory, it was only in recent years that Wetzel and Barrick related the strength of the received signal spectrum directly to the ocean waveheight spectrum evaluated at the Bragg spatial wavenumbers. This enables a quantitative connection between echo strength and sea state which should complement the measured data.

II SUMMARY OF ATTENUATION PREDICTIONS (U)

(U) The problem of attenuation of a surface wave propagation above a rough sea has been attacked in the following manner. First, an effective surface impedance is derived which accounts for the roughness as well as the finite conductivity of sea water. Then this effective surface impedance is used in an ESSA computer program to predict the basic transmission loss between two points over the sea versus sea state.*

(U) The calculation of the effective surface impedance of the sea at HF is facilitated because 1, the ocean waveheight is small compared to wavelength, 2, the surface slopes are small, and 3, the sea water is highly conducting at HF. Consequently, the boundary perturbation approach of Rice was used along with the Leontovich boundary condition for the surface. The results show that the effective impedance (accounting for roughness) consists of two terms, one which is merely the impedance of sea water alone and the other which contains the effect of roughness. The latter involves an integral over the ocean wave-height spectrum. In evaluating the latter numerically, the Phillips wind-wave spectrum for the ocean surface was selected as a "typical" model. The presence of swell is neglected in this model, as well as any actual directionality. One thus obtains results for the effective impedance which are functions of wind speed.

(U) When these effective impedances are employed in the ESSA groundwave program, numbers for basic transmission loss are obtained. To show clearly the effect of sea state, loss difference (in decibels) between a perfectly smooth sea and various conditions of roughness were plotted. Figure 1 shows such an example for 10 MHz, versus range and wind speed. The conductivity of ocean water was taken as 4 mho/m and a 4/3 earth refractivity factor was used in the program. Transmitter and receiver are assumed located on the surface in Figure 1. In Figure 2, the actual basic transmission losses (rather than the differences) are shown from a surface-based source to an elevated receiver. The first number is the loss for a perfectly smooth sea and the second is for sea state 5 (i.e., 25-knot wind).

(U) The results show that sea state effects become more pronounced at greater ranges. For example, at 10 MHz and 100 nmi range, the signal variation due to sea state is of the order of 8 dB for one-way propagation.

---

*A report showing the details and results of this work is available as "Theory of Ground Wave Propagation across a Rough Sea at Dekameter Wavelengths" by D. E. Parrick, Battelle Memorial Institute, January 1970.

III SUMMARY OF CLUTTER CALCULATIONS (U)

(U) The analysis of scatter from the rough ocean surface is approached with the same technique as used for the attenuation calculations: namely, the Rice perturbation analysis along with the Leontovich boundary condition.* The results of this study show that the incremental received power spectral density and absolute power scattered from the patch of sea, ds, can be expressed in the usual radar range equation form as

$$dP_R(\omega) = \frac{4P_T G_T G_R \lambda^2}{(4\pi)^3 R_T^2 R_R^2} F_T'^2 F_R'^2 \sigma(\omega)\, ds \ , \quad dP_R = \frac{4P_T G_T G_R \lambda^2}{(4\pi)^3 R_T^2 R_R^2} F_T'^2 F_R'^2 \sigma^\circ\, dr$$

Transmitted power is P_T, antenna gains are G_T, G_R, distances from transmitter to the patch ds and from the patch ds to receiver are R_T, R_R, and wavelength is λ. The quantities F_T' and F_R' are the Norton attenuation functions from target patch to the transmitter and receiver, respectively. (They approach unity for short ranges.) They can be expressed in terms of the basic transmission loss, L_T (in dB), for example, as

$$F_T' = \frac{2\pi R_T}{\lambda} \cdot 10^{L_T/20}$$

(U) The sea scatter cross section σ° and related spectral density for vertical polarization obtained from the analysis are

$$\sigma(\omega) = \pi k_o^4 \ (1 - \cos\psi)^2 \ W[k_o(\cos\varphi - 1), k_o \sin\varphi, \omega - \omega_o] \ ,$$

$$\sigma^\circ = \pi k_o^4 \ (1 - \cos\varphi)^2 \ W[k_o(\cos\varphi - 1), k_o \sin\varphi]$$

where $k_o = 2\pi/\lambda$, $f_o = \omega_o/2\pi$ is the carrier frequency, φ is the bistatic angle from the forward scatter direction, $W(p, q, \omega)$ is the spatial-temporal waveheight spectrum for the sea and $W(p, q)$ is the spatial waveheight spectrum only. The normalization between power and power spectral density is

$$\sigma^\circ = \tfrac{1}{2} \int_{-\infty}^{\infty} \sigma(\omega)\, d\omega \ .$$

(U) As seen in the above equations for $\sigma(\omega)$ and σ°, the spatial wavenumbers appearing in the waveheight spectra for p and q are precisely those required for Bragg scatter. This confirms the interpretation deduced from measurements.

---

*A report giving derivations of sea scatter and the signal spectrum is in preparation. Most of the derivations are also found in a paper "The Interaction of HF/VHF Radio Waves with the Sea Surface and Its Implications", by D.E. Barrick, presented at AGARD "Electromagnetics of the Sea" Meeting, June 1970.

(U)

UNCLASSIFIED

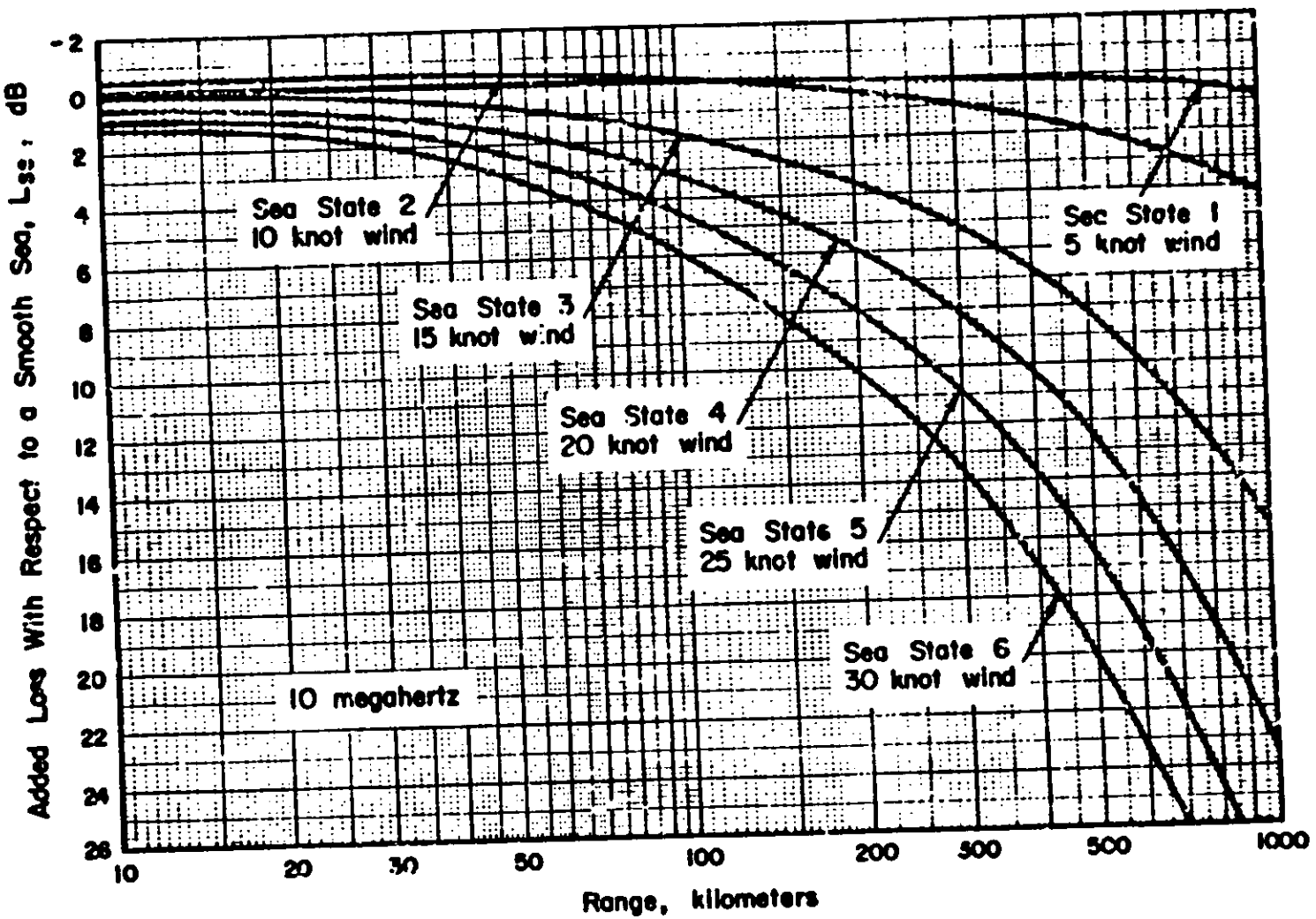

(U) Figure 1. Added Transmission Loss Due to Sea State at 10 MHz. Antennas are Located Just Above Surface. Phillips Isotropic Ocean-Wave Spectrum. (U)

UNCLASSIFIED

UNCLASSIFIED

(U)

(U) Figure 2. Basic Transmission Loss to Points at Various Heights and Ranges above the Ocean at 10 MHz. First Number is for Perfectly Smooth Sea, Second is for Sea State 5 (25 knot wind). Phillips Ocean-Wave Spectrum. (U)

UNCLASSIFIED

(U)

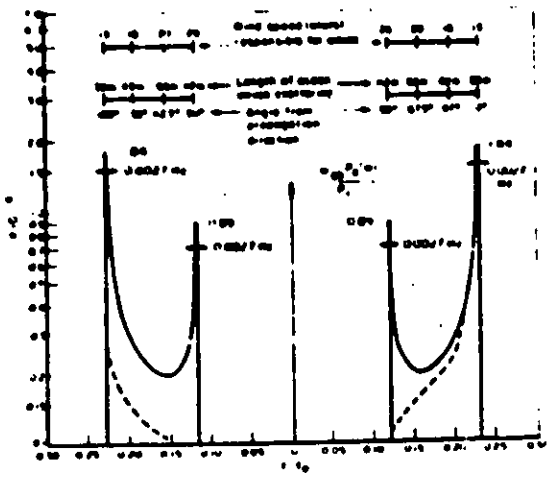

(U) Figure 3. Received Clutter Signal Spectrum at 5 MHz for Bistatic Radar with 100-km Baseline, Effective Pulse Length 12.5 μs, and for Time Delay One Pulse Length Behind Direct Pulse. Phillips Isotropic, Fully Aroused Ocean-Wave Spectrum is Assumed (Solid Line). Dashed Line Represents Likely Measurements from Nonisotropic Sea. (U)

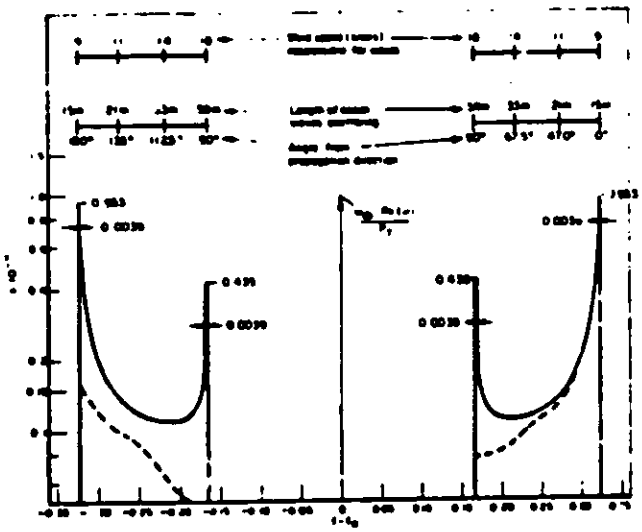

(U) Figure 4. Received Clutter Signal Spectrum at 10 MHz for Bistatic Radar with 100 km Baseline, Effective Pulse Length 12.5 μs, and for Time Delay One Pulse Length Behind Direct Pulse. Phillips Isotropic, Fully Aroused Ocean-Wave Spectrum is Assumed (Solid Line). Dashed Line Represents Likely Measurements for Nonisotropic Sea. (U)

(U) To estimate the level and shape of sea clutter signals, the Phillips isotropic wind-wave spectrum is again employed; σ°, obtained in this manner for bistatic scatter, is -23 dB. This value is more likely an upper limit because the sea in practice is neither isotropic nor fully developed, as implied in the model.

(U) The Phillips isotropic wind-wave model is again used to calculate the clutter spectrum for a bistatic surface-surface radar. The sea is assumed fully developed. The antennas are quarter-wave vertical monopoles, located over sea water, separated by 100 km. The signal permits an effective time (or range) resolution of 12.5 μsec. The elliptical range cell selected corresponds to one pulse length after receipt of the direct signal. Figures 3 and 4 show the expected spectra at 5 and 10 MHz, normalized to the incident power. The frequency, $f_{db} = \omega_{db}/2\pi$ is the cutoff on the outer sides of the clutter pedestals, i.e., 0.228 and 0.322 Hz respectively. The height observed for the "ears" depends upon the processor resolutions; the less the resolution, the shorter the ears.

(U) The interpretation of these bistatic clutter spectra is again in conformance with the Bragg scatter mechanism. The higher frequencies in the pedestals come from the ends of the elliptical resolution cell near the backscatter directions. The lower frequencies in the pedestals come from the sides of the ellipse, nearer the forward scatter region. For larger ellipses corresponding to longer delays, the pedestals collapse to an impulse function centered on f_{db}, the backscatter Doppler.

(U) The total clutter power received in this range cell is about 23 dB below the direct signal. Again, observed clutter signals are likely to be lower because the sea is rarely fully developed and isotropic for these radar frequencies. Therefore, a difference between clutter and direct signal of 30 dB would be expected to be typical.

THIS PAGE INTENTIONALLY LEFT BLANK

BOMEX SEA SCATTER OBSERVATIONS (U)

D. D. Crombie

Institute for Telecommunication Sciences
ESSA Research Labs, Boulder, Colorado 80302

1 INTRODUCTION

(U) Observations were made during the BOMEX project of the coherent backscatter of HF ground waves from the sea, along the east coast of Barbados Island. The data were taken using a multifrequency coherent HF radar system operating in the range of 1.7 to 12.37 MHz. Successive pulse pairs were transmitted in each of eight preselected frequencies in the above range. The demodulated signals were sampled at four ranges (22.5 - 100 km), passed through an A/D converter, and recorded digitally (10 bits) with an incremental tape recorder.

(U) Short vertical broadband monopoles were used for transmission and reception. Two of these were spaced 100 ft. apart and switched alternately to the receiver between each pair of transmitter pulses on the same frequency. Thus, 64 separate sets of data were recorded.

(U) The basic repetition rate of the transmitter was 60 pulses/second and the pulse length was 40 μs. Thus, each set of data (one antenna, one range and one frequency) was sampled 3¾ times per second.

(U) The radiated power and receiver/antenna sensitivity were determined using a field strength meter, and a small target transmitter located several hundred feet from the antennas. Calibrations were made at each operating frequency. Radiated powers ranged from 26 watts at 1.7 MHz to about 1 kW at the higher frequencies.

(U) The transmitting and receiving antennas were situated about 150 ft. from the edge of a cliff which was about 30 ft. above, and 200 ft. away from the water's edge.

II DATA ANALYSIS (U)

(U) Thirty-minute samples of data were taken and subjected to fast Fourier transformation in the computer at Boulder. The program was written to identify the spectral densities and the bandwidths at the -3, -10 and -20 dB levels as well as the frequencies of the spectral peaks. From these data the RMS signal level at each peak could be obtained. Knowing the receiver sensitivity and the radiated power, the scattering cross section, σ, of the sea could be calculated from the following formula.

$$\sigma = \frac{d^4 E_r^2}{2.25 \times 10^4 P} \text{ m}^2$$

where

d = distance of the scatterer in km,
E_r = received field strength in μV/m, and
P = radiated power in kW

(U) This definition of σ, which is particularly appropriate to ground wave radar, results in values which are smaller by a factor of three than free space formula. The factor three arises because it is assumed that the scatterer behaves as a short vertical monopole contributing a factor of 1.5 that re-radiates into the hemisphere above the sea contributing a factor of 2. The effects of ground wave attenuation are not included in this formula.

III OBSERVED SCATTERING CROSS SECTIONS (U)

(U) Some of the values of σ observed at a range of 22.5 km, where ground wave attenuation can be ignored, are shown in Figure 1. The right-hand scale shows the value of relative scattering cross section σ^0 (i.e., cross section per unit illuminated area). The values shown are for approaching waves resulting from partially or fully developed seas at wind speeds of from 10 to 20 kts. The receding components have cross sections about 20 dB smaller. The values shown are averaged over the whole 180° sector illuminated by the transmitter.

IV SPECTRAL DENSITY OF THE SEA SURFACE (U)

(U) Knowing the scattering cross section and the bandwidth of the scattered signal, it is possible to determine the non-directional spectral density, S(f), of the sea surface for the wavelengths observed.

(U)

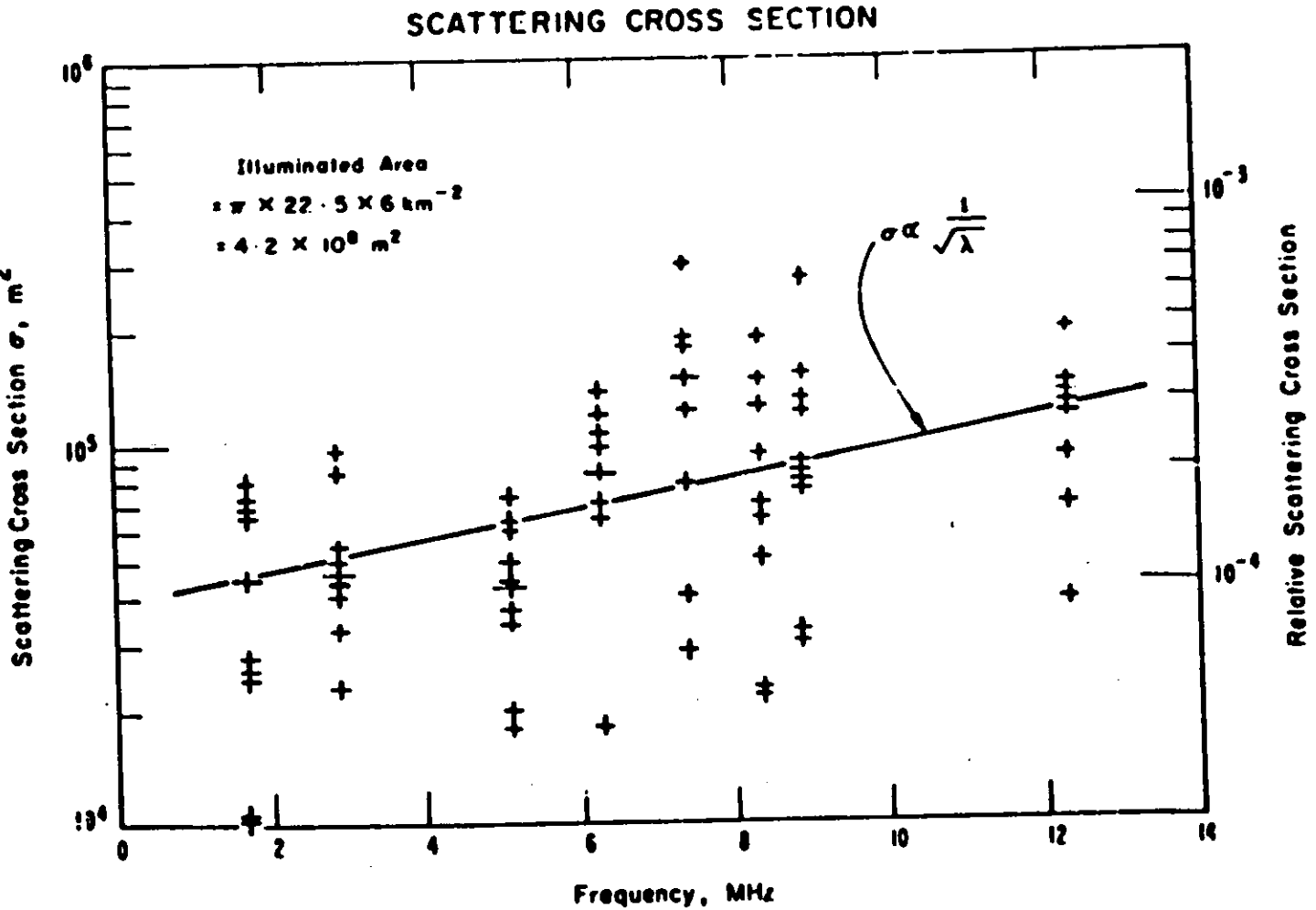

(U) Figure 1. Observed Scattering Cross-sections (U)

UNCLASSIFIED

UNCLASSIFIED

(U)
The required relationship is

$$S(\Omega) = \frac{\sigma L^{2.5}}{g^2 d d_o \sqrt{2\pi}} \quad m^2/sec$$

where σ is the scattering cross section in m^2 at a sea wavelength L meters or a wave frequency of F hertz, d is the range (m), d_o the radial length (m) of the illuminated area, and g is the acceleration of gravity.

(U) Some examples of nondirectional frequency spectra obtained in this way are shown in Figure 2. The lower curve shows an observed spectrum for comparison with Moskowitz's 20-kt synoptic spectrum. The next curve shows the results for a wind believed to be lighter than for the lower curve. The two upper curves show spectra obtained at the same time as the NASA wave-measuring aircraft was flying over the area (in the downwind direction) where the radar data were obtained. Significant wave heights derived from the NASA data are also shown for comparison with those derived from the spectra shown. The agreement is good and although the wave heights are small, the comparison shows that wave heights and spectra can be obtained from backscatter data. However, to be useful under rougher conditions, the radar wavelengths need to be increased.

V BANDWIDTH OF THE BACKSCATTERED SIGNALS (U)

(U) Some representative bandwidths of backscattered signals are shown in Figure 3. The plotted values are the bandwidth 10 dB below the spectral peak. Plots of the spectra show a strong tendency towards a Gaussian shape rather than the sin x/x form expected from simple theory. The points in Figure 3 show that the Doppler bandwidth increases with frequency but that the rate of increase depends on sea state. The points for 11 July represent relatively rough conditions, while those for the 14 and 16 July represent rather quieter seas.

VI SHIP SCATTERING CROSS SECTION (U)

(U) During the BOMEX observations some data was obtained about the cross section of the USCGS ship Mt Mitchell. The revised estimated cross section was ~ 400 m^2 using the definition of σ given in equation 1. The frequency used was 2.9 MHz. Observations at other frequencies were unsuccessful because of the high noise and interference levels present during the nighttime observations.

(U) WAVE SPECTRA

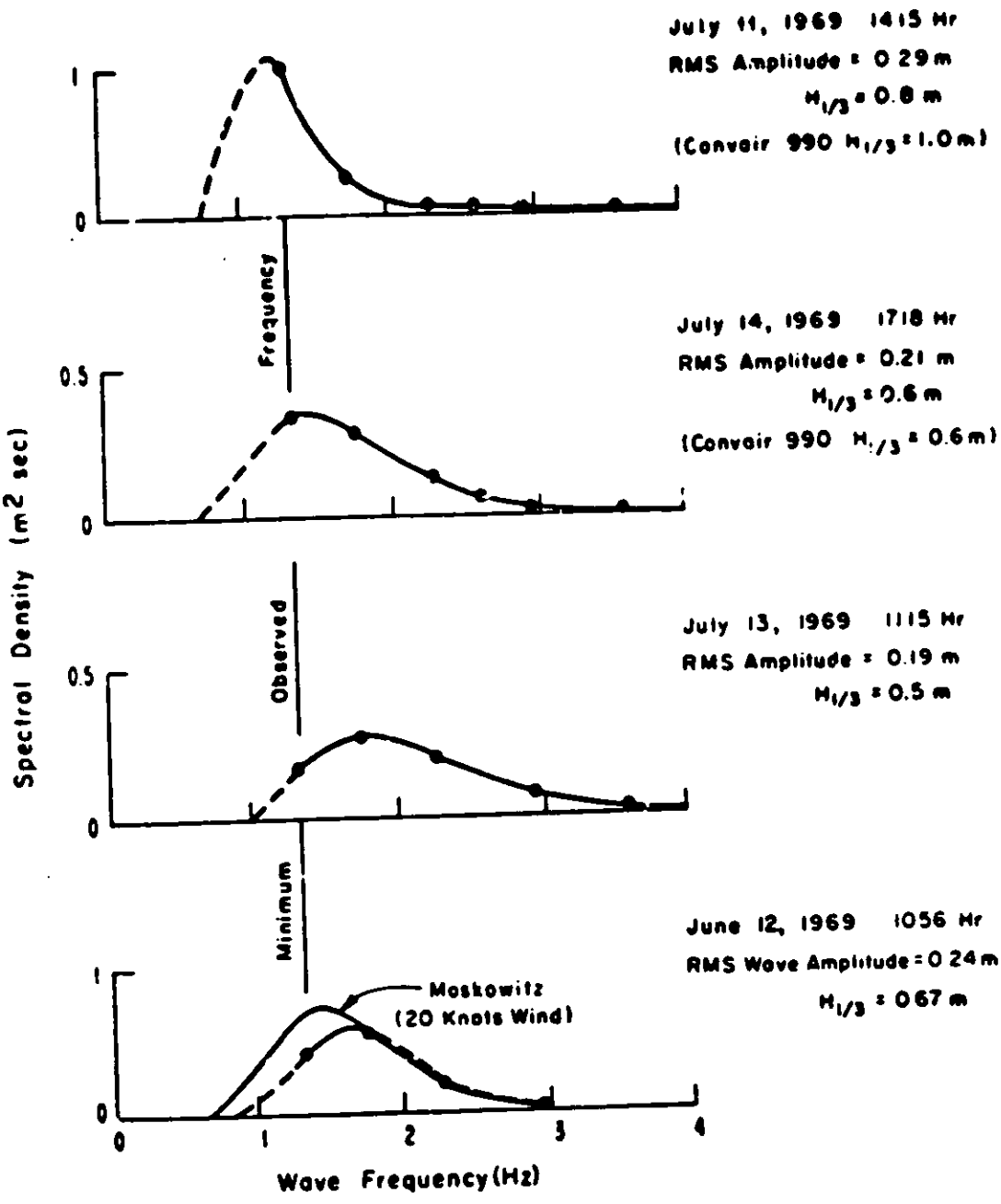

(U) Figure 2. Wave Spectra Deduced from Cross-sections (U)

(U)

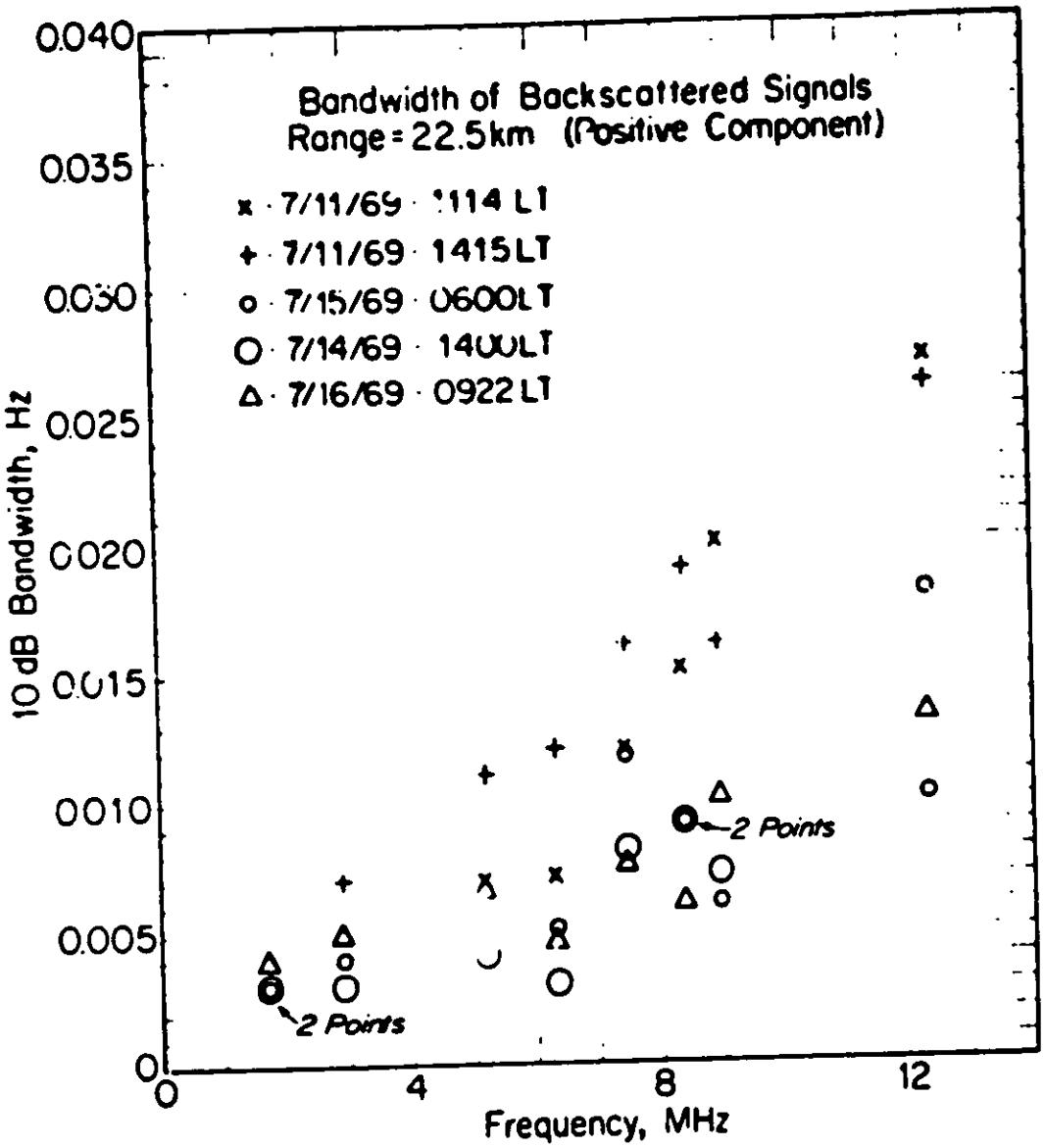

(U) Figure 3. Observed Bandwidths of Backscattered Signals (U)

(U) The Mt. Mitchell has an overall length of 231 feet, beam of 42 feet and a displacement of 1627 tons. The funnel top is approximately 40 feet above the water line, the top of the tallest mast is 70 feet above the water line. The masts are approximately 100 feet apart.

(U) (SI) When the cross section is increased by a factor of 3 to bring it in accordance with conventional free space definitions of σ the value becomes 1200 m^2. Theoretical estimates of the cross section of a dipole 140 feet long in free space, at 2.9 MHz gives ~1000 m^2. The agreement appears good, but the theoretical estimate is strongly dependent on the effective length of the mast.

VII CONCLUSIONS (U)

(U) (SI) The main conclusions from this work using a monostatic backscatter radar are the following.

- The average scattering cross section of the sea can be estimated if the non-directional spectrum of the sea is known.
- The intrinsic bandwidth of the back scattered signals is very small but increases with frequency and sea state.
- It appears that there is reasonable agreement between theoretical estimates of ship cross sections based on mast height, and a measurement (see Section VI).

UNCLASSIFIED

THIS PAGE INTENTIONALLY LEFT BLANK

UNCLASSIFIED

MEASUREMENTS OF PATH LOSS (U)

H. Hoogasian

Raytheon Company
Equipment Division
OHD Advanced Development Department
Spencer Laboratory
Burlington, Massachusetts

I OBJECTIVE (U)

(U) The primary interest of MAY BELL ground wave signal amplitude experiments was to measure path loss on several frequencies, to correlate the signal fluctuations with sea state, and to test the validity of the rough ocean scattering model developed by D. Barrick of BMI.

II APPROACH (U)

(U) Surface wave signal levels were measured on a propagation path between the transmitter site on Carter Cay in the Bahamas and the receiving site at Cape Kennedy. There were two transmitters on Carter, radiating about 1 kW over monopole antennas. During the first three months of 1970 operation was on four frequencies, near 5, 10, 15, and 20 MHz.

(U) Signals were received on the ITT 16-element array on all frequencies during the entire program and with reference monopole antennas on 5, 10 and 15 MHz over a shorter period. All transmitting and receiving antennas were in close proximity to the shoreline so that the propagation path was substantially over an open stretch of ocean for a distance of 300 km between path terminals. However, approximately 80 km of this distance lay inside a shoal line defining a region of low water with depths ranging from 1 to 5 fathoms.

(U) The index for sea state used in making comparisons was taken to be hindcast wave height (see Figure 1). The reference smooth sea datum was Norton's prediction for ocean water with conductivity of 5 mhos/m. In this analysis, computed signal levels were derived from Norton's formulation for a radiating elementary monopole. Estimates for the available power from a receiving monopole were then computed from the free space aperture, using the free space gain of 2 dB for the monopole.

III RESULTS (U)

(U) Path loss data on 5 MHz with monopole reception (see Figure 2) was available for 13 days in March. Signal level fluctuations over a range of 5 dB were measured. The lowest value of signal level was observed around the 9th of March where hindcast data showed a maximum wave height of 13 feet.

(U) On 10 MHz, loss data from the monopole system (see Figure 3) showed little convincing day-to-day correlation with hindcast data with the exception of the period 10 March - 15 March, during which rough seas were reported. During this time, the signal level dropped by approximately 10 dB below the estimate for a smooth sea. The overall spread in power measurements, 0 dB to 10 dB below reference, agrees closely with the Barrick predictions for a distribution of sea states ranging from 0 to 5.

(U) There were 11 days when the 15-MHz signal was received on the BSA. The BSA was calibrated against the 15-MHz monopole and BSA measurements were adjusted accordingly. Although the data base was more restricted, the 15-MHz data displayed trends similar to the 10-MHz data; little or no correlation with hindcast except for the March 10 - March 15 period, and a data spread ranging from 2 dB above to 10 dB below the smooth sea estimate. This compares to Barrick's estimate of about +1 to -14 dB for sea states 1 to 5.

(U) The data base for 20 MHz (see Figure 4) was 6 days. Data was collected on the BSA but a reference monopole was not available for calibration. Consequently, the BSA gain was assumed to include the full 12-dB theoretical array factor. On this basis, the values of received power display a range to 15 dB below the smooth sea estimate. There was insufficient data to search for low signal values in the March 10 - March 15 period.

(U) A comparison was made of hindcast data (see Figure 1) with wind speeds recorded over the same period at GBI and Cape Kennedy. Only a fair correlation was noted. In the hindcast data, the occurence of northerly winds appeared to coincide with the highest values of wave height. This would imply ocean waves travelling in a direction more or less transverse to the propagation path, where the effect on path loss is minimal, and consequently would be expected to produce a decorrelating effect between sea state and signal level on a point-to-point basis.

(U) Skywave contamination proved to be a serious problem on all frequencies. On analysis, a substantial portion (about 40 per cent) of the data was rejected on the basis of suspected biasing by skywave signals. The elimination was accomplished primarily by examining the peaks of the signal spectral density for stability over a relatively long period.

IV SIGNIFICANCE (U)

(U) It is concluded that the measurements showed little day-to-day correlation with hindcast data for the sea except for one high sea state period in March. Treated as a whole, however, the body of data did exhibit an unquestioned frequency behaviour substantially in conformity with the referenced predictions for the sea states encountered.

(U)

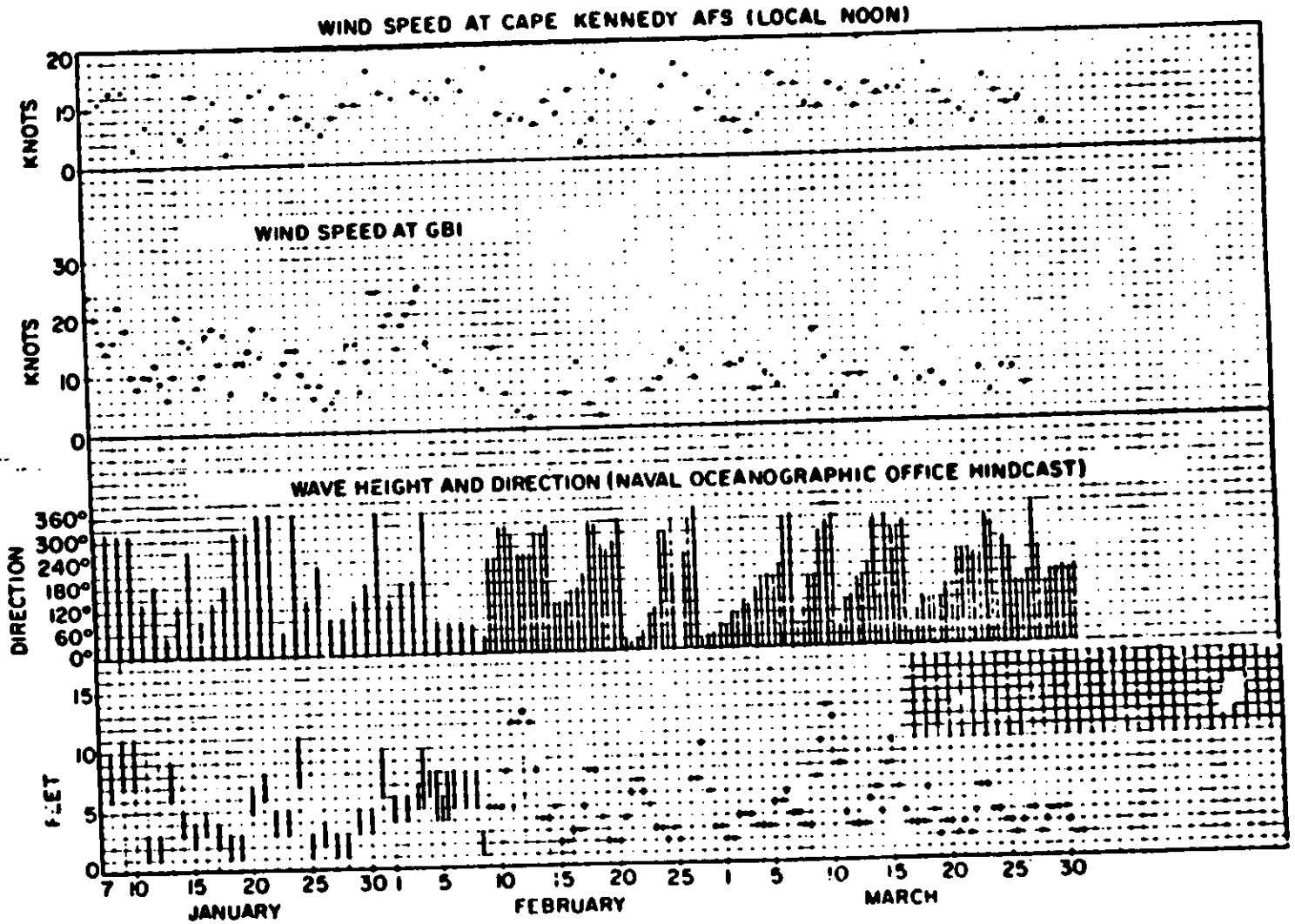

(U) Figure 1. Windspeed and Wave Height, January – March 1970 (U)

UNCLASSIFIED

(U)

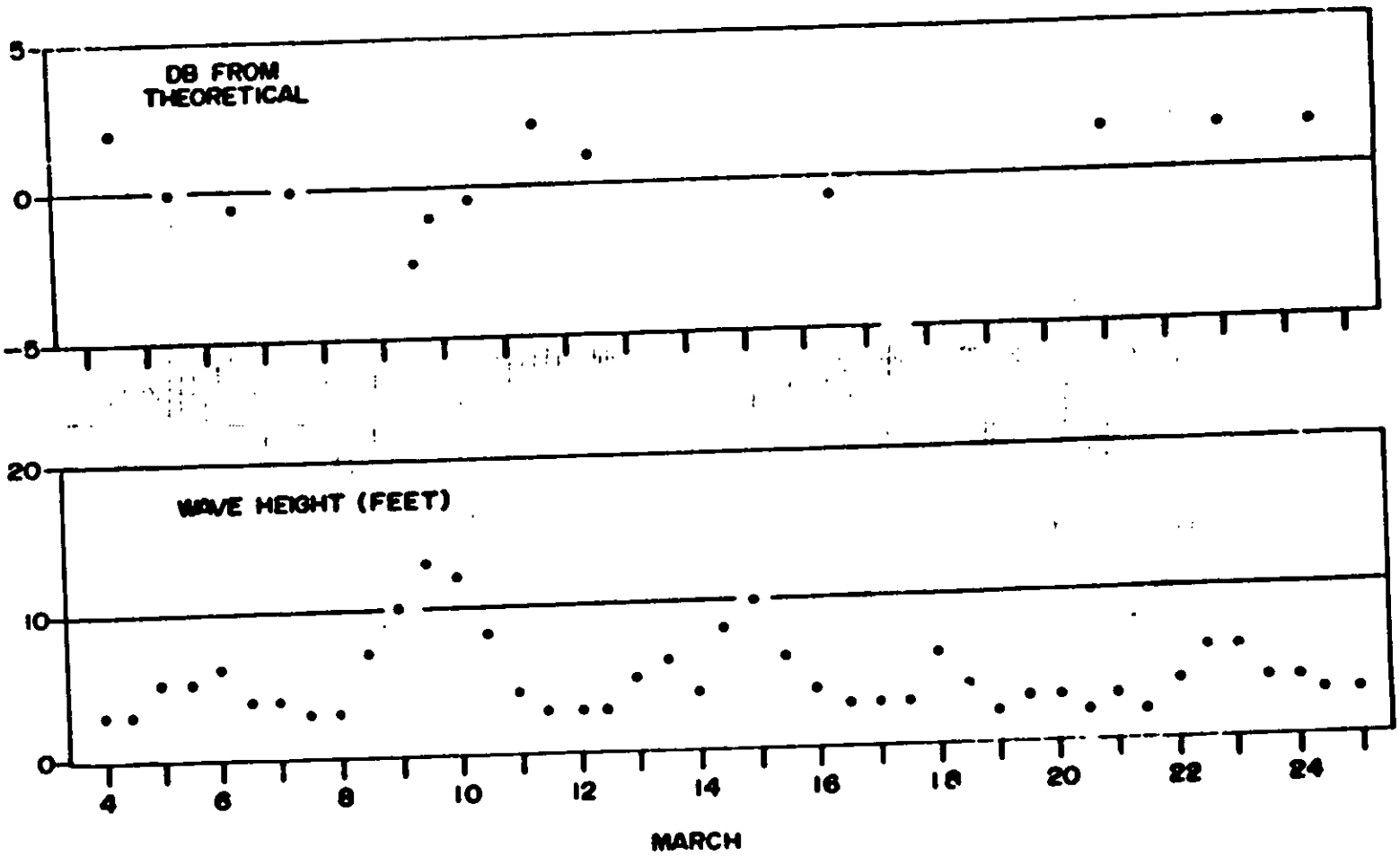

(U) Figure 2. Received Power 5 MHz Monopole vs Hindcast Wave Height (U)

UNCLASSIFIED

UNCLASSIF'D

UNCLASSIFIED

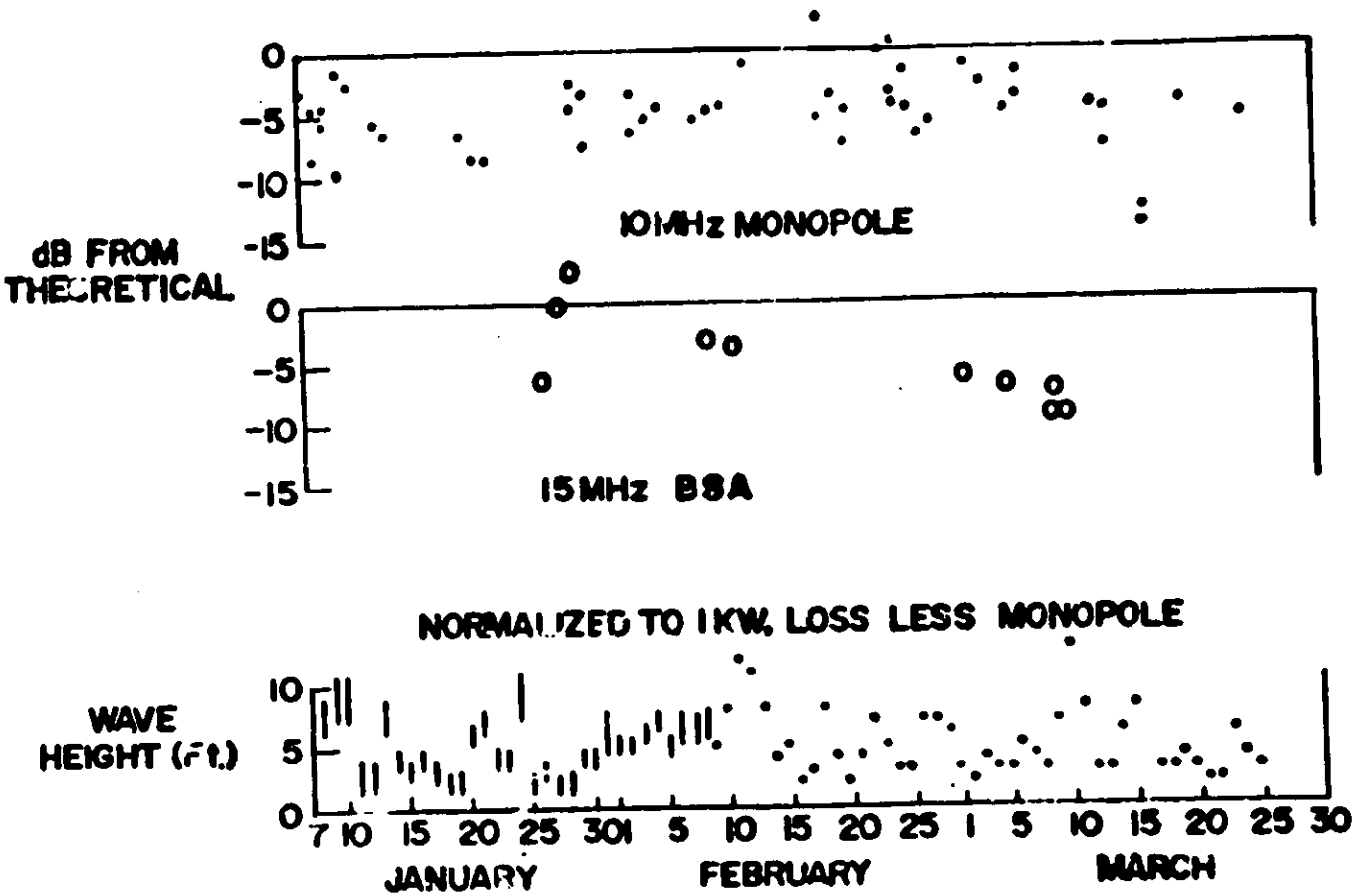

(U) Figure 3. Received Power Measurements on 10 and 15 MHz, January – March 1970 (U)

UNCLASSIFIED

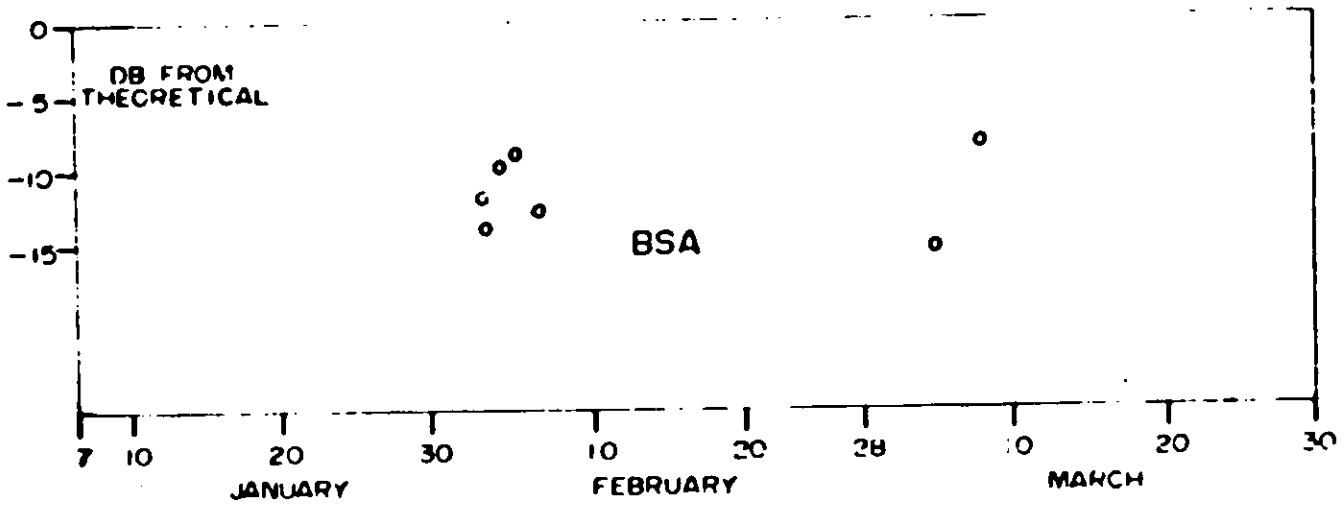

(U) Figure 4. Added Loss, 20 MHz (U)

UNCLASSIFIED

THIS PAGE INTENTIONALLY LEFT BLANK

[redacted]

UNCLASSIFIED

SEA CLUTTER PREDICTIONS AND MEASUREMENTS (U)

Jerald A Grames

Raytheon Company
Equipment Division
OHD Advanced Development Department
Spencer Laboratory
Burlington, Massachusetts

I INTRODUCTION (U)

(U) It has been expected that, in certain applications of a [illegible] radar operating over ocean [illegible] sea clutter from sea waves would under some conditions be a limiting factor [illegible] detections. Consequently, an important part of the Raytheon MAY BELL experiment [illegible] during the early months of [illegible] was to attempt to determine the measured power spectrum of sea clutter under a range of [illegible] graphical, system, and environmental parameters. These experiments constitute a direct test [illegible] as formulated by B Barrick of BMI. Preliminary results are in good agreement with those [illegible]

II PREDICTIONS (U)

(U) Barrick has predicted clutter peaks 23 to 40 dB below the [illegible] signal at [illegible] 0.25 Hz for a 5 800-MHz signal and at [illegible] 0.315 Hz for a 9,250-MHz signal. In each case [illegible] at $\sqrt{2}$ times the original shift are predicted for sufficiently high sea states. Barrick further predicts a maximum clutter frequency equal to $\sqrt{\cos \theta}$ times the maximum (backscatter) shift [illegible] and the scattering ocean waves are in this case approaching or receding perpendicular [illegible] receiver path. A further prediction is the absence of clutter if the maximum ocean wave [illegible] equal to or greater than half the radio wavelength, i.e., low radio frequencies are [illegible]

[redacted]

UNCLASSIFIED

III DATA BASE (U)

(U) The primary data analyzed to date is summarized in relation to Navy Oceanographic Office hind cast wave height and direction in Figure 1. On 17 March the buoy was anchored offshore from the ocean tower site at Cape Kennedy. On 19 March the only other successful operation of the buoy high frequency was recorded from a 120 km range. No buoy transmissions were available during the two highest sea states recorded 18 March. The only significant change in sea state during buoy operation was in wave direction

IV SYSTEM GEOMETRY (U)

(U) Figures 2 and 3 illustrate the buoy transmitter, receiver, and range gate locations along with an indication of the heights of the ellipsoidal range gate regions. Ocean wave, ground and ionospheric scatterme regions are identified in terms of these maps and related to observed returns from each range gate. Most important for clutter analysis is the relation of ocean wave direction on each range gate to physical requirements for scatterme, together with the directivity pattern of the receiving antenna used in this experiment either a narrow beam directed toward the transmitter or a nondirective monopole

V WAVE INFORMATION (U)

(U) Direction and amplitude of ocean waves for periods in which buoy transmissions were recorded are [illegible] in Figure 4. Variability in either parameter is indicated on days when either direction, height, or both were changing significantly. These data are again those from the Navy Oceanographic Office hindcast. Direct determinations of sea state in the areas of interest have not been available. The uncertainties concerning true ocean wave behavior as opposed to best available estimates thereof must be kept in mind in interpreting observed clutter.

VI CLUTTER MEASUREMENTS (U)

(U) To this date sufficient data has been recorded and processed to investigate clutter variation with ocean wave direction, transmitted frequency, directivity of receiver antenna, and ocean wave amplitude. Variations of observed clutter with the specific geometry of individual range gates can also be investigated

(U)

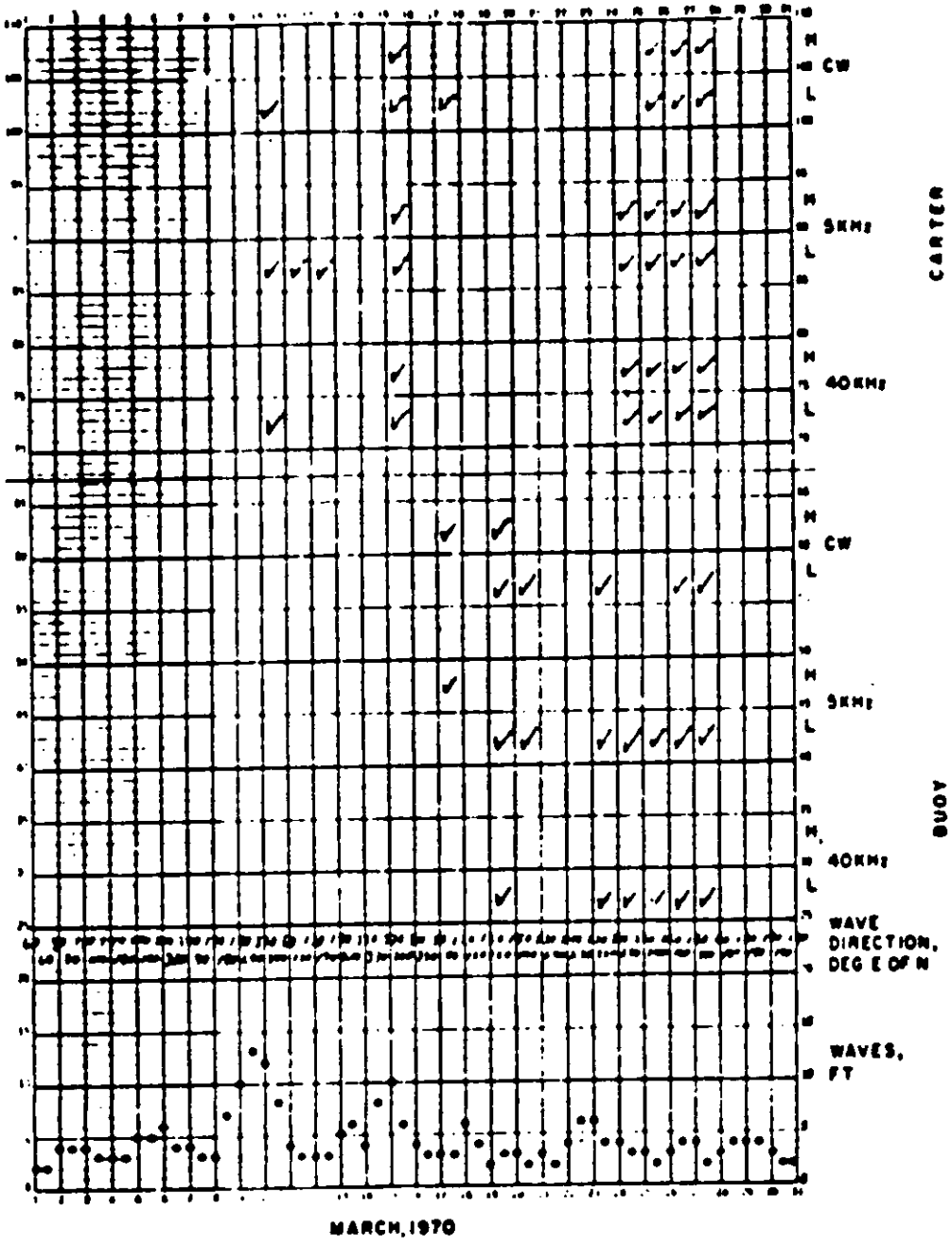

(U) Figure 1. APL Transmissions Recorded in March 1970 (U)

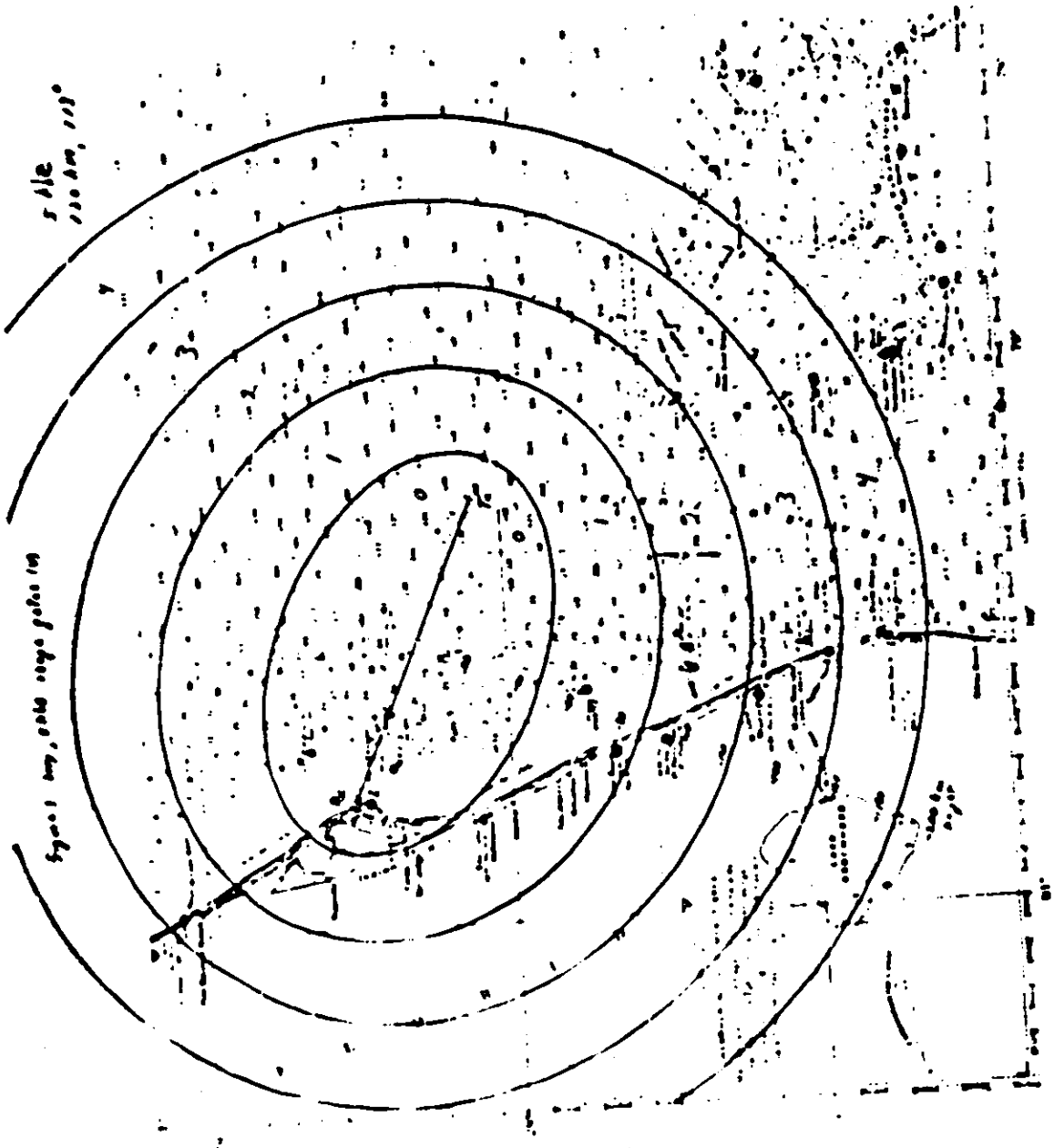

(U) Figure 2. Buoy 5-kHz Range Rates (U)

(U)

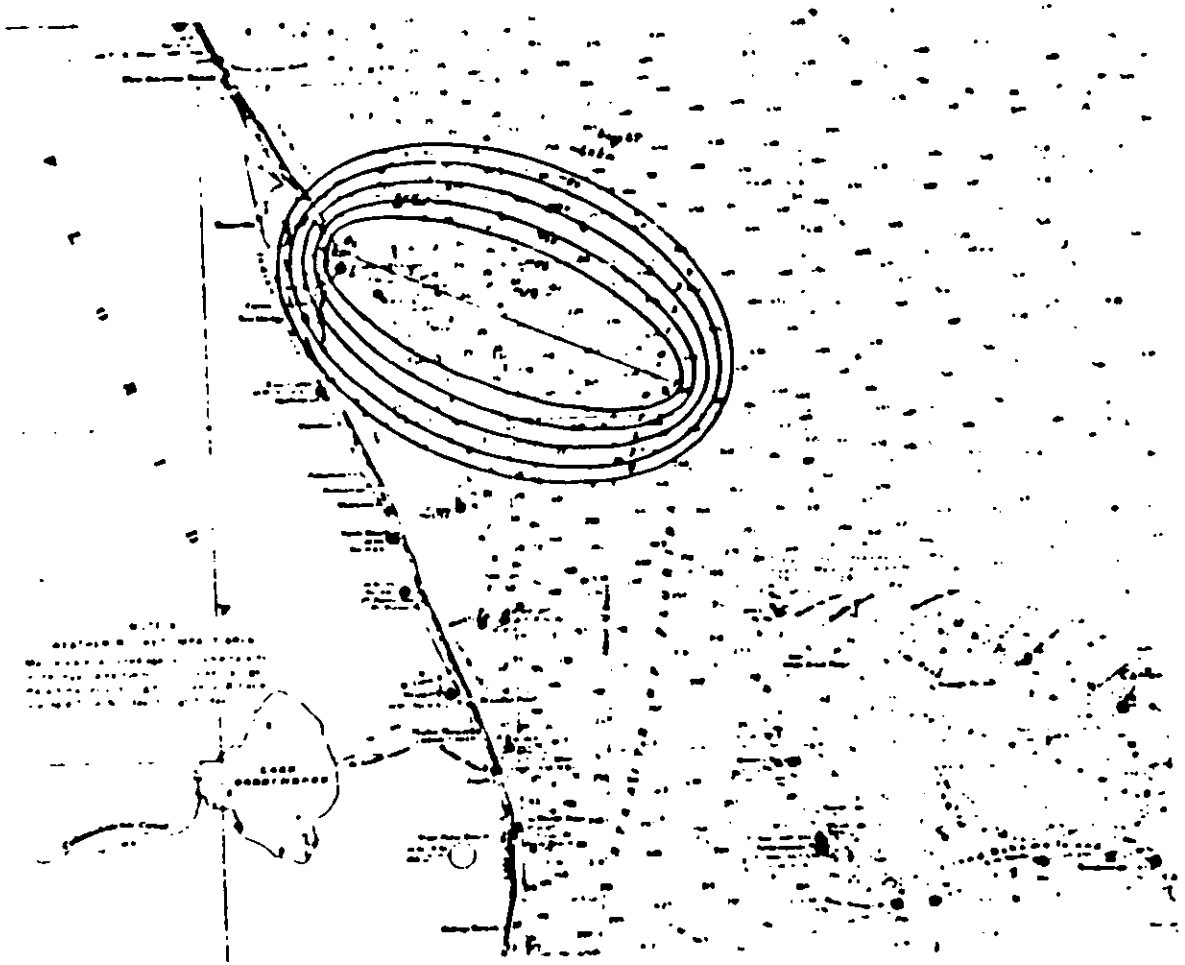

(U) Figure 3. Buoy 40-kHz Range Gates (U)

UNCLASSIFIED

UNCLASSIFIED

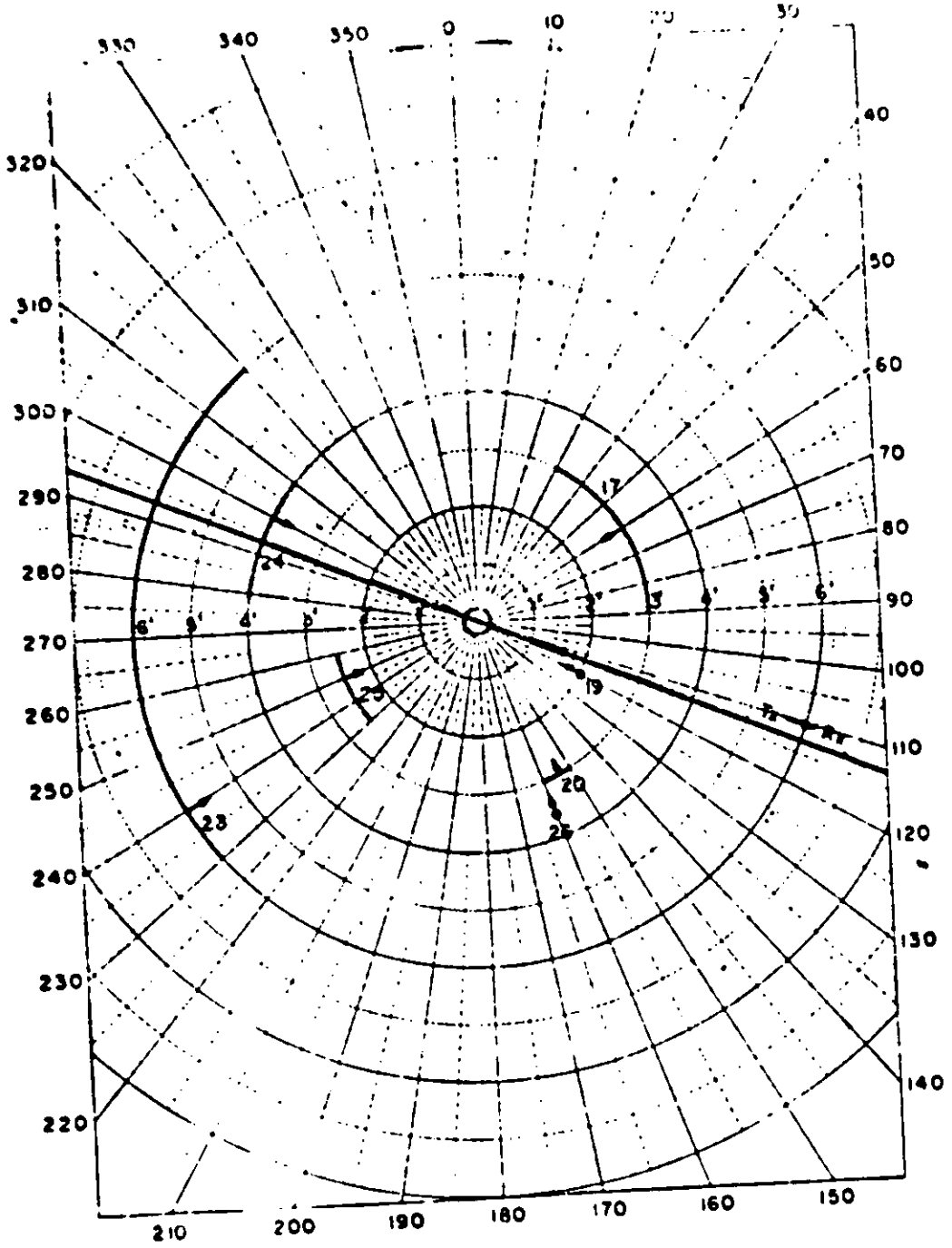

(U) Figure 4. Wave Heights and Directions, March Buoy Data Recorded (U)

(U) Figure 5 illustrates the variation of positive and negative clutter peaks with wave direction. Higher positive clutter is observed for waves approaching the transmitter and receiver, while higher negative clutter is seen for waves receding from the transmitter and receiver, since with the directive BSA and range gate one, the primary scatter region is beyond the transmitter. Figure 6 further illustrates that the detailed behavior of the negative clutter varies with individual range gate areas. Detailed geometrical analysis shows that the observed increase in amplitude of this negative clutter is expected.

(U) The general increase in clutter doppler with higher frequency signals is illustrated in Figure 7. This qualitatively substantiates predictions, and specific data will be sought in which the true maximum shift is observed at two different frequencies so that quantitative comparisons can be made with theory.

(U) Receiving antenna directivity is expected to differentiate between positive and negative clutter or scatter from regions of waves approaching or receding. Figure 8 illustrates that in range gate zero (direct signal included) and range gates one and two as well, both positive and negative clutter is observed by both the directive and monopole antennas. The BSA sees more negative clutter which in this case must come from far off the beam, than did the monopole, which does not favor any azimuthal angle of arrival. The relative positive clutter observed in this case via the monopole is further illustrated, along with the relative signal maximum clutter doppler, on a facsimile display, shown in Figure 9. Note that blackness is higher received power and carrier position is indicated as doppler zero.

(U) A considerably larger data base (three months, four frequencies) is available if we examine the Raytheon CW signals from Cutler, Me. This is particularly valuable for investigating high sea state effects which did not occur with any significance during phase code operations. One preliminary sample was checked for this report, the highest reported sea state of 9 March, and for comparison the low sea state immediately following this on 12 March. The marked effect of this large change in ocean waves is indicated in Figure 10. The combined loss in signal power of several dB and the presence of clutter only about 25 dB down in the case of the high sea state is most evident. The possibility of higher order clutter peaks, further down but with higher doppler shifts, is also indicated in the 9 March power spectrum. In comparison with other data, it is expected that in this case observed energy at about -1 Hz is most likely related to ocean wave effects. Analysis of this and other CW data will continue.

VII CONCLUSIONS

(U) The observed data clearly identifies clutter and, together with the good agreement of Dr. Barrick's predictions with a small sample of data, analyzed in terms of the best available measurements of environmental and system parameters, contributes guidelines to identifying clutter in a much larger set of CW data.

(U) Specific clutter levels and dopplers can be determined for the particular geometries and sea states experienced in this program. Completion of analysis of this data will result in statistics concerning the amplitude and frequency of all identifiable sea clutter in the phase code and CW data and comparison with available sea state data.

(U) Primary limitations to the completeness of this phase of the MAY HILL propagation experiment were the lack of better sea state information, phase code coverage of more varied sea states, and simultaneous high and low frequency signals from the buoy.

(U)

(U) Figure 5. Clutter Variation with Opposite Wave Directions, Runs, low, 5 kHz, Range Gate 1, BSA (U)

UNCLASSIFIED

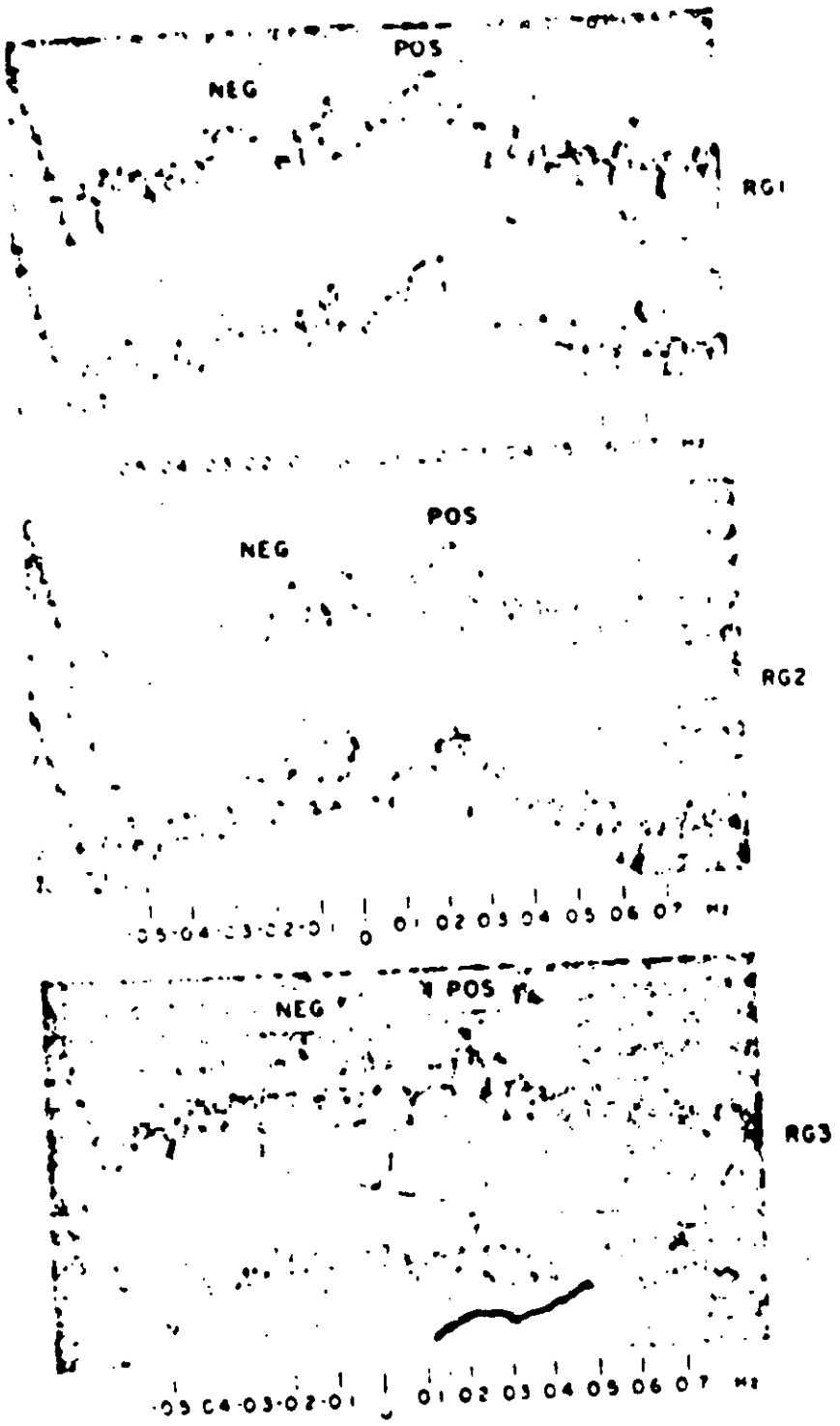

(U) Figure 6. Clutter Variation with Range Gate, Buoy, low, 40 kHz, Range Gates 1, 2, and 3, Monopole (U)

(U)

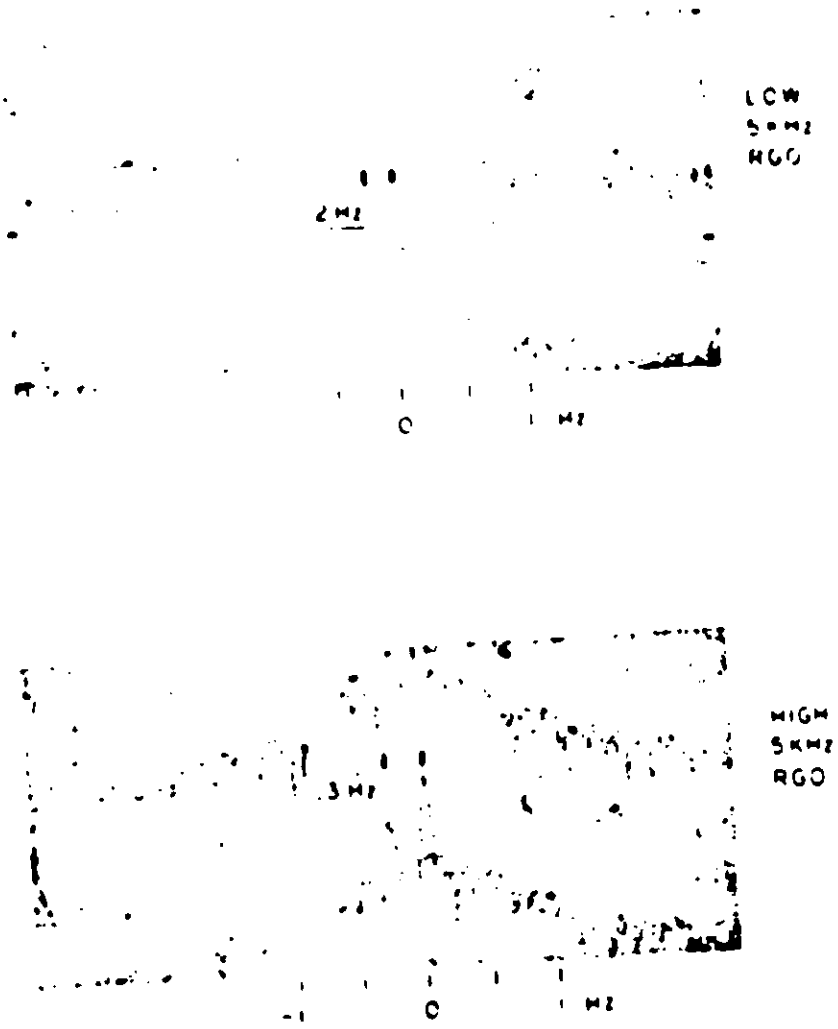

(U) Figure 7 Clutter Variation with Frequency of Transmission, Buoy, 5-kHz, Range Gate 0, BS-5 (U)

(U)

UNCLASSIFIED

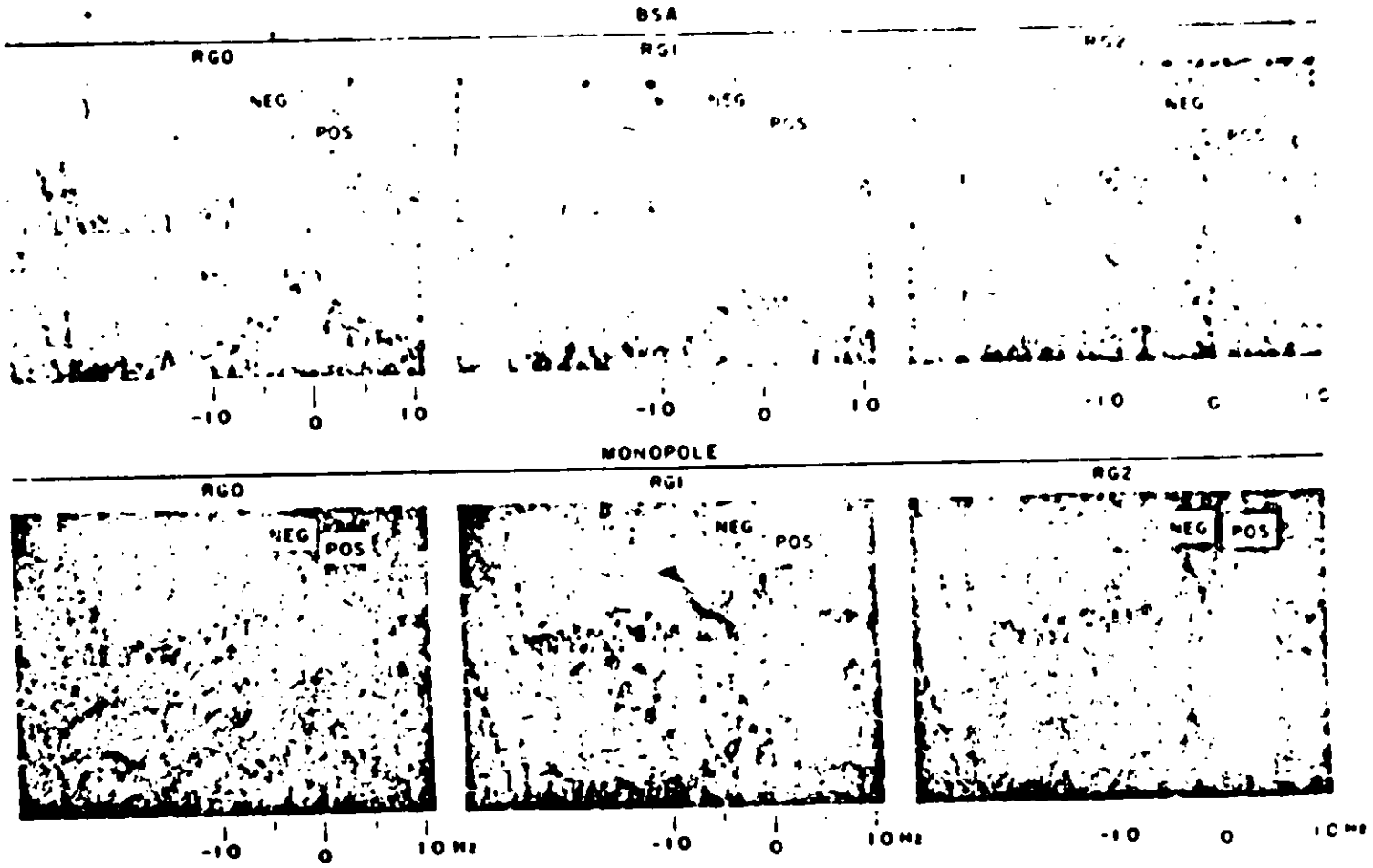

(U) Figure 8. Clutter Variation with Receiving Antenna, Run [illegible], 5-kHz, Range Gates 0, 1 and 2 (U)

UNCLASSIFIED

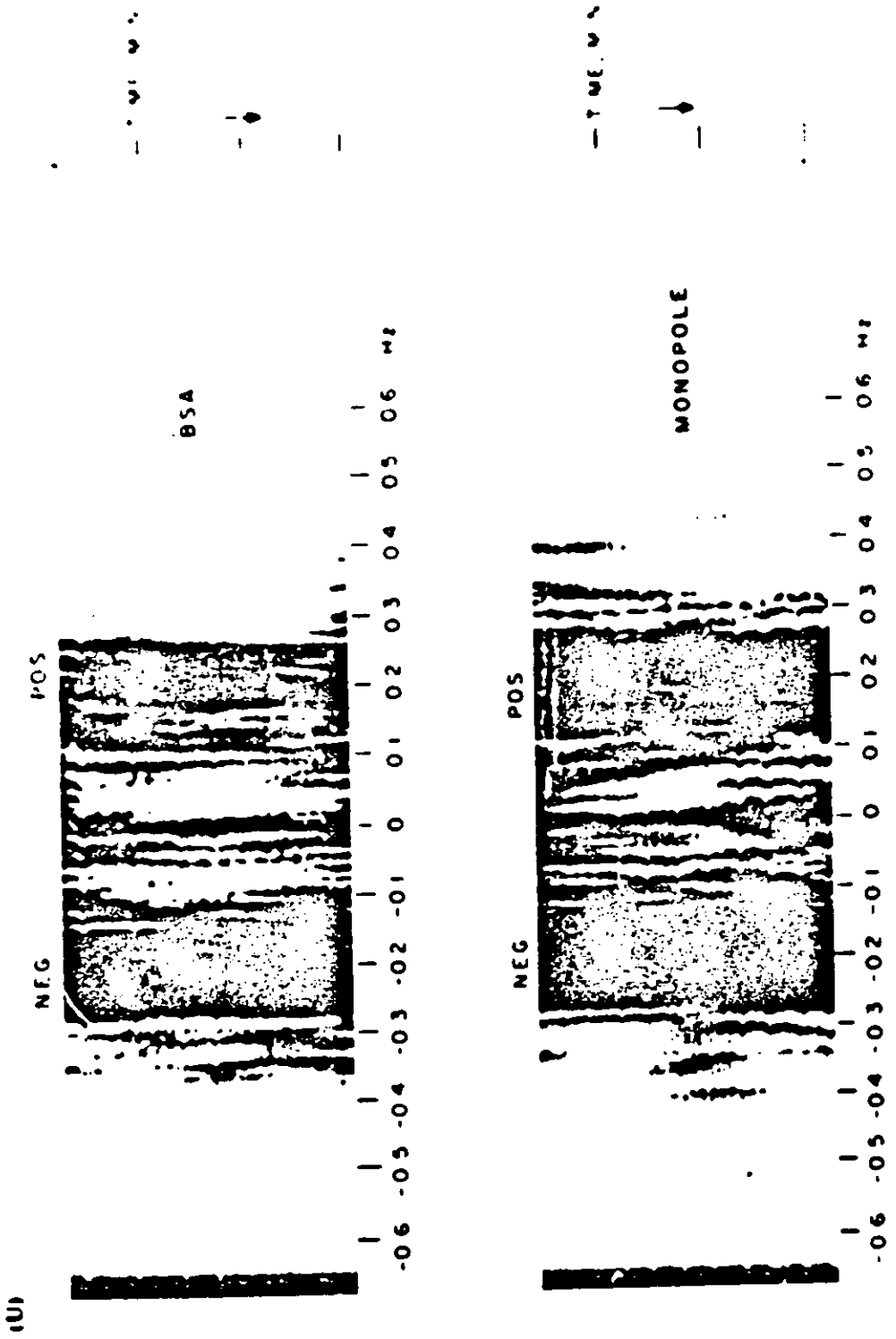

(U) Figure 9. Clutter Variation with Receiving Antenna, Buoy, [illegible] 5 kHz, Range Gate 1, Facsimile Display (U)

UNCLASSIFIED

UNCLASSIFIED

(U) Figure 10. Clutter Variation with Sea State. Raytheon 5 MHz CW Radar, Monopole (U)

THEORETICAL ATTENUATION FOR TERRAIN SEA PATHS (U)

Dr R H Ott

Institute for Telecommunication Sciences
ESSA Research Laboratories
Boulder, Colorado 80302

I INTRODUCTION (U)

(U) Recently [1] an integral equation for calculating the attenuation of radio waves propagating over irregular inhomogeneous terrain was derived. In this paper, the integral equation is applied to four terrain profiles: a Gaussian shaped ridge, a sea-land-sea path, a sea-land-sea path with an island and a slope coast, both at high and low tide. For the case of the Gaussian-shaped ridge, the solution is compared with solutions obtained using classical methods such as diffraction theory.

II EXAMPLES (U)

A A Gaussian Shaped Ridge (U)

(U) The terrain profile is shown in Figure 1. The ridge is 1 km high at a distance of 5 km from the transmitting antenna. This example was chosen as a check on our formula's capability for treating terrain features having large slopes. The slopes for this example are near 45° for some points on the profile. The antenna is vertically polarized and the frequency is 1 MHz. The ground conductivity is 0.01 mho/m and the dielectric constant is 10. In Figure 1 the magnitude of the attenuation function normalized to twice the free space field is plotted versus distance in km from the antenna. The observation point receiving antenna is located on the profile shown in Figure 1. The three sets of data in Figure 1 correspond to three alternative methods for computing the attenuation function and two of these serve as a check on the accuracy of our formulation. The solid circles were computed using our new integral equation. The open circles were computed using the classical Hufford-Lenberg[2] integral equation. The crosses were computed using simple diffraction theory to compute the attenuation function for a

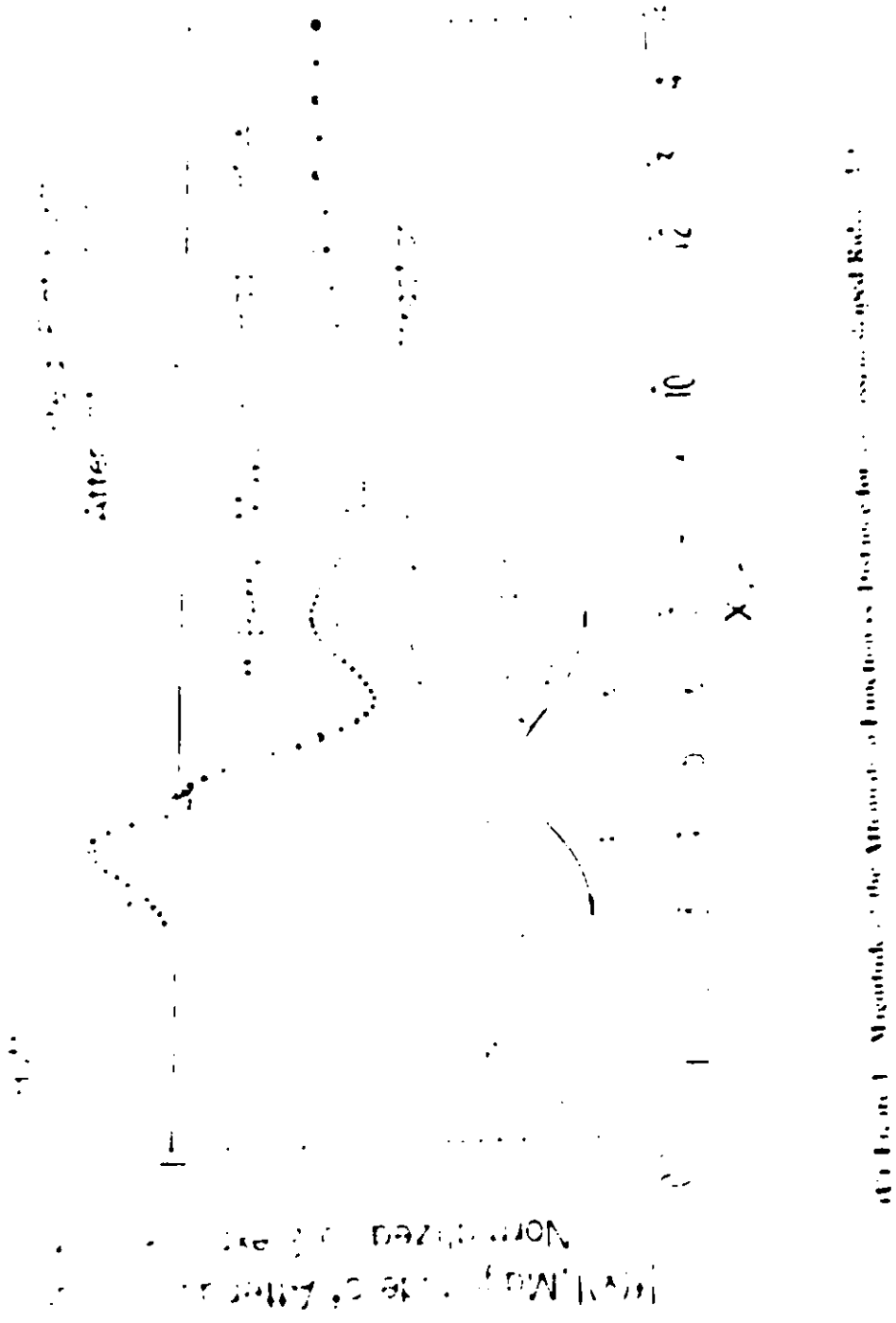

(U)

[illegible] Knife edge model for the ridge. The agreement between the open and solid circles [illegible] this case demonstrates the validity of our new formulation. The advantage of our formulation over the Hufford Embedding formulation is not brought out in this example since the frequency is sufficiently low so that accumulation of roundoff error characteristic of the Hufford Embedding formulation at the receiver does not [illegible] MHz does not occur. Both integral equation solutions agree well with the [illegible] diffraction occurs on the shaded side of the hill. However the diffraction results [illegible] in the attenuation function on the lit side of the hill. This peak in the attenuation [illegible] explained by considering the constructive interference between a direct ray from the [illegible] point near the crest of the hill and a ray which travels along the surface before [illegible] crest. The peak has a magnitude approximately twice the free space field. The field drops [illegible] on the lit side of the hill then gradually recovers as the ray diffracted at the crest is combined with [illegible] surface wave travelling down the slope.

B. A Sea Land Sea Path (U)

(U) The terrain profile is flat in this example and the ground constants have abrupt changes at the sea land sea interfaces. This example was selected as a check on the mixed path capabilities of our [illegible] tion. In Figure 2 the results for the magnitude of the attenuation function normalized to twice the free space field are plotted versus distance from the antenna in km. The antenna is vertically polarized and the frequency is 10 MHz. The solid circles represent the attenuation function computed numerically using our new formulation. The open circles in Figure 2 represent the attenuation function computed by Rasch [ITS 137][3] using a perturbation approach. The data given by the crosses in Figure 2 represent the attenuation function computed using a method based upon the classical residue series. This latter method is exact for the three section earth considered in this example. The agreement between the solid circles representing our new integral equation and the crosses appears to demonstrate the validity of the formulation in treating mixed path propagation problems. The abrupt changes in conductivity and dielectric constant used in this example do not represent a realistic sea land interface. Our formulation is capable of treating a continuous variation of conductivity and dielectric constant.

C. A Sea-Land-Sea Path with an Island (U)

(U) This example is a combination of the terrain features of example A and [illegible] features of example B. The island is drawn to scale in Figure 3 [illegible] elevation is 2 [illegible] nearest point. This elevation may be greater than the elevation of any point on islands of interest [illegible] MAY BELL program however this elevation is much smaller than the elevation on some islands [illegible] Mt. Mauna Loa in Hawaii, which has an elevation of 4 km. The magnitude of the attenuation function normalized to twice the free space field versus distance is plotted in Figure 3. The antenna is vertically polarized and the

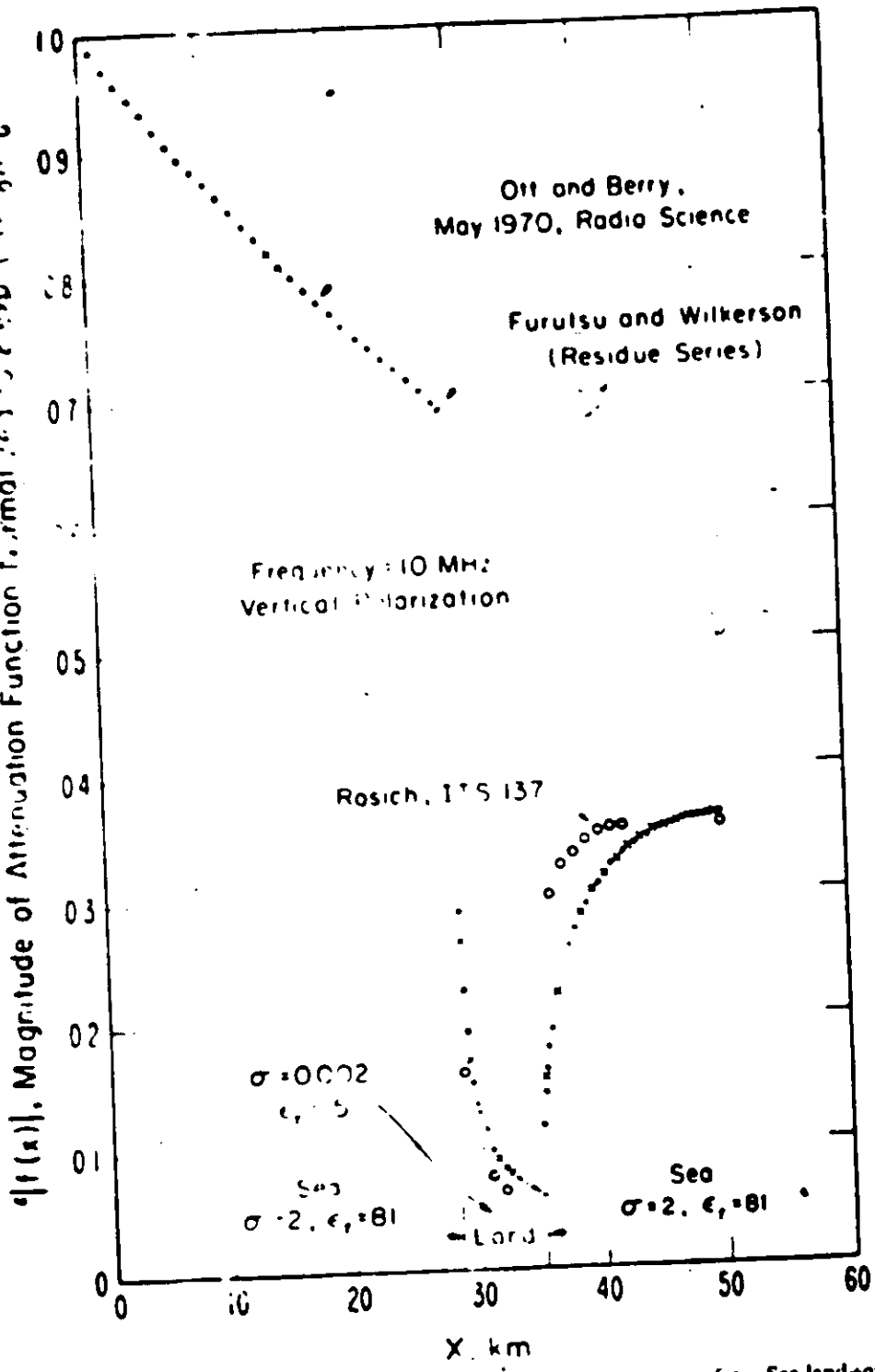

(U) Figure 2. Magnitude of the Attenuation Function vs Distance for a Sea-land-sea Path. (U)

Figure 3. Magnitude of the Attenuation Function vs Distance for a Sea-Land-Sea Path with an Island

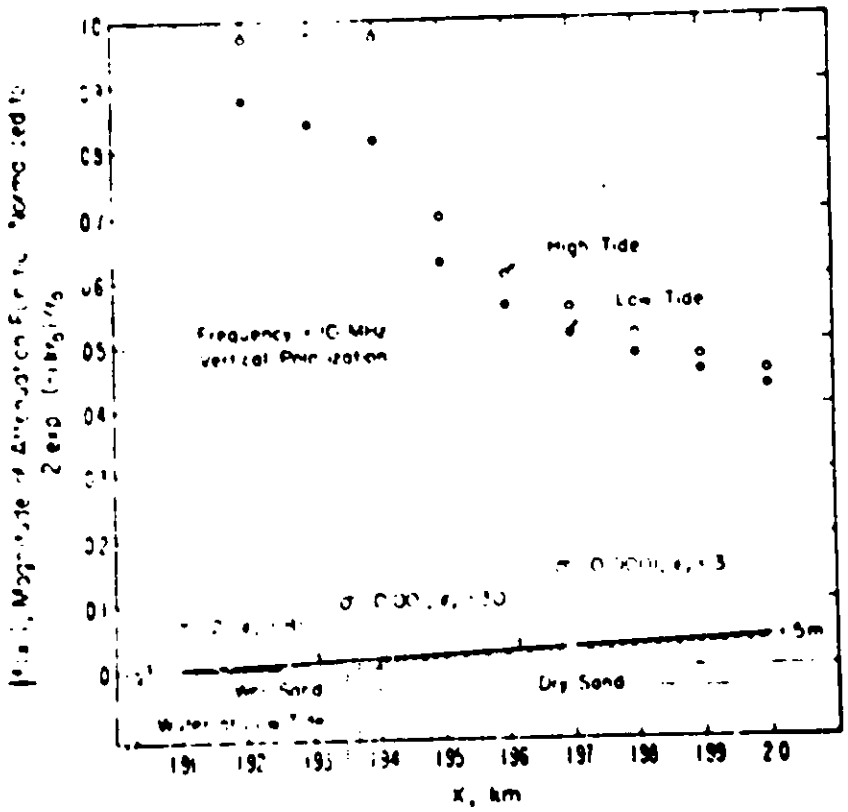

Figure 4. Magnitude of the Attenuation Function vs Distance for a Sloping Beach at High and Low Tide

(U)

...ency is 10 MHz. For comparison the magnitude of the attenuation function for a flat island is also ... in Figure 4. The most interesting feature of Figure 4 is that the terrain profile has a greater effect ... the attenuation function than do changes in the ground constants. This may be an important consider... ... MAN BASED systems since the field strength may be highly attenuated in the shadow of an ... with moderate elevations.

(U) A Sloping Beach at High and Low Tide

... example was brought to the author's attention by Burrick[4]. The terrain profile together with ... ground constants are shown in Figure 4. Figure 4 also shows the attenuation function ... distance. The free space field plotted versus distance from the transmitting antenna is 0 dB. In ... case of water the transmitting antenna may be as far as 120 km from the beach[4], however, for this ... example the transmitting antenna was taken to be 2 km from the beach. This change in location ... antenna merely changes the ordinate scale in Figure 4, but not the general features of ... attenuation function as the radio wave strikes the beach. The antenna is vertically polarized and the ... is 10 MHz. The solid circles represent the attenuation at low tide while the open circles ... attenuation at high tide. The differences in the attenuation function at high tide and low tide ... for observation points right up the beach. This is partially caused by the focusing proper ... for observation points right up on the beach. The model used to study attenuation at high ... is an oversimplification of the true situation. For example, the water table under the dry ... may be less than one skin depth (approximately 16 meters for $\sigma = 0.0001$ mho/m and $f = 10$ MHz) ... surface. This would result in less contrast in σ and ϵ_r as the tide varied. There is the additional ... that the tide comes and goes every 12 hours which makes σ and ϵ_r functions of time. This ... makes the attenuation of the radio wave a function of time. These further complications are however ... on the scope of applicability of our formulation.

III REFERENCES (U)

1. R. H. Ott and L. A. Berry, "An Alternative Integral Equation for Propagation Over Irregular Terrain," Radio Science, May 1970, UNCLASSIFIED.

2. G. A. Hufford, "An Integral Equation Approach to the Problem of Wave Propagation Over an Irregular Terrain," Quart. Appl. Math. Vol. 9, No. 4, pp. 391-404, 1952, UNCLASSIFIED.

3. R. K. Rosich, "High Frequency Ground Wave Attenuation Over Inhomogeneous Path," ESSA Research Lab. Tech. Memo - ITS 137, August 1968, UNCLASSIFIED.

4. D. E. Barrick, Private Communication, UNCLASSIFIED.

PRECEDING PAGE BLANK - NOT FILMED

[redacted]

UNCLASSIFIED

SUBMARINE RADAR CROSS SECTIONS AT HF (U)

G. N. Oetzel

Stanford Research Institute
Menlo Park, California

I INTRODUCTION (U)

(U) The submarine-launched ballistic missile (SLBM) is distinguished as a radar target chiefly by the fact that it is a much smaller and more difficult target than a large ICBM. It is physically smaller at launch since both U.S. and Russian submarines will only accommodate missiles that are about 10 m long. Because of its smaller size there is less engine thrust, and the SLBM generally does not continue the engine burn as high in the ionosphere as the ICBM.

(U) The current Russian SLBM's, the SSN-4 and SSN-5 are very-short-range, liquid-fueled missiles. Both are single stage missiles. The SSN-5, the larger of the two, has a maximum range of about 1300 km. Engine burnout occurs at about 70 km, when the missile velocity is only about 3.5 km/s.

(U) In the future, multi-stage Russian SLBMs with performance comparable with or exceeding that of the Polaris can be expected. The A3 Polaris has a maximum range close to 5000 km, and second-stage burnout termination occurs at about 170 km.

II LOW-ALTITUDE CHARACTERISTICS (U)

(U) When a missile is below 70 or 80 km, the burning engine does not increase the radar cross section very much, if at all. When radar illumination of the vehicle passes through the engine plume, attenuation may occur and reduce the radar cross section (RCS) to extremely small values. Because of this attenuation, a "blackout" of the missile echo is usually observed by backscatter radars located near the missile launch site.

(U) When the missile is viewed from aspects other than the rear, the RCS in the low altitude regime is simply the skin cross section of the vehicle. Samples of the skin cross section, or static RCS, of the Polaris and SSN-5 are shown in Figures 1, 2, and 3. Figure 1 shows the maximum RCS of the Polaris

[redacted]

UNCLASSIFIED

(U) [illegible] below [illegible] frequency. [illegible] the missile and [illegible] assumed to be [illegible] the [illegible] and missile axis at [illegible] aspect [illegible] will reduce the RCS from the values shown.

(U) Figures 2 and 3 show similar [illegible] for the Polaris stage and for the SSN-8. In comparison of these figures shows that the RCS is of the order of 10 m² or less at the frequencies below 30 MHz at all aspects except [illegible] to MAY BELL. Because the SSN-8 is somewhat larger than the [illegible] RCS at 30 MHz may be as large as 100 m² but no enhancement over this value should be [illegible] altitude because of the low altitude of thrust termination.

III. ENHANCEMENT IN THE IONOSPHERE (U)

(U) In a rocket engine thrust termination above 80 km the RCS increases with altitude due to shock [illegible] around the boundary of the exhaust plume. The increased RCS due to this mechanism [illegible] up to an altitude of about 120 km where the mechanism of RCS enhancement changes. In [illegible] RCS values greater than 10^5 m² have been observed on Polaris launches in this altitude [illegible]. However it is not uncommon to find that the RCS never exceeds 10^3 m² on a particular launch [illegible].

(U) Figures 3 and 4 show the range of results obtained by ITT and AVCO RL on the most favorable [illegible] of the 1964 measurement series at MILLER. Of 18 Polaris launches observed, each organization chose to reduce data on just three launches for reasons of economy and because the data quality was [illegible] on the other launches.

(U) Observations of larger missiles, such as the Minuteman, show that the RCS generally rises as the missile [illegible] to burn above 120 to 130 km in the daytime but that the RCS falls dramatically above that altitude at night. The result is a considerable overall difference in detectability between day and night observations.

(U) While the Polaris has been observed to burn above 130 km, the continued rise of RCS in the daytime has not been observed. The large RCS at about 140 km in the ITT data (Figure 3) is apparently associated with separation of the re-entry body. Making allowance for the separation peak, no [illegible] altitude enhancement is seen in the data of Figures 3 and 4.

(U)

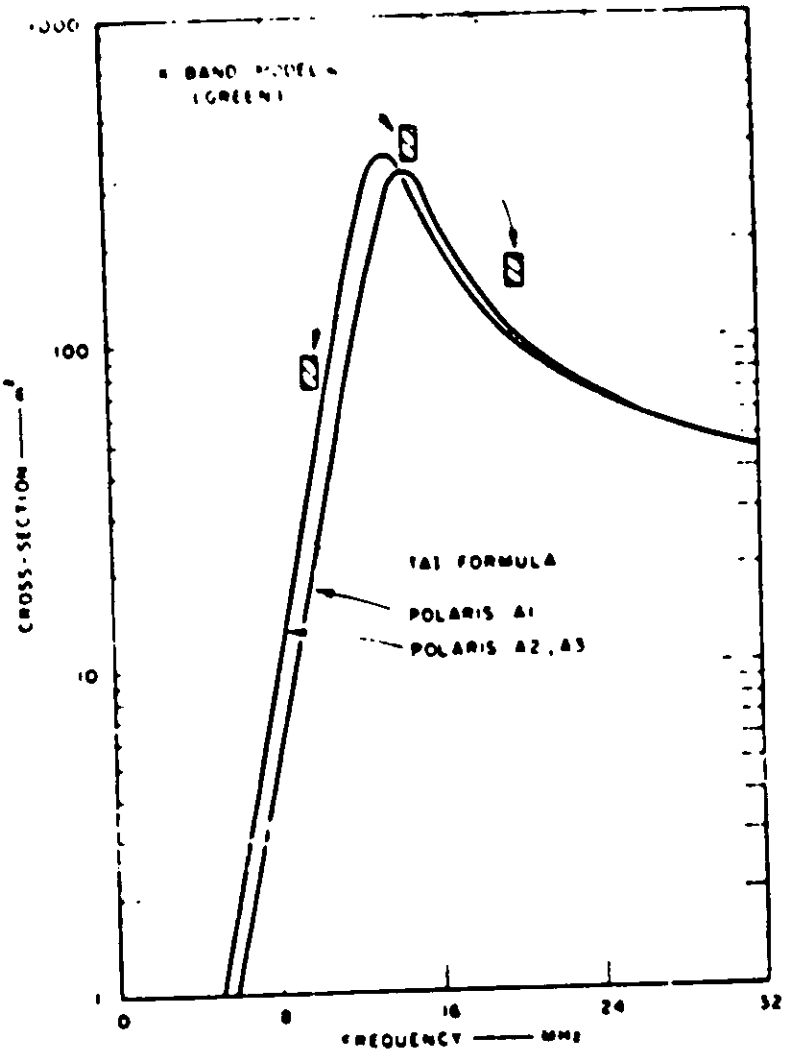

(U)
(S) Figure 1. Comparison of X-Band Model Measurements and Tai Formula Calculation for E-Plane Maximum RCS of Polaris (U)

(U)

UNCLASSIFIED

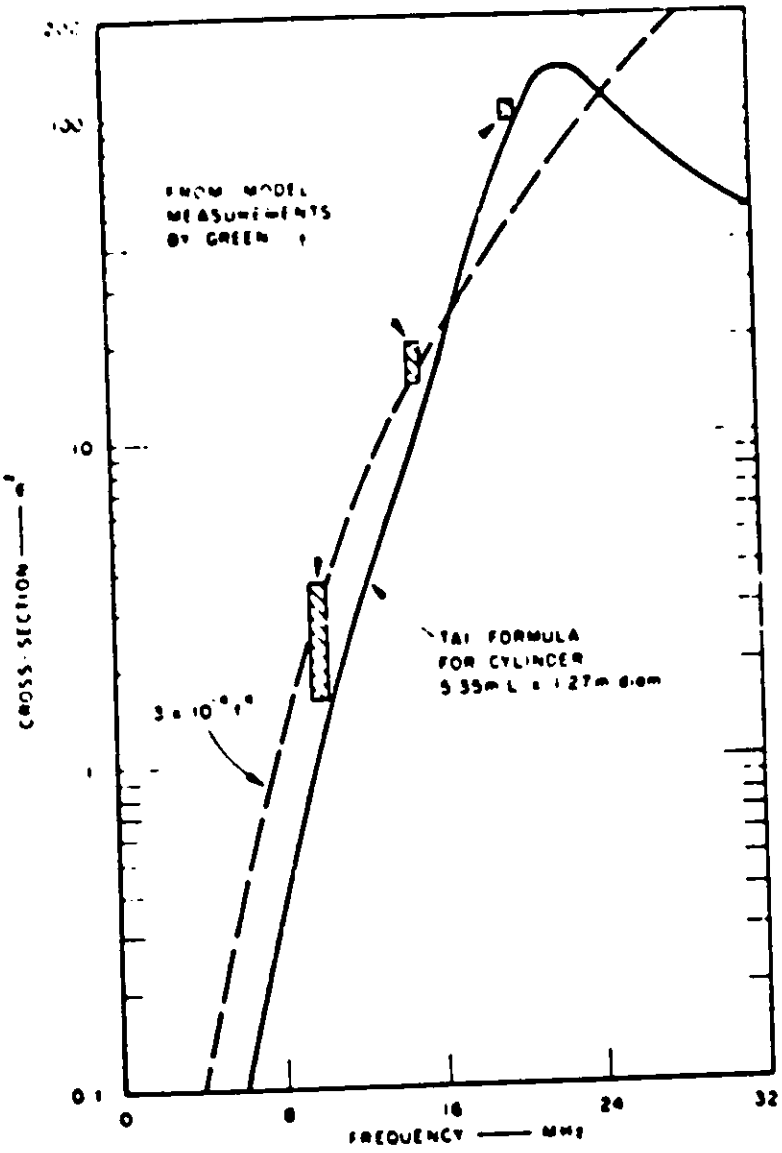

(U) Figure 2. E-Plane Maximum RCS for Polaris after First-Stage Separation [1]

UNCLASSIFIED

(U)

[redacted]

UNCLASSIFIED

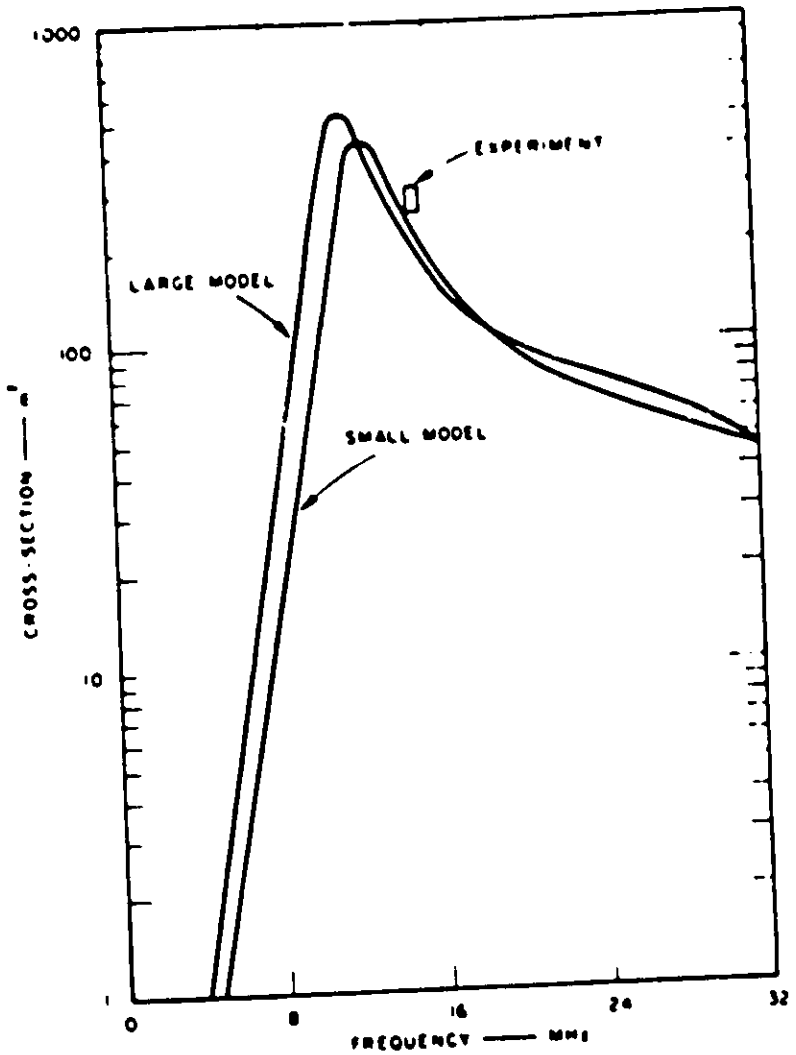

(U)(S) Figure 3. E-Plane Maximum RCS Estimates for the Russian SSN-5 Missile (S)

[redacted]

UNCLASSIFIED

IV IMPLICATIONS FOR MAY BELL (U)

(U) The SLBM is an extremely demanding target for either an OTH system or a semi-OTH system with a low-power illuminating transmitter, such as is contemplated in the BTH W concept. While larger RCS values are obtained on occasion, it seems best to expect the RCS to be of the order of 50 m^2 in the first few km at launch, and 10^{-1} to 10^{-4} m^2 at 100 to 120 km. The enhanced RCS at high altitudes may last for a few seconds only, which provides an additional problem for detection.

(U) Observations prior to the present have generally been made at 12 MHz or above. It would be useful if tests of the MAY BELL equipment would also provide some observations in the 6- to 10-MHz band.

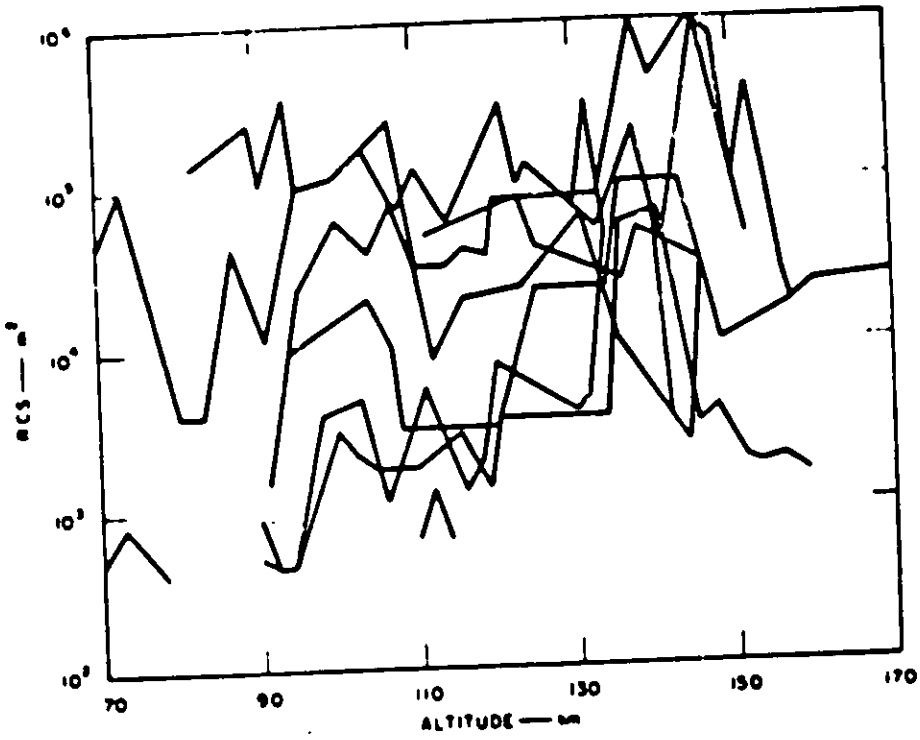

(U) Figure 4. Composite Plot of RCS as a Function of Altitude for the ITT Data from Tests 0324, 2903, and 2955 (U)

[redacted]

(U)

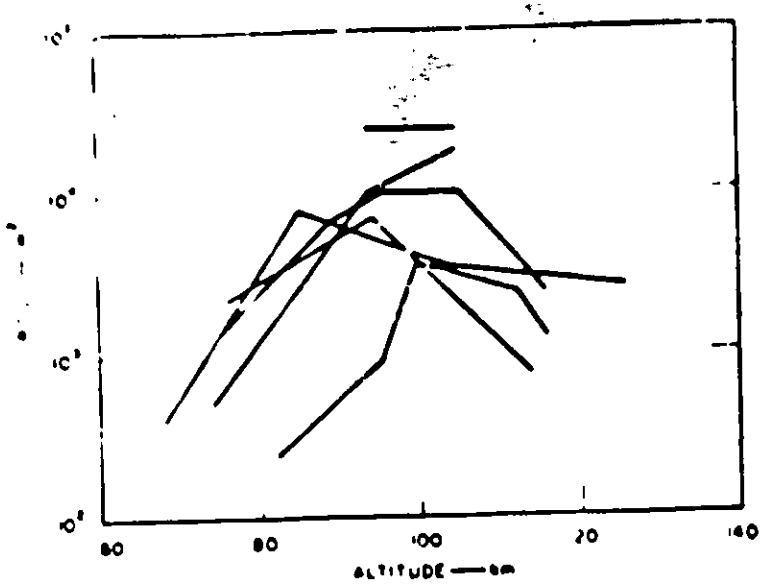

(U) (S) Figure 5 Composite Plot of Ai s RL Observations of Polaris Launches 0038, 2903, and 2955 from GBI (U)

[redacted]

UNCLASSIFIED

[redacted]

MEASURED SHIP CROSS SECTIONS (U)

J. M. Headrick

Naval Research Laboratory
Washington, D. C.

(U) Cross section determinations have been made with the MADRE radar using ground-wave propagation. A quarter-wave monopole located on the Chesapeake Bay has been the gain standard used for antenna calibration. The water conductivity has been measured for each test and a path-loss determination made after the program of L. Berry of ESSA.

(U) Figure 1 shows a MAY BELL buoy that was fitted with a modulated (10-Hz) antenna by EPL-ITT. Figure 2 is an example of the characteristics of this type target. The left column contains, from top to bottom, the echo amplitude of one sideband versus time, the Dopplers (9.5 Hz and 10.5 Hz) versus time, and the amplitudes versus frequency. A one-half Hz offset from zero was used to obtain the above. In the column on the right a similar set of pictures (in different order) are shown but with a true zero frequency reduction. Notice that the two sidebands do interfere both constructively and destructively depending upon the time.

(U) Figure 3 shows the radar return from the final version of the buoy antenna target. The target appears at 7.5 and 8.5 Hz, the level reference at 10.5 Hz. The radar area determined for one sideband was 19 dB m^2. The relation used was

$$\sigma = \frac{P_t\,(4\pi)^3\,R^4\,F^2}{P_t\,G^2\,\lambda^2}$$

where F is the ground-wave loss factor per L. Berry of ESSA.

(U) Figure 4 gives normalized signal levels made using the above techniques on HMS Arethusa, a British frigate. The difference between the curve defined by these points and the plotted loss curve gives the radar area. The droop in the signal levels at the longer ranges due to shielding by Cove Point is seen on Figure 5.

(U) Figure 6 is a picture of the USS Thomas, and Figure 7 gives the radar area determination.

(U) Figure 8 is a picture of the USS Furet, and Figure 9 gives the radar area determination.

UNCLASSIFIED

[redacted]

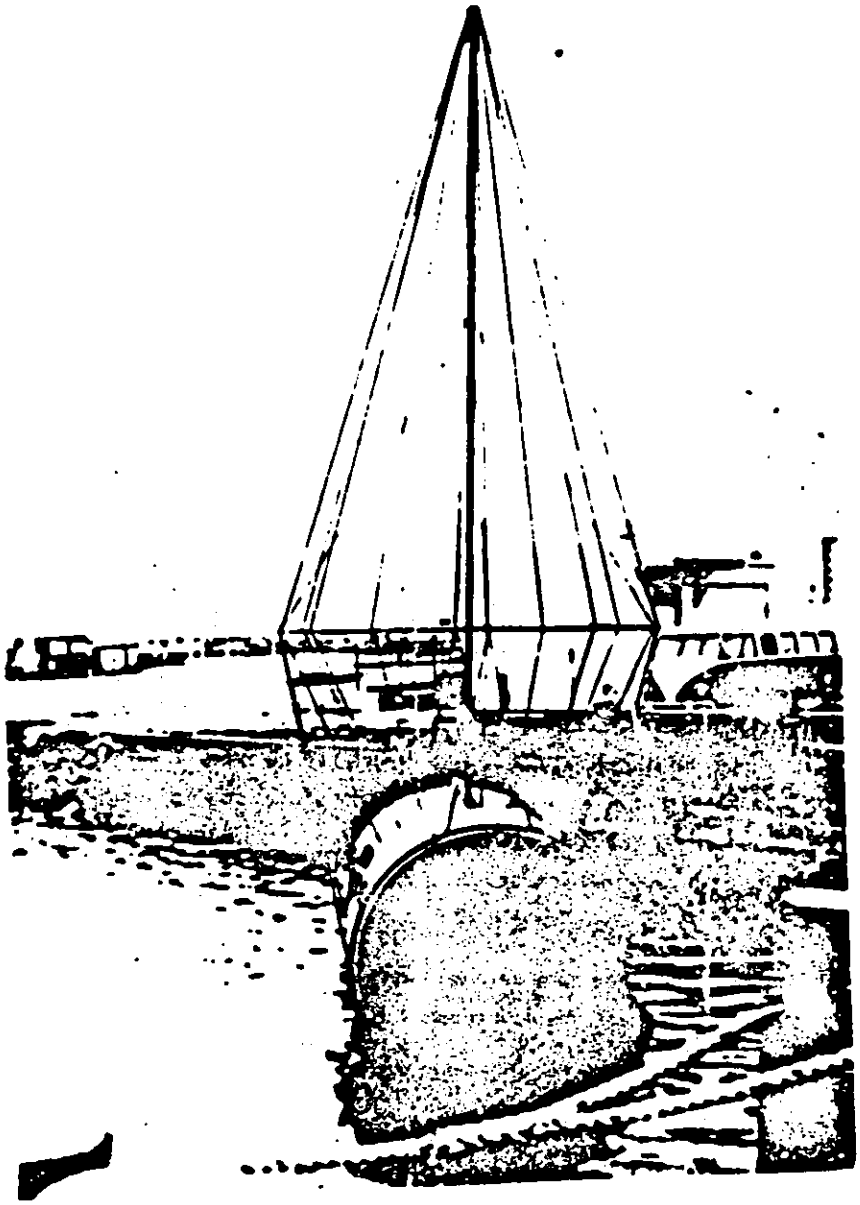

(U) Figure 1. Buoy with Target Antenna (U)

(U)

UNCLASSIFIED

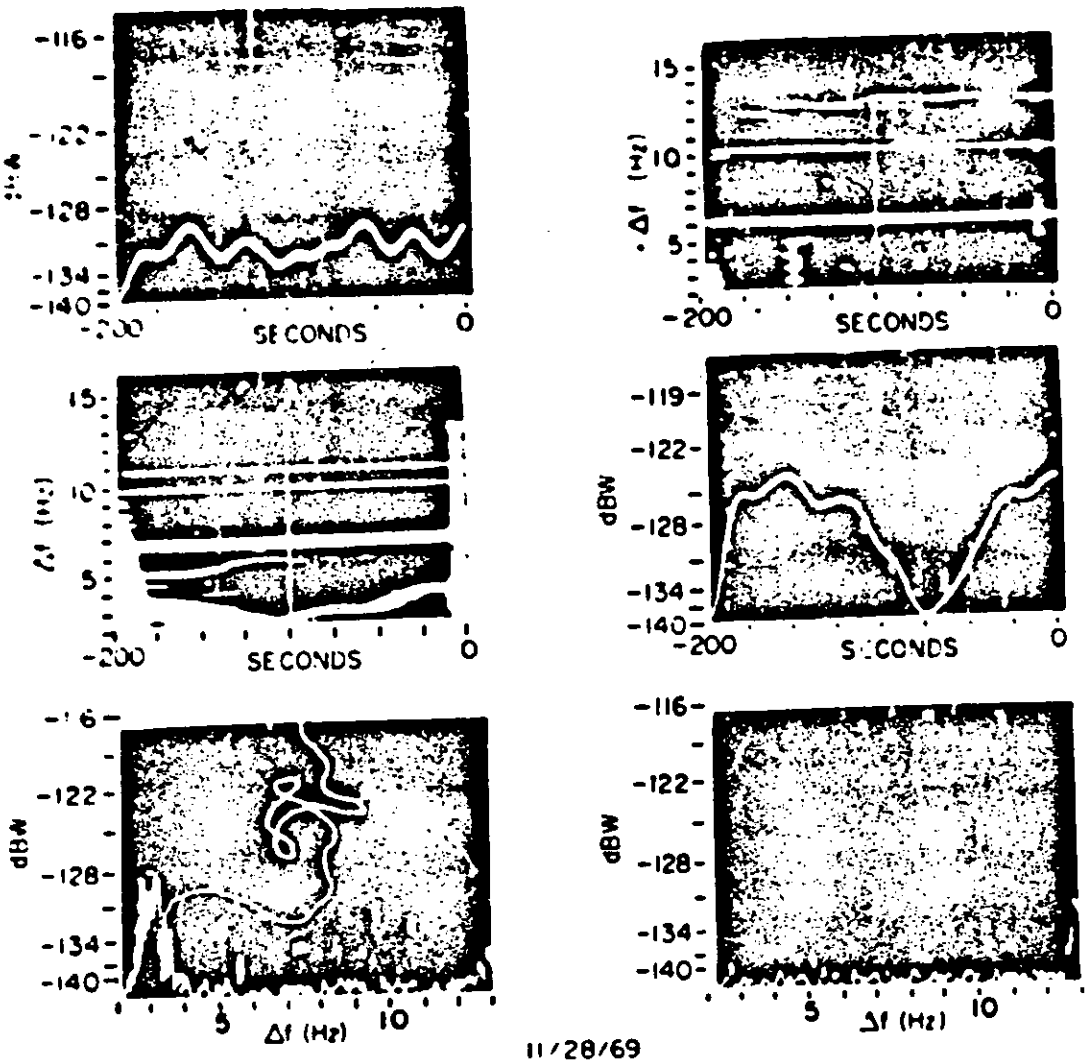

11/28/69

13.687 MHz, 60 dBW, 125 μs, 45 PRF, FTM, 8 kHz Sample rate, 0.15 Hz BW

(U) Figure 2. Buoy Echo (U)

[redacted]

UNCLASSIFIED

UNCLASSIFIED

[redacted]

(U)

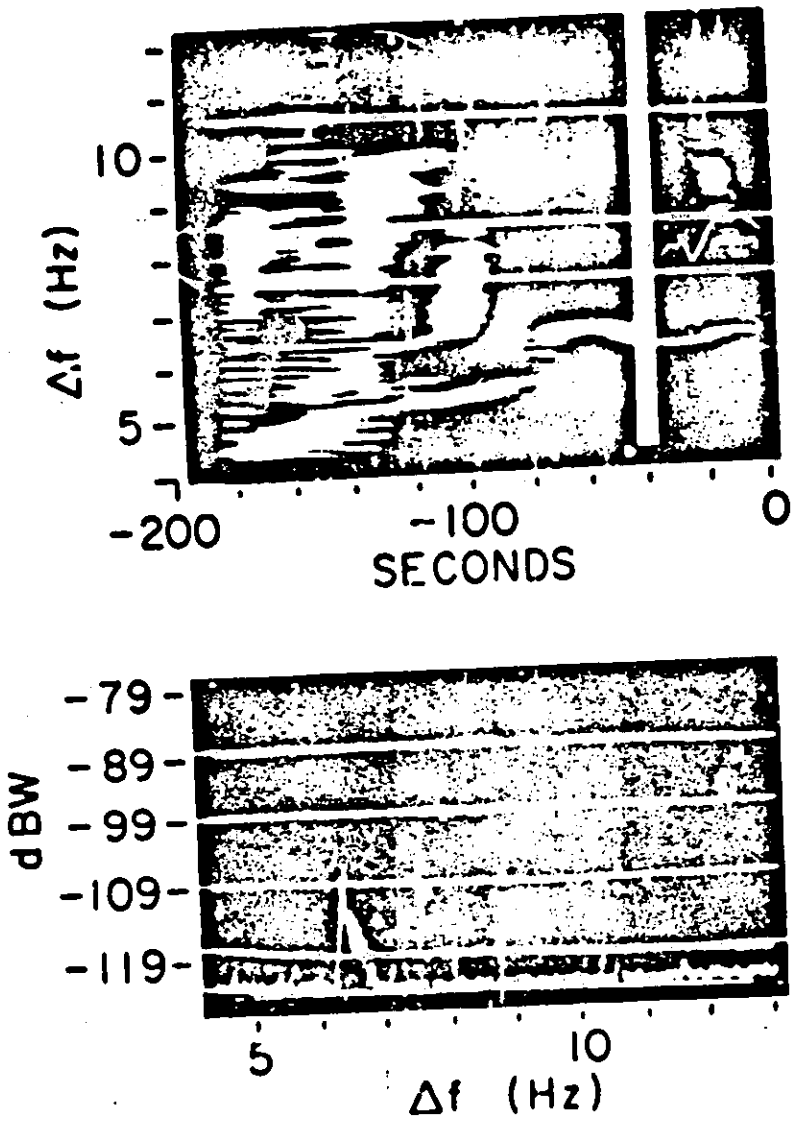

(U) Figure 1 [illegible]

[redacted]

UNCLASSIFIED

(U)

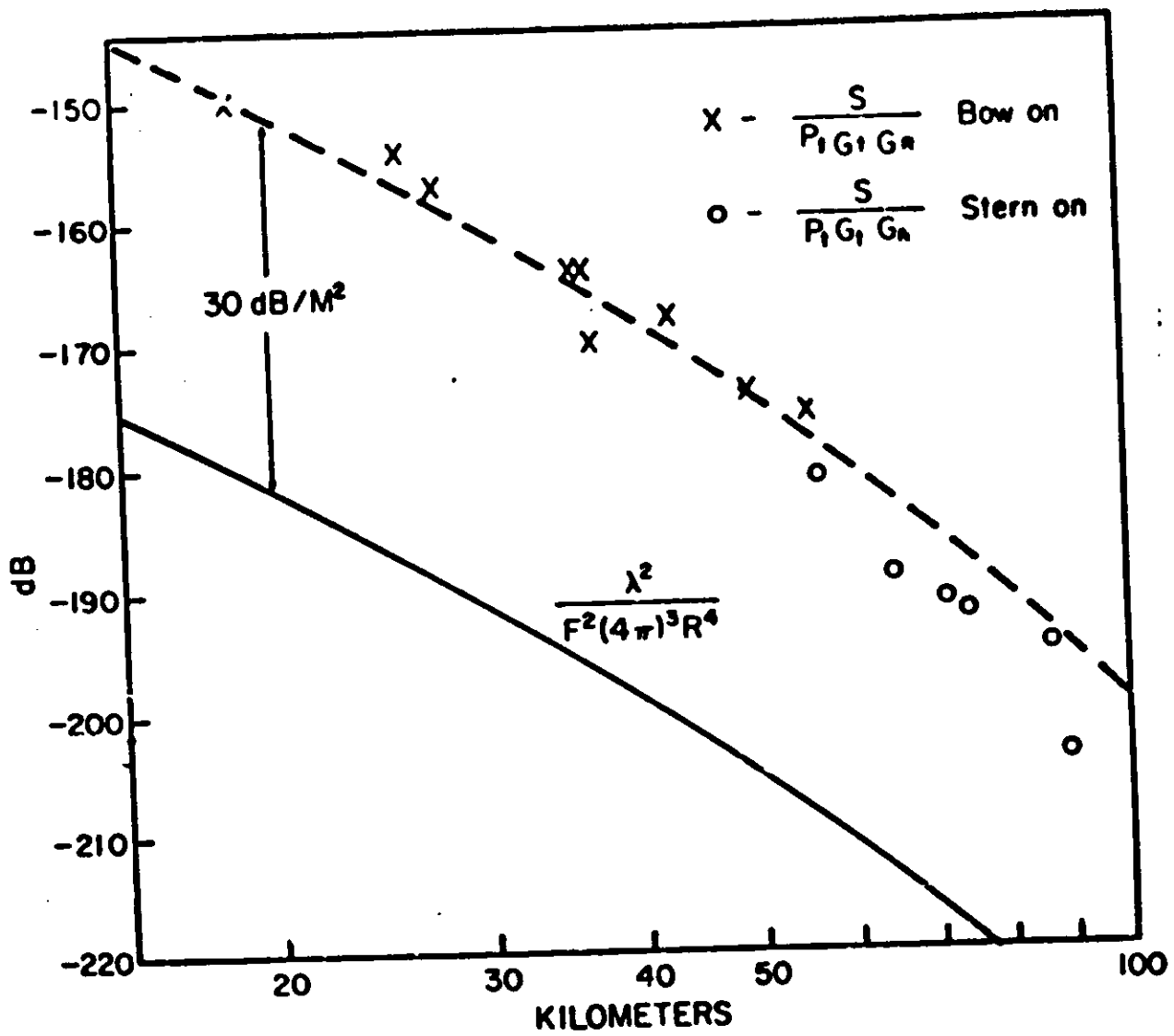

(U) Figure 4 Normalized Signal Levels from HMS Arethusa (U)

UNCLASSIFIED

UNCLASSIFIED

UNCLASSIFIED

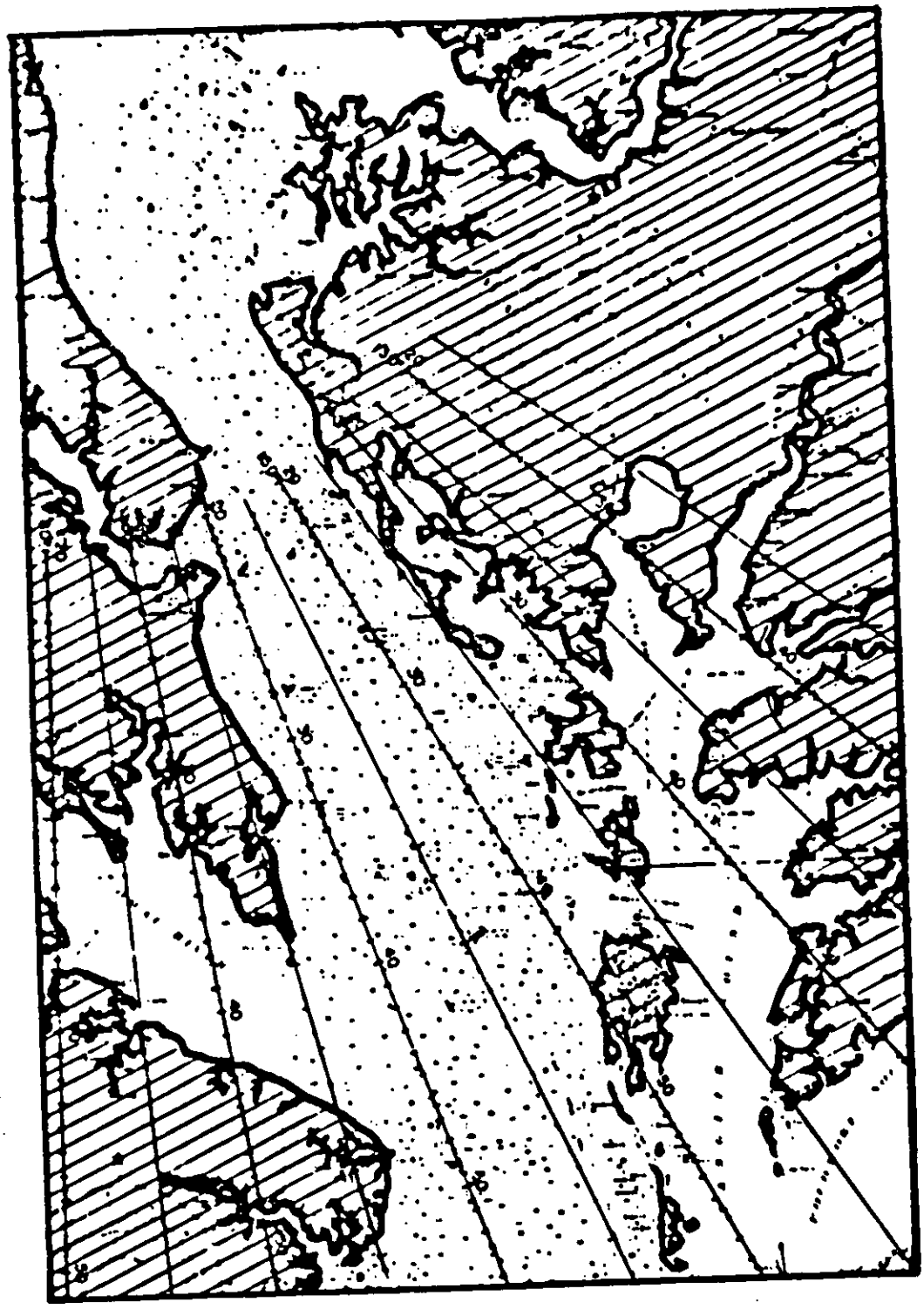

(U) Figure 5. Chesapeake Bay (U)

UNCLASSIFIED

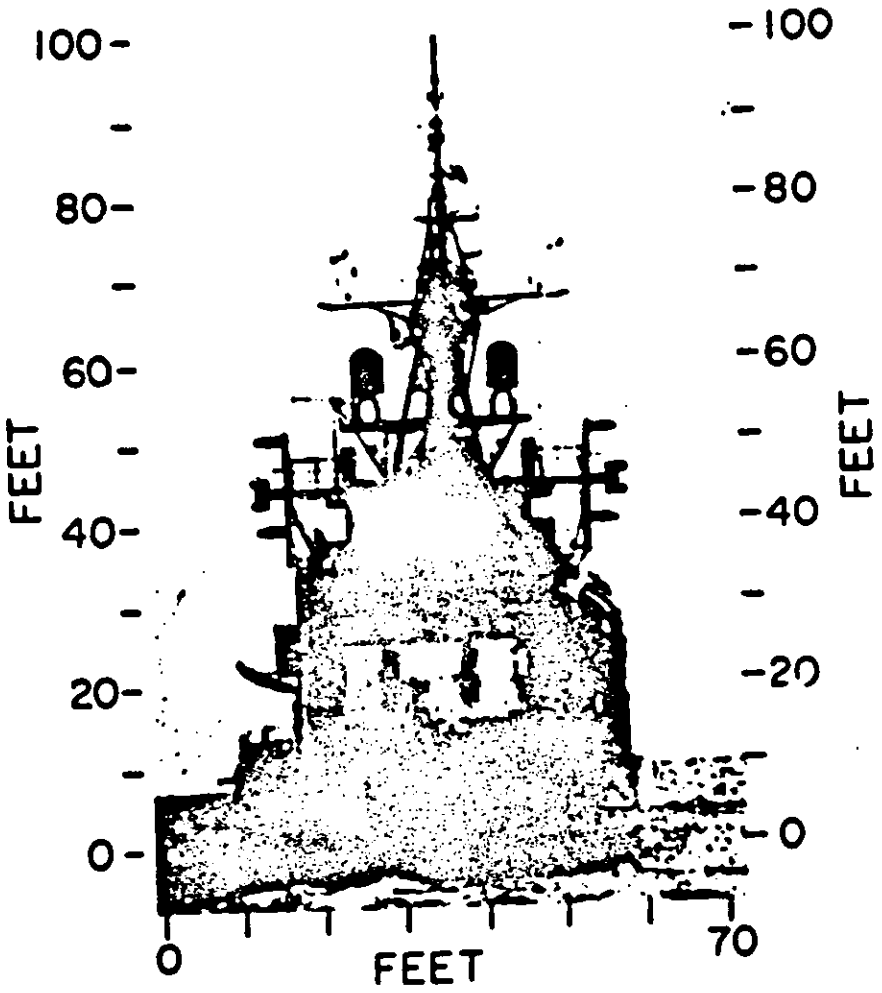

(U) Figure 6. USS Lloyd Thomas, DD-764 (U)

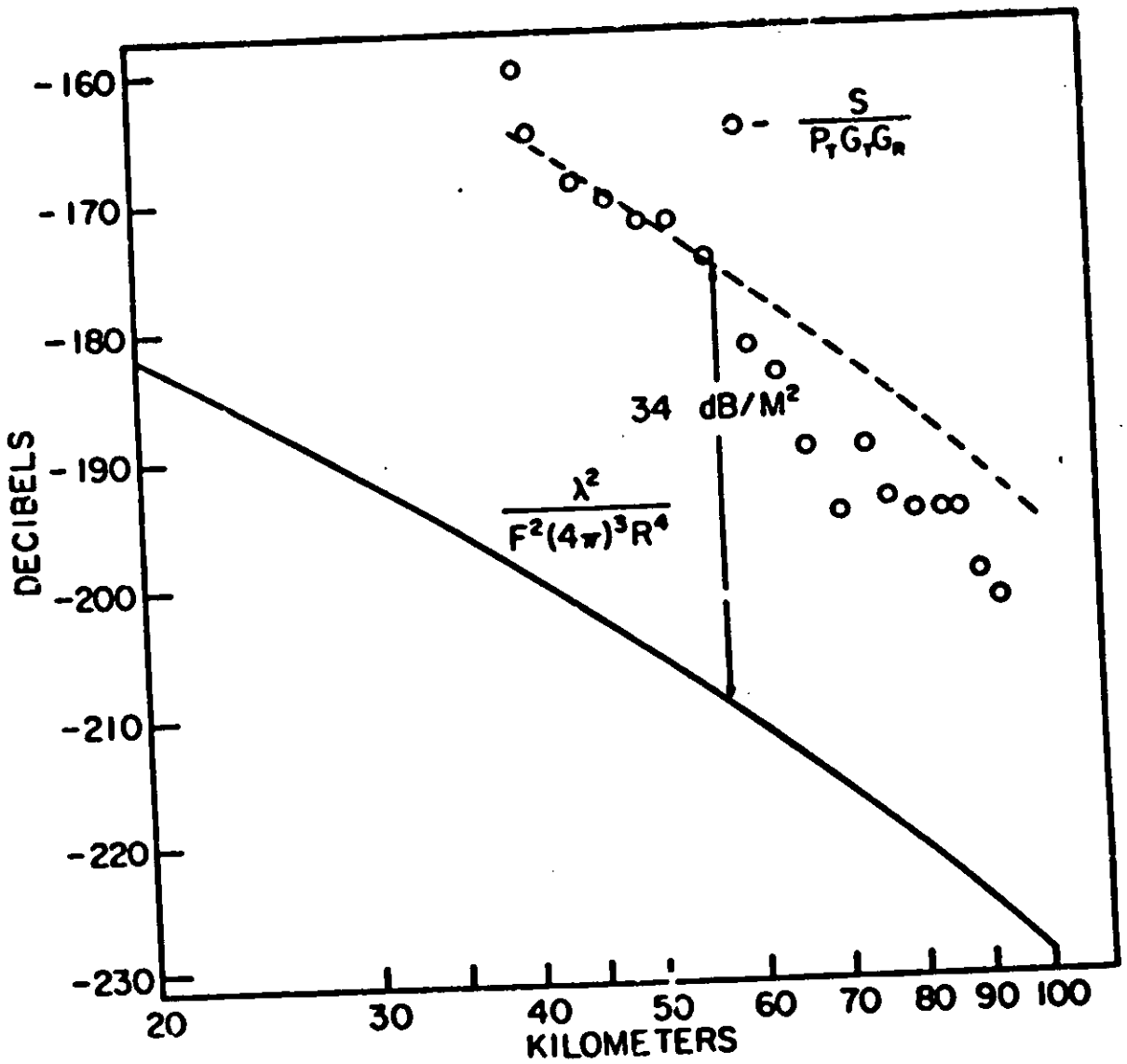

(U) Figure 7. Normalized Signal Levels from USS Lloyd Thomas (U)

UNCLASSIFIED

(U)

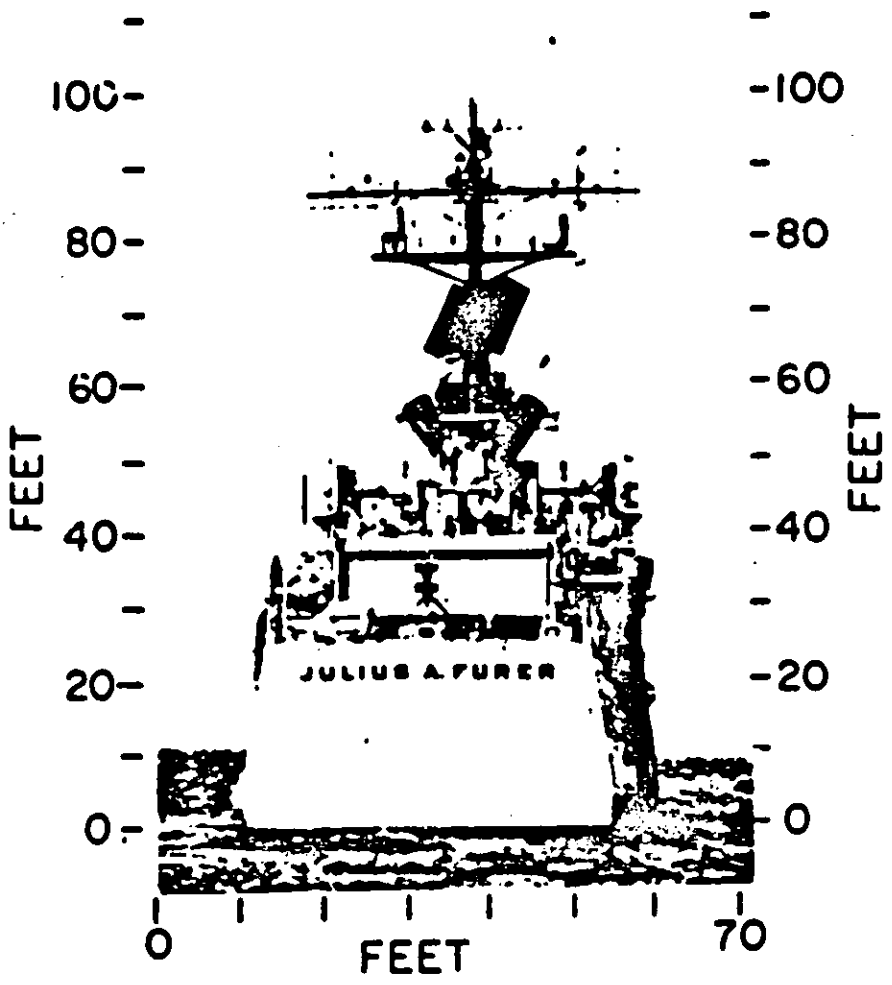

(U) Figure 8. USS Julius A. Furer, DEG-6 (U)

UNCLASSIFIED

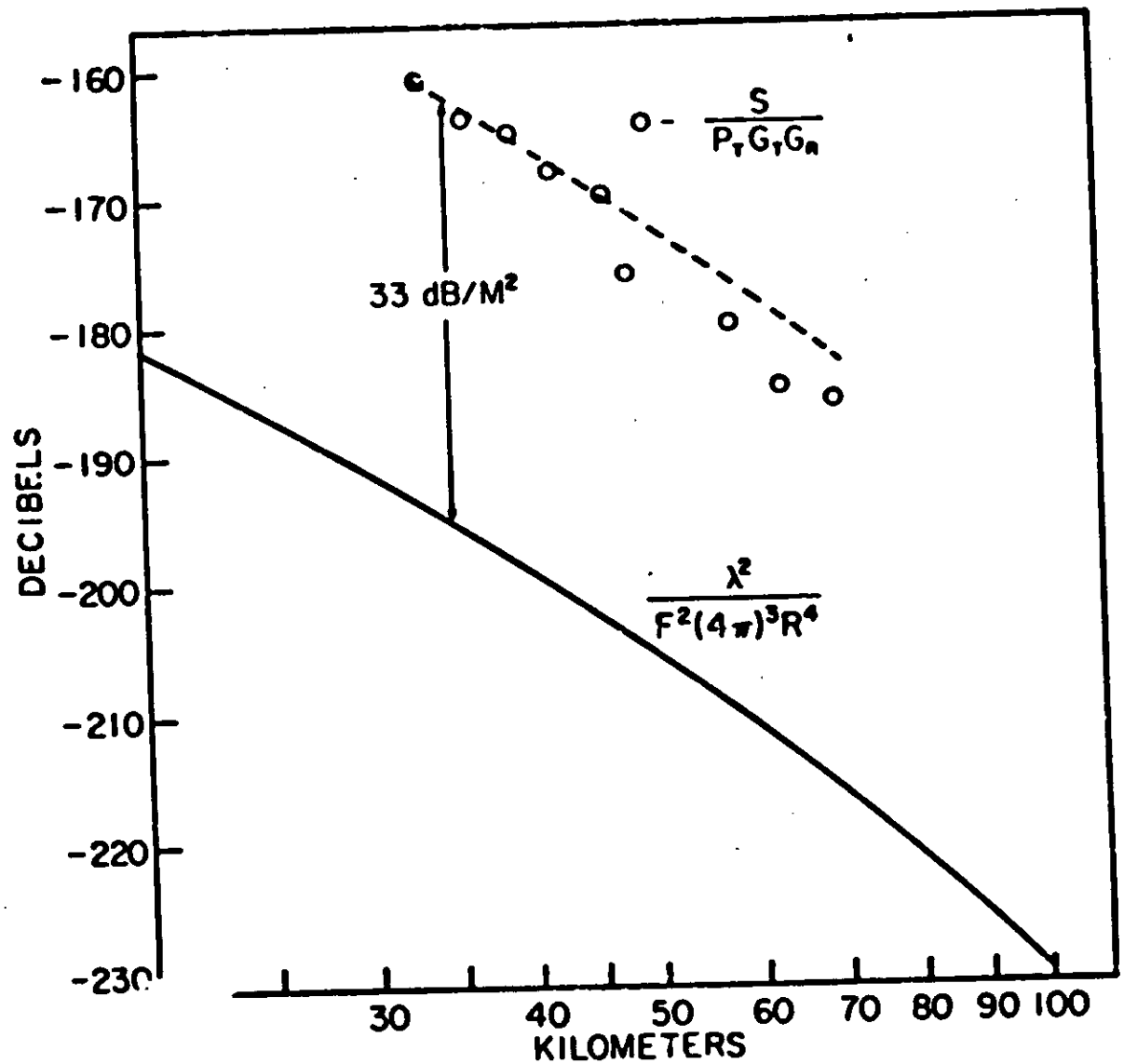

(U) Figure 9. Normalized Signal Levels from USS Julius A. Furer (U)

UNCLASSIFIED

HF BACK SCATTER FROM A SHIP'S WAKE (U)

D. D. Crombie

Institute for Telecommunication Sciences
ESSA Research Labs, Boulder, Colorado 80302

I INTRODUCTION (U)

(U) In 1968 the writer suggested at a Defense Science Board (DSB) meeting that the highly periodic structure of a ship's wake might have a large resonant scattering cross-section. It was also suggested that at some aspects, at least the Doppler shift of signals resonantly scattered from the wake would be different from that of the signals resonantly scattered from the sea. As a result Dr. H. Kurss has investigated how the Doppler shift from a wake depends on the ship's velocity, on the direction of incidence, and how its value at resonance compares with the Doppler shift of the sea clutter. He has also investigated how the scattering cross section depends on the same factors. This note will summarize his results.

II DOPPLER SHIFT (U)

(U) The Doppler shift of the signal backscattered from the sea is given by

$$(\Delta f_r)_s = \pm (2^{1/2} 3^{1/4}/4\pi)(g/v)\,|\cos(\theta \pm \theta_c)|^{1/2}$$

while the Doppler shift of the signal scattered from the wake at resonance is given by

$$(\Delta f_r)_w = (3^{1/2}/4\pi)(g/v)(\cos\theta/|\cos(\theta \pm \theta_c)|)$$

Thus the ratio is given by

$$(\Delta f_r)_w/(\Delta f_r)_s = \pm a\cos\theta/|\cos(\theta \pm \theta_c)|^{1/2}$$

where $a = 3^{1/4}/2^{1/2} = 0.9306$, θ is the angle between the direction of the transmitter, as seen from the ship, and the direction of the ship's motion, and v is the ship velocity while g is the acceleration of gravity. The angle θ_c is the inclination of the cusp lines of the wake to the direction of travel, and has a value $\theta_c = 19^\circ 28'$.

UNCLASSIFIED

UNCLASSIFIED

(U) Equation 1 is plotted in Figure 1, and shows that except when θ is in the region of 20 to 40° there is a significant difference in the two Doppler shifts. This difference should enable a wake echo to be separated from the sea clutter in a properly designed monostatic system.

III SCATTERING CROSS SECTION (U)

(U) Dr Kurss has also developed formulae giving the scattering cross section of the wake. An approximate version, which assumes that the width of the cusp line is $\pi/\sqrt{2}k_w$, is

$$\sigma = \text{const}\,(K/k)^2\, N^{4/3} f(\theta)$$

where the const = 24.1, and

$$K/k = 1.845\, n^{1/3} \zeta_n$$

where ζ_n is the elevation of the nth crest along the cusp line. N is the number of crests along the illuminated portion of the cusp line. The factor $f(\theta)$ contains the angular dependence and is given by

$$f(\theta) = \left| \frac{\sin(\theta - \theta_1)}{\cos(\theta + \theta_c)} \right|$$

where θ, θ_c and θ_1 are shown in Figure 1. The variation of $f(\theta)$ with θ is shown in Figure 2. It is evident that the cross section is zero when $\theta = \theta_1$, but otherwise shows no rapid dependence on θ.

(U) At a ship velocity of 20 knots, the frequency (fr) of resonance with cuspidal components of the wake, along the direction of the ship's velocity, is ~2.0MHz, the wake wavelength (λ_ω) is .75m. If the wake amplitude is 0.75m (1/100 of the wavelength) one wavelength behind the ship, K/k = 1.37. If the illuminated length of the wake is 10km, N = 10,000/75 = 133 and $N^{4/3} \cong 700$. From Figure 1, $f(\theta) \cong 0.74$. Thus the scattering cross section for one component of the wake is ~23,500m², at resonance.

(U) Yim and Tulin indicate that the surface wake of a submarine 30 ft. in diameter, 327 ft. long, at a depth of 82 ft., and having a velocity of 20 knots will have an amplitude of 0.27 meters at 5 wavelengths behind the submarine. Thus,

$$K/k = 1.845\,(5)^{1/3} \times .27 = 1.1.$$

The other parameters being the same, the cross section of one arm of the wake is ~9100m² at resonance.

UNCLASSIFIED

(U)

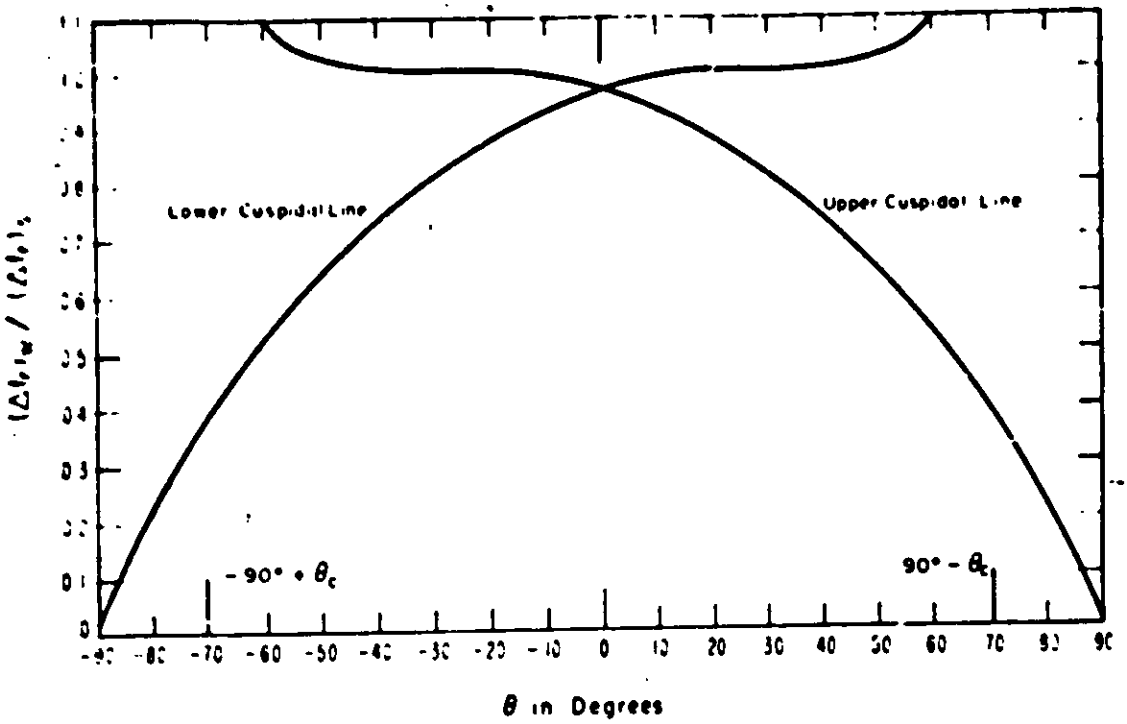

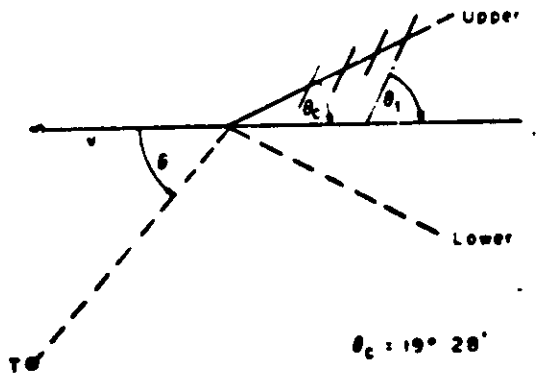

(U) Figure 1. Angular Dependence of the Ratio of Doppler Shifts from a Wake and the Sea at Resonance. (U)

UNCLASSIFIED

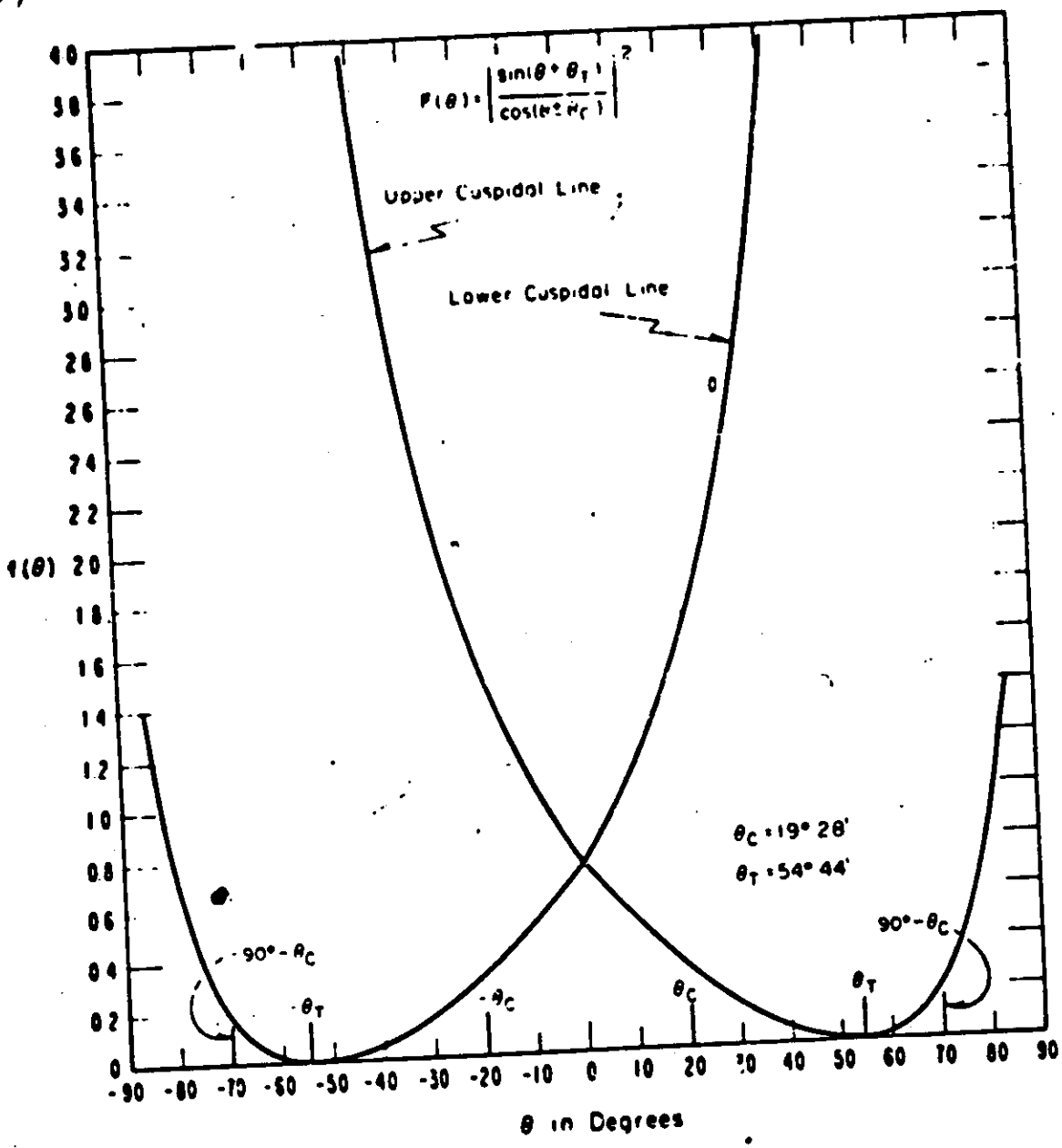

(U) Figure 2. Angular Dependence of the Wake Cross-section at Resonance (U)

UNCLASSIFIED

IV NOTES ON DETECTION OF SUBMARINE AND SHIP WAKES (U)

(U) Current calculations indicate that the radar cross-section of a wake can be very large ($\sim 10^6$ m^2) at resonance.

(U) The frequency of the radar depends quite critically (< 1%) on the ship's velocity and heading. Thus the radar must step with very small changes in frequency.

(U) The Doppler shift of the wake differs significantly from the Doppler shift of the sea over quite a wide range of azimuth angles. However, the differences are such that Doppler resolution of 1/100 Hz or so are required. This implies observation times of a few minutes. The use of a bistatic radar is also contra-indicated.

(U) Submarines produce surface wakes of significant amplitude if they are shallow enough and fast enough. Current calculations suggest that the wakes might be detected for depths of up to 200 ft and for speeds greater than 20 kts (lower speeds require smaller depths).

(U) At such speeds radar frequencies as low as 1 MHz are required. At these frequencies the obtainable radar range is quite large compared with those obtainable at higher frequencies because of the small ground wave attenuation.

(U) Provided the wake Doppler can be separated from the clutter Doppler, a radar for detecting wakes will be noise limited. Thus the minimum wake amplitude which is observable will depend only on ambient noise levels and transmitter power.

(U) I visualize that a radar for detection of wakes would consist of a pulsed monostatic system with 360° illumination. Pulse rates should be as high as possible consistent with avoidance of skywave clutter. Each pulse will be transmitted at a different (by < 1%) frequency from the previous one. The complete frequency scan will be completed within half the period of the Doppler shifts expected. Successive signals at the same frequency will be added coherently.

(U) After signals from one or both "arms" of the wake are detected their bearing can be determined by various methods. It is presumed that the received signals will be processed as indicated above in several range gates.

THIS PAGE INTENTIONALLY LEFT BLANK

FLEET AIR DEFENSE (U)

PRECEDING PAGE BLANK - NOT FILMED

UNCLASSIFIED

[redacted]

FLEET AIR DEFENSE REQUIREMENTS (U)

Paul T. Stine

Radar Division, Naval Research Laboratory
Washington, D.C. 20390

I INTRODUCTION (U)

(U) Our Navy's problem in terms of fleet air defense (FAD) requirements is posed by the fact that fleet units must operate in a hostile environment under constant surveillance by trawlers, submarines, "neutral" shipping vessels, aircraft, certain types of land-based sensors, and possibly satellites, each making use of sensing techniques available as a result of a rapidly advancing technology. In order to operate effectively, our fleet units need improved surveillance data providing detection, identification, and location or track of a threat while sufficient time remains for defensive reaction. This surveillance capability needs to be available under all weather conditions, effective under EMCON operating conditions, highly reliable, and capable of providing data of sufficient accuracy and timeliness as to be useful to shipboard defensive systems. In addition, the surveillance system must not obviate an appropriate offensive defensive balance within fleet units.

II DOCUMENTED REQUIREMENTS (U)

(U) Officially, the Navy's requirements for fleet air defense are covered by General Operational Requirement (GOR) 17 titled "Surface Anti-Air Warfare" which essentially says that all ships must be able to defend themselves against short-range missiles, and large tactical units must be able to counter threats from all sources including space vehicles. Advanced Development Objective (AIXO) 17-23X, "Shipboard Surface Wave Radar" deals more specifically with the probable threat and possible requirements for shipboard surface-wave radar as a means of over-the-horizon (OTH) detection of the threat.

III NATURE OF THE THREAT (U)

(U) The threat as defined by AIXO 17-23X, summarized in Figures 1 and 2, is a low-flying (40 ft altitude) target capable of at least 100-nmi range and having a radar cross section (RCS) of one

[redacted]

UNCLASSIFIED

UNCLASSIFIED

[redacted]

(U) square meter in the high frequency (HF) band. This RCS seems to be reasonable as substantiated by model measurements shown in Figure 3. Along with low-flying attack aircraft and such air launched missiles as the SS-C-2 (SAMLET), the patrol boat-launched SS-N-2 (STYX) missile and the frigate or submarine launched SS-N-3 (SHADDOCK) missile are commonly accepted as being representative of today's threats. The actual range capabilities of the SS-N-2, SS-C-2, and SS-N-3 are 22, 45, and 250 nmi respectively. It is reasonable to expect that the threats of the near future will be capable of flying farther, lower, and faster than the above mentioned missiles.

IV THE REAL NEED (U)

(U) In summary, the Navy's real need seems to be a surveillance system having the following basic characteristics and performance:

- All-weather operating capability.
- Effectiveness under EMCON conditions.
- Large-area coverage (approximately a 300-nmi radius from fleet unit).
- Mobility to cover operating area of interest.
- Compatibility with ships defensive and offensive weapons systems.
- High reliability.
- Ability to detect, identify, and track small (RCS $\approx 1 M^2$), low flying (H $\approx$ 10 ft) targets.
- Azimuthal accuracy of $\pm$ 5° or better (as seen from the fleet unit).
- Range accuracy of $\pm$ 5 nmi or better (as seen from the fleet unit).
- Velocity accuracy of $\pm$ 5 knots or better (relative to fleet unit).

[redacted]

UNCLASSIFIED

(U)

ADO 17-23X: SHIPBOARD SURFACE WAVE RADAR

BRIEF

"To accomplish the development work necessary to prove the military usefulness, technical feasibility, and financial acceptability of a Shipboard Surface Wave Radar."

ULTIMATE OBJECTIVES

a. "To provide early detection of low-flying air targets at a range of 100 miles or more."

b. "To provide azimuth angle and time that the threatening air target will enter the normal defensive radar envelope."

c. "When the objective is achieved, a decision whether or not to continue into Engineering Development will be made by CNO."

(U) Figure 1. ADO 17-23X. Brief and Objectives (U)

ADO 17-23X: SHIPBOARD SURFACE WAVE RADAR

AMPLIFYING DATA SUMMARY

a. Performance Desired

- Detection of low-flying 1-m^2 target at 100-nmi range
- Range resolution of ± 1 nmi
- Azimuth accuracy of ± 5°
- Velocity resolution of ± 10 knots
- Five frequency bands within HF band
- Rapid shifting between frequency bands

b. Constraints

- Lightweight and compact
- Suitable for installation in a DD or larger ship
- Compatible with current shipboard power limitations
- No harmful interference to HF communications systems
- No physical harm to personnel in exposed locations

(U) (S) Figure 2. ADO 17-23X. Summary of Amplifying Data (U)

[redacted]

[redacted]

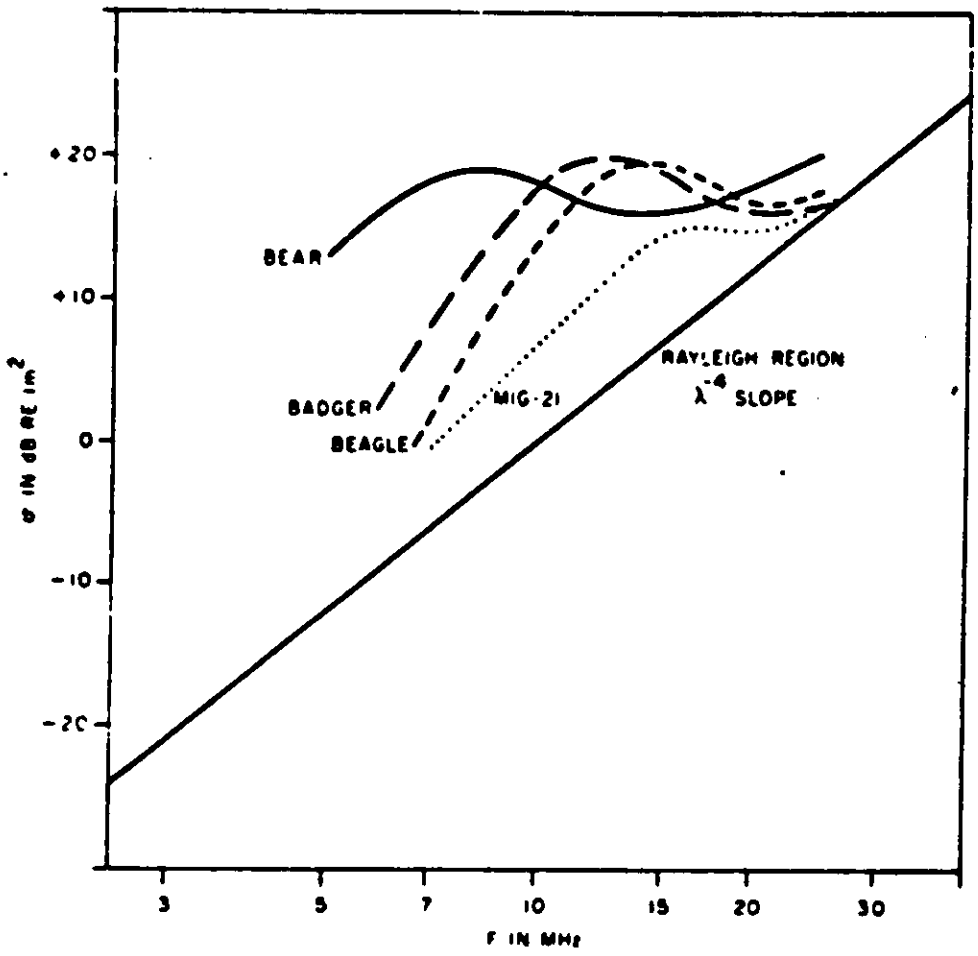

(U) Figure 3. Nose-on (± 30°) Vertically Polarized Radar Cross Sections vs Frequency (U)

[redacted]

V POSSIBLE OTH SOLUTIONS (U)

(U) A list of possible solutions to the Navy's large-area surveillance problem includes AEW radar, helicopter-borne radar, passive ECM satellite surveillance, skywave radar, surface-wave radar, and microwave radar propagating in the evaporative duct. Needless to say, each has its advantages and limitations. Both AEW radar and helicopter radar methods of looking over the horizon suffer from weather and logistics problems. Passive ECM is useless against a non-radiating threat. Satellite surveillance faces severe logistics, weather, and accuracy problems. Skywave radar has range and azimuthal accuracy limitations along with problems of propagation path availability as illustrated in Figure 4. Monostatic surface-wave radars, due to high surface-wave attenuation, would require powerful transmitters and large antennas as illustrated in Figures 5 through 7, would be limited by practical considerations to detection ranges of about 50 to 100 nmi and would not be usable under EMCON conditions. Microwave radar propagation in the evaporative duct would also violate EMCON conditions and is probably limited to ranges of 50 to 100 nmi. In addition, much remains to be learned about the time, space, and thickness variabilities of evaporative ducts.

(S) One other possible solution is a hybrid system in which one or more optimally designed mobile skywave radars each operate monostatically to provide large-area surveillance ($R \geq 500$-nmi radars) around a fleet unit, the surveillance data being transmitted to the fleet unit by regular communication links. Inasmuch as the skywave radars are illuminating the area of interest, fleet units can be equipped to make bistatic detection and location of threats coming within a range of about 50 to 100 nmi as shown in Figures 8 and 9. In this approach, the range accuracy of the bistatic data is quite dependent upon strategic positioning of the skywave illuminators relative to the fleet unit as shown in Figure 10. Although the bistatic range accuracy of such a system leaves something to be desired, it would appear to have all of the desired characteristics listed under Section IV with a high probability of solving the total problem.

VI CONCLUSIONS (U)

(U) (S) It is concluded that the hybrid skywave/surface-wave system suggested above and summarized in Figure 11 offers a practical solution to the Navy's problem of OTH surveillance, and it is recommended that steps be taken toward implementation of such a system.

(U)

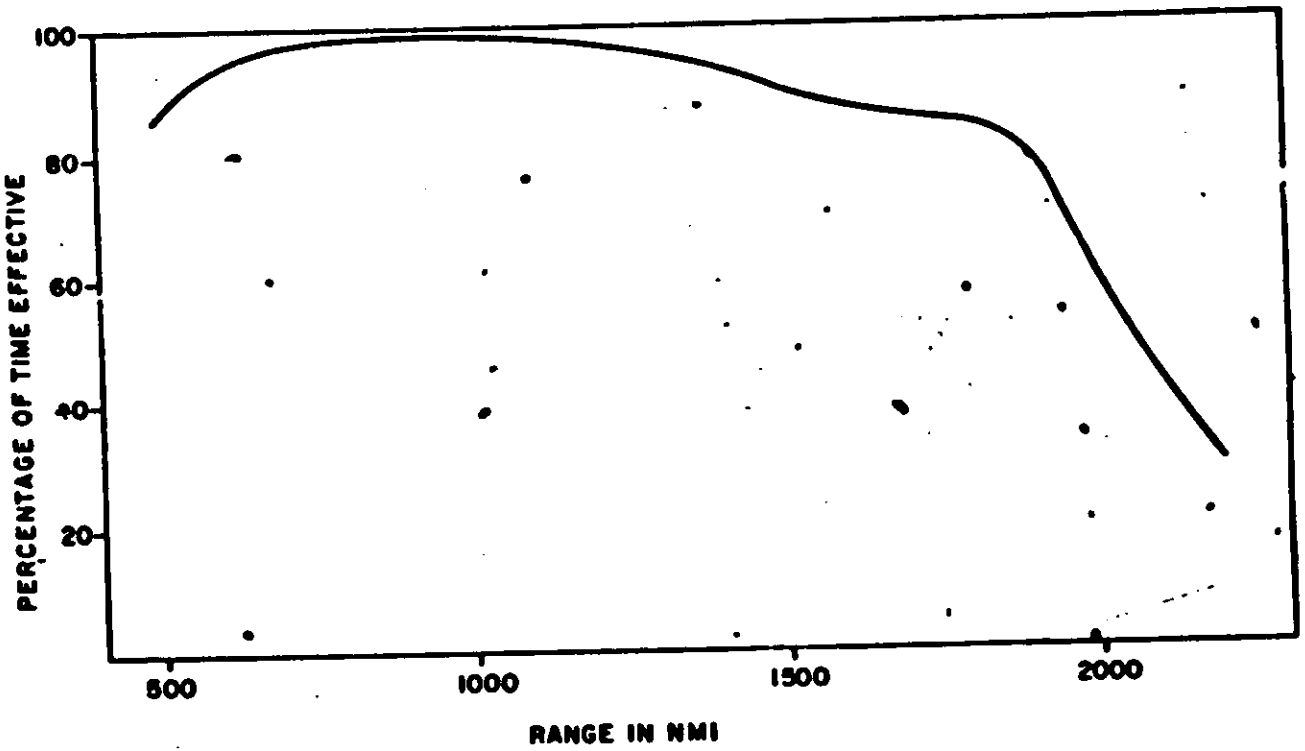

(U) Figure 4. Percentage of Time Radar is Effective as a Function of Range (U)

(U) UNCLASSIFIED

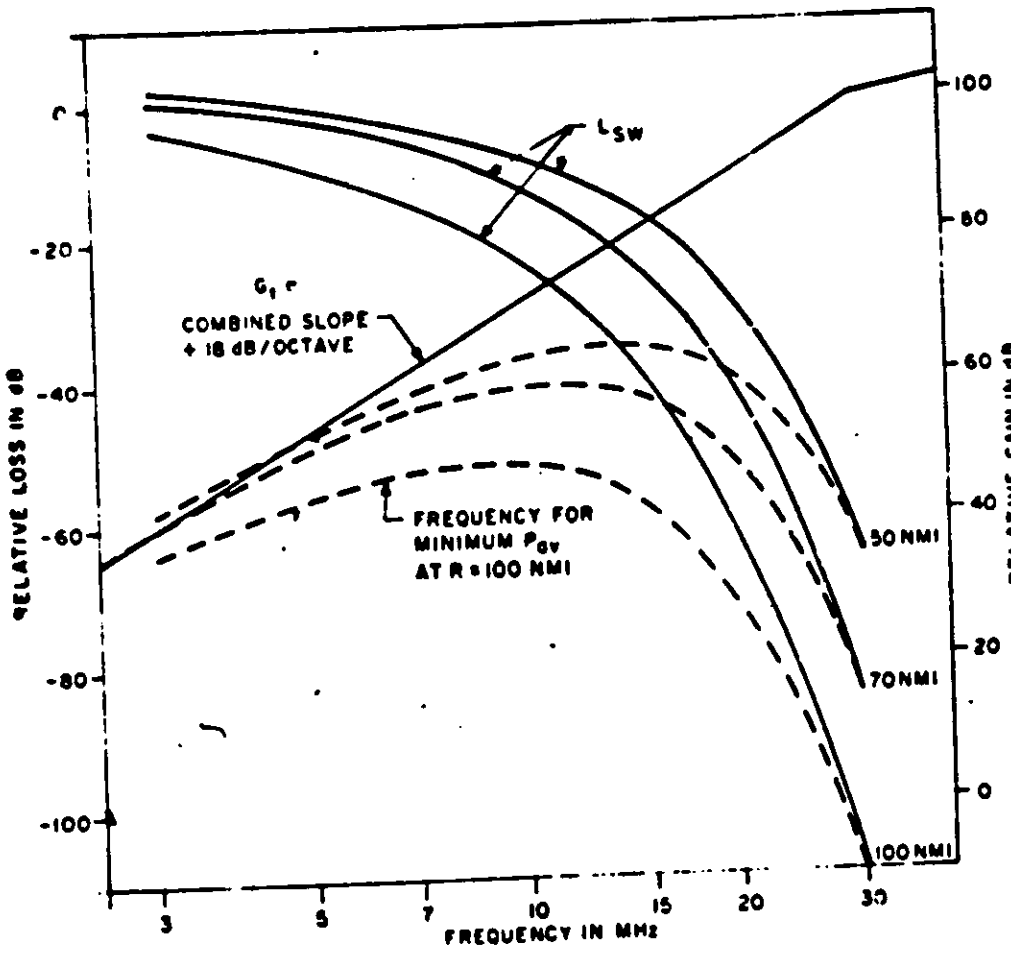

(U) Figure 5. Determination of SSWR Optimum Frequency for Minimum Transmitter Power Requirement (constant antenna aperture assumed with small target in Rayleigh region below 30 MHz) (U)

UNCLASSIFIED

[redacted]

(U)
(S)

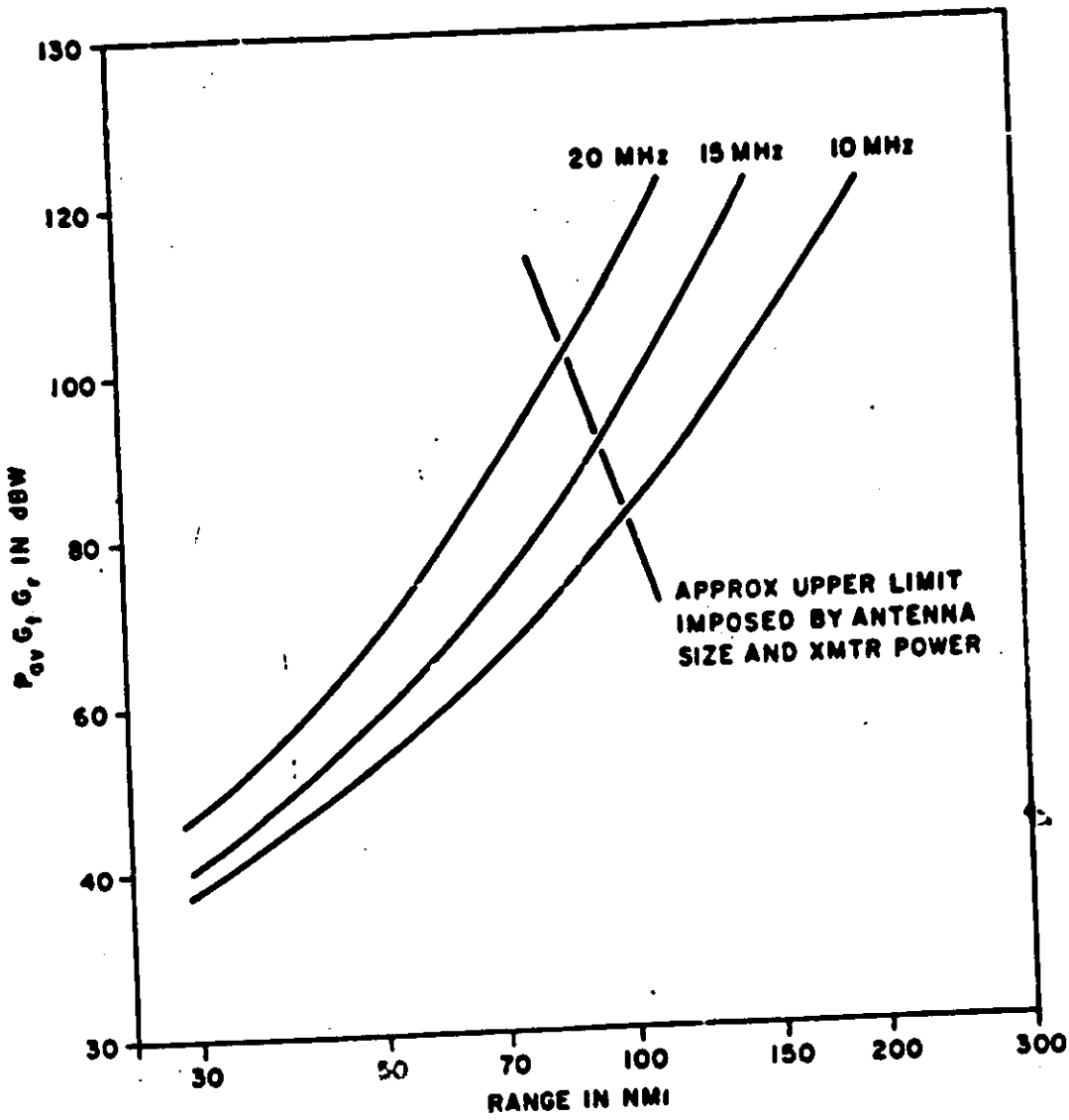

(U) (S) Figure 6. Product of Transmitter Power, Transmitter Antenna Gain, and Receiver Antenna Gain for SJWR (Monostatic)Case (U)

[redacted]

(U)

CHARACTERISTIC	HIGH PERFORMANCE MONOSTATIC SYSTEM	INTERMEDIATE MONOSTATIC SYSTEM	MINIMUM SIZE MONOSTATIC SYSTEM	BISTATIC SYSTEM
Ship Size Req'd.	Mod Light Carrier	Frigate	Destroyer	Destroyer
Probable Shipboard Antenna	Large Dipole Array	Rotatable Log Periodic Array	Rotatable Log Periodic Array	Crossed Spaced Loop
Avg. Transmitter Power	100 kW	30 kW	10 kW	200 kW (Remote)
Primary Power Req'd	300-500 kW	120-200 kW	60-100 kW	10-20 kW
"Below Deck" Weight	15 Tons	10 Tons	7.5 Tons	5 Tons
"Below Deck" Space Req'd	1000 $ft.^2$	700 ft^2	550 ft^2	350 ft^2
Range Capability (On 1-M^2 Low Flying Target)	100 nmi	80 nmi	60 nmi	60 nmi
Range Accuracy	±1 nmi	±1 nmi	±1 nmi	Depends on Geometry
Azimuth Accuracy	±3°	±10°	±15°	±5°

(U) Figure 7. Estimated Characteristics of Shipboard Surface Wave Radar Systems (U)

(U)

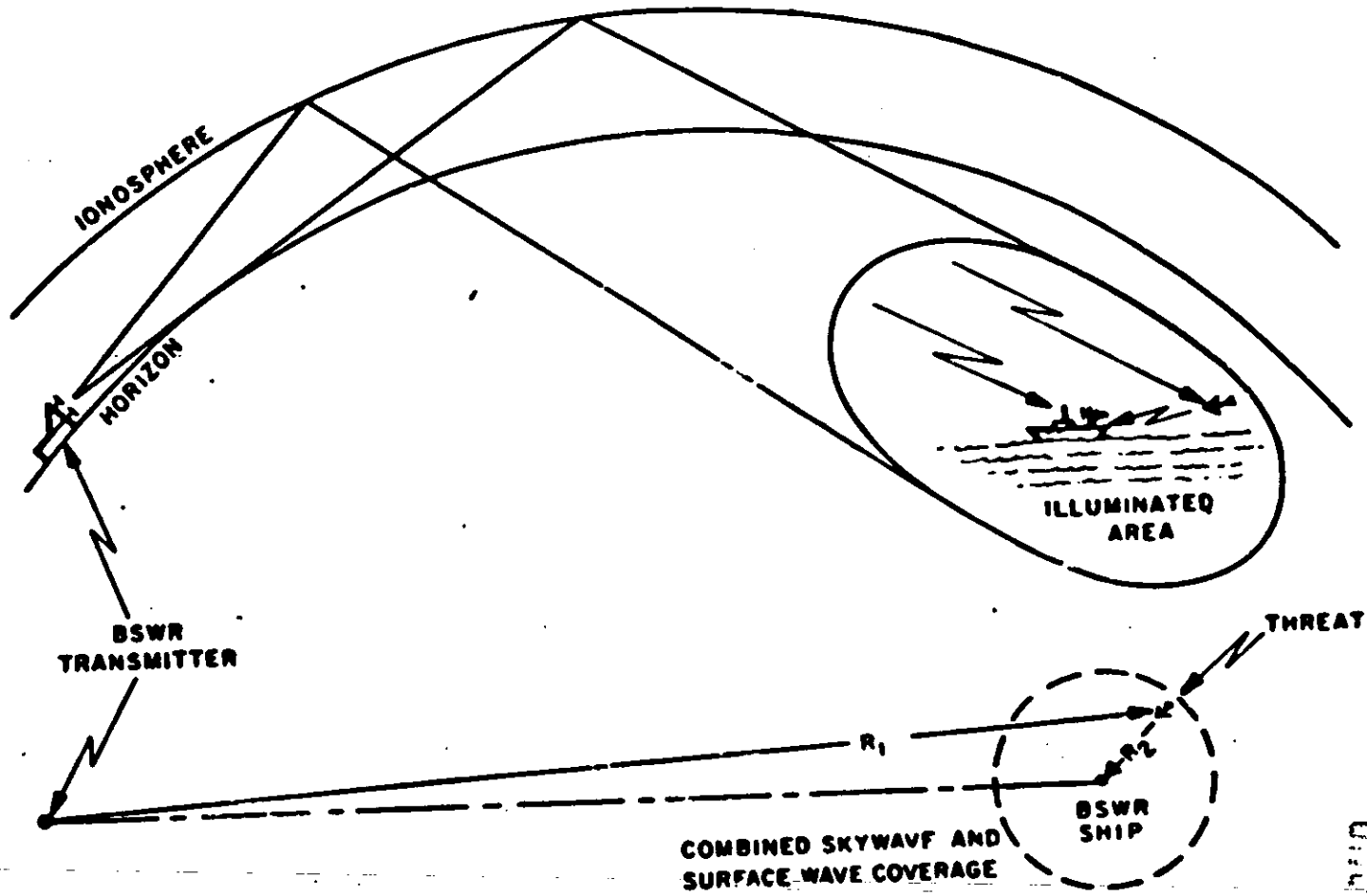

(U) (S) Figure 8. Bistatic Surface Wave Radar Concept and Geometry (U)

(U) UNCLASSIFIED

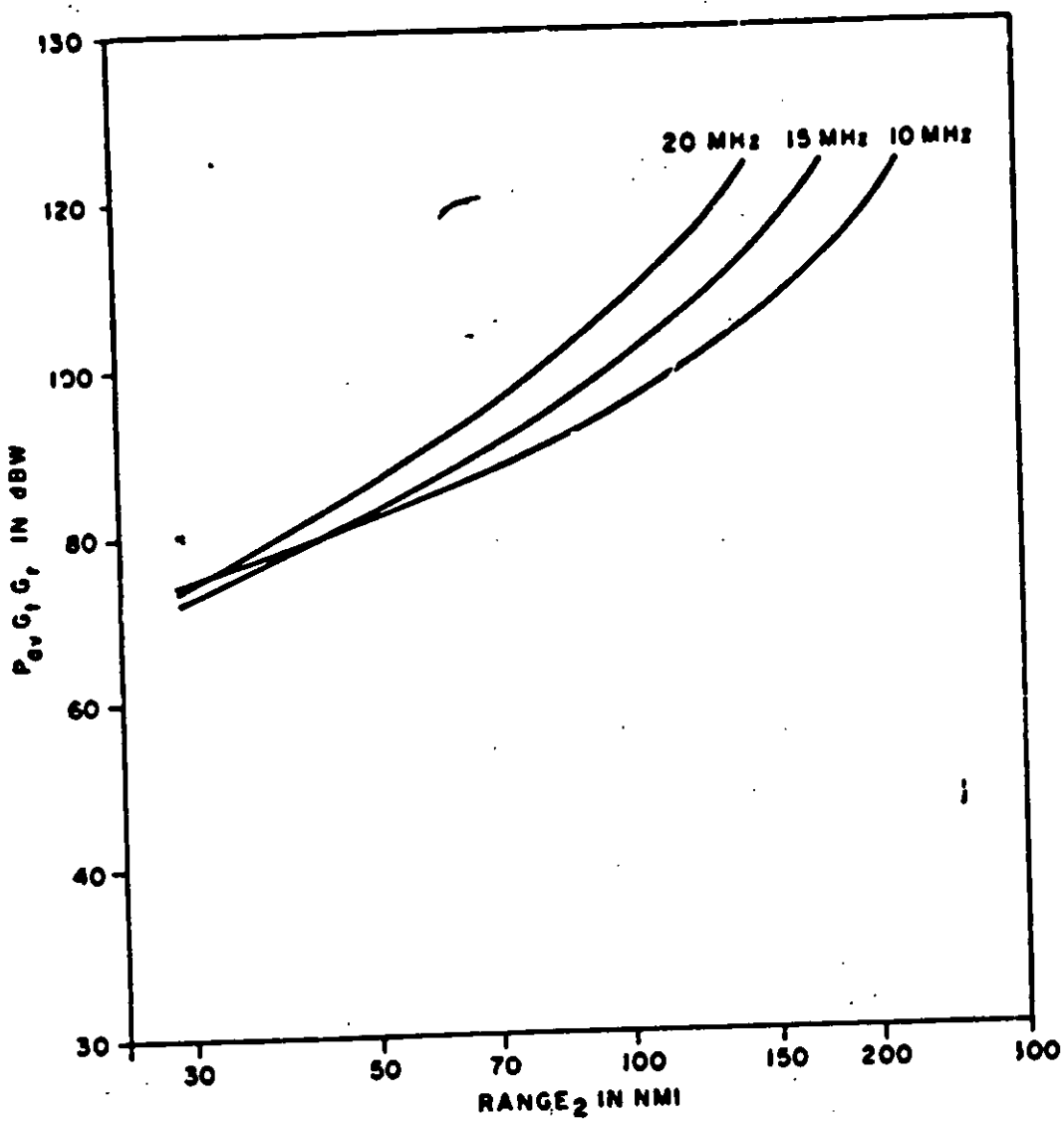

(U) Figure 9. Product of Transmitter Power, Transmitter Antenna Gain, and Receiver Antenna Gain vs Range from Ship to Target for BSWR Case (U)

UNCLASSIFIED

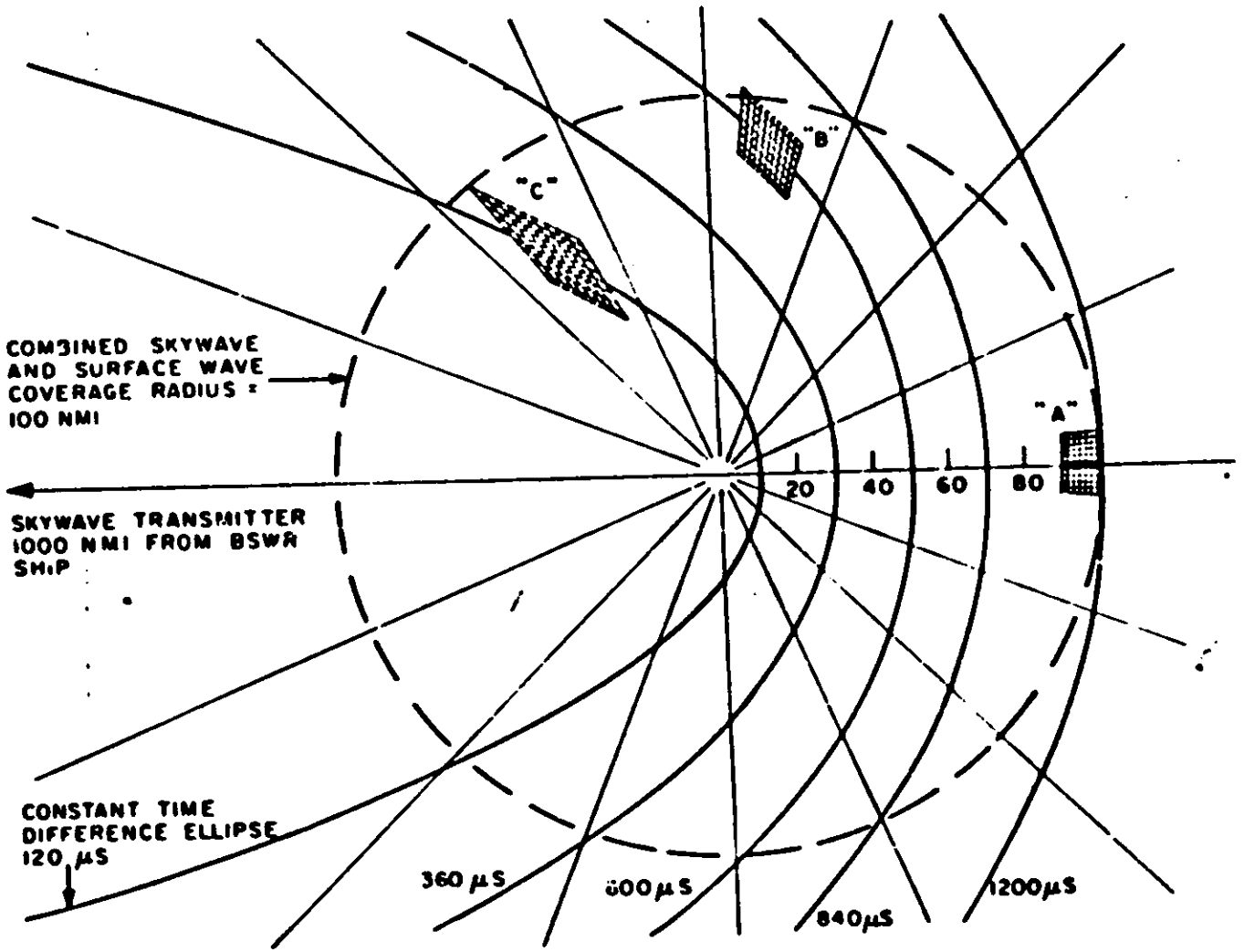

(U) Figure 10. Illustration of Geometric Limitations of BSWR Range Accuracy (U)

(U)

PROPOSED METHOD OF OTH THREAT DETECTION

1. Use a remotely located OTH skywave radar to detect and locate a threat and possibly to communicate this "early warning" to the ship or task force under attack.

2. Equip one or more ships in a task force with a bistatic surface wave radar capability such that they can make use of the illumination of the threat by the skywave radar.

3. Equip one or more ships in a task force with a monostatic surface wave radar capability to provide improved data on OTH targets which have been identified as threats.

(U) Figure 11. Hybrid System for OTH Surveillance (U)

[redacted]AL

FLEET AIR DEFENSE REQUIREMENTS FOR EARLY WARNING (U)

Richard J. Hunt

The Johns Hopkins University
Applied Physics Laboratory
8621 Georgia Avenue
Silver Spring, Maryland 20910

I INTRODUCTION (U)

(U) This paper discusses gross requirements for detection and alerting of a Naval Task Force against the primary anti-ship cruise missile threat. A system which adequately meets this threat will almost certainly satisfy requirements of lesser threats. An example of a coordinated missile attack which might be expected against a Task Force in the open ocean is discussed to highlight the salient features of the various types of weapons available to the enemy. To provide adequate AAW defense against such an attack, the AAW force commander requires warning of an impending attack with enough time so that he may use his defensive AAW weapons in the best way. The actions that need to be taken to prepare the defense, together with factors affecting decisions, are outlined. Gross requirements for threat recognition, time and bearing are given. Because of the need to communicate early warning information, a functional description of an intership communication system based on NTDS is provided (Figure 1).

(U) The ensuing discussion follows each of the charts in the presentation.

II COORDINATED MISSILE ATTACK (FIGURE 2) (U)

(C) The Soviet Navy has been growing considerably during the last 10 years with the introduction of many new types of ships, missiles and aircraft. The anti-ship missile threat has now reached a level of quality, diversity, force size and geographical deployment that establishes it as a major constraint on U S fleet operations. The threat, although developing in detail, is established in general pattern and cannot be expected to change radically any more than the U S could easily diverge from the attack Carrier Task Force concept.

(U) A well coordinated missile attack in open seas might be expected as shown in Figure 2.

[redacted]

(U)

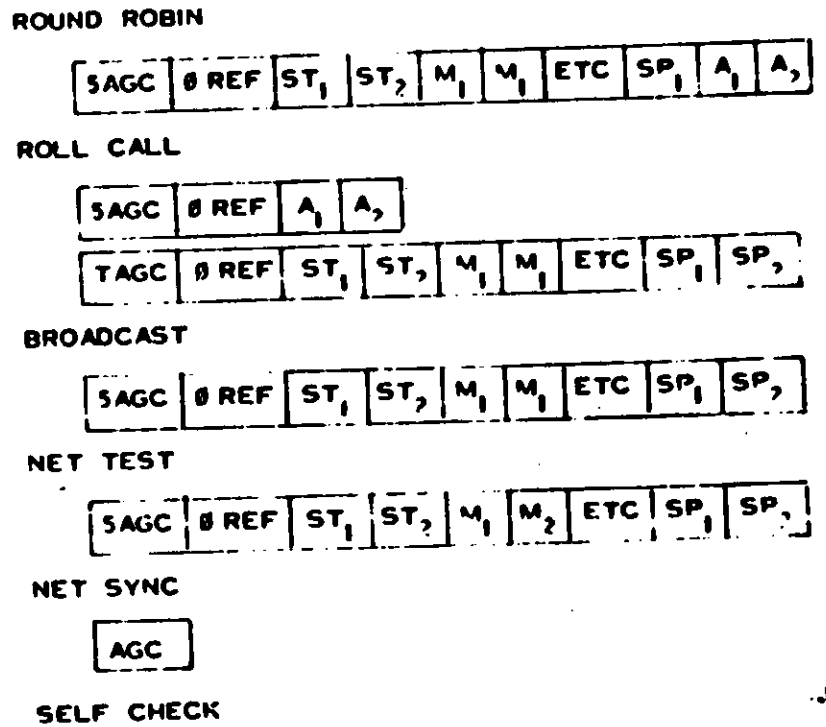

(U) Figure 1. NTDS Modes of Net Operation (U)

(this page unclassified)

[redacted]

(U) This group is capable of launching 45 to 55 missiles at the USN force within a period of about 5 to 10 minutes. About 40 to 45 missiles will be successfully flying objects and will enter the air space about the USN force. Approximately 25-35 should be operable seeking missiles. It should be noted that 40 to 45 missiles are engageable targets since the defenses cannot know which seekers are operable. The defenses are thus faced with about 5 to 11 targets per minute if the attack is well coordinated. These targets may be approaching the defense over about as large as 120° angular sector.

(U) It should be noted that roughly half the missiles came from submarines, meaning the surfaced launch platforms are essentially undetectable until 2 to 3 minutes before launch.

(U) The enemy can be expected to support such an attack with high levels of stand-off barrage jamming. In addition, air traffic density will be high and can be expected as a normal part of the environment. Traffic density will be variable depending primarily on distance to shore. Typically, on the order of 50-100 friendly air tracks can be expected for operations close in to shore and 20-50 friendly tracks for open ocean situations.

III FUNCTION OF EARLY WARNING (FIGURE 3) (U)

(U) The primary purpose of early warning is to provide timely information to the AAW force commander so as to ensure that the actions necessary for preparing weapon systems to best cope with an attack have been taken. The actions that are taken will depend on the information available to the commander and the level of confidence he has in the validity of the information.

(U) The most critical factor in a good defensive posture is bringing system manning levels to GQ. Commanders are reluctant to take this action unless timely and positive threat recognition can be provided. Recent fleet exercises have demonstrated that detection of targets with modified condition 3 watches is the single most limiting factor in defensive capability against simulated high density raids.

(U) To bypass the many normal sequential steps in the processing of targets, SAM and EW systems are being built today (some elementary systems have already been installed) with so-called 'Threat Responsive Modes' of operation. Basically, this system concept depends on adequate recognition or identification of the threat. Some thoughts on providing positive threat recognition are shown on the next chart. If the fleet has chosen to use EMCON as a deceptive measure and positive threat recognition can be obtained, doctrine should be established to remove radiation silence.

(U) Some of the actions which will enhance detection and target processing are to employ limited azimuth search by the operators of radar consoles, to use fire control radars in automatic sector search and to bring the force PIM to a direction which will unmask radars and launchers. These actions depend on an adequate knowledge of attack bearing.

[redacted]

[redacted]

UNCLASSIFIED

(U) JCT

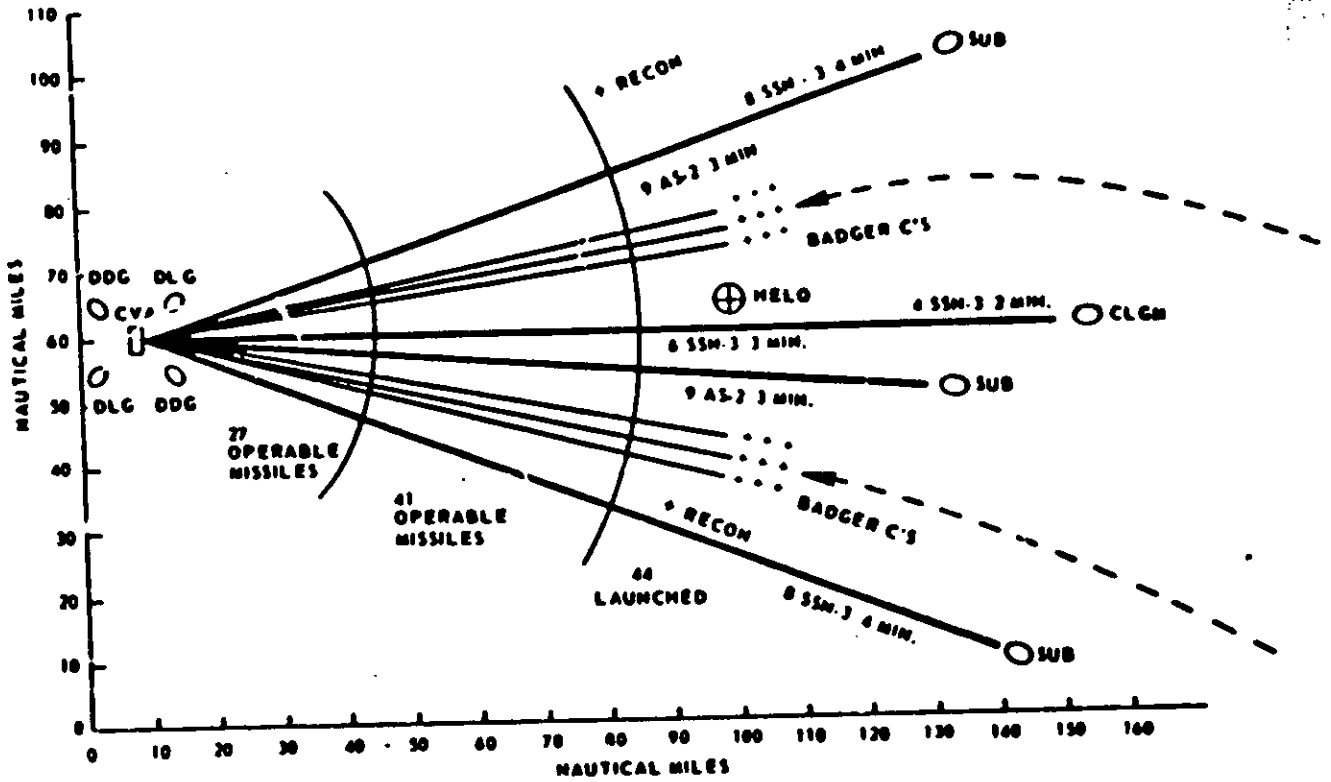

(U) JCT Figure 2. Well Coordinated Missile Attack (U)

UNCLASSIFIED

(U) per

- PROVIDE INFORMATION WHICH WILL ASSIST THE AAW FORCE COMMANDER IN BRINGING SHIPS EQUIPMENTS & SYSTEMS TO BEAR IN THE BEST WAY

FACTORS AFFECTING DECISIONS	ACTION ITEMS
POSITIVE THREAT RECOGNITION & TIME AVAILABLE	GQ MANNING LEVELS
POSITIVE THREAT RECOGNITION	EMPLOY THREAT RESPONSIVE MODES REMOVE EMCON STATUS
ATTACK BEARING	CONCENTRATED AZIMUTH SEARCH USE OF FCR SECTOR SEARCH PATTERNS UNMASKING EQUIPMENT
ATTACK BEARING & TIME AVAILABLE	INTERCEPTOR & ASW AIRCRAFT DEPLOYMENT DISPOSITION OF SURFACE ELEMENTS

(U) per (C) Figure 3. Function of Early Warning (U)

(U) The use of interceptors, both CAP and DLI, depends on sufficient time to bring these systems to bear against a known attack bearing. Interceptors can play a primary role in destroying launch vehicles prior to missile launch, destroying jamming aircraft and assisting in the identification process. Timely knowledge of an attack bearing can help the force commander in redeployment of surface elements in a way to best defend the high-value target. Redeployment may be particularly appropriate if ships have been disposed in missile traps or are on ASW missions and the threat information clearly establishes that the attack is vectored to the high-value target.

IV THREAT RECOGNITION (Figure 4) (U)

(U) Since the key element in taking actions for a good defensive posture depends on positive threat recognition, it is useful to examine characteristics of the threat appropriate to the system under consideration which may be germane to identification. The most striking characteristics of the missile threat, independent of radiation signatures, are the Doppler separation from the launch vehicle and the kinematic profile of the target. The airlaunched missiles current today are discernible by a Doppler of about 50 knots which probably will not be smaller than this in the future. Subs will surface prior to launch for a few minutes and are subject to detection before missiles are fired so that the Doppler from surfaced vessels is a threat indication. Obtaining velocity vector to within 10° will give the force commander an indication of the success or failure of missile traps and dictate the need for ship redeployment.

V GROSS REQUIREMENTS TO ALERT FORCE TO IMMINENT ATTACK (Figure 5) (U)

(U) Time and bearing requirements for the several defensive systems are shown on this chart. Time requirements translate into range based on current missile speeds of about M1.0 and possibly M2.0 in the future. The limiting factor in time is the delay associated with bringing ships to GQ. Ten minutes implies a range from the task force of the order of 100-200 nmi which corresponds roughly to possible missile launch range and is therefore compatible with the requirements for positive threat recognition. Time requirements for poor ship disposition, however, are not satisfactory for the force commander to alter deceptive deployment tactics.

(U) Bearing requirements for search radars are based on limited experience in fleet exercises which show that operators do not detect targets from simultaneous bearings separated more than 90°. Fire control radar bearing accuracies should be within the automatic sector search patterns of these radars which vary from 15° to 20°.

Declassified

(U) UNCLASSIFIED

- SOME CHARACTERISTICS OF THREAT
  - SEPARATION OF ATTACKING MISSILE FROM LAUNCH CRAFT
    - AIRPLANE (DISCERNIBLE BY ~ 50 KNOT DOPPLER RESOLUTION
      - WITH A 50 NM RANGE RESOLUTION
    - SURFACED SUBMARINE
    - SURFACE VESSELS
  - TARGET PROFILE
    - SPEED
    - ALTITUDE
    - VELOCITY VECTOR (<10°)
- CAPITALIZE ON ABOVE CRITERIA TO KEEP PROBABILITY OF FALSE ALARM LOW

(U) UNCLASSIFIED

(U) Figure 4. Threat Recognition (U)

(U)

SAM GUN & EW SYSTEMS

TIME	TRANSIT	~5-10 MIN	WITH GOOD SHIP DISPOSITION
		~1-2 HR	WITH POOR SHIP DISPOSITION
	ON-STATION	~1-5 MIN	WITH GOOD SHIP DISPOSITION
		~1-2 HR	WITH POOR SHIP DISPOSITION
BEARING	FOR SEARCH RADAR		~60°
	FOR FCR	WITHIN REASONABLE FCR SECTOR SEARCH	~15°-20°

INTERCEPTOR SYSTEMS

TIME	CAP	~3 MIN FROM 100 NM CAP STATION	
	DLI	~15 MIN	
BEARING		WITHIN AI RADAR SCAN	~20°

(U) Figure 5. Gross Requirements to Alert Force to Imminent Attack (U)

[redacted]

For intercepts, a CAP station at about 100 nmi requires seven to eight minutes to achieve intercept of the target aircraft prior to missile launch. Greater detection ranges will permit the interceptors to arrive on the scene of final identification and could well provide the information in time for force redeployment for effective defensive action. Beyond-the-horizon interceptors should be within the AI radar scan

VI POSSIBLE COMMUNICATION CONTROL (Figure 6) (U)

(U) With regard to intership communication of detection information, the critical question is: Is the force under EMCON? If there is high confidence in threat identification, then independent of EMCON status the doctrine should be to use the normal communication channels. If routine detections occur in the system without positive threat indications, then if the force is not in EMCON, normal communications should be used. On the other hand, if the force is in EMCON, intership communications should not be used but the control ship should have the computer capacity in data terms essential for correlation of detections on threat hostility.

VII INFORMATION FLOW TO PROVIDE INPUTS TO THE ID PROCESS (U)

(U) Systems of the future will use more sophisticated computational schemes to correlate observations and intelligence and planning information. A variety of actions must be integrated to improve the ID process. Each combat unit which must engage contacts or assist in identification must perform the subprocesses of identification as shown in Figure 7.

(U) The initial ingredients in the process are the plans, codes, and information available concerning friendly forces. These provide part of the inputs to the correlation process of the ID function. The observations made on contacts provide the other inputs. Out of this then comes the degree of correlation between the data on hand and the observations which is then applied to an inductive or inference-making device to derive an estimate of the degree of hostility of the contact.

(U) This identification process must supply the degree of hostility information to the threat evaluation function to ensure that there is an efficient processing of targets, i.e., that weapons can be assigned to hostile targets in a timely manner. Identification should also carry through to the weapon commitment stage so as to provide a final estimate of contact hostility when a weapon is committed.

[redacted]

- IF HIGH CONFIDENCE OF THREAT DISCLOSURE, THEN USE NORMAL COMMUNICATIONS
- IF ROUTINE DETECTIONS WITH NO POSITIVE THREAT INDICATIONS THEN
  - FOR FORCE NOT IN EMCON USE NORMAL COMMUNICATIONS
  - FOR FORCE IN EMCON NO INTERSHIP COMMUNICATIONS BUT CONTROL SHIP SHOULD HAVE COMPUTER CAPACITY & APPROPRIATE ALGORITHMS FOR COMPUTATION OF INFERENCE ON HOSTILITY

(U) Figure 6. Possible Communication Control (U)

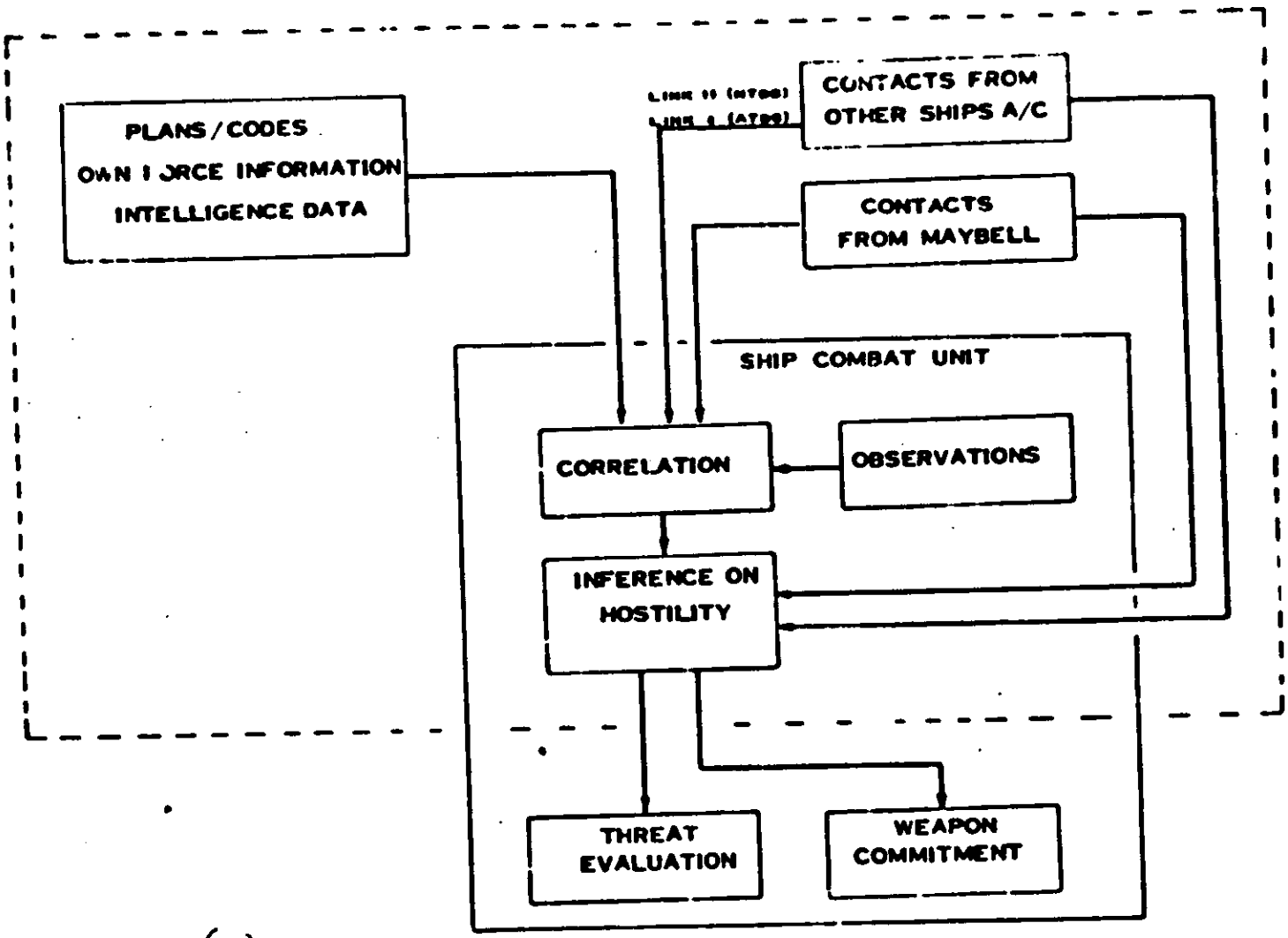

Figure 7. Information Flow to Provide Inputs to Identification Process (U)

PRECEDING PAGE BLANK - NOT FILMED

[redacted]

FAD HISTORY (U)

J. M. Headrick

Naval Research Laboratory
Washington D. C.

(U) The missile threat to ships was the inspiration for considering bistatic HF radar. The method was to use remote sky-wave illumination of low-altitudes targets near a ship and to detect the target-scattered energy by a ground-wave path to a ship-mounted receiving radar station. Some sample calculations were made in 1967 that suggested feasibility. Figure 1 gives expected monostatic sky-wave radar performance for a set of assumed radar and target parameters. The ionospheric model was per IISA-1. Figure 2 gives expected monostatic ground-wave radar performance for three operating frequencies spread over a greater frequency range than the set required in Figure 1. In Figure 3 bistatic performance is given for the required frequency extremes. These computations indicate the bistatic method has possibilities; the analysis is treated in more detail in an appendix of the MSDS Group Secret Report "Missile-Threat Ship Defense Study" (U) of 8 May 1968.

(U) A series of experimental tests have been made using ESSA transmissions for illumination and the MADRE facility on Chesapeake Bay for reception. Figure 4 is an early example that shows resonant wave echoes received by ground wave. Figure 5 is a later example with higher power. In addition, some tests have been conducted using the ESSA-received signal as a reference.

(U) The ARPA FAD experiments were planned to completely demonstrate the basic feasibility of low-altitude bistatic detection and to explore both the capabilities and required system design features.

(U) It is felt that the ARPA FAD tests have demonstrated the basic bistatic feasibility of detection of the low flyer [illegible] fleet but such a detection capability may have several applications. However, the sky-wave illumination should also be used as a monostatic radar, and it can complement the bistatic system since greater range detection and fill blind azimuths. In some cases it may be desirable to have the fleet unit operate [illegible] monostatic after the first missile detections.

[redacted]

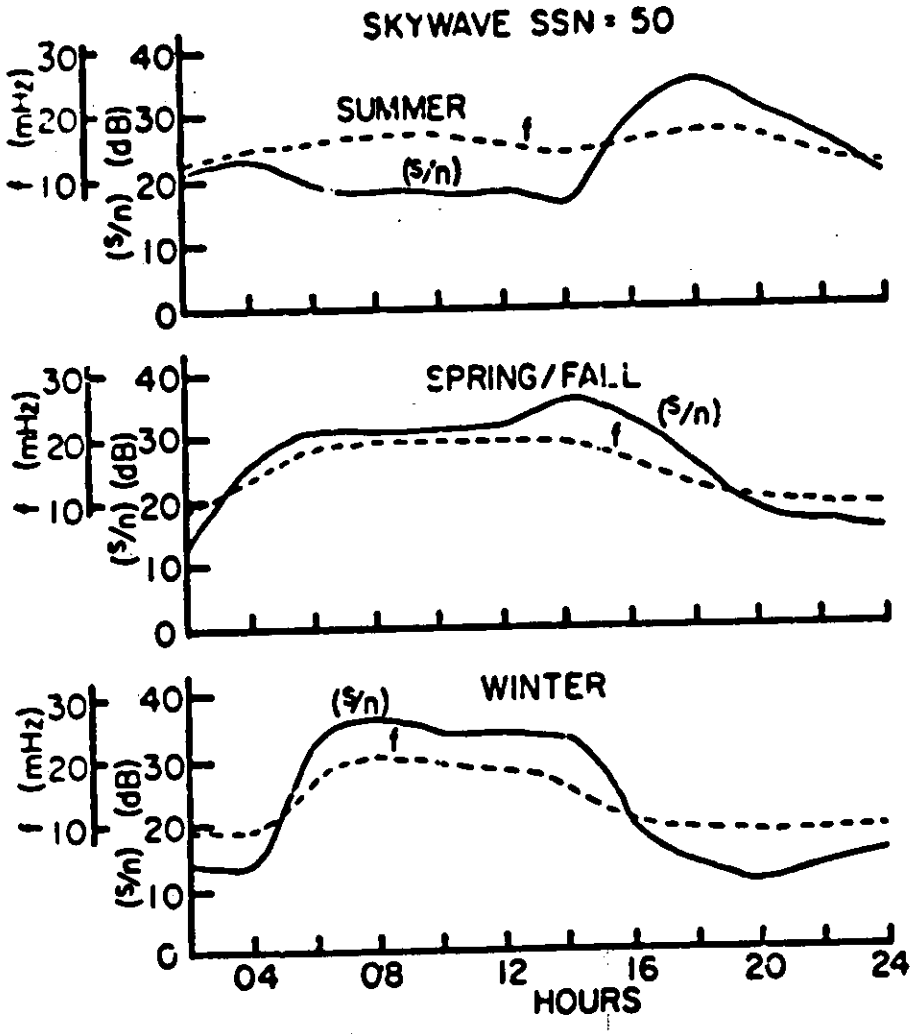

(U) Figure 1 Monostatic Radar Performance Prediction for 1000-nmi Range σ = 40 Log (f/5), P = 53, T = 10, G = 24 + 5 Log (f/10), N = 148-12.6 ln (f/3) (U)

UNCLASSIFIED

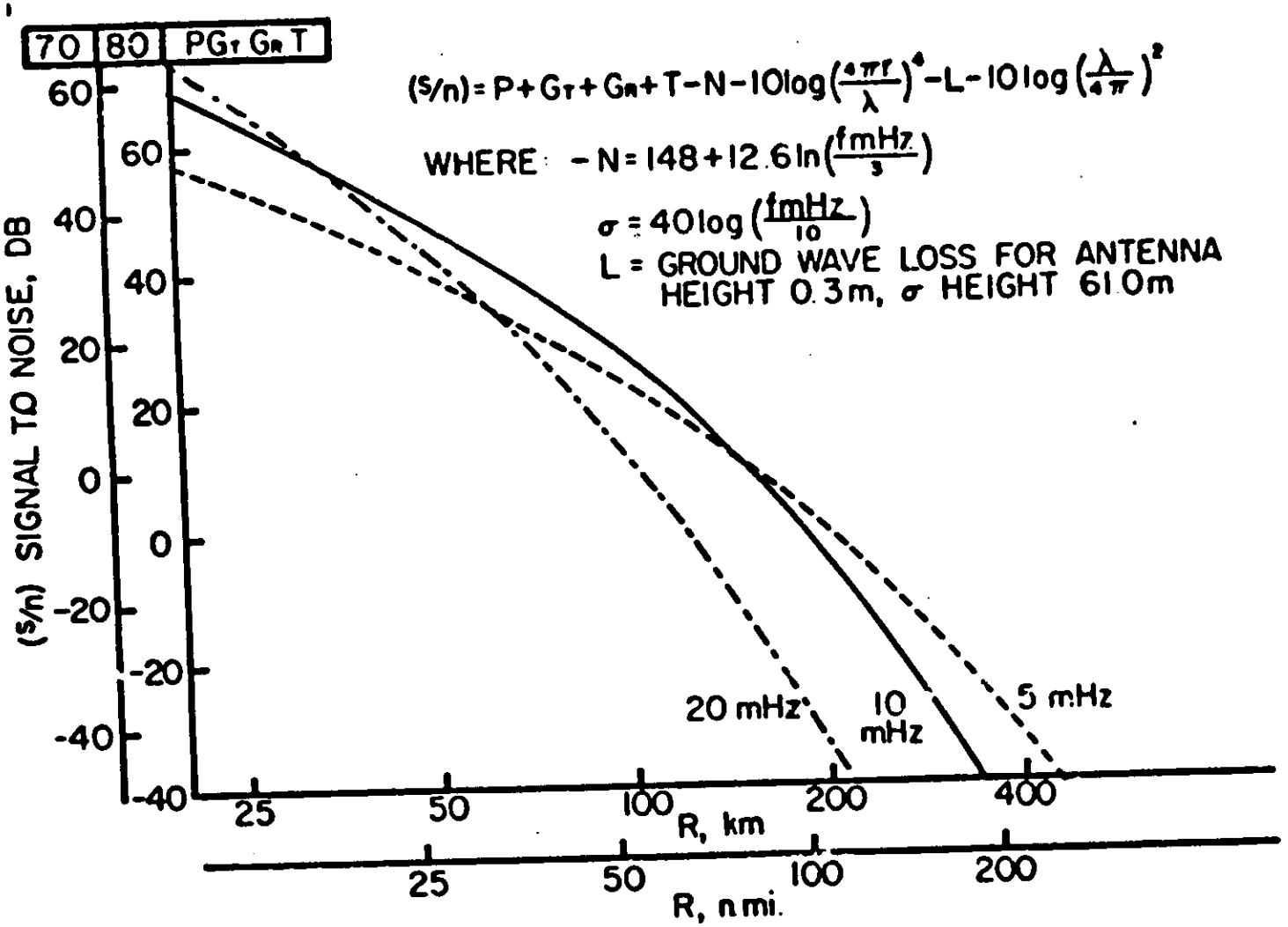

(U) Figure 2. Monostatic Surface Wave Radar (U)

UNCLASSIFIED

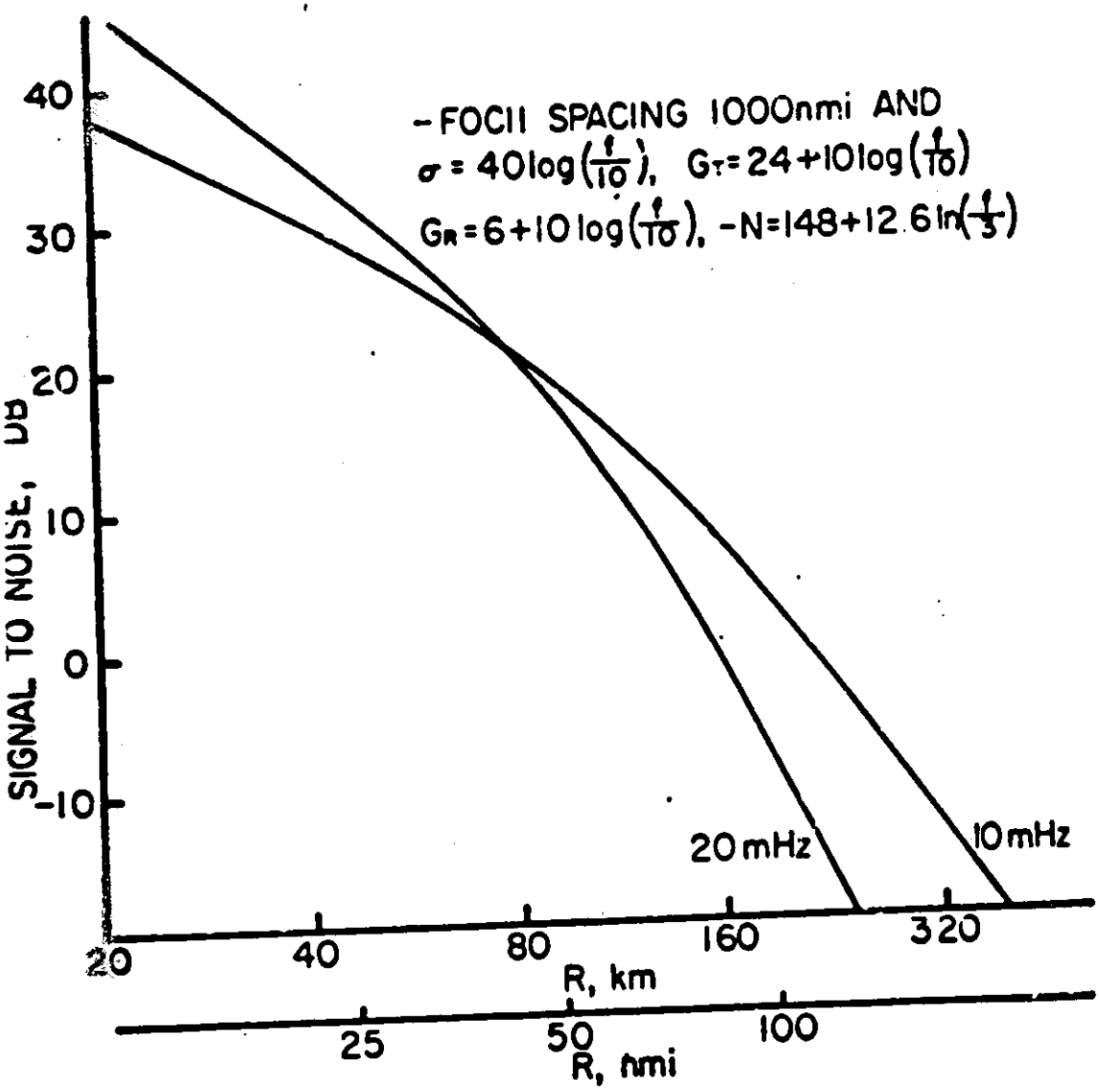

(U) Figure 3. Bistatic Performance Example (U)

UNCLASSIFIED

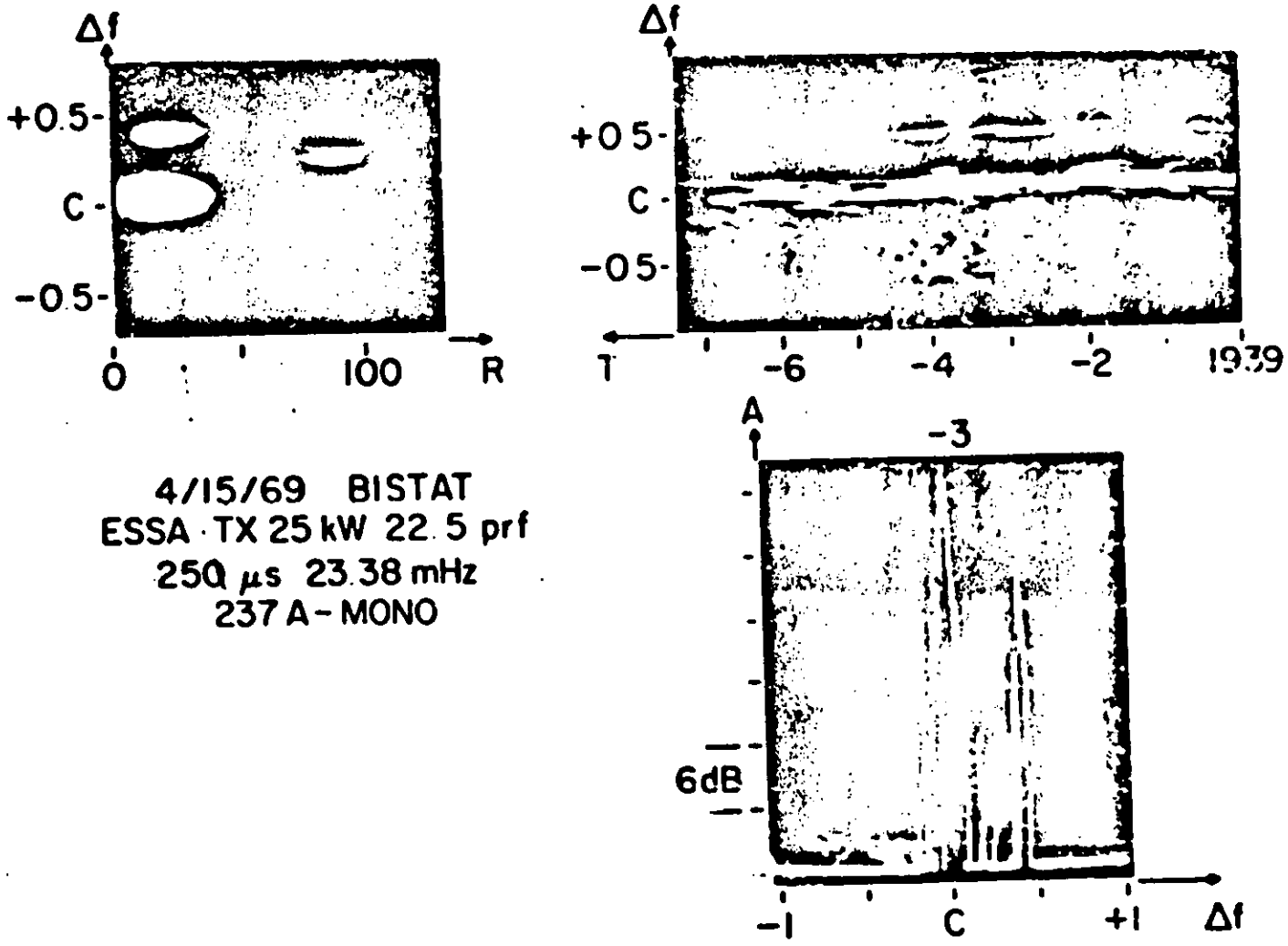

(U) Figure 8 Bistatic ESSA, T = 25 kW, 22.5 prf, 250 μs, 23.38 MHz, 237 A Mono, 4 15 69 (U)

UNCLASSIFIED

UNCLASSIFIED

[redacted]

NRL DATA ANALYSIS (U)

J. M. Hudnall

Naval Research Laboratory
Washington, D. C.

(U) It was planned that NRL 1) illuminate for part of the Fleet Air Defense (FAD) tests, 2) develop computer programs for signal analysis using I and Q plus monopulse channels including methods of display, and 3) after-the-fact examine and analyze the data using both the MADRE signal processor and a computer plus the developed programs. The contribution would be a capability for fine-frequency and long-storage-time analysis plus a variety of displays.

(U) To accomplish task (3) NRL required that the data be recorded on 7-track tape in an IBM-compatible format. Due to a long series of events, not one reel of tape meeting the requirements exists. Thus only Tasks 1 and 2 have been done plus considerable unexpected work in trying to achieve Task 3. Since the FAD source of a clutter versus frequency description was to be NRL's, some fragments of data will be shown here that do give pertinent examples.

(U) Figures 1 through 6 are the examples. In general the signal exhibited two or three amplitude peaks as a function of frequency. It is hoped that weather and sea-state conditions can be compared with the energy distribution.

(U) In Figure 1, doppler (Hz) time delay (pseudo range) is shown at 16:52:50Z, on 10 February 1970. The analysis bandwidth is 2.14 Hz.

(U) In Figure 2, a doppler time history is given for an 0.25-ms range gate starting on the time delay of the second earliest strobe of Figure 1. A short aircraft track is evident. The bandwidth is 4.14 Hz.

(U) Figure 3A was made with an 0.25-ms range gate starting at the earliest strobe of Figure 1. Figure 3B was started on the second strobe.

(U) Figure 4 A and B show amplitude versus Doppler displays made for the last two strobes of Figure 1. The resolution bandwidth is 1/28th.

(U) Figure 5A and B show displays similar to those of Figure 3, but made for operation on 16.16 MHz.

(U) Figure 6 shows computer-generated spectra for 27 February 1970.

[redacted]

UNCLASSIFIED

[redacted]

(U)

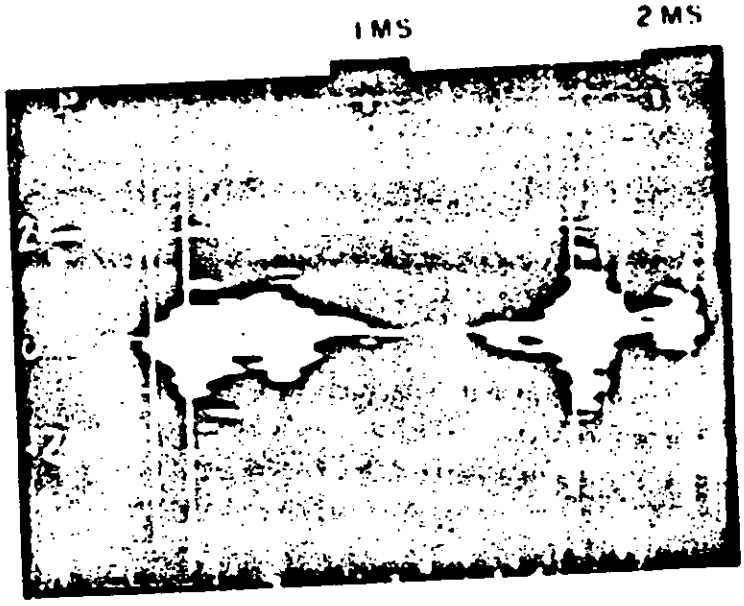

(U) Figure 1 Doppler Time Delay Space, 10 February 1970

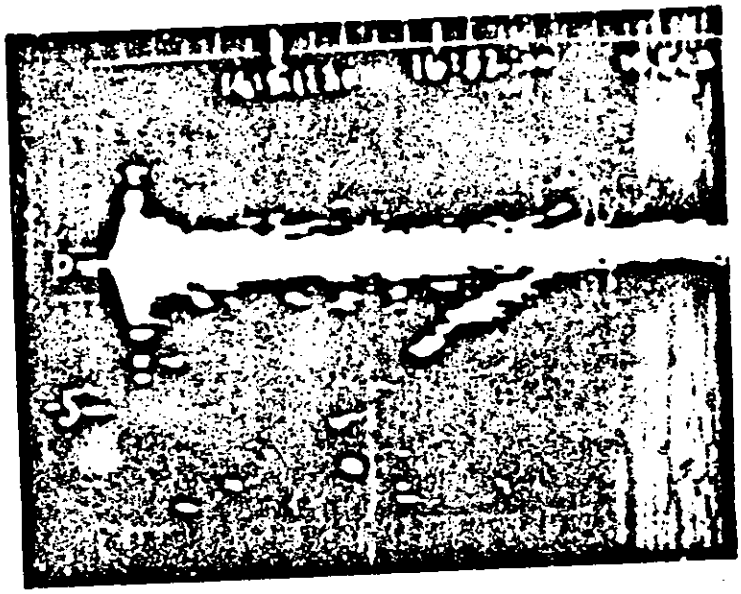

(U) Figure 2 Doppler Time History for an 0.25 ms Range Gate

[redacted]

UNCLASSIFIED

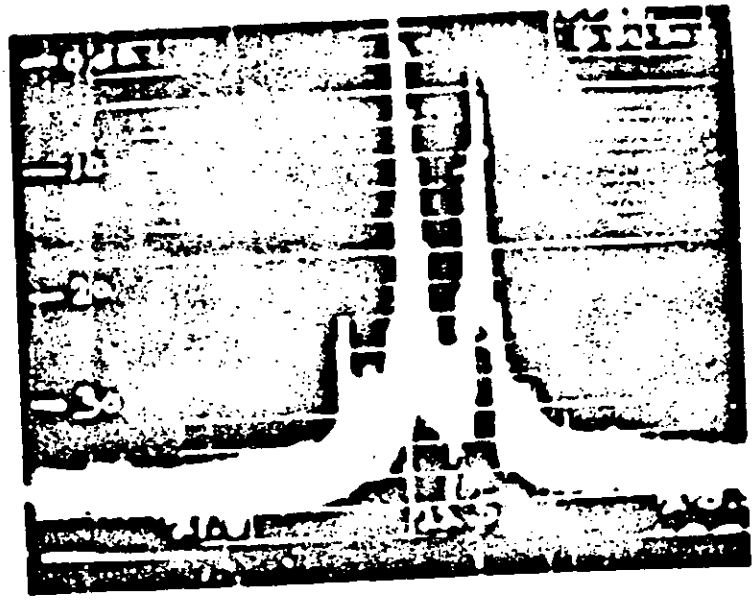

BANDWIDTH 1/28 Hz

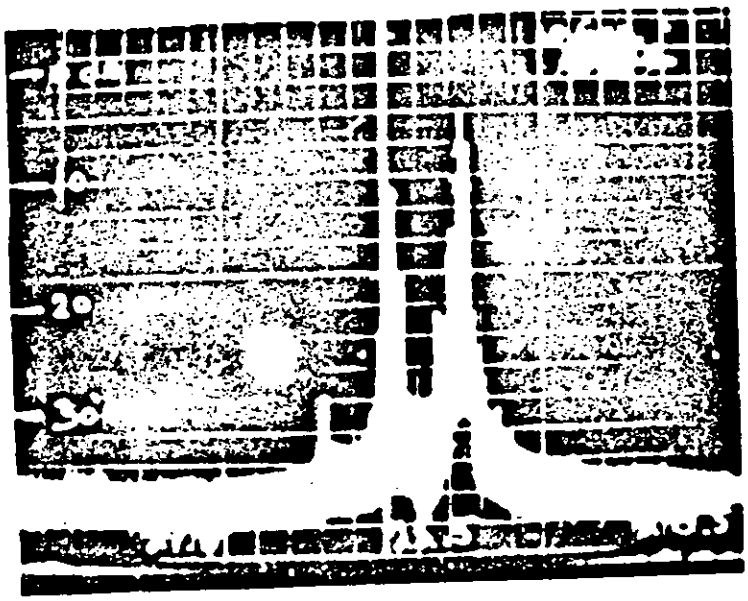

10.087 MHz

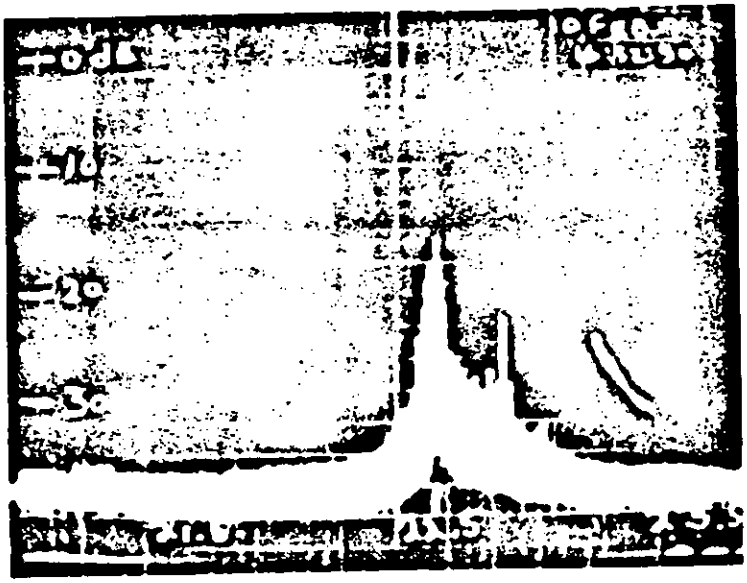

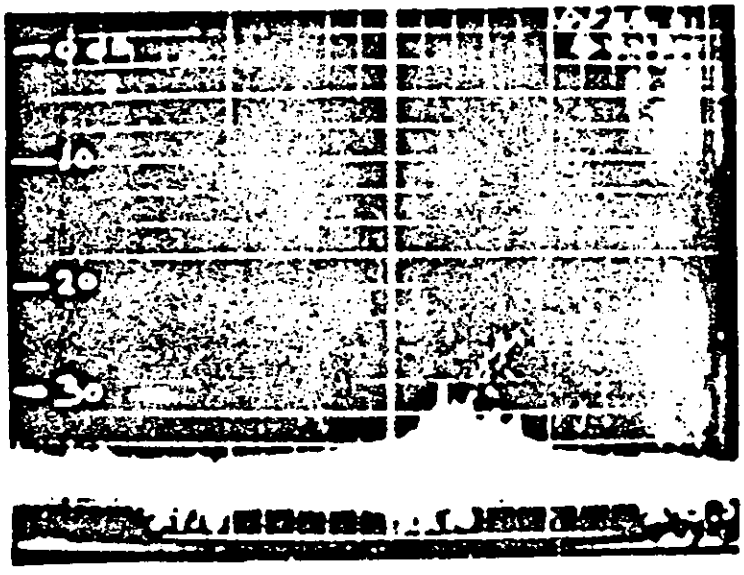

Figure 4 Amplitude vs Doppler Displays

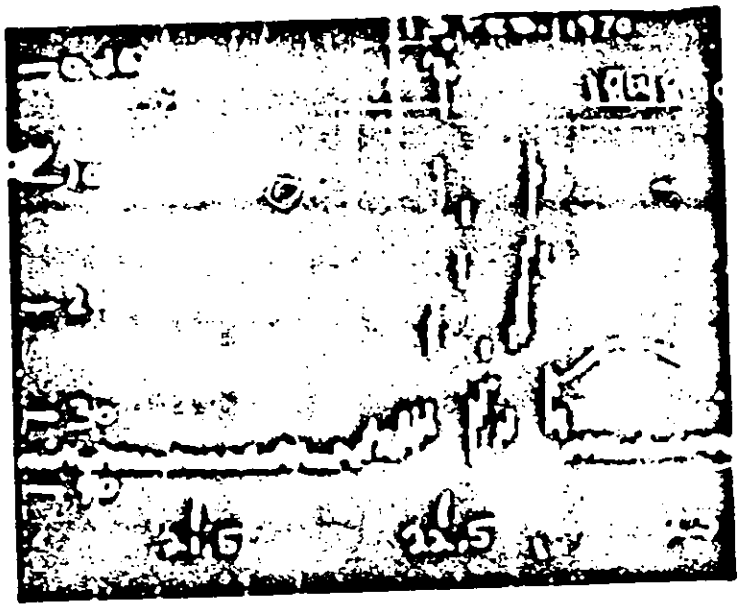

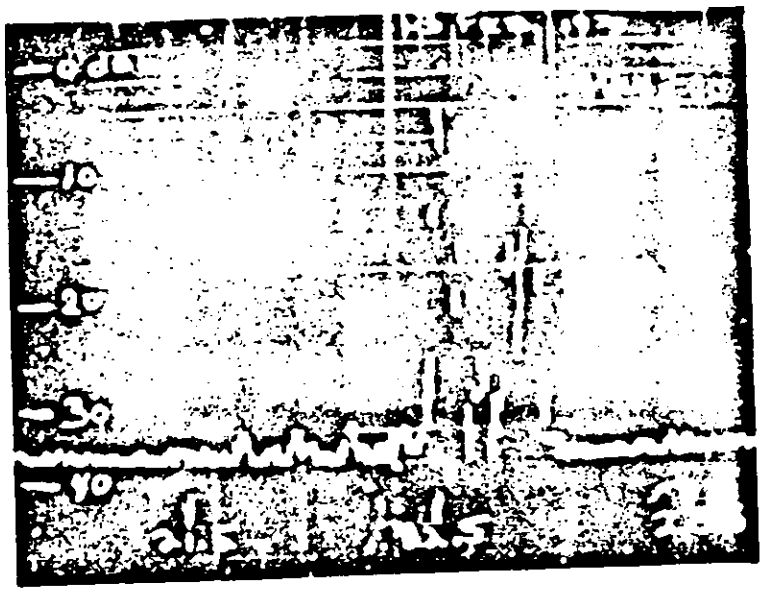

UNCLASSIFIED

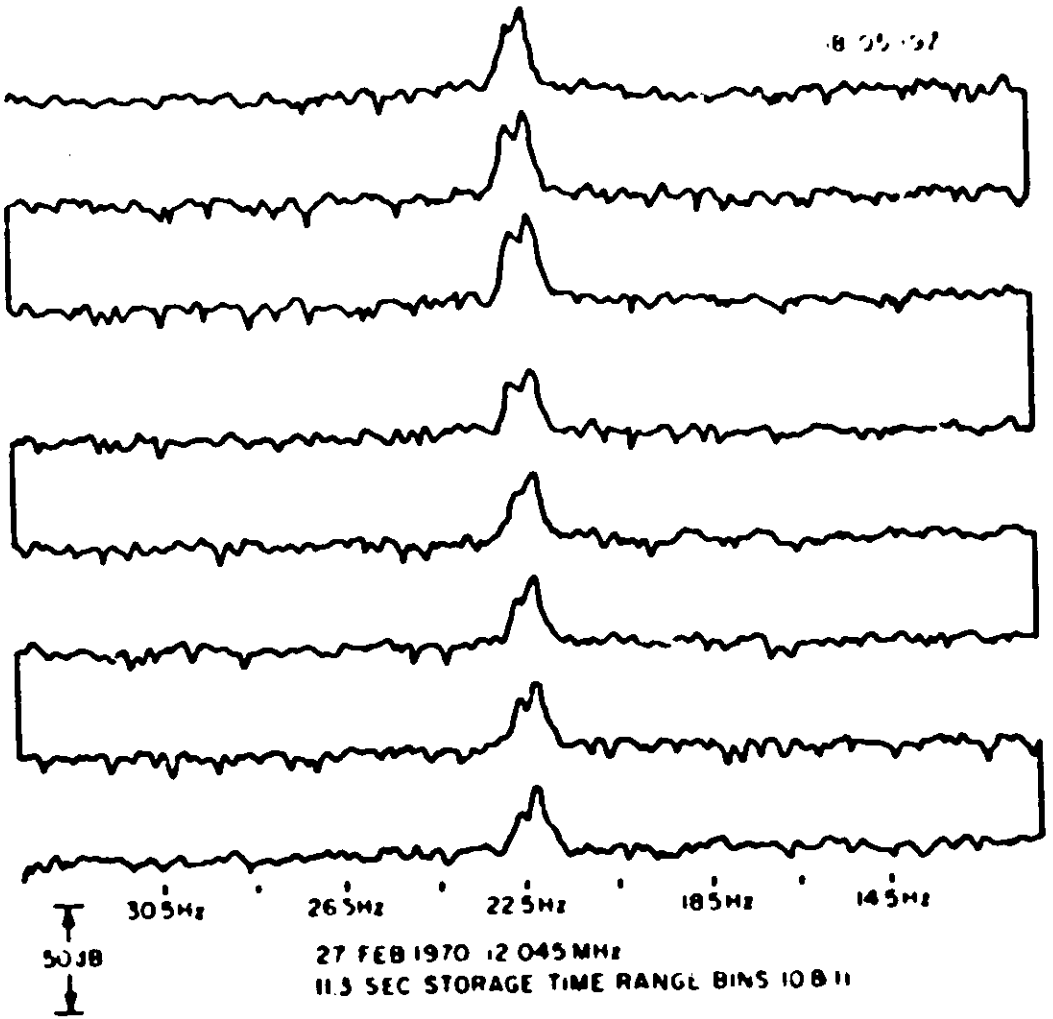

(U) Figure 6 Computer Generated Spectra, 27 February 1970 (U)

UNCLASSIFIED

[redacted]

[redacted]

FAD EXPERIMENT OF FEBRUARY 1970 (U)

Thomas D Scott

ITT Electro Physics Laboratories Inc
3355 52nd Avenue
Hyattsville, Maryland 20781

I INTRODUCTION (U)

(U) The Fleet Air Defense Experiment which was conducted in January and February of [illegible] a skywave HF radar signal from the ARPA ONR CHAPEL BELL facility at WHITEHOUSE Virginia to illuminate the area around a receiving field site at Cape Kennedy Florida The receiving site recorded both the incident skywave field strength from WHITEHOUSE and bistatic radar reflections from a Navy P3B aircraft flying on prescribed flight paths between 20 and 120 km offshore from Cape Kennedy A large portion of these paths were over the radar horizon from the receiving site because the airplane was at a very low altitude.

II EQUIPMENT (U)

(U) The skywave illumination was provided by a 500 kW CW HF high power transmitter with an antenna with approximately 9 dB gain at the angles and frequencies used The bistatic echoes were received on a 17 dB gain antenna at Cape Kennedy. The transmission format was a binary phase coded 1 ms pulse which was compressed to a length of 50 μs Pulse doppler and monopulse processing at the receiving site provided range doppler frequency (velocity) and azimuth tracking of the target Modulated reflectors were installed on two buoys which were anchored 25 and 50 km offshore served as control targets and provided frequency range and azimuth calibrations Communications via HF radio were maintained at all times between the transmitter receiver and the aircraft

III RESULTS (U)

(U) Successful detection of the target aircraft was made out to a range of 1000 km from the receiving site even with the more optimized system used for this experiment

[redacted]

[redacted]

UNCLASSIFIED

(U) An example of the tracking results is given in Figure 1 which shows a typical zig zag flight path on the upper left corner. In the upper right corner is an azimuth versus time plot calculated on the basis of [illegible] data collected on board the aircraft along with the azimuth versus time record made at the [illegible] site. This record illustrates the azimuthal tracking capability of the equipment. The graphical data on the bottom of Figure 1 show the computed and observed doppler frequency histories of the aircraft echo as it executes its zig zag path.

(U) In addition to the preceding results on aircraft detection and tracking, data were gathered to permit the determination of path loss, noise, and bistatic target cross sections. The bistatic cross section of the P3B aircraft was found to be between 5 m^2 and 100 m^2 and was a function of angle. The noise [illegible] a 20 kHz system were generally about 7 dB larger than those predicted by CCIR for a quiet rural setting in the daytime and about 10 dB larger at night. The path losses on the sky wave path agreed quite well with predictions.

IV CONCLUSIONS (U)

(U) The main purpose of the experiment was to test the feasibility of a hybrid sky wave surface wave system for passive detection of low flying aircraft at ranges beyond conventional ship radar coverage limits. The experiment proved the feasibility of this fleet air defense concept and provided data on some of the problems and limitations of such a system.

UNCLASSIFIED

(U)

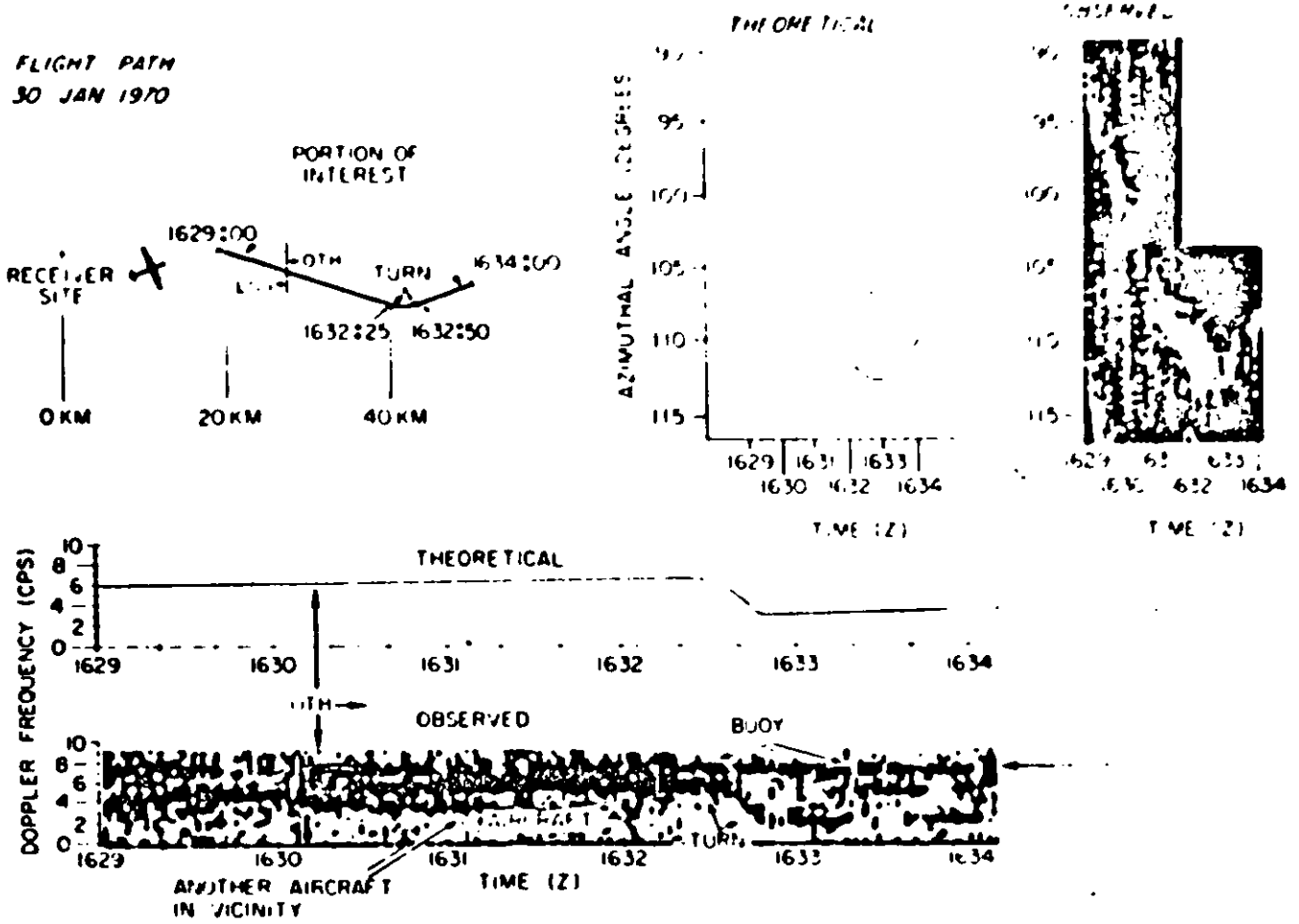

(U) Figure 1. Passive Detection of Over-the-Horizon Aircraft during the Fleet Air Defense Tests (S)

CLASSIFIED

PRECEDING PAGE BLANK - NOT FILMED

[redacted]

FAD RADAR SYSTEM STUDY (U)

Wesley N. Mollard

ITT Electro-Physics Laboratories, Inc.
3355 52nd Avenue
Hyattsville, Maryland 20781

I INTRODUCTION (U)

(U) In a paper titled "FAD Experiment of February, 1970 (U)" presented at this workshop, Thomas D. Scott gave some results of the Fleet Air Defense (FAD) experiments which were carried out in January and February of this year. Those results clearly demonstrated the feasibility of the hybrid, skywave surface wave radar concept.

(U) Following this demonstration of feasibility, ARPA has directed this contractor to undertake a preliminary system study directed toward a potential tactical system employing such a hybrid-mode radar for fleet air defense. It was clear at the outset that such a radar system would provide the fleet with the critical function of maintaining an early warning surveillance capability while still preserving complete electromagnetic-radiation silence. This joint capability would protect the fleet against a surprise attack, and at the same time deny an enemy the use of fleet-generated radiation for the purposes of fleet location or weapons guidance.

(U) The overall objectives of this study are to investigate the application of the hybrid mode radar to the problem of fleet air defense, and to determine the future actions necessary to permit the development of an operational system. The first step in reaching these objectives is to inter-relate the nature of the potential threats with the characteristics of the defensive systems available to the fleet in order to ascertain the performance criteria which must be met by the hybrid-mode radar. From these performance criteria, it is then possible to generate meaningful engineering specifications for such a radar. The above analysis will then help to identify those areas which still require research, development test, and evaluation (RDT&E) efforts, indicating the areas which constitute the state-of-the-art, those which require further study, and, especially, the principal areas of risk.

(U) This current study draws upon past study efforts to the greatest extent possible. In particular, considerable use is being made of certain of the results from a previous ITT-EPL study of a CONUS OTH (Over-The-Horizon Backscatter) system conducted for the USAF. The CONUS study is especially useful

[redacted]

UNCLASSIFIED

(U) [redacted] [illegible] and ORIII performance criteria are considered. Although [illegible] the past studies differ with respect to the mode of radar operation and the overall problem, there are important areas of commonality such as the primary terminal ranges of doppler [illegible] targets, target types, etc. In addition, maximum use will be made of other completed studies on particular facets, such as threat models and defensive systems. By drawing on this extensive background of existing information, it will be possible to [illegible] a modest study effort to ensure coverage of the problem to a depth that establishes meaningful bounds on the important parameters entering into the problem.

(U) [redacted] Figure 1 shows a general outline of the LAD system study as it is being directed by [illegible]. The flow chart in Figure 2 illustrates more clearly the interrelationships among the various parts of the study effort. The major elements making up the flow chart are summarized in the following discussion.

II KEY STUDY AREAS (U)

A Threat Considerations (U)

(U) [redacted] The various threat models which are officially postulated to be in enemy inventories in the 1970 - 1980 era are being investigated. The threat models include both specific weapon characteristics and attack scenarios. The individual weapons extend from aircraft attacking with short-range weapons, aircraft employing long-range, air-to-surface missiles, and surface-to-surface missiles launched by surface vessels or submarines. The variety of scenarios will extend from small-scale sneak attacks through large-scale engagements. These threat models are being integrated to establish threat-missile [illegible] envelopes which define such parameters as altitude-versus-range, range-versus-time history, [illegible] density attackers, etc.

B Defensive System Considerations (U)

(U) [redacted] The defensive systems available for fleet use in the 1970 - 1980 era include sensors and active defense weapons. Among the sensors are shipboard radars for acquisition, tracking, and fire control, airborne radars and other possible sensors (such as LWIR). The active defensive weapons include air-to-air missiles carried by carrier-launched aircraft, surface-to-air missiles, and anti-aircraft artillery. The various capabilities of these respective elements of the defensive systems are being organized into performance envelopes which indicate the accuracy and timeliness required from an early warning system so that effective use can be made of the defensive systems. An additional aspect of the consideration of the defensive systems is the important feature of the "hand-off" from the early warning system to the shipboard terminal defense system. This and other specific interaction between the LAD system and the other fleet defensive systems lead to a set of "interface requirements" which must be met to ensure effective cooperation among the various defensive systems.

[redacted]

(U)
1ST

I. INTRODUCTION
- STATEMENT OF PROBLEM AND ROLE OF FAD

II. OVERALL SYSTEM CONCEPTS

III. THREAT CONSIDERATION
- MISSILE TARGETS
- AIRCRAFT TARGETS

} HF SIGNATURES

IV. SHIPS RADAR DEFENSES

V. INTERFACE OF FAD RADAR WITH SHIPS RADARS

VI. FAD RADAR REQUIREMENTS

VII. CONCLUSIONS-RECOMMENDATIONS

(U)
1ST Figure 1 Topical Outline of FAD Radar System Study (U)

(U)

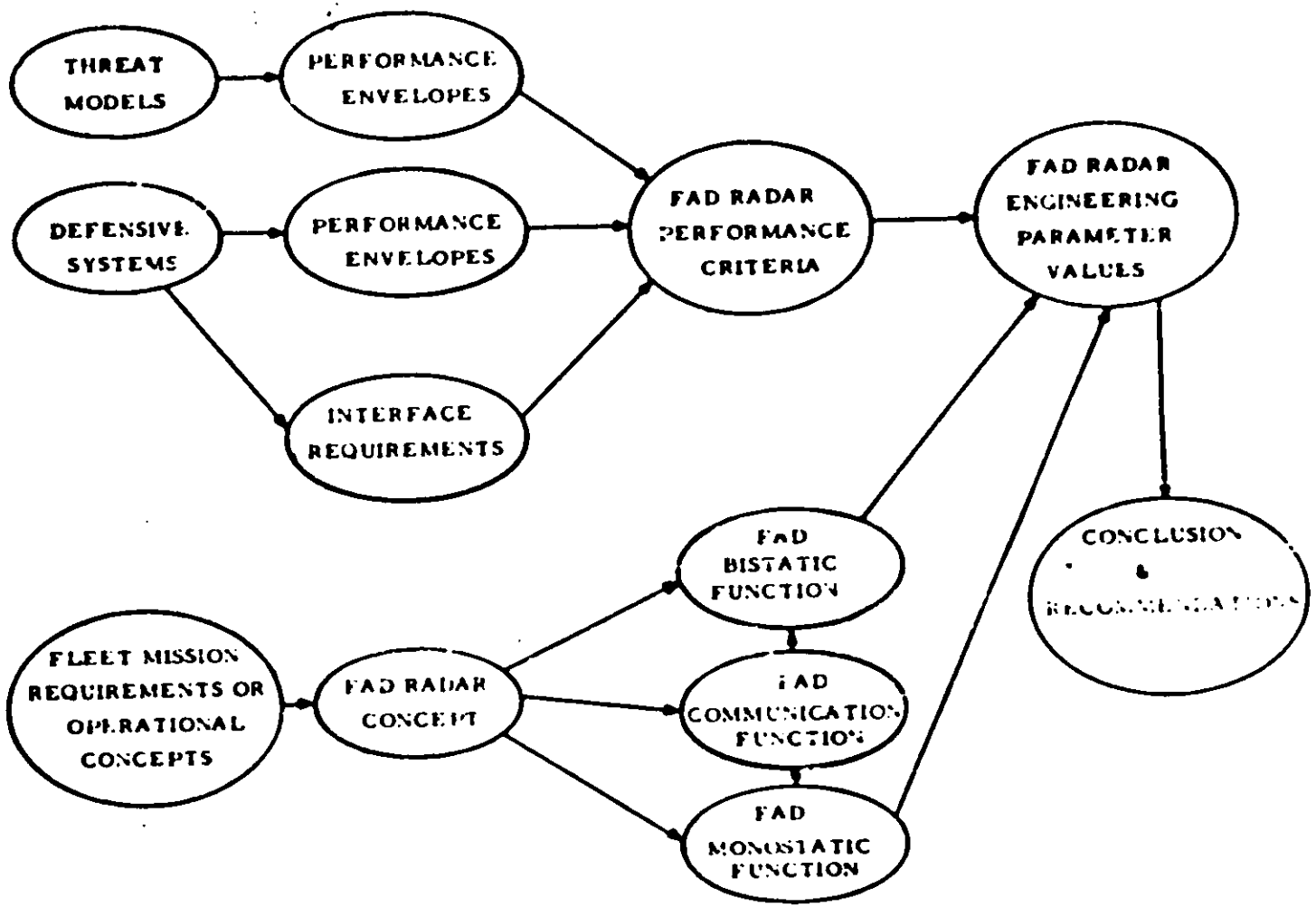

(U)

Figure 2. FAD Radar System Study Flow Chart (U)

[redacted]

c. FAD Radar Performance Criteria (U)

(U) The performance envelopes of the threat models and the defensive systems and the [illegible] will then be used to establish definitive performance criteria for the FAD system so that it can play an effective role in fleet defense.

d. Fleet Mission (U)

(U) Clearly the use of a naval fleet is not limited to a single easily categorized type of operation. It is therefore necessary to consider a variety of fleet operational concepts in order to determine possible scenarios in which the FAD concept can be applied in the various circumstances. Among the aspects requiring consideration is the question of whether the FAD system should be simply added to ships readily in service, or whether it should be deployed on special purpose dedicated vessels or [illegible] alternatives between these extremes. Another important consideration is the extent to which the FAD system must be employed in a special-purpose communication system simultaneously with its radar [illegible]

e. FAD Radar Function (U)

(U) The nature of the sky wave illumination in the present FAD concept is such that it is clear that the illuminator can also act as a monostatic radar. The addition of this function could provide early warning information at greater ranges than could be hoped for in the bistatic configuration with, however, offering the self-contained capabilities provided by the bistatic radar. It is important in the study to define the optimum roles for each of the two possible modes of operation.

f. FAD Radar Engineering Parameter Values (U)

(U) The net output of the FAD performance criteria and the fleet mission requirements will then be a definitive presentation of the necessary engineering specifications of a FAD system which can provide effective early warning to the fleet in event of attack threats originating beyond the range of other sensors, a range which may be set physically because of the radar horizon, or operationally by considerations of electromagnetic control.

III CONCLUSIONS AND RECOMMENDATIONS (U)

(U) The output of the study will be a report in which the FAD engineering specifications are defined and in which recommendations are made for action in areas requiring additional RDT&E.

[redacted]

UNCLASSIFIED

UNCLASSIFIED

PRECEDING PAGE BLANK - NOT FILMED

SECRET

SHIP DETECTIONS (U)

J. L. Ahearn

Naval Research Laboratory
Washington, D. C.

(U) The first positive HF radar ship detection by NRL was made on 29 June 1968. The detection was by skywave at 15.595 MHz, 22.5 prf, 072 T ± 7° with an approximate $\cos^2$ shaped pulse about 700 μs long. Figure 1 is a set of pictures illustrating these observations. The ship can be seen at -0.8 Hz. It was later identified as the Grotedyk, length 534 ft, beam 67 ft and with a KAMM-M superstructure. The ship was observed for 5 hours from 10 AM to 3 PM local time. The maximums of received signal gave a radar area of about 1500 m^2.

(U) A second example of ship detection is given in Figure 2. Operating parameters were 15.595 MHz, 22.5 prf, 084 T ± 7°. This target was the Forrestal, length 1034 ft, beam 250 ft. Maximums in signal strength yielded a radar area of about 13,000 m^2. The target is at -1.5 Hz and the clutter amplitude (given in relative dB) versus frequency characteristic is an example of how well behaved it can be. Note that a 10:1 reduction in pulse width would make the ship detectable at any speed except that of the resonant waves.

(U) Figure 3 is a ground-wave amplitude versus frequency plot made at 30-nmi range, and this is shown to exhibit frequency resolving capability without ionospheric effects. In this example a 50-second time sample was used.

(U) Another example of doppler resolving capability is given in Figure 4. This gives doppler versus range for a 50-μs pulse length and only 10 seconds dwell time.

(U) It is felt that by adapting to (or taking out) undesired ionospheric effects there are genuine potential gains for ship traffic plotting by HF radar.

UNCLASSIFIED

SECRET

UNCLASSIFIED

UNCLASSIFIED

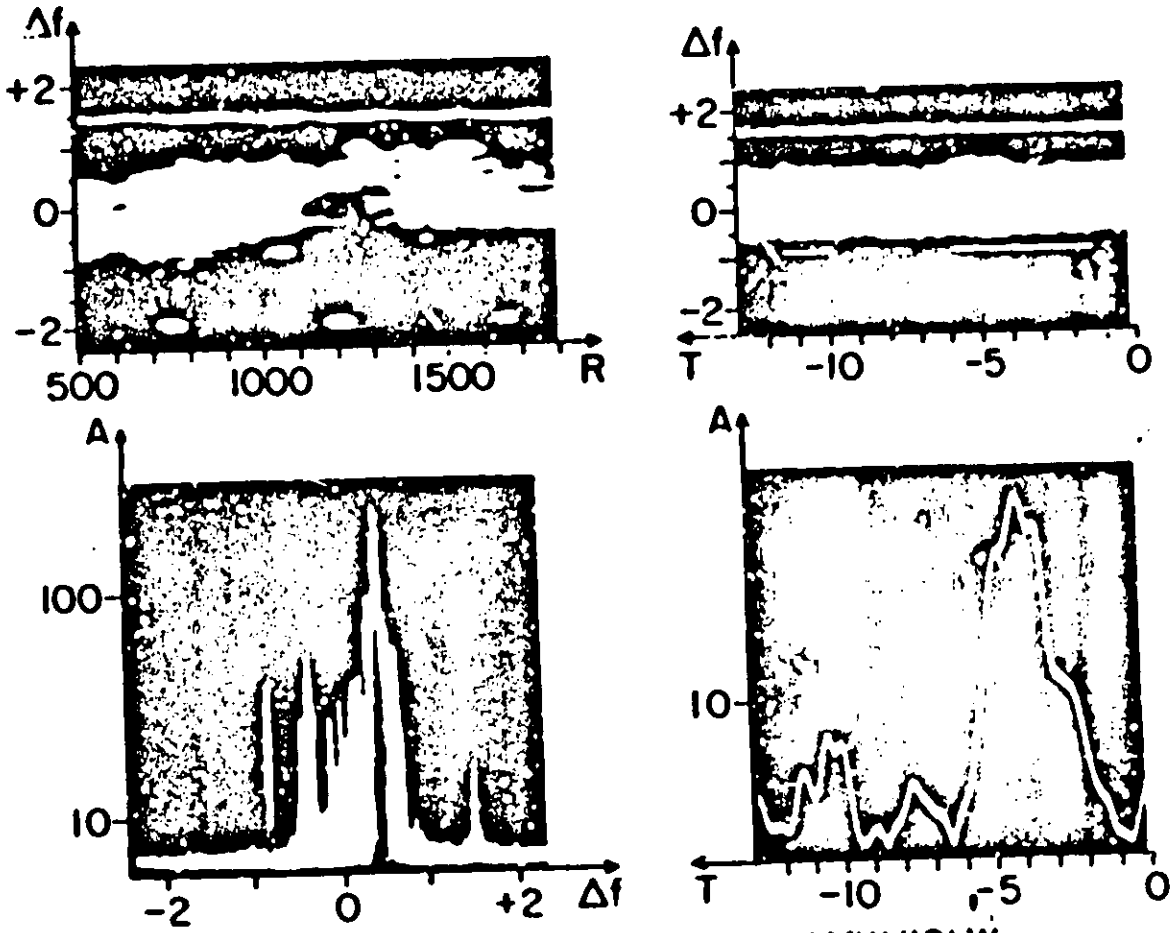

1715, 6/29/68, 072°, 15.595 MHz, 1 MW/10kW

(U) Figure 1. 6/29/68, 1715, 070°, 15.595 MHz, 1 MW/10 kW (U)

(U)

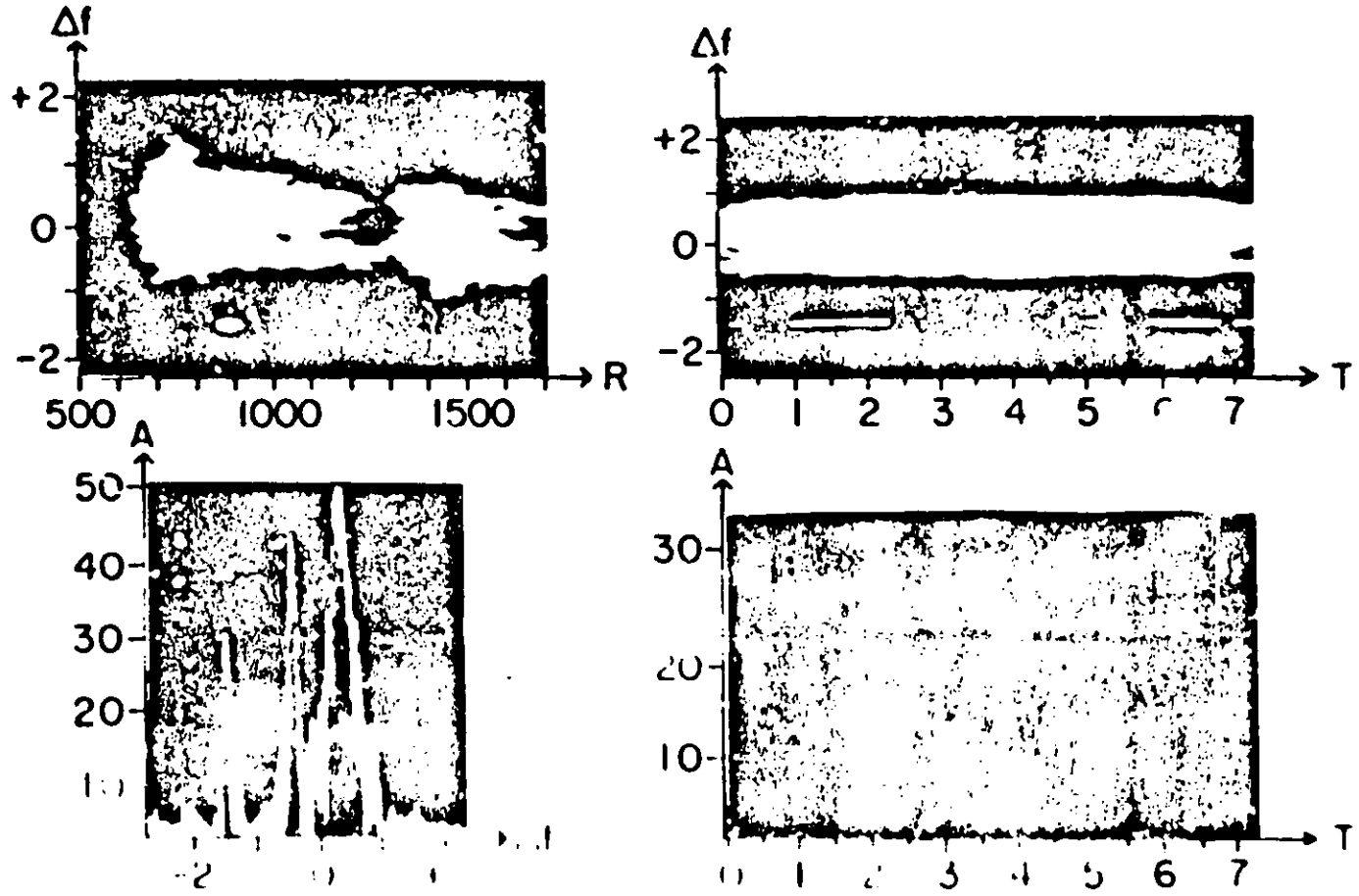

[illegible], 0848, 15 595 MHz, 2 3MW/10kW

(U) [illegible] 1848.084 15 595 MHz, 2 3MW 10kW (U)

UNCLASSIFIED

UNCLASSIFIED

UNCLASSIFIED

(U)

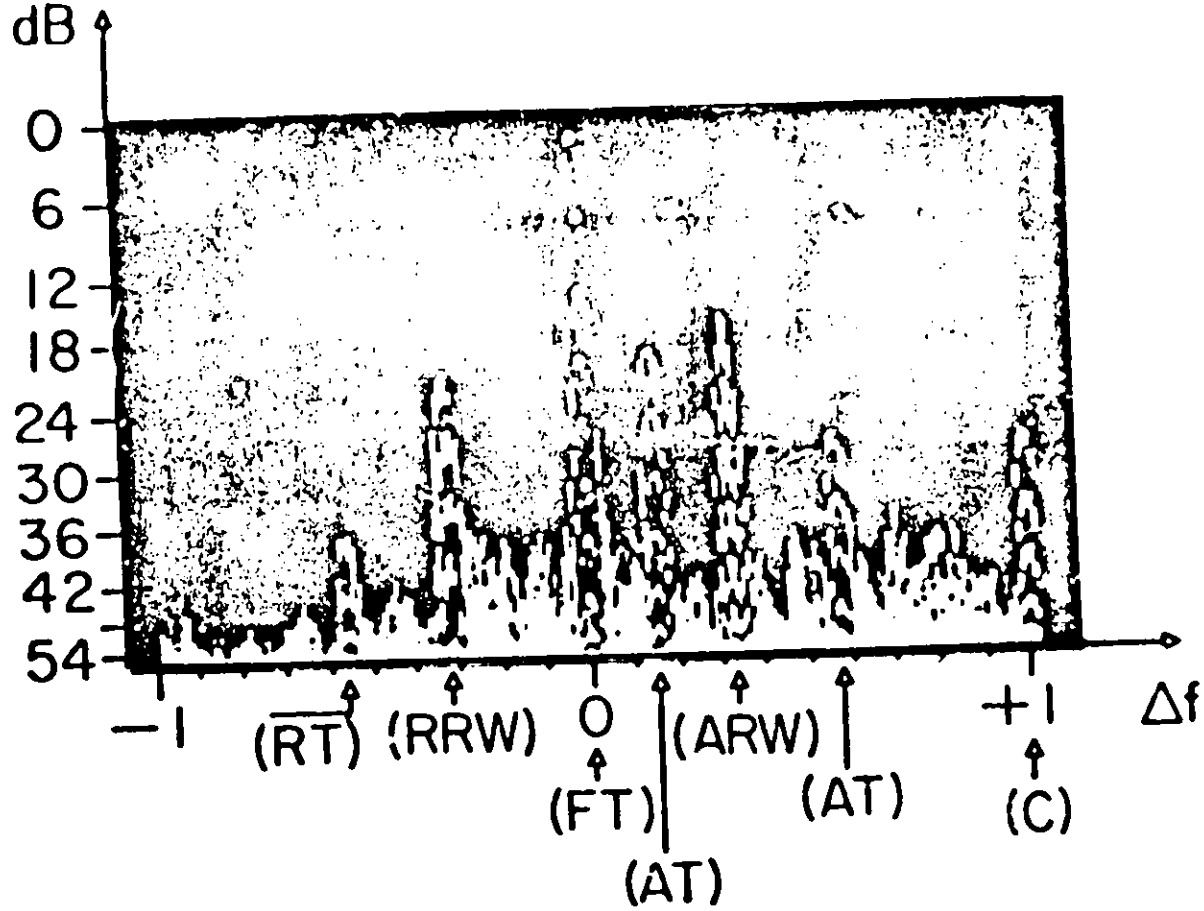

03:03:33 GMT 8/12/69

(U) Figure 1 - S 12 69 03 03 33 GMT (U)

UNCLASSIFIED

UNCLASSIFIED

(U)

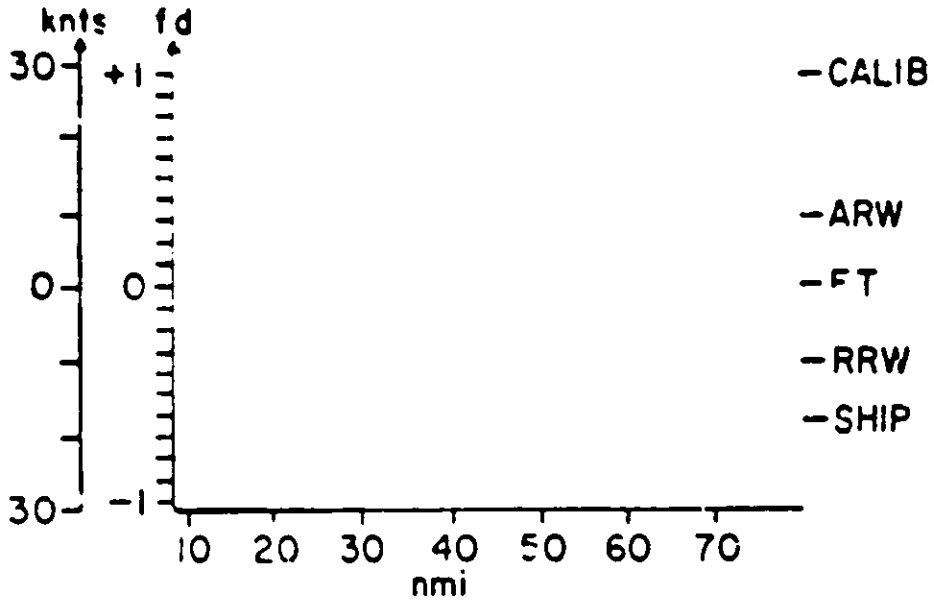

(U) (S) Figure 4. Ground Wave Doppler Resolving Capability (S)

UNCLASSIFIED

PRECEDING PAGE BLANK - NOT FILMED

[redacted]

HIGH RESOLUTION SEA BACKSCATTER (U)

J. R. Barnum

Radioscience Laboratory
Stanford, California 94305

I INTRODUCTION (U)

(U) (S) Stanford University's part in Project MAY BELL has been to study the feasibility of detecting ships OTH by means of sweep-frequency CW radar while receiving on a very wide aperture antenna array. It has become necessary to know the HF radar cross-sections of typical ships at sea, and to measure the properties of sea clutter using sky-wave propagation. A partially-controlled experiment was also run, in which the detection of a 500-foot cargo ship was attempted. The purpose here is to summarize these topics, and to specify what further work is necessary.

II SHIP CROSS SECTIONS AT HF (S)

(U) (S) Under a subcontract from Stanford, Technology for Communications International (TCI) measured the backscatter from ship models at the Naval Electronics Labs (NEL).

(U) (S) A total of 99 radar cross-section (σ) patterns for a DE-1030 destroyer and a Forrestal Carrier were obtained at frequencies between 3 and 22 MHz, for elevation angles between 3.5 and 20 degrees. Bistatic and surface wave measurements were also performed at 3 and 7 MHz. The data were obtained using 1:48-scale models at 48 times the HF value. The correspondence to the realistic (full-size) cases at HF should be close.

(U) (S) For vertical polarization, the cross-sections are 10^3 to 10^5 m^2 for the destroyer, and 10^4 to 10^6 m^2 for the carrier. Horizontally-polarized cross sections are down 3 to 19 dB for the destroyer (depending on ship orientation), and 0 dB for the carrier, at a 20-degree elevation angle. The "surface wave" cross-sections are of the same magnitude as the above, and when the radar becomes bistatic, the scatter is only 0 to 5 dB lower in amplitude.

[redacted]

[redacted]

(U) The number of nulls in all the patterns increase with frequency, but at a faster rate for the ship. Bistatic patterns contain fewer nulls.

(U) The accuracy in measurement of max σ is usually ±3 dB. For 20 to 30 percent of the patterns a slight to moderate error in pattern null structure occurs, however, enough data was taken so that further measurements of this type are unnecessary.

III SKY WAVE PROPAGATED SEA CLUTTER (U)

(U) The radar cross-section of a sea patch was measured in the Gulf of Mexico using a portable repeater operated on board a cargo ship. Using high azimuthal resolution (½-degree beamwidth) and small equivalent pulses (4-10 μs) the sea cross-section was reduced to 10^4 m^2. The sea's cross-section per unit area was then calculated to lie between 10^{-3} and 10^{-2}.

(U) Fixed frequency experiments have been performed to ascertain the effect of controlled transmitter polarization on backscatter amplitude as a function of range in the Pacific Ocean. The results show that it is possible to reduce the clutter by about at least 10 dB by switching the transmitter between vertically and horizontally polarized antennas, while receiving on the 2.5-km Los Banos array. The effect is not observed when using a 4-degree beamwidth antenna, which was explained using swept azimuth data and computer-raytracing backscatter synthesis to show that polarization rotation is very sensitive to azimuth changes.

(U) It is now concluded that such a control over sea clutter magnitude should aid in ship detection. The sea reflects the characteristic (ordinary and extraordinary) waves to the receiver such that time delay of all received modes are constrained to be equal. By contrast, a ship represents a discrete target and reflects these modes while keeping the ground range constant. Because of this difference, one could simultaneously null out the sea clutter while maximizing the ship's return. It is therefore clear that some control over the radar's polarization will help detect ships at sea, i.e., when the sounder's antenna is large enough, and when the ionosphere permits the polarization phenomena to occur.

IV OTH SHIP DETECTION (S)

(S) On the basis of the results described in Parts I and II (above), it is probable that a ship could be detected on a total power basis using the ARPA-ONR Wide-Aperture Research Facility (WARF). This follows from the measurement of a 10^4 m^2 total sea cross section, which is less than σ's for broadside ships. The control of the sounder's polarization may facilitate this detection.

[redacted]

(U) Detection-oriented experiments have shown that oil platforms (or groups of them) were seen in the Gulf of Mexico. When a 10^5 m^2 cross-section repeater was operated on a 500-foot cargo ship between New Orleans and Houston, the repeater's echo was visible 90 percent of the time. Echoes from the ship's position (other than the delayed repeater echo) were also seen occasionally, but these may have been from platforms.

(U) The experimental results demonstrate that 1- to ½-degree azimuthal, and 4- to 10-μs time delay resolutions are obtainable using the WARF system, as predicted. Targets with cross-section comparable to those for broadside ships have been detected on a total power basis using the system. It has not yet been proved, however, that a ship was detected.

V FUTURE WORK (U)

(U)

- Measure more sea clutter magnitudes and polarization dependence at HF
- Study ways to use polarization control in OTH ship detection
- Run several well-controlled ship detection experiments
- Investigate use of repeaters as permanently-stationed reference targets at sea
- Develop Doppler-filtering for sea backscatter data processing on the SFCW waveform

PRECEDING PAGE BLANK - NOT FILMED

[redacted]

BUOY TACTICAL EARLY WARNING (S)

[redacted]

PRECEDING PAGE BLANK - NOT FILMED

[redacted]

BTEW CONCEPTS (U)

Allen M. Peterson

Stanford Research Institute
Menlo Park, California

(U) (S) Surface-wave beyond-the-horizon radar dates back to work undertaken before 1950 in the United Kingdom.[1] Shortly thereafter a program was started by Raytheon[2] and continued by MIT Lincoln[3] Laboratory until 1957. The final report by Lincoln Laboratory clearly demonstrated the feasibility of beyond-the-horizon detection even in the 1950-1960 time frame.

(U) (S) A renewed interest in Surface-wave radars was initiated in the 1968 IDA JASON Summer Study[4] during a review of OHD radar techniques. This study occurred in La Jolla, California and the possibility of using anchored, buoy-mounted transmitters of relatively low power levels ($\simeq$ 100 watts) arose in discussions with personnel from Scripps Institution of Oceanography. Low power appeared possible since buoys could be distributed along a "fence-line" or in an array so that the distance from the transmitter to the target (aircraft or missile) could be kept small and the large surface wave losses could be limited to the path from target to a land-based receiving installation.

(U) (S) Following the 1968 JASON Study ARPA initiated a research program to investigate the possibilities of the surface wave systems including the buoy-based transmitters. A number of "catamaran" buoys were procured from Scripps and instrumented by APL. Detection experiments were implemented by Raytheon for the BTEW technique.

(U) (S) In addition, surface wave propagation measurements were implemented to study the relationship of losses to "sea state" conditions. This appeared essential based on theoretical studies carried out by Barrick[5] who found that, under rough sea conditions, 10 dB or more signal losses would occur in the desireable frequency range near 10 MHz. Losses of this amount, which appear to have been confirmed, certainly make the system application more difficult.

(U) (S) Sea clutter caused by resonant or "Bragg" scattering from sea waves was also raised as a source of concern in system applications. Studies now appear to show that the Bragg-scattered signals are sufficiently confined in frequency extent that they will not seriously limit system performance for aircraft or missile detection because of the larger Doppler shifts associated with these targets.

[redacted]

[redacted]

(U) One potentially desirable feature of surface wave techniques is their immunity to nuclear propagation blackout. In fact, sufficiently widespread nuclear blackout could cause a reduction in background noise level and ionospherically propagated interference.

(U) It appears probable that enough has been learned during the BTEW experimental program to permit meaningful system studies in the near future. Certainly it should be possible to define required future experiments based on the research which is being reviewed today.

REFERENCES

1. [redacted]

2. [redacted]

3. [redacted]

4. [redacted]

5. D. E. Barrick, "Theory of Ground-Wave Propagation Across A Rough Sea at Dekameter Wavelengths" (U), Research Report, Battelle Memorial Institute, Columbus, Ohio, January 1970. UNCLASSIFIED

[redacted]

BTEW-1 FEASIBILITY TESTS (U)

Bruce B. Whitehead

Raytheon Company
Equipment Division
OHD Advanced Development Department
Spencer Laboratory
Burlington, Massachusetts

I INTRODUCTION (U)

(U) (S) The BTEW-1 Feasibility tests were carried out during the period January-March 1970 in the vicinity of the Raytheon transmitter site on Carter Cay in the Bahamas. A total of eight flight tests were made, one was chosen for detailed analysis. This paper describes that analysis and draws conclusions that may be used in a system design using the BTEW-1 concept.

II NOMINAL SYSTEM AND TEST PARAMETERS (U)

(U) (S) For the selected test the system parameters are summarized in Figure 1. The aircraft flight plan is shown in Figure 2. The aircraft made successive passes from CC to G3 and returned at altitudes ranging from 250 feet to 14,000 feet. All passes were made at speeds of approximately 250 knots.

III OBSERVED AND PREDICTED DOPPLER (U)

(U) (S) Figure 3 shows the observed and predicted Doppler for the CC-G3 flight at 6000 feet. This and all the Doppler predictions were based on the measured true ground speed of the aircraft. All computed Dopplers are for a ground wave propagation path from the transmitter to the target. Two possible propagation paths have been taken into account for the target to receiver path. These two return paths result in two predicted dopplers. In Figure 3 only the ground wave prediction is shown and it can be seen that the observed Doppler clearly corresponds to this mode. In Figure 4, a composite predicted Doppler is illustrated. The Doppler track with the largest frequency excursion is the ground wave mode whereas the

[redacted]

UNCLASSIFIED

NOMINAL SYSTEM AND TEST PARAMETERS

RECEIVER SITE	--	CAPE KENNEDY
TRANSMITTER SITE	--	CARTER CAY
AIRCRAFT	--	NAVY P3V (LOCKHEED PROP-JET ELECTRA)
ANTENNAS	--	RX ANT 16 ELEMENT BSA TX ANT λ/4 MONOPOLE $G_T G_r$ = 16 db
ALTITUDES	--	250' — 14,000' LINE OF SIGHT -- 17,000'
FREQUENCY	--	10.167 MHZ
TRANSMITTED POWER	--	2.25 KW

(U) (S) Figure 1. Nominal System and Test Parameters (U)

[redacted]

UNCLASSIFIED

(U) (S)

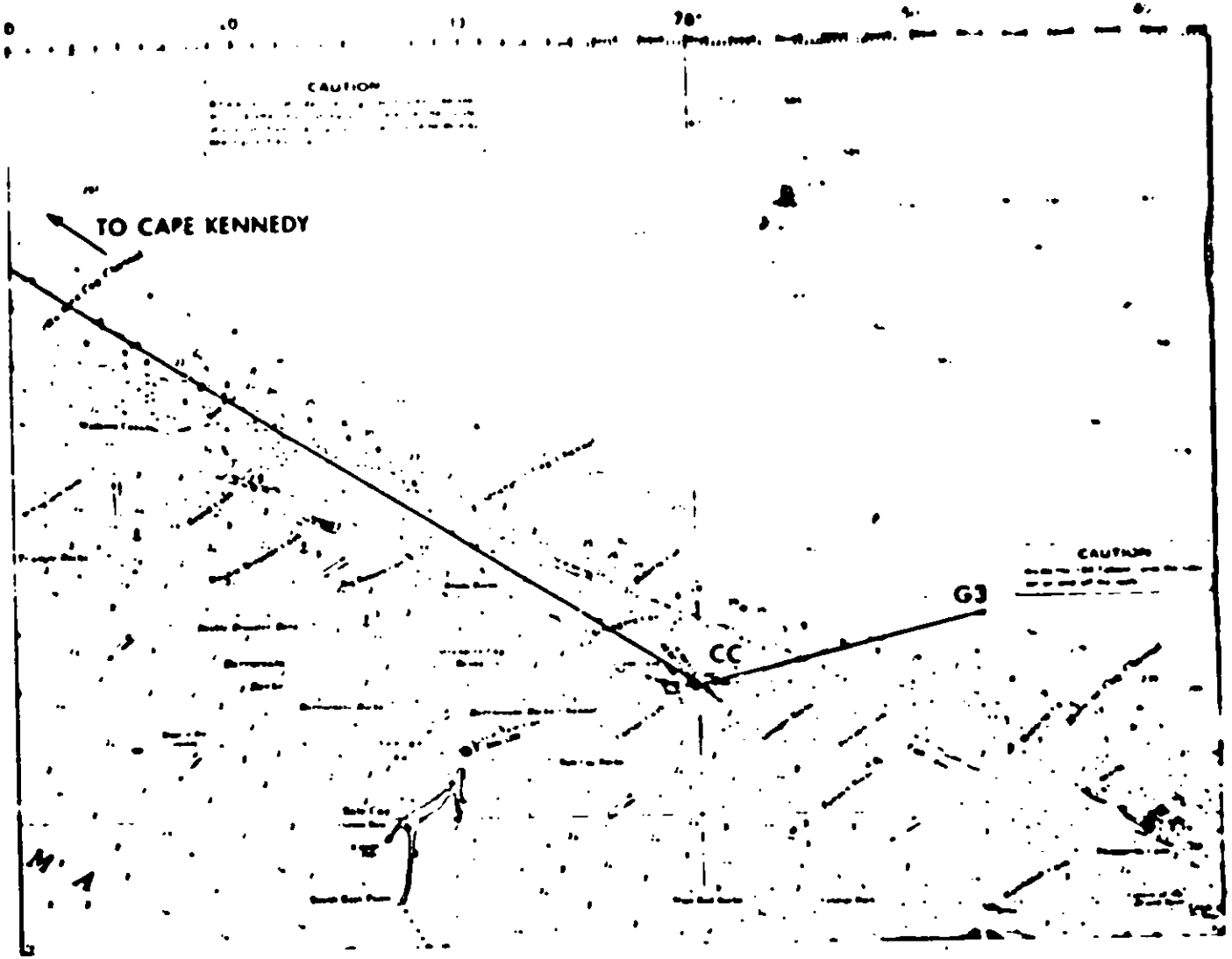

(U) (S) Figure 2. Map of CC-G3 Flight Path (U)

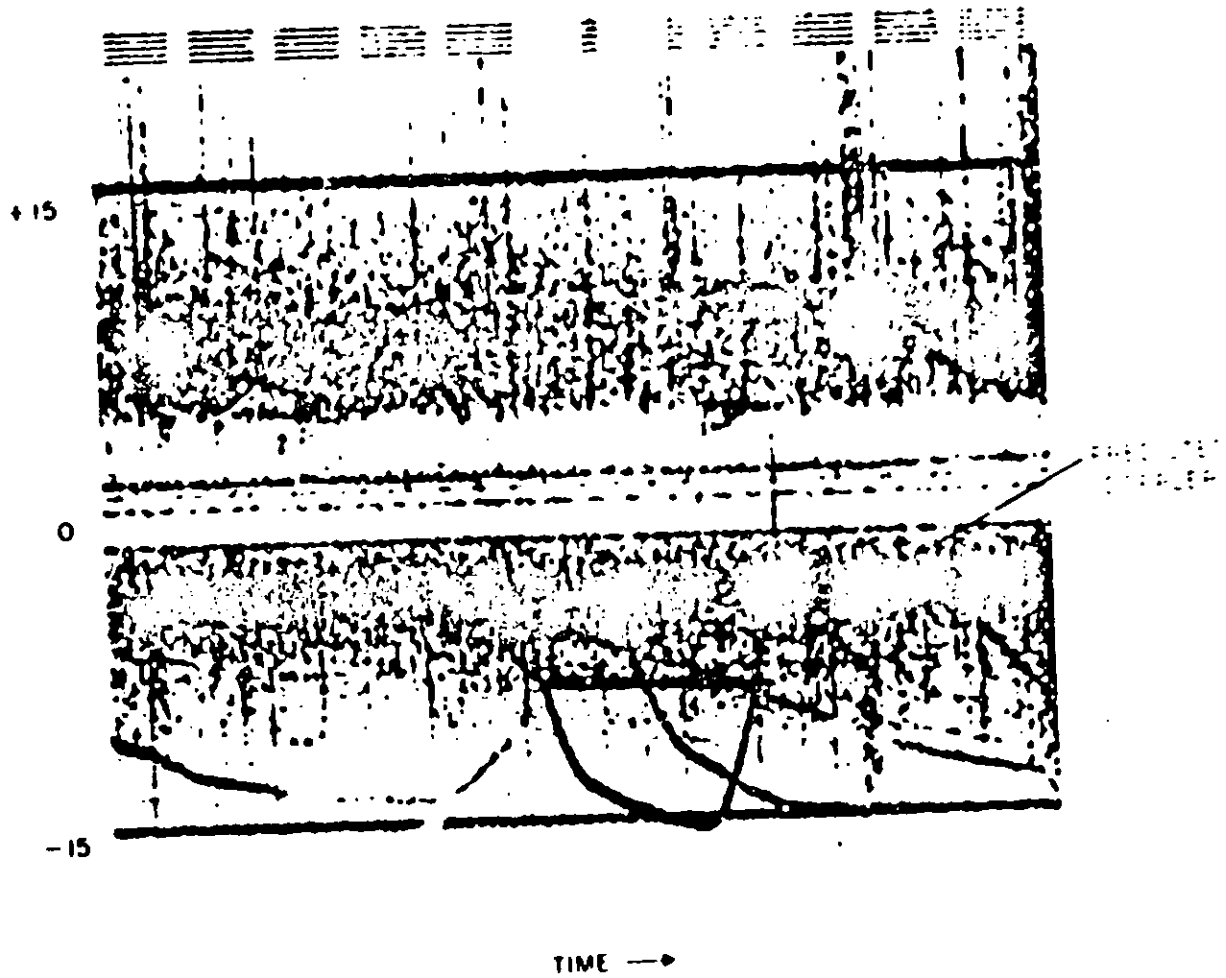

(U) Figure 3. Observed Facsimile Target Signal Path, [redacted] Altitude [redacted]

similar Doppler track has been calculated using a single hop F layer (300-km) return mode. It can be seen that the largest observed Doppler track is clearly due to the ground wave mode. However, a small track corresponding exactly to the sky wave return is also clearly visible.

(U) Figure 5 illustrates the simultaneous detection of a controlled aircraft on 10 MHz and 15 MHz. This detection was made when there were few other aircraft in the area and hence the absence of other doppler tracks. With the addition of a ranging capability similar results could be achieved for the previous illustration.

(U) Of further interest is the presence of sky wave on the 10 MHz track whereas 15 MHz shows no sky wave detection at all.

(U) The observed presence of both modes reaffirms the fact that a purely ground wave mode of detection is being realized.

IV OBSERVED AND PREDICTED TARGET SCATTERED RECEIVED POWER (U)

(U) Predicted target scattered received power was computed using the following parameters:

a. Path loss attenuation as given by Dr. D. Barnick for Sea State 0.

b. System parameters as shown in Figure 1.

c. A reference target cross-section of 200 square meters.

(U) Figure 6 shows the predicted and observed received power for the pass from CC-G3 at 6000 feet (the scale on the left has been referenced to the input of a calibrated receiver and hence does not reflect the actual received power at the antenna). It can be observed that there is an approximate 10 dB discrepancy between the predicted received power for a 200-m^2 target and the observed signal power for the P3V aircraft.

(U) Since it is expected that the cross-section of an aircraft changes with its aspect, it is instructive to eliminate this variable by plotting it against the observed difference in received power from a prediction using a constant cross-section (e.g. 200-m^2).

(U) This has been done in Figures 7 and 8. The abscissa shows the difference in the observed received power below that which would be predicted for a 200-m^2 target. The ordinate is the angle of illumination in degrees below an azimuthal plane parallel to the surface of the earth.

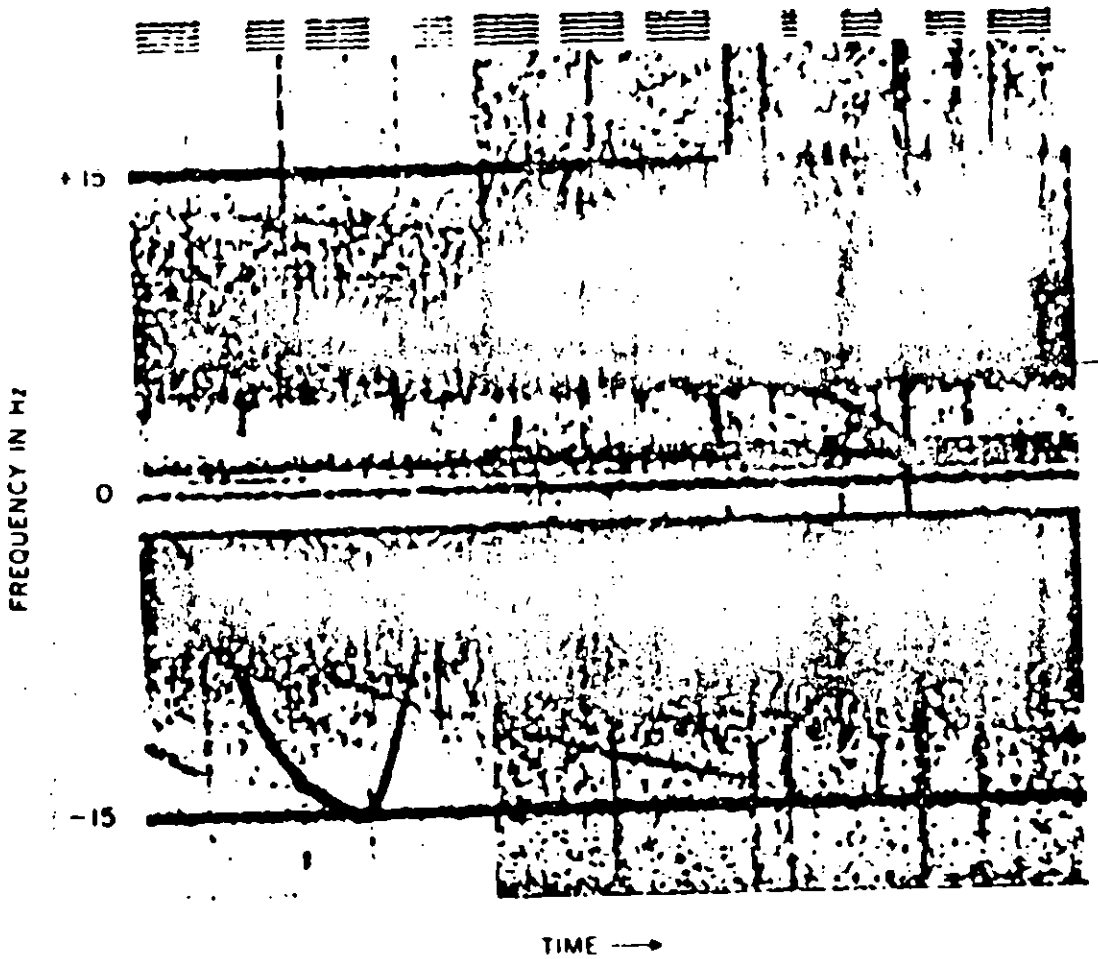

(U) Figure 4. Observed Facsimile Target Signal Path G14CC, Altitude 250 [illegible]

(U)

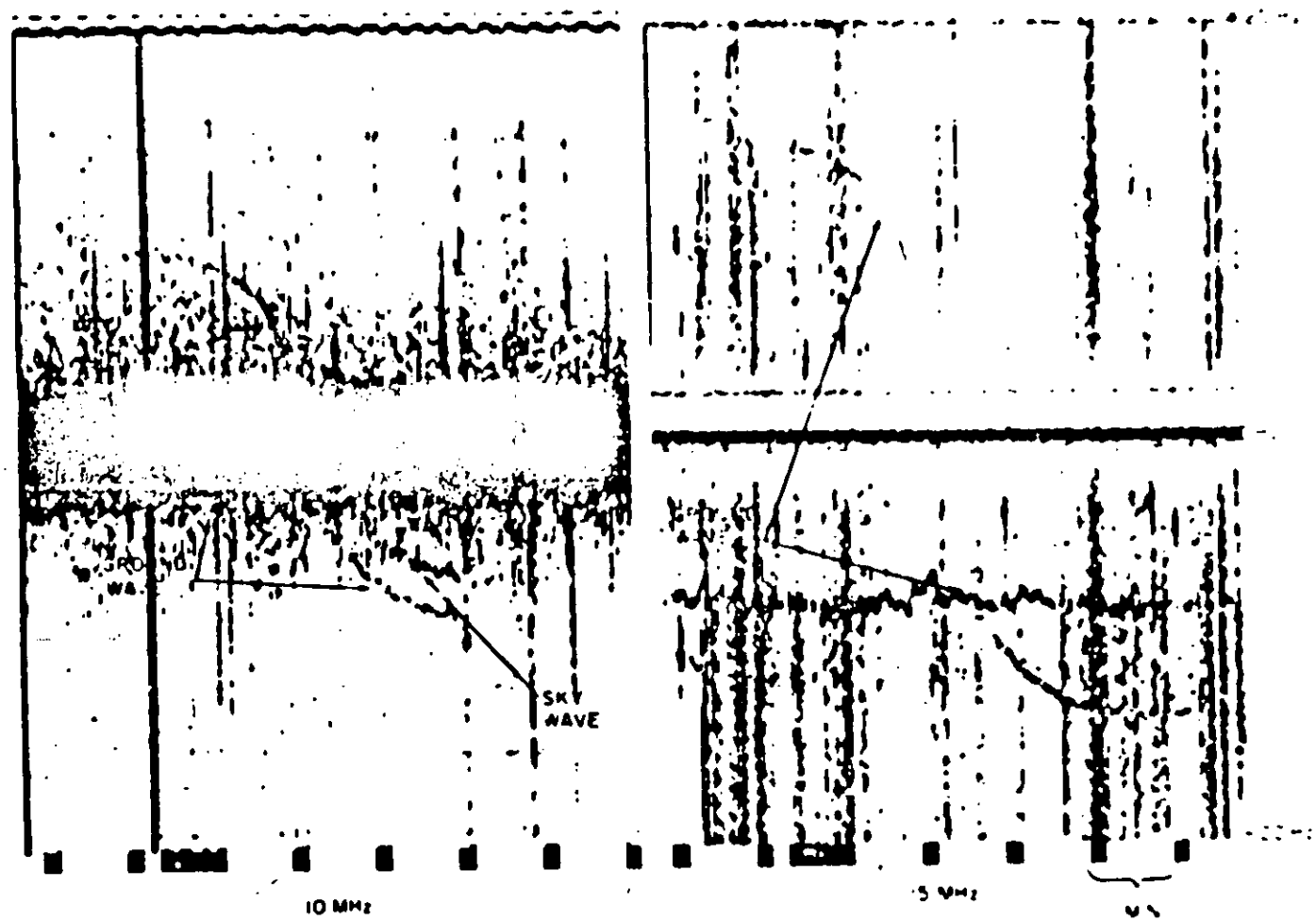

(U) Figure 5. Simultaneous Aircraft Detections at 10 MHz and 15 MHz (C)

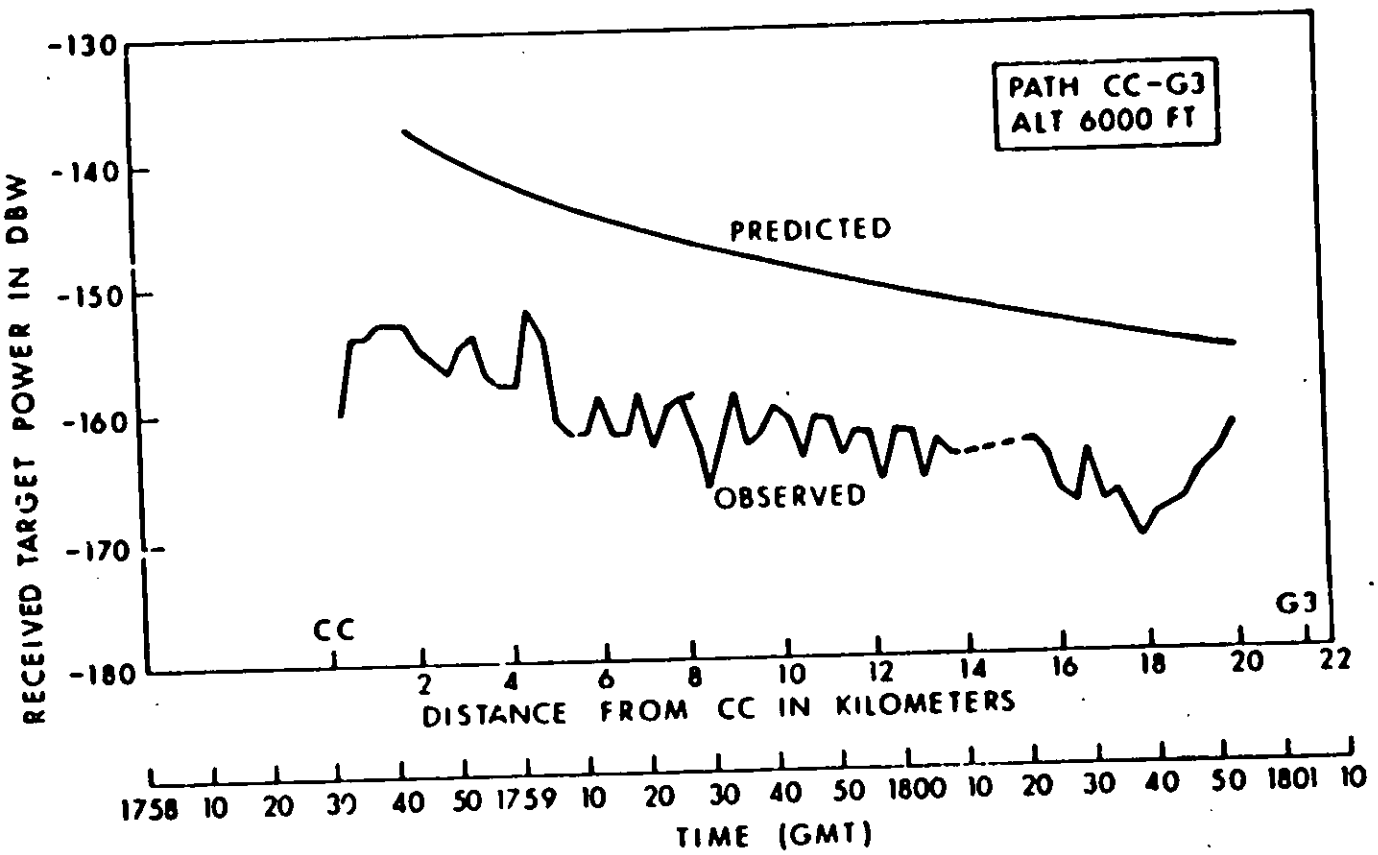

(U) Figure 6. Target Received Power Predicted vs Observed (U)

[redacted]

These plots can be looked at as correlograms. Assuming all other parameters to be constant, all observed points at a given angle should yield the same received power. As can be clearly seen, a least squares fit of all observed points would yield a line about which the deviation would be only about ±2 dB. This is well within experimental error.

Figure 9 shows the least square plot for each of Figures 7 and 8. The abscissa has been changed to reflect observed cross-section in square meters. Two additional points have been shown on this graph. They are monostatic cross-sections obtained from a laboratory model study by ITT-EPL. They are shown here to illustrate the compatibility of the two independent observations.

V CONCLUSIONS (U)

It has been shown the the BTI W-1 concept is phenomenologically feasible. The results of the flight tests indicate a strong correlation between observed and predicted values of received power and Doppler excursion. This implies then that a system design using the above techniques should yield results commensurate with predictions.

[redacted]

(U)

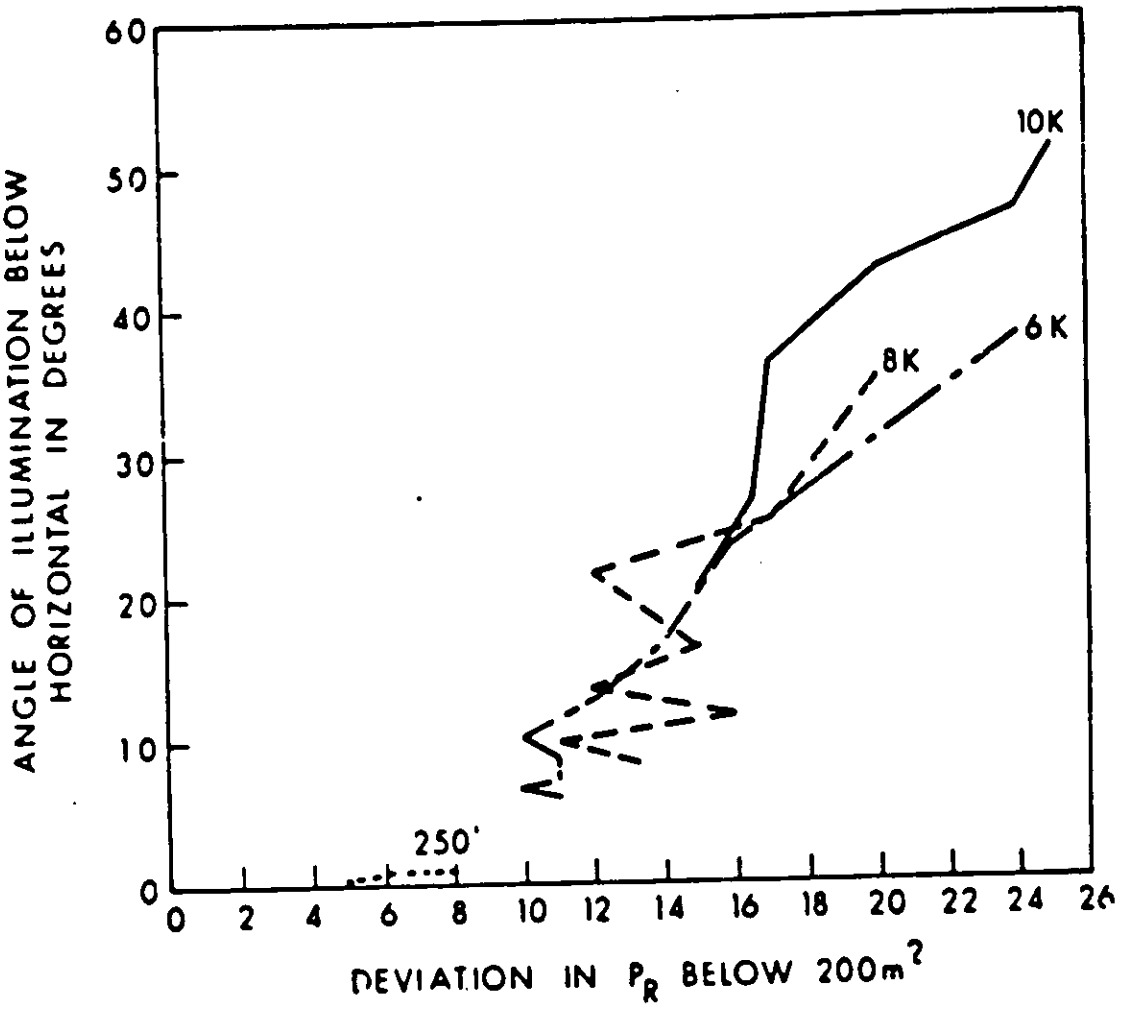

(U) Figure 8. G3-CC Data Summary Correlogram (U)

(U)

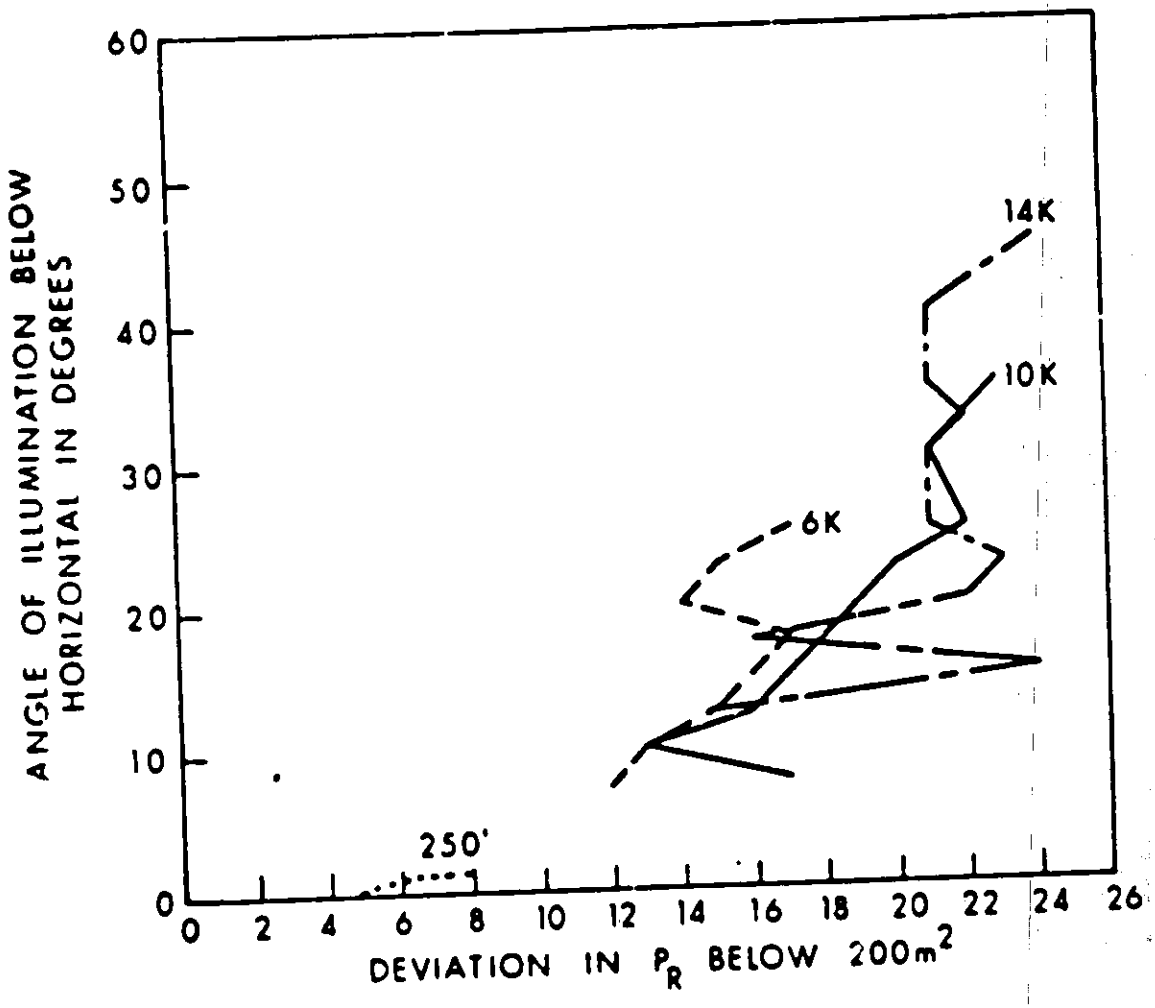

(U) Figure 7. CC-G3 Data Summary Correlogram (U)

[redacted]

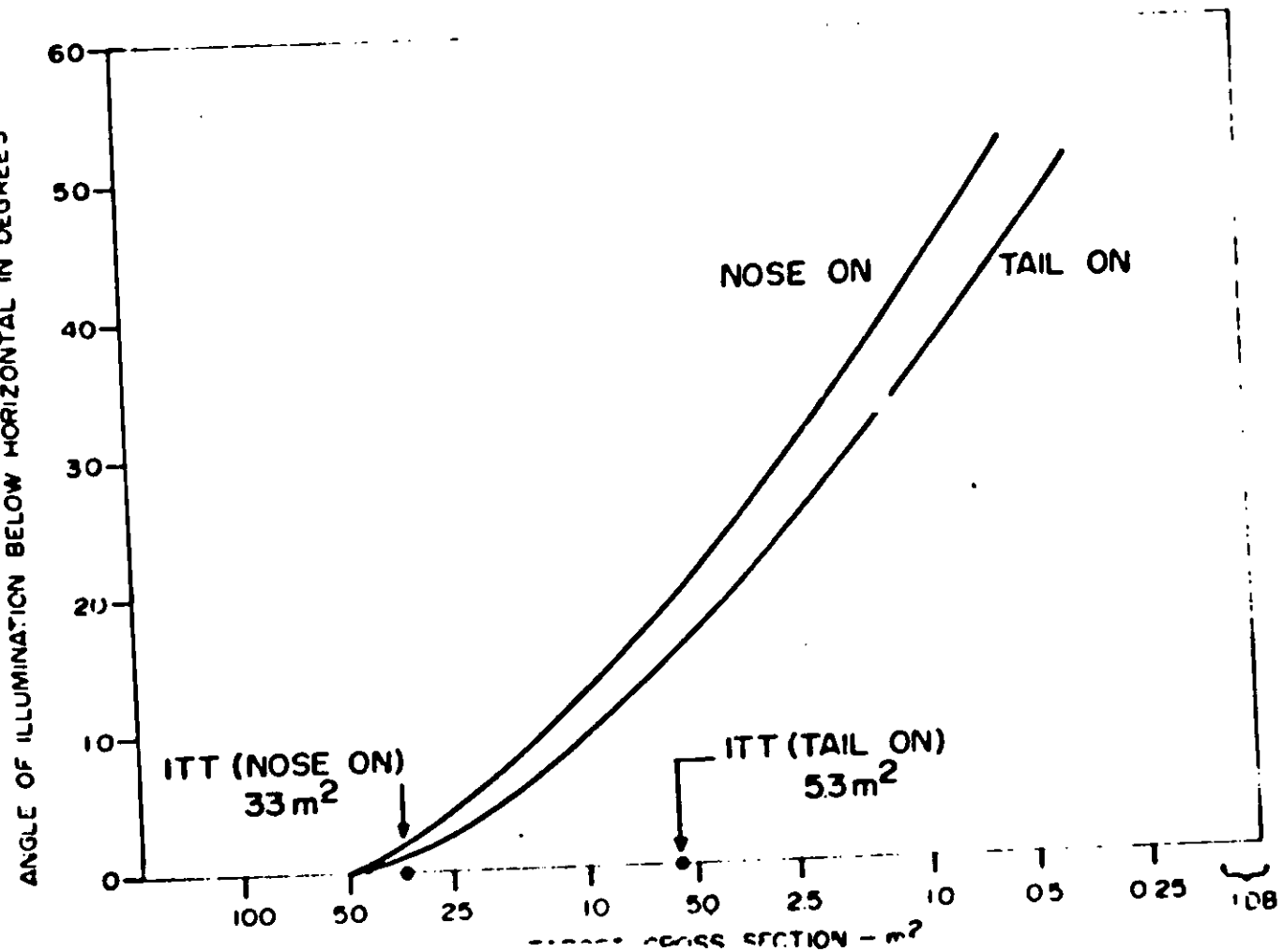

(U) (S) Figure 9. Smoothed Target Cross Section vs Angle of Illumination (U)

[redacted]

[redacted]

SLBM OBSERVATIONS (U)

Henry M. Baker

Raytheon Company
Equipment Division
OHD Advanced Development Department
Spencer Laboratory
Burlington, Massachusetts

(U) (S) In addition to the detection of aircraft, as discussed in other MAY BELL workshop papers, the BTEW system can be used for the detection of submarine-launched ballistic and cruise missiles (SLBM, SLCM). During the data take in Florida, the opportunity to collect data during one SLBM launch occured. This event, ETR Test 2989, was a Poseidon missile. It was launched from the USS Observation Island on 24 March 1970 at a range of 55 km from the receiver site. During this launch, two CW frequencies were being transmitted (5.152, 10.167 MHz) from Carter Cay, BWI. The frequencies were monitored at the Cape Kennedy receiving site using the vertically polarized quater-wave-length monopole antennas.

(U) (S) The facsimile display of the spectral content of the 5.152 MHz signal is shown in Figure 1. There are three distinct portions of the missile-induced signature. These are the hard echo (T+40 to T+100 sec), wide-band noise-like burst (110-170 sec) and an ionospheric echo effect (180-480 sec). The hard echo is the skin track of the missile; the wide-band noise-like burst is a staging echo; and the ionospheric perturbation is standard.

(U) (S) The ±15 Hz sidebands observed in the data were present during many days of the data recording. They occured on each frequency being observed and at first were thought to be associated with the ITT passive modulator buoys. ITT personnel indicated, however, that their equipment was not producing the side-bands at these frequencies. A complete test was made on the Raytheon equipment and the results indicated the sidebands were not produced in the receiving equipment. Therefore, the source of these sidebands remains an unknown.

(U) (S) A predicted Doppler frequency shift for this test was obtained using the missile post flight data. As can be seen in Figure 2, the observed skin track did agree closely with these predictions.

(U) (S) Figure 3 shows that the same type of data was observed on the 10.167 MHz frequency. Again three portions of the signature are present, with a more pronounced hard echo. The predicted doppler

[redacted]

[redacted]

(U)

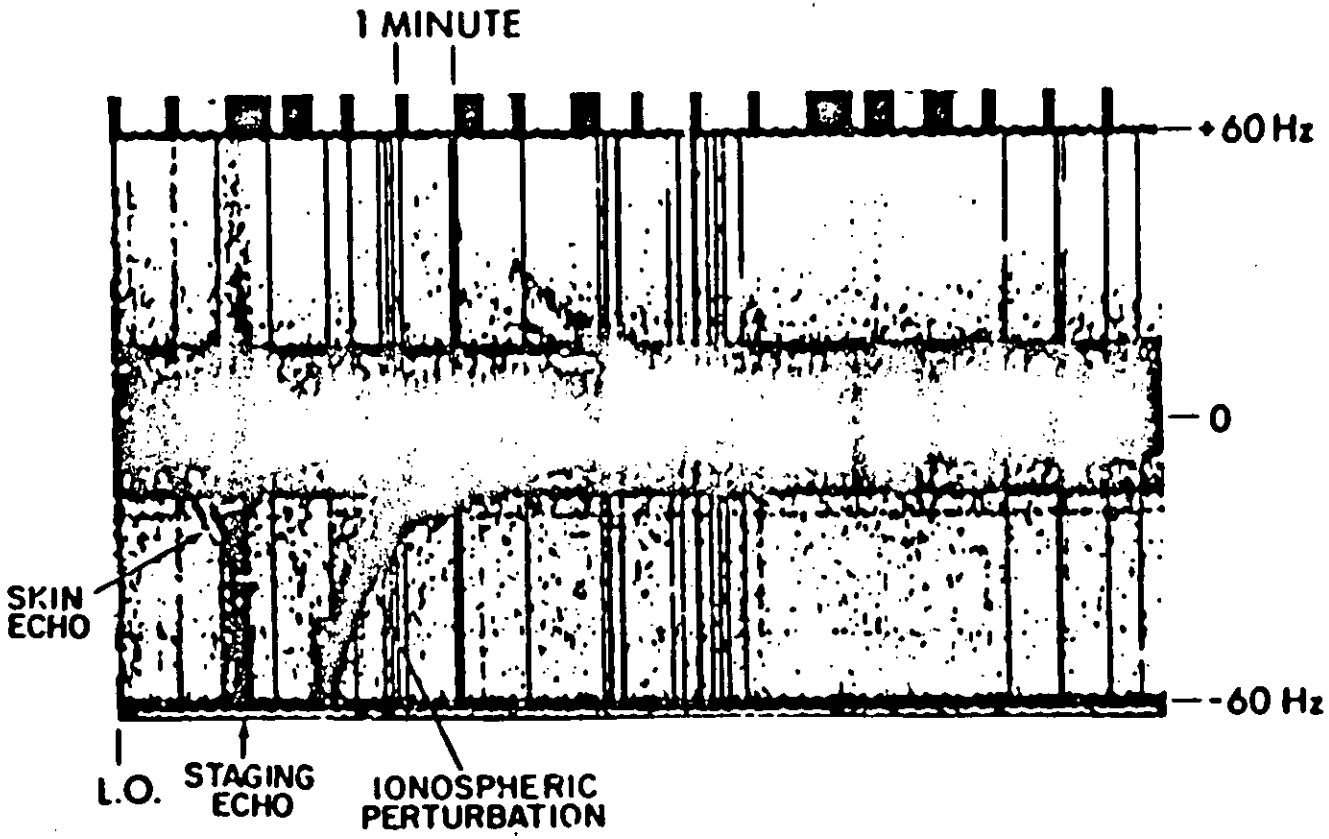

(U) Figure 1. Spectral Data Observed on 5.152 MHz (U)

(U) (S)

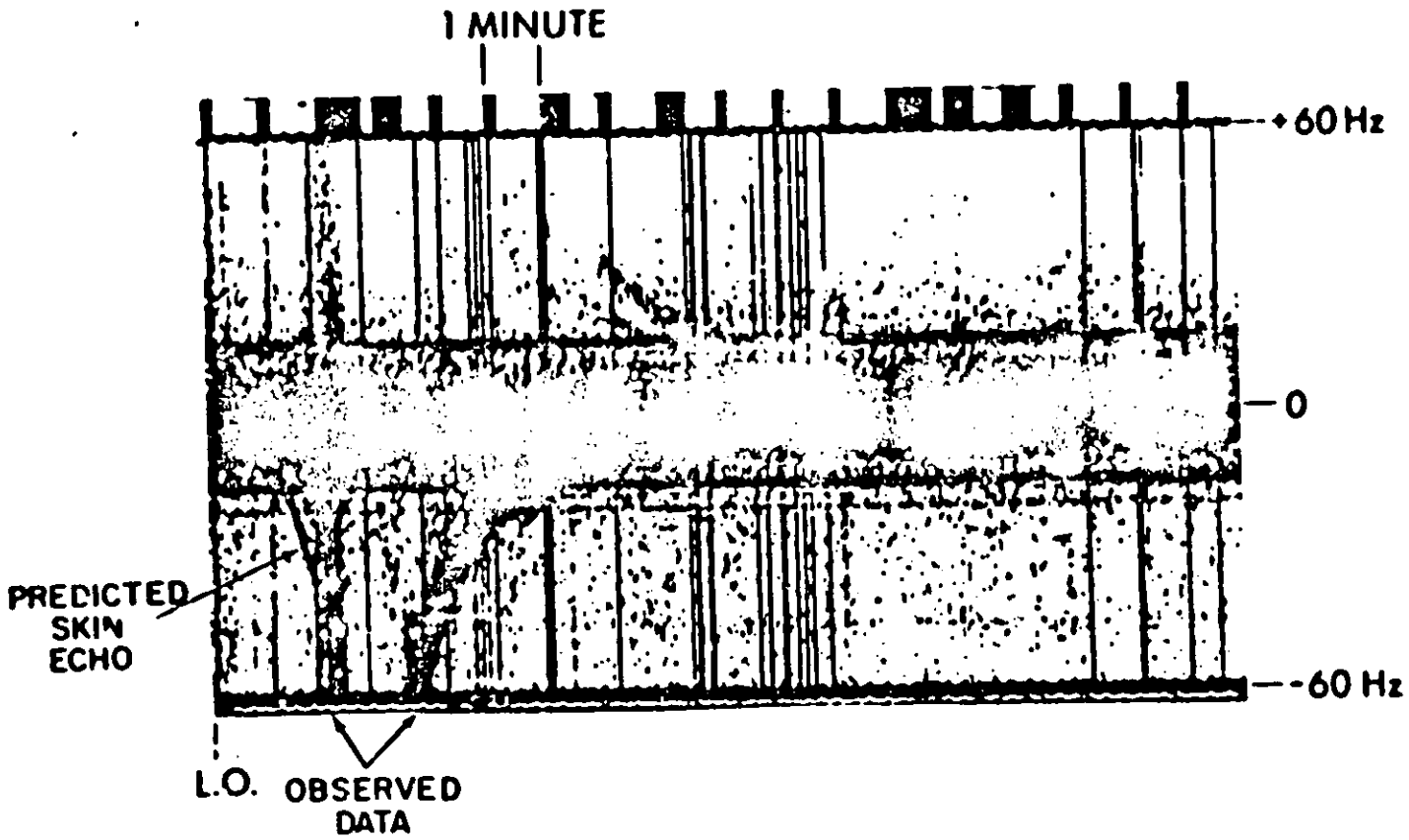

(U) (S) Figure 2. Spectral Data Predicted on 5.152 MHz (U)

(U) (S)

shift again shows good correlation with the received hard echo, Figure 4. Notice that the received carrier masks the initial 40 seconds of the predicted signature.

(U) (S) The geometry associated with the event is shown in Figure 5. The tick marks on the trajectory show the altitude of the vehicle and the time of flight. Note the region 40 to 100 seconds where the hard echo was observable. At the signature onset (T + 40 seconds) the missile had travelled a horizontal distance of only 5.5 km. By the time of signature drop-out at 100 seconds, a total range of 87 km had been traversed.

(U) (S) The altitude and velocity plots versus time for the vehicle are shown in Figure 6. Tick marks on these curves indicate the onset and the portion of the hard echo seen in the data.

(U) (S) The lower plot of Figure 7 shows the comparison of a computed and the observed signature received power on the two frequencies. The computed received power is based on a $1m^2$ target cross-section and was normalized to the existing system parameters. The 5 MHz computed and the actual power received curves agree closely. This indicates that the observed cross-section on the 5-MHz frequency was on the order of $1m^2$. The upper plot of Figure 7 shows the measured cross section on the 10-MHz frequency versus time. At signature onset, the cross-section was $57m^2$ and as the missile's altitude increased the cross section decreased. It is assumed that this decrease in cross-section is due to the mismatch between the polarization of the vertical transmitting and receiving antennas and the missile orientation which becomes more horizontal as the vehicle moves downrange. This polarization mismatch was also observed by SRI and has been reported.[1]

CONCLUSIONS (U)

(U) (S) A BTEW system is capable of detecting SLBM missiles at a very low altitude.

(U) (S) Because the carrier masks the very low doppler frequencies, the altitude of earliest detection is dependent on the geometry involved. A means of reducing the carrier spread without a loss of system sensitivity or a means of cancelling the carrier would allow a Doppler signature of less than ± 2 Hz to be observed and permit the missile to be detected at a lower altitude.

(U) (S) The three observable portions of the missile related signature are created by independent effects; therefore, the probability of at least one of the three portions of the signature being detected is very high and if more than one portion of the signature is observed a missile launch warning can be issued with a very high confidence.

[redacted]

(U) (S) With a deployed multi-station BTEW system where the hard echo is observed on three or more independent paths, missile trajectory information can be derived in real-time from analysis of the Doppler records for the observing paths.

REFERENCE

1. [redacted]

[redacted]

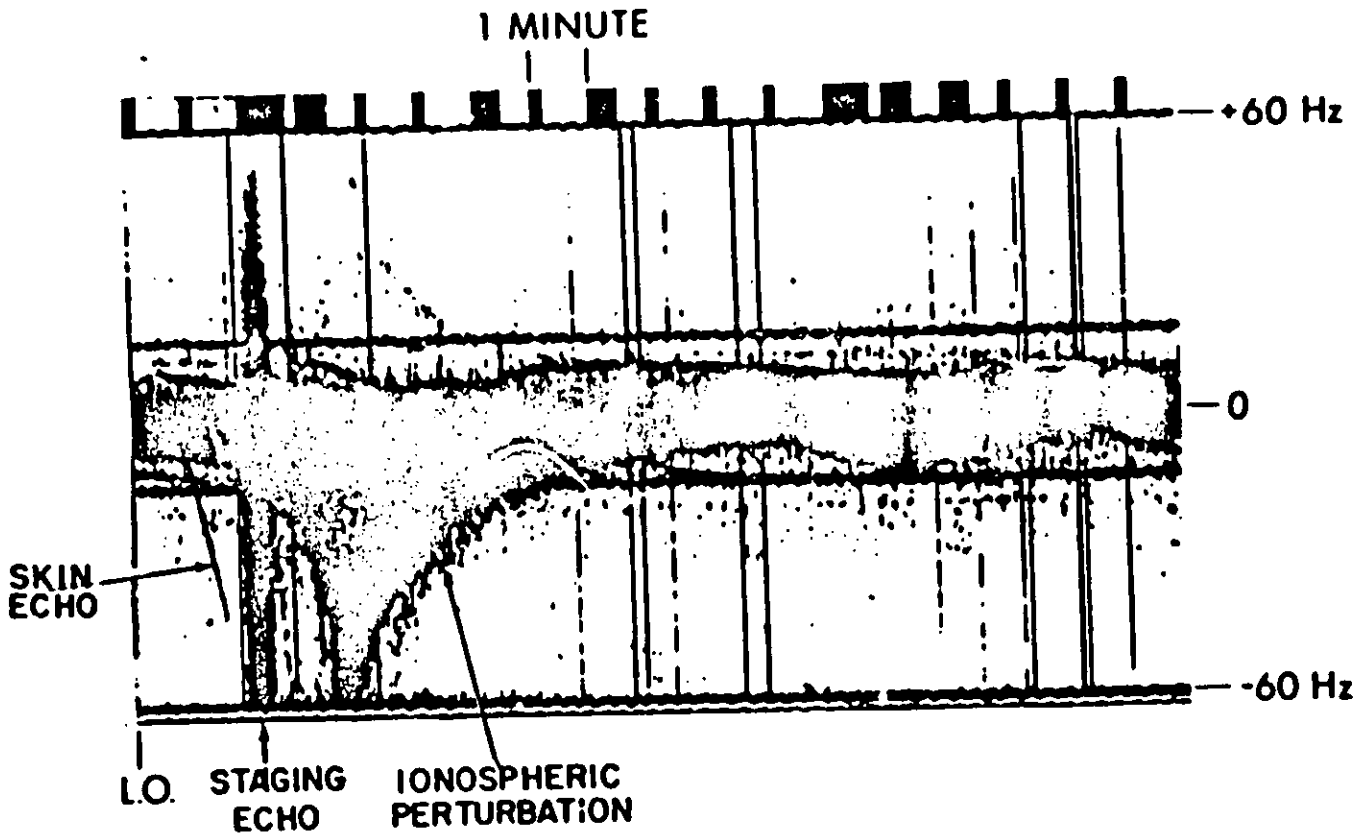

(U) (S) Figure 3. Spectral Data Observed at 10.167 MHz (U)

(U) SR

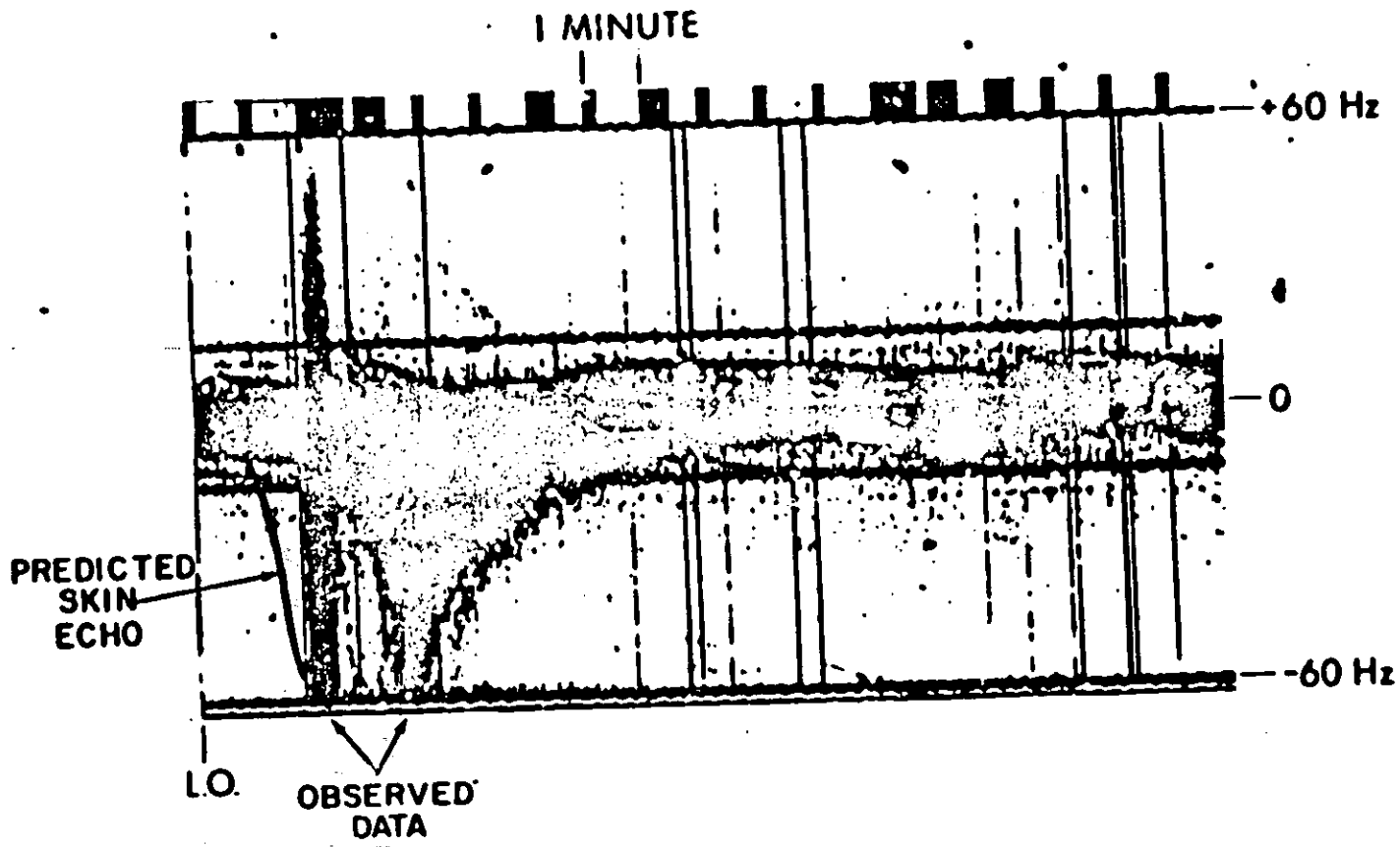

(U) (S) Figure 4. Spectral Data Predicted on 10.167 MHz (U)

(U) (S)

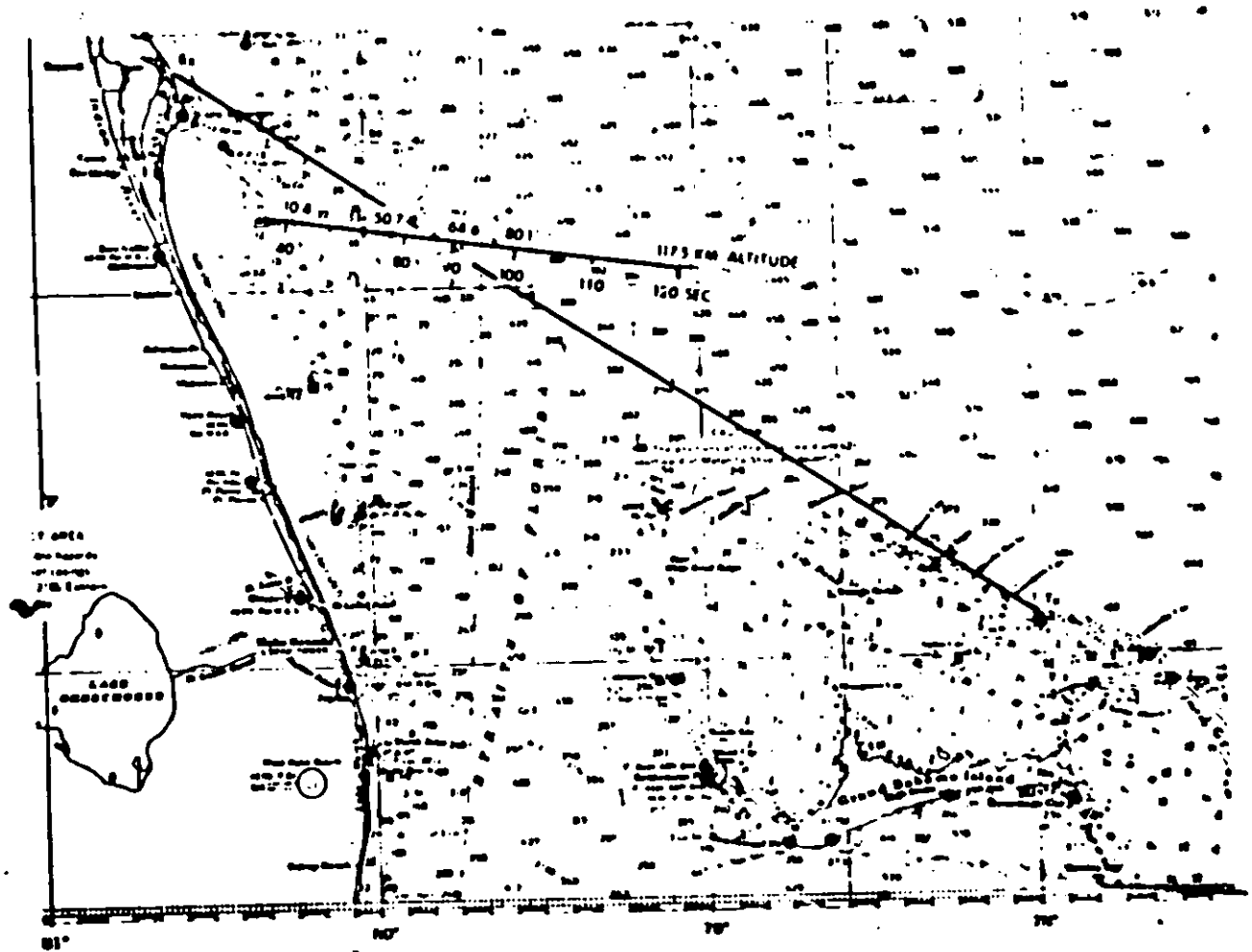

(U) (S) Figure 5. Geometry of ETR Test 2989 (U)

(U)
151

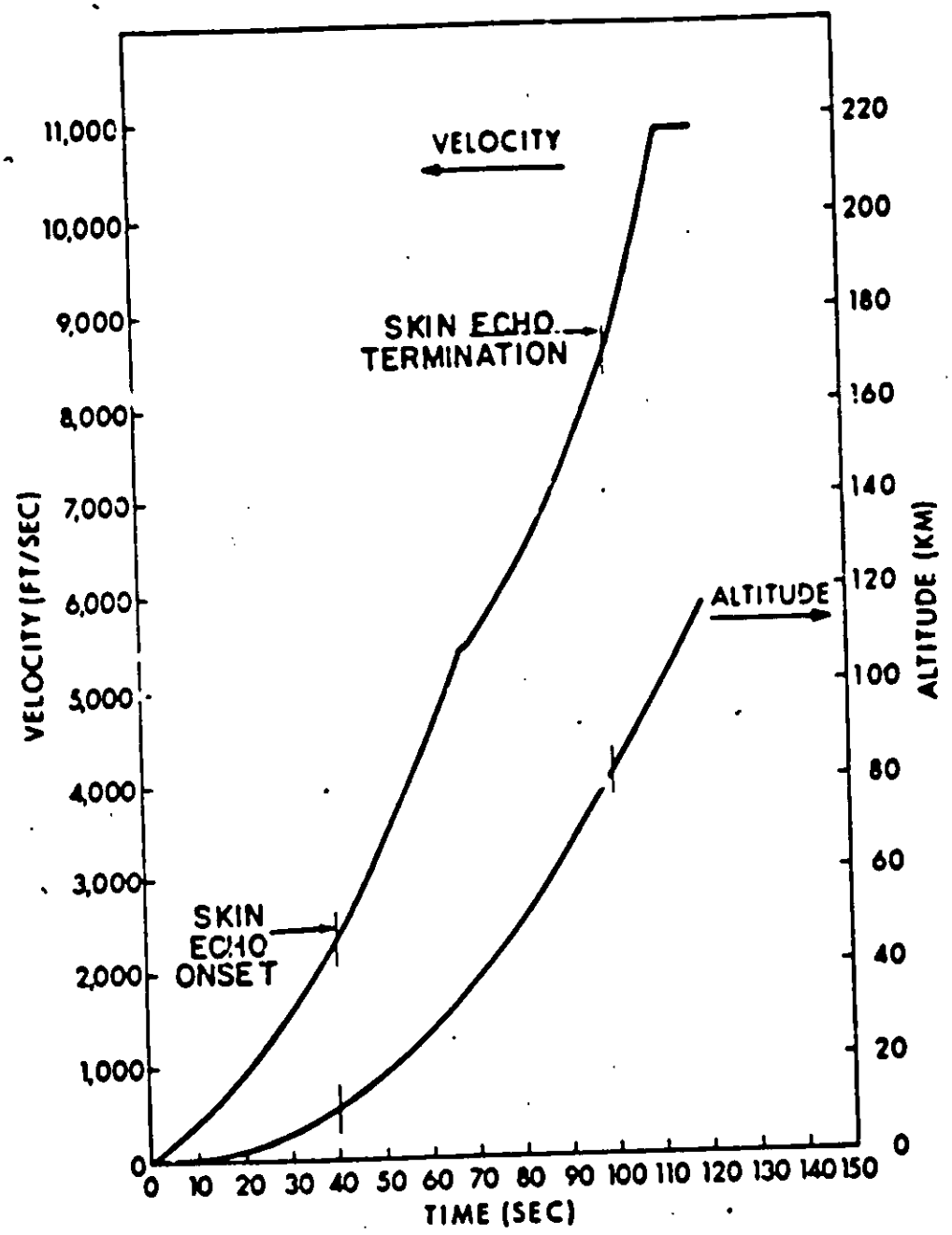

(U) (S) Figure 6. Missile Altitude and Velocity vs Time (U)

UNCLASSIFIED

[redacted]

(U)

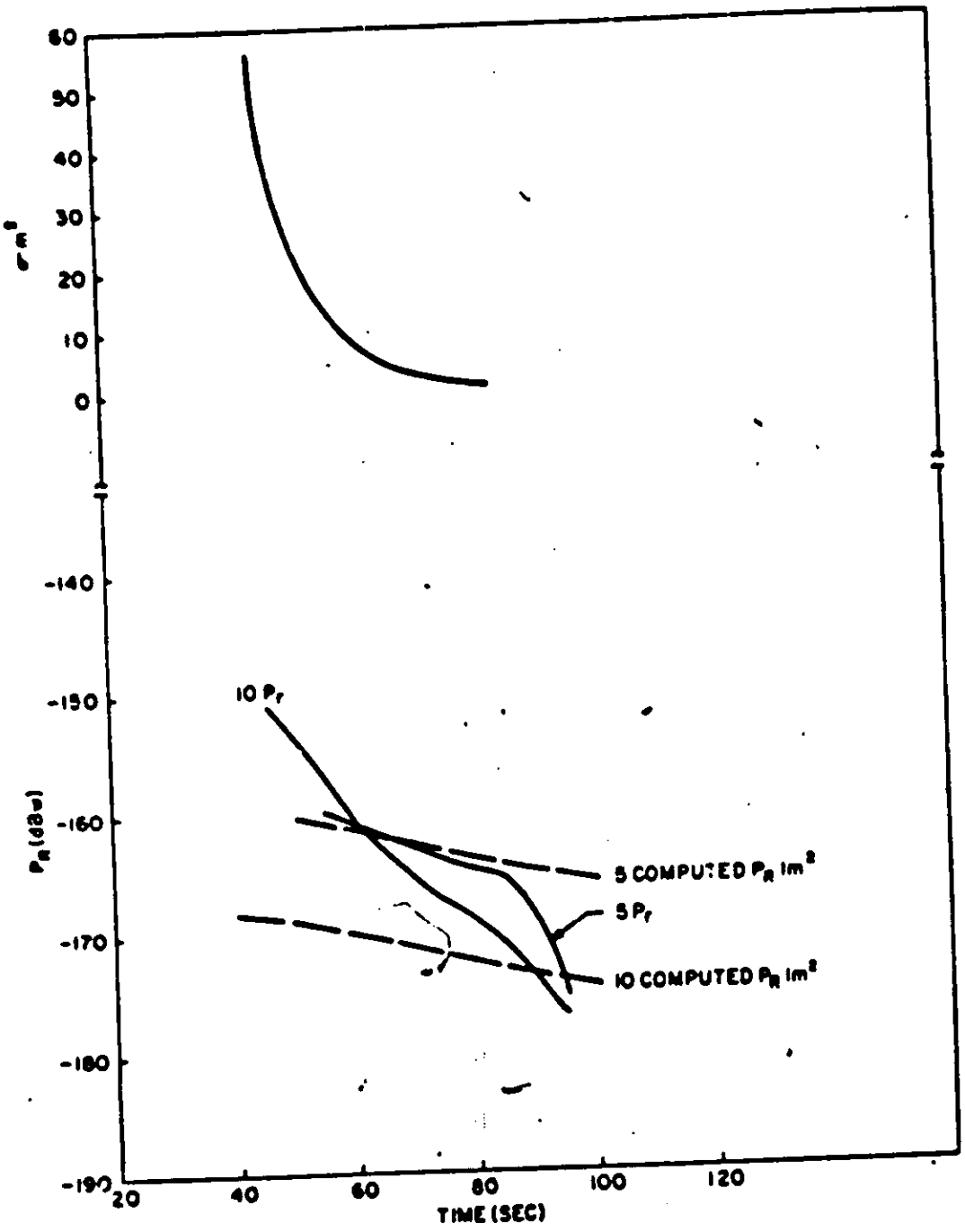

(U) (S) Figure 7. Cross-section (U)

[redacted]

UNCLASSIFIED

[redacted]

PROJECT AQUARIUS (BTLW-2) (U)

K. D. Snow

Sylvania Electronic Systems - West
Mountain View, California 94040

I INTRODUCTION (U)

(U) UST Project Aquarius is a part of the ARPA-sponsored ocean surveillance program under Project MAY BELL. The primary goals of the project as shown in Figure 1 are to experimentally demonstrate the feasibility of detecting submarine launched ballistic missiles and low flying aircraft, and to compare the experimentally observed detection ranges. The results of the experimental work completed to date indicate that target aircraft can be detected at the theoretically predicted range and that the concept is feasible providing there is sufficient radiated power from the transmitter.

II EXPERIMENTAL NETWORK (U)

(U) UST The experimental setup consists of using a bistatic HF continuous wave radar consisting of a low power ocean-based bouy transmitter and high sensitivity receivers located on the coast. A detection is made by observing the doppler-shifted signal that is scattered from a moving target such as an airplane or an SLBM. The target is illuminated by line-of-sight or groundwave energy from a transmitter. The scattered doppler-shifted return is received by ionospheric skywave as illustrated in Figure 2.

(U) UST The experimental system geometry is shown in Figure 3 with the bouy transmitter located approximately 120 kilometers off the Cape Kennedy coast. A high power set of transmitters is located at Carter Cay in the Bahaman Islands and the high sensitivity receiving system at Vint Hill Farms Station in Virginia.

[redacted]

PROJECT AQUARIUS

GOALS

- PARTICIPATE IN MAYBELL PROGRAM -- BTEW-2
- DETERMINE BTEW-2 FEASIBILITY
- DETECT LOW FLYING AIRCRAFT USING BOUY-GROUND WAVE-SKYWAVE CONCEPT
- DESIGN A DETAILED BTEW-2 EXPERIMENT

RESULTS

- DETECTED TEST AIRCRAFT AT PREDICTED RANGE
- BTEW-2 FEASIBLE WITH SUFFICIENT TRANSMITTER POWER OR ANTENNA GAIN

Figure 1. Project Aquarius Goals and Results (U)

(U) (S)

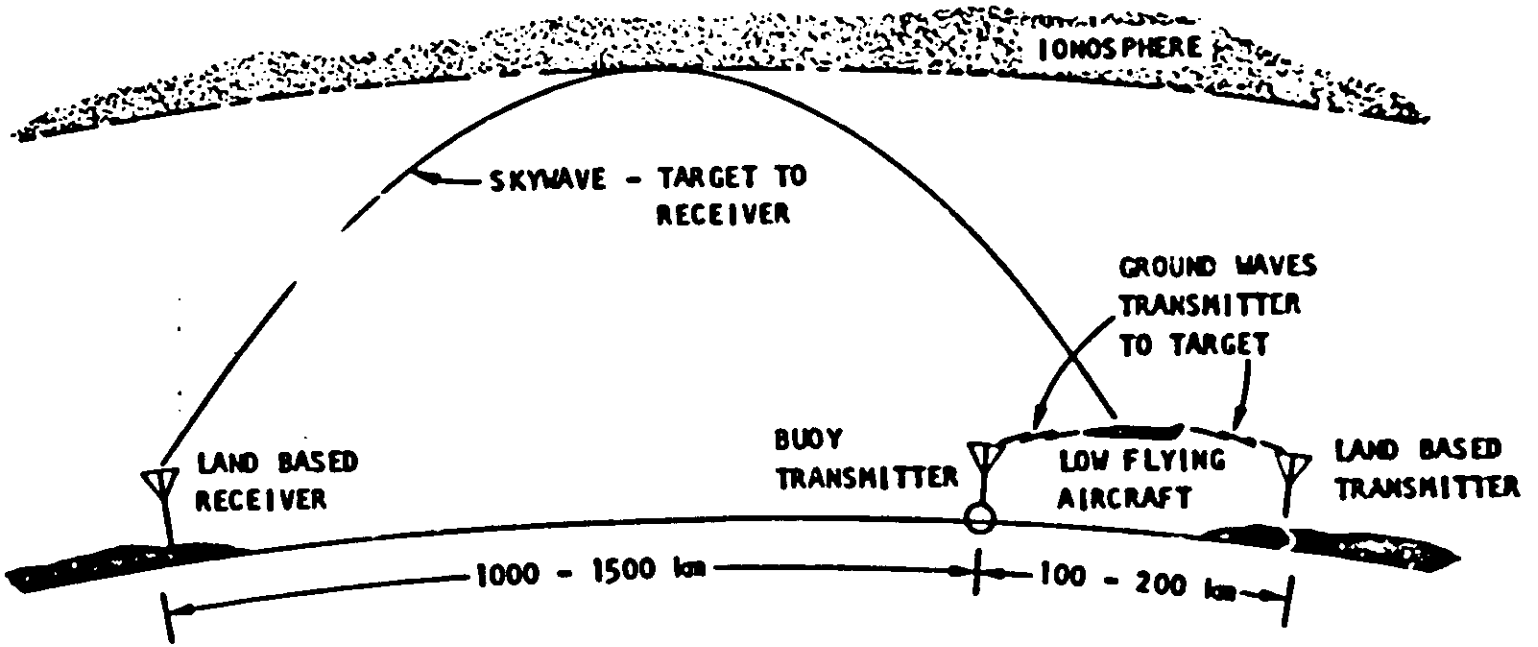

(U) (S) Figure 2. Project Aquarius, Basic System Concept (U)

(U)

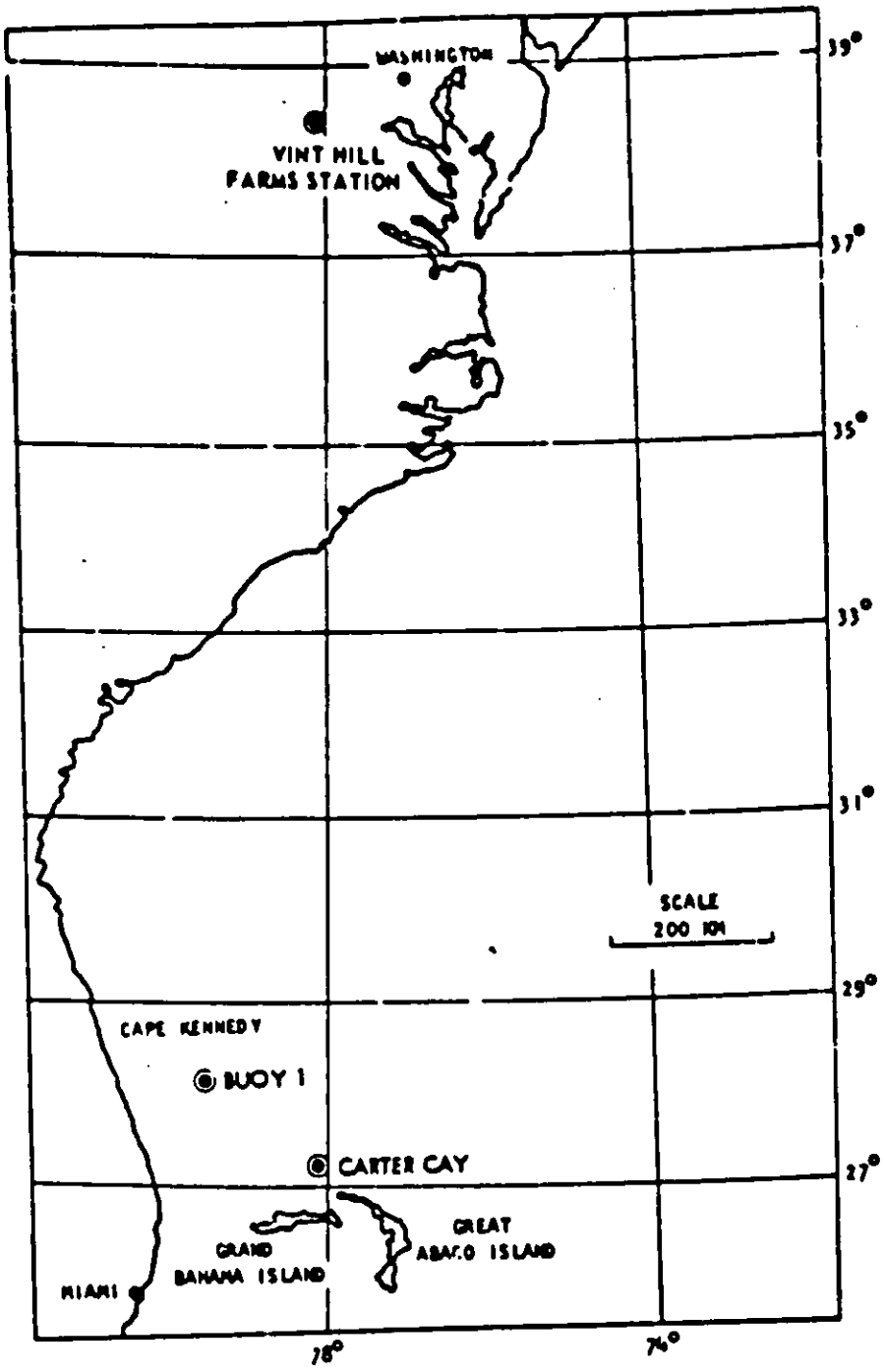

(U) Figure 3. Network Geometry (U)

[redacted]

UNCLASS

III RECEIVING SITE (U)

(U) The block diagrams of the two receiving systems are shown in Figures 4 and 5. Figure 5 shows a 12-channel receiving system, including a DF set connected to an LUAA steerable antenna. The twelve analog receiving channels use R-390A receivers and drive a real-time analog spectral display and a twelve-channel analog tape recorder. The other receiving system is a van-mounted high dynamic range digital processing system containing synthesizer controlled receivers, digital spectrum analysis and both an analog and digital PCM recording capability.

IV AIRCRAFT TESTS (U)

(U) (S) Figure 6 lists the operations of aircraft flights and hearability tests through 10 February 1970. On 27 January during the controlled tests, the P3B controlled aircraft was detected at two different times on two different frequencies. The flight path and the detection regions for this 27 January flight are shown in Figure 7. The data collected in real-time is shown in Figure 8. The data at the top of the figure shows the detected doppler signature lasting for a period of approximately 30 seconds for the 10.167 MHz frequency. The detection is at a range of approximately 9 kilometers from Carter Cay and exists during the time when the plane banks following a turn over checkpoint C5. The lower half of the figure shows the second detection on the 15.595 MHz frequency, again lasting for approximately 16 kilometers from Carter Cay. The same characteristic signature exists and is also present at the time when the plane is banking during a turn over checkpoint D4. Both of these signatures seem to be at times when there is specular reflection from the transmitter at Carter Cay to the receiver at Vint Hill Farms Station. Figure 9 is an expanded view of the flight path and includes the detection regions for these two detections. By assuming turns are completed by first flying over the checkpoint and then making a maximum turn rate for the next checkpoint, the doppler shifts predicted from this type of flight plan match very closely to the actual observed data as shown in Figure 8.

V SUMMARY (U)

(U) (S) To summarize, the goals of the project have essentially been met; that of demonstrating the feasibility of the bouy tactical early warning system. However, to make this system useful for detections at any range beyond a few kilometers, the effective radiated power from the transmitter will have to exceed the 2000 watts used for the Carter Cay detections of the controlled aircraft flights.

[redacted]

UNCLASSIFIED

(U)

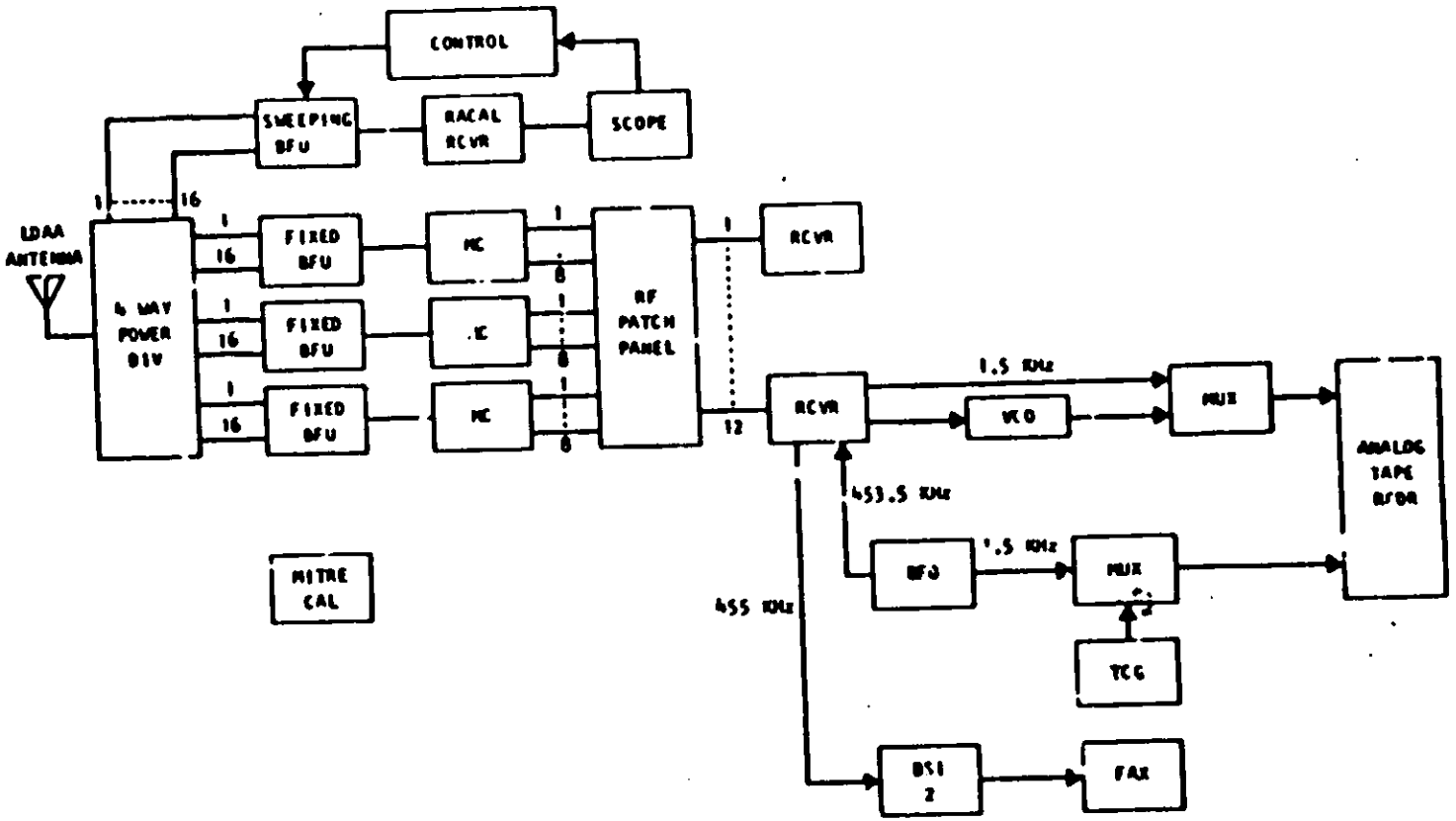

(U) Figure 4. Analog System Block Diagram (U)

(U)

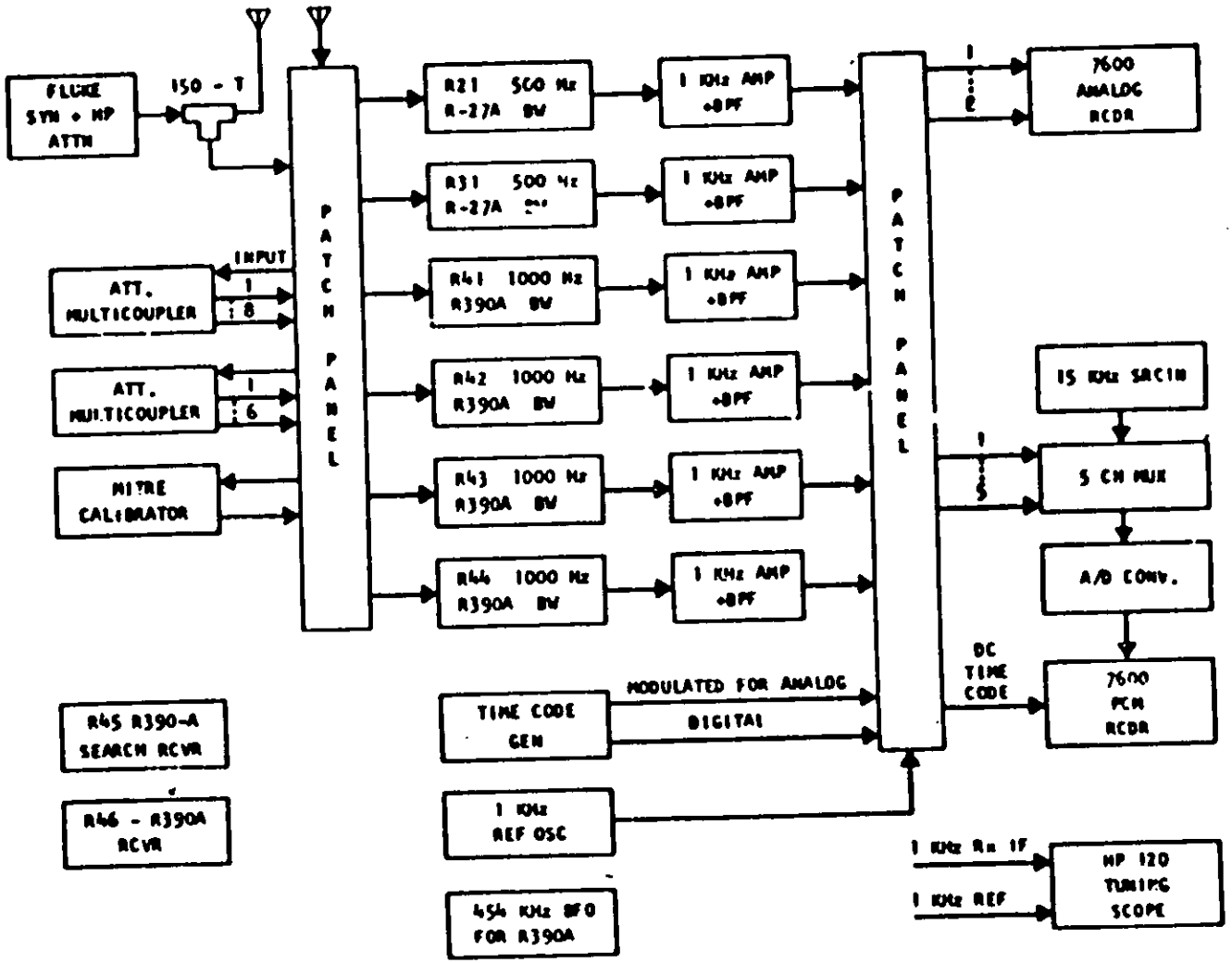

(U) Figure 5. System Block Diagram (U)

UNCLASSIFIED

DATE	TYPE	FREQUENCIES (MHz)	MEASUREMENT OR DETECTION TIMES (GMT)
18 DEC 69	AC	5.8	1750-1755 2000-2005
	AC	9.259	ND
	AC	10.167	ND
27 JAN 70	AC	15.595	1656
27 JAN 70	AC	10.167	1712
5 FEB 70	HB	20.250	1500
	HB	10.167	1500
	HB	10.167	2100
	HB	20.250	2100
10 FEB 70	HB	9.259	1430
	HB	5.8	1430

AC - AIRCRAFT ND - NOT DETECTED HB - HEARABILITY

(U) Figure 6. Summary of Operations (U)

UNCLASSIFIED

(U)

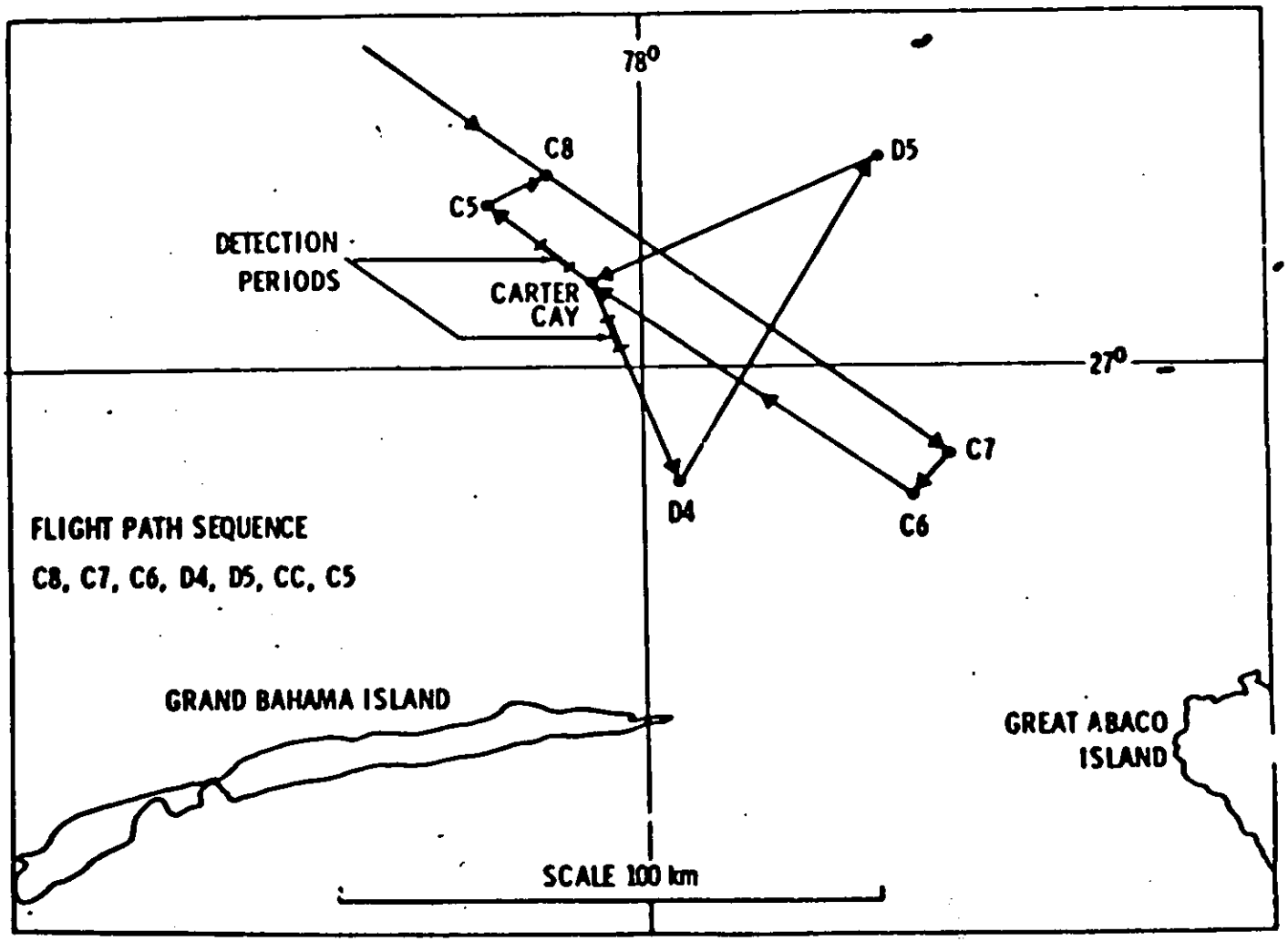

(U) Figure 7. Controlled Aircraft Flight, 27 January 1970 (U)

(U)

1715 - 1715 zulu 27 JANUARY 1970
CARTER CAY - VINT HILL FARMS STATION
10.167 MHz

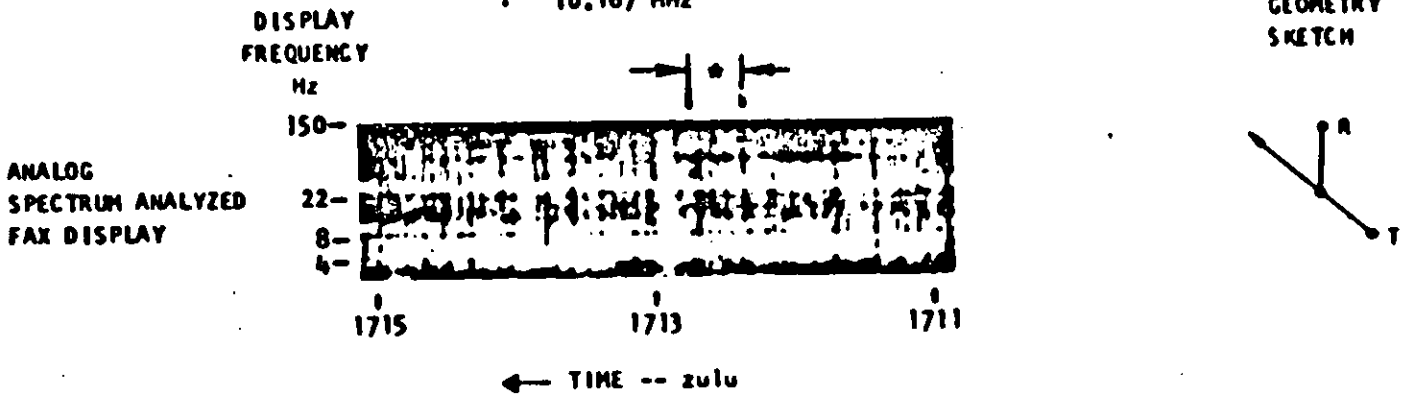

1652 - 1659 zulu 27 JANUARY 1970
CARTER CAY - VINT HILL FARMS STATION
15.595 MHz

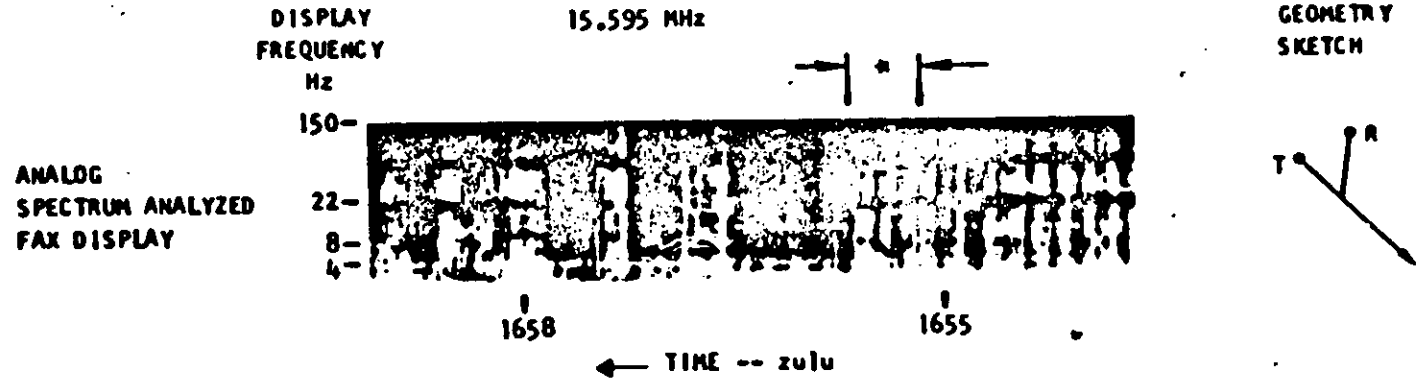

*DOPPLER SIGNATURE REGION

(U) (S) Figure 8. Aircraft Detections (U)

UNCLASSIFIED

(U)
(S)

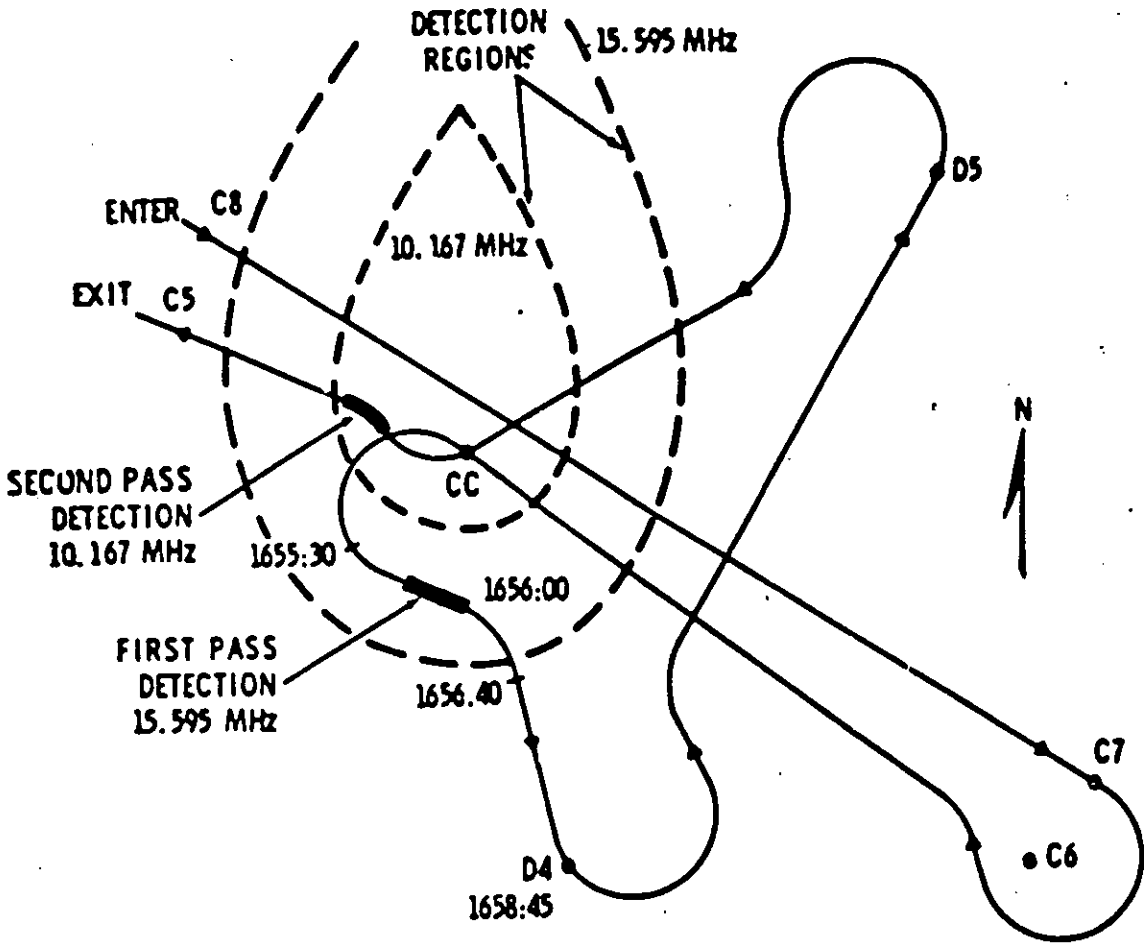

FREQ •	10.167 MHz	15.595 MHz
σ •	100 m^2	100 M^2
NOISE •	-137 dbw	-145 dbw
GAIN •	17 db	25 db
POWER •	2 kw	2 kw

(U)
(S) Figure 9. Predicted and Observed Detection Regions (S)

UNCLASSIFIED

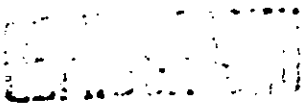

UNCLASSIFIED

APR 27 1993

Pages 186 thru 197 missing

(U) In calculating the received signals, the basic transmission loss is used to describe propagation. This quantity was discussed in a paper titled "Theory of Attenuation and Clutter (U)" presented by this author at another session of this workshop. Curves of loss across the sea were presented in that report. For this problem, Sea State 2 is assumed in entering the loss curves.

(U) As applied to the aircraft, the radar range equation can be rewritten in terms of L_1 and L_R, the basic transmission losses from transmitter-to-target and target-to-receiver, as follows:

$$L_o = -10 \log_{10} \frac{P_R}{P_1} = L_1 + L_R - G_1 - G_R - 10 \log_{10} \left(\frac{4\pi\sigma}{\lambda^2} \right)$$

where

P_R = Received power
P_1 = Transmitted power
L_o = Overall transmission loss
G_1 and G_R = The free-space antenna gains
σ = The radar cross section of the aircraft. The latter is taken to be 40 m^2 throughout the problem.

(U) The above equation is expressed in decibels. Figure 1 shows a possible radar-target geometry in which the aircraft is approaching on a course 20° from the baseline. Its range from the receiver is 370 km. The receiving antenna beam is pointed directly at the aircraft. For this single configuration, the overall loss L_o is 201 dB. Actually, L_o is computed versus range for the aircraft approaching on two courses, 20° from the baseline and on the baseline. The receiving antenna is pointed at the target in both cases.

(U) To compute the received clutter signal, the same procedure is applied to a target which in this case is a patch of sea of area $R_R \Delta R_R \Delta\theta$, as shown in Figure 2. Here, the sea has an average bistatic scattering cross section per unit area, σ^o, of -30 dB; this number is somewhat lower than its fully developed value of -23 dB, so as not to be overly pessimistic. A numerical integration must be performed, summing the powers received from all patches. Figure 2 shows how the overall transmission loss is computed for a particular patch, the i, j-th patch. The receiver beam is pointed 20° off the baseline. Figure 3 shows the contents of all such patches in their contributions to the total received clutter. The total loss for all of the clutter, computed by summing the absolute power received from each patch, is 143.5 dB. This clutter calculation is also performed for the receiver beam pointed along the baseline as well, in which case the overall clutter loss is 125.8 dB.

(U) Finally, the power in the direct signal from the transmitter to the receiver is computed. The latter is done for beam positions 20° and 0° from the baseline. The loss corresponding to these two cases is 142.4 dB and 94 dB.

UNCLASSIFIED

(U) These numbers are then used to compute the target signal to clutter ratio for the aircraft approach over the two paths as a function of range. The results are shown in Figures 4 and 5. In Figure 5 the notch at 160 km occurs when the aircraft passes directly over the buoy, in which case the target signal becomes very large. Hence the signal to clutter ratio drops at this point.

(U) Figures 6 and 7 show the target-signal to direct-signal ratios for the same two approach courses.

III CONCLUSIONS (U)

(U) Several conclusions can be drawn from these curves. For one thing, the target must be close to the buoy fence before the two ratios drop below about -60 dB. This latter number might be taken as a state of the art dynamic range for a radar receiver and processor, although by no means the ultimate possible.

(U) Another conclusion is that the worst approach path is the one along the baseline. There, the strong direct signal would tend to swamp the weak aircraft signal, except possibly when the aircraft passes over the transmitter. Over most of the path, the target echo will be 80 dB or more below the direct signal. Of course, the better ratio for the 20° path is only possible here because the beam of the receiving antenna is pointed away from the buoy, and hence the direct signal is weaker. A non-directional receiving antenna would result in a bad ratio for both aircraft courses.

(U) The above ratios become better for the buoy fence closer to the shore, and also for the aircraft target at a higher altitude. Studies similar to that done here are to be undertaken for fences at different locations and also for more realistic antenna patterns and target cross sections. Phase-coded signals, which permit exclusion of signals from all except the desired range cell, will certainly offer improvement over a CW system, and are to be included in further studies.

UNCLASSIFIED

(U)

AIRCRAFT BISTATIC CROSS SECTION AT 7MHz ≃ 40 m²

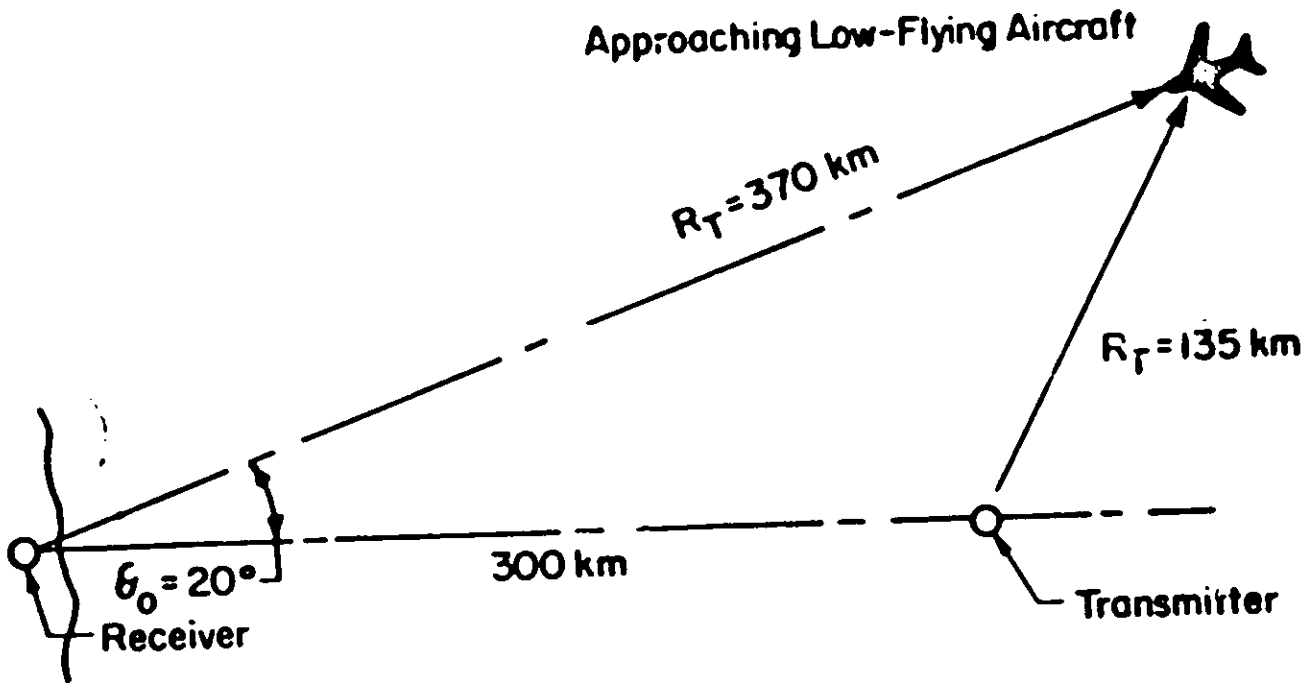

L_{OA} = Overall transmission loss to aircraft target

L_{OA} = −201 dB

S/C = $L_{OC} - L_{OA}$ = −57.5 dB = Signal to Clutter Ratio

(U) Figure 1. Sample Calculation of Overall Transmission Loss for Signal Reflected from Aircraft Target at 370 km Range (U)

(This page confidential)

UNCLASSIFIED

(U)

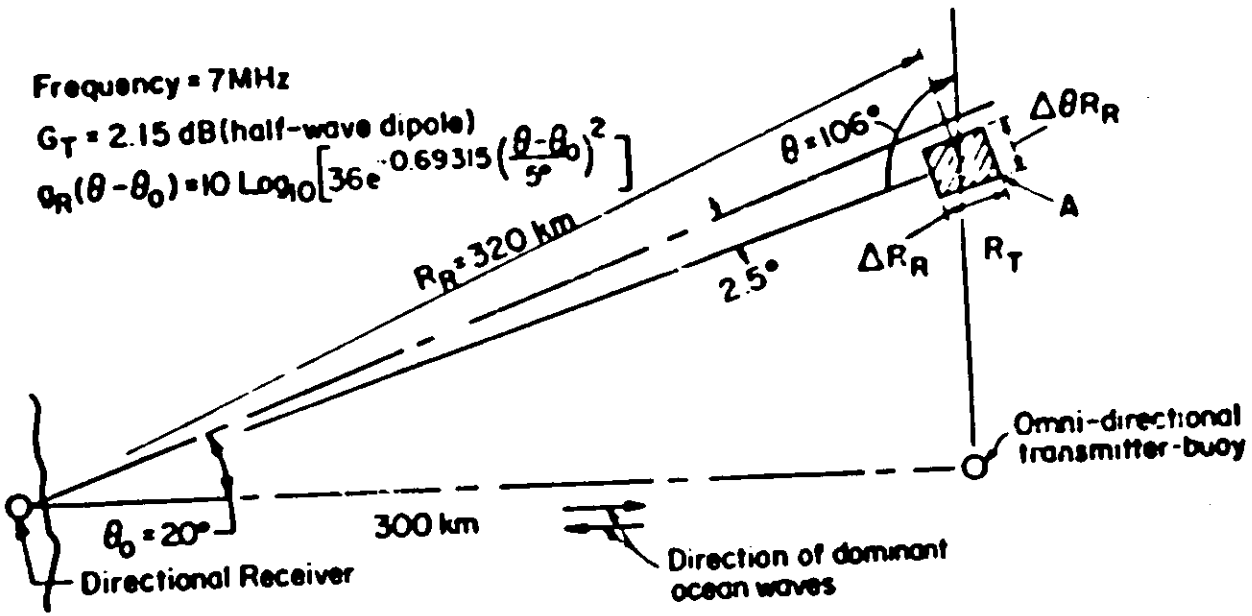

$\sigma_c^0 = -30.4$ dB (Sea State 2)

$A = R_R \Delta R_R \Delta\theta \simeq 280\ \mathrm{km}^2$ (ΔR = 20 km, $\Delta\theta$ = 2.5°)

$g_R(\theta-\theta_0)$ = gain function for directional receiving antenna, an array of half-wave dipoles of length 750 feet, it has a 10° beamwidth. A gaussium pattern is used for convenience.

For Sea State 2 (10 knot wind)

L_{oij} = 157.7 dB for patch shown (i, j th patch)

(U) Figure 2. Example of Calculation of Received Clutter Power (Expressed as Overall Transmission Loss) from One Patch of Sea. Receiver Beam is Pointed 20° from the Baseline. (U)

UNCLASSIFIED
UNCLASSIFIED
UNCLASSIFIED

(U)

UNCLASSIFIED

UNCLASSIFIED

UNCLASSIFIED

RELATIVE WEIGHTS OF L_{oij} FROM VARIOUS SEA CLUTTER PATCHES

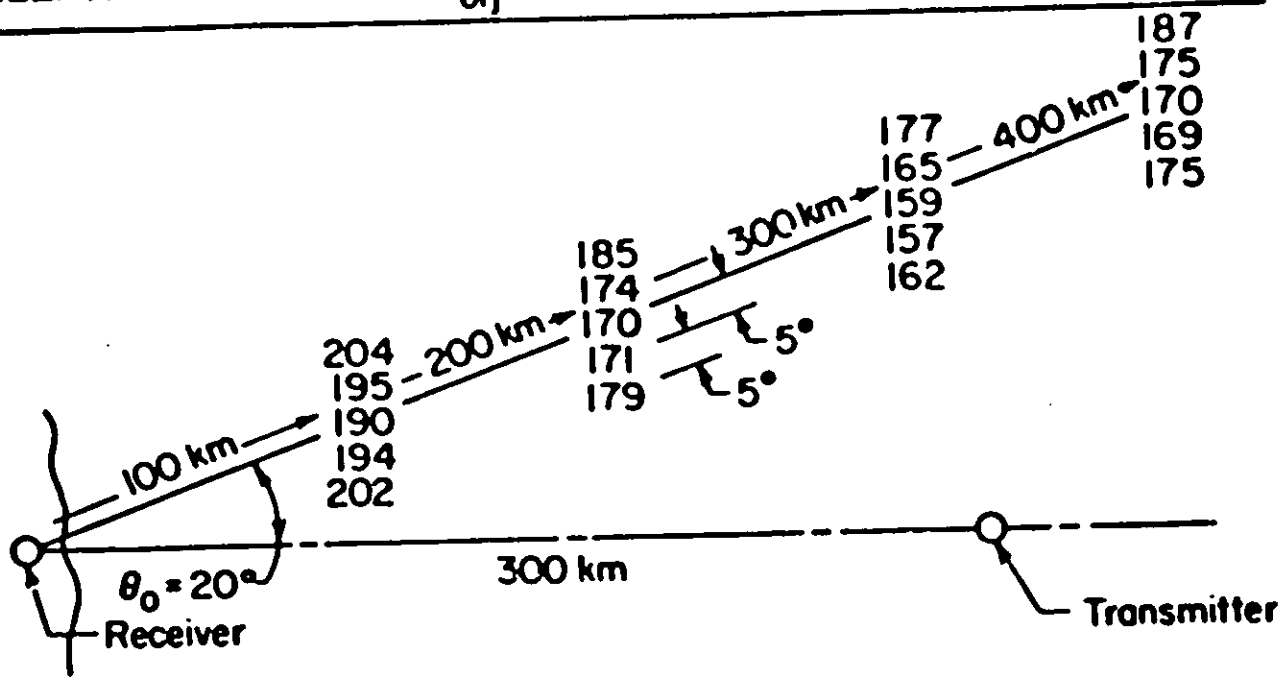

L_{oc} = 143.5 dB for summation of all significant patches

(U) Figure 3. Relative Weights of Overall Losses for Various Patches of Clutter. A High Number (in dB) Indicates Weaker Received Signal. (U)

[redacted]

UNCLASSIFIED

(U)

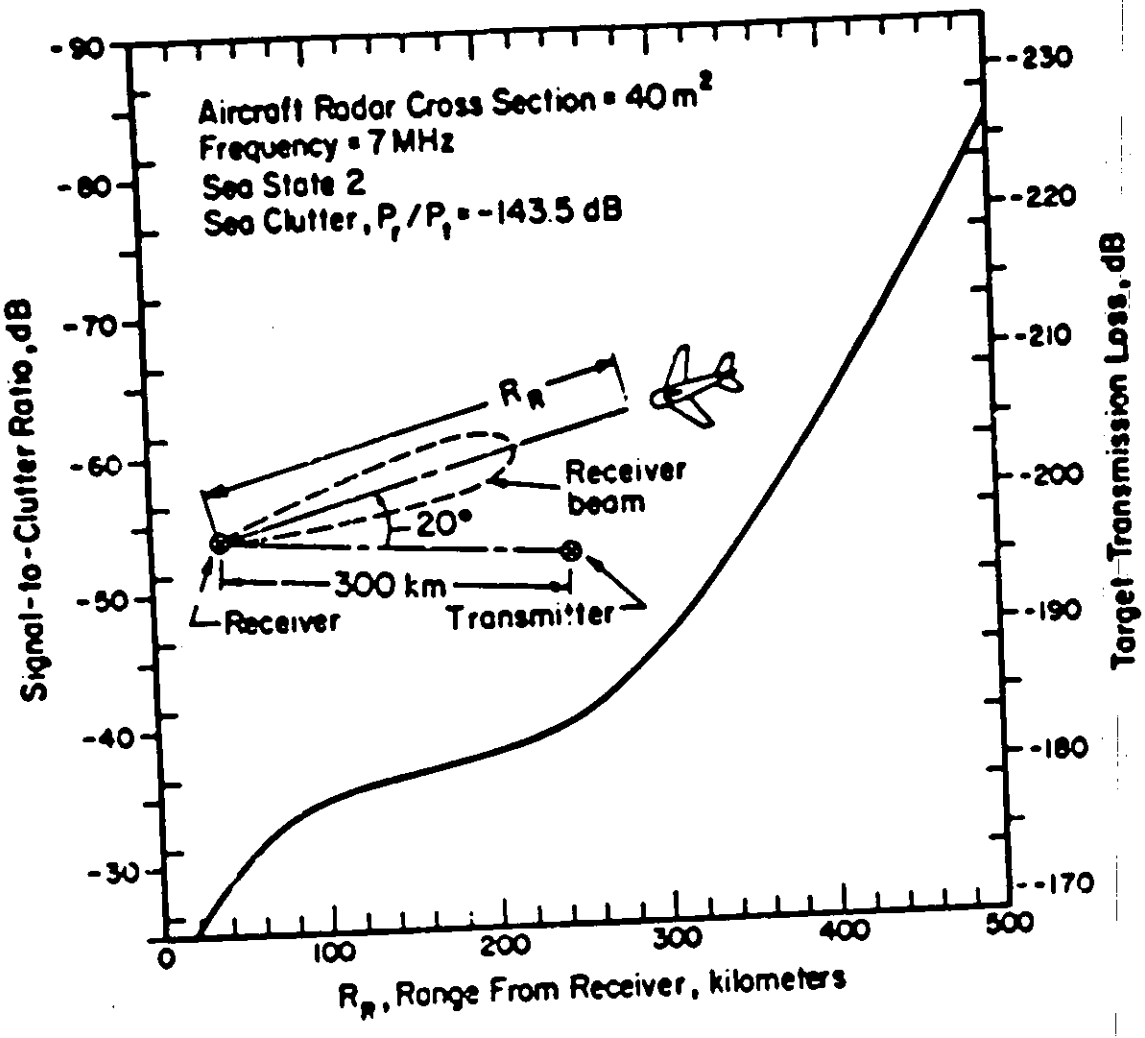

(U) Figure 4. Target Signal-to-Clutter Ratio vs Range for Aircraft and Antenna Beam on 20° Line from Baseline (U)

[redacted]

UNCLASSIFIED

UNCLASSIFIED

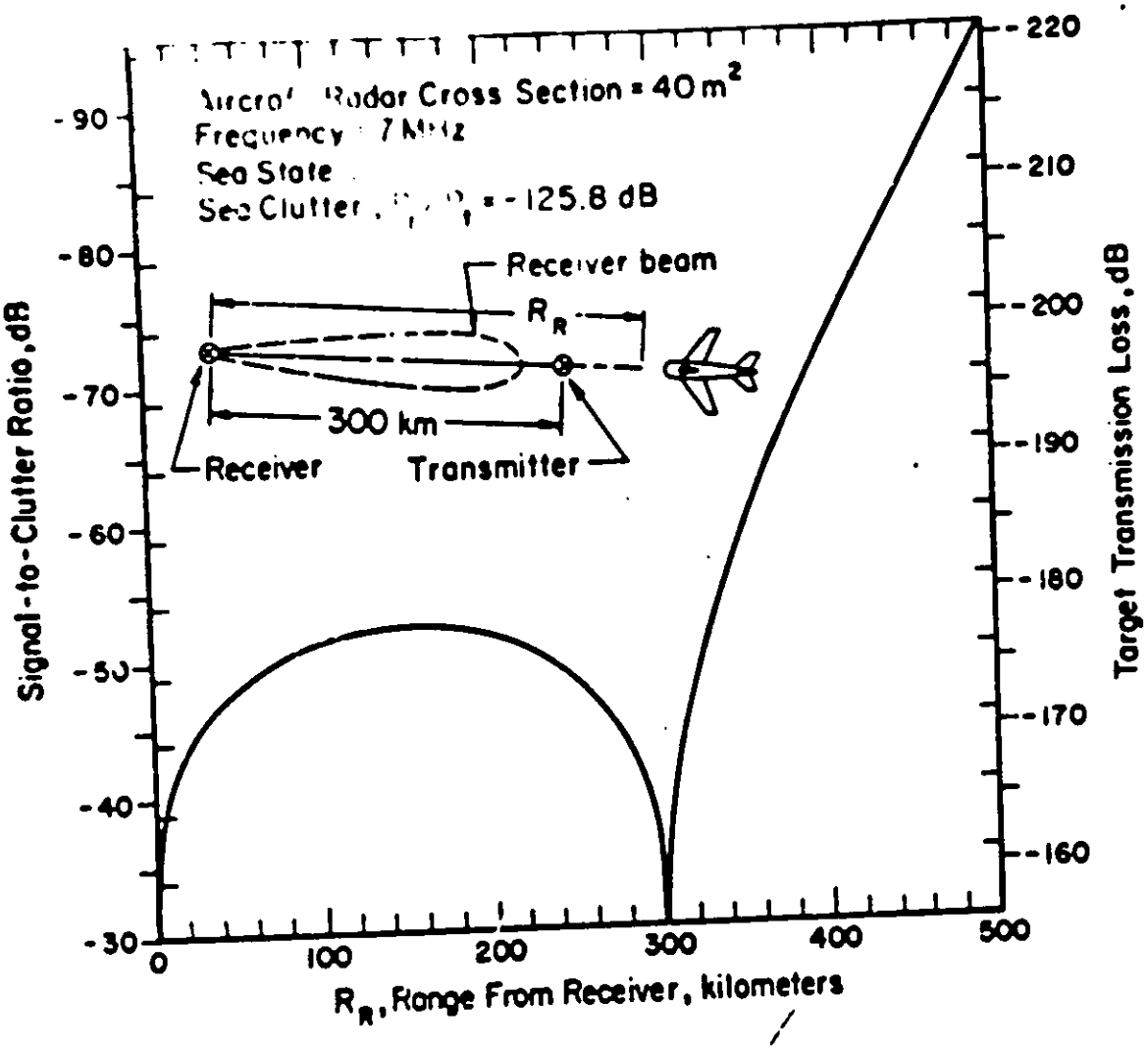

(U) Figure 5. Target Signal-to-Clutter Ratio vs Range for Aircraft and Antenna Beam along the Baseline. (U)

UNCLASSIFIED

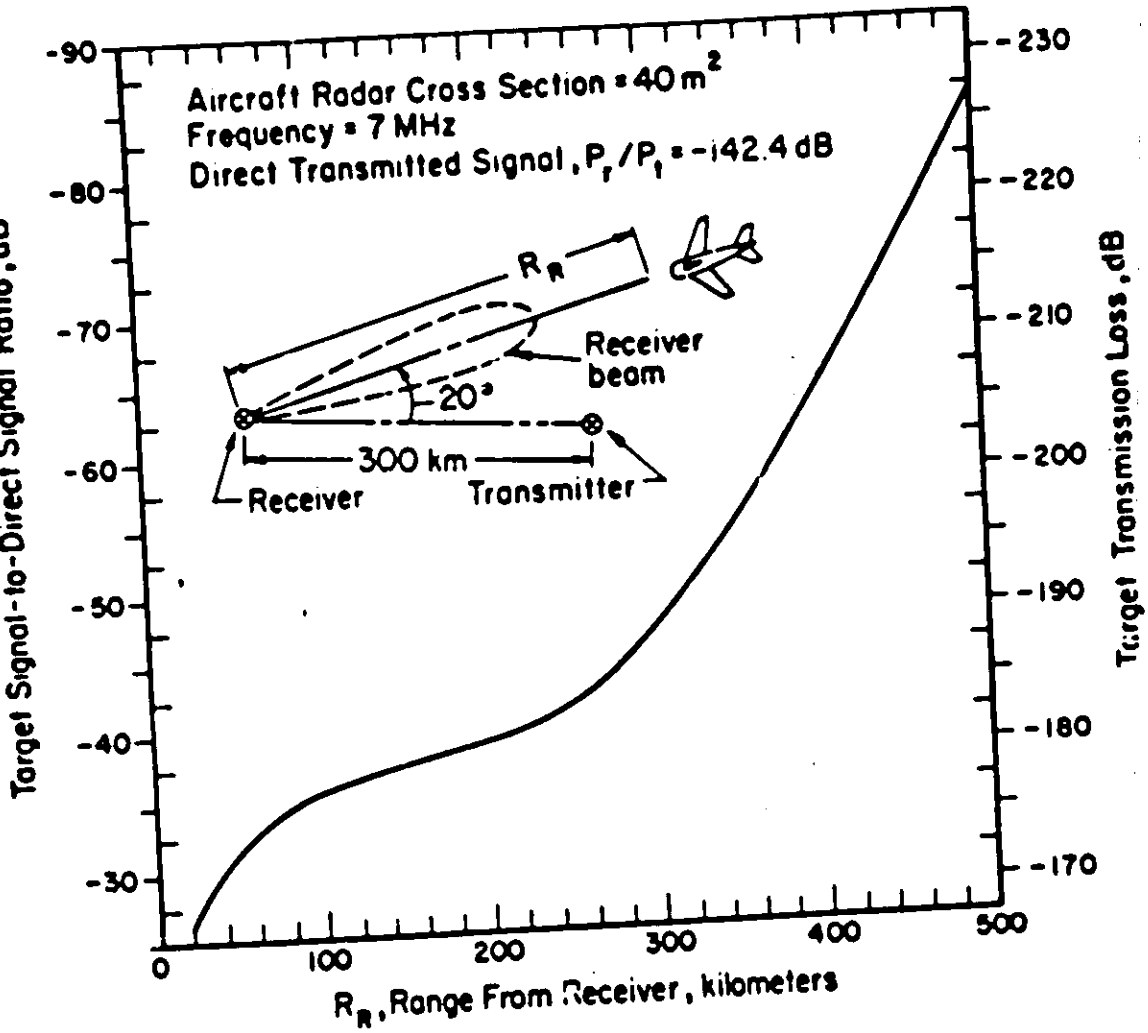

Figure 6. Target Signal-to-Direct Signal Ratio vs Range for Aircraft and Antenna Beam on 20° Line fromBaseline. (U)

CLASSIFIED

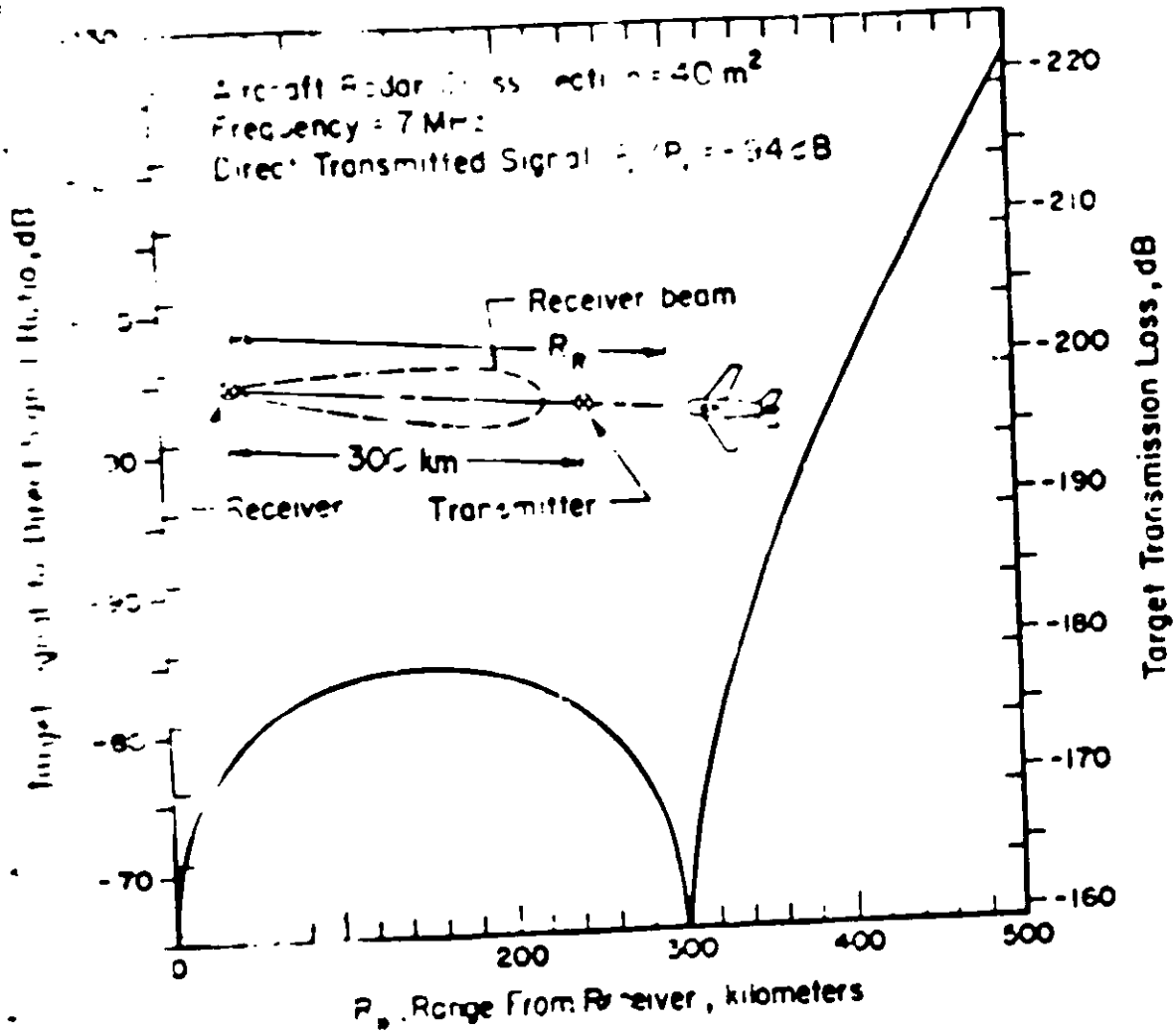

(U) Figure [illegible] Target Signal to Direct Signal Ratio vs Range for Aircraft and Antenna Beam Along the Baseline

UNCLASSIFIED

[redacted]

UNCLASSIFIED

THE BUOY TACTICAL EARLY WARNING SYSTEM CONCEPT, BTEW-I (S)

L. Edwards

Raytheon Company
Equipment Division
OHD Advanced Development Department
Spencer Laboratory
Burlington, Massachusetts

(U) (S) The BTEW concept orginally evolved from the thought that OTH surveillance might be achieved, even during times of nuclear blackout, by using a system based upon ground wave propagation. Such a system would, in fact, enjoy increased range and sensitivity at time of nuclear blackout because lesser amounts of noise would reach the receiver via ionospheric paths.

(U) (S) Monostatic Ground Wave Radar systems had been considered in the past, however, it was well known that such systems achieve long range coverage only at the cost of very high power. To overcome this disadvantage it was suggested that a buoy terminal in a bistatic mode might permit long range detection while power and system gain factors were kept to levels more attractive from a cost viewpoint.

(U) (S) Lacking a specifically defined performance requirement it was decided to take the approach of attempting to define the capabilities, or potential capabilities, of the concept as a function of system gain.

(U) (S) In general it is desired to determine the practical usefulness of the concept as applied to the entire coastal defense problem, as well as to the defense of specific strategic areas such as the Florida straits or the Northeast industrial complex.

(U) (S) The propagation and feasibility tests that were conducted off the Florida coast demonstrated that standard radar calculation techniques, coupled with Barrick's loss model, could be used to describe coverage areas. Actually to calculate coverage areas, it is necessary to define the deployment concept being examined, the various system parameters and the threat or expected target. Four different deployment concepts were examined:

- The monostatic radar case
- A shore transmitter and buoy receiver
- A buoy transmitter and shore receiver
- Buoy-to-buoy pairs

[redacted]

UNCLASSIFIED

[redacted]

...pected threat envelope covers targets from the SLCM size to larger bombers and SLBM's. At a ...ground wave operating frequency of 10 MHz the cross sections of these targets range from about ... the SLCM, about 100 m² for the attack bombers, and about 10^4 m² for an SLBM when it ... the lower ionosphere. The system parameters chosen for each of the deployment concepts ex... are shown in Figure 1.

The coverage by the monostatic system is shown in Figure 2. The map area shown covers the ...coast from Boston and the Massachusetts Cape area down to the Washington-Baltimore ... The system is shown located on the lower end of Long Island. The inner concentric ... circle out to 125 km where detection could be achieved by simply pulse modulating ...0 kW transmitter with a 100 μs pulse. The outer sector represents the area that could be covered ... using a 1 ms (long) pulse with a 10:1 pulse compression code that allowed range resolution ...out 15 km. With 5-degree azimuthal resolution provided by the antennas this would allow target ...ion to within about a 15 km square at a range of about 200 km.

The additional coverage that would be afforded by adding a buoy receiver to the complex is ...rated in Figure 3. This variation provides coverage out to 300-350 km from the shore station.

The coverage provided by the Bistatic II Buoy Transmitter - Shore Receiver system is described in ...e 1 and shown in Figure 4. Three shore receiver stations and seven buoys provide a radar fence at 225 km range from the Massachusetts Cape area down the coast to the Washington Area.

The Bistatic III buoy-to-air concept provides limited aircraft coverage. The ...ys can be spaced at about 100-km intervals; but using either ground wave or ...ellite telemetry modes back to shore, they could provide warning at greater ...shore distances plus offering the greater surveillance of SLBM's. A possible ...st coast buoy fence system is illustrated in Figure 5.

Figure 6 has been prepared to illustrate the magnitude of a system designed to provide surveillance the entire Eastern coast of the United States. Ten shore stations operating both monostatically and ...tically with about 30 off-shore buoy receivers would provide continuous coverage from Nova Scotia ...n around the tip of Florida out to a range of about 350 km.

The basic feasibility of the BTEW-I concept has been successfully demonstrated. A system of ...fest size, and therefore presumably much lower cost, can provide off-shore detection coverage out to ...ges of 300 to 400 kms. SLBM coverage can be obtained to significantly greater ranges.

[redacted]

[redacted]

(U)

MONOSTATIC SYSTEM PARAMETERS	BISTATIC I BUOY RECEIVER - SHORE TRANSMITTER
G_T = 22 dB G_R = 22 dB F = 10 MHz σ = 100 m^2 P_T = 100 kW (200 kW PEP) 3 dB efficiency loss None = -154 dBW/1-Hz band P_R = Noise + 9 dB = -145 dBW SEA STATE 3	G_T = 22.5 dB G_R = 1 dB (2 dB - 1 dB) F = 10 MHz σ = 100 m^2 P_T = 100 kW 3 db efficiency loss None = -154 dBW/1-Hz band P_R = Noise + 9 dB = -145 dBW SEA STATE 3
BISTATIC II **BUOY TRANSMITTER - SHORE RECEIVER**	**BISTATIC III** **BUOY TRANSMITTER - BUOY RECEIVER**
G_T = 1 dB G_R = 22 dB F = 10 MHz σ = 100 m^2 P_T = 1 kW 3 dB efficiency loss None = -154 dB 1-Hz band P_R = Noise + 9 dB SEA STATE 3	G_T = 1 dB G_R = 1 dB F = 10 MHz σ = 100 m^2 P_T = 1 kW None = -154 dBW/Hz band P_R = Noise + 14 dB SEA STATE 3

(U)

Figure 1. System Parameter Tabulation (U)

[redacted]

(U)

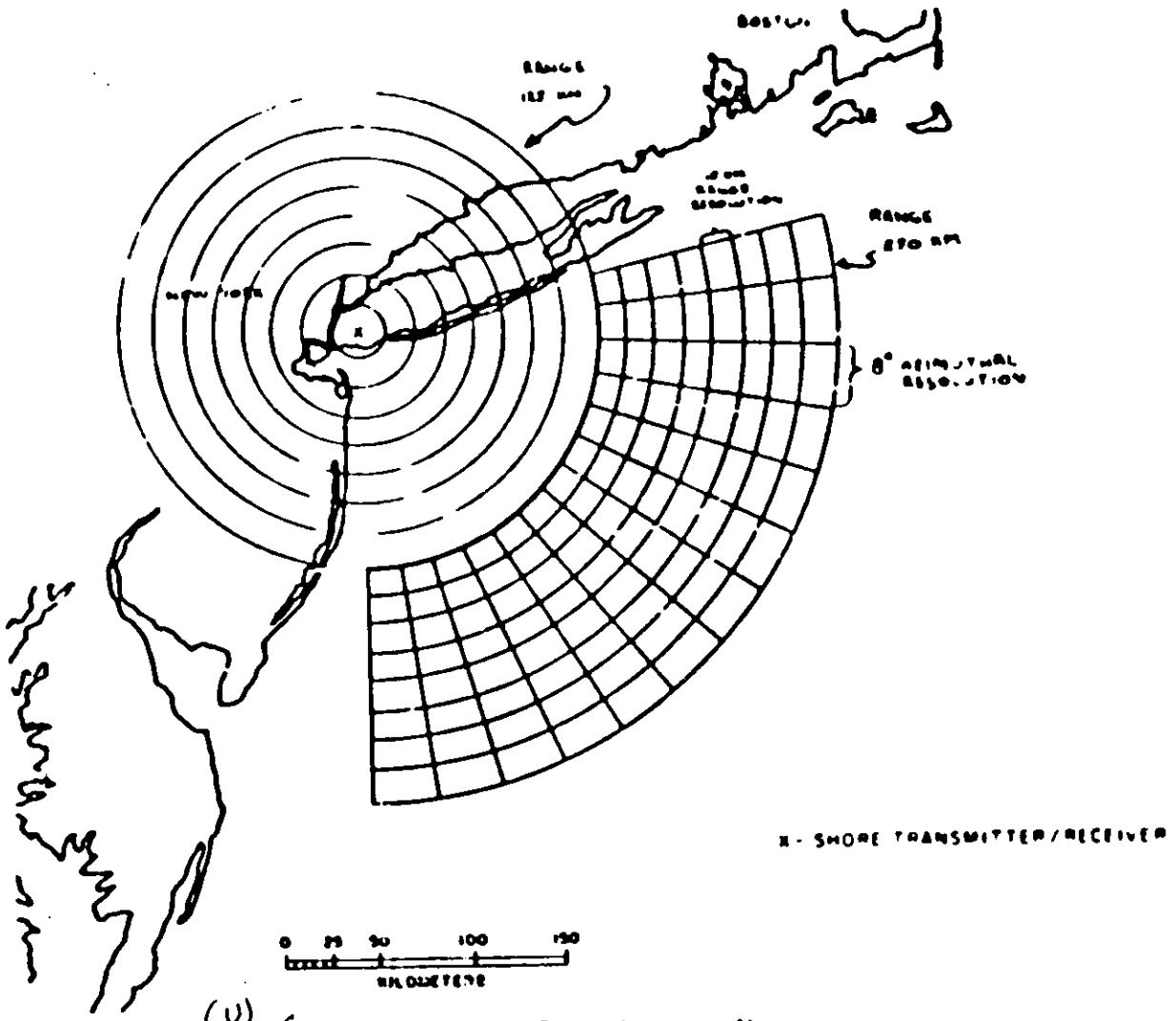

(U) Figure 2 Monostatic System Coverage (U)

Figure 3. Extending Coverage by Adding a Buoy Receiver (C)

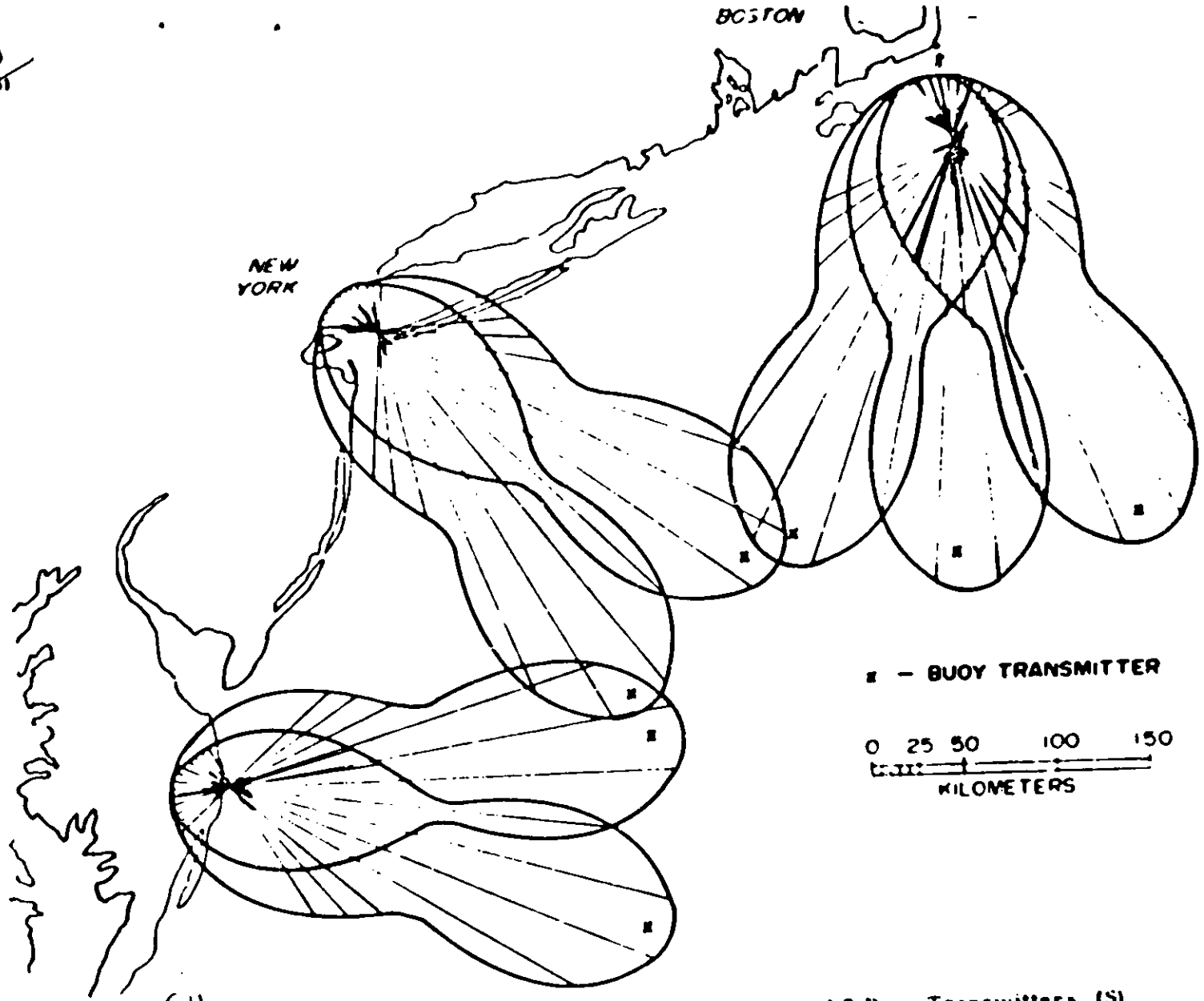

(U) (S) Figure 4. Coverage Using 3 Receiver Stations and 7 Buoy Transmitters (S)

UNCLASSIFIED

[redacted]

(U)

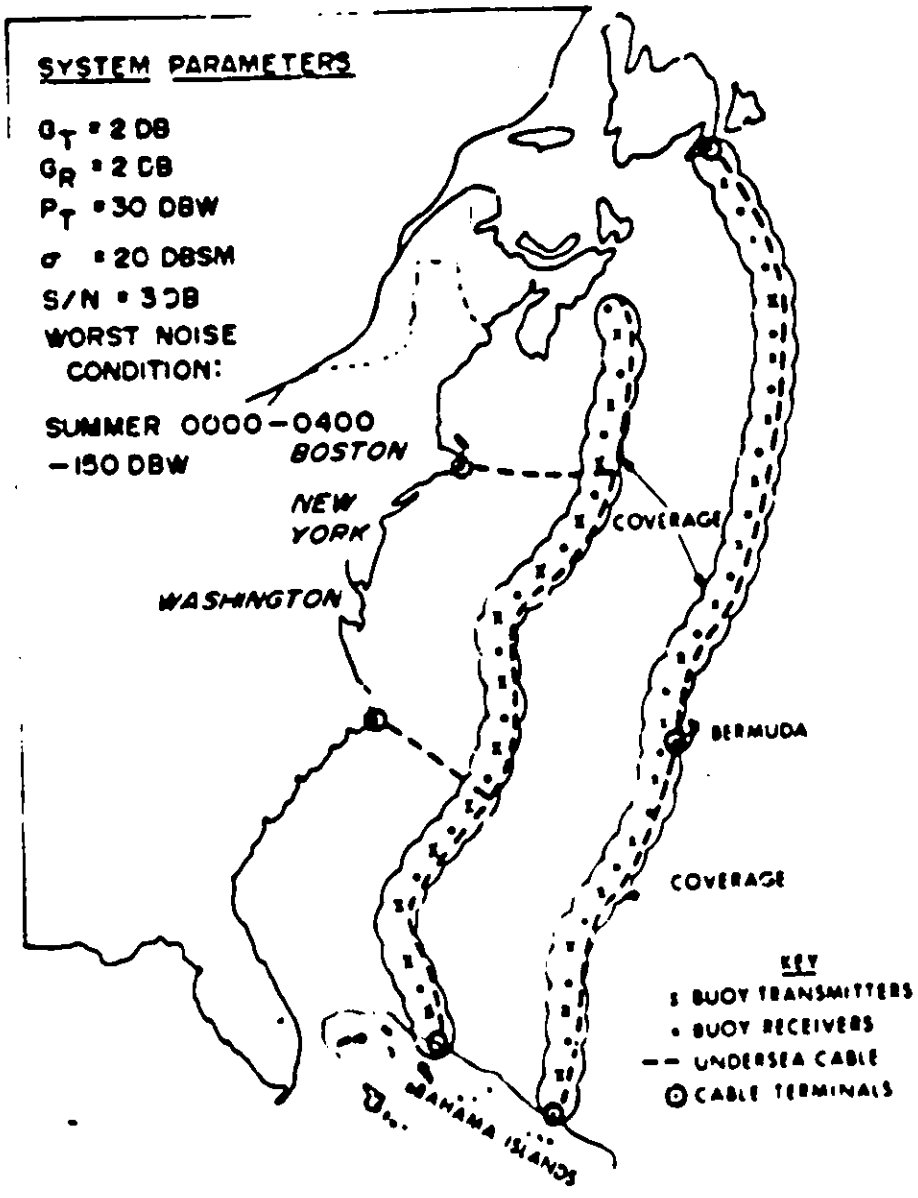

(U) Figure 5. Coverage Map of Fence Radar Using Buoy Pairs (U)

[redacted]

UNCLASSIFIED

UNCLASSIFIED

(U)

(U)
(S) Figure 6. East Coast Coverage Using 10 Monostatic Shore Stations and About 30 Buoy Receivers (S)

UNCLASSIFIED

[redacted]

UNCLASSIFIED

COMPARISON OF SEVERAL BTEW SYSTEM CONFIGURATIONS (U)

J. W. Follin, Jr.

Applied Physics Laboratory
The Johns Hopkins University
8621 Georgia Avenue
Silver Spring, Maryland 20910

(U) A relative comparison of different system configurations can be made without detailed target and ambient noise conditions by comparison of illuminating power at the target for several geometries. For example, Figure 1 shows the power delivered to a buoy from a shore radar with an aperture of 1 kilometer and an average power of 1 megawatt as a function of range to the target. Also shown are the powers delivered to a target from a buoy radiating one kilowatt isotropically. By comparing these cases for which the power on target is identical, it is possible to determine the buoy spacing for which the signal-to-noise at the land-based receiver is the same for both systems. It must be realized that the target aspect, and hence its radar cross section, may differ; and the Doppler shift expected, especially for SLBMs, will also differ.

(U) The second set of curves in Figure 2 shows a comparison in which the system is run backward, transmitting from land and receiving on the buoy. This system has an advantage of 30 dB in average power while all of the antenna gains are comparable. In addition, it is probable that the ambient noise in the vicinity of the buoy is less than that in the vicinity of the land-based radar, perhaps by 10 dB. This shows that, for system ranges of 500 kilometers from shore, a buoy spacing of 400 kilometers gives comparable performance directly between adjoining buoys, and improved performance closer to the individual buoy locations.

(U) For the skywave case we oversimplified the ionospheric path to the line-of-sight minus 10 dB, and the illumination density, as shown in Figure 3. Figure 4 shows the comparison of monostatic versus bistatic. It is apparent that rather high buoy densities are required to compete with the monostatic radar skywave case.

[redacted]

UNCLASSIFIED

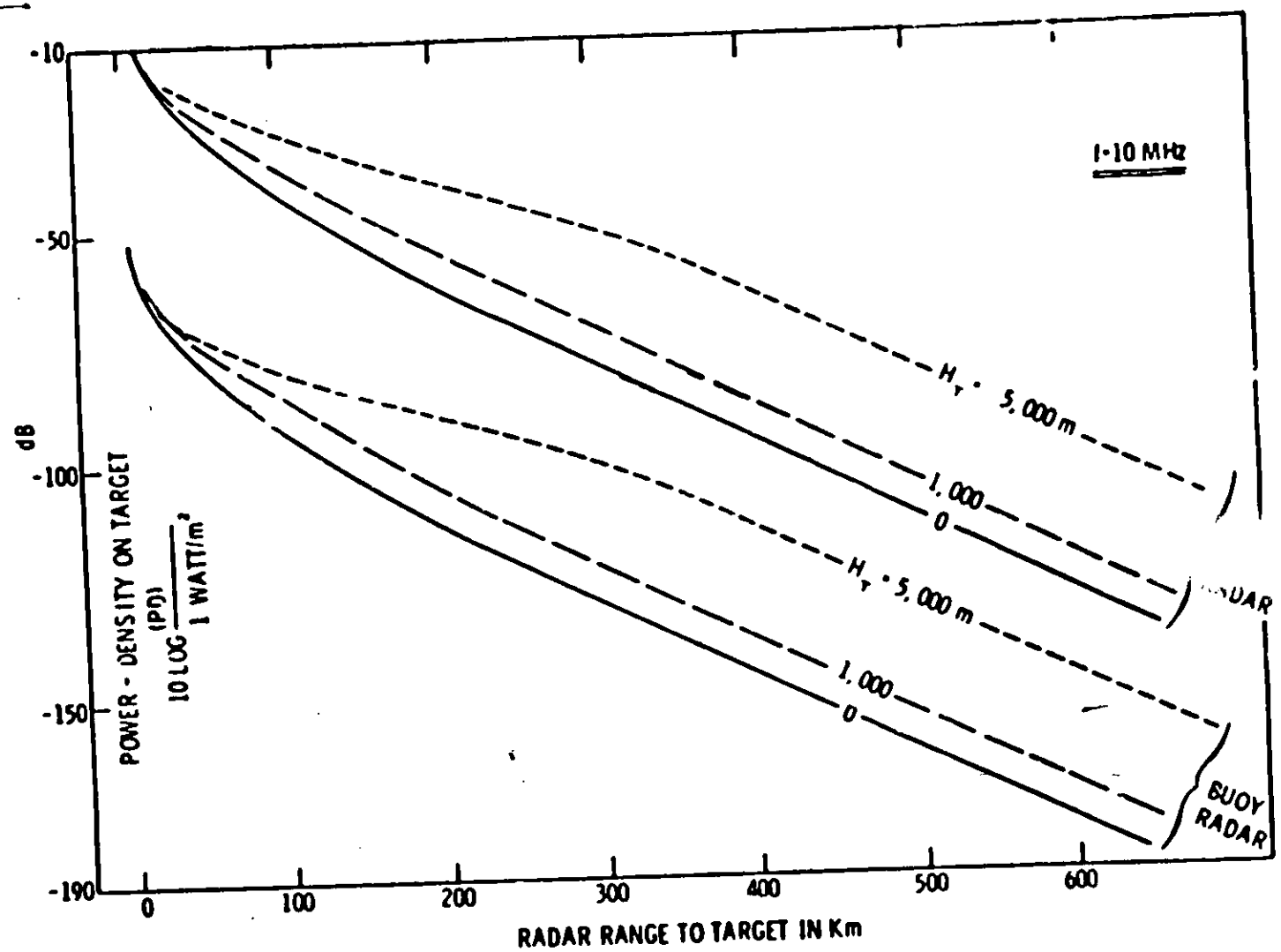

(C) Figure 1. Power Densities on Target for Ground Wave Transmission of Shore Radar (U)

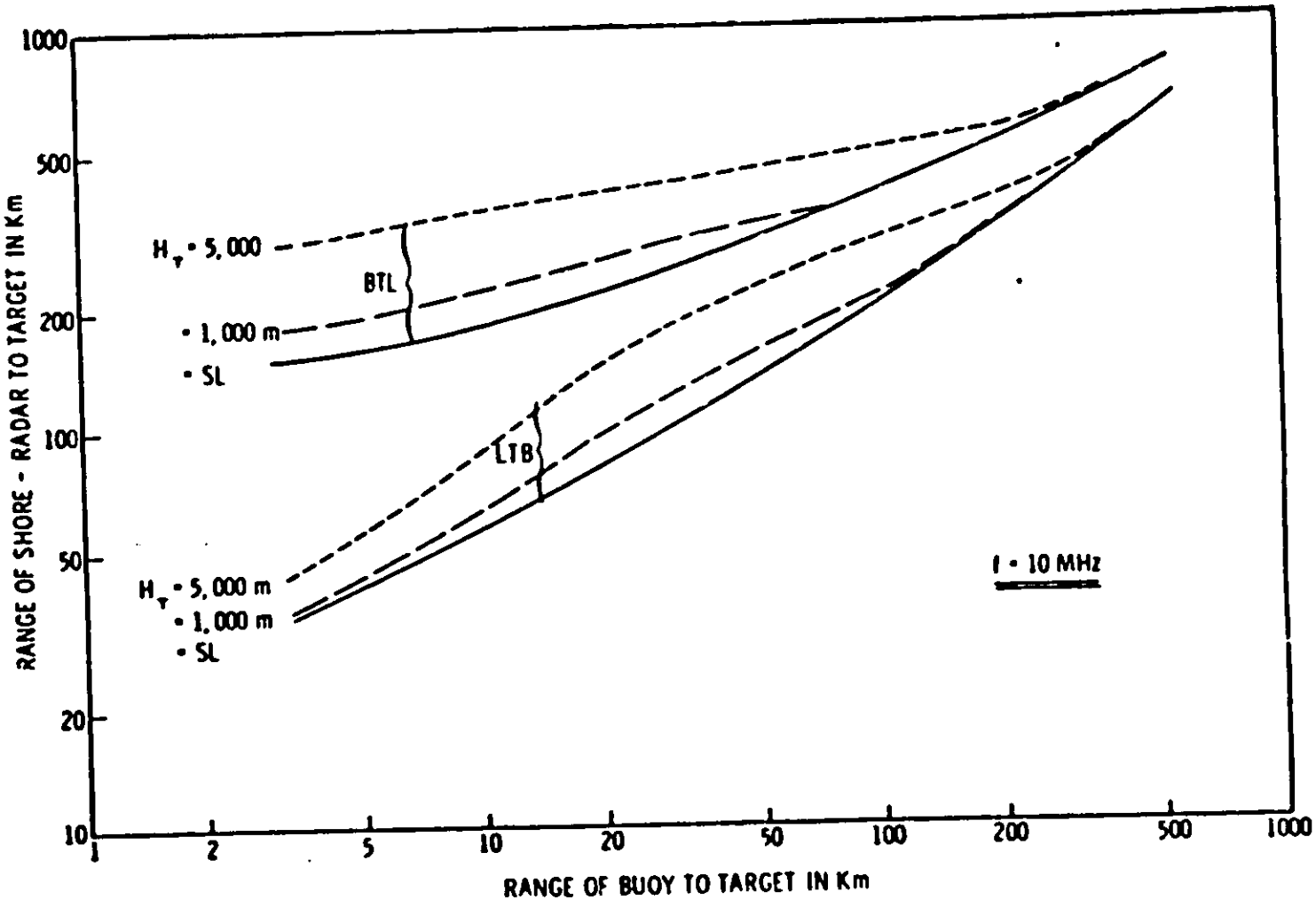

(U) Figure 2. Comparison of Various Systems for Ground Wave Transmission of Shore Radar (U)

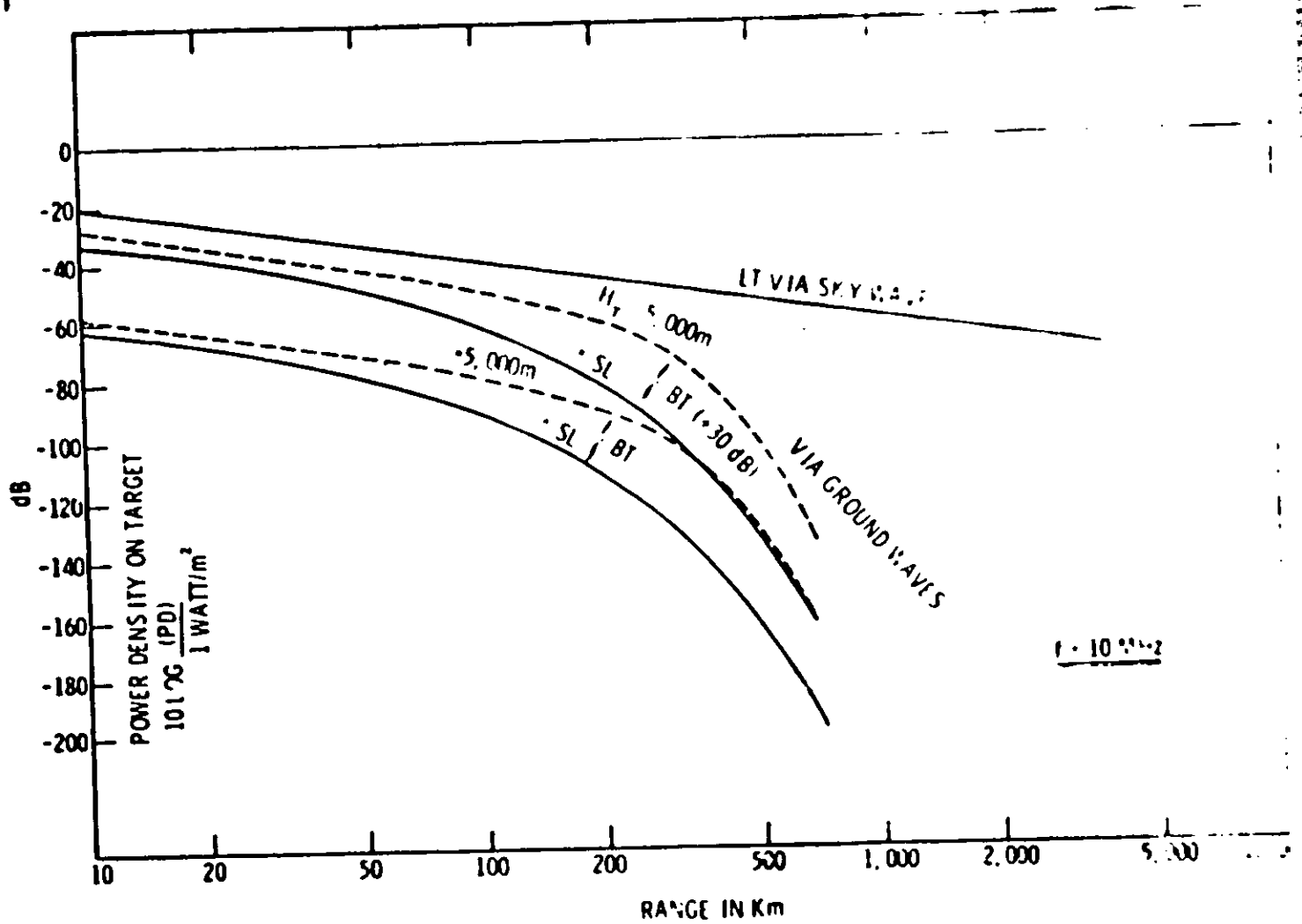

(C) Figure 3. Comparison of Power Densities on Target (U)

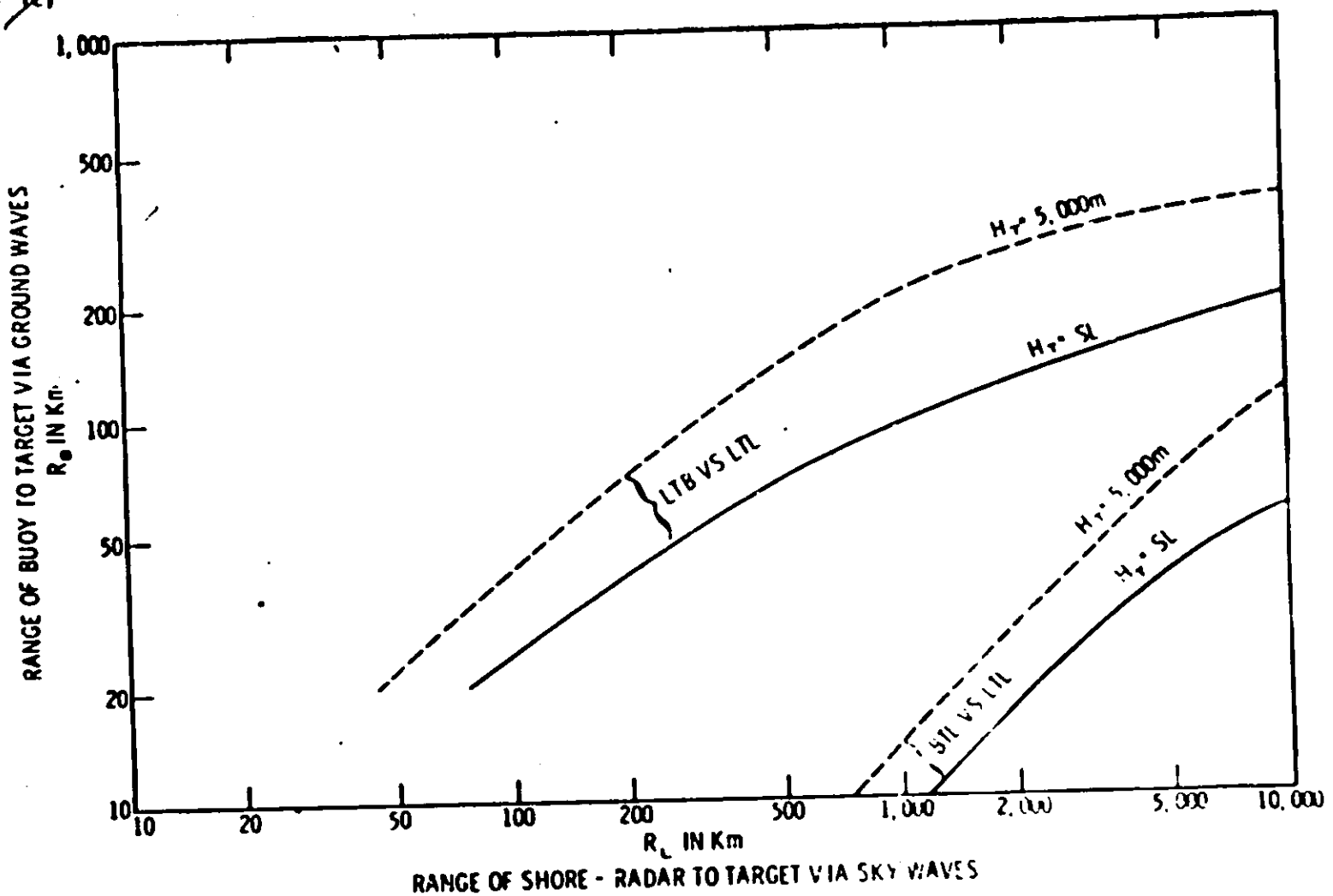

(U) (C) Figure 4. Comparison of Various Systems at 10 MHz on the [illegible]

UNCLASSIFIED

[redacted]

These comparisons between systems only suggest which one is preferable, not whether it can in cut the mustard, and more detailed calculations such as those presented by the preceding speakers needed to determine system effectiveness. However, before final conclusions can be drawn it seems a conclusion to draw that HTH W surface wave systems are useful, but for the skywave case much analysis is required, especially with a disturbed ionosphere.

[redacted]

UNCLASSIFIED

SECTION 3

PANEL REPORTS (U)

PANEL REPORTS (U)

I CONCLUSION (U)

A Path Loss (from Carter Cay) (U)

(U) Average absolute received path loss compares well with predicted average loss (Sea State 4) to 1.2 dB

(U) Total spread on received path loss at 5 and 10 MHz compares well with predicted variations with sea state by Barrick, i.e., about 3 dB at 5 MHz and about 9 dB at 10 MHz. At 15 and 20 MHz, the data points are too few to permit any conclusions.

(U) Day-to-day correlation between measured path loss and predictions based on hindcast wind and wave data is generally poor, except for two or three days when there were significant changes in sea state. However, day to day correlation of the three sources of hindcast data is also poor. Hence in the absence of actual ocean spectrum measurements, day to day correlation of measurements with predictions is not expected to be a meaningful test of sea state dependence.

(U) Correlation between 5, 10, 15 and 20 MHz path loss measurements on a day-to-day basis should provide some test of dependence on sea state. If most data points can be obtained at 5, 15 and 20 MHz, such correlations will be meaningful.

(U) Day to day variations in path loss due to equipment systematic errors are believed to be less than 2 dB (Dr. L. Wetzel provided rough calculations to document this conclusion).

(U) Conductivity variations of the sea water (based on analyses) had no important role in received signal loss variations.

(U) Possible effects of ducting are completely unknown. No way is known of assessing this factor from existing measurements, nor are any predictions or even estimates available (to anyone's knowledge) on the seriousness of ducting over the sea at HF.

(U) There is some evidence of possible direct signal spectral broadening due to the moving sea surface, especially at the highest frequencies. However, limited high sea state occurrences and possible contamination by sky-wave make any final conclusions about spectral broadening impossible.

B Sea Clutter (from the Buoy and Carter Cay) (U)

(U) Comparisons of clutter measurements with wave heights and directions are meaningful primarily for the buoy measurements, too much of the area in the various range gates around Carter Cay consists of land, shoals or shallow water, especially the significant backscatter region behind the transmitter. Hence, correlations are to be based primarily on buoy data.

(U) Buoy measurements were restricted to only the 5-MHz data for about 10 days in March. Some possibility exists for examining clutter spectra at 10 MHz from the December measurements.

(U) Clutter spectra permit detailed analyses only in the 1/2-Hertz mode, i.e., spread out so that the resonant Bragg scatter ocean waves whose Dopplers lie within one Hertz of the carrier can be observed.

(U) On the basis of existing measurements, the predicted mechanism is well confirmed from the "clutter occupancy" of the spectrum. The "pedestals" predicted for bistatic geometries are present, and their width and position varies exactly as predicted throughout the different range gates, phase code rates, and frequencies.

(U) Correlation of 5-MHz spectra with expected spectra based upon ocean wave height and direction hindcast data for several days shows excellent agreement and again confirms the predicted mechanism.

(U) Total scatter cross section, σ^0, as deduced from measurements on several days with moderate seas, agrees reasonably well with predictions and with measurements of Crombie, Headrick and others. There remain differences of definition of σ^0, but these will be resolved so that more of these independent comparisons can be made directly.

(U) Little can be deduced from the measurements about the region between the carrier and the clutter pedestals during higher sea states. While some records for higher sea states show this region well filled in compared to similar records for calm seas, too few such comparisons are available. No present first-order theory offers estimates for this region either.

(U) Measurements at 5 MHz show higher clutter levels than would have been deduced from the "tail" of the wind-wave models. Often the latter models on the days in question would have predicted no scatter because of the absence of resonant ocean waves. Thus the measurements show that the standard windwave models are not reliable in the lower regions because of the presence of some longer ocean waves, or swell.

(U) Agreement between theory, the Raytheon measurements, and the measurements of others is so good that the theoretical models can be used reliably for system design purposes at HF. This is especially true in aircraft or SEEMD sense where high Doppler shifts are expected. Use of the models for low-velocity target systems (such as ship detection) must be tempered somewhat by uncertainties in clutter level around the first-order spectral pedestals of the model.

6. Sea-State Observations (U)

(U) There were three significant regions of sea involved in the Carter Cay - Cape Kennedy propagation path: 1). shallow water near the Florida coast (about 30 km), 2) the moving currents of the Gulf Stream, and 3). the shoal waters near the Bahamas (about 55 km). Distinctly different ocean wave conditions were consistently observed from the surveying aircraft in these three regions.

(U) Wind speed and direction has been plotted on a daily basis at both Cape Kennedy and Grand Bahama Island. Wave hindcast data showing waveheight and direction for the general region of the Atlantic has also been plotted on a daily basis.

(U) The possible sources of information about the state of the sea mentioned above correlated poorly on a day-to-day basis.

(U) Aerial photographs of the sea wave were made for 18 days. The goal of these flights was the direct construction of isotropic water-wave spectra using the Stilwell coherent optics technique. Due to the use of the wrong type of film, such spectra cannot be computed from any of the photographs.

(U) The above photographs can and will be used to deduce rough information about ocean-wave directionality.

(U) Laser profilometer measurements were also recorded along the propagation path during the 18 flights. Because of uncertainties involving aircraft motion contaminating the height data, no usable ocean wave spectra have yet been available.

(U) Aircraft motions were recorded during the eighteen flights as an accelerometer output. NRL personnel have stated that this accelerometer output will be analyzed and the knowledge of the resulting aircraft motion spectrum will be used to obtain the true ocean-wave spectrum. They have promised that these spectra will be processed within one month.

(U) Hindcast data show that over the three-month measurement period, the seas were relatively calm with a Sea State 6 being reported only once. Average conditions appeared to be Sea State 1 to Sea State 3.

(U) Accelerometer and inclinometer data telemetered from the buoy is of insufficient quantity and reliability to allow the inference of sea state conditions.

II RECOMMENDATIONS (U)

A Additional Measurements (U)

(U) The Committee on Theory and Measurements recommends additional path loss measurements. The suggestion was initiated by Dr. Allen Peterson and discussed in some detail by the committee. The reasons that additional path loss measurements were felt necessary are listed below.

- (U) Path loss measurements at 5, 15 and 20 MHz at present appear too few and sporadic to permit conclusions or even trends to be established.
- (U) Overlapping days, i.e., days on which path loss at more than one frequency was obtained, are very few. Overlap on the days with high sea states or high weather conditions (i.e., conducive to possible ducting) does not exist. Without many such overlapping days, effects of the environment cannot be studied or related to measurements.
- (U) Spectral widening of the direct signal by the moving sea during high sea states appears to be a possibility from one or two records, but again too little data is available during high seas to permit any conclusions about this important phenomenon.
- (U) Much of the time the ground-wave signal was contaminated by sky-wave. It was only near the end of the three-month period that phase-coded emissions at 5 and 10 MHz permitted positive separation of ground wave from sky-wave.
- (U) The weather in the area from January through March does not normally undergo great changes. Temperature and seas appear to vary less about a mean than during warmer summer months and hurricane seasons.
- (U) Nearly one-third of the path crosses shoals, while much of the remainder crosses the Gulf Stream. Hence, most of the path consists of water whose surface is not typical of deep-water ocean.

(U) The suggested investigation would consist of and emphasize the following parts:

- (U) A long path over deep water would be selected, preferably with end points on land so as to reduce expense of the measurements. The path should be 300 to 400 km long. A possible path considered and recommended stretches between

(U)
Cape Cod and northern Maine, near the Bay of Fundy, over 90 percent of this path is over water more than 500 feet deep. Reported seas in this area are quite high and often influenced by Northeasterly storms blowing nearly parallel to the propagation path.

(U) • (U) Phase-coded, highly stable signals at 5, 10, 15 and 20 MHz should be employed. The phase-code is necessary to ensure separation of the ground-wave from the sky-wave.

• (U) Path-loss measurements should be made twice daily over a period of five months. The measurement period chosen should include both summer and winter weather.

• (U) Field-strength probes should be used daily to calibrate the main transmit and receive antennas. The field structure from the main antenna out along the beach and into the water should also be probed, at least once during the period.

• (U) The main antennas should be kept simple, i.e., vertical quarter-wave monopoles.

(U) • (U) Path-loss signals for the ground-wave should be measured in Range Gate 0, i.e., the range gate corresponding to the arrival time of the direct signal. Spectral processing should be available so as to allow better than 0.01-Hertz resolution. This will permit a study of direct signal broadening due to sea wave motion and (possibly) atmospheric turbulence.

• (U) Range Gates 1, 2, 3, 4, etc. should also be spectrally examined (occasionally) to permit study of sea clutter and sky-wave signals.

(U) • (U) One wave spar should be used to measure and telemeter the isotropic ocean wave spectrum somewhere near the path midpoint.

• (U) Pulsed sea backscatter measurements should be made near the receiver site, in the manner reported by Crombie in his papers presented in these proceedings. These measurements appear to allow fairly accurate and inexpensive calculation of the isotropic ocean waveheight spectrum.

• (U) Hindcast wind and wave data should be collected. Also, quantitative meterological data versus altitude and position should be gathered where possible to permit calculation and study of the refractivity.

• (U) Signal strength versus range should be measured at least once during the experiment. This could be done with a transmitter on a small boat or from various other shore points.

• (U) Horizontal polarization near the receiving antenna should be measured several times, especially during high seas. This will indicate the presence of any de-polarization from steeply sloping ocean waves.

B. Additional Processing of Existing Data (U)

(U) NRL should be asked to complete analysis of wave data from their profilometer records for the 18 flights. This ocean-wave data should be plotted beside the path loss measurements for the same days.

(U) Raytheon should, where possible, process and plot more points of path loss on 5, 15 and 20 MHz.

(U) The total number of reliable path-loss points on each frequency should be calculated.

(U) The mean and variance of the path loss signals on each frequency should be calculated.

(U) Mean and variance of expected (or predicted) path loss should be calculated for each frequency based on the hindcast waveheight data on the days of observations.

(U) Averages of several clutter spectral records in the 1½-Hertz mode should be made, especially for days such as March 23 and March 26 when clutter is clearly in evidence. These averages should be made over a duration for several independent samples (an independent sample in the 1½-Hertz mode is 162 seconds long).

SECTION 4

TASK ABSTRACTS (U)

TASK ABSTRACTS (U)

THEORETICAL STUDIES: CALCULATIONS SURFACE WAVE (U)

Organization (U)

(U) Battelle Memorial Institute

Specific Objective (U)

(U) Determination of surface wave attenuation and clutter as a function of sea state, range, frequency and aspect angle.

System Concept-Relation and Importance (U)

(U) Important to all concepts where surface wave propagation is involved in predicting the clutter amplitude and doppler of the sea and the range performance.

THEORETICAL STUDY-ATTENUATION OVER IRREGULAR INHOMOGENOUS TERRAIN (U)

Organization (U)

(U) ESSA

Specific Objective (U)

(U) Development and application of theoretical techniques for determining the surface wave attenuation over surfaces having different dielectric constants and conductivities.

System Concept-Relation and Importance (U)

(U) Applicable in predicting system performance where surface wave is used and land sea interfaces occur. Typical examples involve an antenna located on land and using surface wave for transmission or reception; or where energy used in surface wave mode must traverse an island. This is important in determining system losses that reduce range or cause shadow zones (e.g., islands).

[redacted]

UNCLASSIFIED

BISTATIC SEA ATTENUATION AND CLUTTER MEASUREMENTS (U)

Organization (U)

(U) Raytheon

Specific Objectives (U)

(U) Substantiated the theoretical calculations of attenuation and clutter of surface wave propagation as a function of sea state, frequency, distance, and aspect angle.

System Concept-Relation and Importance (U)

(S) Applicable in predicting the performance of all systems where ocean surface wave is used in propagating to and/or from target.

[redacted]

UNCLASSIFIED

MONOSTATIC SEA CLUTTER MEASUREMENTS (U)

ganization (U)

) ESSA

ecific Objective (U)

U) Determine and correlate with sea state the monostatic clutter spectrum as a function of range -150 km) and frequency.

stem Concept-Relation and Importance (U)

U) Important in predicting range performance and clutter rejection requirements of a land ted or ship based monostatic radar.

[redacted]

[redacted]

UNCLASSIFIED

SLBM CROSS-SECTION (U)

Organization (U)

(U) Stanford Research Institute

Specific Objective (U)

(U) Compile and summarize the available data on the theoretical calculation and measurements of SLBM cross sections.

System Concept-Relation and Importance (U)

(U) Required for the design and performance prediction of HF radar systems against SLBMs.

[redacted]

UNCLASSIFIED

[redacted]

SHIP CROSS-SECTION MODEL MEASUREMENTS (U)

Organization (U)

(U) Stanford University

Objective (U)

(U) (S) Calculate theoretically and measure experimentally cross-sections of two representative scale-model ships as a function of frequency, aspect angle and polarization at HF.

System Concept-Relation and Importance (U)

(U) (S) Required to determine ship detection system performance calculations.

[redacted]

SHIP CROSS-SECTION MEASUREMENTS (U)

Organization (U)

(U) Naval Research Laboratory

Objective (U)

(U) Measure cross-sections of actual ships at specific aspect angles and frequencies with the MADRE radar.

System Concept-Relation and Importance (U)

(U) Demonstrates that ships can be detected using pulse Doppler Radar. Provides check points at specific frequency and aspects to correlate with model measurements. Provides input for system performance calculations.

[redacted]

WAKE STUDY (U)

Organization (U)

(U) ESSA

Specific Objective (U)

(U) (S) Determine theoretically the size, aspect, frequency, and spectral characteristics of ship and submarine wakes applicable to HF radar.

System Concept-Relation and Importance (U)

(U) (S) Ship wakes may be of sufficient size and spectral characteristics so as to enhance the nominal ships cross-section and increase the capability to detect and track ships.

(U) (S) Under certain high speeds and shallow depths of travel submarines may produce wakes that are detectible with HF radar.

[redacted]

[redacted]

UNCLASSIFIED

FLEET AIR DEFENSE (FAD) TEST NO. 1A (U)

Organization (U)

(U) ITT-Electro Physics Laboratory/Naval Research Laboratory

Objective (U)

(U) To conduct an initial demonstration of the feasibility of detecting and tracking aircraft with the Fleet Air Defense (FAD) concept using distant sky-wave illumination from a ground-based transmitter and receiving the target reflected energy via a surface wave to a land-based receiver. Compare the concept using two different signal formats.

System Concept-Relation and Importance (U)

(U) An important initial demonstration to ensure there are no major problems in the basic concept prior to proceeding with a shipborne receiver installation. Ensures that dynamic range, target cross-polarization cross-section and clutter can be handled by known technology. The concept is important in providing a silent fleet surveillance capability.

[redacted]

UNCLASSIFIED

UNCLASSIFIED

MONOSTATIC DOPPLER SEA CLUTTER MEASUREMENTS (U)

Organization (U)

(U) Naval Research Laboratory

Specific Objective (U)

(U) Determine the Doppler characteristics of sea clutter using the MADRE radar.

System Concept-Relation and Importance (U)

(U) Provides typical Doppler sea clutter records for the design of pulse Doppler ocean surface surveillance radars. Measurements are limited in frequency range (10-26 MHz) and at a specific fixed frequency at any one time.

UNCLASSIFIED

UNCLASSIFIED

MONOSTATIC HIGH RESOLUTION SEA CLUTTER MEASUREMENTS (U)

Organization (U)

(U) Stanford University

Specific Objective (U)

(U) (S) Determine the amplitude and polarization characteristics of sea scatter in azimuth and FM/CW high resolution techniques.

System Concept-Relation and Importance (U)

(U) (S) It may be possible to detect ships on the surface of the ocean on a power basis. That is if resolution cell size is reduced in range and azimuth until its cross section due to sea clutter is less than that of the ship.

UNCLASSIFIED

[redacted]

SHIP AHOY NO. 1A (U)

Organization (U)

(U) Stanford University

Objective (U)

(U) (S) Investigate the feasibility of detecting ships using an FM/CW technique on a power-only basis by reducing the size of the range azimuth cell.

System Concept-Relation and Importance (U)

(U) (S) The Doppler radar technique will not detect ships with low radial velocities or that are stationary. This concept will permit detection of ships under such circumstances.

[redacted]

BUOY TACTICAL EARLY WARNING (BTEW) TEST NO. 1 (S)

Organization (U)

(U) Raytheon

Objective (U)

(U) (S) Conduct an initial demonstration of detecting aircraft and missiles using the BTEW concept, transmitter on a buoy with a land-based receiver in real-time at short ranges using surface wave propagation.

System Concept-Relation and Importance (U)

(U) (S) The use of the BTEW concept can provide coverage beyond microwave radar coverage and in the skip zone of OHD backscatter skywave radar coverage for CONUS defense and special tactical applications. The technique is not dependent on the ionosphere and can operate after a nuclear detonation. In fact after a nuclear detonation, galactic and other user noise will decrease and coverage of this concept will be increased.

BUOY TACTICAL EARLY WARNING (BTEW) TEST NO. 2 (S)

Organization (U)

(U) Sylvania

Objective (U)

(S) Conduct an initial demonstration of the detection of aircraft using the BTEW concept. transmitter on a buoy with a land-based receiver in real-time at long ranges using surface wave ; ;agation from transmitter to aircraft and sky-wave from aircraft to receiver.

System Concept-Relation and Importance (U)

(U) (S) The use of the BTEW long range concept should extend the range of SLBM and aircraft coverage beyond the range of OHD sky-wave backscatter radar.

END

DATE
FILMED
5-71

UNCLASSIFIED
~~SECRET~~

#196
AD 509068 ✓

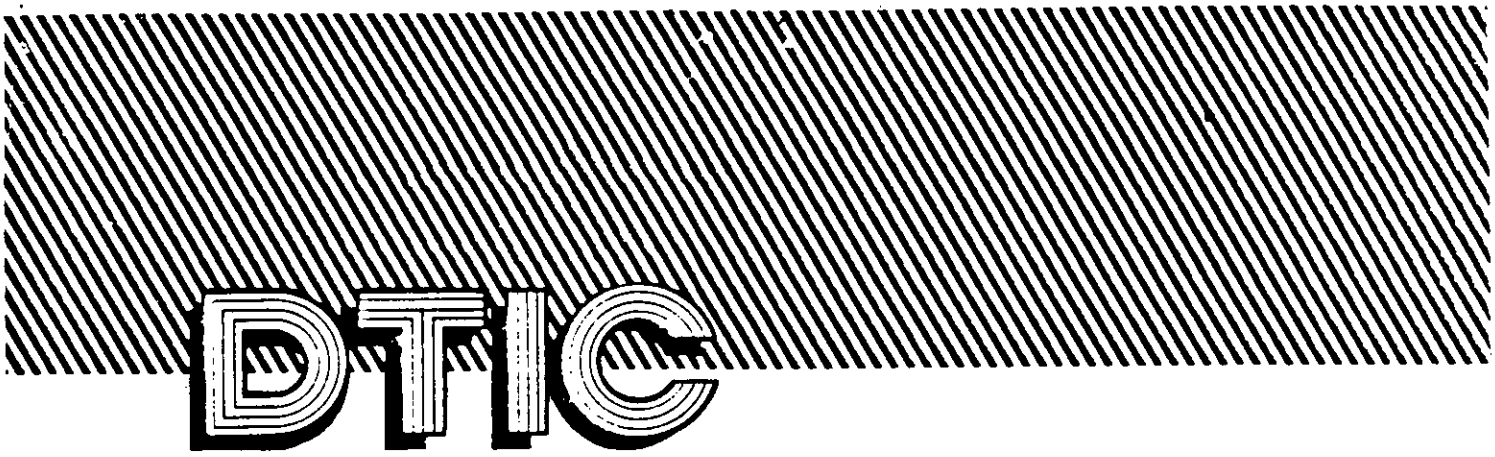

EXCISED UNDER THE PROVISIONS OF THE
FREEDOM OF INFORMATION ACT 5USC552
(b) (1)

Technical Report

THIS DOCUMENT HAS BEEN DOWNGRADED
TO UNCLASSIFIED
Per Director DIA, SAIO/TIO

NOV 17 1992

distributed by

PP 10-15

Defense Technical Information Center
DEFENSE LOGISTICS AGENCY
CAMERON STATION, ALEXANDRIA, VIRGINIA 22304-6145

UNCLASSIFIED
~~SECRET~~

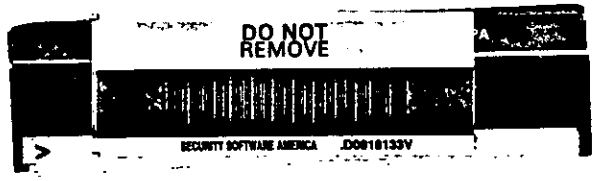

NOTICE

We are pleased to supply this document in response to your request.

The acquisition of technical reports, notes, memorandums, etc., is an active, ongoing program at the Defense Technical Information Center (DTIC) that depends, in part, on the efforts and interests of users and contributors.

Therefore, if you know of the existence of any significant reports, etc., that are not in the DTIC collection, we would appreciate receiving copies or information related to their sources and availability.

The appropriate regulations are Department of Defense Directive 3200.12, DoD Scientific and Technical Information Program; Department of Defense Directive 5200.20, Distribution Statements on Technical Documents (amended by Secretary of Defense Memorandum, 18 Oct 1983, subject: Control of Unclassified Technology with Military Application); Military Standard (MIL-STD) 847-B, Format Requirements for Scientific and Technical Reports Prepared by or for the Department of Defense; Department of Defense 5200.1R, Information Security Program Regulation.

Our Acquisition Section, DTIC-DDAB, will assist in resolving any questions you may have. Telephone numbers of that office are: (202)274-6847, 274-6874 or Autovon 284-6847, 284-6874.

FEBRUARY 1984

☆ U.S. Government Printing Office 1985—461-169/35047

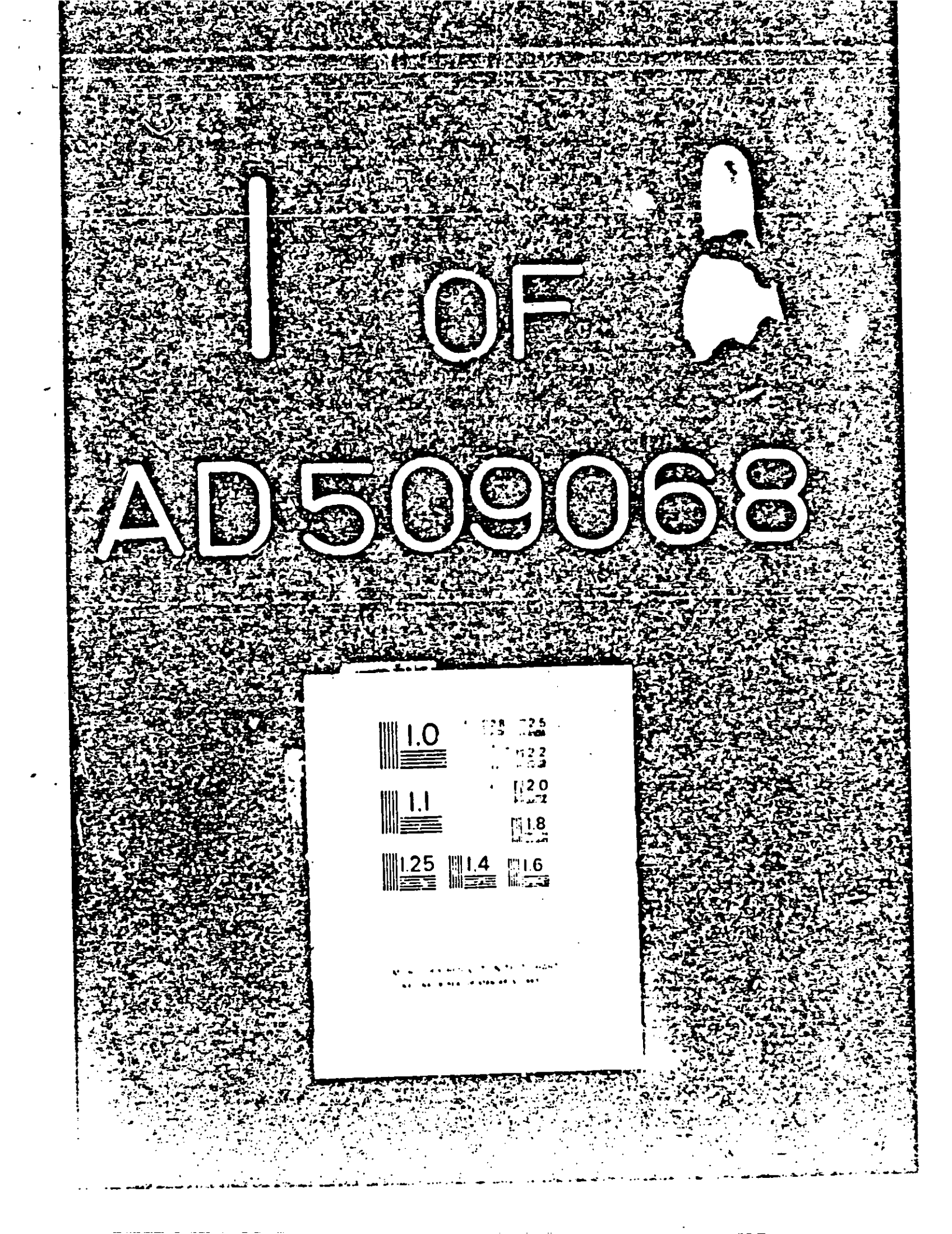
1 OF
AD509068
1.0
1.1
1.25
1.4
1.6
1.8
2.0

SECURITY MARKING

The classified or limited status of this report applies to each page, unless otherwise marked.
Separate page printouts MUST be marked accordingly.

THIS DOCUMENT CONTAINS INFORMATION AFFECTING THE NATIONAL DEFENSE OF THE UNITED STATES WITHIN THE MEANING OF THE ESPIONAGE LAWS, TITLE 18, U.S.C., SECTIONS 793 AND 794. THE TRANSMISSION OR THE REVELATION OF ITS CONTENTS IN ANY MANNER TO AN UNAUTHORIZED PERSON IS PROHIBITED BY LAW.

NOTICE: When government or other drawings, specifications or other data are used for any purpose other than in connection with a definitely related government procurement operation, the U.S. Government thereby incurs no responsibility, nor any obligation whatsoever; and the fact that the Government may have formulated, furnished, or in any way supplied the said drawings, specifications, or other data is not to be regarded by implication or otherwise as in any manner licensing the holder or any other person or corporation, or conveying any rights or permission to manufacture, use or sell any patented invention that may in any way be related thereto.

~~SECRET~~

UNCLASSIFIED

EDL-Q915

COPY NO. ___ OF 30 COPIES

AD509068

PROJECT AQUARIUS ANNUAL REPORT (U)

By
R. KRULEE
K. SNOW

THIS DOCUMENT HAS BEEN REDOWNGRADED
TO UNCLASSIFIED
Per Director DNA SEC/TTO
NOV 17 1992

1 JUNE 1970

DDC
RETURNED
JUN 4 1970
RELEASED
DDC CONTROL
NO. 01602

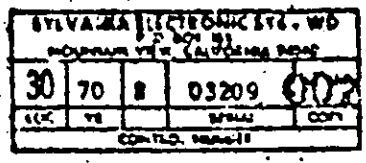

[redacted]

[redacted]

UNCLASSIFIED

Sylvania Electronic Systems-Western Division
Electronic Defense Laboratories
Mountain View, California

EDL-G915

Project AQUARIUS Annual Report (U)

Principal Investigator R. Krulee 415/966-2904
Project Engineer K. Snow 415/966-3186

ARPA Order No. 1459
Effective Date of Contract: 2 June 1969
Contract Expiration Date: 30 June 1970
Amount of Contract: $118,864

This document contains information affecting the national defense of the United States within the meaning of the espionage laws, Title 18 U.S.C. Sections 793 and 794. The transmission or the revelation of its contents in any manner to an unauthorized person is prohibited by law.

This research was supported by the Advanced Research Projects Agency of the Department of Defense and was monitored by the Office of Naval Research under Contract No. N00014-69-C-0446

(U) TABLE OF CONTENTS (U)

Section	Title	Page
1.	INTRODUCTION	1
2.	SYSTEM CONSIDERATIONS	3
3.	STATEMENT OF PROBLEM AREAS	7
3.1	Effective Radiated Power	7
3.2	Surface Wave Losses	7
3.2.1	Surface Waves Region I	7
3.2.2	Medium Height Antenna Region II	10
3.2.3	High Antenna Region III	10
3.3	Effective Target Area	12
3.4	Sky Wave Propagation	17
3.5	Noise at Receiver	21
3.6	Receiving Antenna	21
4.	EXPERIMENT DESIGN	23
5.	ANALYSIS	29
6.	SUMMARY	30
7.	RECOMMENDATIONS	32
8.	REFERENCES	33

(U) TABLES (U)

Table	Title	Page
1	Monostatic HF Backscatter Radio Cross Sections	14
2	Reflected Power from Target	25
3	Incident Skywave Signal Power (dbm)	28

Figure	Illustrations	Page
1	Areas of Coverage for Buoy-Mounted Transmitter	4
2	Basic Transmission Loss for Ground Wave Along the Ocean. Propagation in Upwind-Downwind Direction.	9
3	The Variation of Field Intensity with Numerical Antenna Intensity with Numerical Antenna Height for Low Antennas.	11
4	Typical Diurnal Variation of Critical Frequency for January at Latitude 40 Degrees. (From Ref. 2)	18
5	Typical Values of Midday Ionospheric Absorption. (From Ref. 2)	20
6	Typical Average Noise Level in a 6-Kc Band. (Ref. 2)	22
7	Sketch of Basic Propagation Model.	25

Section 1.

1. (U)(S) INTRODUCTION (U).

For the past year several companies have joined in Project MAY BELL under ARPA sponsorship to investigate the feasibility of detecting low-flying aircraft and Submarine Launched Ballistic Missiles by use of high frequency electromagnetic waves. In particular, a number of tests have been made by Raytheon using a shore-mounted transmitter for generating a surface wave mode while Sylvania has conducted a smaller number of tests using a buoy-mounted transmitter with reception being accomplished via sky-wave at a remote site in Virginia. The transmitters and surface wave receiving sites as well as the controlled aircraft flight patterns have all been on or near the East coast of Florida.

The results of the initial tests of this target detection technique were presented in an earlier report written during this project. In that report it was shown that an aircraft flying approximately 20 km from a 2000 watt low power HF transmitter could be detected. While sufficient detections of aircraft were accomplished to demonstrate the feasibility of such a system, insufficient data has been gathered to date to permit development of a proper system concept to provide a complete coastal defensive system. In particular, there are many parameters that inter-relate the ground-wave-sky wave mode that have not been examined or tested in detail These include variations in frequency, path loss with time of day, season, etc. A firm understanding of how a system can be developed to provide the necessary operational capability does not yet exist.

In this report, the basic parameters that can lead to a system definition for the surface wave-sky wave mode are considered by first evaluating known theory and experimental data. A set of experiments is then

UNCLASSIFIED

1. (U) (S) -- Continued.

proposed that can provide the additional details necessary to complete the definition phase of the program. This will involve measurements of the variation in total path loss with respect to

1) Time
2) Season
3) Frequency
4) Target Aspect Angle
5) Sea State
6) Distance
7) Propagation Mode

The resultant data, when coupled with suitable analysis will provide the necessary evaluation of the following basic system requirements:

1) Probability of detection
2) False Alarm Rate
3) Time Availability
4) Volume of Coverage
5) Number of Sites
6) Power Requirements

UNCLASSIFIED

2. (U) (S) SYSTEM CONSIDERATIONS (U).

Since the purpose of this portion of the program is to detect low flying aircraft and missiles at low altitude in order to provide early warning along the sea coasts, where the basic method involves both a surface wave over sea water plus a sky wave to the receiver, it is apparent that a single transmitter will provide essentially a circle of coverage; and hence, many such overlapping circles are needed for reliable detection as shown in Figure 1. It is apparent that more than one receiver site will be required since skip zones are known to exist for sky wave propagation.

More importantly, from a system standpoint, it is necessary to provide a good probability of detection for a significant portion of time while, at the same time, maintaining a reasonable false-alarm rate. Thus, the parameters of the system must be determined in terms of the system requirements with various trade-offs being possible to maximize the cost-effectiveness.

In order to determine the system parameters it is necessary to combine available data with experimentation in such a way that new data is generated with sufficient statistical accuracy to place bounds on the parameters. This process consists of the following steps:

1) State the problem.
2) Formulate the hypotheses.
3) Devise experimental techniques.
4) Examine possible outcomes with reference back to the reason for the problem to assure the experiment provides adequate information.

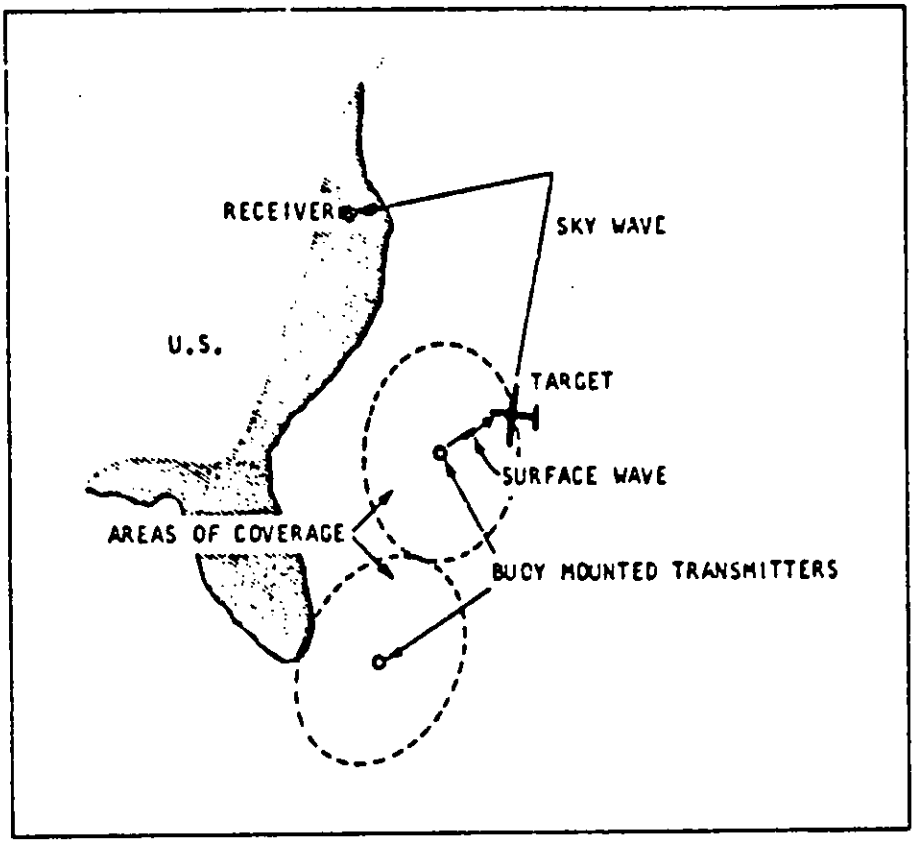

Figure 1. (U) Areas of Coverage for Buoy-Mounted Transmitters (U)

2. (U) -- Continued.

5) Consider the possible results as well as the statistical methods to be applied, to assure that the conditions necessary for the methods to be valid are satisfied.

6) Do the experiment.

7) Apply the statistical methods to the collected data.

8) Draw conclusions, with measures of reliability and confidence limits included, and with due care as to the validity of the conclusions as they apply to the problem and results.

While the above sequence appears to lead in a straight-forward manner to the required results (in this case, the system specifications and parameters), a serious problem arises due to the time-varying statistics of the various paths. For example, the propagation of radio waves over water has been studied in the past by many people (7, 8, 11) however, variations in the path loss occur because of sea state, wind, etc. and the statistics of these variations do not obey any simple law. The same problem of statistical variation will also occur in the radiation patterns from the transmitter antenna, the sky-wave mode and the scattering coefficient of the target.

It should also be noted that the available data on these problem areas does not, in general, represent average values, but usually applies only to the best conditions with a non-zero mean associated with the variations. It should also be noted that most of the data concerning propagation over a sky-wave mode is time dependent with very large changes occurring both for time of day and season of the year. It has also been found that the values are dependent upon geometry and geographical location.

UNCLASSIFIED

2. (9) (8) -- Continued.

In summary then, the purpose of this set of experiments is to evaluate the statistical variations of the system so that suitable parameters can be selected to provide a good probability of detection for an acceptable percentage of time with a reasonable false alarm rate. The desired parameters will thus have to be selected to accommodate essentially "worst-case" conditions, and these are obviously not changed by taking more data.

UNCLASSIFIED

Section 3.

3. (U) STATEMENT OF PROBLEM AREAS. (U)

Consider a model which contains a buoy-mounted transmitter with a vertical antenna, a reflecting target flying over the ocean and a receiving site with a high-gain antenna located sufficiently far from the target so that propagation occurs via sky-wave.

The basic problem is to specify the parameters so that a predetermined signal to noise ratio will be exceeded with high confidence at the receiving site. The following six areas should be investigated:

1) Effective radiated power and antenna coupling.
2) Surface-wave losses to target.
3) Scattering or reflection coefficient of target.
4) Sky-wave losses to receiver.
5) Effective noise at receiver.
6) Receiver antenna gain.

3.1 (U) Effective Radiated Power.

The first problem, that of effective radiated power includes the variations of received power due to motion of the ocean. Thus, if the transmitter power, feedline and antenna efficiencies are known, the far field can be measured and compared with numerous field intensity charts such as those of reference 2. Variations will occur since the sea at these frequencies acts as a reflector which unfortunately is moving with time.

3.2 (U) Surface Wave Losses.

While the surface wave attenuation must be valuated, it may to some extent be inseparable from the above antenna gain problem unless a calm sea and a stable platform are used. A number of theories exist for ground wave propagation and they also include the effects of an elevated target or receiver. It should be noted, that the purpose of this experiment is not to develop a new theory but rather to determine the variations in path loss so that reliable detections can be achieved.

Norton [7] has studied propagation over a spherical earth and has shown that there is significant variation in field strength of a surface wave as a function of height; he considers three regions

$$h = 0$$
$$h \leq (2000/f^{2/3}) \text{ feet}$$
$$h > (2000/f^{2/3}) \text{ feet}$$

where f is in megahertz.

3.2.1 (U) Region 1 - Surface Wave.

When both transmitting and receiving antenna (or target) are near the ocean surface the direct and reflected waves cancel and only the surface wave exists. The important component is the one for vertical polarization because of the high conductivity of sea water which attenuates the horizontal component. Thus, the surface wave attenuation approaches the values given by theory for a perfectly conducting sphere. Barrick [11] has also included the effects due to roughness and has published detailed data for various sea states and frequencies as shown in Figure 2. It should be noted that the basic loss is for a sphere and not a perfectly conducting plane.

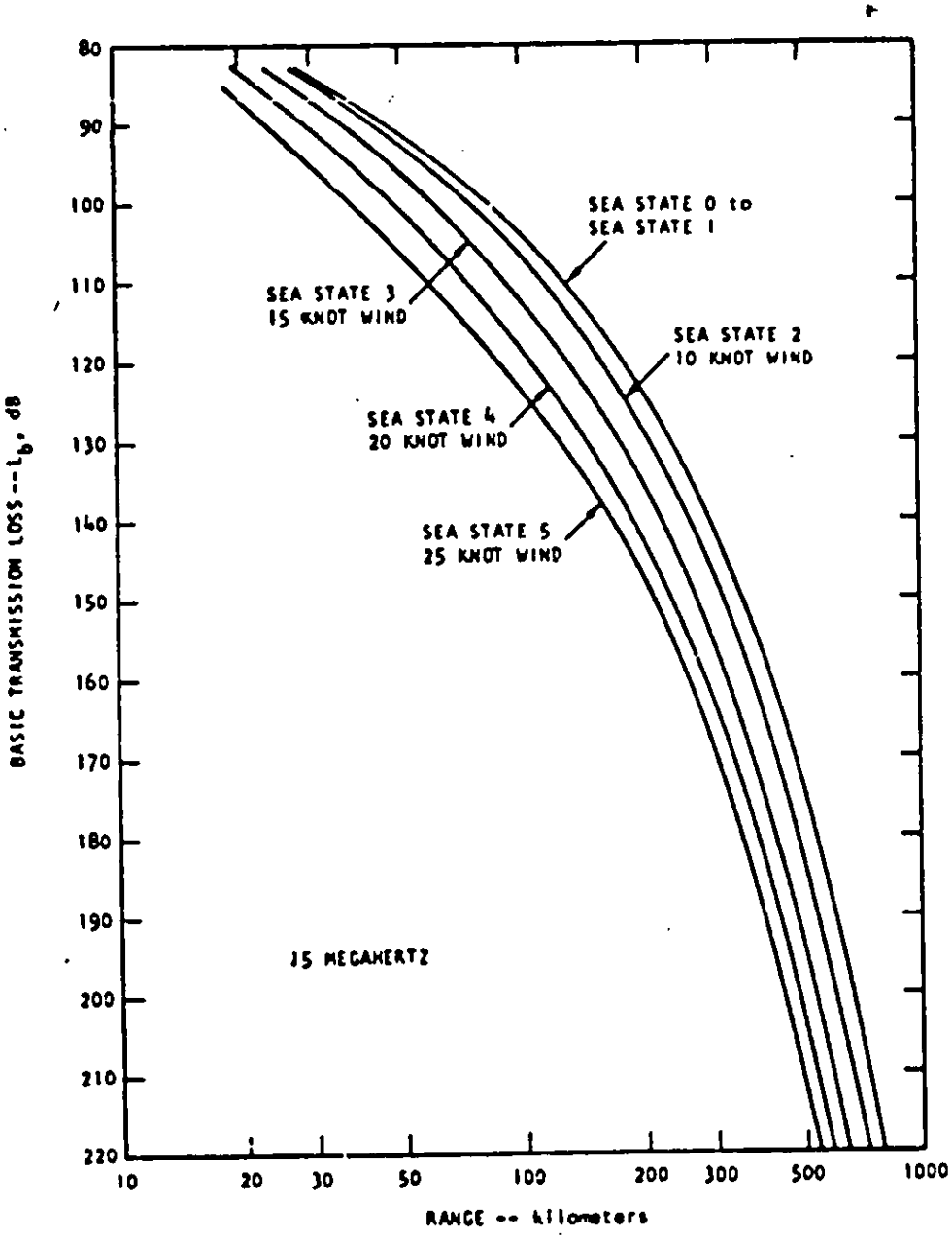

Figure 2. (U) Basic Transmission Loss for Ground Wave Along the Ocean. Propagation in Upwind-Downwind Direction. (U)

3.2.2 (U) Region II - Medium Antenna Heights.

In this region Norton [7] has determined a height-gain function and it is only necessary to multiply the surface wave field by the functions $f(q_1)$, $f(q_2)$ defined by Norton for the transmitting and receiving antenna heights as shown in Figure 3.

3.2.3 (U) Region III - High Antenna.

When the transmitting and/or receiving antenna are high, the earth's curvature affects the field strength both within and beyond line-of-sight points. The basic ground-wave field strength must be multiplied by a factor depending upon whether the path is line-of-sight or not. At sufficiently high altitudes the field intensity has been found to decay exponentially with increasing height.

At points within line-of-sight the earth's curvature must be considered since the plane wave reflection coefficient is different for a curved surface than for a plane. Also the curved surface reflection causes the energy to diverge more than is indicated by the inverse square law, and hence a divergence loss factor must be included. It is apparent that these factors affect not only the transmitter to target path but also the target to receiver path since the target acts as a radiator after reflection. Barrick [11] has also modelled a surface wave and calculated the path loss variations with sea state and height for the HF band. His results are very similar to Norton.

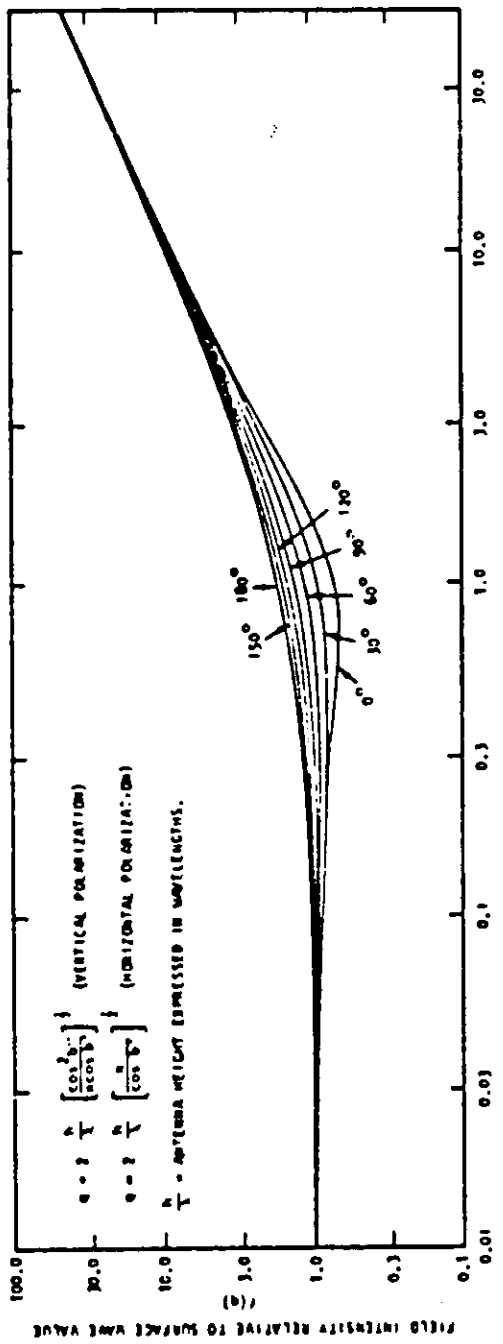

Figure 3. (U) The Variation of Field Intensity with Numberical Antenna Height. (U)

3.3 (U) Effective Target Area.

The evaluation of a meaningful target cross-section for an aircraft is difficult, since a complex target such as an aircraft may be considered as madeup of a large number of independent objects which scatter energy in all directions. Skolnik[9] has shown that the cross-section fluctuation from a "simple" scatterer can vary over a ratio of 4 to 1 which would introduce scintillation in the signal and hence doppler spreading.

Target aspect angle (TAA) can have considerable impact upon the reflected or scattered RF energy impinging on the target. Some of the information available at EDL on the HF radar cross-sections of aircraft and missiles is contained in references 4 and 5, however, it should be emphasized that these measurements were made for back-scattered energy and may not be correct for forward or sideward scattering. The difficulty is that the target area not only affects the amount of required transmitter power, but also because the sizes of typical aircraft and missiles are on the order of a wavelength at these frequencies that the choice of operating frequency may be influenced. Thus, appropriate targets must be evaluated in terms of the goals of this program. Some of their conclusions are:

1. The fine structure (nose cone, tail fins, etc) with dimensions considerably smaller than a wavelength has negligible effect on the cross-section at any aspect, except in the direction of deep nulls where the depth of the null is somewhat affected.

2. The HF broadside cross-sections of rockets and large aircraft are of the order of several hundred square meters.

(U)

3.3 (U) -- Continued.

3. The particular cylinders studied showed a deep null end-on if the length of the cylinder is less than one wavelength. If the length is greater than one wavelength, another null develops at 20° from broadside.

4. The depths of the above nulls can exceed 30 db below the broadside response.

5. The cylinder aspect ratios studied had length to diameter ratios L/D = 10 to 14. A rotation of the cylinder about an axis normal to its longitudinal axis and parallel to the Poynting vector resulted in a slowly varying response (polarization sensitivity) with nulls not exceeding 6 db.

Table I is taken from Reference 5 and shows nulls, null depths, and cross-sections as a function of frequency. Great variations in null depths are shown - as well as large variations between peaks and nulls. For example, the peak-to-null variation of the KC-135 shows 27.3 + (-15) db or a total variation of 42.3 db. It is obvious from these results that both aircraft and missiles present scintillating targets with wide signal variations.

It is interesting to note tha. only two out-of-plane measurements were made - these on the KC-135. They showed -15 to -19 db nulls at the same frequency. The apparent cross-section did not change significantly, however. Since the impinging RF energy from the buoy antenna will not always be exactly in-plane for an aircraft target, an even more complex null structure can be expected as the out-of-plane angle varies.

TABLE I. (U) ~~(S)~~ MONOSTATIC HF BACKSCATTER RADIO CROSS SECTIONS FOR AIRCRAFT TARGETS BASED ON X-BAND MODEL RANGE STUDIES (U). (Reference 5)

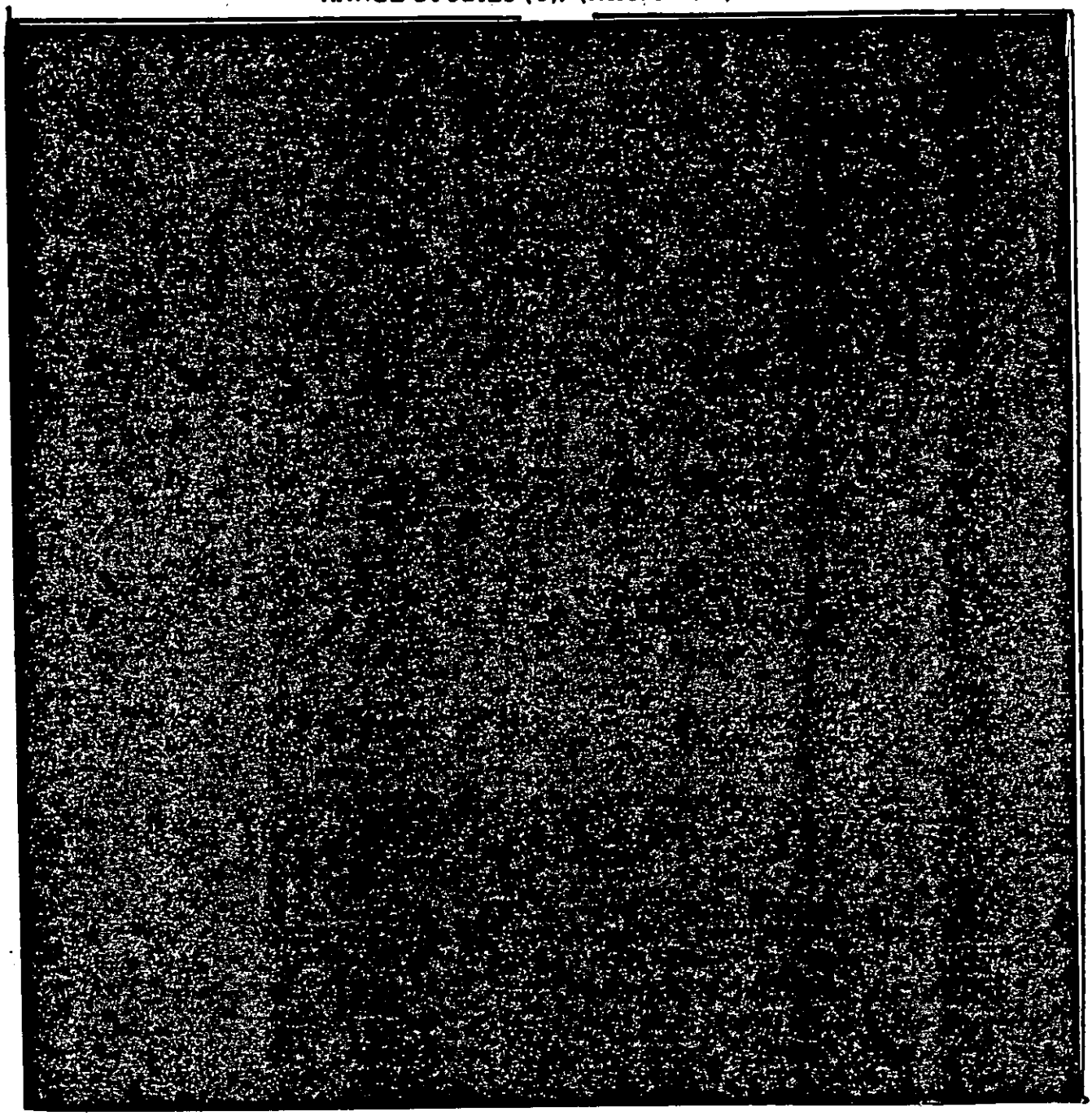

TABLE I (U) -- Continued.

[redacted]

Soviet			
BISON	E Polarization	15	1200 (max) -18 db (min)
	H Polarization	15	164 (max) -12 db (min)
BEAR	E Polarization	15	1800 (max)
	H Polarization	15	1010 (max)
TU-104	E Polarization	15	215 (max) -12 to -15 db (min)
TU-16	H Polarization		762 (max) -12 db (min)

(U)

TABLE I (S) -- Continued.

MIG 19	E Polarization	15	450 (max)
	H Polarization	15	50.5×10^{-6} (max) min at -17 db
MIG 21	E Polarization	6	388 (max) -22 db nulls at ±90°
	H Polarization	8.56	816 (max) -25db nulls at ±90° several nulls at ± 90°
MIG 21	E Polarization	15	258 (max) -18 db nulls)
	H Polarization	15	12.4 (max) min of -9 db no nulls

3.4 (U) Sky-Wave Propagation.

The frequency chosen for this experiment must be examined carefully so that the disadvantages of HF propagation are minimized. Some of the disadvantages of using HF are:

1) The variability of propagation conditions which could require changes in operating frequency.

2) The large number of possible propagation paths with resulting time dispersion of the signal due to multiple modes of propagation.

3) The large and rapid phase fluctuations.

4) The possibility of high interference rates due to multiple modes of propagation.

For example, Figure 4 shows the typical diurnal variation of the critical frequency at one specific latitude and season for high and low sunspot numbers.

A low frequency is needed to get below the nighttime maximum useable frequency (MUF), and a higher frequency is needed in the daytime that is both below the MUF yet above the region of high absorpiton. Implicit in this discussion of first-order factors is the fact that a lower useable frequency (LUF) exists and is a function of absorption, incident field strengths, receiver noise levels, and receiving site noise environment.

At medium frequencies, it is possible that the groundwave and skywave ranges overlap with the result that severe fading can occur when the two signals are of comparable amplitude. The path length is thus a consideration as well as the frequency chosen for the experiment.

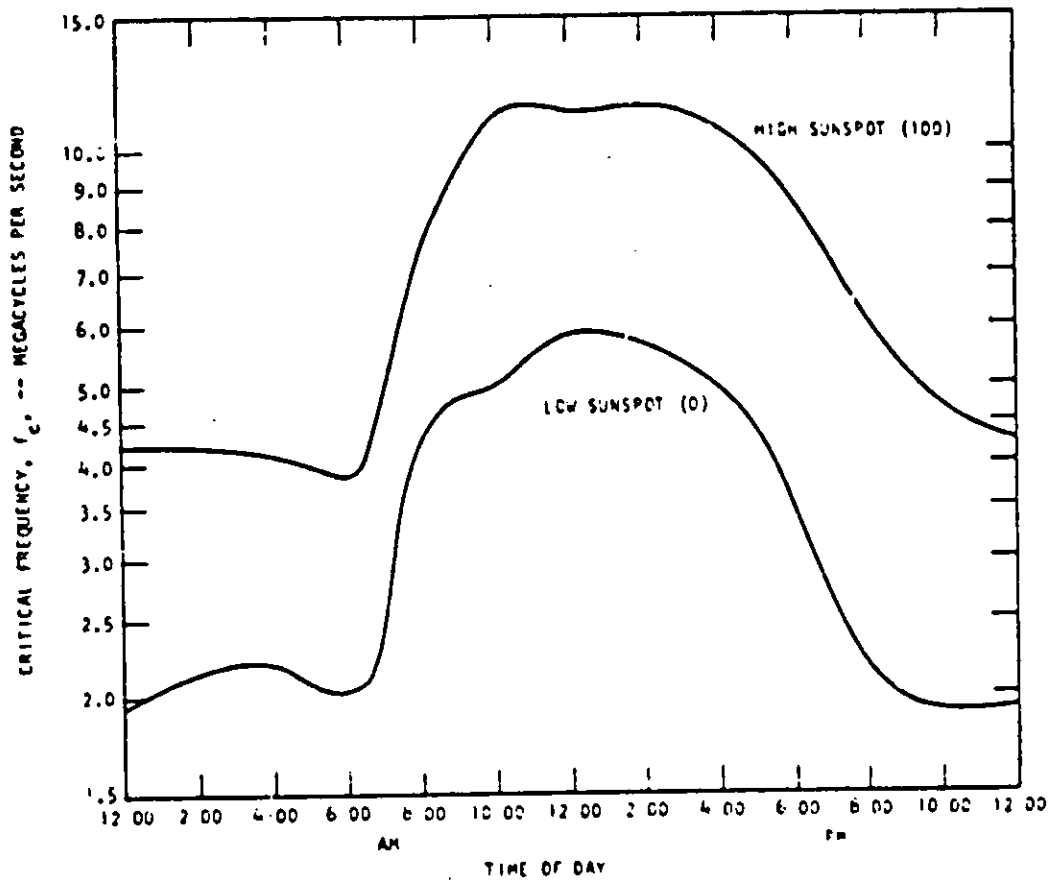

Figure 4. Typical Diurnal Variation of Critical Frequency for January at Latitude 40 degrees (From Ref. 2). (U)

3.4 (U) -- Continued.

Where Figure 4 showed diurnal variations of critical frequency at one latitude for one season of the year, Figure 5 shows typical values of absorption at midday. This is a maximum and depends upon the angle of the sun in relation to the horizon. On short paths, this is the actual path length and not the distance along the earth.

In order to evaluate the proper frequencies of operation, it will be necessary to determine experimentally the variation in path loss with frequency. Certain assumptions can be made to limit the amount of experimentation needed for a manageable program. These are:

1) The receiver site noise environment and minimum detectable signal threshold are accurately known.

2) The effective radiated power (ERP) of the buoy-mounted transmitter and antenna is accurately known or can be predicted.

3) The HF radar cross-section of target aircraft is at least 20 meters^2 at all aspect angles.

4) The receiving site antenna gain is known accurately.

5) The midpoint of the skywave path is known or can be predicted.

6) The ionosphere midpoint is stable or its variation can be predicted.

7) The instrumental inaccuracies are known or can be controlled.

8) The buoy swing or sea state will not affect the measurements of path loss.

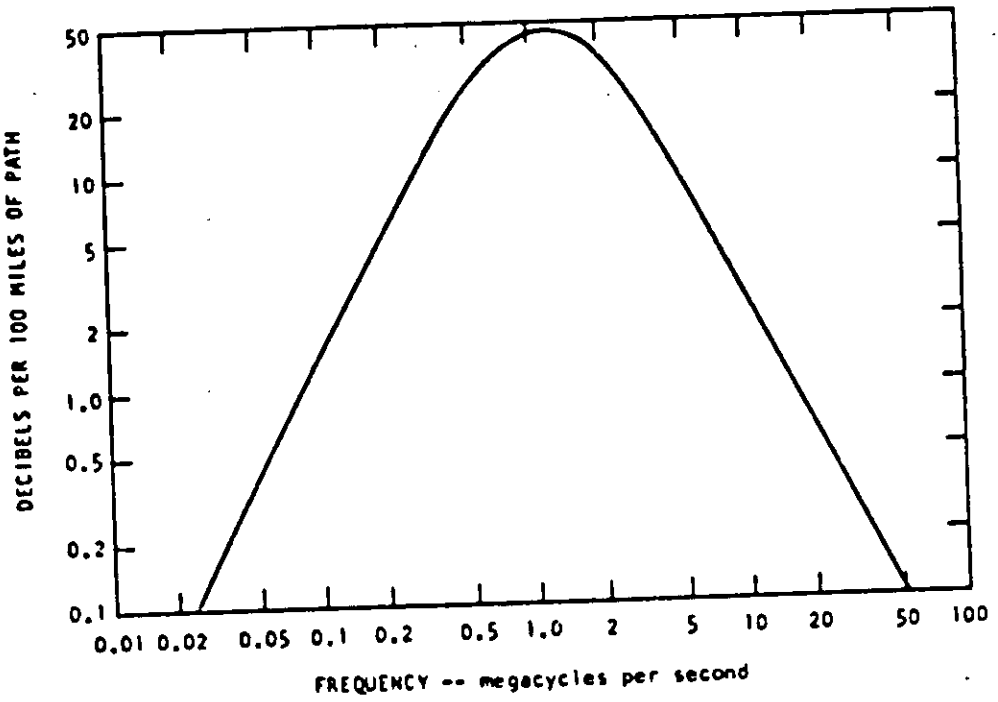

Figure 5. (U) Typical Values of Midday Ionospheric Absorption (From Ref 2) (U)

3.4 (U) -- Continued.

9) The weather effects on the atmospheric refractive index are negligible.

3.5 (U) Noise at the Receiver.

Figure 6 shows typical noise in a 6-kc bandwidth for a latitude of 40° averaged over a year. Summer averages will be a few db higher while winter averages will be a few db lower. The noise level will vary with latitude, however, the particular receiving site is fixed so that more accurate noise determinations could be made and a suitable correction factor applied to any experimental results.

3.6 (U) Receiving Antenna.

The transmitting antenna will be by necessity limited to a simple vertical and may be quite short compared to a wavelength so that its efficiency as a radiator will be low. The receiving antenna can be quite efficient providing the chosen frequency is not too low. Depending upon the spatial separation of arriving signals from more than one buoy, the receiving antenna may have to be rotatable -- or consist of a steerable array so that optimum receiving conditions can exist. The better the receiving antenna, the greater the depression of the LUF.

UNCLASSIFIED

Figure 6. (U) Typical Average Noise Level in a 6-kc Band (Ref 2) (U)

UNCLASSIFIED

4. (U) EXPERIMENT DESIGN (U).

Because the end measurement of this experiment is related to doppler shift, it becomes apparent that a slow moving vehicle -- such as a surface vessel -- is of limited use as a target in evaluating path loss. In addition, a helicopter platform is considered less desirable because of low speed, unknown cross-section, and rotor modulation effects. A relatively high speed aircraft -- up to Mach 1 as a target vehicle -- appears to be a viable solution, but is subject to some contraints. The aircraft should be large enough to assure an adequately large cross-section, and for over-water operations it should be multi-engined. Since the target is passive, it need not require more than a single seat aircraft, such as the F-101. The cross section of the target aircraft should be known accurately from model measurements.

To cover the effects of diurnal variation, flights must be made often enough during every 24 hours to provide sufficient statistical data. In addition, seasonal variations require that experiments must also be carried out over a period of months so that seasonal effects may be taken into account. It may be possible to linearly interpolate for values over longer period effects such as sunspot number variation, but this is mere conjecture at this time. Additional study is needed to determine the length and frequency of tests.

Since the target aspect angle is a vital parameter, many flight paths may be necessary -- at different altitudes -- to provide sufficient statistical data which may be processed to provide meaningful results. The aircraft should be flown in constant radius circles around the buoy to provide general contours. Cross-hatch flight paths can then be used to provide the

4. (U) ~~(S)~~ -- Continued.

variable aspect angle data as well as provide check points where the circular paths are intersected. Again, it should be realized that these flights must take place at several different altitudes and should be numerous as possible to provide a sufficient data base for statistical analysis. Reference to Table I included earlier in this report shows the larger values of cross-section are 1800 meters^2 so that an assumed 20m^2 in the equation below represents a worst case.

The reflected power can be expressed as

$$P_{ref} = \frac{P_t G_t \sigma}{(4\pi D)^2} \qquad (3)$$

where:

P_{ref} = Power reflected from the target

P_t = Power of the transmitter

G_t = Gain of the transmitting antenna

σ = Target cross section

D = Distance from transmitter to target (same units as σ)

The reflected power (P_{ref}) is calculated for various distances D in Table II assuming an effective radiated power ($P_t G_t$) of 1000 watts. Table II shows the large variation in reflected power with distance or volume of coverage.

UNCLASSIFIED

4. (U) -- Continued.

TABLE II. REFLECTED POWER FROM TARGET. (U)

Distance in Miles	Reflected power in dbm
1	-12
2	-18
5	-26
10	-32
20	-38
50	-46
100	-52

A sketch of the basic propagation model is shown in Figure 7 below with various portions of the path labelled.

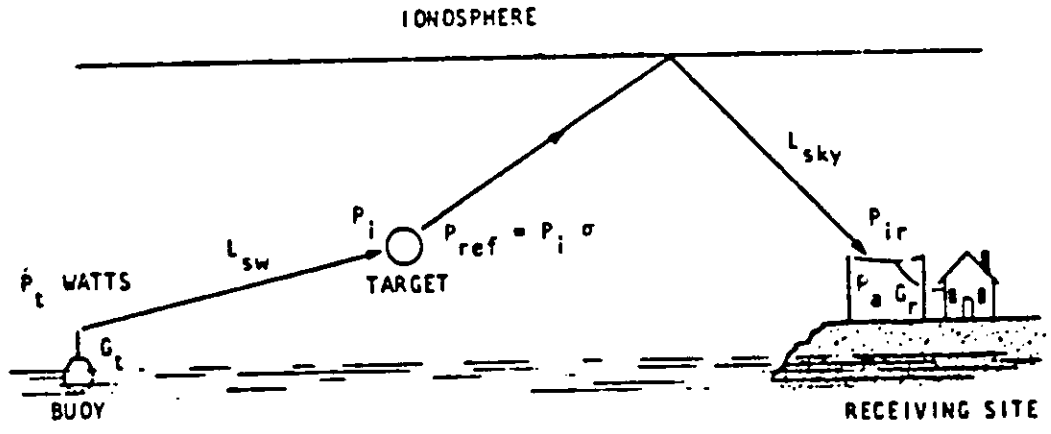

Figure 7 (U) Sketch of Basic Propagation Model. (U)

4. (U) (S) -- Continued.

The following equations apply to this model.

$P_r = T_p - L_{loss} + G_t$ = ERP (in dbm)

T_p = Transmitter Power, L_{loss} = Line loss, and G_t = Antenna Gain

L_{sw} = Surface Wave Losses

P_i = Power Incident on Target

P_{ref} = P_i times Target Reflection Coefficient (see Table II)

L_{sky} = Skywave Path Loss (including ionospheric losses)

P_{ir} = Skywave power incident at receiver antenna

P_a = P_{ir} time G_r = Total Signal Power at receiver ($P_{ir} + G_r$ in dbm)

$$P_a = P_{ref} - L_{sky} + G_r \quad (4)$$

$$P_{ref} = (P_i)\ (\text{Reflection Coefficient}) \text{ where } P_i = P_r - L_{sw} \quad (5)$$

Note that this does not take into account receiver noise figures, bandwidths, nor interference. The standard logarithmic form for free-space transmission loss, L between two isotropic antennas is given by:

$$L = 20 \log_{10} D + 20 \log_{10} f + 36.581 \quad (6)$$

where D is in miles and f is in megahertz. Path loss cannot be less than the free-space loss so that one can, after Norton (8), state the following:

$$L_{trans} = L - G_t - G_r + A \quad (7)$$

where L_{trans} - System Transmission Loss

G_t, G_r = Transmitting and Receiving Antenna gains above isotropic

A = Propagation path loss relative to the free-space value L.

4. (U) (S) -- Continued.

In cases where it is possible to determine the effective values of transmitting and receiving antenna gain, equation (7) may be used to determine the value of A. It becomes impossible, however, to separate the antenna gains under conditions of multipath ionospheric propagation. With multipath propagation the only values that can be measured are P_r and P_a. Thus, one must be satisfied with only an overall transmission path loss value.

To see why this is so, let d_j denote the distance and a_j the voltage attenuation factor corresponding to the j-th ionospheric path. Let g_{tj} and g_{rj} denote the power gains of the transmitting and receiving antennas for this particular path. The average signal power available from the receiving antenna P_a, is then (from Norton - Ref. 8):

$$P_a = P_r \lambda^2 \sum_{j=1}^{m} a_j^2 \, g_{tj} g_{rj} / (4\pi d_j)^2 \qquad (8)$$

This is the generalized form of equation (7) above and is obtained by summing the signal powers available from the separate paths. It is impossible to extract the transmitting and receiving gains from the summation sign, and so it is impossible to separate out either an inverse distance factor, ERP, or the received field intensity.

Referring to Figure 2 and Equations (4) and (5), it appears that one could measure (or calculate) both ERP and the surface wave loss, L_{sw}. The figures given in Table II show total reflected power. If it is assumed that this is equivalent to the power that is reflected toward the ionosphere in the direction of the receiving site, then the target can be considered as a "virtual" transmitter with those values in Table II as the ERP. The sky wave loss, L_{sky}, can be calculated by assuming no other losses than the free-space

4. (U) -- Continued.

loss. This would be approximately true for nighttime conditions, but an absorption factor would have to be added for any portion of the path which is in daylight.

Taking the values from Table II as the target ERP and calculating the path loss for 100, 500, 1000, and 1500 mile skywave distances for a 5 Mcs transmission frequency, we obtain the incident skywave signal power (dbm) at the receiving site (see Table III).

TABLE III (U) INCIDENT SKYWAVE SIGNAL POWER (dbm) (U)

Target ERP dbm	Transmission Distance in Miles			
	100	500	1000	1500
-12	-107	-121	-127	-131
-18	-123	-127	-133	-137
-26	-121	-135	-141	-145
-32	-127	-141	-147	-151
-38	-133	-147	-153	-157
-46	-141	-154	-161	-165
-52	-147	-161	-167	-171

Included in the above table is the assumption of a single hop skywave propagation mode as well as an arbitrary 4 db loss due to ionospheric reflection. This number is conservative since it depends upon the reflection coefficient of the ionosphere, and could be significantly higher (10). In addition any receiving antenna gain is not included in the table.

UNCLASSIFIED

Section 5.

5. (U) ANALYSIS.

As mentioned before, the purpose of any experimental program is to develop systems specifications. Therefore, the data taken at best represents sample points from the total possible variation for the various portions of the model. It will then be necessary to apply standard statistical techniques to determine the mean values and the various percentiles about the mean. This in turn can be readily translated into the more usual parameters of power, antenna gain, volume of coverage, etc.

In addition, to the usual analysis, it will be necessary to examine the data to evaluate whether dependence exists on the various portions of the path and also to determine variations with time, geographical location, etc., since it is quite likely that any system would require a control link in order to maintain optimum parameters while accommodating the known variations in the system.

UNCLASSIFIED

UNCLASSIFIED

Section 6.

6. (U) (S) SUMMARY.

The following parameters contribute the most uncertainty to the experiment.

1. Frequency - must be chosen to minimize interference yet provide a sufficiently stable signal with time. In all probability, at least two frequencies will be necessary -- one for daytime use and one for nighttime use.

2. Path Length - the path length must be chosen so as to minimize any possible self-interference problems -- i.e., the ground wave coverage area must not include the receiving site, but the skywave path should be long enough for reliable modes.

3. Target Aspect Angle - the only data available on TAA is data which was taken in the horizontal plane. As such any inclined plane nulls are not plotted, except in two cases on the KC-135 aircraft. Since incident RF energy on the target will not always fall exactly in the horizontal plane (broadside) cross-sections will vary over some unknown range.

4. Null Depth Variations - a given target has shown null variations of over 30 db, therefore, any flight path will have to be carefully controlled so the effects of the nulls may be accounted for.

5. Receiving site Noise Environment - this is not expected to seriously affect the experiment since the mean value and seasonal variations of ambient noise should be available from CCIR 322.

6. Absorption - this is a variable correction factor and is proportional to the sun's angle with the horizon as well as being frequency sensitive.

UNCLASSIFIED

6. (U) (S) -- Continued.

7. Platform - the recommended platform is a multi-engine, high performance aircraft, and preferably one whose cross-section is known.

8. Altitudes - several altitudes for the target will be necessary because the field strength is both altitude and frequency sensitive.

9. Measurement Tolerances - some determination of the possible ranges of tolerance will be needed in all areas of implementation, not only to size the experiment, but to judge its impact on the collected data.

10. Interference - HF interference is a great unknown quantity since it varies considerably from hour to hour and day to day. It may require more than just two frequencies to conduct the experiment. Using higher power sources would decrease the interference problem.

UNCLASSIFIED

Section 7.

7. (U) RECOMMENDATIONS.

In summary it is recommended that the proposed experimental program be accomplished in four phases. First, analysis and measurements are needed to evaluate the coupling between the buoy-mounted transmitter and the surface wave which, of course, is vertically polarized. To do this, a variable frequency transmitter will be operated with a shore receiving station to minimize the variables.

Second, additional analysis will be made for target cross-sectional area. This is best accomplished by modelling. Model experiments will also be conducted to evaluate the difference between backscatter and forward scatter.

Third, the path loss must be evaluated. To do this, an airborne transmitter will be used and both the sky wave via the ionosphere and the surface wave will be measured. In this phase, sufficient data must be taken to validate the theoretical results of previous workers (2, 3, 7, 8 and 11) in order to all prediction of time availability with reasonable accuracy. Mode and frequency of propagation will also be optimized during this phase.

Fourth, a preliminary system will be defined as a result of the above investigations. This design will include coverage area, control requirements, and an estimate of detection probability and false alarm rate.

UNCLASSIFIED

REFERENCES

1. O. Kempthorne, The Design and Analysis of Experiments, 1952, Wiley and Sons.

2. K. Bullington, Radio Propagation Fundamentals BSTJ, Vol. XXXVI, May 1957.

3. Ionospheric Radio Propagation, NBS Monograph 80, April 1965.

4. [redacted]

5.

6.

7. K. A. Norton, The Calculation of Ground-Wave Field Intensity Over a Finitely Conducting Spherical Earth, Pro. IRE, December 1941.

8. K. A. Norton, Transmission Loss in Radio Propagation, Proc. IRE, January 1953.

9. M. T. Skolnik, Introduction to Radar Systems, McGraw-Hill, 1962.

10. Antenna Systems for the 1.5 to 30 Mcs Frequency Range, News from Rohde and Schwarz, No. 22, 1967.

11. Barrick, D. E. "Theory of Ground-Wave Propagation Across a Rough Sea at Tekameter Wavelengths" January 1970, Battelle Memorial Institute, Columbus Laboratories.

12. E. M. Kennaugh, "Polarization Properties of Radar Reflections", Antenna Lab., Ohio State Research Foundation, Rpt. No. 389-12, March 1952, prepared under Contract AF28(099)-90, RADC Rome, N.Y.

13. J. R. Copeland, "Radar Target Classification by Polarization Properties", Proc. IRE, July 1960.

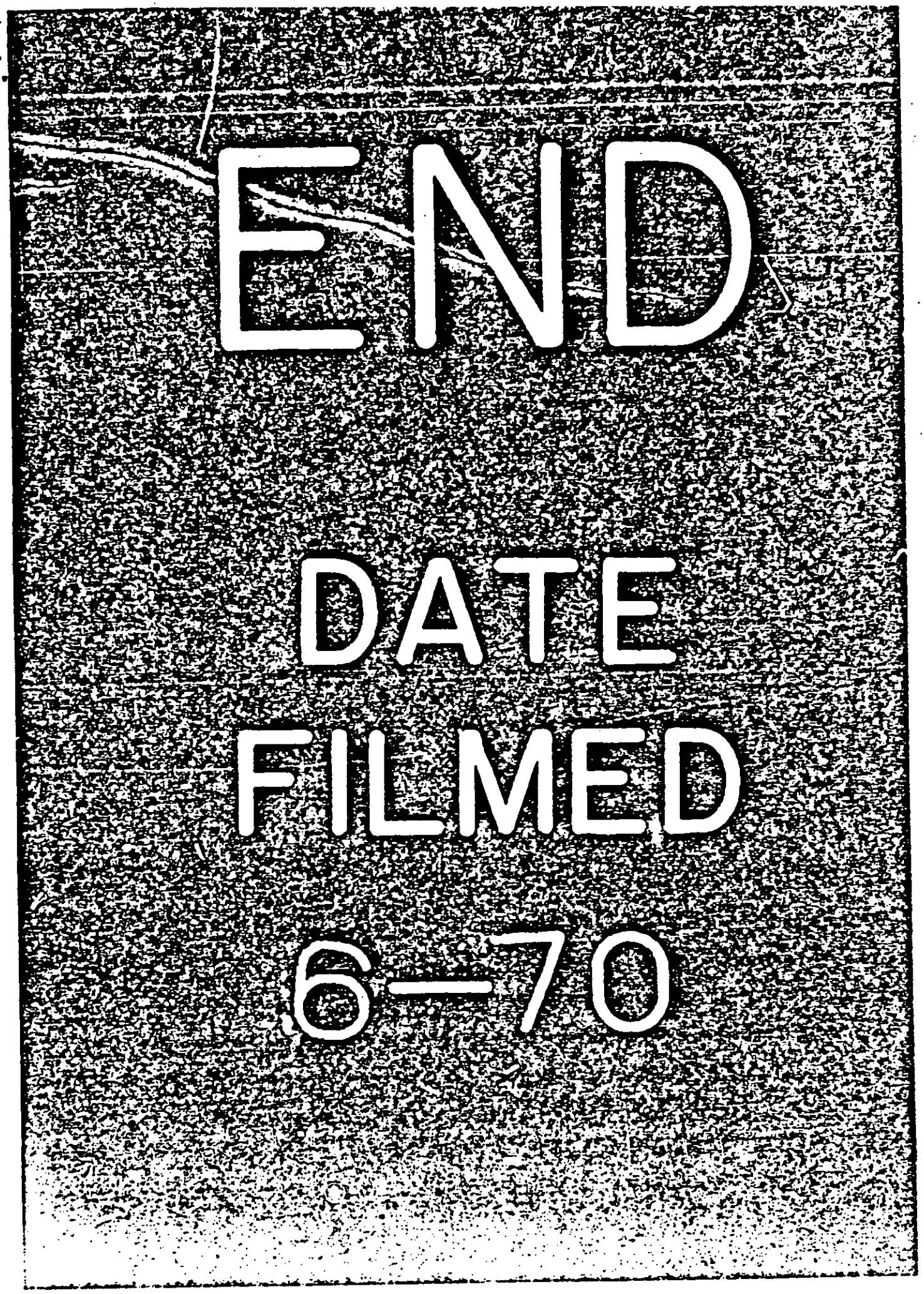
END
DATE
FILMED
6-70

UNCLASSIFIED
~~SECRET~~

#196
AD 513725
33 pgs.

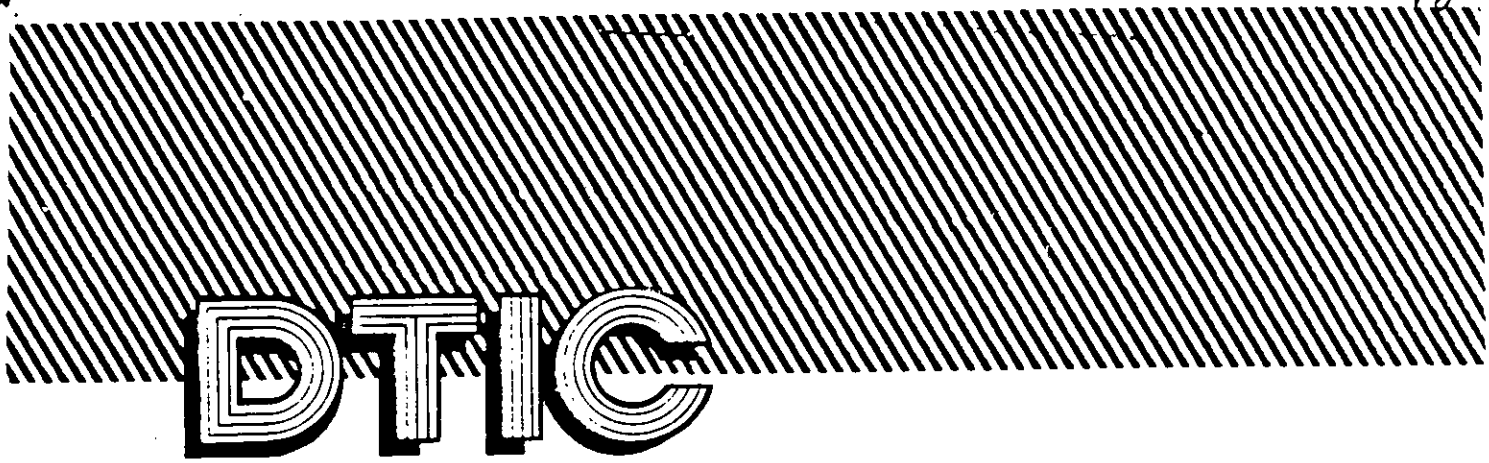

Technical Report

THIS DOCUMENT HAS BEEN DOWNGRADED
TO UNCLASSIFIED
Per Director DARPA, SEIO/TIO
NOV 10 1992

distributed by

Defense Technical Information Center
DEFENSE LOGISTICS AGENCY
CAMERON STATION, ALEXANDRIA, VIRGINIA 22304-6145

UNCLASSIFIED
~~SECRET~~

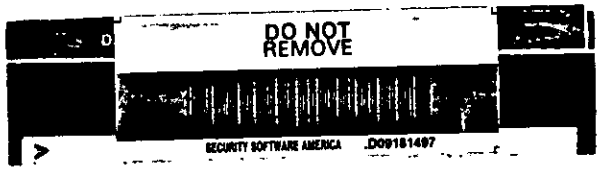

NOTICE

We are pleased to supply this document in response to your request.

The acquisition of technical reports, notes, memorandums, etc., is an active, ongoing program at the Defense Technical Information Center (DTIC) that depends, in part, on the efforts and interests of users and contributors.

Therefore, if you know of the existence of any significant reports, etc., that are not in the DTIC collection, we would appreciate receiving copies or information related to their sources and availability.

The appropriate regulations are Department of Defense Directive 3200.12, DoD Scientific and Technical Information Program; Department of Defense Directive 5200.20, Distribution Statements on Technical Documents (amended by Secretary of Defense Memorandum, 18 Oct 1983, subject: Control of Unclassified Technology with Military Application); Military Standard (MIL-STD) 847-B, Format Requirements for Scientific and Technical Reports Prepared by or for the Department of Defense; Department of Defense 5200.1R, Information Security Program Regulation.

Our Acquisition Section, DTIC-DDAB, will assist in resolving any questions you may have. Telephone numbers of that office are: (202)274-6847, 274-6874 or Autovon 284-6847, 284-6874.

FEBRUARY 1984

☆ U.S. Government Printing Office: 1985—461-169/35047

SECURITY MARKING

The classified or limited status of this report applies to each page, unless otherwise marked.
Separate page printouts MUST be marked accordingly.

THIS DOCUMENT CONTAINS INFORMATION AFFECTING THE NATIONAL DEFENSE OF THE UNITED STATES WITHIN THE MEANING OF THE ESPIONAGE LAWS, TITLE 18, U.S.C., SECTIONS 793 AND 794. THE TRANSMISSION OR THE REVELATION OF ITS CONTENTS IN ANY MANNER TO AN UNAUTHORIZED PERSON IS PROHIBITED BY LAW.

NOTICE: When government or other drawings, specifications or other data are used for any purpose other than in connection with a definitely related government procurement operation, the U.S. Government thereby incurs no responsibility, nor any obligation whatsoever; and the fact that the Government may have formulated, furnished, or in any way supplied the said drawings, specifications, or other data is not to be regarded by implication or otherwise as in any manner licensing the holder or any other person or corporation, or conveying any rights or permission to manufacture, use or sell any patented invention that may in any way be related thereto.

AD 513725

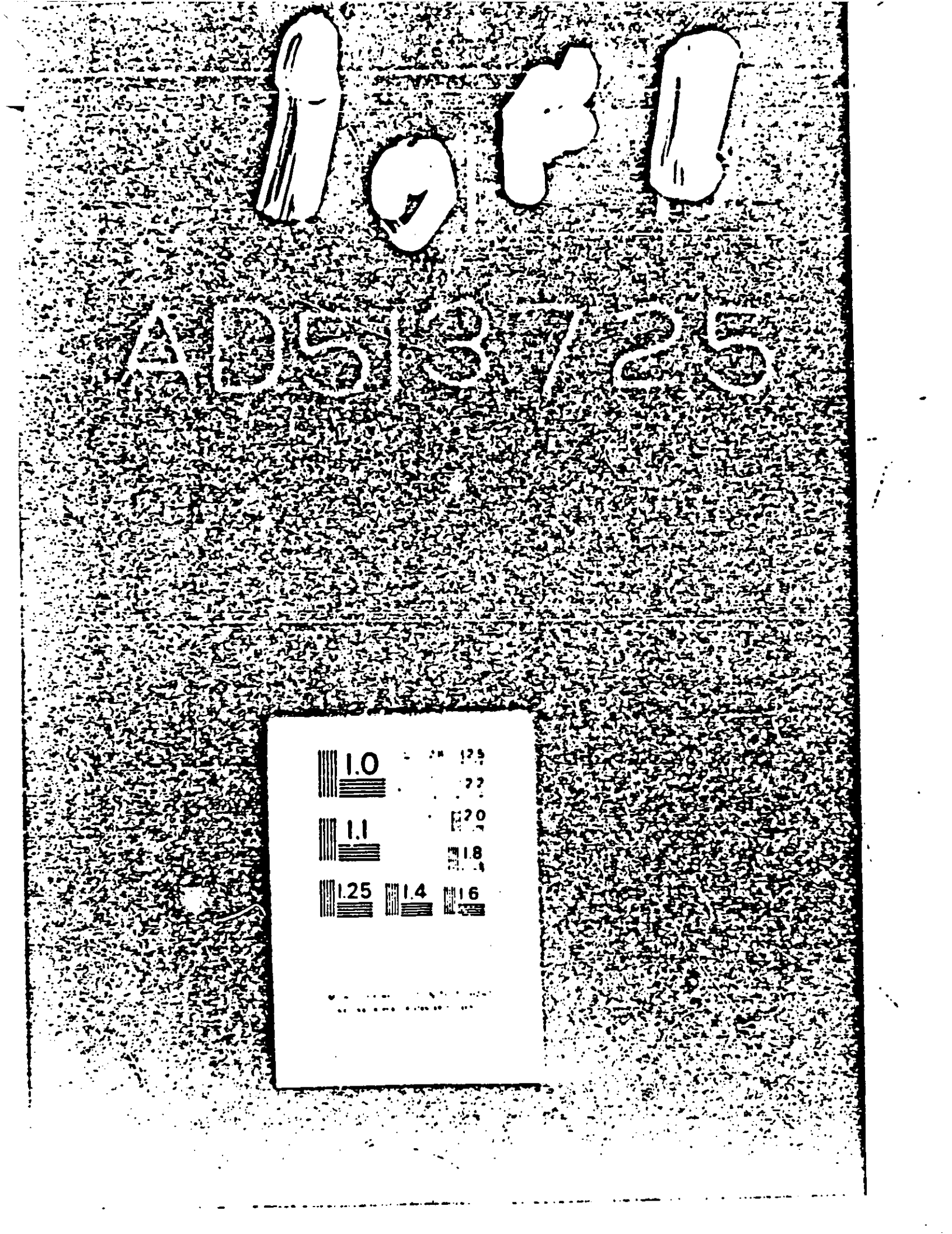
AD-A183 725
1.0
1.1
1.25
1.4
1.6

UNCLASSIFIED

SECURITY REMARKING REQUIREMENTS
DOD 5200.1-R, CHG 3
REVIEW ON 01 DEC 91

UNCLASSIFIED

GTE SYLVANIA INCORPORATED

P. O. Box 205

Mountain View, California 94040

[illegible] AUTHORITY
[illegible] DOD DIR 5200.10
[illegible]

EDL-M1380

Project AQUARIUS Special Report (U)

Principal Investigator S. Richmond 415/966-3771
Project Engineer K. Snow 415/966-3186

DDC
RECEIVED
FEB 18 1971
[illegible]
D

ARPA Order No. 1459
Effective Date of Contract: 2 June 1969
Contract Expiration Date: 31 March 1971
Amount of Contract: $118,864

THIS DOCUMENT HAS BEEN DOWNGRADED
TO UNCLASSIFIED
Per Director DARPA STIO/TIO
NOV 10 1992
[illegible] DOD DIR 5200.10
[illegible]
DDC CONTROL
[illegible]

This research was supported by the Advanced Research Projects Agency of the Department of Defense and was monitored by the Office of Naval Research under Contract No. N00014-69-C-0446

ABSTRACT

This report discusses an investigation of the feasibility of defending surface vessels against low-flying threats. Various models and techniques based on them for the estimation of threat trajectories are derived using a polystatic radar approach wherein targets are illuminated with skywave and surface-wave modes and reflections are received by a shipborne receiving system via the surface-wave mode. Two of the models were tested via simulation: a two-transmitter, one-receiver (double baseline) case and a one-transmitter, one-receiver (single baseline) case. The results of the investigation indicate that of the models tested only the double baseline approach may be a feasible method. However, further analysis is needed before a final conclusion can be reached.

Two configurations that might be feasible for the shipborne hardware required to perform the azimuthal and Doppler measurements are discussed: the multiple-baseline/pattern-recognition system and the switched linear array Doppler direction finding system. It is concluded that the relative advantages of the two systems should be investigated to select the one most appropriate to the specific application desired.

CONTENTS

Section		Title	Page
		ABSTRACT	ii
1		INTRODUCTION	1
	1.1	Background	1
	1.2	Feasibility Study	1
	1.3	Summary	2
	1.4	Conclusions	3
	1.5	Report Organization	4
2		DERIVATION FOR AIRCRAFT TRAJECTORY ESTIMATION	5
	2.1	General	5
	2.2	Models Used	5
	2.2.1	Double-Baseline, Two-Measurements Model	9
	2.2.2	Double-Baseline, One-Measurement Model	13
	2.2.3	Single Baseline Model	16
3		SIMULATION AND MODEL TESTING	20
	3.1	Models Simulated	20
	3.2	Double-Baseline, One-Measurement Model	20
	3.2.1	The Simulation	20
	3.2.2	Simulation Results for Double Baseline Model	22
	3.2.3	Sources of Error	23
	3.2.4	Sensitivity to Measurement Error	24
	3.2.5	Single Baseline Model	24
	3.2.6	Summary and Conclusions	25
4		DETECTION SYSTEM	27
	4.1	General System Considerations	27
	4.2	Doppler Measurement	27
	4.3	Shipborne DF Considerations	27
	4.3.1	Multiple Baseline/Pattern Recognition System	30
	4.3.2	Switched Linear Array Doppler (SLAD) Direction Finding System	32
	4.4	Comparison of MB/PR and SLAD Systems	32

ILLUSTRATIONS

Figure	Title	Page
1	Double-Baseline, Two-Measurements Model	6
2	Double-Baseline, One-Measurement Model	7
3	Single Baseline Model	8
4	Variables for Double-Baseline, Two-Measurements Model	10
5	Variables for Double-Baseline, One-Measurement Model	14
6	Variables for Single Baseline Model	17
7	Geometry of Situation Being Simulated	21
8	A Typical Single-Channel Receiving and Processing System	28

TABLES

Table	Title	Page
1	Actual and Estimated Quantities for Case 1	22
2	Actual and Estimated Quantities for Case 2	23
3	Estimated Range with Measurement Error (Case 1)	25
4	General Requirements for a Shipborne HF DF System	31

Section 1

INTRODUCTION

1.1 (U) (S) BACKGROUND.

The detection of low-flying threats to surface vessels at a range sufficient to give useful warning time and tracking information is a problem which must be solved if the surface navy is to survive. In detecting these threats the enemy must not be given the opportunity to use simple direction finding techniques to locate fleet units. Thus, it is desirable that target detection not require radiation from the fleet and that the fleet operate under complete electromagnetic control (EMCON).

The feasibility of using a hybrid (skywave/surface-wave) system to help solve this problem has been demonstrated as part of the MAY BELL Program. In this concept, the target is illuminated by skywaves from transmitters (either shipborne or land-based) located at over-the-horizon (OTH) ranges. Surface waves which propagate from the target to a receiving system aboard a ship permit detections to be made even when the target is below the line-of-sight radar horizon.

Experiments performed at Cape Kennedy, Florida, with a shore-based receiving station simulating the shipboard environment, a Navy P3V aircraft as a controlled target, and illumination provided by the MADRE (pulse) and CHAPEL BELL (phase code) transmitters, located respectively in Maryland and Virginia, have shown the technique to be feasible. For most of the flights of the target its altitude was 200 feet, and detections were made at ranges as great as 100 kilometers (km) from the receiver.

1.2 (U) (S) FEASIBILITY STUDY.

As an application of the hybrid-system, fleet air-defense technique, a feasibility study under Project AQUARIUS has been conducted to determine the practicality of defending the Mediterranean Fleet against low flying aircraft and cruise missiles using over-the-horizon detection (OHD) skywave--surface-wave and surface-wave--surface-wave techniques. A parallel effort within this study was to determine if simple continuous wave (CW) rather than range code transmissions could be used which might then result in a simpler, more mobile system.

UNCLASSIFIED

1.2 (U) (S) --CONTINUED.

It was determined that shore-based HF (CW) sources could be used for skywave and surface-wave target illumination and shipboard receivers used to detect the surface-wave Doppler shifted signal scattered by the target. Assuming reasonable powers (10,000 W), vertical antennas and 100 m^2 cross sections, a target detection range of approximately 100 km from the ship is typical.

Although the Doppler detection provides some information about the target velocity and direction, because of symmetry, targets flying near the transmitter may give the same Doppler shift as those flying near the ship. Thus a means of discriminating between threatening and non-threatening targets may be as important as detecting the targets themselves, at OTH ranges.

This report describes the derivation and presents simulation results for three straight-forward techniques which allow OTH target detection and tracking while maintaining EMCON.

1.3 (U) (S) SUMMARY.

Derivations have been made of techniques to provide location estimates of low-flying targets using a polystatic radar approach in which the targets are illuminated with skywave and/or surface-wave modes from a land-based HF CW transmitter and the reflections from the targets are received by a shipborne receiving system via surface wave mode. The models used have been examined for two configurations: a two-transmitter, one-receiver (double baseline) case and a one-transmitter, one-receiver (single baseline) case. For the double baseline case two models were developed, one to represent azimuthal and Doppler measurements made at two different time points for each baseline and a second to represent a single set of measurements for each baseline. For the single baseline case a third model requiring two sets of azimuthal and Doppler measurements was developed.

The second and third models were simulated for aircraft detection in the Mediterranean for two situations: one in which the aircraft flies directly at the ship and a second in which it flies at an angle of 30° from the ship. The influences of bearing error measurements on the trajectory estimation were examined.

1.3 (U) --CONTINUED.

Implementation considerations indicate that Doppler resolutions of 0.1 Hz and azimuthal accuracies of 1.? degrees RMS are feasible.

Two configurations--the multiple-baseline/pattern-recognition system (MB/PR) and the switched linear array Doppler direction finding system (SLAD)--that might be feasible for the shipborne hardware required to perform the azimuthal and Doppler measurements are discussed.

1.4 (U) CONCLUSIONS

The results of the investigation indicate that the double baseline approach wherein a single set of measurements is made for each baseline is superior to the single baseline approach. The necessary assumption required by the single baseline method introduces large errors in practice and makes this formulation of the method unacceptable. An estimation accuracy of 1 km in range is achievable for the ideal double-baseline case where there are no measurement errors. Inaccurate azimuthal measurements result in greater errors in range estimates than do inaccurate Doppler measurements. A preliminary error analysis indicates that errors of $\pm 2^{\circ}$ in bearing measurement result in range errors of 1 - 5 km.

From the foregoing results it is concluded that the double baseline approach appears to be a feasible method for estimating the location of low-flying aircraft using a polystatic HF system. However, additional analysis is required in

(a) detailed error analysis of the double baseline (single measurement) method,

(b) a simulation and error analysis of the double baseline (multiple measurement) method,

(c) location estimation of high flying aircraft/missiles (the case for which a flat earth and two dimensional model is no longer valid),

(d) system design for implementing the double baseline (single measurement) method, and

(e) analysis of other formulations of the single baseline approach.

1.4 (U) (S) --CONTINUED.

It is also concluded that the two possible shipborne hardware systems should be further investigated to select the one most appropriate to the specific application desired.

1.5 (U) REPORT ORGANIZATION.

This report consists of four sections. The first presents introductory background information concerning previous work done on the detection of low-flying threats to surface vessels. It also introduces the feasibility study described in this report and gives a summary of the study and the conclusions reached. The second section describes the models used and the derivations of the various techniques, based on the models, for estimation of missile/aircraft trajectories. Section 3 discusses the simulation and testing that was performed on two of the models and points out sources of error in each. Estimates of the effects of errors in the measured parameters on the results are also given. Finally, Section 4 discusses ways of designing and constructing the shipborne hardware required to provide the azimuth and Doppler measurement information necessary to the application of the derived techniques.

Section 2

DERIVATION FOR AIRCRAFT TRAJECTORY ESTIMATION

2.1 (U) GENERAL.

As described in Section 1, protection of the fleet against low flying aircraft and/or cruise missiles may be accomplished using a bistatic radar with a shore-based transmitter for target illumination combined with passive shipboard reception. In fact, over-the-horizon warning may be accomplished without active shipboard radiation (i.e., with electromagnetic control, EMCON). The techniques considered in this study appear to eliminate two fundamental problems associated with CW-Doppler bistatic radar:

a. Target signal amplitude gives no indication of whether the target is near the transmitter or the receiving ship because the bistatic radar range equation is symmetric about the transmitter-target and receiver-target ranges.

b. Single Doppler measurements alone cannot provide unambiguous target location since single Doppler measurements have a four-fold location ambiguity caused by the geometric symmetry between the transmitter, receiver and target.

Three separate derivations will be given describing techniques which may be used to locate and track low flying targets which may threaten a surface fleet.

2.2 (U) MODELS USED.

For the two-dimensional (flat earth, low flying) situation being considered here, two geometries are worth investigating: a two-transmitter, one-receiver (double baseline) case and a one-transmitter, one-receiver (single baseline) case. For the double baseline case, two models were developed. One model requires that, for each baseline, azimuth and Doppler measurements be taken at two different time points. The other model requires only one azimuth and Doppler measurement for each baseline. The geometries for these two models are illustrated in Figures 1 and 2. The single baseline model requires azimuth and Doppler measurements at two different time points; the geometry for this model is shown in Figure 3.

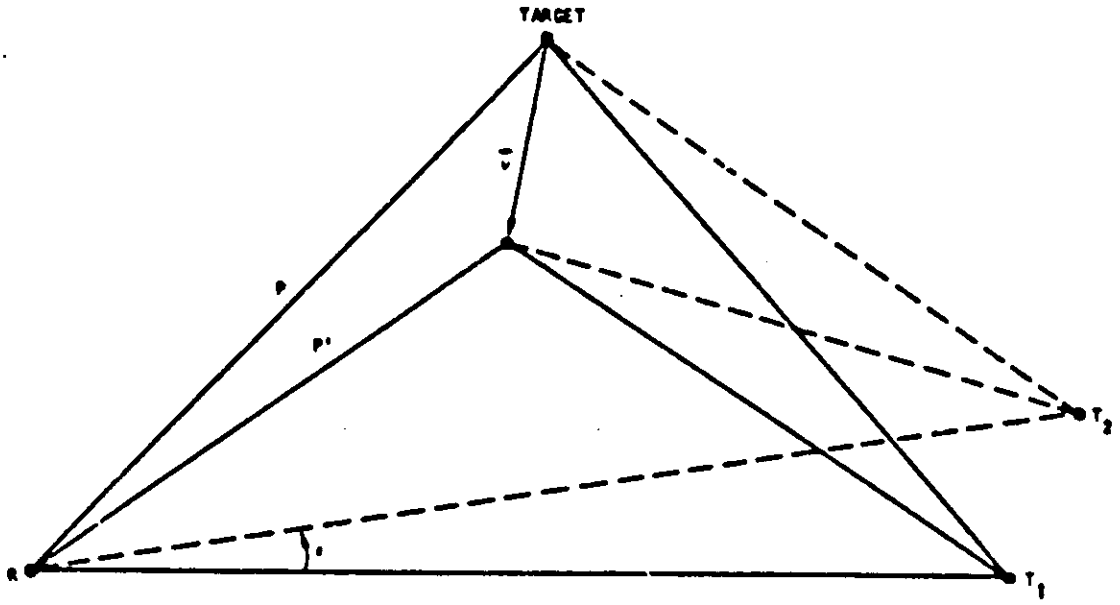

Figure 1. (U) Double-Baseline, Two-Measurements Model. (U)

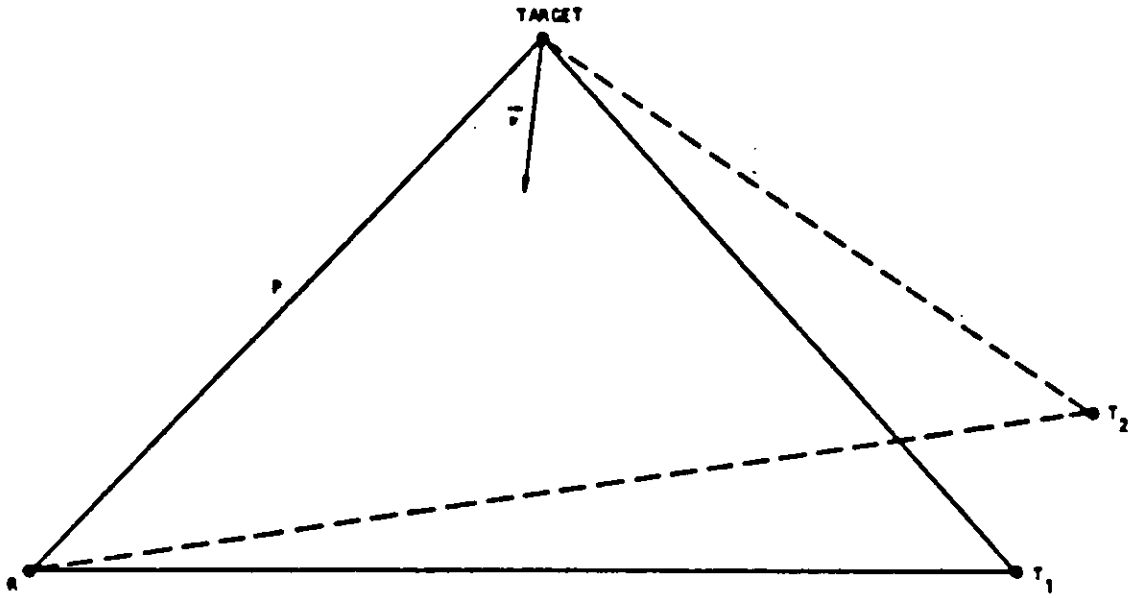

Figure 2. (U) Double-Baseline, One-Measurement Model. (U)

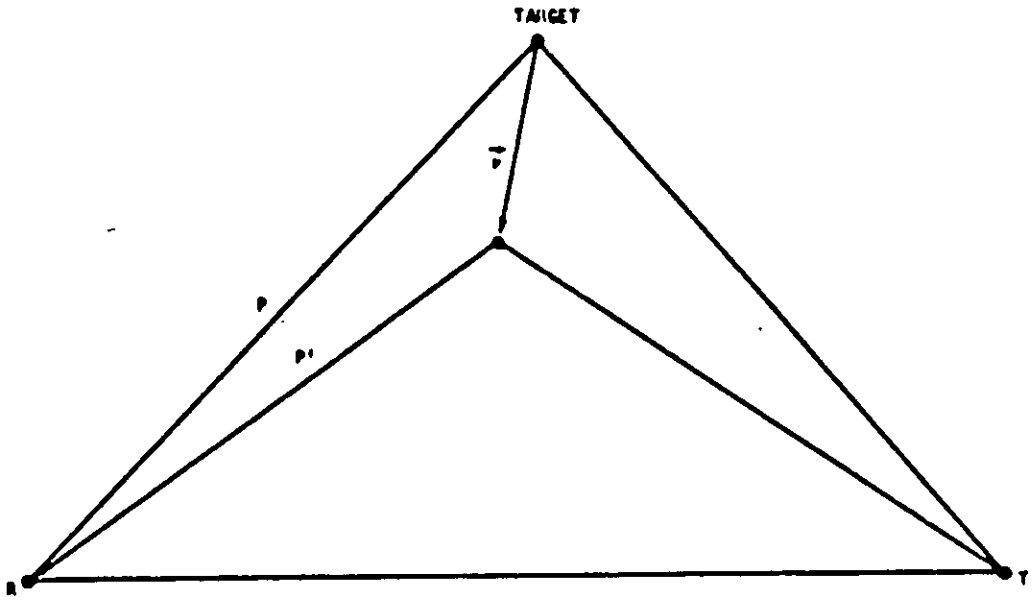

Figure 3. (U) Single Baseline Model. (U)

2.2 (U) --CONTINUED.

Of the three models, the single baseline case is the most desirable from an operational point of view because it requires monitoring only one transmitter. Of the double baseline models, the one-measurement case is the simplest and the easiest to implement. The following derivations describe how trajectory information may be obtained using each of these models. All models assume that the aircraft of interest has constant velocity and direction. Flat earth geometry is also assumed, a valid simplification for low flying targets.

2.2.1 (U) Double-Baseline, Two-Measurements Model.

Consider the single baseline, one time point situation shown in Figure 4, where a vehicle is moving at an unknown velocity $\hat{v}$, the distance between the transmitter and the receiver is assumed known to be D, and the transmitter is broadcasting on a known wavelength λ. The azimuth angle of the target at the receiver, α, and the Doppler shift, Δf, are measured.

The received Doppler shift for this geometry may be written as

$$\Delta f = -\frac{\hat{v}}{\lambda}(\hat{r}_1 + \hat{r}_2)$$

$$= -\frac{v}{\lambda}(\cos\theta_1 + \cos\theta_2)$$

Angles θ_1 and θ_2 can also be written:

$$\theta_1 = 90 + \alpha + \delta$$

$$\theta_2 = 90 + \beta - \delta$$

Therefore,

$$\Delta f = \frac{v}{\lambda}[\sin(\alpha+\delta) + \sin(\beta-\delta)]$$

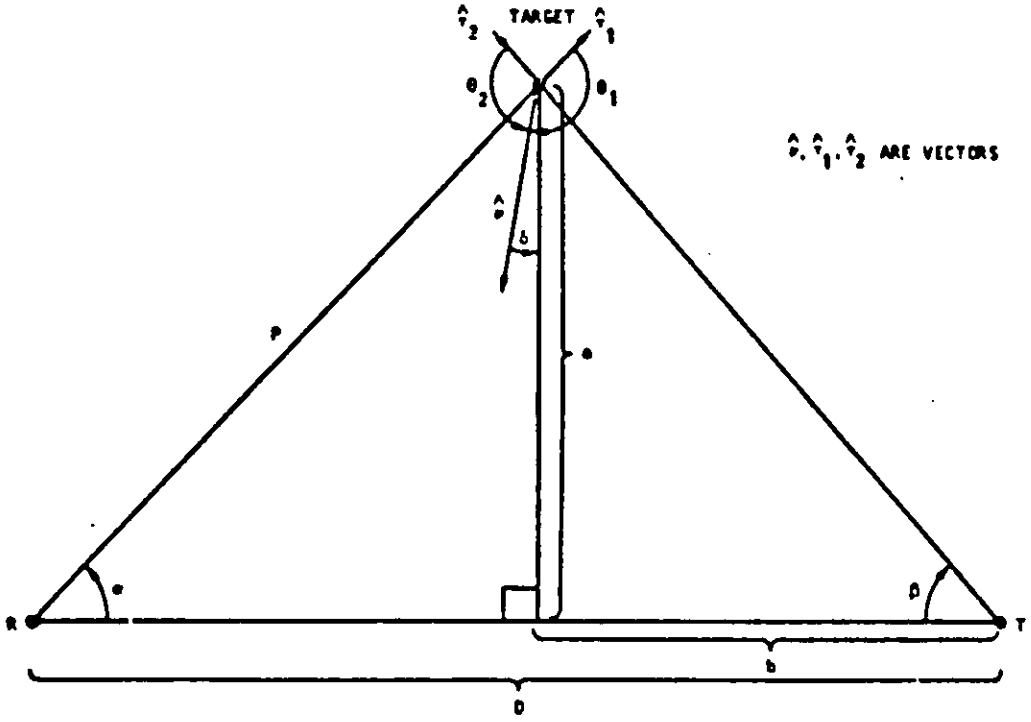

Figure 4. (U) Variables for Double-Baseline, Two-Measurements Model. (U)

2.2.1 (U) -Continued.

Also,

$$\beta = \tan^{-1}\left(\frac{a}{b}\right)$$

$$= \tan^{-1}\left[\frac{a}{D - \frac{a}{\tan\alpha}}\right] = \tan^{-1}\left[\frac{a \tan\alpha}{D \tan\alpha - a}\right]$$

If there are two transmitter geometries, which shall be distinguished using subscripts, then the following three equations can be written:

$$\Delta f_1 = \frac{v}{\lambda_1}\left\{\sin(\alpha_1+\delta_1) + \sin\left[\tan^{-1}\left(\frac{a_1 \tan\alpha_1}{D_1 \tan\alpha_1 - a_1}\right) - \delta_1\right]\right\} \quad (1)$$

$$\Delta f_2 = \frac{v}{\lambda_2}\left\{\sin(\alpha_2+\delta_2) + \sin\left[\tan^{-1}\left(\frac{a_2 \tan\alpha_2}{D_2 \tan\alpha_2 - a_2}\right) - \delta_2\right]\right\} \quad (2)$$

and

$$\delta_2 = \delta_1 + \epsilon \quad (3)$$

where ϵ is the angle between the two baselines, as shown in Figure 1. The value of ϵ may be calculated because the coordinates of the two transmitters and the receivers are assumed known.

If additional azimuth and Doppler measurements are made for these same two geometries at some time Δt later, then four more equations can be written. This set of equations is distinguished by a superscript prime.

$$\Delta f_1' = \frac{v}{\lambda_1}\left\{\sin(\alpha_1'+\delta_1) + \sin\left[\tan^{-1}\left(\frac{a_1' \tan\alpha_1'}{D_1 \tan\alpha_1' - a_1'}\right) - \delta_1\right]\right\} \quad (4)$$

$$\Delta f_2' = \frac{v}{\lambda_2}\left\{\sin(\alpha_2'+\delta_2) + \sin\left[\tan^{-1}\left(\frac{a_2' \tan\alpha_2'}{D_2 \tan\alpha_2' - a_2'}\right) - \delta_2\right]\right\} \quad (5)$$

2.2.1 (U) --Continued.

$$a_1' = a_1 - v\,\Delta t\,\cos\delta_1 \qquad (6)$$

$$a_2' = a_2 - v\,\Delta t\,\cos\delta_2 \qquad (7)$$

The last two equations are a result of the constant velocity and direction assumption. All seven equations can be combined into a system of four equations in four unknowns by eliminating δ_2 from the equations. The results are:

$$\Delta f_1 = F_1(v, a_1, \delta_1)$$

$$\Delta f_2 = F_2(v, a_2, \delta_1)$$

$$\Delta f_1' = F_3(v, a_1, \delta_1)$$

$$\Delta f_2' = F_4(v, a_2, \delta_1)$$

where the $F_i(\cdot)$ are different functions of the argument parameters.

The unknowns are v, a_1, a_2 and δ_1. The measured quantities are α_1, α_2', α_1', α_2, Δf_1, $\Delta f_1'$, Δf_2, and $\Delta f_2'$. The quantities known a priori are D_1, D_2, λ_1, λ_2, Δt, and ϵ. The above set of simultaneous equations may be solved for the unknowns and the ground range from the receiver to the target could be calculated by

$$p = \frac{a_1}{\sin\alpha_1}$$

Although this procedure yields four independent equations which may be solved for the target position, a slight reformulation of the problem can reduce the number of equations by two as described below.

2.2.2 (U) Double-Baseline, One-Measurement Model.

The variables for the double-baseline, one-measurement model are defined in Figure 5. As in the previous case, the transmitter-receiver distances, D_1 and D_2, and the transmitter wavelengths, λ_1 and λ_2, are assumed known a priori. The azimuths, α_1, and α_2, and Doppler shifts, Δf_1 and Δf_2, are the only quantities requiring measurement.

From another form of the Doppler equation,

$$\Delta f_1 = \frac{-1}{\lambda_1} (\dot{p} + \dot{n}_1)$$

$$\Delta f_2 = \frac{-1}{\lambda_2} (\dot{p} + \dot{n}_2)$$

where $\dot{p} = dp/dt$ and $\dot{n}_i = dn/dt$

From the law of cosines,

$$n_1 = (p^2 + D_1^2 - 2pD_1 \cos \alpha_1)^{1/2}$$

so

$$\dot{n}_1 = \frac{(p\dot{p} - \dot{p}D_1 \cos \alpha_1 + pD_1 \dot{\alpha}_1 \sin \alpha_1)}{(p^2 + D_1^2 - 2pD_1 \cos \alpha_1)^{1/2}} \quad (8)$$

where $\dot{\alpha}_1 = d\alpha_1/dt$

Similarly

$$\dot{n}_2 = \frac{(p\dot{p} - \dot{p}D_2 \cos \alpha_2 + pD_2 \dot{\alpha}_2 \sin \alpha_2)}{(p^2 + D_2^2 - 2pD_2 \cos \alpha_2)^{1/2}} \quad (9)$$

Note that $\dot{\alpha}_1 = \dot{\alpha}_2 = \dot{\alpha}$. The quantity $\dot{\alpha}$ can be estimated using the previous azimuth measurements as follows:

$$\dot{\alpha} = \frac{[\alpha_1(t) - \alpha_1(t-\Delta t)] + [\alpha_2(t) - \alpha_2(t-\Delta t)]}{2\Delta t}$$

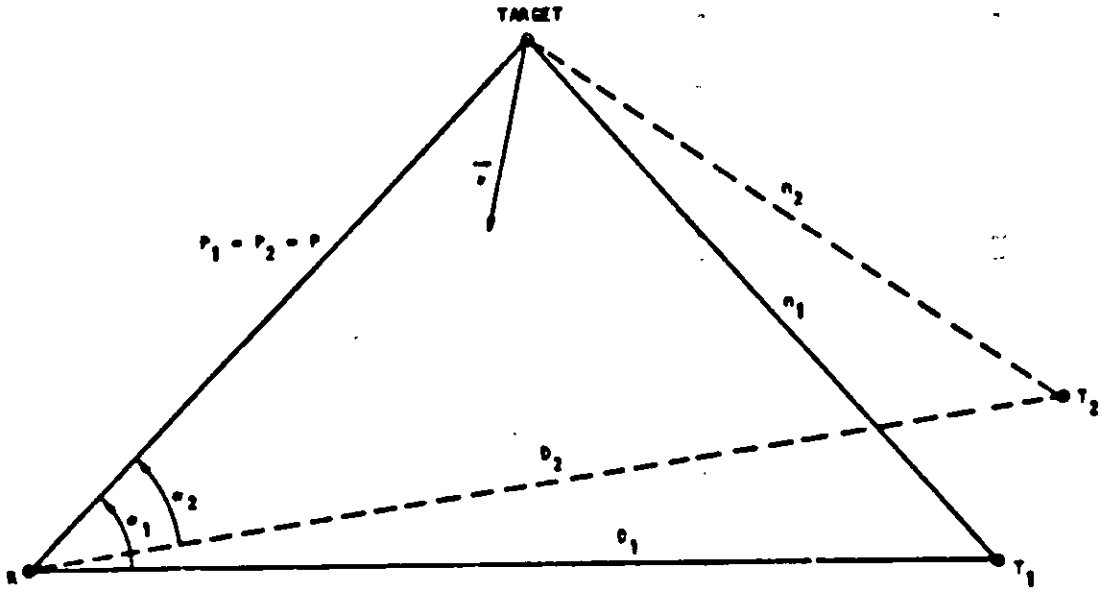

Figure 5. (U) Variables for Double-Baseline, One-Measurement Model. (U)

2.2.2 (U) --Continued.

Now define h_1, q_1, r_1, and s_1 as follows:

$$h_1 = (p^2 + D^2 - 2pD_1 \cos \alpha_1)^{1/2}$$

$$q_1 = \Delta f_1 \lambda_1$$

$$r_1 = D_1 \cos \alpha_1$$

$$s_1 = D_1 \dot{\alpha} \sin \alpha_1$$

The quantities h_2, q_2, r_2, and s_2 are similarly defined. Equations (8) and (9) can then be written as

$$\dot{n}_1 = \frac{p\dot{p} - \dot{p} r_1 + ps_1}{h_1}$$

$$\dot{n}_2 = \frac{p\dot{p} - \dot{p} r_2 + ps_2}{h_2}$$

So Δf_1 can be written

$$\Delta f_1 = \frac{-1}{\lambda_1} \left[\dot{p} + \frac{\dot{p}(p - r_1) + ps_1}{h_1} \right]$$

Similarly

$$\Delta f_2 = \frac{-1}{\lambda_2} \left[\dot{p} + \frac{\dot{p}(p - r_2) + ps_2}{h_2} \right]$$

Solving for $\dot{p}$.

$$\dot{p} = -\frac{(q_2 h_2 + ps_2)}{(h_2 + p - r_2)} \qquad (10)$$

2.2.2 (U) --Continued.

Also,

$$-q_1 h_1 = \dot{p}\, h_1 + \dot{p}\,(p - r_1') + p\, s_1$$

and so

$$p = \frac{-[q_1 h_1 + \dot{p}\,(h_1 - r_2')]}{s_1 + \dot{p}} \qquad (11)$$

Equations (10) and (11) form a system of two equations in two unknowns (p and $\dot{p}$) that may be solved using standard iterative techniques. Note also that, for this formulation, the assumption of constant velocity and direction are not necessary.

2.2.3 (U) Single Baseline Model.

The final derivation to be considered is that involving the model using only one transmitter. The variables for the single baseline model are defined in Figure 6. As before, the transmitter-receiver distance, D, and the transmitter wavelength, λ, are assumed known. The azimuths, α and α', and Doppler shifts Δf and $\Delta f'$, are measured quantities where the primes signify measurement at some time Δt after the first (unprimed) measurements. The velocity, v, of the vehicle is not known.

From the Doppler equation,

$$f = \frac{-1}{\lambda}\,(\dot{p} + \dot{n})$$

$$f' = \frac{-1}{\lambda}\,(\dot{p}' + \dot{n}')$$

From the law of cosines,

$$n = (p^2 + D^2 - 2pD\cos\alpha)^{1/2}$$

$$\dot{n} = \frac{(p\dot{p} - \dot{p}D\cos\alpha + pD\dot{\alpha}\sin\alpha)}{(p^2 + D^2 - 2pD\cos\alpha)^{1/2}}$$

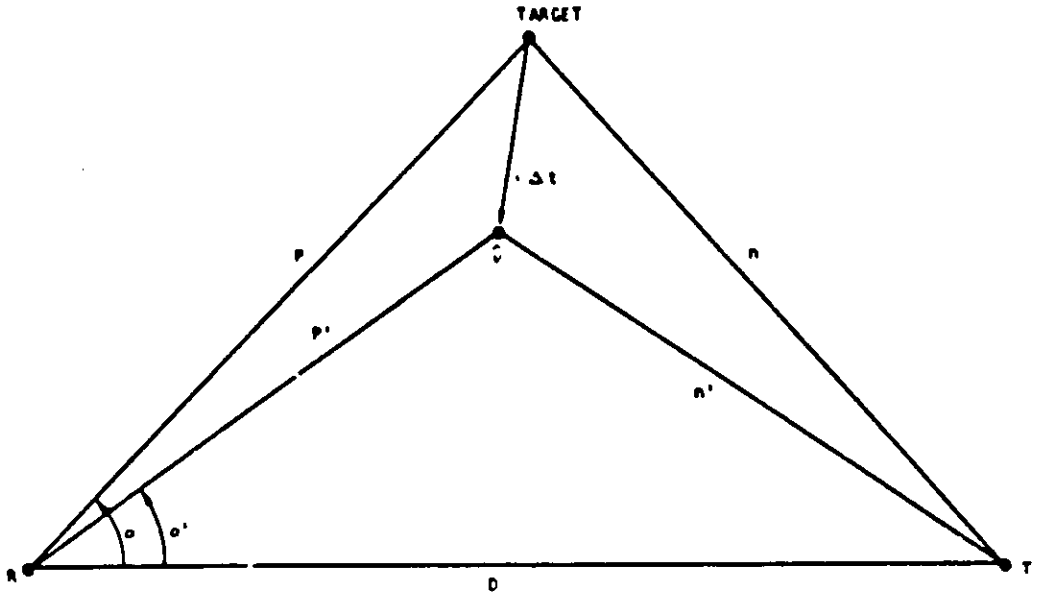

Figure 6. (U) Variables for Single Baseline Model. (U)

2.2.3 (U) --Continued.

Similarly,

$$\dot{h}' = \frac{(p'\dot{p}' - \dot{p}' D\cos\alpha' + p' D\dot{\alpha}' \sin\alpha')}{(p'^2 + D^2 - 2p' D\cos\alpha')^{1/2}}$$

In order to find a solution using only one baseline, two approximations have to be made

(a) $\dot{p}$ is constant; i.e., $\dot{p}' = \dot{p}$ and, furthermore,

$$p = p' - \dot{p}\,\Delta t$$

(b) $\dot{\alpha}$ is constant; i.e., $\dot{\alpha}' = \dot{\alpha}$

Over short time intervals (small Δt) these assumptions are reasonable. The angular velocity $\dot{\alpha}$ can be estimated as follows:

$$\dot{\alpha} = \frac{\alpha' - \alpha}{\Delta t}$$

These approximations are strictly true if the target is flying on a radial path, toward or away from the ship.

Combining the equations and approximations above gives

$$-\Delta f\lambda = -q = \dot{p} + \frac{\dot{p}(p-r) + ps}{h}$$

where

$$q = \Delta f\lambda$$

$$r = D\cos\alpha$$

$$s = D\dot{\alpha}\sin\alpha$$

$$h = (p^2 + D^2 - 2pD\cos\alpha)^{1/2}$$

2.2.1 (U) --Continued.

Substituting $p = p' - \dot{p}\,\Delta t$, squaring to eliminate square roots and algebraic manipulation of the results yields the cubic equation

$$A\dot{p}^3 + B\dot{p}^2 - C\dot{p} + D = 0 \qquad (12)$$

where

$$A = 2\Delta t^2 (q-s)$$

$$B = \Delta t^2 (q^2-s^2) + \Delta t (4qr-4qp') + 2s\Delta t (2p'-r) + D^2 - r^2$$

$$C = \Delta t (2q^2 r-2q^2 p'+2p's^2) + 2p'^2 (q-s) + 2p'r (s-2q) + 2qD^2$$

$$D = p'^2 (q^2-s^2) + q^2 (D^2-2p'r)$$

This cubic equation can be solved for $\dot{p}$ and the correct root chosen. Also note that $\dot{p}$ is still a function of the single unknown p'.

In similar fashion,

$$\Delta f' = \frac{-1}{\lambda} (\dot{p}'+\dot{h}')$$

or

$$-\Delta f' = -q' = \dot{p} + \frac{\dot{p}(p'-r') + p's'}{h'}$$

Where h', q', r' and s' are defined similarly to h, q, r and s.

Now

$$-q'h' - \dot{p}(h'-r') = p'(\dot{p}+s')$$

or

$$p' = \frac{-q'h' - \dot{p}(h'-r')}{\dot{p}+s'} \qquad (13)$$

Equations (12) and (13) form a set of simultaneous equations in the two unknowns p' and $\dot{p}$ which may be solved for the target position.

Software simulations have been written to estimate the target location accuracy to be expected by using these techniques. The results of these simulations are discussed in the next section.

Section 3

SIMULATION AND MODEL TESTING

3.1 (U) MODELS SIMULATED.

The results of simulations of realistic trajectory estimation situations are detailed below for the double-baseline, one-measurement model and the single baseline model. The double-baseline, two-measurement model was not simulated.

3.2 (U) DOUBLE-BASELINE, ONE-MEASUREMENT MODEL.

An algorithm was developed for solving sets of nonlinear simultaneous equations such as equations (10) and (11) in Section 2. The algorithm is based on a standard iterative procedure for solving equations of the form $p = f(p)$ (see, for example, Introductory Computer Methods and Numerical Analysis, by Ralph H. Pennington, The MacMillan Co., 1965). This procedure consists of estimating a solution p_o and using this estimate to get a new estimate p_1, where $p_1 = f(p_o)$. A new estimate p_2 is obtained from $p_2 = f(p_1)$, and so on until $|p_n - p_{n-1}| < \epsilon$, where ϵ is some small number. At this point the process is judged to have converged with a solution $p = p_n$. In practice, each successive p_i is transformed slightly so as to guarantee convergence.

Graphically, this technique amounts to finding the intersection of the plots of $y_1 = f(p)$ and $y_2 = p$. The point of intersection is where the algorithm converges. In actual practice, there may be more than one intersection. However, the correct root may be determined by examining the sign of $\dot{p}$ and the trend of the previous values of p.

3.2.1 (U) The Simulation.

The situation simulated is that of a ship in the Mediterrenean sea at 37°N., 25°E. and an aircraft at a range of 180 kilometers, due north, flying at 720 km/hour (about Mach 0.66). Two cases are considered as shown in Figure 7. In the first case the aircraft is merely flying at a 30° angle by the ship, whereas in the second case it is on an attack course, heading straight for the ship. In both cases, the speed and direction of the aircraft are constant. The transmitters are assumed to be located at Rhodes and Athens.

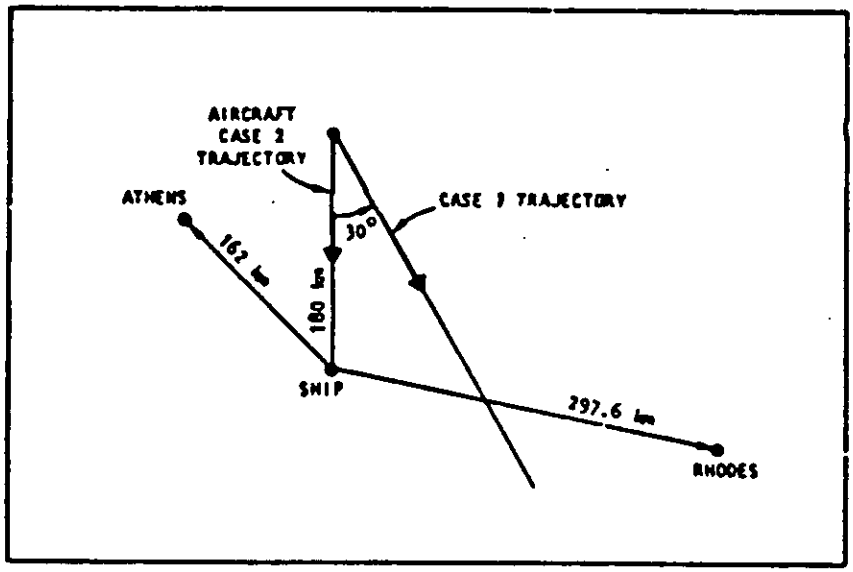

Figure 7. (U) Geometry of Situation Being Simulated. (U)

3.2.2 (U) Simulation Results for Double Baseline Model.

The results of the two simulations are presented in Tables 1 and 2. These tables give the actual and estimated range, p, and the actual and estimated derivative of range, $\dot{p}$, at intervals of 60 seconds for the two cases.

TABLE 1. (U) ACTUAL AND ESTIMATED QUANTITIES FOR CASE 1. (U)

Time (seconds)	σ_1 (degrees)	σ_2 (degrees)	Range, p (km)	Estimated (km)	$\dot{p}$ (km/sec)	Estimated (km/sec)
0	100.9	44.6	180.0			
60	98.9	42.6	169.7	170.2	-.169	-.171
120	96.6	40.3	159.7	160.2	-.165	-.166
180	94.0	37.7	149.9	150.4	-.160	-.161
240	91.1	34.8	140.5	141.0	-.154	-.155
300	87.7	31.4	131.5	132.1	-.146	-.147
360	83.9	37.6	123.0	123.6	-.136	-.138
420	79.5	23.2	115.2	115.7	-.125	-.127
480	74.5	18.2	108.1	108.7	-.111	-.112
540	68.9	12.6	101.9	102.5	-.094	-.096
600	62.6	6.3	96.9	97.4	-.074	-.083
660	55.8	-0.5	93.1	92.6	-.051	-.025
720	48.4	-7.9	90.8	91.1	-.026	-.056
780	40.8	-15.5	90.0	90.0	+.000	-.001
840	33.2	-23.1	90.8	90.5	+.027	+.026
900	25.9	-30.4	93.2	92.5	+.052	+.052
960	19.0	-37.3	97.0	96.0	+.074	+.075
1020	12.8	-43.5	102.0	100.7	+.094	+.095
1080	7.2	-49.1	108.2	106.7	+.111	+.111
1140	2.2	-54.1	115.3	113.8	+.125	+.125
1200	-2.2	-58.5	123.2	121.6	+.137	+.136
1260	-6.0	-62.3	131.7	130.2	+.146	+.146
1320	-9.3	-65.6	140.7	139.3	+.154	+.153
1380	-12.2	-68.6	150.1	148.9	+.160	+.160
1440	-14.8	-71.1	160.0	158.7	+.165	+.165
1550	-17.1	-73.4	170.0	169.0	+.170	+.169

TABLE 2. (U) ACTUAL AND ESTIMATED QUANTITIES FOR CASE 2. (U)

Time (seconds)	α_1 (degrees)	α_2 (degrees)	Range, p (km)	Estimated (km)	$\dot{p}$ (km/sec)	Estimated $\dot{p}$ (km/sec)
0	100.9	44.6	180.0			
60	100.9	44.6	168.0	168.0	-0.200	-0.200
120	100.9	44.6	156.0	156.0	-0.200	-0.200
180	100.9	44.6	144.0	144.0	-0.200	-0.200
240	100.9	44.6	132.0	132.0	-0.200	-0.200
300	100.9	44.6	120.0	120.0	-0.200	-0.200
360	100.9	44.6	108.0	108.0	-0.200	-0.200
420	100.9	44.6	96.0	96.0	-0.200	-0.200
480	100.9	44.6	84.0	84.0	-0.200	-0.200
540	100.9	44.6	72.0	72.0	-0.200	-0.200
600	100.9	44.6	60.0	60.0	-0.200	-0.201
660	100.9	44.6	48.0	48.0	-0.200	-0.201
720	100.9	44.6	36.0	36.0	-0.200	-0.201
780	100.9	44.6	24.0	24.0	-0.200	-0.202
840	100.9	44.6	12.0	12.0	-0.200	-0.202
900	100.0	44.6	0.0	0.0	-0.200	-0.202

3.2.2 (U) --Continued.

The most accurate results were obtained for case 2, the attack case. For case 1, the fly-by, errors in the range estimate are on the order of 0.5 to 1.0 kilometers. The reasons for these differences are discussed below.

3.2.3 (U) Sources of Error.

The sources of error include the linear estimate of rate of change of azimuth ($\dot{\alpha}$) and measurements of azimuth and Doppler frequency. Of these, the main source of error in determining the range is that due to $\dot{\alpha}$, given in Section 2. For example, in case 1 at 400 seconds the estimated value of $\dot{\alpha}$ is 1.271×10^{-2} radians/second, while the actual value is 1.300×10^{-3} radians/second. Using the estimated value of $\dot{\alpha}$, a solution of $p = 118.28$ km was obtained. Using the correct value of $\dot{\alpha}$, however, yielded a solution $p = 117.51$ km. The actual solution is $p = 117.72$ km.

3.2.3 (U) --Continued.

For some situations, a plot of $y = f(P)$ shows that it is very close to the function $y=p$ for a wide range of p. In this range, the small errors in f(p) caused by the small errors in estimating $\dot{\alpha}$ produce drastic differences in where the two curves intersect, and hence produce errors in the range estimate. Normally, however, the set of conditions that would produce this problem occurs only for targets outside the detection range and would not affect a practical trajectory determination scheme.

It is now apparent why the trajectory estimation for case 2 was more accurate than for case 1; in case 2 the azimuth is constant, hence $\dot{\alpha} = 0$ and errors due to estimating $\dot{\alpha}$ disappear. It follows that it is during the most critical situations that the greatest accuracy can be expected.

3.2.4 (U) Sensitivity to Measurement Error.

During the simulations discussed above, it was assumed that the azimuth and Doppler measurements were exact. During normal operation in a shipboard environment great accuracy is not possible. To test the sensitivity of the model to measurement errors, range estimates were obtained for various combinations of errors in measuring azimuth angles α_1, and α_2, and Doppler shifts Δf_1 and Δf_2. The measurement errors and the corresponding range estimate are tabulated in Table 3. The estimates were made at time = 400 seconds in case 1.

The errors in measuring Δf_1 and Δf_2 have the least effect on the range estimate. The percentage error in the range estimate is about the same as the percentage error in these measurements. However, the errors in measuring azimuth have much greater effect. Here the errors in the range estimates are considerable. This is mainly due to the azimuth errors yielding very inaccurate $\dot{\alpha}$ estimates, which has the effect noted in the previous section. The subject of measurement error and error sensitivity needs further investigation.

3.2.5 (U) Single Baseline Model.

Simulations of the two cases described in 3.2.1 were also done using the single baseline model. The model failed to give good range estimates in nearly every situation. The probable reason for this is error introduced by the assumption of constant $\dot{p}$ and $\dot{\alpha}$ over the interval Δt. At the present time it is not clear whether or not the single baseline model is practical. However, further simulations using this technique will be investigated.

TABLE 3. (U) ESTIMATED RANGE WITH MEASUREMENT ERROR (CASE 1). (U)

Error in α_1 (degrees)	Error in α_2 (degrees)	Error in Δf_1 (Hertz)	Error in Δf_2 (Hertz)	Actual p (km)	Estimated p (km)
0.0	0.0	0.0	0.0	117.2	118.3
0.0	0.0	0.0	0.2	117.2	122.2
0.0	0.0	0.0	-0.2	117.2	114.7
0.0	0.0	-0.2	0.0	117.2	120.2
0.0	0.0	0.2	0.0	117.2	116.6
0.0	0.0	-0.2	0.2	117.2	124.1
0.0	0.0	0.2	-0.2	117.2	112.8
2.0	0.0	0.0	0.0	117.2	136.5
-2.0	0.0	0.0	0.0	117.2	102.3
0.0	-2.0	0.0	0.0	117.2	106.2
0.0	2.0	0.0	0.0	117.2	131.9
2.0	-2.0	0.0	0.0	117.2	122.6
-2.0	2.0	0.0	0.0	117.2	113.8
2.0	-2.0	-0.2	0.2	117.2	127.9
-2.0	2.0	0.2	-0.2	117.2	107.9

NOTE:

Exact α_1 = 82.49°
Exact α_2 = 26.19°
Exact Δf_1 = 6.174 Hz
Exact Δf_2 = 4.636 Hz
Time = 400 seconds

3.2.6 (U) Summary and Conclusions.

In summary, the double-baseline, one-measurement model yielded reasonably accurate trajectory estimates for two different simulations. The model was found to be more accurate when the azimuth was not changing ($\dot{\alpha} = 0$). It is much more sensitive to azimuth measurement error than it is to Doppler-shift measurement error. Since azimuth measurement is likely to be a difficult task in a practical implementation of this technique, investigation of ways to minimize the effect of azimuth errors should be initiated. This model should be tested further to uncover any undetected difficulties.

3.2.6 (U) --Continued.

At the present time the single baseline model has not been shown to be feasible. The double-baseline, two-measurement model has not been tested.

Section 4

DETECTION SYSTEM

4.1 (U) GENERAL SYSTEM CONSIDERATIONS.

The analysis and simulation results discussed in Sections 2 and 3 were developed with the implicit assumption that the hardware to provide the necessary azimuth and Doppler measurements could be made available. In fact, an HF prototype system for tracking low-flying targets at distances beyond radar line of sight can be built with available hardware. The item of greatest concern in implementing such a system is the difficulty of building an accurate shipboard HF direction finding system. The following subsections describe the techniques and hardware that could be used to implement the system.

4.2 (U) DOPPLER MEASUREMENT.

Precise target Doppler measurements (within 0.1 Hz) have long been made by both R&D and operational over-the-horizon (OTH) radar systems. A block diagram of a typical single channel receiving and data processing system is illustrated in Figure 8. Digitally tuned, synthesizer controlled receivers are preferred for their frequency stability. Each receiver output would be digitally spectrum analyzed with 0.1 Hz resolution with approximately a 50 Hz bandwidth to cover the maximum expected target Doppler shift. The Doppler shift would be displayed on a hard copy fax in the standard time-frequency-intensity format. The Doppler shift as measured from the direct path carrier could be scaled manually by the operator or scaled digitally for direct computer input using a x-y digitizing arm.

4.3 (U) SHIPBORNE DF CONSIDERATIONS.

Direction finding (DF) from a shipborne platform involves many of the problems encountered by shore based DF systems such as dense signal environment, multimode effects, and reradiation from nearby obstacles. It is also constrained by the practical size of HF DF antenna arrays that can be employed. The signal environment varies according to radio frequency (RF) band of operation and geographical location of the platform. For operations in the middle of the Atlantic and Pacific oceans

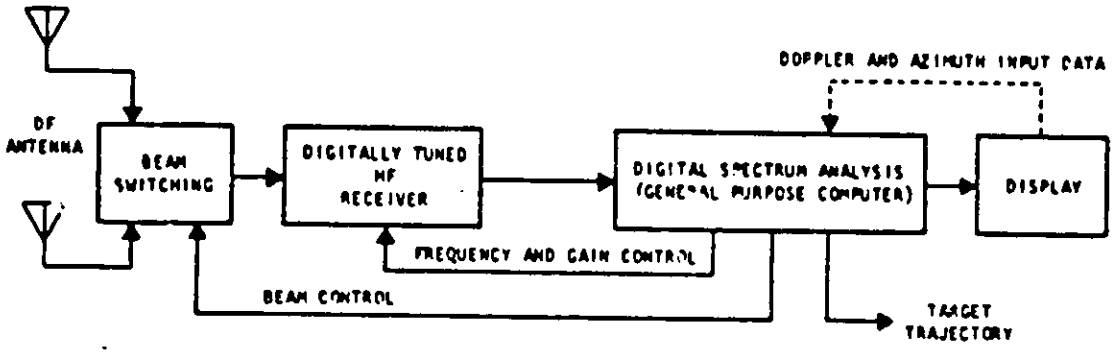

Figure 8. (U) A Typical Single-Channel Receiving and Processing System. (U)

4.3 (U) -- Continued.

a dense signal environment may not exist. However, for DF operation in the Mediterranean and near urban regions this problem area can become severe. Narrow bandwidths (e.g., 300-3000 Hz) can be used on DF receivers to minimize this problem. In addition, azimuth and elevation discrimination can be employed in the antenna system design to extract the DF information from the signal of interest in a dense environment.

The multimode effect can become a problem when a skywave as well as surface wave of approximately equal amplitude impinges on the DF system. Because of the phase shift due to the difference in path lengths, reinforcement and cancellation of signals occur that will make DF measurements difficult for any HF DF array. Because the signal reflected from the target is expected to be principally a surface wave, its greater amplitude will help to minimize any multimode effects.

The most severe problem of shipborne DF systems is that due to the reradiation of an incoming wave from the various superstructure elements. Many solutions have been attempted but most seem to be unsatisfactory because of the constraints and requirements placed on a shipborne DF system. These constraints are concerned with --

(a) the size of the antenna array and

(b) the location/space for DF system components

The size of the HF DF array is limited by the dimensions of the ship. Because the principal dimension (length) is on the order of 400 feet (destroyer class ship) and much of this length is not available for a DF system, a wide aperture HF DF antenna array (greater than 200 feet) is not generally feasible. The conventional wide-aperture antenna system has the dual advantage of achieving a high signal-to-noise ratio (from the gain of the antenna array) and high DF resolution (from the directivity of the array). Such a system has the additional advantage that a certain amount of reradiation rejection is possible from the directivity of the array. The size constraint of shipborne arrays prevents these advantages from being realized. One alternative is to employ a narrow aperture system. For this approach, which is very susceptible to reradiation effects, a location on the top of a mast away from superstructure elements is required. However, the premium for mast and topside space make this alternative infeasible in most cases.

4.3 (U) --Continued.

The requirements that must be met for shipborne HF DF systems vary according to application but generally may be stated as shown in Table 4. Many of the existing and proposed systems meet the majority of these requirements. The principal requirements that are difficult to completely satisfy are the DF accuracy and the azimuth and elevation coverages. This is due to the reradiation effects that cause DF errors as described above for both amplitude and phase comparison systems.

To date only two approaches appear promising for satisfying the shipborne DF requirements. These are:

(a) the multiple-baseline/pattern-recognition (MB/PR) system and

(b) the switched linear array Doppler (SLAD) direction finding system.

The characteristics of these two systems and their applicability to the early warning (EW) problem are described below. The references in footnotes 1 and 2 below contain more detailed descriptions of the systems.

4.3.1 (U) Multiple Baseline/Pattern Recognition System.

The multiple baseline/pattern recognition (MB/PR) system was initially suggested by D. Marx at Naval Electronic Laboratory Center (NELC) and employs an array of antenna elements distributed around the ship. The phase difference between pairs of elements is measured to form an input or signal vector. This vector is compared against a calibration matrix to determine the direction of arrival of the incoming signal. Model measurements were made by NELC for an HF system consisting of 15 antenna elements.[3] These measurements have been analyzed using the MB/PR approach. The results indicate that, for low angle (85.5° from zenith) signals, root-mean-square (RMS) accuracies of better than 3.3° are obtainable. For skywave signals unacceptable accuracies (greater than 10°) resulted. For the surface-wave mode, for which the polarization is essentially vertical, the RMS accuracy improves to 1.8° (or less). For low-flying target detection applications

1 K. E. Spencer, S. N. Watkins, J. Greisser, A Study of the Switched Linear Array Doppler Direction-Finding System, SES-WD M1372, November 1970. (UNCLASSIFIED publication).

2 C. Cornwell, Shipboard HF DF Final Report, SES-WD G-942, January 1971. (UNCLASSIFIED publication).

3 NELC Technical Document No. 72.

Table 4. (U) GENERAL REQUIREMENTS FOR A SHIPBORNE HF DF SYSTEM. (U)

Parameter	Specification
Maximum dimension	150 feet
System location	on deck
DF accuracy	4 degrees RMS or better
System sensitivity	8-10 μV/m
Azimuth coverage	360°
Elevation coverage	70° (above horizon)
Dependence on signal characteristics	independent of modulation and multiple signals

4.3.1 (U) -- Continued.

where the primary propagation mode is a surface wave the MB/PR approach appears to be promising in terms of satisfying the DF accuracy requirement and overcoming the reradiation problem aboard ships.

4.3.2 (U) Switched Linear Array Doppler (SLAD) Direction Finding System.

The switched linear array Doppler (SLAD) direction finding system is a method of determining the direction of arrival of a signal by processing the outputs of two simulated orthogonal moving antennas and a reference antenna. The simulated movement in each direction is accomplished by rapid switching between elements of a linear array. The azimuthal and elevation angles of arrival can be determined from the Doppler frequencies measured along the two orthogonal axes. This approach provides a method of overcoming the reradiation problems aboard ships as well as providing elevation angle-of-arrival information. A worst-case analysis of the DF accuracy was made by Spencer, Watkins and Greiser[4] by considering the reradiation due to a resonant mast. The azimuthal angle errors were determined to be 16.3 degrees RMS at 4 MHz and 4.3 degrees RMS at 8 MHz for a CW signal.

To employ this approach for a target Doppler signal (i.e., a signal source whose frequency changes with time) the frequency of the target signal at the times the Doppler measurements are made must be separately obtained (e.g., from the reference antenna). These measurements then can be processed in a manner similar to that for a CW source.

4.4 (U) COMPARISON OF MB/PR AND SLAD SYSTEMS.

The MB/PR technique has the potential to provide much better DF accuracy than the SLAD approach for surface waves. However, the MB/PR method does not perform well against skywave signals and does not provide elevation angle-of-arrival information. The storage requirements of MB/PR processing are more severe than the SLAD technique because of the size of the calibration matrix. In contrast, the SLAD approach provides the capability to use skywave information and does determine elevation angle of arrival. However, because of its comparatively poor DF accuracy it does not meet the general DF requirements.

4 Op. cit.

UNCLASSIFIED

4.4 (U) -- Continued.

Both approaches should be investigated in more detail before one method is selected over the other for a specific application. The MB/PR technique is expected to be tested using data from an experimental shipborne DF antenna array. A demonstration of this technique is expected to occur sooner than one for the SLAD technique.

UNCLASSIFIED

UNCLASSIFIED

END

DATE
FILMED

3-71

AD 507423 ✓
#156

UNCLASSIFIED
~~SECRET~~

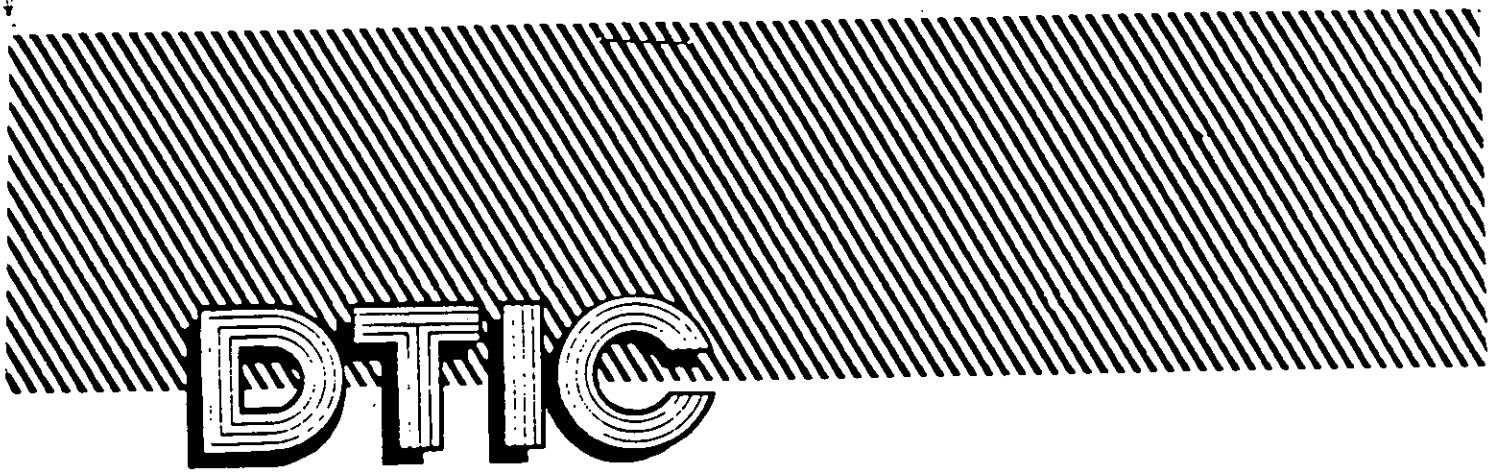

THIS DOCUMENT HAS BEEN DOWNGRADED
TO UNCLASSIFIED
Per Director, DARPA S&IO/TIO
NOV 17 1992

Technical Report

distributed by

Defense Technical Information Center
DEFENSE LOGISTICS AGENCY
CAMERON STATION, ALEXANDRIA, VIRGINIA 22304-6145

UNCLASSIFIED
~~SECRET~~

DO NOT REMOVE
SECURITY SOFTWARE AMERICA D0918134Y

NOTICE

We are pleased to supply this document in response to your request.

The acquisition of technical reports, notes, memorandums, etc., is an active, ongoing program at the Defense Technical Information Center (DTIC) that depends, in part, on the efforts and interests of users and contributors.

Therefore, if you know of the existence of any significant reports, etc., that are not in the DTIC collection, we would appreciate receiving copies or information related to their sources and availability.

The appropriate regulations are Department of Defense Directive 3200.12, DoD Scientific and Technical Information Program; Department of Defense Directive 5200.20, Distribution Statements on Technical Documents (amended by Secretary of Defense Memorandum, 18 Oct 1983, subject: Control of Unclassified Technology with Military Application); Military Standard (MIL-STD) 847-B, Format Requirements for Scientific and Technical Reports Prepared by or for the Department of Defense; Department of Defense 5200.1R, Information Security Program Regulation.

Our Acquisition Section, DTIC-DDAB, will assist in resolving any questions you may have. Telephone numbers of that office are: (202)274-6847, 274-6874 or Autovon 284-6847, 284-6874.

FEBRUARY 1984

* U.S. Government Printing Office 1985—461 169 38041

1 OF 1
AD507423

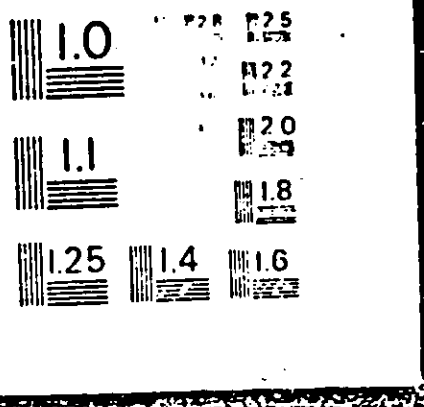

SECURITY MARKING

The classified or limited status of this report applies to each page, unless otherwise marked.
Separate page printouts MUST be marked accordingly.

THIS DOCUMENT CONTAINS INFORMATION AFFECTING THE NATIONAL DEFENSE OF THE UNITED STATES WITHIN THE MEANING OF THE ESPIONAGE LAWS, TITLE 18, U.S.C., SECTIONS 793 AND 794. THE TRANSMISSION OR THE REVELATION OF ITS CONTENTS IN ANY MANNER TO AN UNAUTHORIZED PERSON IS PROHIBITED BY LAW.

NOTICE: When government or other drawings, specifications or other data are used for any purpose other than in connection with a definitely related government procurement operation, the U.S. Government thereby incurs no responsibility, nor any obligation whatsoever; and the fact that the Government may have formulated, furnished, or in any way supplied the said drawings, specifications, or other data is not to be regarded by implication or otherwise as in any manner licensing the holder or any other person or corporation, or conveying any rights or permission to manufacture, use or sell any patented invention that may in any way be related thereto.

UNCLASSIFIED

AD507423

PROJECT AQUARIUS
QUARTERLY REPORT (U)

By
R. STANDLEY
K. SNOW

THIS DOCUMENT HAS BEEN DOWNGRADED
TO UNCLASSIFIED
Per Director, DARPA, SEIO/TIO
NOV 17 1992

D D C
MAR 9 1970
D

2 MARCH 1970

SPONSORED BY
ADVANCED RESEARCH PROJECTS AGENCY
ARPA ORDER NO. 1459

DDC CONTROL NO. [illegible]

SYLVANIA
ELECTRONIC DEFENSE LABORATORIES
Mountain View, California

[redacted]
DOES NOT APPLY
[redacted]
30 | 70 | S | 01415 | 1
LOC | YR | SERIAL | COPY
CONTROL NUMBER
[redacted]
GROUP 4
EXCLUDED FROM AUTOMATIC DOWNGRADING AND DECLASSIFICATION
[redacted]

UNCLASSIFIED

UNCLASSIFIED

Sylvania Electronic Systems-Western Division
Electronic Defense Laboratories
Mountain View, California

(S) Project AQUARIUS Quarterly Report (U)

Principal Investigator R. Standley 415/966-3731
Project Engineer K. Snow 415/966-3186

ARPA Order No. 1459
Effective Date of Contract: 2 June 1969
Contract Expiration Date: 30 June 1970
Amount of Contract: $118,864

This research was supported by the Advanced Research Projects Agency of the Department of Defense and was monitored by the Office of Naval Research under Contract No. N00014-69-C-0446

DDC CONTROL NO.

SECRET

UNCLASSIFIED

(U) TABLE OF CONTENTS (U)

Section	Title	Page
1.	INTRODUCTION	1
1.1	Report Organization	3
2.	EQUIPMENT AND TECHNIQUES	4
2.1	Transmitter Characteristics	4
2.2	Receive Site Characteristics	5
2.3	Receiver System Calibration	5
2.4	Propagation Prediction	8
3.	PREDICTED SYSTEM PERFORMANCE	12
3.1	Missile Detection Performance	12
3.2	Aircraft Detection Areas	13
4.	DATA ANALYSIS	24
4.1	Event 1	24
4.2	Events 2 and 3	27
4.3	Event 4	34
4.4	Event 5	35
5.	SUMMARY	36
6.	REFERENCES	37

(U) ILLUSTRATIONS (U)

Figure	Title	Page
1.	Buoy Tactical Early Warning Concept	2
2.	Block Diagram of High Dynamic Range Receiving System	6
3.	Block Diagram of Twelve Channel Analog Receiving System	7
4.	Sample Detection Regions	21
5.	Network Geometry	25
6.	Event 1 Flight Pattern	28
7.	Experimentally Collected Data	29
8.	Experimentally Collected Data	30
9.	Experimentally Collected Data	32
10.	Flight Path for Events 2 and 3	33

(U) TABLES (U)

Table	Title	Page
1	Predicted System Performance for November, 1969 for Buoy 1 at 100 km Range from Cape Kennedy	14
2	Predicted System Performance for November, 1969 for Buoy 2 at 200 km Range from Cape Kennedy	15
3	Predicted System Performance for November, 1969 for Buoy 3 at 300 km Range for Cape Kennedy	16
4	Predicted System Performance for November, 1969 for Carter Cay Transmitter	17
5	Predicted System Performance for November, 1969 for Carter Cay Transmitter Using Frequencies near the MUF	18
6	Summary of Detection Region Calculations	22
7	Event 1 Summary	24
8	Summary of Operation	26
9	Event 2 and 3 Summary	31
10	Comparison of Predicted and Observed Carrier and Noise Levels	34
11	Comparison of Predicted and Observed Carrier and Noise Levels	35

UNCLASSIFIED

SECTION 1.

(U) INTRODUCTION (U)

Project AQUARIUS is a part of the ARPA sponsored ocean surveillance program under Project MAY BELL. The primary goals of Project AQUARIUS are to experimentally demonstrate the feasibility of detecting both submarine launched ballistic missiles and low-flying aircraft and to compare the experimentally observed detection ranges to theoretically predicted detection ranges. The experimental set-up consists of using a bistatic HF continuous wave radar with low power ocean based buoy transmitters and high sensitivity receivers located on the coast. A detection is made by observing the doppler shifted signal that is scattered from moving targets. In this particular experiment the target is illuminated by line-of-sight or ground wave energy from the transmitter. The scattered doppler shifted target return is received by an ionospheric sky-wave as illustrated in Figure 1.

There has been a continuing requirement for this type of long range detection of small targets since a Cuban pilot flying a MIG penetrated the U.S. radar network and was first spotted by the air controller at the Miami airport.

The experimental results of the controlled aircraft tests have been fairly encouraging and indicate that long range aircraft detection is possible using this low power bistatic radar concept. There appears to be a fair agreement between the predicted detection regions and the regions for which the aircraft has been detected. During a total of three controlled aircraft tests, four detections have been made, two of which are detections of the controlled aircraft. However, during one period, that of 18 December, the detected aircraft does not appear to correspond in time or location with

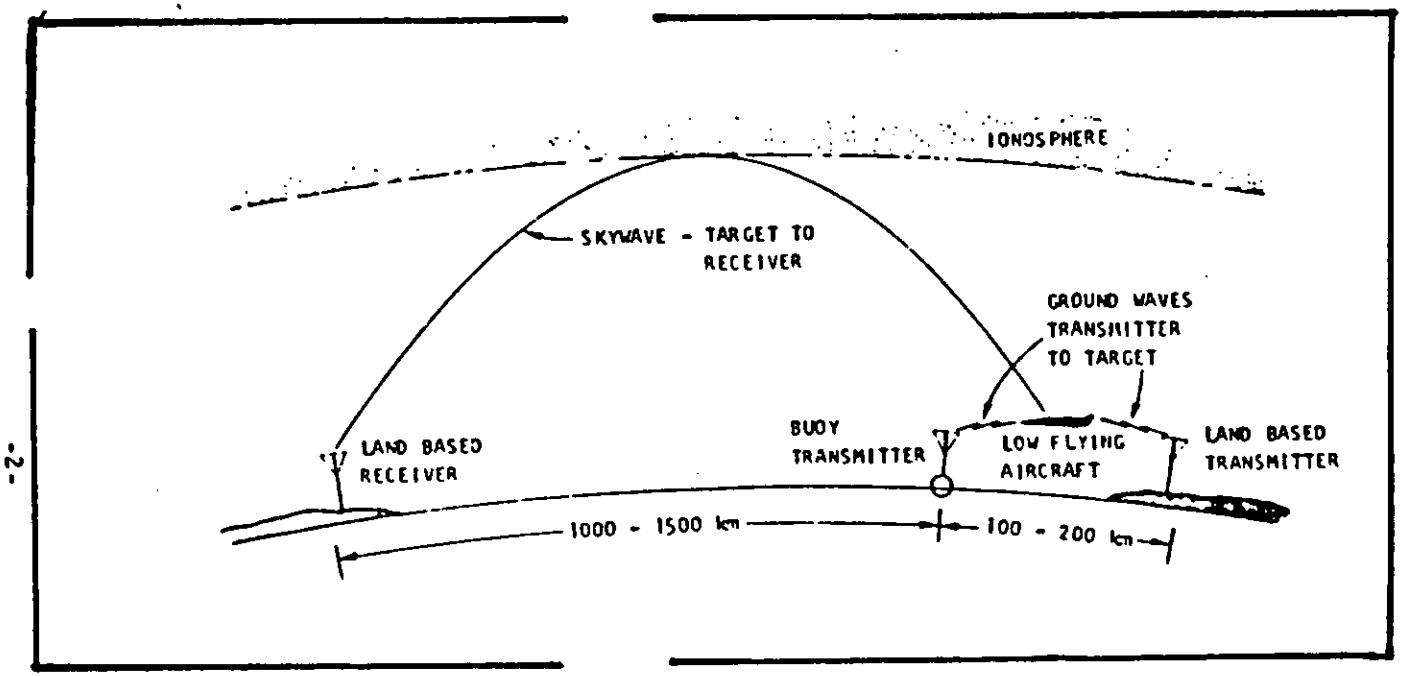

(U)

Figure 1. (S) Illustration of Buoy Tactical Early Warning Concept (U).

UNCLASSIFIED

UNCLASSIFIED

1.0 (U) (S) -- Continued.

that of the controlled aircraft. It is surmised that these detections were of an aircraft flying near the receiver rather than the transmitter.

UNCLASSIFIED

1.1 (U) (S) Repor. Organization.

In Section 2 of this report the basic technique and the hardware being employed for these tests are described. The basic geometry, transmitter and receiver configuration, calibration techniques, propagation calculations, and a description of the propagation program are given in this section. Section 3 contains the description of the detection prediction of Poisedon launchings from Cape Kenendy using the buoys located approximately 100, 200 and 300 km from the launch area. For that particular geometry and the ranges involved, it is observed that the probabilit. of detecting an SLBM is virtuall negligible until the target rises into the ionosphere and acquires a substantiall enhanced cross section. Section 4 contains a description of the controlled aircraft tests, flight plans and the detection observations made. Also, in this section is a tabulation of predicted and observed carrier strengths and noise levels. The purpose of these comparisons is to observe with what reliability these parameters can be predicted with the object of accurately predicting system performance. Finally, Section 5 contains a summary of the problems and the basic results obtained to date.

SECRET

UNCLASSIFIED

UNCLASSIFIED

(U) (S) EQUIPMENT AND TECHNIQUES (U)

Due to the nature and the time frame of this project, all of the data collection hardware has been obtained by using equipment developed by other Project MAY BELL participants or by using hardware developed for other programs. Both the buoy and the CW transmitters at Carter Cay used in these tests, are also used for the groundwave measurements which Raytheon is conducting. The receiving system in use belongs to the LSASA field station located at Vint Hill Farms Station, Va. and consists of a linear disposed antenna array and multi-channel HF receiving and recording equipment.

2.1 (U) (S) Transmitter Characteristics.

Two different types of transmitters have been used in the experiment to date. Those tests conducted prior to December used a buoy mounted transmitter of approximately 10 watts radiating at 5.8 and 9.259 MHz. The antenna on the buoy consists of a top-loaded vertical monopole cut for a quarter wave length at 7.5 MHz. This buoy was anchored off the coast of Florida approximately 120 kilometers down range and at an azimuth of 113 degrees from Cape Kennedy. The tests conducted in January and February have used the CW transmitters on Carter Cay. The power of these CW transmissions has ranged from 100 watts up to 2.3 kilowatts depending upon time and the particular transmitter in use. All of these transmissions radiate into quarter wave vertical monopoles cut for the frequency in use.

SECRET

UNCLASSIFIED

UNCLASSIFIED

2.2 (U) (S) Receiver Site Characteristics.

Two separate receiving systems have been used at the receiver site located at Vint Hill Farms Station. One receiving system is a van mounted high dynamic range digital processing system containing synthesizer controlled receivers (Sylvania R-27A receivers);digital spectrum analysis* using a CDC 1700 general purpose computer and both analog and digital PCM recording capability. The second receiver system is located in two back-to-back house trailers, and consists of a DF set connected to an LDAA steerable beam antenna and 12 analog receiving channels using R390A receivers. The R390A receivers connect to both a real time analog spectral display and a 12 channel analog tape recorder. The block diagrams of these two receiving systems are shown in Figures 2 and 3.

2.3 (U) (S) Receiver System Calibration.

One of the more important goals of this project is to be able to predict the detection performance of the buoy tactical early warning system. Thus, it is desired to compare predicted signal and noise values to actual measured data. Then, if there exist significant discrepancies between the actual and observed data, the predictions must be modified to correct this difference.

The standard calibrations that are performed on the system are to measure the received carrier strength and also the received noise power referenced to a 1 Hertz bandwidth. The process of measuring the received carrier strength is a simple procedure of comparing the receiver IF output signal level when it is connected to the antenna, to the IF output level when the receiver is connected to a synthesizer having the same HF frequency as the carrier signal being measured. The average IF output level for that

* Digital Spectrum Analysis not available after January, 1970 due to termination of the computer lease.

UNCLASSIFIED

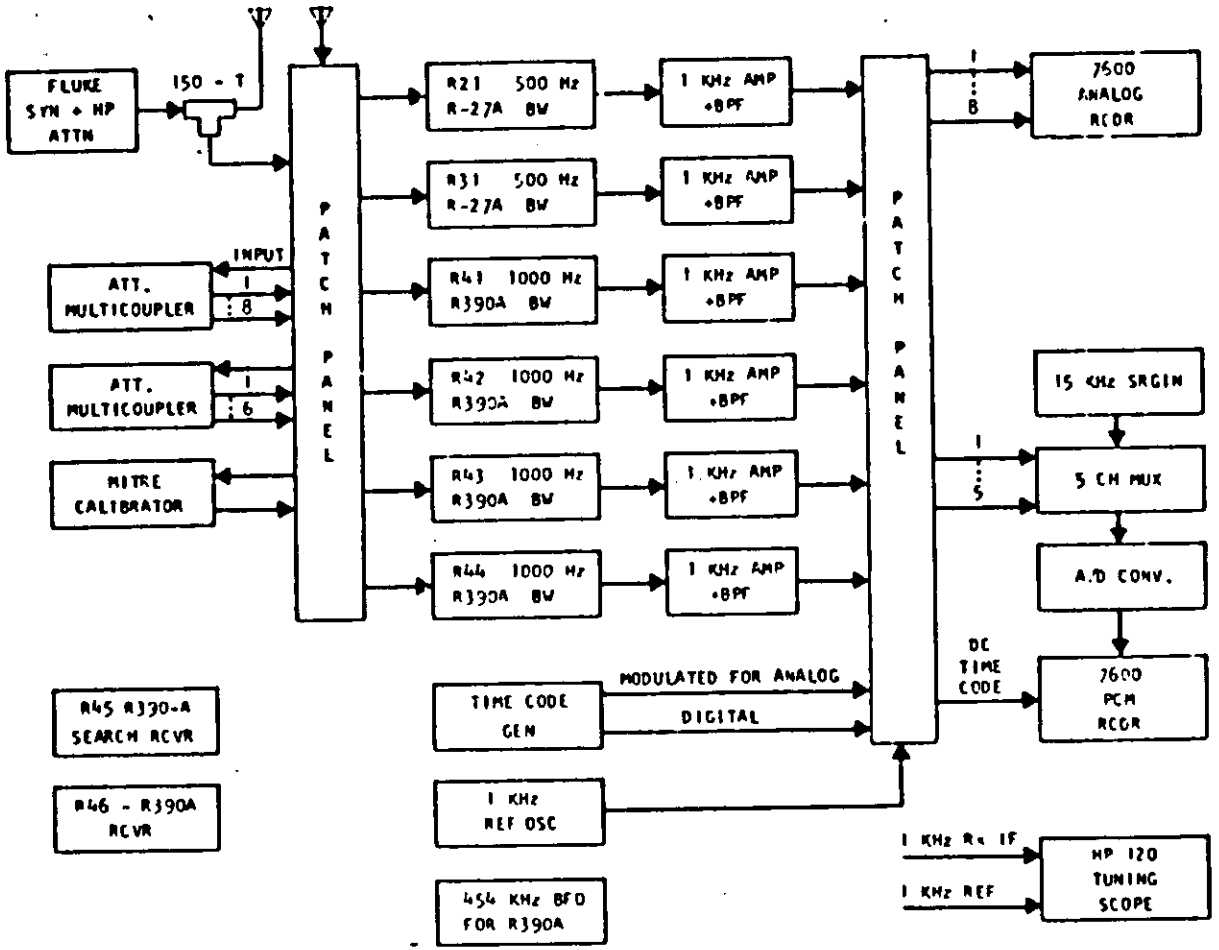

Figure 2. (U) Block Diagram for High Dynamic Range Receiving System (U).

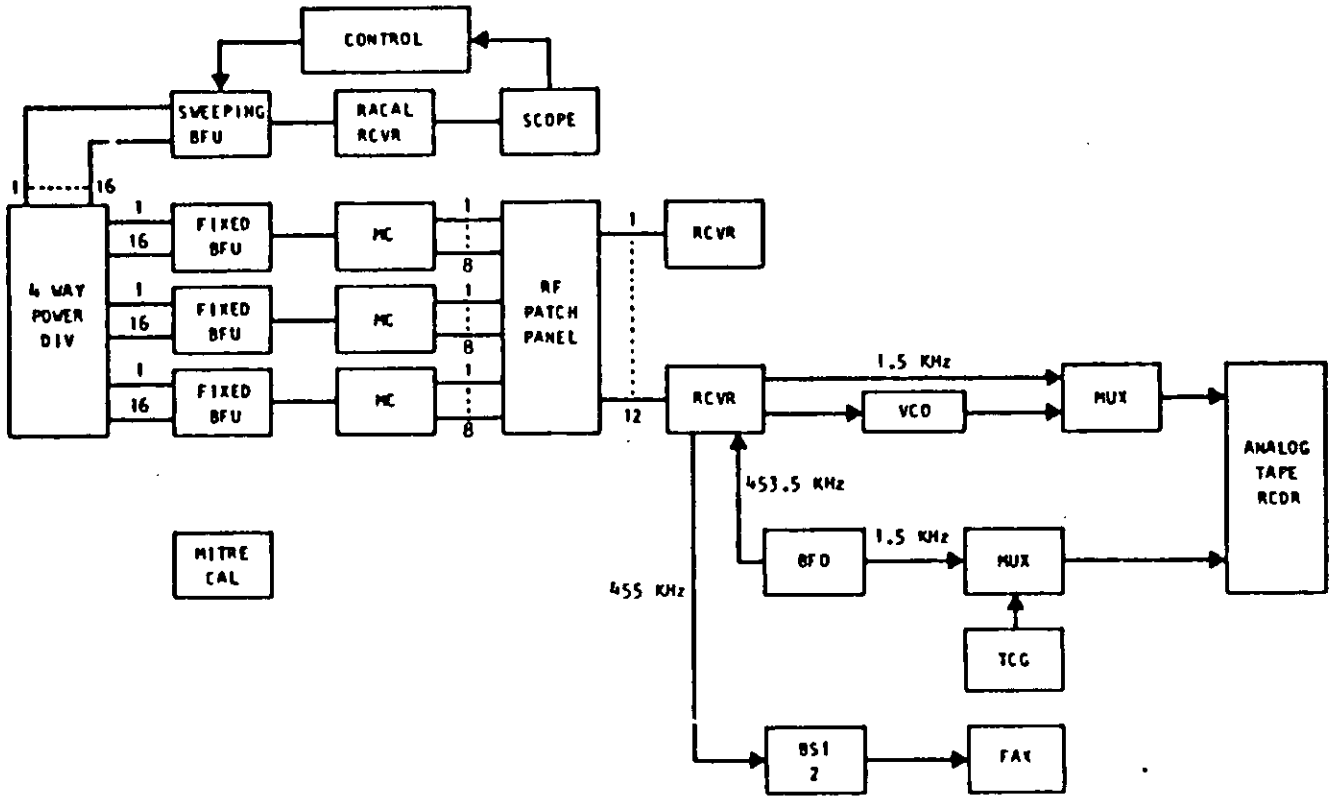

Figure 3. (U) Block Diagram of Twelve Channel Analog Receiving System (U).

UNCLASSIFIED

2.3 (U) (S) -- Continued.

particular carrier signal is noted. Then the synthesizer at the same frequency is input to the antenna terminals and the output amplitude adjusted until the receiver IF output signal strength is the same. The synthesizer signal level is then measured, and converted to db with respect to a watt. Thus this signal substitution method gives the received carrier strength in dbw and is measured within the narrow IF receiver bandwidth.

The determination of the noise level at frequencies near the carrier is done by AM modulating the on-air carrier signal with an audio frequency square wave using a very small percentage modulation. The amplitude of these modulation tones is observed at the output of the real time spectrum analysis display. The modulation percentage is reduced until the modulation tones disappear into the background noise of the display. Since the modulation percentage is easily converted to signal level in db below the carrier and the spectrum analysis bandwidth is 1 Hz, then the relative carrier-to-noise power is directly obtained referenced to a 1 Hz bandwidth. Thus, if the calibration tone disappears into the noise at a level of 64 db below the carrier, it is assumed that the noise value is also 64 db below the carrier value. This carrier-to-noise ratio is then added to the received carrier strength to obtain the measured noise power in dbw per Hz.

2.4 (U) (S) Propagation Prediction.

The propagation prediction program used to estimate the system performance basically combines a modified version of the ITSA/ESSA HF propagation prediction program for mode and mode amplitude prediction; the bistatic radar range equation to predict the received scatter path power; and an ITSA/ESSA noise prediction program to estimate atmospheric, man made, and galactic noise at the receiver site.

SECRET

UNCLASSIFIED

UNCLASSIFIED

2.4 (U) -- Continued.

The prediction program package consists of individual computer programs that (a) compute a target trajectory, (b) predict propagation mode structure and mode amplitude; and (c) predict the Doppler and missile cross-section.

The trajectory simulation program estimates the missile or aircraft trajectory based upon fitting the flight profile to a functional form using a least-squares fit technique. The required inputs to generate the model profile are liftoff and burnout times, launch azimuth, apogee, and range. The program then computes altitude, range, latitude, longitude, velocity, the speed of sound, Mach number, Mach angle, local target bearings, local target elevation angles, and acceleration. The computed parameters serve as inputs to the propagation prediction program to determine mode structures with a time varying terminal point on the trajectory.

The ITSA/ESSA propagation prediction program has been modified to allow for non-congruent hop structures and for propagation to and reflection from a point above the earth. The program predicts the mode structures that meet ionospheric propagation conditions on each of the three paths: the direct path, the transmitter-target half path, and target-receiver half path. In addition, the propagation losses and antenna gains for each mode are determined. For each mode predicted on the transmitter-missile half path, an "incident" (at the target) elevation angle, measured from the local horizon, is found. For each mode predicted on the target-receiver half path, the "scattered" elevation angle is also found. These parameters are then used with a modeled profile to predict Doppler frequencies.

SECRET

UNCLASSIFIED

UNCLASSIFIED

2.4 (U) (S) -- Continued.

Propagation predictions are based on empirically derived world-wide numerical maps of vertical ionosonde data. The results are monthly ionospheric coefficients which can be used with the parabolic layer assumption (parabolic electron density variations in the E and F layers) to predict monthly average ionospheric conditions affecting a specific ray path at any hour of the day.

In the prediction model, all line of sight, E and F propagating modes are determined between the transmitter and the target, between the receiver and the target, and between the transmitter and the receiver. The determination of these "half paths" is a generalization of the ground-to-ground prediction technique to include the case of ground-to-elevation-point predictions.

After the mode structures that meet the ionospheric conditions are identified, (those between horizontal screening and ionospheric penetration) propagation losses and antenna gains are determined. The losses calculated are free space loss (inverse square law), D-layer absorption loss, and ground reflection loss. The NBS empirical adjustment factor is included on the direct-path predictions to account for non-calculated losses. This factor is statistical and varies with season, path length, and earth location of the path. No similar adjustment factor is used or known for the half paths. The antenna types are specified for the system and the appropriate gain routines or gain tables are used.

The target scattering model for missile targets above 100 km is a hyperboloid compressed-ambient ionization in the exhaust-plume bow shock wave. The shock-wave scattering surface is considered hyperboloidal from photographic observations which have shown that the shock-wave surface could be described by a second order function and that the shock-wave surface should be asymptotic to the Mach cone.

SECRET

UNCLASSIFIED

UNCLASSIFIED

2.4 (U) (S) -- Continued.

The direction of the rays for the transmitter-missile and receiver-missile propagation paths uniquely define a plane tangent to the hyperboloidal surface which has the proper orientation for a reflection, provided the incident ray encounters a high enough electron density for reflection.

Since little definitive work has been done to accurately model missile cross sections below 100 km or aircraft cross sections at HF, a constant (adjustable) cross section is used for aircraft and missile targets below 100 km.

The antenna gain patterns for both the monopole transmitter antennas and the LDAA receiving antenna are part of the program. The gain pattern for the LDAA was obtained from data supplied by ITT by using azimuth patterns predicted by the array factor technique for 16 monopole elements and the elevation patterns from scaled model measurements.

SECRET

UNCLASSIFIED

UNCLASSIFIED

SECTION 3.

(U) PREDICTED SYSTEM PERFORMANCE (U)

Propagation calculations to predict system performance using a modified version of the ESSA skywave propagation program described in the previous section have been made for both the direct and the scatter-paths between the receiver site at VHFS, and the buoy transmitters off the Florida coast. The purpose of these calculations was to estimate the feasibility of detecting SLBM missile launchings from Cape Kennedy and controlled aircraft targets using the geometry previously established of buoys at ranges of 100, 200 and 300 km from Cape Kennedy.

3.1 (U) Missile Detection Performance.

Several sets of calculations using the computer predictions were performed. The receiving antenna at Vint Hill Farms Station used for all tests is a tulip element LDAA built by ITT with an assumed maximum gain of 16 dbi. A constant scattering cross section of 100 m^2 was assumed for the missile at all altitudes below 100 km. At altitudes above 100 km the bistatic cross section was modelled using a hyperboloid compressed ambient shock surface. The assumed cross section then changes from 10^2 m at low altitude to values of 10^4 to 10^5 m^2 above 100 km. The three buoy transmitter locations are at 100, 200 and 300 km directly down range from the 105° Cape Kennedy launch azimuth. The Carter Cay transmitters are approximately 285 km down range at a 123° azimuth from Cape Kennedy. The transmitted frequencies for the buoys were the presently assigned values of 5.8 and 9.295 MHz. These frequencies, plus frequencies of 15 and 20 MHz were assumed for the Carter Cay transmitters. The buoys were assumed to have

SECRET

UNCLASSIFIED

3.1 (U) (S) -- Continued.

a transmitting power of 100 watts radiating from monopole antennas. Similarly, the Carter Cay transmitters were assumed to be radiating 5 kw into monopole antennas.

Tables 1 through 5 summarize the results of the propagation calculations. Tables 1 through 4 show target signature-to-noise ratio and carrier-to-signature ratio. Because of the low power and relatively low frequency from the buoy transmitters, the signal-to-noise ratio is almost always negligible below 100 km for any time of the day for either frequency. Only above 100 km with the enhanced target cross section does there appear to be any substantial chance of detection using the buoy transmitters. However, with the Carter Cay transmitter using 5 kw and transmitting on frequencies near the MUF as shown in Table 5 the signature-to-noise ratio and thus the probability of detection at even low altitudes is quite substantial. In fact, there are many cases for which the signal-to-noise ratio exceeds 15 db. Thus, if the high power Carter Cay transmitters continue to operate and transmit on frequencies near the 1 F hop MUF between Carter and VHFS then low altitude SLBM detections in the afternoon should be possible.

3.2 (U) (S) Aircraft Detection Areas.

Even though the probability of detecting SLBM launchings from Cape Kennedy is quite low (due to the relatively long range from the buoy to the target) it is important to determine whether or not aircraft flying controlled patterns near the buoys and Carter Cay can be detected. A way to evaluate this and to clearly display the results is to compute expected detection regions around the transmitter position. Variables that must be considered when calculating detectability regions are bistatic geometry, frequency, transmitter power, target cross section, skywave hop structure, sea state, local time of day and noise level. By choosing median values for

Table 1.

(U) Predicted System Performance for November, 1969

for Buoy 1 at 100 km Range from Cape Kennedy (U)

Altitude	Frequency (MHz)		00:00Z	04:00Z	08:00Z	12:00Z	16:00Z	20:00Z
5km	5.8	S/N	-3.6	-12.2	-14.4	-11.0	-42.6	-30.3
		PC/SB	80.5	80.5	81.3	82.1	83.5	82.6
	9259	S/N	-2.3	-8.8	-7.7	-3.4	-14.3	-5.0
		PC/SB	79.1	79.1	79.9	79.7	79.7	80.3
10km	5.8	S/N	-2.5	-12.1	-14.3	-11.0	-40.5	-31.2
		PC/SB	79.4	80.4	81.2	82.0	81.5	83.6
	9.259	S/N	-2.2	-8.7	-7.6	-3.3	-14.8	-5.0
		PC/SB	79.0	79.0	79.7	79.6	80.3	80.3
40km	5.8	S/N	-2.1	-11.5	-13.8	-10.7	-40.0	-31.9
		PC/SB	79.0	79.9	80.7	81.7	81.0	84.2
	9259	S/N	-0.6	-8.0	-6.9	-1.9	-18.5	-5.0
		PC/SB	77.4	78.4	79.1	78.2	83.9	80.2
119km	5.8	S/N	49.9	10.9	8.6	18.5	37.7	-1.8
		PC/SB	27.0	57.5	58.3	52.5	78.7	54.2
	9.259	S/N	41.5	2.8	3.89	48.1	23.0	24.6
		PC/SB	35.3	67.5	68.4	28.2	42.4	50.6

S/N = Target Signal-to-Noise Ratio (db)

PC/SB = Carrier-to-Target Signal Ratio (db)

UNCLASSIFIED

Table 2.

(U) Predicted System Performance for November, 1969
for Buoy 2 at 200 km Range from Cape Kennedy (U)

Altitude	Frequency (MHz)		00:00Z	04:00Z	08:00Z	12:00Z	16:00Z	20:00Z
5 km	5.8	S/N	-9.9	-18.5	-20.7	-17.3	-49.0	-36.5
		PC/SB	84.9	83.9	84.7	85.0	86.4	86.0
	9.259	S/N	-8.6	-15.1	-14.0	-9.7	-20.6	-11.3
		PC/SB	76.6	76.6	77.3	78.0	76.7	77.6
10 km	5.8	S/N	-8.9	-18.4	-20.7	-17.3	-46.9	-37.6
		PC/SB	93.9	83.9	84.7	85.0	84.4	87.0
	9.259	S/N	-8.5	-15.0	-13.9	-9.7	-21.2	-11.4
		PC/SB	76.5	76.5	77.2	77.9	77.3	77.6
40 km	5.8	S/N	-8.6	-18.1	-20.3	-17.2	-44.4	-33.5
		PC/SB	83.6	83.5	84.3	84.9	81.9	82.9
	9.259	S/N	-7.1	-14.5	-13.4	-8.4	-20.7	-11.5
		PC/SB	75.1	76.1	76.7	76.7	78.8	77.8
119 km	5.8	S/N	20.6	11.9	7.6	7.7	-49.1	-18.5
		PC/SB	54.4	53.6	54.4	60.0	86.6	68.0
	9.259	S/N	13.5	3.1	4.15	27.6	22.0	27.6
		PC/SB	54.7	58.5	59.2	40.6	34.1	38.6

S/N = Target Signal-to-Noise Ratio (db)

PC/SB = Carrier-to-Target Signal Ratio (db)

UNCLASSIFIED

Table 3.

(U) Predicted System Performance for November, 1969

for Buoy 3 at 300 km Range from Cape Kennedy (U)

Altitude	Frequency (MHz)		00:00Z	04:00Z	08:00Z	12:00Z	16:00Z	20:00Z
5km	5.8	S/N	-20.3	-30.4	-32.8	-28.3	-70.7	-55.2
		PC/SB	89.7	90.3	91.3	90.0	102.2	98.9
	9.259	S/N	-19.3				-34.9	-24.6
		PC/SB	78.4				82.0	82.2
10km	5.8	S/N	-12.5	-22.0	-24.3	-21.0	-50.5	-41.2
		PC/SB	81.9	81.9	82.8	82.7	82.0	85.0
	9.259	S/N	-12.2	-18.6	-17.5	-13.3	-24.8	-15.0
		PC/SB	71.2	71.2	72.3	72.9	82.5	72.6
40km	5.8	S/N	-12.4	-21.8	-24.1	-21.0	-48.1	-37.3
		PC/SB	81.8	81.7	82.5	82.7	79.7	81.0
	9.259	S/N	-10.9	-18.3	-17.2	-12.1	-23.9	-15.3
		PC/SB	70.0	70.9	72.0	71.7	71.6	72.9
119km	5.8	S/N	-10.0	2.3	-0.7	12.7	-56.9	-27.2
		PC/SB	59.5	57.6	59.1	49.0	88.4	70.6
	9.259	S/N	3.3	-4.3	-4.8	16.7	7.7	13.7
		PC/SB	55.7	56.9	59.6	42.9	39.4	43.9

S/N = Target Signal-to-Noise Ratio (db)

PC/SB = Carrier-to-Target Signal Ratio (db)

UNCLASSIFIED

Table 4.

(U) Predicted System Performance for November, 1969.

for CARTER CAY Transmitters (U)

Altitude	Frequency (MHz)		00:00Z	04:00Z	08:00Z	12:00Z	16:00Z	20:00Z
5km	5.8	S/N	0.7	-7.8	-10.1	-6.7	-38.3	-25.9
		PC/SB	84.9	83.9	84.7	85.0	85.9	85.1
	9.259	S/N	2.1	-4.4	-3.3	0.9	-10.0	-0.7
		PC/SB	80.4	79.5	80.2	80.8	79.0	80.0
10km	5.8	S/N	1.8	-7.8	-10.0	-6.7	-36.2	-26.9
		PC/SB	83.5	83.9	84.7	85.0	83.9	86.1
	9.259	S/N	2.1	-4.3	-3.2	1.0	-10.5	-0.7
		PC/SB	80.3	79.4	80.1	80.8	79.6	80.1
40km	5.8	S/N	2.0	-7.5	-9.7	-6.6	-33.8	-22.9
		PC/SB	83.6	83.6	84.3	84.9	81.5	82.1
	9.259	S/N	3.5	-3.9	-2.8	2.2	-10.1	-0.9
		PC/SB	79.0	79.0	79.7	79.5	79.2	80.3
119km	5.8	S/N	36.8	27.3	24.8	21.5	-40.7	-10.4
		PC/SB	48.8	48.8	49.8	56.8	68.4	69.1
	9.259	S/N	29.2	21.0	20.1	45.2	24.7	25.3
		PC/SB	53.3	54.1	56.7	36.5	44.4	54.1

S/N = Target Signal-to-Noise Ratio (db)

PC/SB = Carrier-to-Target Signal Ratio (db)

TABLE 5.

(U) Predicted System Performance for November, 1969
for Carter Cay Transmitter Using Frequencies near the MUF. (U)

Altitude	Frequency		0000Z	MUF	0400	MUF	0800	MUF	1200	MUF	1600	MUF	2000	MUF
5 KM	15 MHz	S/N	9.93	13.56	-		-		-		13.4	21.80	10.4	21.07
		PC/SB	60.3		-		-				59.2		60.7	
	20 MHz	S/N	-		-		-		-		16.5	21.77	11.3	21.03
		PC/SB	-		-		-				73.3		74.8	
10 KM	15 MHz	S/N	10.0	13.65	-		-		-		12.3	22.07	10.4	21.28
		PC/SB	60.2		-		-				60.2		60.7	
	20 MHz	S/N	-		-		-		-		16.5	22.00	11.3	21.21
		PC/SB	-		-		-				73.4		74.8	
40 KM	15 MHz	S/N	11.3	14.20	-		-		19.3	12.99	12.0	22.73	9.2	22.60
		PC/SB	59.0		-		-		60.6		60.6		61.8	
	20 MHz	S/N	-		-		-		-		18.2	23.51	13.2	22.38
		PC/SB	-		-		-				71.7		72.9	
119 KM	15 MHz	S/N	26.7	15.83	-		-		47.1	14.70	33.5	14.53	51.1	26.40
		PC/SB	43.6		-		-		32.8		39.2		20.0	
	20 MHz	S/N	18.6	15.55	-		-		-		56.6	28.16	48.7	25.80
		PC/SB	190.4		-		-		-		33.2		37.4	

S/N = Target signal-to-noise ratio (db)

PC/SB = Carrier-to-target signal ratio (db)

3.2 (U) (C) -- Continued.

all the variables and changing the values of a single variable at a time, regions where detections are most likely to occur can be generated, as well as obtaining an understanding of how a particular variable affects the overall detection area.

Detectability regions have been calculated for various frequencies, hop structures and noise levels using a buoy located 120 km from Cape Kennedy as the transmitter and VIIFS, Va. as the receiver. A sea state of 5, transmitter power of 50 watts, groundwave propagation from transmitter to target and skywave propagation from target to receiver and a required signal to noise ratio of 3 db have been assumed.

The following technique is applied to find the area of detectability: From the radar range equation

$$L_R = L_{BT} + L_{BR} - G_T - G_R - \left[10 \log \frac{4\pi\sigma}{\lambda^2}\right]$$

where L_R = total loss

L_{BT} = spreading loss from transmitter to target (db)

L_{BR} = spreading loss from target to receiver (db)

G_T = gain of the transmitter antenna (dbi)

G_R = gain of the receiver antenna (dbi)

σ = cross section of target in m^2

λ = wave length

G_T, G_R and $10 \log \frac{4\pi\sigma}{\lambda^2}$ are known and L_R is calculated by assuming a value for atmospheric noise, adding to it the transmitter power and the required 3 db signal-to-noise ratio. Substituting the calculated value for

3.2 (U) (S) -- Continued.

L_R into the equation, $L_{BT} + L_{BR}$ is calculated. By taking the total spreading loss, subtracting the loss contributed by the D layer loss and skywave propagation loss from target to receiver, a value for the spreading loss in the target-transmitter leg is obtained. This loss is the propagation loss incurred by a groundwave and can be converted to the range required for this loss to occur using Barrick's[1] groundwave transmission loss tables. This technique was used to calculate the detection area around the transmitter for various frequencies and atmospheric noise conditions. The results of the detection area calculations are tabulated in Table 6 and a vertical projection of some of the regions onto the ground is shown in Figure 4. The reason for the egg-like shape is that the area boundary is the locus of points such that the product $R_1 R_2$ is equal to a constant.

Referring to Figure 4 we see that the largest area of detection is for 2F hop cases for both 5.8 and 9.259 MHz, as compared to the 1E hop situation. This is because there is substantially less D-layer loss for the 2F hop mode than the 1E hop mode due primarily to the different path lengths in the D-region itself. With higher modes the incident angle through the D-layer is higher, thus the loss on these paths due to D-layer absorption is smaller. For the 2F hop modes the region at 5.8 MHz is larger than the region at 9.259 MHz. This is due to the fact that the loss on the R1 path is smaller at lower frequencies because the spreading loss is directly proportional to the wavelength and as one would expect the larger region for detection exists for the lower frequency. However, on the 1E modes we find the situation is reversed, the higher frequency is also the larger area of detection. This is because the D-layer loss on the 5.8 MHz frequency is substantially more than the D-layer loss at 9.259 MHz and this overcomes the groundwave propagation advantage at the lower frequency.

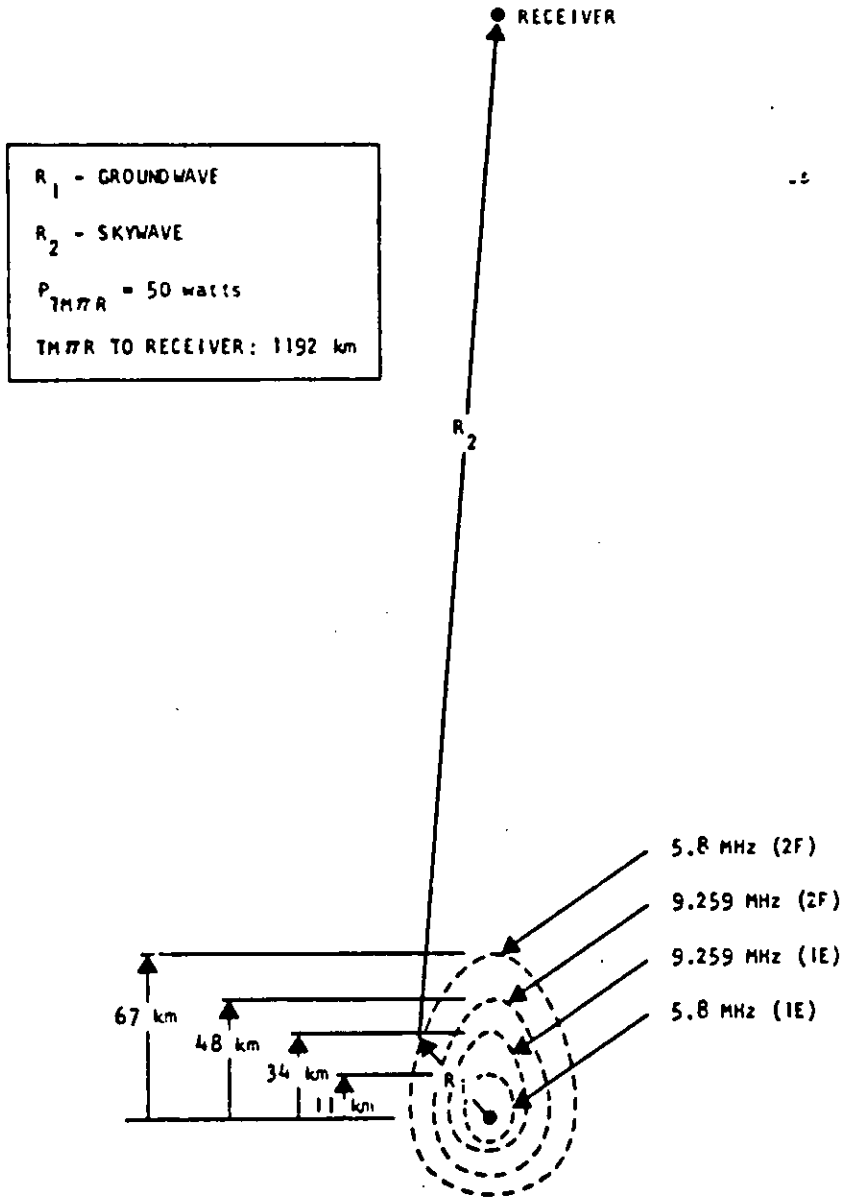

Figure 4. (U) Sample Detection Regions (U).

Table 6.

(U) Summary of Detection Region Calculations (U)

Freq MHz	Hop Structure	R_1 Km	R_1 Loss db	$L_{BT}+L_{BR}$ Loss db	D-Layer Loss db	R_2 Loss db	Atmos Noise dbw
5.8	1E	11	61	211.7	48.5	102.2	-180(B)
5.8	2F	67	79.1	211.7	30.4	102.2	-180(B)
5.8	1E	10	59.5	195.7	34	102.2	-153(M)
9.259	1E	34	80.1	210.7	21.9	108.7	-172(B)
9.259	2F	48	86.2	210.7	15.8	108.7	-172(B)
9.259	1E	44	84.7	208.7	15.3	108.7	-169(M)
9.259	1F	65	90.8	208.7	9.2	108.7	-169(M)
15.00	1F	60	101	216.9	4.0	112	-174(M)
15.00	1F	67	103.6	221.5	5.9	112	-176(B)
20.0	1F	66	113.9	231.5	3.1	114.5	-186(B)
20.0	1F	66	113.6	230.1	2.1	114.5	-185(M)

B = Best noise case 0800-1200 Local Time

M = Medium noise case 1600-1200 Local Time

UNCLASSIFIED

3.2 (U) (S) -- Continued.

From Table 6 we see that the detectability radii (R_1) tend to increase with increasing transmitted frequency. However, once the frequency increases to approximately 15 MHz, the R_1 spreading losses cancel the effect of decreasing D-layer loss and decreasing atmospheric noise so that the growth of the detectability region virtually stops. Note that the detectable radii are approximately the same for 15 and 20 MHz. It is also observed that varying transmitter power and transmitter or receiver antenna gains have the same effect on the size of the detectability regions. That is a db of gain or loss whether generated from varying transmitter power or antenna gain enters the radar range equation in the same way.

UNCLASSIFIED

UNCLASSIFIED

(U) SECTION 4.

(S) DATA ANALYSIS (U)

In this section, two events involving a controlled aircraft flight of a Navy P3B aircraft and two propagation measurements between Carter Cay and VHFS are presented with their specific geometry, predicted and measured results and conclusions derived from the results. These operations are summarized in Table 7 and a map of the network geometry is shown in Figure 5.

4.1 (U) (S) Event 1.

Event 1 on 18 December, 1969, involved a Navy P3B aircraft flying at an altitude between 300 to 600 feet, speed between 200 and 400 knots and used the buoy transmitter located 120 km from Cape Kennedy on an azimuth of 113°. The flight path of the aircraft, along with time (GMT) is shown in Figure 6. The receiver location for this event, as with all Aquarius events, was VHFS, Virginia. The two buoy frequencies of 5.8 and 9.259 MHz were monitored by the receiver. A signature detection was made on 5.8 MHz between 1750-1755Z and 2000Z-2005Z. The propagation conditions are summarized below:

Table 7 (U)
Event 1 Summary (U)

Frequency (MHz)	Carrier Level (dbw)	Noise Level (dbw)	Transmitter Power (W)	Calculated Detection Radii (km)	Hop Structure
5.8	- 92	-160	10	3	1E
				6	2F
9.259	-130	-157	2.5	11	1F
				6	1E

SECRET

UNCLASSIFIED

UNCLASSIFIED

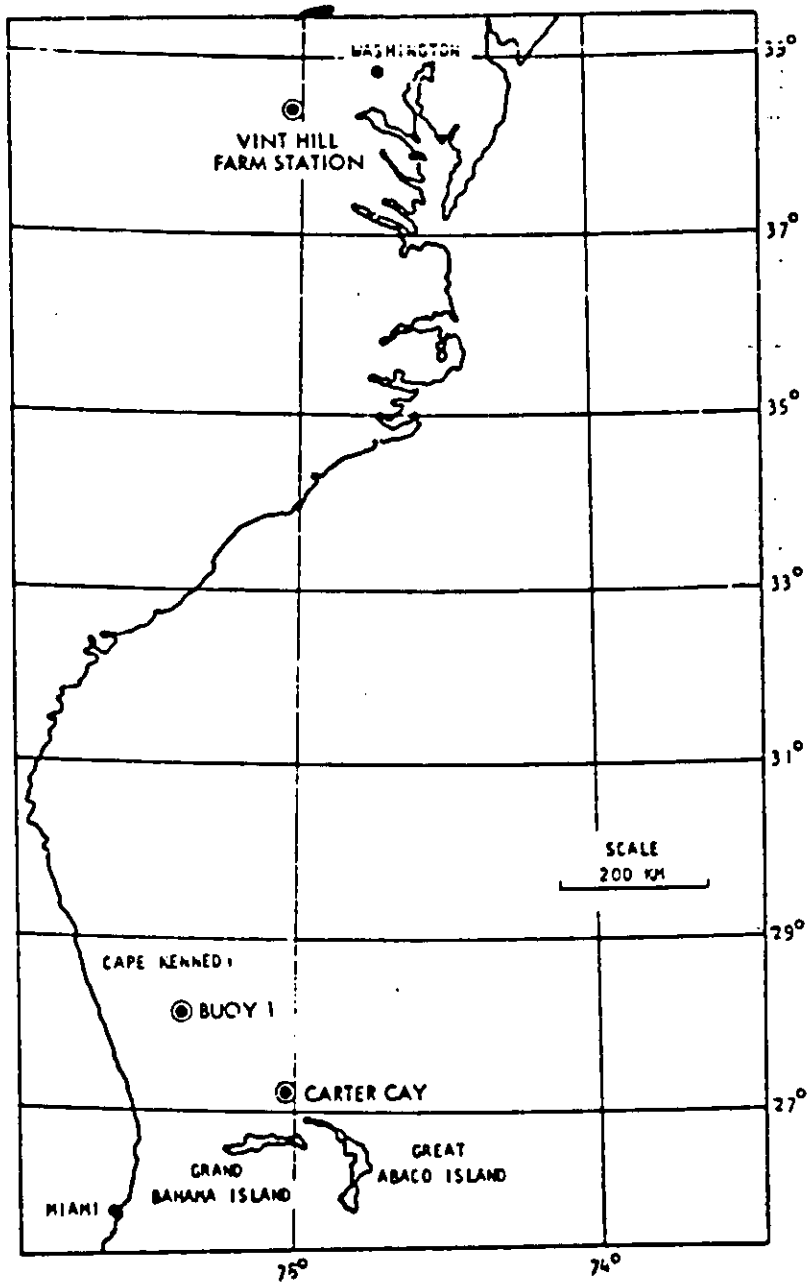

Figure 5. (U) Network Geometry (U).

UNCLASSIFIED

Table 8.

(U) Summary of Operations (U)

EVENT	DATE	TYPE	FREQUENCIES (MHz)	MEASUREMENT OR DETECTION TIMES (GMT)
1	18 Dec 69	AC	5.8	1750-1755 2000-2005
		AC	9.259	ND
		AC	10.167	ND
2	27 Jan 70	AC	15.595	1656
3	27 Jan 70	AC	10.167	1712
4	5 Feb 70	HB	20.250	~1500
		HB	10.167	~1500
		HB	10.167	~2100
		HB	20.250	~2100
5	10 Feb 70	HB	9.259	~1430
		HB	5.8	~1430

AC - Aircraft

ND - Not Detected

HB - Hearability

UNCLASSIFIED

4.1 (U) (S) -- Continued.

It is felt that the detected signature is not the Navy P3B aircraft used in this test but on aircraft flying near the receiver at VHFS. The predicted detectability region for this day extends at best to only 11 km. The P3B aircraft approaches the buoy within only 30 km. The period of the first Doppler signature's sign change occurs 5.2 minutes later than predicted closest approach and the period of the second Doppler signature sign change occurs 2.8 minutes earlier than predicted closest approach. The Doppler signatures obtained shown in Figures 7 and 8 were of the proper frequency for an aircraft but were much stronger than could be expected from a 10 watt transmitter. Thus, due to inconsistant timing, distances of aircraft from the transmitter, strength of detected signatures, and the low power of the transmitters, it is concluded that signature detected was not the P3B aircraft used in the experiment but rather another plane flying over the receiving antenna.

4.2 (U) (S) Events 2 and 3.

Events 2 and 3 on January 27, 1970 involved an aircraft (P3B) climbing to an initial altitude of 24,000 feet and spiralling down to 2000 feet while holding a precise test pattern and maintaining ground speed between 200-300 knots. The aircraft flew the pattern described by Figure 10. Initially approaching the Carter Cay area on its way from CP C3 to CP C8, the aircraft proceeded to fly the pattern C8 to C7 to C6 to Carter Cay to D4 to D5 to Carter Cay to C5 and repeating for altitudes of 24,000, 14,000, 12,000 and 2000 feet. The transmitters were again located on Carter Cay. The frequencies monitored by the receiver at Vint Hill Farms Station were 10.167 and 15.598 MHz. Detection was made at 1712Z on 10.167 MHz and

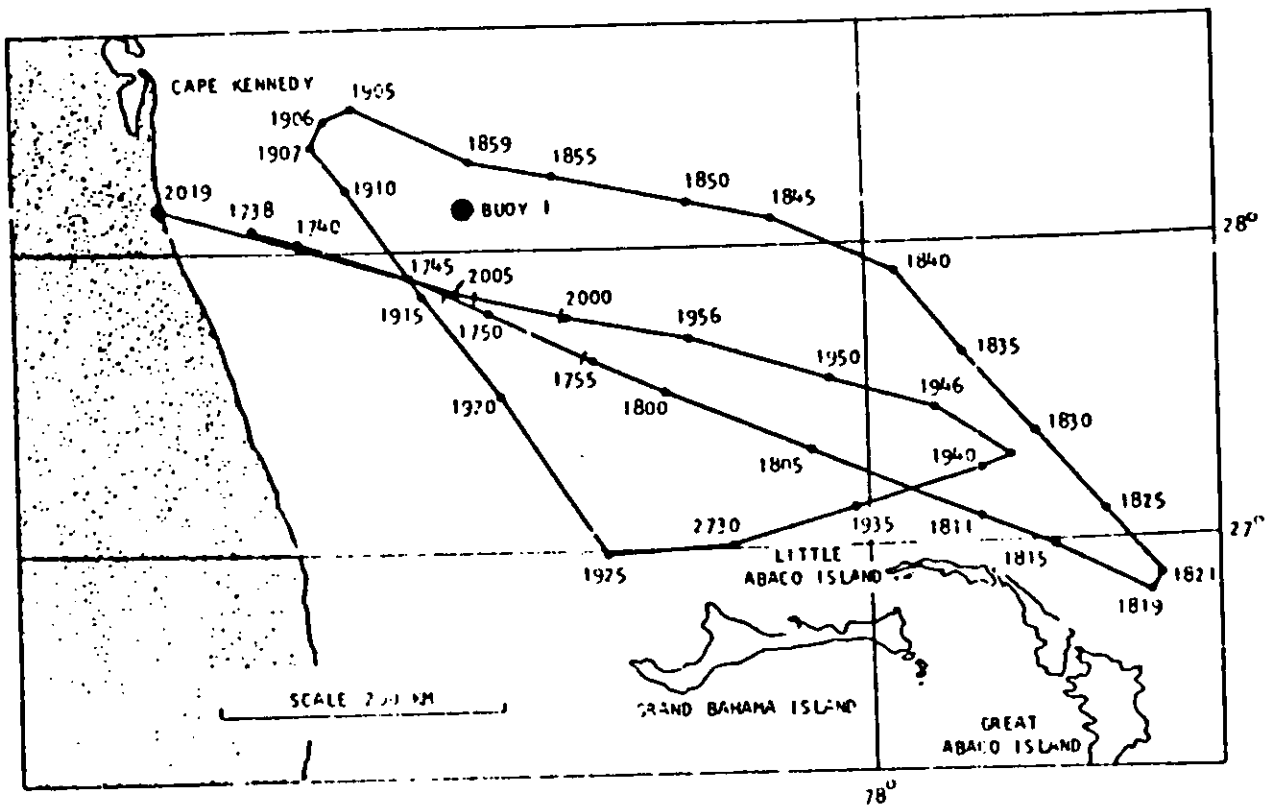

Figure 6. (U) Event 1 Flight Pattern (U).

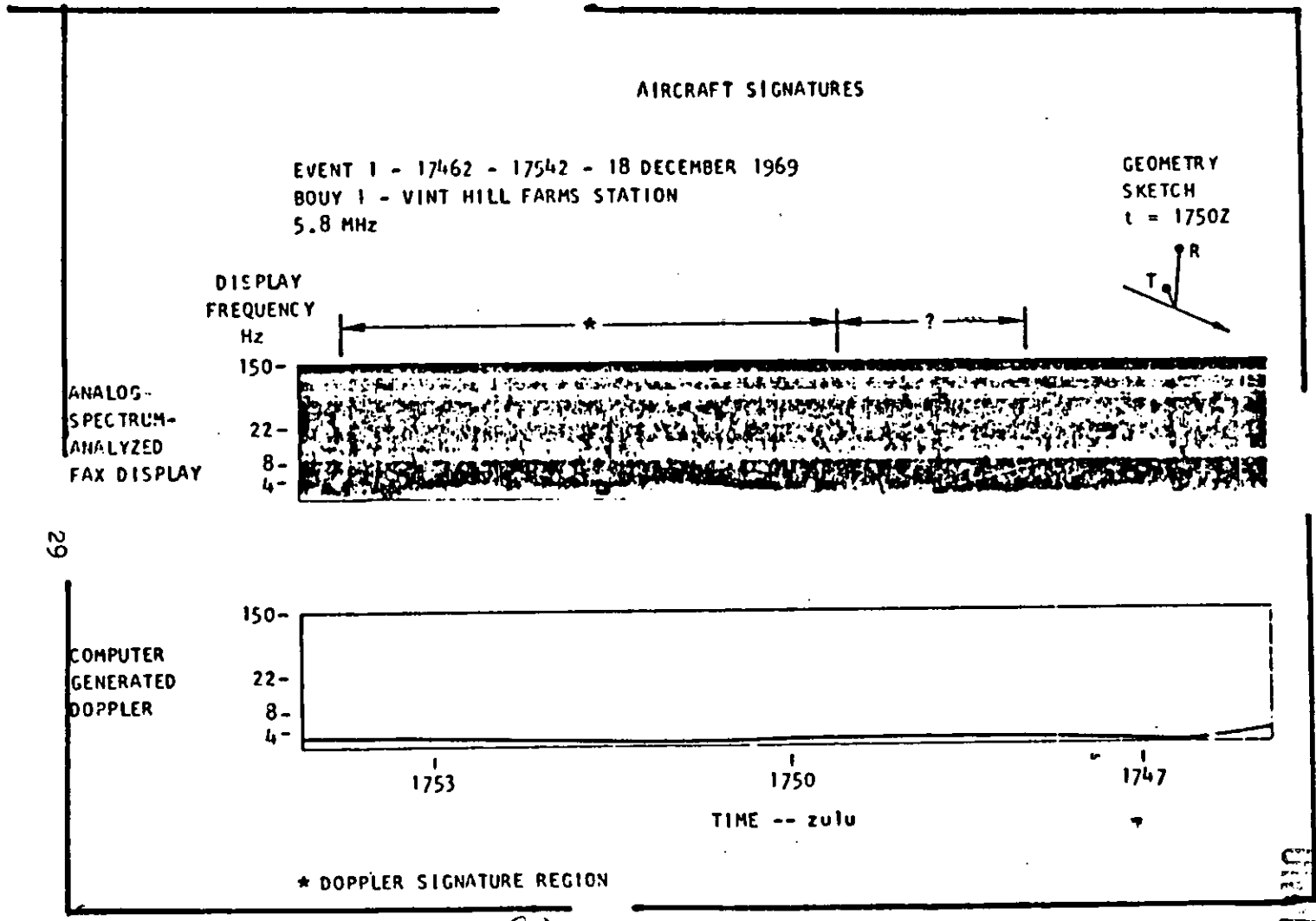

(U)

Figure 7. (~~SECRET~~). Experimentally Collected Data (U).

SECRET
SECRET
DECLASSIFIED
DECLASSIFIED

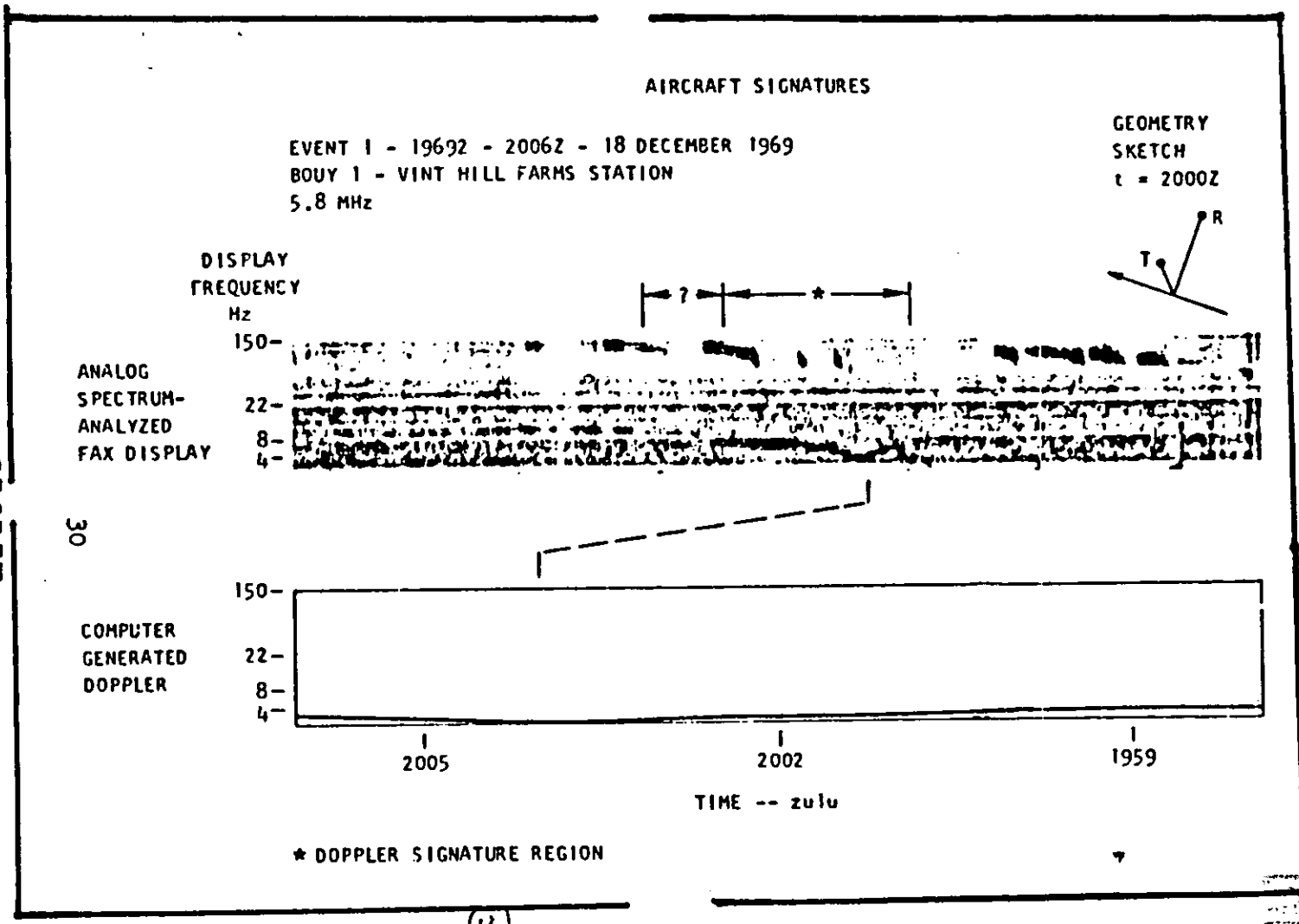

Figure 8. (U) (~~SECRET~~). Experimentally Collected Data (U).

DECLASSIFIED
EDL-C900

UNCLASSIFIED

4.2 (U) (S) -- Continued.

at 15.595 MHz as shown on Figure 9. The propagation conditions for these events are summarized below:

Table 9. (U)

Event 2 and 3 Summary

Frequency (MHz)	Carrier Level (dbw)	Noise Level (dbw)	Tx Power (w)	Detection Time (Z)
10.167	-112	NA	3000	1712
15.595	NA	-145	3000	1655

The signatures detected on this event represent the scattered and doppler shifted energy from the target aircraft during the time of close approach to Carter Cay. However, accurate doppler predictions have not yet been made due to the inexact knowledge of the flight path and the fact that the detections appear to be made during the end of the turning maneuver over Carter. The present doppler modelling for aircraft is being modified to handle out of plane maneuvers and from this improved model, accurate doppler matches will be possible.

We observe from Figure 10 that the detections for both passes on Carter were slightly late with respect to the time that the aircraft indicates it was directly over the transmitter. There is a good possibility that the aircraft flew exactly over the transmitting antenna and thus was in the vertical pattern antenna null. Being in the null of the antenna explains the loss of signature for times over the transmitter. The signatures are detected at the completions of the turning maneuvers over Carter Cay. Signatures for both detected passes of the aircraft are almost identical in both timing and frequency. Thus, the frequency excursion, time correlation, nearness of the aircraft to the transmitter, radiated power from the Carter Cay transmitters, and the weak signature strength make the

SECRET

UNCLASSIFIED

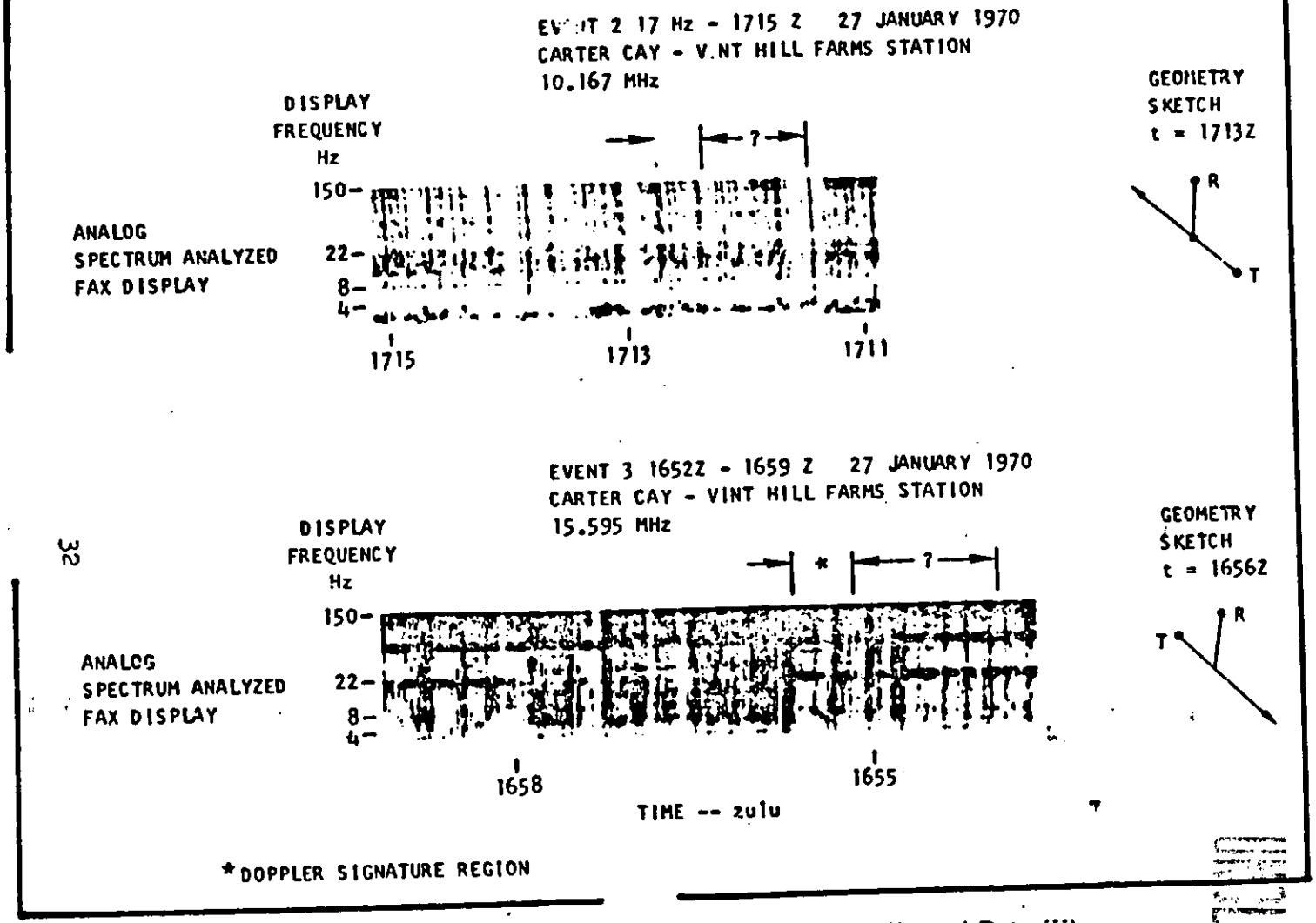

Figure 9. (~~SECRET~~) Experimentally Collected Data (U).

(U)

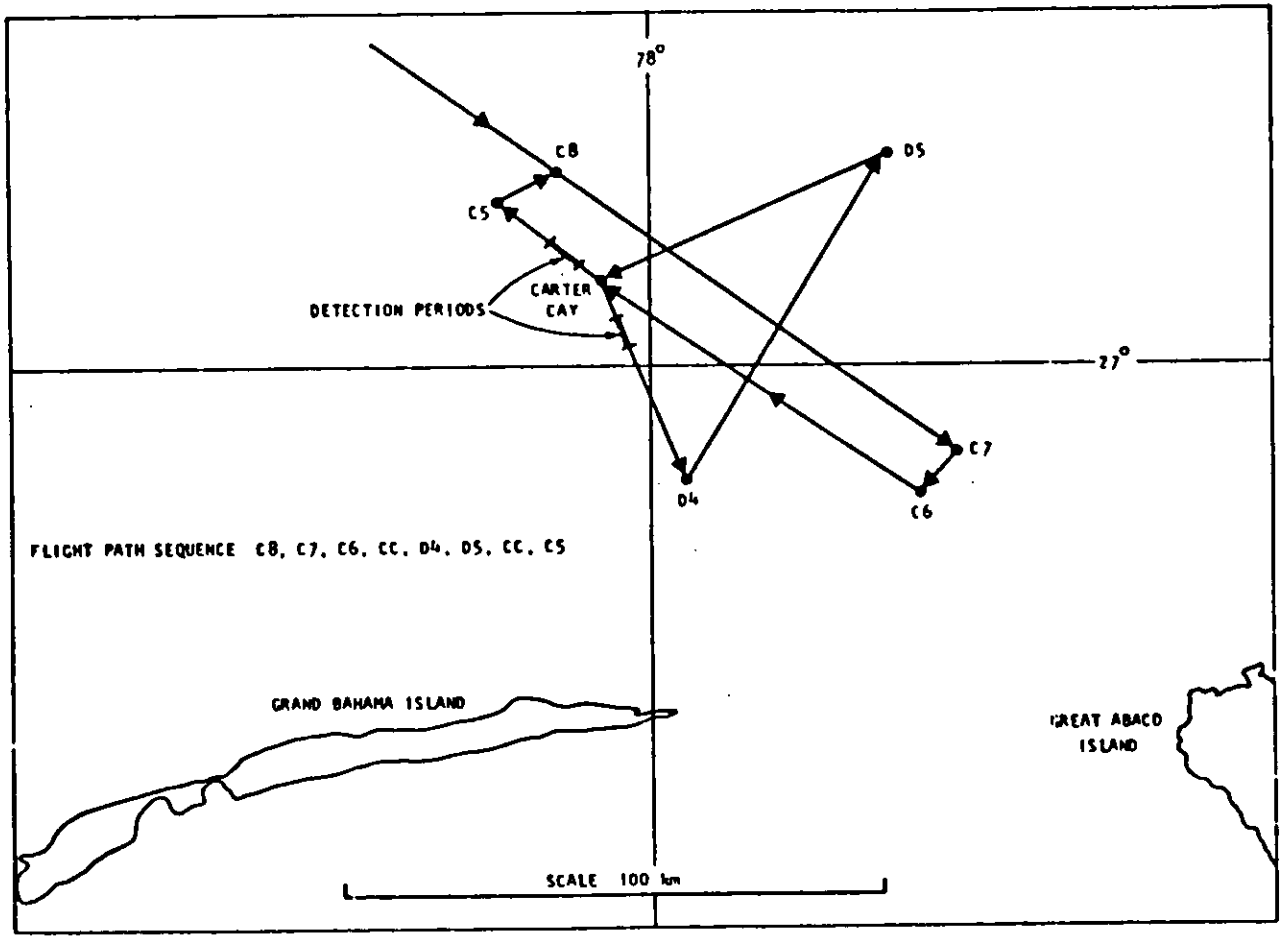

Figure 10. (U) Flight Path for Events 2 and 3 (U).

4.2 (U) -- Continued.

identification of the signature as the target P3B aircraft. The conclusion is that aircraft below 2K feet and within the predicted detectability regions can be detected using this buoy concept if sufficient power is transmitted (3 kw in this case).

4.3 (U) Event 4.

Event 4 was a hearability test, performed on 5 February at 1600 and 1000 hours local, measuring the propagation characteristics from Carter Cay transmitters to the Vint Hill Farms Station receiver. The purpose of the hearability test was to determine how accurately present prediction techniques correlate with measured values and to estimate the hop structures for various frequencies. Tests were performed for two frequencies 10.167 and 20.250 MHz and at two times during the day. It was found that for an assumed 1E hop structure at 10.167 MHz and an assumed 1F hop structure at 20.250 MHz good agreement between predicted and observed carrier levels was obtained. However, the noise predictions were consistently lower than measured values as shown in Table 10. The difference between the predicted and observed noise levels is typically due to co-channel interference which is significantly higher than atmospheric noise.

Table 10 (U)

Comparison of Predicted and Observed Carrier and Noise Levels (U)

Date/Time	Frequency (MHz)	Assumed Hop Structure	Tx Power (kw)	Carrier (dbw) Pred.	Carrier (dbw) Obs.	Noise (dbw) Pred.	Noise (dbw) Obs.
Feb 1600L	10.167	1E	2.1	-79	-76	-162.8	-144
Feb 1000L	10.167	1F	2.1	-58.9	-90	-163	-158
Feb 1600L	20.250	1F	2.1	-62.7	-66	-179.1	-134

4.4 (U) Event 5.

Event 5 was also a hearability test, performed on 16 Feb. at 1430 local time, with the same geometry and purpose as Event 4. Tests were performed for 5.8 and 9.259 MHz. As shown in Table 11, best correlation between measured and observed carrier levels was obtained for an assumed 2F hop structure at 5.8 MHz and an assumed 1E hop structure at 9.259 MHz. As in Event 4, the noise predictions were consistantly lower than measured values. The conclusions from Events 4 and 5 is that 1E, 1F and 2F appear to be the dominate hop structures for 10, 20, 5 MHz respectively. It is also concluded from this limited data base that the propagation prediction is fairly accurate for predicting the received carrier levels, but due to high co-channel interference consistently predicts lower noise levels than are measured.

Table 11.

Comparison of Predicted and Observed Carrier and Noise Levels (U)

Date/Time	Frequency (MHz)	Assumed Hop	Transmitter Power	Carrier (dbw) Pred.	Carrier (dbw) Obs.	Noise (dbw) Pred.	Noise (dbw) Obs.
Feb. 1430L	5.8	1E	75w	-128.2	-110	-160.3	-160
Feb. 1430L		2F	75w	-124.6	110	-162.3	-160
Feb. 1430L	9.259	1E	75w	- 93.2	- 95	-162.8	-139
Feb. 1430L		2F	75w	-104	- 95	-162.8	-139

UNCLASSIFIED

Section 5.

(U) ~~(S)~~ SUMMARY (U)

The operations covered to date include both controlled aircraft tests and hearability tests. The remainder of the operations have not been analyzed because all data on the events including flight paths and transmitter power have not yet been collected at Sylvania for analysis. The most significant conclusion is from Event 2 which seems to demonstrate that the buoy transmitter concept works (with sufficient transmitter power).

The predictions of carrier levels made for the hearability tests on 5 February and 10 February seem to align rather well with measured values. Predictions of noise level is not as successful, being consistently weaker than measured values. This is probably due to local interference and the assumption that the receiving site at VHFS is a "rural" man-made radio noise area. Identification of the receiver site as a "suburban" area is probably more accurate. This would raise the predicted noise level by approximately 20 db thus making it align with measured values much more closely.

SECRET

UNCLASSIFIED

SECTION 6.
REFERENCES

1. Banich, Donald E., "Theory of Ground-Wave Propagation Across a Rough Sea at HF/VHF", Battelle Memorial Institute, Draft Report.

UNCLASSIFIED

END

DATE

FILMED

4-70

UNCLASSIFIED
[redacted]

AD515 288L
#196

DTIC

690602

EXCISED UNDER THE PROVISIONS OF THE FREEDOM OF INFORMATION ACT 5USC552
(b) (1)

Technical Report

APR 22 1993
THIS DOCUMENT HAS BEEN DOWNGRADED TO UNCLASSIFIED
Per Director, ARPA SEIO/TIO

12418

distributed by

Defense Technical Information Center
DEFENSE LOGISTICS AGENCY
CAMERON STATION, ALEXANDRIA, VIRGINIA 22304-6145

DARPA DO NOT REMOVE DARPA
EDARPA00052482A
%DDARPA00031435L

UNCLASSIFIED
[redacted]

NOTICE

We are pleased to supply this document in response to your request.

The acquisition of technical reports, notes, memorandums, etc., is an active, ongoing program at the Defense Technical Information Center (DTIC) that depends, in part, on the efforts and interests of users and contributors.

Therefore, if you know of the existence of any significant reports, etc., that are not in the DTIC collection, we would appreciate receiving copies or information related to their sources and availability.

The appropriate regulations are Department of Defense Directive 3200.12, DoD Scientific and Technical Information Program; Department of Defense Directive 5200.20, Distribution Statements on Technical Documents (amended by Secretary of Defense Memorandum, 18 Oct 1983, subject: Control of Unclassified Technology with Military Application); Military Standard (MIL-STD) 847-B, Format Requirements for Scientific and Technical Reports Prepared by or for the Department of Defense; Department of Defense 5200.1R, Information Security Program Regulation.

Our Acquisition Section, DTIC-DDAB, will assist in resolving any questions you may have. Telephone numbers of that office are: (202)274-6847, 274-6874 or Autovon 284-6847, 284-6874.

FEBRUARY 1984

★ U.S. Government Printing Office 1984—461 189 38047

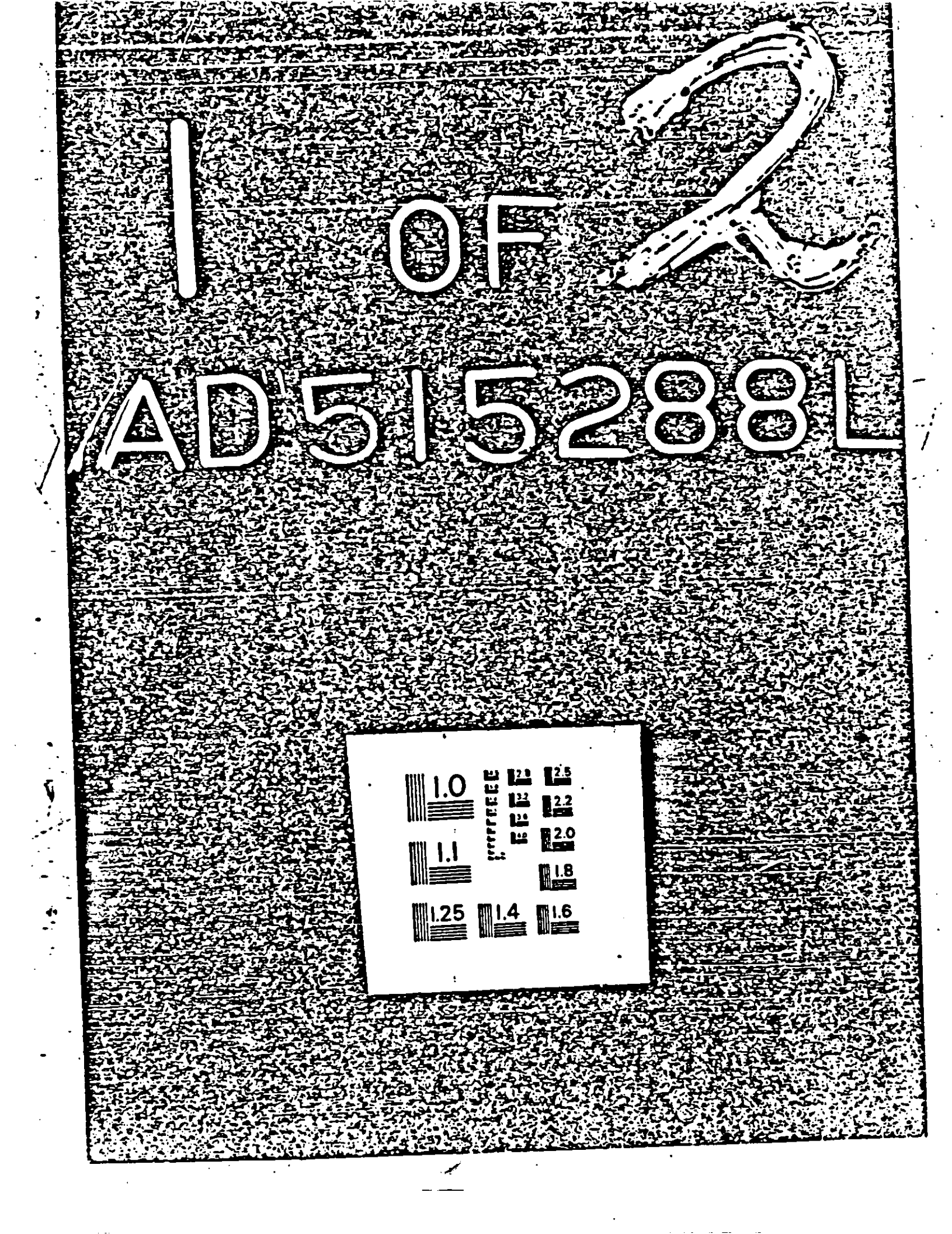
1 OF 2
AD515288L
1.0
1.1
1.25
1.4
1.6
1.8
2.0
2.2
2.5

SECURITY MARKING

The classified or limited status of this report applies to each page, unless otherwise marked.
Separate page printouts MUST be marked accordingly.

THIS DOCUMENT CONTAINS INFORMATION AFFECTING THE NATIONAL DEFENSE OF THE UNITED STATES WITHIN THE MEANING OF THE ESPIONAGE LAWS, TITLE 18, U.S.C., SECTIONS 793 AND 794. THE TRANSMISSION OR THE REVELATION OF ITS CONTENTS IN ANY MANNER TO AN UNAUTHORIZED PERSON IS PROHIBITED BY LAW.

NOTICE: When government or other drawings, specifications or other data are used for any purpose other than in connection with a definitely related government procurement operation, the U.S. Government thereby incurs no responsibility, nor any obligation whatsoever; and the fact that the Government may have formulated, furnished, or in any way supplied the said drawings, specifications, or other data is not to be regarded by implication or otherwise as in any manner licensing the holder or any other person or corporation, or conveying any rights or permission to manufacture, use or sell any patented invention that may in any way be related thereto.

UNCLASSIFIED

[redacted]

Sylvania Electronic Systems-Western Division
Electronic Defense Laboratories
Mountain View, California

APR 22 1993

THIS DOCUMENT HAS BEEN DOWNGRADED
TO UNCLASSIFIED
Per Director, ARPA, S&IO/TIO

EDL-E184

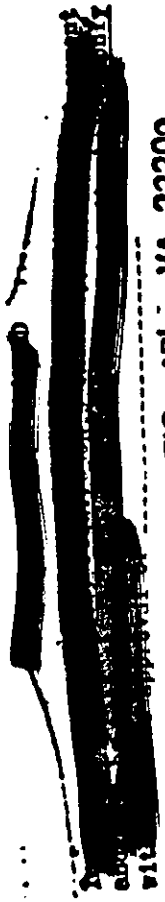

ARPA - TIO ARL: VA 22209

Project Aquarius Final Report (U)

Project Engineer: K. Snow 415/966-3186

DDC
RECEIVED
MAY 24 1971
D

ARPA Order No. 1459
Effective Date of Contract: 2 June 1969
Contract Expiration Date: 31 May 1971
Amount of Contract: $118,864

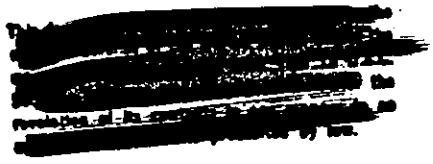

This research was supported by the Advanced Research Projects Agency of the Department of Defense and was monitored by the Office of Naval Research under Contract No. N00014-69-C-0446

DDC CONTROL NO. 11391

[redacted]

UNCLASSIFIED

(U) TABLE OF CONTENTS (U)

Section	Title	Page
1.	INTRODUCTION AND SUMMARY	1-1
1.1	General	1-1
1.2	Early Warning System - Summary	1-3
1.3	Fleet Air Defense - Summary	1-8
1.4	Recommendations	1-12
2.	EARLY WARNING SYSTEMS	2-1
2.1	Predicted Detection Performance	2-1
2.2	Detection Experiment	2-8
2.3	Conclusions of EW Study	2-16
3.	FLEET AIR DEFENSE	3-1
3.1	Polystatic System Detection Feasibility	3-1
3.2	Target Location Methods	3-16
3.3	Error Analysis	3-33
4.	EXPERIMENTAL TESTING OF FAD POLYSTATIC TECHNIQUES	4-1
4.1	Objectives	4-1
4.2	Experimental Considerations	4-2
4.3	System Design	4-8
4.4	Design Concept	4-11
4.5	Detailed Design Specifications	4-14
4.6	Computer Hardware Description	4-19
	APPENDIX A	A-1

(U) ILLUSTRATIONS (U)

Figure	Title	Page
1-1	Basic Geometric Configurations	1-2
1-2	Illustration of Buoy Tactical Early Warning Concept	1-4
1-3	Network Geometry	1-5
1-4	FAD Polystatic System	1-9
2-1	Detection Regions	2-7
2-2	Block Diagram for High Dynamic Range Receiving System	2-10
2-3	Block Diagram of Twelve Channel Analog Receiving System	2-11
2-4	Event 1 Flight Pattern	2-13
2-5	Predicted and Observed Detection Regions	2-14
3-1	FAD Polystatic System	3-2
3-2	Located Sources	3-5
3-3	Source Schedule	3-6
3-4	Typical Geometry	3-7
3-5	Basic Transmission Loss for a Groundwave Along the Ocean	3-9
3-6	Typical Fleet Protection Areas in the Mediterranean Ocean	3-11
3-7	Skywave-Groundwave Example	3-13
3-8	Skywave-Groundwave Coverage	3-14
3-9	Double-Baseline, Two-Measurements Model	3-17
3-10	Double-Baseline, One-Measurement Model	3-18
3-11	Single Baseline Model	3-20
3-12	Variables for Double-Baseline, Two-Measurements Model	3-21

(U) ILLUSTRATIONS (U)

--Continued.

Figure	Title	Page
3-13	Variables for Double-Baseline, One-Measurement Model	3-25
3-14	Variables for Single Baseline Model	3-28
3-15	Variables for Doppler Location Finder	3-32
3-16a	Range Estimation Errors for Double Baseline, Single Measurement Technique--Geometry No. 1	3-40
3-16b	Range Estimation Errors for Double Baseline, Single Measurement Technique--Geometry No. 2	3-40
3-16c	Range Estimation Errors for Double Baseline, Single Measurement Technique--Geometry No. 3	3-41
3-16d	Range Estimation Errors for Double Baseline, Single Measurement Technique--Geometry No. 4	3-41
3-16e	Range Estimation Errors for Double Baseline, Single Measurement Technique-- Geometry No. 5	3-42
3-16f	Range Estimation Errors for Double Baseline, Single Measurement Technique--Geometry No. 6	3-42
3-16g	Range Estimation Errors for Double Baseline, Single Measurement Technique--Geometry No. 7	3-43
3-16h	Range Estimation Errors for Double Baseline, Single Measurement Technique--Geometry No. 8	3-43
3-17	Range Estimation Errors for Single Baseline, Double Measurement Technique	3-46
3-18	Range Estimation Errors for Single Baseline, Double Measurement Technique	3-46
3-19	Location Error for Doppler Location Finder-- Geometry No. 1	3-50
3-20	Location Error for Doppler Location Finder-- Geometry No. 2	3-50
3-21	Location Error for Doppler Location Finder-- Geometry No. 3	3-51

(U) ILLUSTRATIONS (U)

--Continued.

Figure	Title	Page
3-22	Location Error for Doppler Location Finder--Geometry No. 4	3-51
3-23	Location Error for Doppler Location Finder--Geometry No. 5	3-52
3-24	Location Error for Doppler Location Finder--Geometry No. 6	3-52
3-25	Location Error for Doppler Location Finder--Geometry No. 7	3-53
3-26	Location Error for Doppler Location Finder--Geometry No. 8	3-53
3-27	Location Error for Doppler Location Finder--Geometry No. 9	3-54
3-28	Location Error for Doppler Location Finder--Geometry No. 10	3-54
4-1	System Block Diagram	4-10
4-2	Artist's Concept of Data Collection System	4-15
4-3	Fathometer Display	4-20

(U) TABLES (U)

Table	Title	Page
2-1	Predicted System Performance for November 1969 for Carter Cay Transmitter Using Frequencies near the MUF	2-3
2-2	Summary of Detection Region Calculations	2-6
3-1	Mediterranean Transmitters	3-4
3-2	Additional Transmitters	3-15
4-1	Experimental Factors	4-3
4-2	Candidate Sources for FAD Polystatic Experiment	4-4
4-3	Typical Aircraft and Missile Threats	4-5
4-4	Test Parameters for Experiment	4-9
4-5	Spectrum Analysis Specifications	4-14
4-6	Computer Core Requirements	4-18

Section 1

INTRODUCTION AND SUMMARY

1.1 (U) [redacted] GENERAL. (U)

Project AQUARIUS is a part of the Advanced Research Projects Agency (ARPA) sponsored ocean surveillance and tactical early warning program under Project MAY BELL. The primary goal of Project MAY BELL was to investigate the feasibility of detecting and tracking aircraft, missiles, and ships at over-the-horizon distances using high frequency (HF) monostatic and bi-static radars. Concepts using the basic geometric configurations shown in Figure 1-1 have been explored. The MAY BELL program emphasis has been directed towards determining the attenuation, clutter and propagation aspects that apply to concepts using surface waves; and investigating the basic feasibility of detecting and tracking aircraft and SLBM's for Fleet Air Defense (FAD) and Buoy Tactical Early Warning.

Sylvania's primary efforts under Project AQUARIUS have been to determine the feasibility of:

(1) detecting both submarine launched ballistic missiles (SLBMs) and aircraft using surface wave propagation to the target and sky wave propagation from the target to the receiver, and

(2) providing detection and tracking information under electromagnetic control (EMCON) conditions for FAD using shore-based HF (CW) sources and shipboard receivers.

Both analytical and experimental work have been accomplished to arrive at the conclusions included in this report. The principal results of the investigation are summarized in the remainder of this section: results related to early warning (EW) systems and results associated with Fleet Air Defense. The detailed presentation is included in Sections 2 and 3, respectively. Based on these findings recommendations are made in Section 4 for subsequent experiments and investigations associated with aircraft tracking under EMCON conditions using a polystatic configuration.

The concepts explored under Project AQUARIUS can be applied to tactical early warning systems employed against aircraft and submarine

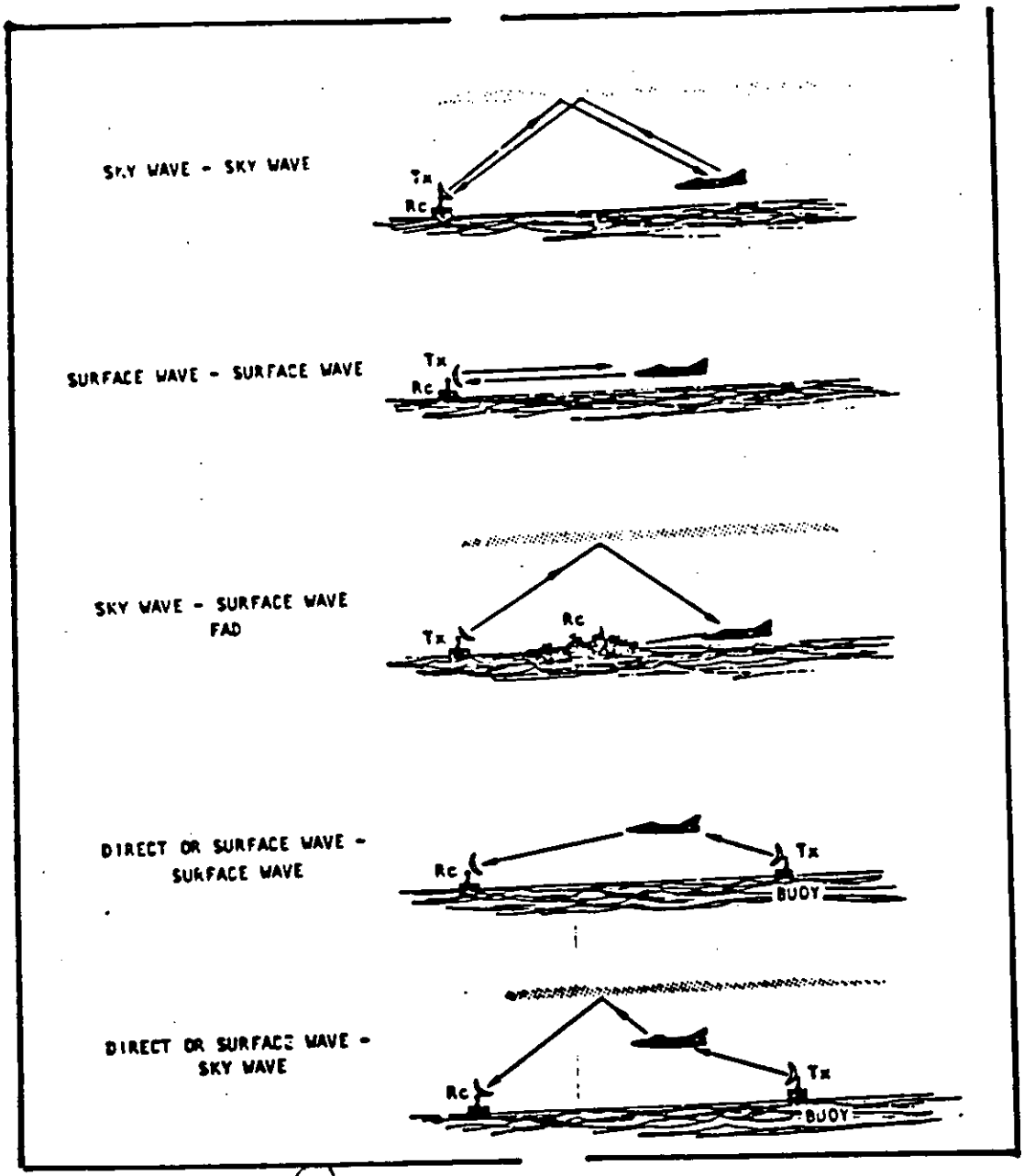

Figure 1-1 (U) Basic Geometric Configurations. (U)

1.1 (U) [redacted] --Continued.

launched ballistic missiles (SLBMs) and fleet air defense (FAD) systems that must cope with hostile aircraft and missiles under both friendly and enemy EMCON conditions.

1.2 (U) [redacted] EARLY WARNING SYSTEM - SUMMARY. (U)

The early warning system configuration considered under Project AQUARIUS is depicted in Figure 1-2. It consists of low power buoy and land based transmitters that illuminate the target (an aircraft or SLBM) via a ground or surface wave. Target detection is accomplished via a sky wave reflection to a highly sensitive receiver located on the coast. The primary goals of this effort were to experimentally demonstrate the feasibility of detecting both SLBMs and low-flying aircraft and to compare the experimentally observed detection ranges to theoretically predicted detection ranges. The targets were detected by observing the scattered doppler shifted signal from the moving targets.

1.2.1 (U) [redacted] Predicted Detection Performance. (U)

Propagation calculations to predict system detection performance using a modified version of the ESSA skywave propagation program were made for both the direct and the scatter-paths between the receiver site at Vint Hill Farms Station (VHFS) and the buoy transmitter off the Florida coast and the Carter Cay transmitter (see Figure 1-3). Separate prediction analyses were made for SLBMs and aircraft.

A constant scattering cross section of 100 M^2 was assumed for the SLBM at all altitudes below 100 km. Above 100 km altitude enhanced cross section values of 10^4 to 10^5 m^2 were used. Because of the relatively low (10 watts) powers (and low frequency) of the buoy transmitters, the signal-to-noise ratio of the reflected doppler is almost negligible below 100 km altitude for any time of the day for either 5.8 or 9.295 MHz (the frequencies used in the experiment). Only above 100 km with the enhanced target cross section is there any substantial chance of SLBM detection using buoy transmitters. However, with the Carter Cay transmitter using 3 kw and transmitting on frequencies near the MUF, the signal-to-noise ratio and thus the probability of detection even at low altitudes is generally above 0.8. Thus, the Carter Cay transmitters operating on frequencies near the 1F hop MUF between Carter Cay and VHFS, should provide low altitude SLBM detections in the afternoon.

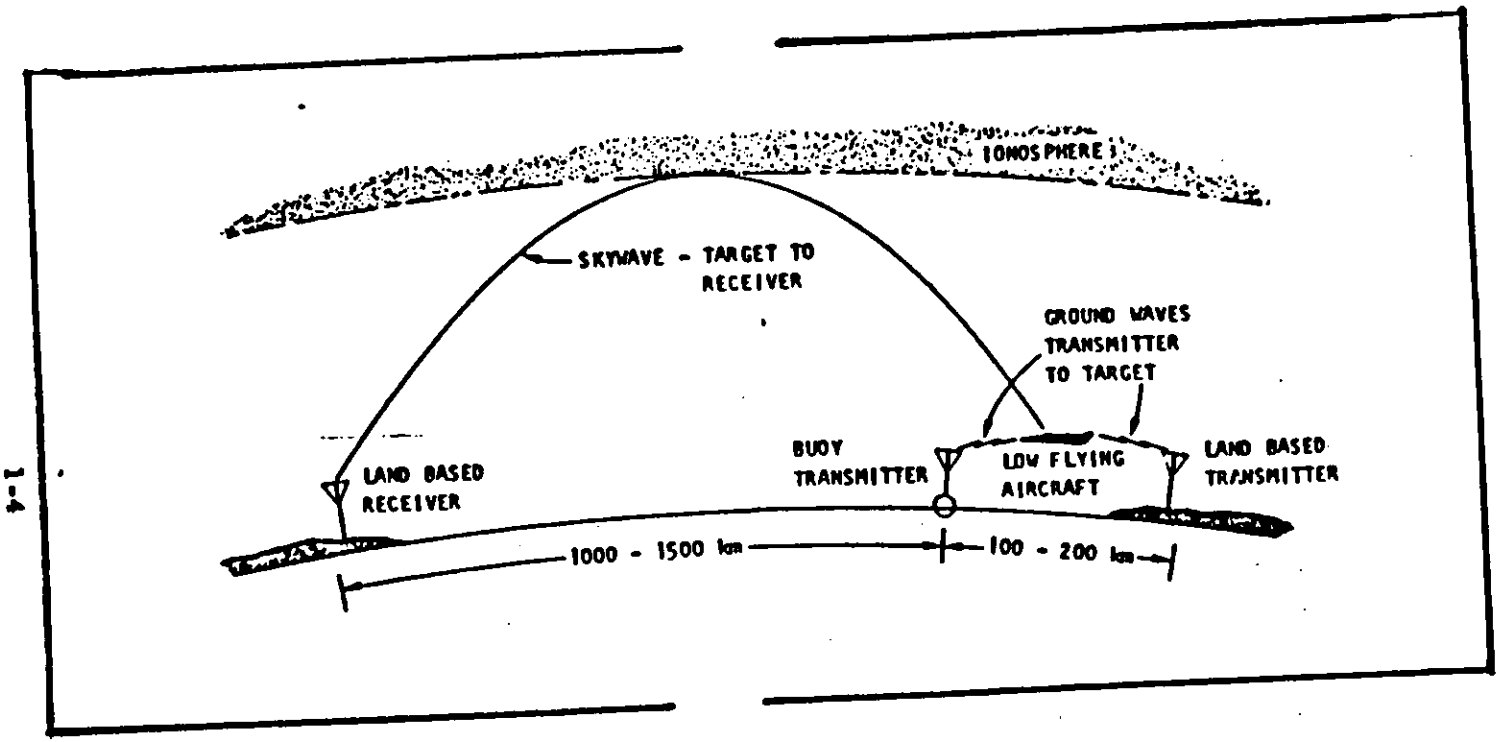

Figure 1-2. (U) Illustration of Buoy Tactical Early Warning Concept (U).

UNCLASSIFIED
UNCLASSIFIED

[redacted]

(This page is UNCLASSIFIED)

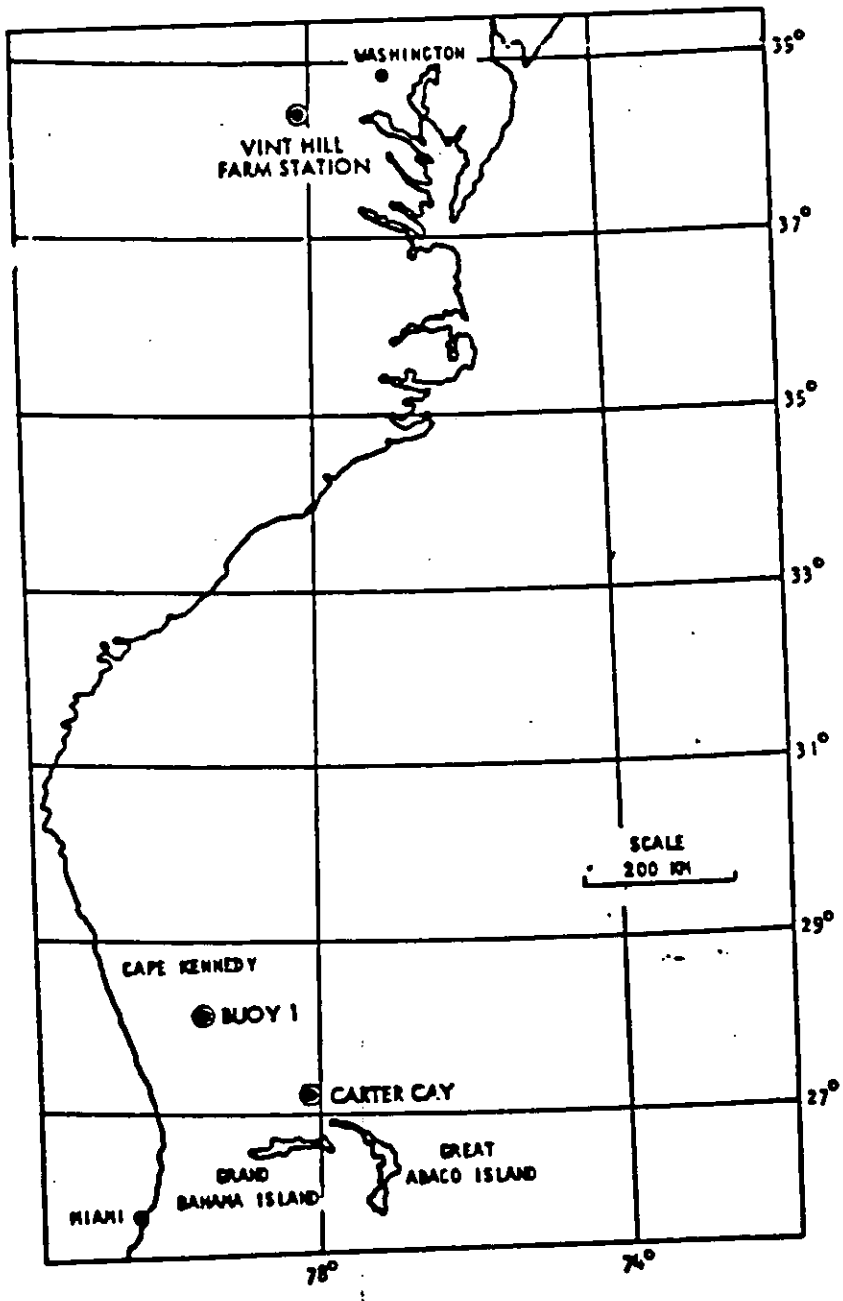

Figure 1-3. (U) Network Geometry (U).

[redacted]

1.2.1 (U) [redacted] --Continued.

The predicted detection performance for low flying aircraft was also examined because it is important to determine whether or not aircraft flying controlled patterns near the buoys and Carter Cay can be detected. This was done by computing the expected detection regions around the transmitter using median operating values. The results indicate that aircraft with 100 m^2 cross sections can be expected to be detected at distances in the range of 11-67 km from the transmitter; depending on the frequency and time of operation and hop structure.

1.2.2 (U) [redacted] Experimental Results. (U)

The principal experiments consisted of two separate controlled aircraft flights of a Navy P3B aircraft to examine the detection capability of the bistatic configurations and two propagation measurements between the Carter Cay transmitter and the Vint Hill Farm Station receiver. Figure 1-3 describes the network geometry.

The first flight employing a 10-watt buoy transmitter resulted in a detected aircraft doppler signature. However, it was not the P3B aircraft used in the test but an aircraft flying near the receiver at VHFS. This conclusion is reached because the time of the signature does not coincide with the time the P3B was closest to the buoy. Also, the predicted detectability region for the existing operating conditions (noise, etc.) extended at best to only 11 km while the P3B aircraft approached the buoy to within only 30 km. Thus, due to timing, geometry, and transmitter power constraints, the detected signature is not considered to be due to the test aircraft.

The second flight test employed the higher powered (3 kw) Carter Cay transmitter to illuminate the aircraft flying at several altitudes from 2,000 to 24,000 feet. From this test it was concluded that aircraft below 2,000 feet and within the predicted detectability regions (approximately 11 km from the transmitter) can be detected using the buoy concept if at least 3 kw is transmitted.

Signal strength tests were performed to determine how accurately the prediction techniques correlate with measured values and to estimate the hop structures for various frequencies. Tests were performed for two frequencies and at two times during the day. It was found that there was good agreement between predicted and observed carrier levels for 1E, 1F, and 2F hop structures.

[redacted]

1.2.3 (U) [redacted] System Parameter Considerations. (U)

While the experimental results described herein indicate the basic feasibility of the ground-wave/sky-wave configuration, there remains a need for additional information to design a complete coastal defensive system. In particular, there are many parameters that inter-relate the ground-wave/sky-wave mode that were not examined or tested in detail during this experiment. These include variations in frequency, path loss with time of day, season, etc. To perform an adequate design of an early warning system an examination of six areas was required:

(1) effective radiated power and surface wave from a buoy mounted antenna,

(2) surface-wave losses to the target,

(3) scattering or reflection coefficient of the target,

(4) sky-wave losses to the receiver,

(5) effective noise at the receiver, and

(6) receiver antenna gain.

These areas were examined and the specific parameters that contribute the most uncertainty in specifying system design values were identified. They include frequency, path length, target aspect angles, null depth variations, receiving site noise environment, absorption, target altitude measurement tolerances, and interference. A proposed experimental program was recommended that could be accomplished in four phases. First, analysis and measurements are to be made to evaluate the coupling between the buoy-mounted transmitter and the surface wave which is vertically polarized. Second, additional analysis using modeling experiments is to be carried out to evaluate the difference between backscatter and forward scatter target cross section. Third, the path losses for both sky wave and surface wave are to be measured for an optimal set of frequencies and modes of propagation. Fourth, a preliminary system is to be defined as a result of the first three phases. This design would include coverage area, control requirements, and an estimate of detection probability and false alarm rate.

[redacted]

UNCLASSIFIED

1.3 (U) FLEET AIR DEFENSE - SUMMARY. (U)

In lieu of pursuing the experiments needed to specify a coastal tactical early warning system, Sylvania was redirected to focus attention on the Fleet Air Defense (FAD) problem.

The detection of low-flying threats to surface vessels at a range sufficient to give useful warning time and tracking information is a problem which must be solved if the surface navy is to survive. In detecting these threats the enemy must not be given the opportunity to use simple direction finding techniques to locate fleet units. Thus, it is desirable that target detection not require radiation from the fleet and that the fleet operate under complete electromagnetic control (EMCON).

The feasibility of using a hybrid (skywave/surface-wave) system to help solve this problem has been demonstrated as part of the MAY BELL program. In this concept, the target is illuminated by skywaves from transmitters (either shipborne or land-based) located at over-the-horizon (OTH) ranges. Surface waves which propagate from the target to a receiving system aboard a ship permit detections to be made even when the target is below the line-of-sight radar horizon.

Experiments performed at Cape Kennedy, Florida, with a shore-based receiving station simulating the shipboard environment, a Navy P3B aircraft as a controlled target, and illumination provided by the MADRE (pulse) and CHAPEL BELL (phase code) transmitters, located respectively in Maryland and Virginia, have shown the technique to be feasible. For most of the flights of the target its altitude was 200 feet, and detections were made at ranges as great as 100 kilometers (km) from the receiver.

Sylvania's investigations in this area were divided into two parts. The first was to examine the feasibility of using transmitters of opportunity as sources for a polystatic doppler radar system for FAD in the Mediterranean Sea. The second part consisted of examining target tracking methods for use with such a doppler radar problem. Recommendations for follow-on experiments were then made to verify the tracking techniques (Section 4.2).

1.3.1 (U) Polystatic System Detection Feasibility. (U)

The polystatic radar system that employs HF broadcast transmitters of opportunity and a shipborne receiver (see Figure 1-4) was examined to determine the availability of sources for illuminating airborne threats to the U. S. fleet so that a shipborne receiver can be employed to detect the target

UNCLASSIFIED

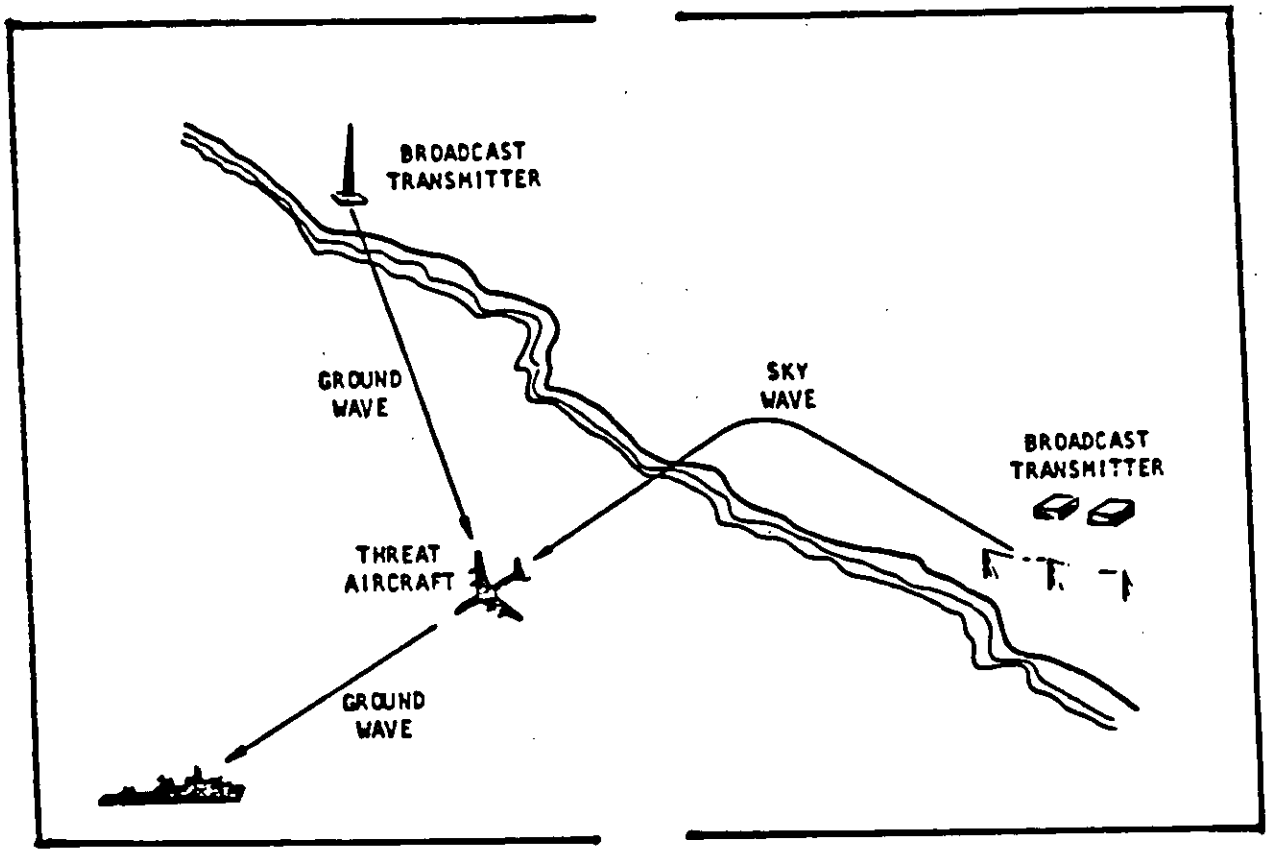

Figure 1-4 [redacted] (U) FAD Polystatic System. (U)

1.3.1 (U) [redacted] --Continued.

at over-the-horizon (OTH) ranges. This study was constrained to the Mediterranean region. The sources were examined to determine the effective radiated power of the transmitter in various directions, especially over the Mediterranean Sea, the propagation modes, and the operating schedule of the transmitter. Propagation losses from the transmitter to the target, loss due to the scattering geometry, and losses from the target to the receiver were examined to determine predicted detectability regions. The results indicate that the sources studies can provide sufficient coverage for the fleet over approximately one half of the Mediterranean Sea some of the time. More study is needed to evaluate other sources with different transmission schedules to provide round-the-clock coverage. The large number of known transmitters that have not yet been evaluated and tentative knowledge of their characteristics and schedules appear to be sufficient to provide the additional coverage needed. The studies indicate that detection ranges on the order of 100 km from the fleet should be possible. Section 3.1 contains the details of this analysis.

1.3.2 (U) [redacted] Target Location Methods. (U)

To provide tracking information for FAD, target location techniques using the basic polystatic configuration described previously were examined. For low-flying aircraft (below 1000 feet) and surface-wave propagation for the target-receiver half path, the location estimation problem can be considered to be a two-dimensional problem. Models for location estimation were developed for three configurations: a two-transmitter, one-receiver (double baseline) case, a one-transmitter, one-receiver (single baseline) case, and a four transmitter, one-receiver case (doppler location finder). For the double baseline case two techniques were developed, one in which azimuthal and doppler measurements are made at two different time points for each baseline and a second to represent a single set of measurements for each baseline. For the single baseline case a third technique requiring two sets of azimuthal and doppler measurements was developed. For the four-transmitter, one-receiver case, four doppler measurements are made to provide an estimate of target range and azimuth. Section 3.2 contains a detailed description of the techniques.

1.3.3(U) [redacted] Error Analysis. (U)

A detailed error analysis was conducted of three of the four techniques. This effort excluded an examination of the first technique (double baseline, double measurement) because the other techniques are simpler to implement.

For the double baseline, single measurement technique it is shown that although the technique is not completely satisfactory under all circumstances, it is fairly successful for certain geometries and parameters. Both bias and random errors arise because of the need for approximations and measurement errors. For RMS measurement accuracies of 1 degree in azimuth and 0.1 Hz in doppler frequency range estimate errors of less than 15 percent of the true range can be achieved.

For the single baseline, double measurement technique range estimate errors of less than 15 percent can also be achieved for the same bearing and doppler measurement accuracies (1 degree and 0.1 Hz). However, the error is especially sensitive to transmitter-target-receiver geometry for this technique. Errors in excess of 80 percent can arise when the shipborne receiver is located between the target and the transmitter. Bias errors are eliminated for target trajectories aimed directly at the ship.

The errors associated with the doppler location finder technique were examined for a doppler measurement accuracy of 0.1 Hz RMS. The RMS range estimate error is less than 15 percent in many cases and the RMS bearing estimate error is less than 6°. In one case the range estimate error is less than 5 percent. This latter case assumes that four transmitters are distributed at the corners of a square centered around the ship with the target approaching from outside the square. This technique results in no bias errors and the random errors are generally less than those for the other techniques. If bearing measurements with 1 degree RMS error are used with the doppler location finder technique then the location accuracies are quite good.

The principal conclusions that can be drawn from the error analysis is that target location can be estimated with reasonable accuracy (15 percent of true target range) using a number of techniques for a variety of FAD operational conditions. The most promising approach for implementation is a hybrid of the techniques considered. For example, for a given transmitter-receiver geometry the doppler location finder that estimates range and azimuth from four doppler measurements may be used with separate azimuthal measurements to estimate a target's location. Because each of the techniques is sensitive to transmitter-target-receiver geometry,

1.3.3 (U) [redacted] --Continued.

the target location system should include an algorithm for selecting the estimation method(s) for a set of operating conditions and combining the estimated results using tests for accuracy. The estimation method(s) would be selected to minimize the errors for targets from different quadrants around the ship for a given transmitter-receiver configuration. The results of the different estimation methods would be compared and combined to provide the "best" estimate.

Section 3.3 contains the details of the error analysis.

1.3.4 (U) Prototype Aircraft Detection System Design. (U)

The results of the investigation of transmitter sources for the FAD system and the evaluation of target location methods were employed as inputs for a prototype aircraft detection system design. This system would provide a test bed to verify the detection capability of the polystatic doppler radar system for FAD. In addition, the prototype system can be used to demonstrate the accuracies of the various target location techniques and select parameters for a final FAD system. Section 3.4 contains the details of the prototype system design.

1.4 (U) [redacted] RECOMMENDATIONS. (U)

Based on the early warning and Fleet Air Defense (FAD) investigations under Project AQUARIUS recommendations are made that apply principally to FAD systems. They include the development of a prototype aircraft detection system, the experimental testing of the FAD polystatic techniques using this system, and the conduct of subsequent investigations necessary for system implementation.

The prototype system and experimental tests are necessary to demonstrate the detection range of the polystatic technique and to verify the accuracies of the target location estimation methods examined under Project AQUARIUS. The prototype system to be employed for the tests can be readily implemented as described in Section 3.4. As mentioned previously, such a system can provide a test bed for final system parameter selection, expecially in the areas of man-machine interface. In addition, it can be used to evaluate hardware and software tradeoffs prior to the final system design.

1.4 (U) [redacted] --Continued.

The subsequent FAD investigations recommended, based on the results of this study are to evaluate transmitter sources for use in the polystatic system for fleet operations in other parts of the world, to refine the target location techniques, and to examine the multiple signature discrimination problem. The source evaluation effort is needed to identify transmitters to be used for fleet early warning when the fleet operates in other areas of the world. The target location technique refinement study is intended to employ the results of the four methods examined under Project AQUARIUS for the development of a hybrid target location system that will perform satisfactorily under a greater variety of fleet operating geometries. The study should incorporate the four techniques to develop a composite method for reducing the sensitivity of target location estimation accuracy to transmitter-target-receiver geometry. The experimental tests that are recommended should be closely coordinated with this effort so that the refined target location techniques can be tested.

The multiple signature discrimination problem consists of the need to identify threats to the US Fleet and to distinguish them from other aircraft, objects, and false alarms. Investigation of methods to efficiently discard the false alarms and to verify that an aircraft is hostile needs to be conducted.

A more detailed description of these recommendations is included in Section 4.

UNCLASSIFIED

This Page Intentionally Blank

UNCLASSIFIED

Section 2

EARLY WARNING SYSTEMS

(U) [redacted] As described in Figure 1-2, the early warning system configuration considered for investigation under Project AQUARIUS consists of low power HF buoy and land-based transmitters that illuminate the target (an aircraft or SLBM) via a ground or surface wave and a highly sensitive receiver located on the coast that detects the sky-wave target reflection from the target. The primary goals of this effort were to experimentally demonstrate the feasibility of detecting both SLBMs and low-flying aircraft and to compare the experimentally observed detection ranges to theoretically predicted detection ranges. The early warning system investigation was divided into three parts:

a. a predicted detection performance evaluation,

b. experimentation in the field to meet the primary goals of demonstration and verification of theoretically predicted detection ranges, and

c. evaluation of early warning system parameters for design.

These efforts are described in the following subsection, (Sections 2.2 and 2.3). The conclusions of these efforts are contained in Section 2.4.

2.1 (U) [redacted] PREDICTED DETECTION PERFORMANCE. (U)

Propagation calculations to predict early warning system performance using a modified version of the ESSA skywave propagation program (described in Appendix A) have been made for both the direct and the scatter paths between the receiver site at Vint Hill Farm Station and the buoy transmitters off the Florida coast. The purpose of these calculations was to estimate the feasibility of detecting SLBM missile launchings from Cape Kennedy and controlled aircraft targets using buoys at ranges of 100, 200 and 300 km from Cape Kennedy and the Carter Cay transmitter. The geometry and parameters were selected to provide theoretically predicted detection ranges for comparison with experimental results.

[redacted]

UNCLASSIFIED

2.1.1 (U) [redacted] Missile Detection Performance. (U)

Several sets of calculations using the computer predictions were performed. The receiving antenna at Vint Hill Farms Station used for all tests is a tulip element LDAA built by ITT with an assumed maximum gain of 16 dbi. A constant scattering cross section of 100 m^2 was assumed for the missile at all altitudes below 100 km. At altitudes above 100 km the bistatic cross section was modelled using a hyperboloid compressed ambient shock surface. The assumed cross section then changes from 10^2 m at low altitude to values of 10^4 to 10^6 m^2 above 100 km. The three buoy transmitter locations are at 100, 200 and 300 km directly down range from the 105° Cape Kennedy launch azimuth. The Carter Cay transmitters are approximately 285 km down range at a 123° azimuth from Cape Kennedy. The transmitted frequencies for the buoys were the presently assigned values of 5.8 and 9.295 MHz. These frequencies, plus frequencies of 15 and 20 MHz were assumed for the Carter Cay transmitters. The buoys were assumed to have a transmitting power of 100 watts radiating from monopole antennas. The Carter Cay transmitters were assumed to be radiating 3 kw into monopole antennas.

Because of the low power and relatively low frequency from the buoy transmitters, the target signal-to-noise ratio was generally found to be negligible when the target is below 100 km for any time of the day for either frequency. Only above 100 km with the enhanced target cross section does there appear to be any substantial chance of target detection using the buoy transmitters. However, with the Carter Cay transmitter using 3 kw and transmitting on frequencies near the MUF as shown in Table 2-1 the signature-to-noise ratio and thus the probability of detection at even low altitudes is quite substantial. In fact, there are many cases for which the signal-to-noise ratio exceeds 15 db. Thus, if the high power Carter Cay transmitters continue to operate and transmit on frequencies near the 1 F hop MUF between Carter and VHFS then low altitude SLBM detections in the afternoon should be possible.

2.1.2 (U) [redacted] Aircraft Detection Areas. (U)

Even though the probability of detecting SLBM launchings from Cape Kennedy is quite low (due to the relatively long range from the buoy to the target) it is important to determine whether or not aircraft flying controlled patterns near the buoys and Carter Cay can be detected. A way to evaluate this and to clearly display the results is to compute expected detection regions around the transmitter position. Variables that must be considered when calculating detectability regions are bistatic geometry, frequency, transmitter power, target cross section, skywave hop structure, sea state, local time of day and noise level. By choosing median values for all the variables and changing the values of a single variable at a time, regions where detections

[redacted]

UNCLASSIFIED

TABLE 2-1.

(U) Predicted System Performance for November 1969
for Carter Cay Transmitter Using Frequencies near the MUF. (U)

Altitude	Frequency		0000Z	MUF	0400	MUF	0800	MUF	1200	MUF	1600	MUF	2000	MUF
5 KM	15 MHz	S/N	9.93	13.56	-		-		-		13.4	21.80	10.4	21.07
		PC/SB	60.3		-		-		-		59.2		60.7	
	20 MHz	S/N	-		-		-		-		16.5	21.77	11.3	21.03
		PC/SB	-		-		-		-		73.3		74.8	
10 KM	15 MHz	S/N	10.0	13.65	-		-		-		12.3	22.07	10.4	21.28
		PC/SB	60.2		-		-		-		60.2		60.7	
	20 MHz	S/N	-		-		-		-		16.5	22.00	11.3	21.21
		PC/SB	-		-		-		-		73.4		74.8	
40 KM	15 MHz	S/N	11.3	14.20	-		-		19.3	12.99	12.0	23.73	9.2	22.60
		PC/SB	59.0		-		-		60.6		60.6		61.8	
	20 MHz	S/N	-		-		-		-		18.2	23.51	13.2	22.38
		PC/SB	-		-		-		-		71.7		72.9	
119 KM	15 MHz	S/N	26.7	15.83	-		-		47.1	14.70	33.5	14.53	51.1	26.40
		PC/SB	43.6		-		-		32.8		39.2		20.0	
	20 MHz	S/N	18.6	15.55	-		-		-		56.6	28.16	48.7	25.80
		PC/SB	190.4		-		-		-		33.2		37.4	

S/N = Target signal-to-noise ratio (db)

PC/SB = Carrier-to-target signal ratio (db)

(This page is UNCLASSIFIED)

2.1.2 (U) [redacted] -- Continued.

are most likely to occur can be generated, as well as obtaining an understanding of how a particular variable affects the overall detection area.

Detectability regions have been calculated for various frequencies, hop structures and noise levels using a buoy located 120 km from Cape Kennedy as the transmitter and VHFS, Virginia, as the receiver. A sea state of 5, transmitter power of 50 watts, ground-wave propagation from transmitter to target and sky-wave propagation from target to receiver and a required signal-to-noise ratio of 3 db have been assumed.

The following technique is applied to find the area of detectability. From the bistatic radar equations*, the total power loss over the scatter path is:

$$L = P_T - P_R = L_T + L_R + L_S - G_T - G_K - 10 \log \frac{4\pi\sigma}{\lambda^2} \qquad (2\text{-}1)$$

where: P_T = power transmitted;

P_R = power received;

L_T = loss over transmitter half path, T;

L_R = loss over receiver half path, R;

L_S = system loss;

G_T = gain of transmitter antenna;

G_R = gain of receiver antenna;

σ = target cross-section (meters); and

λ = wavelength (meters).

Assuming a minimum allowable scatter path signal-to-noise ratio of 3 db, the required power received would be at least N + 3 db, where N is the noise level at the receiver.

*See Skolnik, Merill I., Introduction to Radar Systems, McGraw-Hill Book Company, Inc., New York, New York, 1955.

2.1.2 (U) [redacted] -- Continued.

$$P_R = N + 3 \text{ db} \quad . \tag{2-2}$$

From (2-1)

$$L = P_T - P_R$$

and hence:

$$L = P_T - N - 3 \text{ db} \quad . \tag{2-3}$$

Substituting equation (2-3) into equation (2-1) and solving for $L_T + L_R$, results in:

$$L_T + L_R = P_T - N - 3 - L_S + G_T + G_R + 10 \log \frac{4\pi\sigma}{\lambda^2} \quad . \tag{2-4}$$

Equation (2-4) provides an expression for calculating the total allowable scatter path loss between a transmitter and receiver while still maintaining sufficient signal strength to detect the target. Using different values for D layer loss and sky-wave propagation over the transmitter-target half path, $\sigma = 100$ m^2, and the appropriate transmitter/receiver gain parameters, the maximum loss associated with the target-receiver half path (L_R) can be obtained for various conditions. These L_R losses can be converted to receiver-target ranges using Barrick's loss tables* and the detection regions can be obtained. This technique was used to calculate the detection area around the transmitter for various frequencies and atmospheric noise conditions. The results of the detection area calculations are tabulated in Table 2-2 and a vertical projection of some of the regions onto the ground is shown in Figure 2-1. The reason for the egg-like shape is that the area boundary is the locus of points such that the product $R_1 R_2$ is equal to a constant (see Section 3.1.3 for a more detailed description of the evaluation method).

Referring to Figure 2-1 we see that the largest area of detection is for 2F hop cases for both 5.8 and 9.259 MHz, as compared to the 1E hop situation. This is because there is substantially less D-layer loss for the 2F hop mode than the 1E hop mode due primarily to the different path lengths in the D-region itself. With higher modes the incident angle through the D-layer is higher, thus the loss on these paths due to D-layer absorption is smaller.

*Barrick, D. E., "Theory of Ground-Wave Propagation Across a Rough Sea at VHF/UHF", Battelle Memorial Institute, Draft Report (1970).

Table 2-2

(U) Summary of Detection Region Calculations (U)

Freq MHz	Hop Structure	R_1 Km	R_1 Loss db	D-Layer Loss db	R_2 Loss db	$L_{BT}+L_{BR}$ Loss db	Atmos Noise dbw
5.800	1E	11	61.0	48.5	102.2	211.7	-180(B)
5.800	2F	67	79.1	30.4	102.2	211.7	-180(B)
5.800	1E	10	59.5	34.0	102.2	195.7	-153(M)
9.259	1E	34	80.1	21.9	108.7	210.7	-172(B)
9.259	2F	48	86.2	15.8	108.7	210.7	-172(B)
9.259	1E	44	84.7	15.3	108.7	208.7	-169(M)
9.259	1F	65	90.8	9.2	108.7	208.7	-169(M)
15.000	1F	60	101.0	4.0	112.0	216.9	-174(M)
15.000	1F	67	103.6	5.9	112.0	221.5	-176(B)
20.000	1F	66	113.9	3.1	114.5	231.5	-186(B)
20.000	1F	66	113.6	2.1	114.5	230.1	-185(M)

B = Best noise case 0800-1200 Local Time

M = Medium noise case 1600-1200 Local Time

See Figure 2-1 for R_1 and R_2 definition

(This page is UNCLASSIFIED)

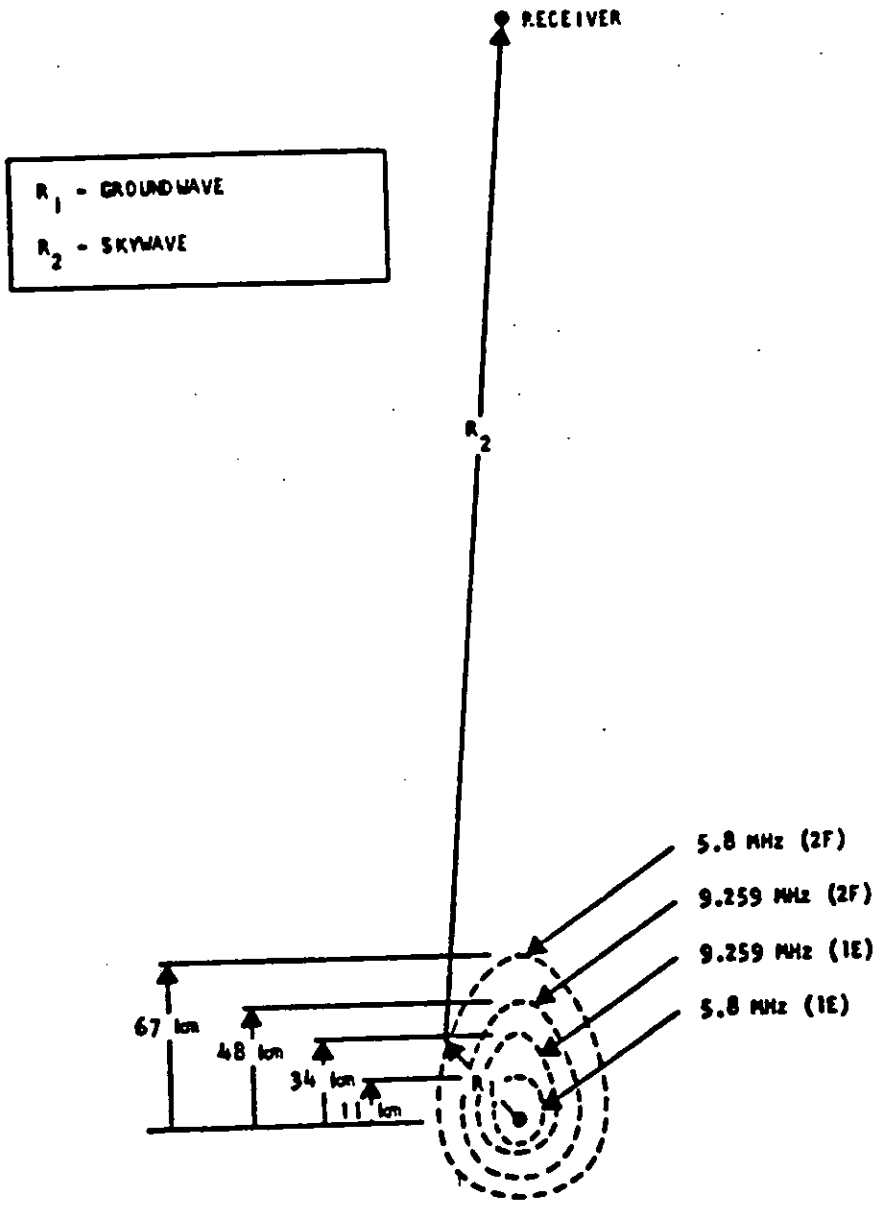

Figure 2-1. (U) Detection Regions (U).

UNCLASSIFIED

2.1.2 (U) [redacted] -- Continued.

For the 2F hop modes the region at 5.8 MHz is larger than the region at 9.259 MHz. This is due to the fact that the loss is greater at higher frequencies. However, for the 1E modes the situation is reversed. The higher frequency also results in the larger detection area. This is because the D-layer loss on the 9.259 MHz frequency is substantially less than the D-layer loss at 5.8 MHz and this dominates the ground-wave propagation advantage at the lower frequency.

From Table 2-2 we see that the detectability radii (R_1) tend to increase with increasing transmitted frequency. However, once the frequency increases to approximately 15 MHz, the spreading losses over the transmitter-target half path cancel the effect of decreasing D-layer loss and decreasing atmospheric noise so that the growth of the detectability region virtually stops. Note that the detectable radii (R_1) are approximately the same at 15 and 20 MHz for the best noise case. It is also observed that varying transmitter power and transmitter or receiver antenna gains have the same effect on the size of the detectability regions. That is a db of gain or loss whether generated from varying transmitter power or antenna gain enters the radar range equation in the same way.

2.2 (U) [redacted] DETECTION EXPERIMENT. (U)

2.2.1 (U) [redacted] General. (U)

Due to the nature and the time frame of this project, the experimental data were collected by using equipment developed by other Project MAY BELL participants or by using hardware developed for other programs. Both the buoy and the CW transmitters at Carter Cay used in these tests, were also used for the ground-wave measurements which Raytheon was conducting. The receiving system in use belongs to the USASA field station located at Vint Hill Farms Station, Virginia, and consisted of a linear disposed antenna array and multichannel HF receiving and recording equipment.

In the description of the detection experiment the transmitter and receiver site characteristics are first described. Then the receiving system calibration and experimental geometry are discussed. The results of the experiment are then presented.

2.2.2 (U) [redacted] Transmitter Characteristics. (U)

Two different types of transmitters were used in the experiment. Those tests conducted prior to December 1969 used a buoy-mounted transmitter of approximately 10 watts radiating at 5.8 and 9.259 MHz. The

2.2.2 (U) [redacted] -- Continued.

antenna on the buoy consists of a top-loaded vertical monopole cut for a quarter wavelength at 7.5 MHz. This buoy was anchored off the coast of Florida approximately 120 kilometers downrange, and at an azimuth of 113 degrees from Cape Kennedy. The tests conducted in January and February 1970, used the CW transmitters on Carter Cay. The power of these CW transmissions ranged from 100 watts up to 3 kilowatts depending upon time and the particular transmitter in use. All of these transmissions radiate into quarter-wave vertical monopoles cut for the frequency in use.

2.2.3 (U) [redacted] Receiver Site Characteristics. (U)

Two separate receiving systems were used at the receiver site located at Vint Hill Farms Station. One receiving system was a van-mounted high dynamic range digital processing system containing synthesizer controlled receivers (Sylvania R-27A receivers); digital spectrum analysis* using a CDC 1700 general-purpose computer and both analog and digital PCM recording capability. The second receiver system is located in two back-to-back house trailers, and consists of a DF set connected to an LDAA steerable beam antenna and 12 analog receiving channels using R390A receivers. The R390A receivers connect to both a real-time analog spectral display and a 12 channel analog tape recorder. The block diagrams of these two receiving systems are shown in Figures 2-2 and 2-3.

2.2.4 (U) [redacted] Receiver System Calibration. (U)

One important goal of this project is to be able to predict the detection performance of the buoy tactical early warning system. Thus, it is desired to compare predicted signal and noise values to actual measured data. Then, if there exist significant discrepancies between the actual and observed data, the predictions must be modified to correct this difference.

The standard calibrations performed on the system included a measurement of the received carrier strength and also the received noise power referenced to a 1-Hertz bandwidth. The process of measuring the received carrier strength was a simple procedure of comparing the receiver IF output signal level when it was connected to the antenna, to the IF output level when the receiver was connected to a synthesizer having the same HF frequency as the carrier signal being measured. The average IF output level for that

* Digital Spectrum Analysis not available after January, 1970, due to termination of the computer lease.

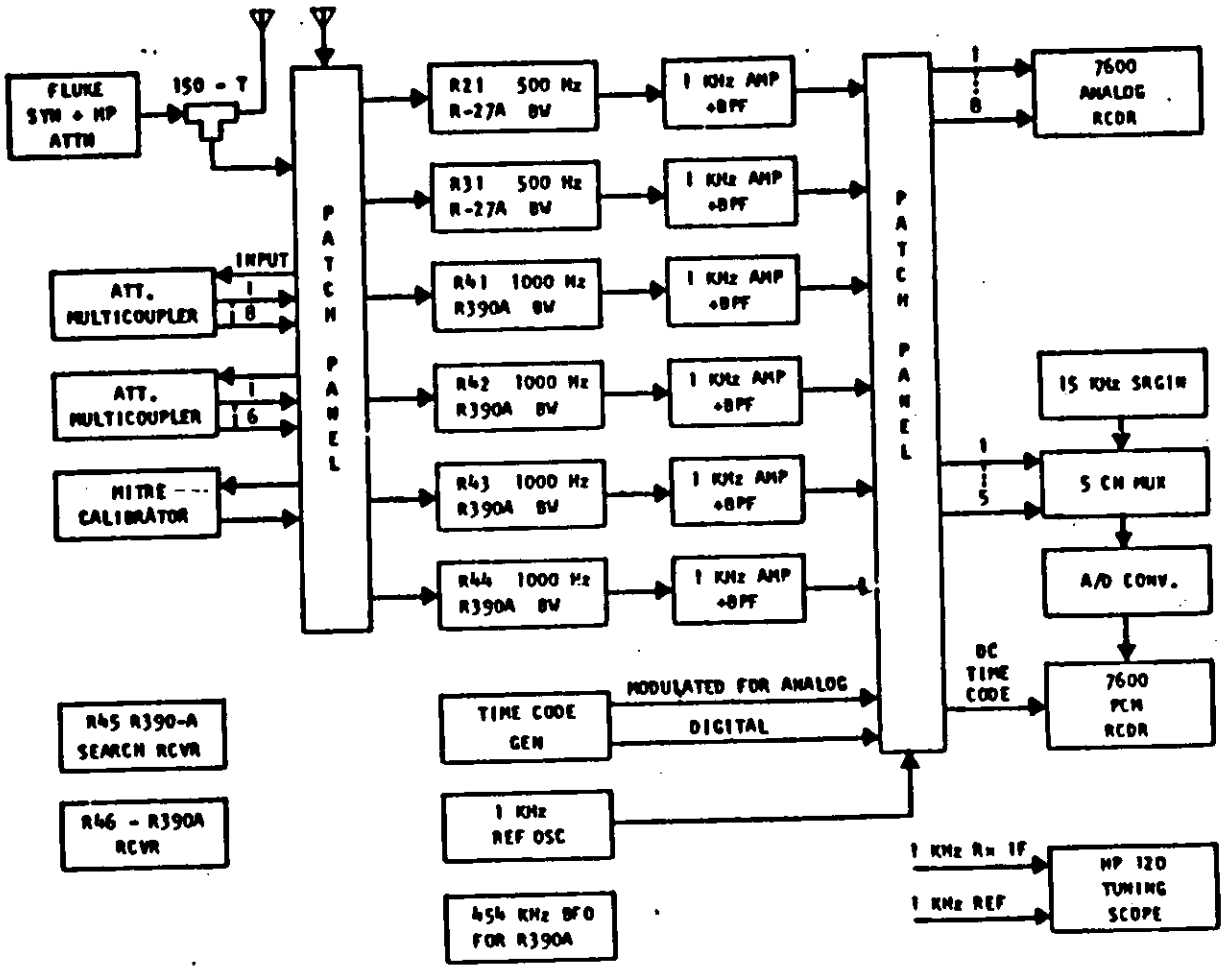

Figure 2-2. (U) Block Diagram for High Dynamic Range Receiving System (U).

(This page is UNCLASSIFIED)

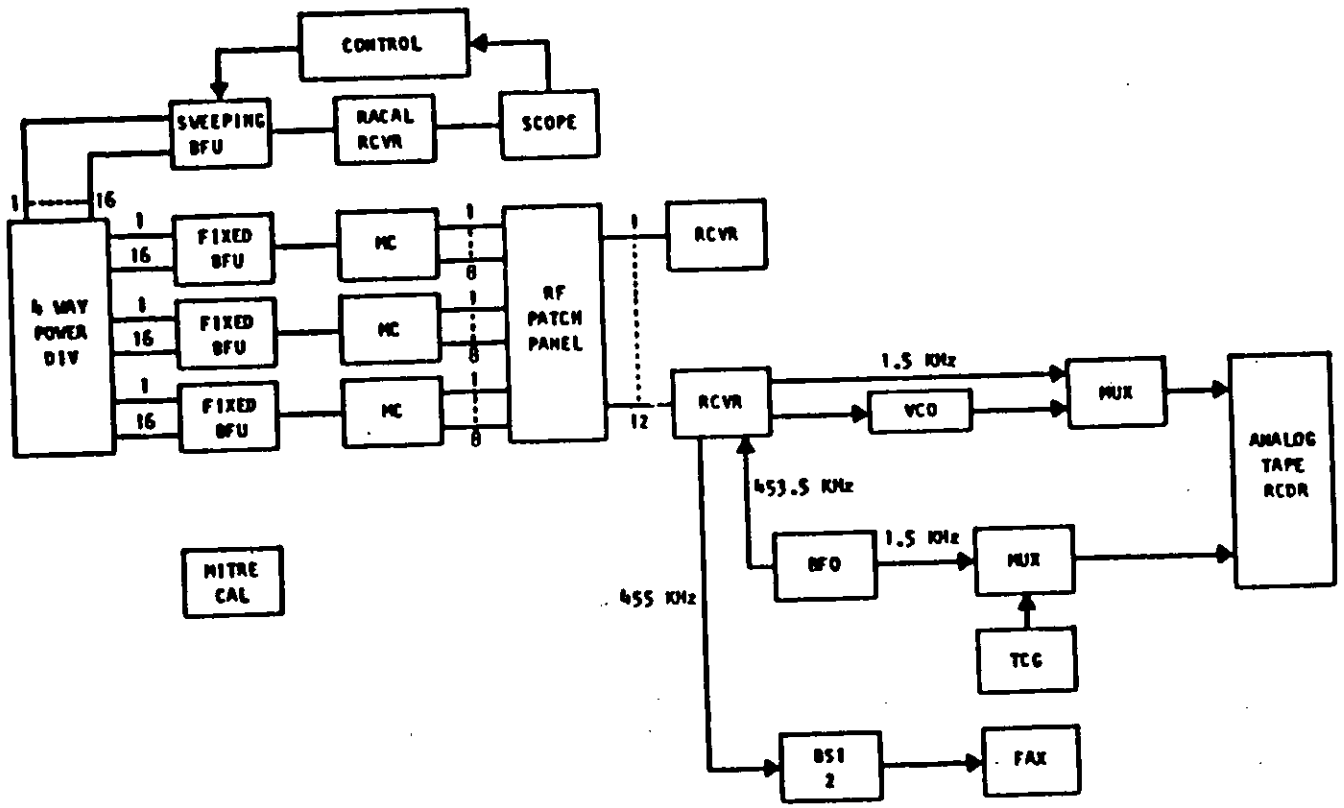

Figure 2-3. (U) Block Diagram of Twelve Channel Analog Receiving System (U).

(This page is UNCLASSIFIED)

[redacted]

UNCLASSIFIED

2.2.4 [redacted] (U) -- Continued.

particular carrier signal was noted. Then the synthesizer at the same frequency was fed to the antenna terminals and the output amplitude adjusted until the receiver IF output signal strength was the same. The synthesized signal level was then measured and converted to db with respect to a watt. This signal substitution method gave the received carrier strength in dbw and was measured within the narrow IF receiver bandwidth.

The determination of the noise level at frequencies near the carrier was done by AM modulating the on-air carrier signal with an audio frequency square wave using a very small percentage modulation. The amplitude of these modulation tones was observed at the output of the real-time spectrum analysis display. The modulation percentage was then reduced until the modulation tones disappear into the background noise of the display. Because the modulation percentage is easily converted to signal level in db below the carrier and the spectrum analysis bandwidth was 1 Hz, the relative carrier-to-noise power was directly obtained referenced to a 1 Hz bandwidth. Thus, if the calibration tone disappeared into the noise at a level of 64 db below the carrier, it was assumed that the noise value was also 64 db below the carrier value. This carrier-to-noise ratio was then subtracted from the received carrier strength to obtain the measured noise power in dbw per Hz.

2.2.5 [redacted] (U) Results of Experiment. (U)

The principal experiments consisted of two separate controlled aircraft flights of a Navy P3B aircraft to examine the detection capability of the bistatic configurations, and two propagation measurements between the Carter Cay transmitter and the Vint Hill Farm Station receiver. The two flights, denoted as Events 1 and 2, are shown in Figure 2-4 and 2-5, respectively. The network geometry is shown in Figure 1-3.

The first event on 18 December 1969 employed a 10-watt buoy transmitter (instead of a 100-watt transmitter as examined in the prediction analysis*) located 120 km from Cape Kennedy on an azimuth of 113°. A Navy P3B aircraft was flown at an altitude between 300 to 600 feet, and speed between 200 and 400 knots, along the flight path shown in Figure 2-4. A signature was detected on 5.8 MHz between 1750-1755Z and 2000-2005Z. The propagation conditions are summarized below--

RF: 5.8 MHz
Transmitter Power: 10 W.
Carrier Level: -92 dbw
Noise Level: -160 dbw
Calculated detection radii: 3 km (1E Hop), 6 km (2F Hop)

*The 10-watt buoy transmitter was built after the analysis using the 100-watt value was completed.

[redacted]

UNCLASSIFIED

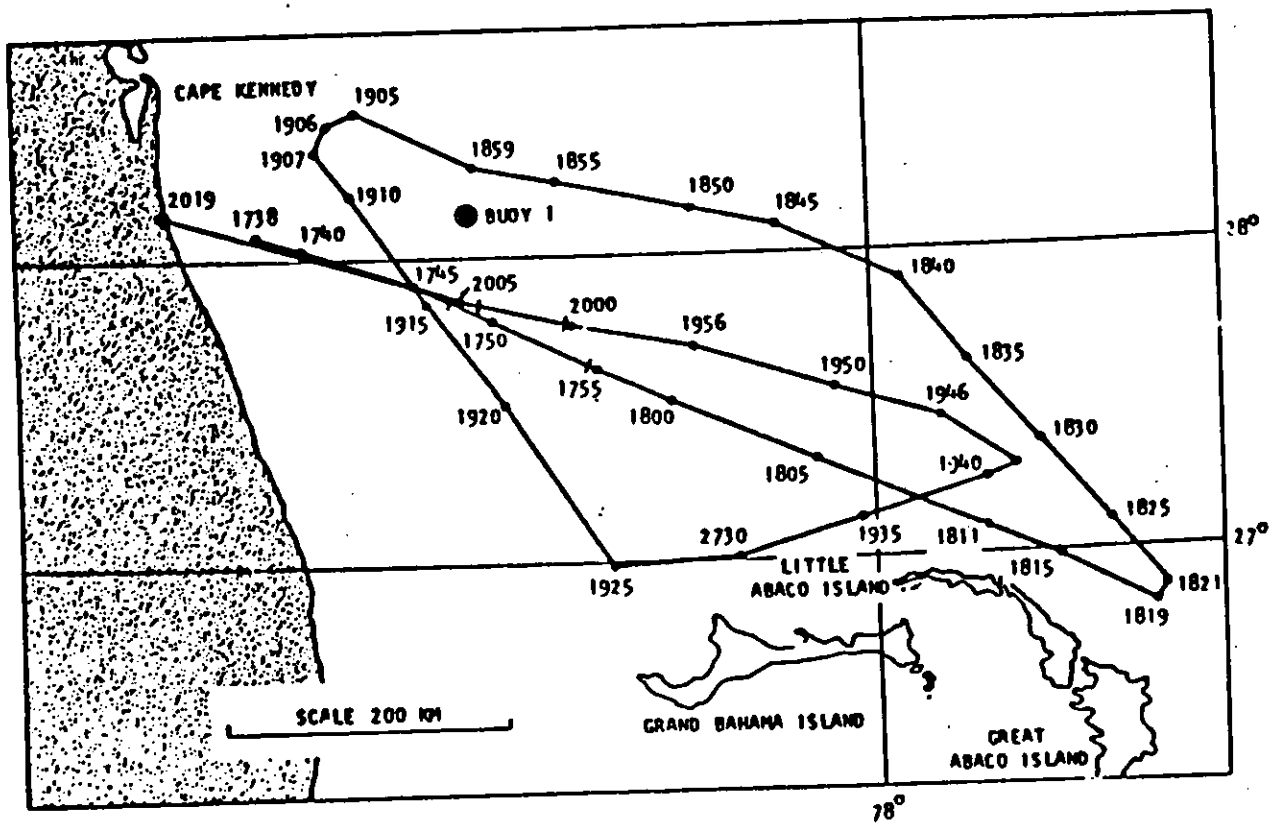

Figure 2-4. (U) Event 1 Flight Pattern (U).

(This page is UNCLASSIFIED)

UNCLASSIFIED

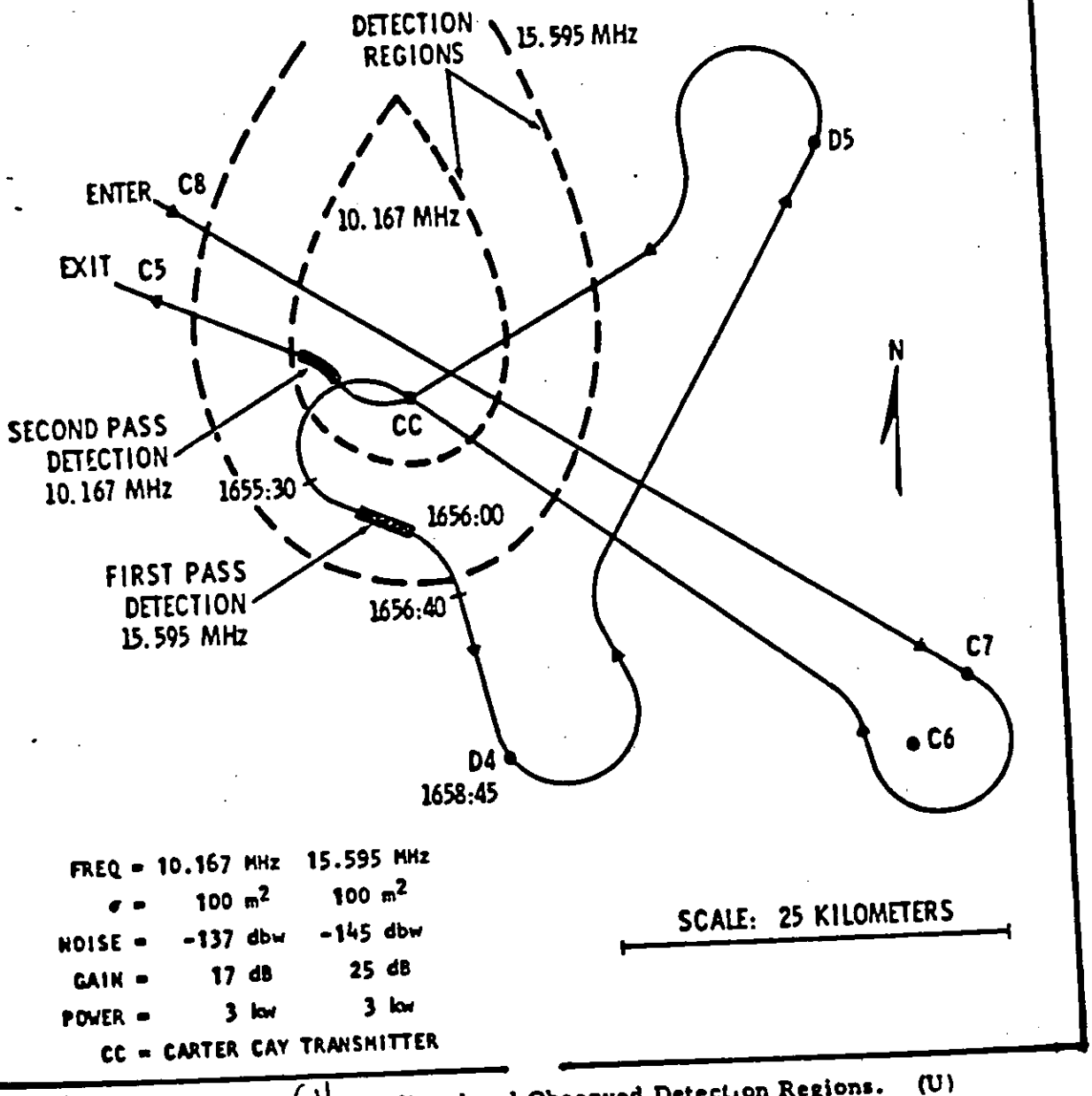

Figure 2-5 (U) Predicted and Observed Detection Regions. (U)

UNCLASSIFIED

2.2.5 (U) [redacted] -- Continued.

The detected signature is not considered to be the P3B test aircraft, but an aircraft flying near the receiver at VHFS. The predicted detectability region for this day extends at best only to 11 km. The P3B's closest approach to the buoy is only 30 km. Also, the period of the first Doppler signature's sign change occurs 2.8 minutes earlier than the predicted closest approach. In addition, the Doppler signatures obtained (although consistent with those for an aircraft) were much stronger than could be expected from the test aircraft using a 10-watt transmitter to illuminate the target. Therefore, because of inconsistent timing the distances of aircraft from the transmitter and receiver, and the strength of the detected signatures using a 10-watt transmitter, it is concluded that the detected signatures were not the P3B test aircraft, but rather another aircraft flying over the receiving antenna.

The second event on January 27, 1970, employed the 3 kw Carter Cay transmitter and a P3B test flight at a speed between 200-300 knots. The aircraft flew the pattern shown in Figure 2-5 at successive altitudes of 24,000, 14,000, 12,000, and 2,000 feet. The propagation conditions are summarized below:

RF (MHz)	XMTR Power (watts)	Receiving Antenna Gain (db)	Noise Level (dbw)
10.167	3,000	17	-137
15.595	3,000	25	-145

The detections for the first and second passes of the aircraft near the transmitter at 15.595 MHz and 10.167 MHz, respectively, are shown in Figure 2-3. The predicted detection regions for these frequencies are also included in the figure for comparison. The experimental data generally agree with the predicted results except that the detections are expected sooner during the flight. The lack of a signature during aircraft flight at high altitudes (e.g., 20,000 ft.) over the Carter Cay transmitter may be attributed to aircraft flight in the vertical null of the antenna. Both signatures were obtained for aircraft flight below 2,000 feet. Therefore, it can be concluded that aircraft detection below this altitude and within the predicted detectability regions can be detected using the buoy concept if sufficient power is transmitted (e.g., 3 kw).

[redacted]

2.3 (U) [redacted] CONCLUSIONS OF EW STUDY. (U)

The conclusions derived from the early warning system study are:

a. Detection of SLBMs at altitudes below 100 km is unlikely using buoy transmitters with 100 watts or less, and a landbased receiving system for the network geometry shown in Figure 1-3. However, with the missile at altitudes above 100 km (at which the missile radar cross section is enhanced) detection appears possible.

b. For buoy (or landbased) transmitters with 3 kw power and transmitting near the MUF, SLBM detection is probable for the network geometry in Figure 1-3 at both low and high altitudes.

c. Aircraft detection regions can be estimated with fair accuracy because the experimental results generally agree with the predicted results. Using a 3 kw transmitter (Carter Cay) aircraft can be detected at distances as great as 60 km with a receiving site at VHFS.

The conclusions indicate that it is basically possible to detect aircraft and SLBMs using a bistatic HF radar configuration in which a buoy transmitter is employed with ground- or surface-wave propagation to the target and sky-wave propagation between the target and the receiver. However, transmitter power on the order of 3 kw or more is required. In addition, it may be necessary to judiciously select the frequency of operation to minimize the D-layer and spreading losses for target detection under different transmitter-target-detection geometries.

[redacted]

[redacted]

Section 3

FLEET AIR DEFENSE

[redacted] (U) The detection of low-flying threats to surface vessels at a range sufficient to give useful warning time and tracking information is a problem for which over-the-horizon detection (OTHD) systems can offer a solution. A polystatic system such as portrayed in Figure 3-1 is especially desirable because it not only provides greater lead time for fleet air defense (FAD) by detecting targets at long ranges, but also provides the detection information without requiring active radiation from the fleet. Thus, the enemy is not given an opportunity to locate the fleet by employing direction-finding techniques against a fleet monostatic radar transmitter.

[redacted] (U) The results of the investigations for FAD are presented in four parts. The first describes the feasibility of using a polystatic system to protect the fleet in the Mediterranean Sea. Aircraft detection regions are examined for transmitters of opportunity that presently exist, and receivers located in the fleet. In addition, the operating schedules of the transmitter sources were examined to determine the degree of 24 hour coverage possible. The second part of the FAD investigation describes target location methods that can be employed using the basic polystatic configuration. Equations are derived for each technique to show how the target range can be estimated using measured and known parameters. The third part is the results of an error analysis of those target location techniques that are feasible. The bias and random errors associated with each technique are discussed. The fourth part describes the design for a prototype aircraft detection system. This system can serve as the test bed for experimental verification of polystatic techniques and system evaluation to select the parameters for the final system design.

3.1 (U) [redacted] POLYSTATIC SYSTEM DETECTION FEASIBILITY. (U)

3.1.1 (U) [redacted] General. (U)

The polystatic system for FAD consists of HF broadcast transmitters of opportunity for illuminating the target and a shipborne receiver (see Figure 3-1) for detecting the target-reflected Doppler signature. The detectability of this system was investigated for FAD operations in the Mediterranean Sea.

Two types of propagation mechanism were considered. The first consists of ground-wave propagation between the transmitter and the target

[redacted]

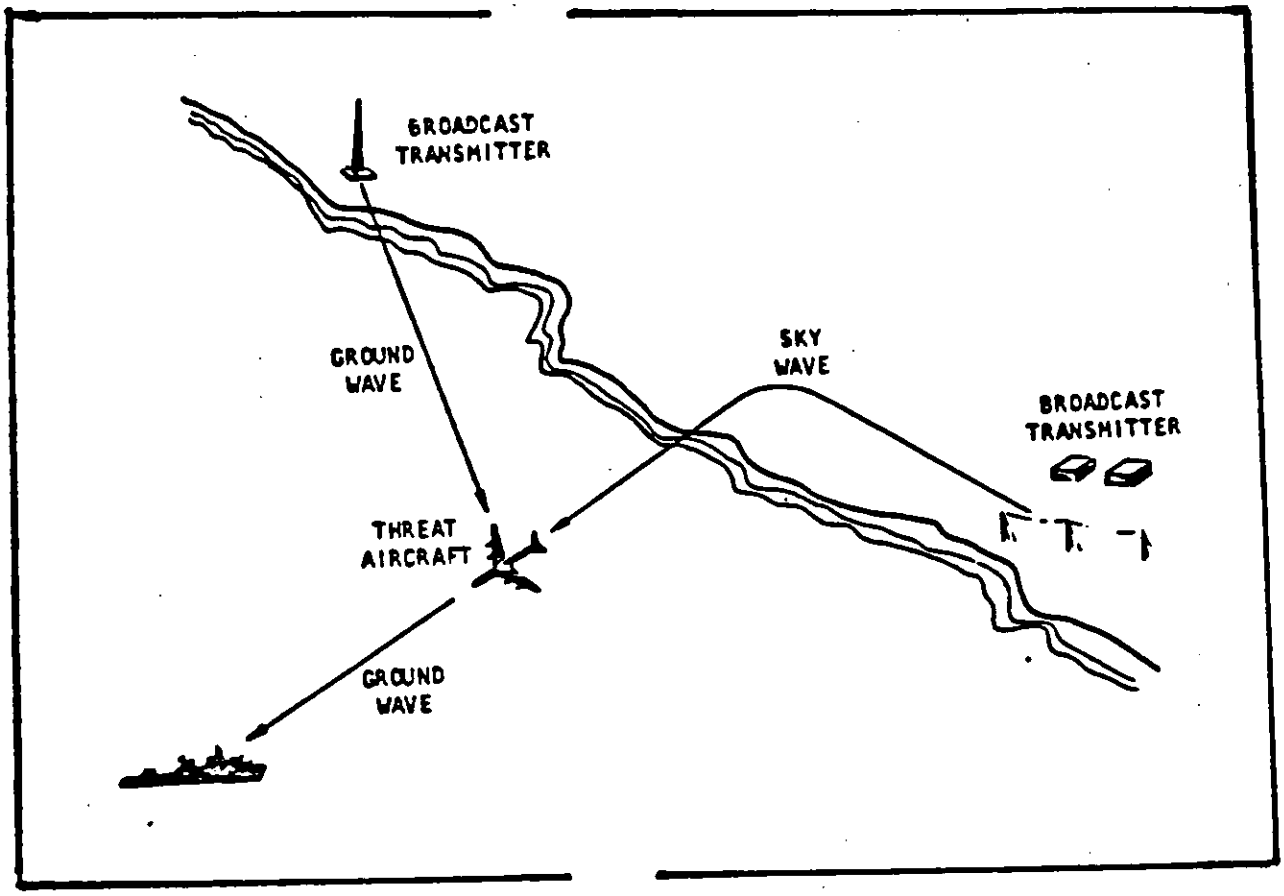

Figure 3-1 (U) FAD Polystatic System. (U)

3.1.1 (U) [redacted] -- Continued.

and also between the target and the shipborne receiver. The second consists of sky-wave propagation between the transmitter and the target and ground-wave propagation between the target and receiver. These two types are denoted as ground-ground and sky-ground modes, respectively.

To accomplish this feasibility study the efforts considered three aspects: source availability, the operating schedules of sources, and the coverage provided by available sources. These are described below.

3.1.2 (U) [redacted] Available Transmitters. (U)

The transmitters were categorized into two groups based on the polarization of their radiated signals. Horizontally polarized signals were considered for sky-wave propagation only on the transmitter-target half path since the attenuation of the horizontal component of a ground-wave over sea water is very large. The vertically polarized signals, on the other hand, were considered for both sky-wave and ground-wave propagation for the transmitter-target half path.

Table 3-1 lists some of the transmitters in the immediate vicinity of the Mediterranean which have been evaluated along with transmitter location, selected frequencies, transmitter power, beam information and polarization. The locations of the transmitters are displayed in Figure 3-2.

Transmitter scheduling is also an important factor in the evaluation of these transmitters. Historical records of scheduling were examined along with current information from FBIS to determine the schedules for each transmitter. Figure 3-3 shows the scheduling for the transmitters in Figure 3-2. Transmitters are available around the clock for coverage of some areas of the Mediterranean, but more sources must be located to provide complete around-the-clock coverage of the Mediterranean.

3.1.3 (U) [redacted] Coverage. (U)

Figure 3-4 illustrates the geometry for a bistatic radar detection. Several requirements must be satisfied in order to make a detection. First, the received scatter path signal, T-R, must be above the noise level present at the receiver. Second, the direct path signal must be received. (In the case of transmitters with sufficient frequency stability, a synthesizer signal can be used where the direct path signal cannot be received.) Third, the ratio of the dirct path to scatter path signals must fall within the dynamic range limitations of the receiver.

[redacted]

(This page is UNCLASSIFIED)

TABLE 3-1 (UNCLASSIFIED). MEDITERRANEAN TRANSMITTERS (U).

City	Latitude	Longitude	Frequency	Power - kw	Azimuth	Polarization
Caltanisseta	37° 30'	14° 04'	6060	25	ND	VER
			7175	5	ND	VER
Rome	41° 48'	12° 31'	5960	50	ND	VER
			6060	5	ND	VER
			7175	5	ND	VER
Athinai	38° 02'	23° 42'	6045	5	ND	VER
Ioannina	39° 40'	20° 49'	6090	1	ND	VER
			7240	1	ND	VER
Kozani	40° 24'	21° 48'	7215	1	ND	VER
Larisa	39° 32'	22° 25'	5922	2	ND	VER
Rhodos	36° 27'	28° 16'	6015	35	ND	VER
			7125	35	ND	VER
			7260	35	ND	VER
Serrai	41° 08'	23° 35'	7160	2	ND	VER
			7165	2	ND	VER
Tripolis	37° 35'	22° 23'	6005	1	ND	VER
Beruit	33° 52'	35° 25'	5980	100	ND	HOR
Damascus	33° 30'	36° 07'	6165	50	ND	HOR
Tel Aviv	32° 0'	34° 50'	6318	20	ND	HOR
			7189	20	ND	HOR
Cairo			7050			
			7075			
Tripoli	32° 42'	13° 12'	7165	100	ND	HOR
Tunis	36° 50'	9° 56'	5985	50	102-252	HOR
Algiers	37°	3°	6080	50	ND	HOR
			9510	50	ND	HOR
Tangier	35° 41'	5° 56'	6170	100	40°	HOR
			6190	100	40°	HOR
			7225	100	40°	HOR
Lisbon	38° 45'	8° 40'	6025	50	54	HOR
Madrid	40° 18'	3° 31'	6130	100	300	HOR
Tirane	41° 30'	20°	5945	50	ND	ND
			6020			
			7060			
Sofia	43°	24°	5920	50	ND	ND
			6020			
			7670			

ND: Non-Directional

[redacted]

[redacted]

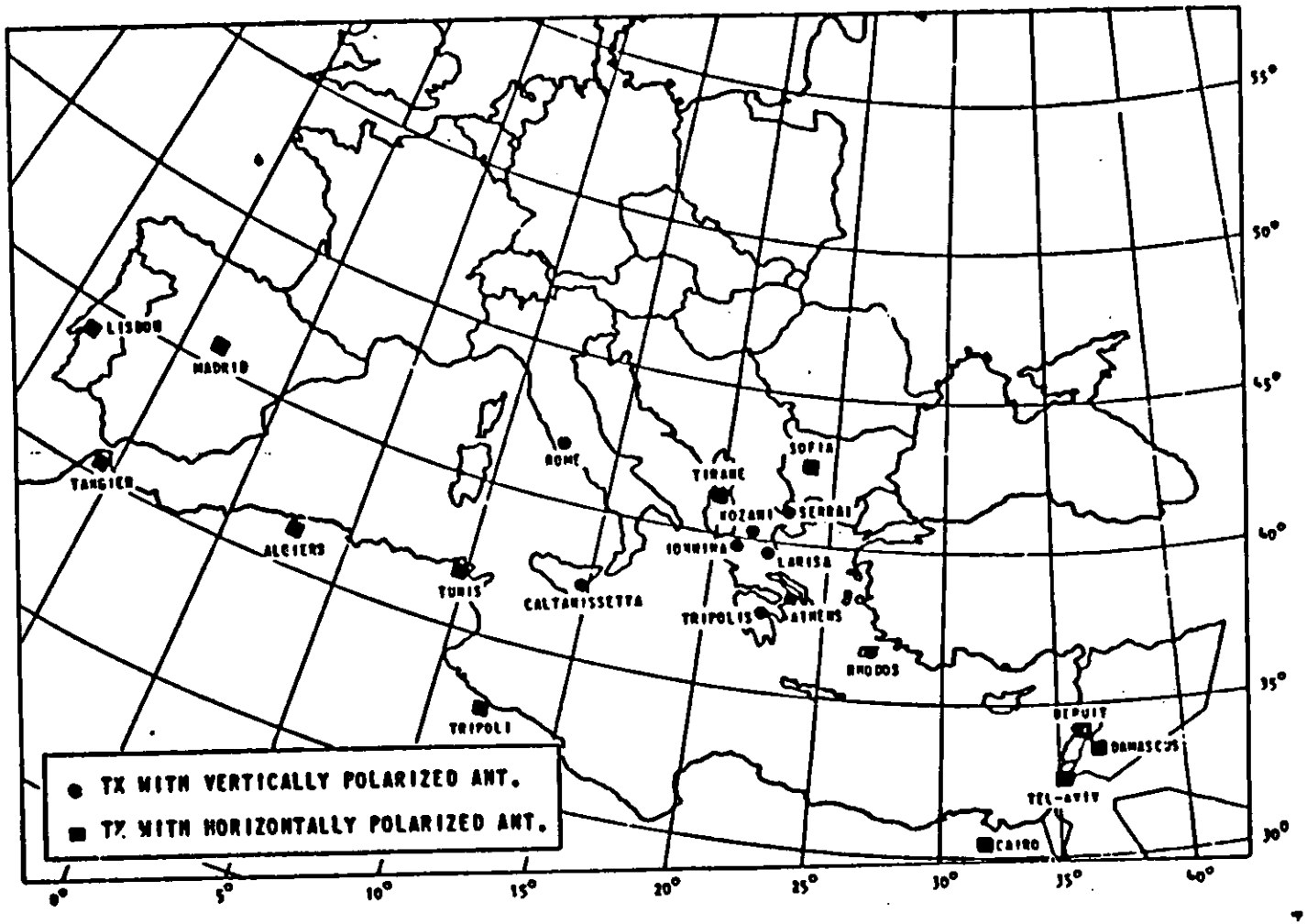

Figure 3-2 (UNCLASSIFIED). Located Sources (U).

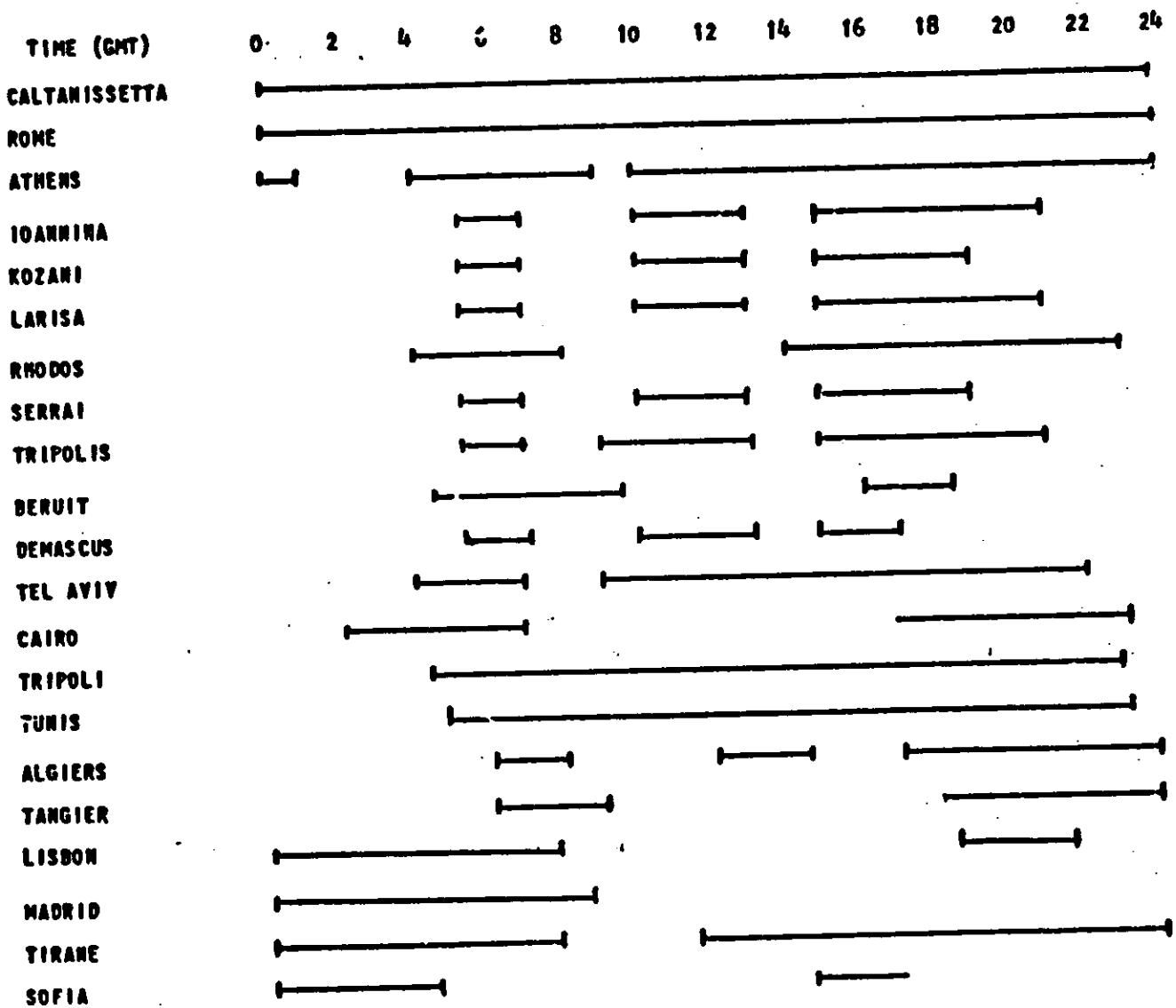

Figure 3-3 (UNCLASSIFIED). Source Schedule (U).

[redacted]

(This page is UNCLASSIFIED)

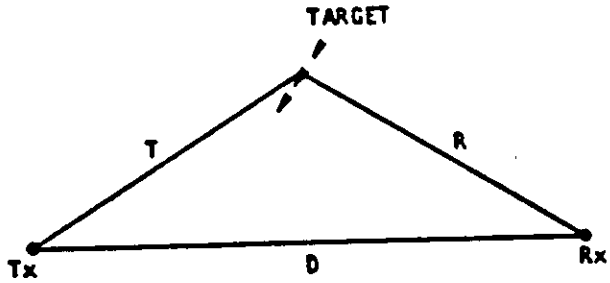

Figure 3-4 (U). Typical Geometry. (U)

[redacted]

UNCLASSIFIED

[redacted]

3.1.3.1 (U) [redacted] Evaluation. (U)

Actual propagation losses for each half path have been calculated for selected transmitter-target-receiver geometries to evaluate the coverage available to the fleet. For sky-wave propagation, the losses were calculated using the propagation prediction package by ITSA ESSA*. For ground-wave propagation, the losses are taken from Barrick's table**.

Figure 3-5 shows an example of one of Barrick's tables. This particular table is for 7 MHz, Sea State 4, 20-knot wind, and propagation in the upwind-downwind direction. The effect of each of these parameters is that increasing frequency increases the loss, rougher sea state increases the loss, and propagation in a crosswind direction has less loss than upwind-downwind propagation.

For organization ease, the Mediterranean was divided into 5 sections. Each section was evaluated individually to determine the amount of coverage protection afforded to a ship while it was located within that area. Evaluations were made for representative transmitter-aircraft-ship positions to see if the detection system was feasible.

3.1.3.2 (U) Ground Wave-Ground Wave Propagation. (U)

For the case in which ground-wave propagation occurs over both half paths, the coverage provided by transmitters with vertically polarized signals was evaluated using the following parameters:

a. target cross-section σ = 100 M^2 ;

b. $G_T = G_R$ = 0 db;

c. N = -150 dbw and -170 dbw;

d. frequency--7 MHz, and

e. system loss L_S = 3 db .

* Barghousen, A. F., et al, Predicting Long-Term Operational Parameters of High Frequency Skywave Telecommunication Systems, ESSA Technical Report, ERL 110-ITS 78, U.S. Department of Commerce; May 1969.

** Barrick, D. E., "Theory of Groundwave Propagation Across a Rough Sea at Dekameter Wavelengths", Battelle Memorial Institute, Columbus Laboratories; January 1970.

[redacted]

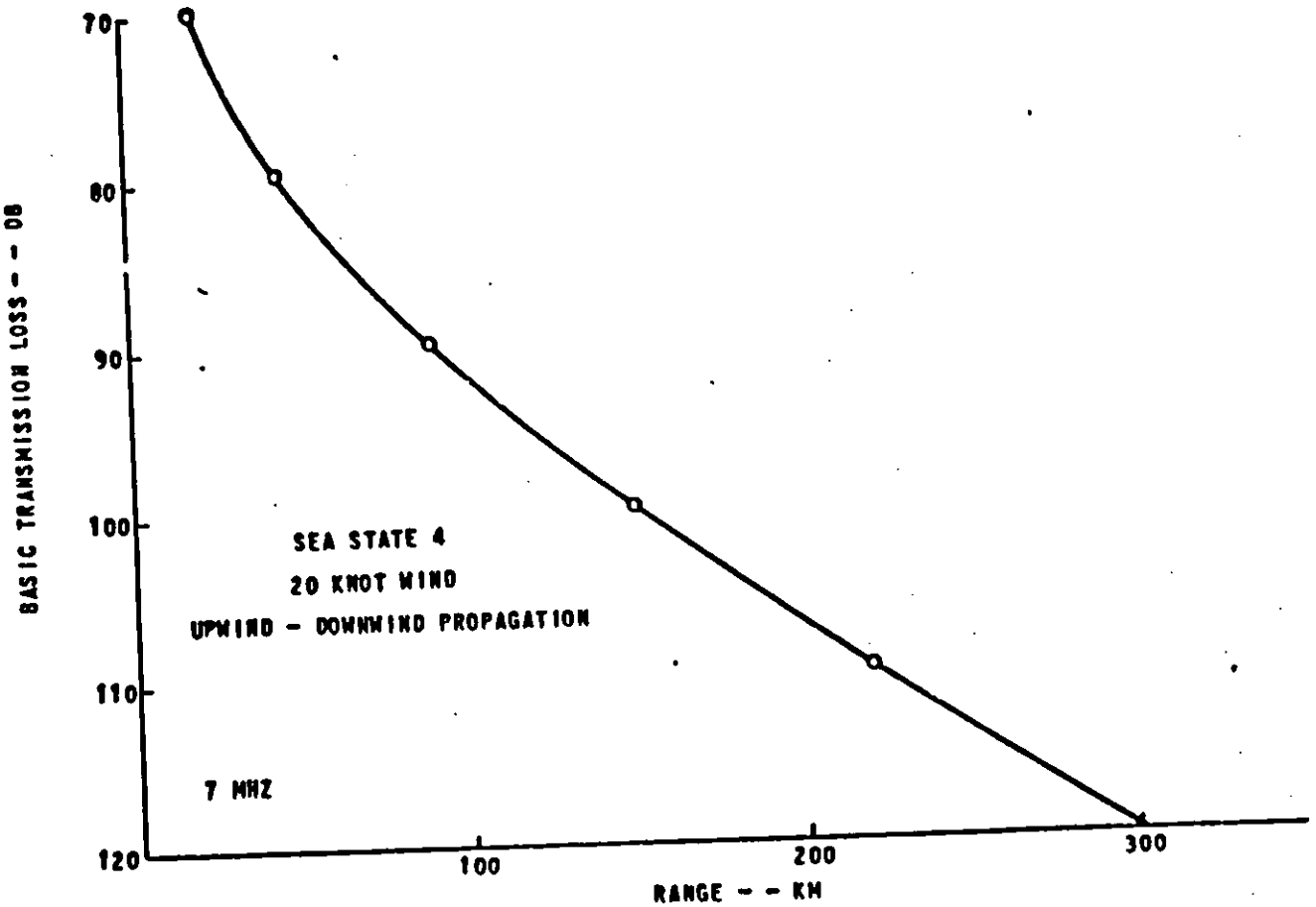

Figure 3-5 (U). Basic Transmission Loss for a Groundwave Along the Ocean (U).

3.1.3.2 (U) -- Continued.

The two noise levels account for diurnal changes in the noise level of the receiver. The frequency of 7 MHz was selected since it is low enough to provide reasonable ground-wave losses and high enough to have reasonably low noise levels for the detection of aircraft. To determine the region of coverage provided by this propagation mechanism, the shipboard receivers were assumed to be 200 km from the transmitters. With this assumption, a contour of constant sensitivity (Oval of Cassini) was constructed around the transmitter and receiver which determines the region of detectability of an aircraft for that transmitter-receiver combination. This was done in a number of transmitter-receiver cases and the results (Figure 3-6) indicate that coverage is quite good in the northern central part of the Mediterranean Ocean.

3.1.3.3 (U) Sky Wave-Cround Wave Propagation. (U)

For each of the five areas in the Mediterranean, propagation predictions were made for selected transmitters to evaluate the use of sky-wave propagation. Target illumination by line of sight and one F-hop propagation is feasible for detection purposes, but hop structures with more than 1 F-hop for the date and time evaluated incur too much loss over the transmitter half path to afford any reasonable protection. Noise calculations and propagation conditions were calculated for 15 September 1970 at 0800Z (N = -165 dbw).

Five aircraft positions were evaluated with shipboard receivers located at selected positions around the aircraft. The regions of detectability for each transmitter-receiver combination (Ovals of Cassini) were not calculated at this time, but as a first estimate of the protection provided by each transmitter, the following technique was used. For a specific aircraft position (altitude 3,000 feet), loss over the transmitter-target half path was evaluated from the ITSA ESSA prediction program. L_R was then calculated and converted into a distance D_R, using Figure 3-5. Assuming the target scatters equally in all directions, a circle of coverage can be drawn around the aircraft of distance D_R. Any receiver located within the circle should detect the aircraft.

For example, consider transmitters located at Algiers and Madrid, an aircraft located at 37-99N, 2-07E, and a receiver located at 38N, 0E. The predicted losses over the transmitter half path are 116 db for the 1 F-hop mode from Madrid and 91 db for a line-of-sight mode from Algiers. Solving for L_R and converting to a target-receiver distance from Figures 3-4 gives 70 km for the Madrid signal and 205 km for the Algiers

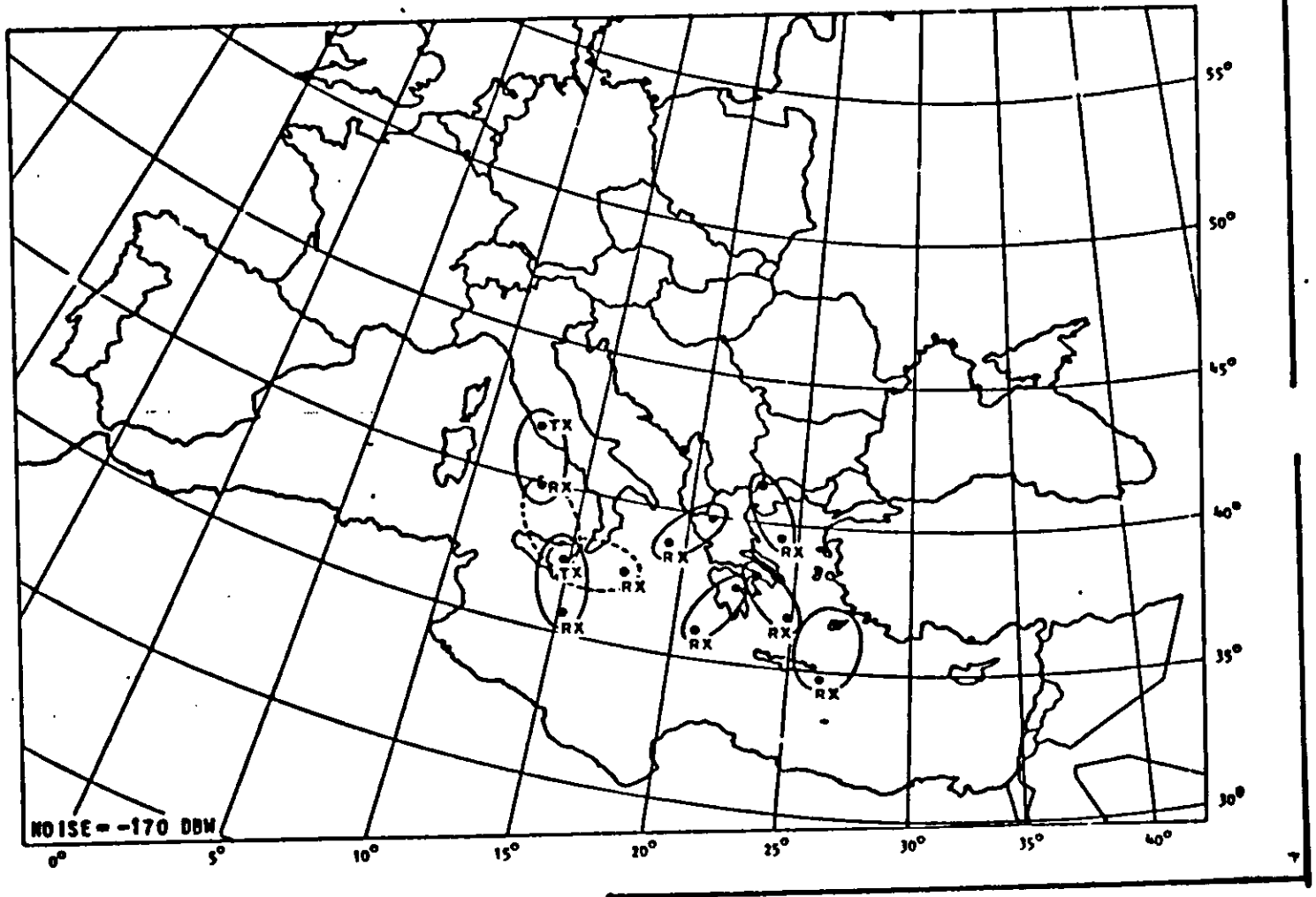

Figure 3-6 (U) Typical Fleet Protection Areas in the Mediterranean Ocean. (U)

3.1.3.3 (U) -- Continued.

signal. Any receiver within these distances from the aircraft should be able to detect the aircraft. Figure 3-7 illustrates this example. In this example the shipboard receiver located at 38N, 0E, would detect the aircraft on the Algiers frequency, but not on the frequency from Madrid. As the aircraft closed on the ship, the Madrid frequency would also make a detection.

Using these methods to evaluate the coverage for each area, the following results were found (see Figure 3-8). For area one, transmitters located at Lisbon, Madrid, Tangier, and Algiers were evaluated for the receiver and target position given in the example. The transmitters afforded protection at distances from this aircraft of 10, 20, 70, and 205 km, respectively.

For area 2, transmitters located at Algiers and Rome were evaluated for two different ship positions. Algiers provided detectability at 70 km from the aircraft while Rome provided detectability at 100 km.

For area 3, transmitters were evaluated at Caltanessetta, Alma Ata, Rome, Tunis, Tirane, and Tripoli. Tripoli provided the greatest detection range at 80 km with Rome and Tirane giving 50 km detection range.

For areas 4 and 5, the greatest detection range for the transmitters evaluated was 100 km in each case.

In addition to the transmitters evaluated, a great number of possible transmitters at other locations still remain to be evaluated around the coast of the Mediterranean. Table 3-2 is a partial listing of these locations. Transmitters with power as low as 1 kw can be used for line-of-sight coverage along the coast and 1F hop propagation into the interior of the sea. Development of these sources is necessary for round-the-clock coverage as well as multiple channel coverage (i.e., on several transmitter frequencies) of a ship at any point in the Mediterranean.

The conclusion that can be drawn from this analysis is that the use of transmitters of opportunity as part of a polystatic HF radar system is feasible for FAD in the Mediterranean Sea. However, before a system is implemented, there is a need to evaluate the transmitter sources that have not been examined to identify the specific transmitters that should be employed by the fleet during operation in different areas of the Mediterranean Sea.

UNCLASSIFIED

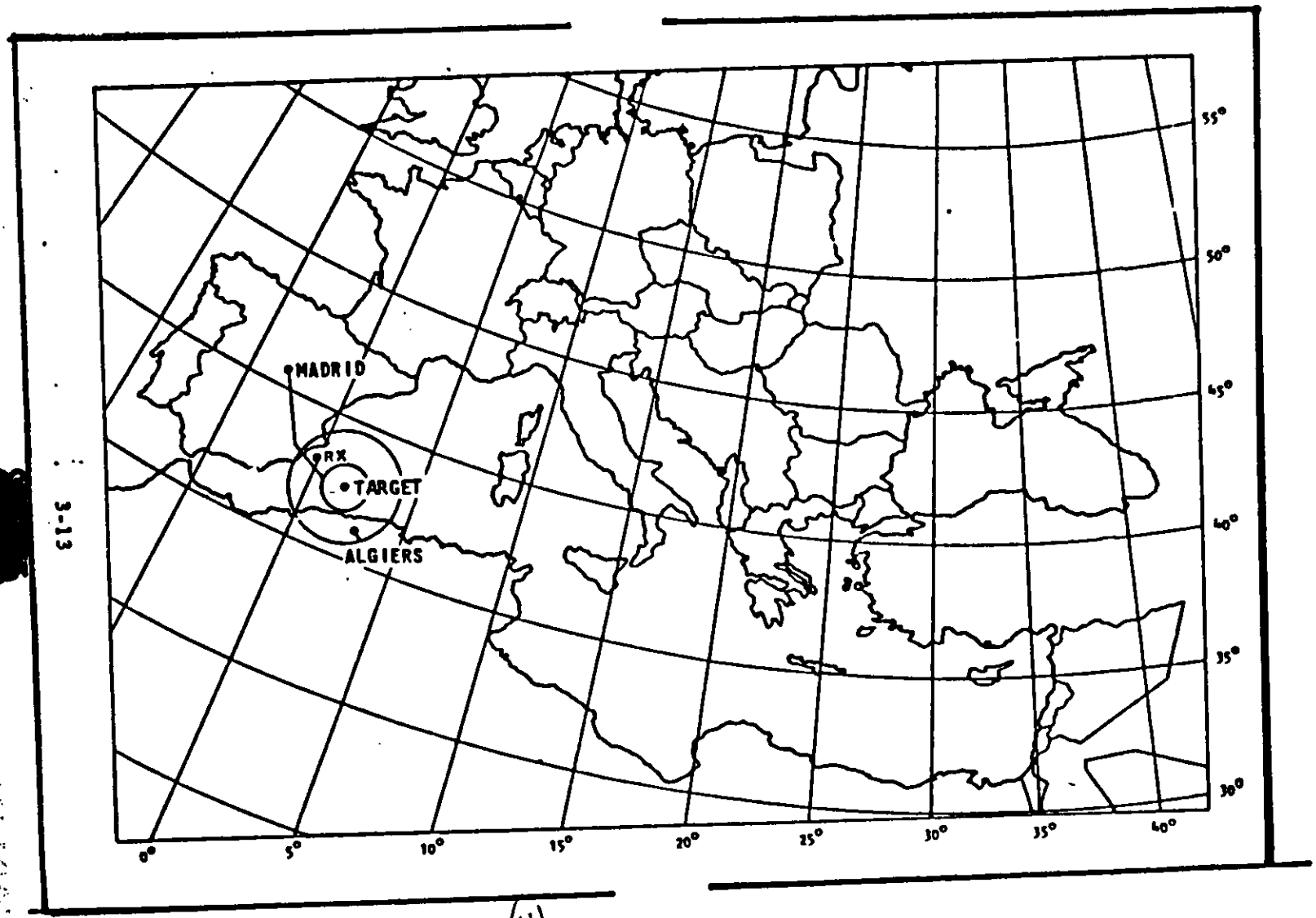

Figure 3-7 (U) Skywave-Groundwave Example. (U)

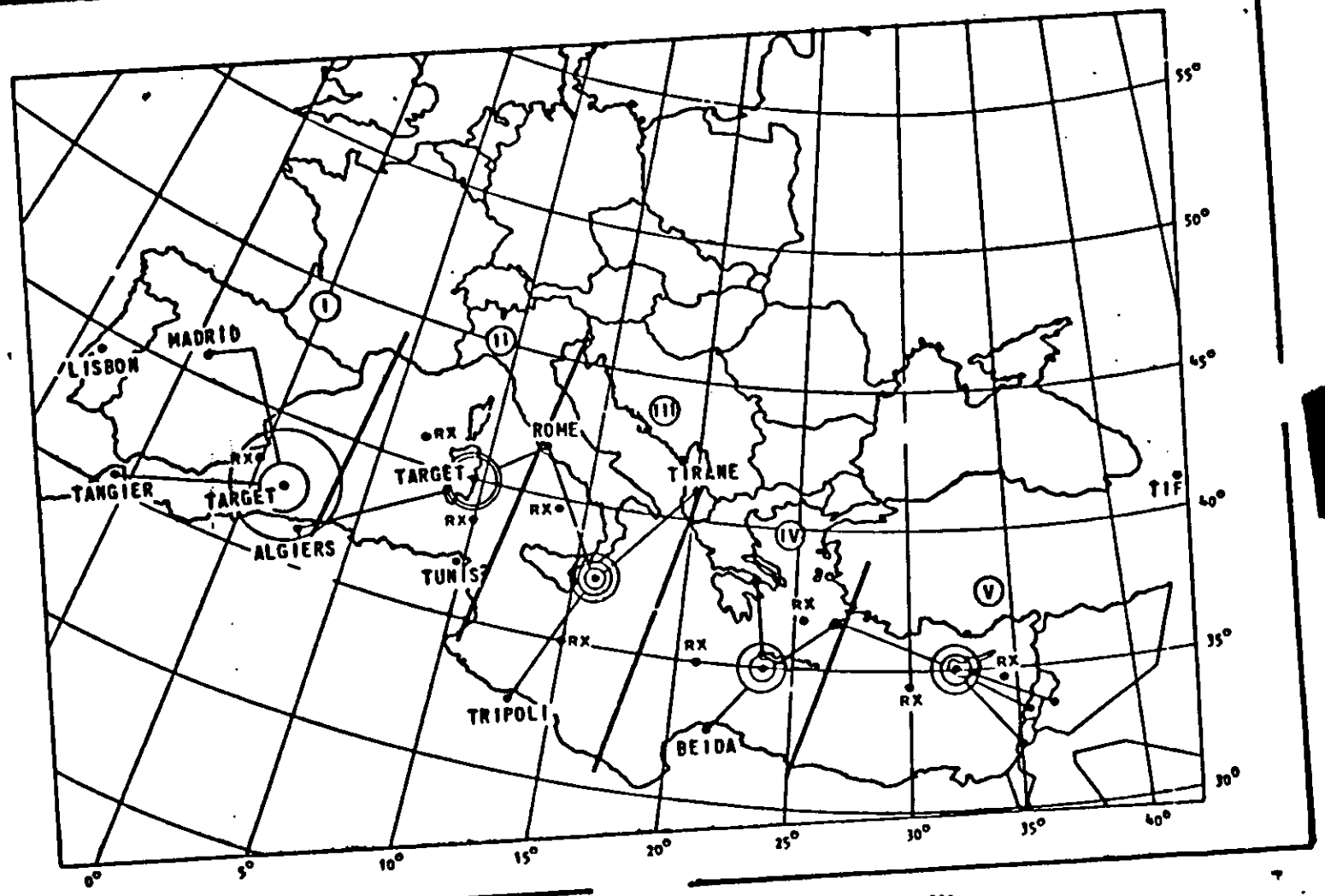

Figure 3-8 (U) Skywave-Groundwave Coverage. (U)

(This page is UNCLASSIFIED)

Table 3-2

(U) Additional Transmitters (U)

Malaga, Spain	Tobruk, Lybia
Cartagena, Spain	Beida, Lybia
Valencia, Spain	Bengazi, Lybia
Barcelona, Spain	Annaba, Tunesia
Marseille, Frances	Safaqis, Tunesia
Nice, France	Oran, Algeria
Pisa, Italy	Melilla, Morroco
Naples, Italy	Balearic Island
Izmir, Turkey	Corsica
Latakia, Syria	Sardinia
Port Said, UAR	Crete
Alexandria, UAR	Cyprus

UNCLASSIFIED

[redacted] UNCLASSIFIED

3.2 (U) [redacted] TARGET LOCATION METHODS. (U)

As described previously, protection of the fleet against low-flying aircraft and/or cruise missiles may be accomplished using a bistatic radar with a shore-based transmitter for target illumination combined with passive shipboard reception. The target location methods considered in this section appear to eliminate two fundamental problems associated with CW-Doppler bistatic radar:

a. Target signal amplitudes gives no indication of whether the target is near the transmitter or the receiving ship because the bistatic radar range equation is symmetric about the transmitter-target and receiver-target ranges.

b. Single Doppler measurements alone cannot provide unambiguous target location since single Doppler measurements have a fourfold location ambiguity caused by the geometric symmetry between the transmitter, receiver and target.

Four separate derivations are given describing techniques which may be used to locate and track low-flying targets which may threaten a surface fleet. They all assume a two-dimensional (flat earth) situation that is reasonably accurate (see Section 3.3.4) for low-flying aircraft and cruise missiles. The four techniques are:

a. the double baseline, double measurement range estimator,

b. the double baseline, single measurement range estimator,

c. the single baseline, double measurement range estimator, and

d. the Doppler location finder.

The first two techniques employ two transmitters and one receiver as shown in Figures 3-9 and 3-10, respectively. For the first method (double baseline, double measurement range estimator) two target-scattered Doppler returns and their directions of arrival are measured at two different points along the target's flight trajectory. Eight measurements are employed to estimate the target's location. For the second method (double baseline, single measurement range estimator) the estimate is essentially made using the two Doppler returns and their associated directions of arrival measured at one flight point. The third technique (single baseline, double measurement range estimator) uses two sets of Doppler returns and associated direction of arrival

[redacted] UNCLASSIFIED

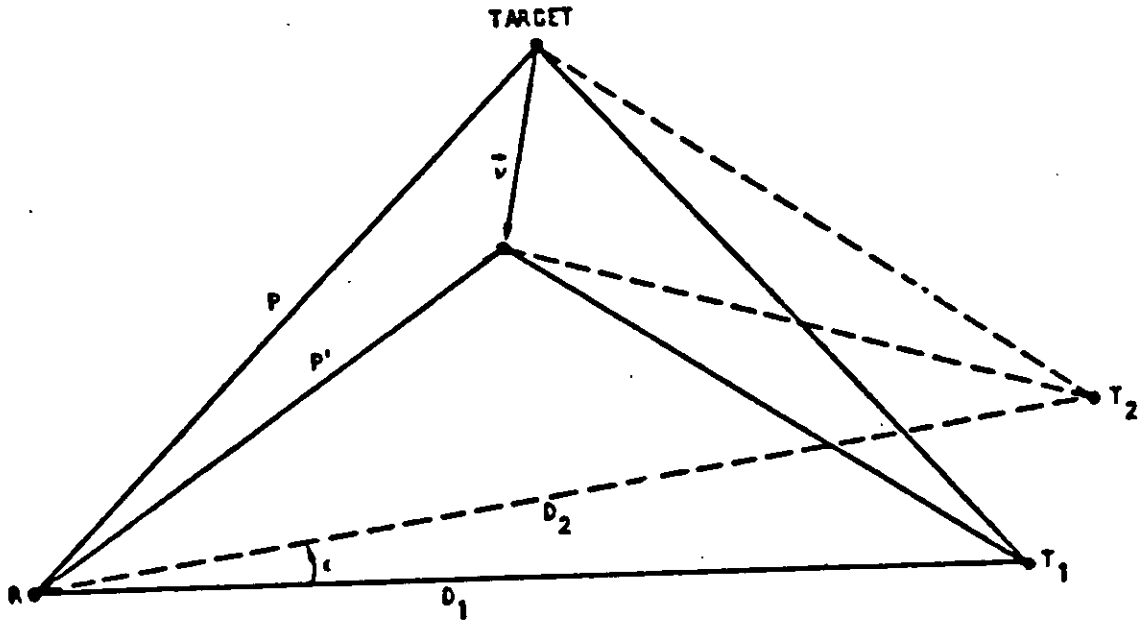

LEGEND:

P, P^1	=	GROUND RANGE FROM RECEIVER TO TARGET AT TWO POINTS ON TARGET PATH
$\vec{v}$	=	TARGET VELOCITY VECTOR
ϵ	=	ANGLE AT THE RECEIVER BETWEEN THE TWO LOCATION BASELINES
R	=	RECEIVER
T_1, T_2	=	TRANSMITTER 1 AND 2, RESPECTIVELY
D_1, D_2	=	ARE THE DISTANCES BETWEEN THE RECEIVER AND TRANSMITTERS T_1 AND T_2 RESPECTIVELY (KNOWN A PRIORI)

Figure 3-9 (U). Double-Baseline, Two-Measurements Model. (U)

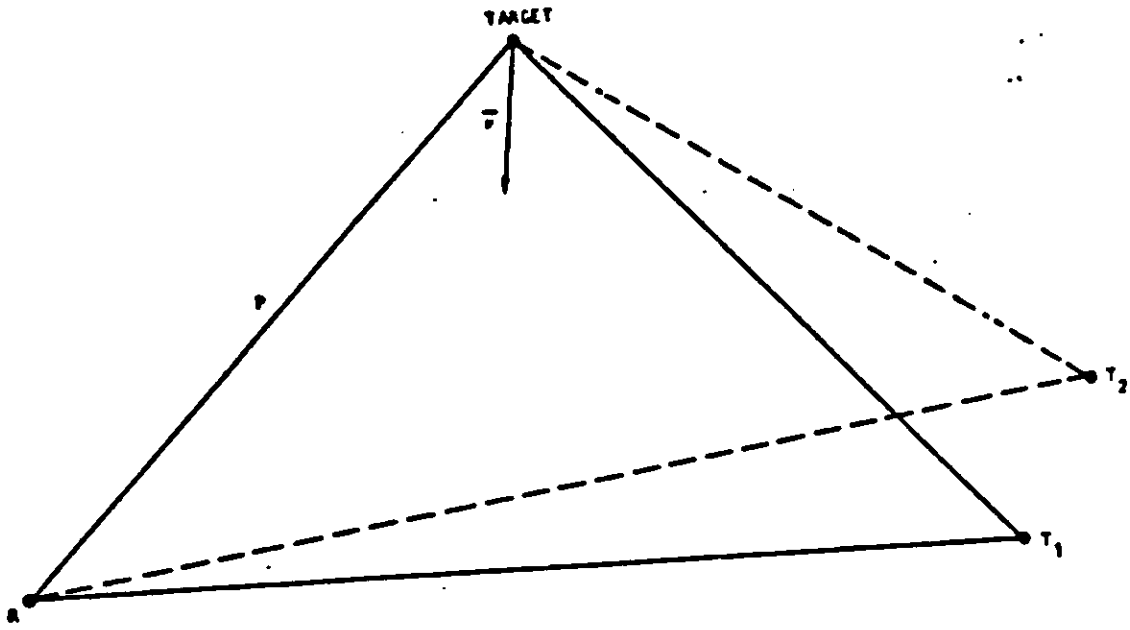

Figure 3-10 (U). Double-Baseline, One-Measurement Model. (U)

and a single transmitter source to estimate the target's range. This method, which uses the configuration in Figure 3-11, is operationally preferred to the first two because of the need for fewer measurements and transmitter sources. The fourth technique (Doppler location finder) employs the Doppler returns from the target illuminated by four transmitters to estimate both range and azimuth. All four techniques provide location information on the detected target.

The derivation of equations for each of the four methods is included below.

3.2.1 (U) Double-Baseline, Two-Measurements Range Estimator. (U)

Consider the single baseline, one time point situation shown in Figure 3-12, where a vehicle is moving at an unknown velocity $\hat{U}$, the distance between the transmitter and the receiver is assumed known to be D, and the transmitter is broadcasting on a known wavelength λ. The azimuth angle of the target at the receiver, α, and the Doppler shift, Δf, are measured.

The received Doppler shift for this geometry may be written as

$$\Delta f = -\frac{\hat{U}}{\lambda}(\hat{r}_1 + \hat{r}_2)$$

$$= -\frac{U}{\lambda}(\cos\theta_1 + \cos\theta_2) .$$

Angles θ_1 and θ_2 can also be written:

$$\theta_1 = 90 + \alpha + \delta$$

$$\theta_2 = 90 + \beta - \delta .$$

Therefore,

$$\Delta f = \frac{U}{\lambda}[\sin(\alpha + \delta) + \sin(\beta - \delta)]$$

[redacted]

(This page is UNCLASSIFIED)

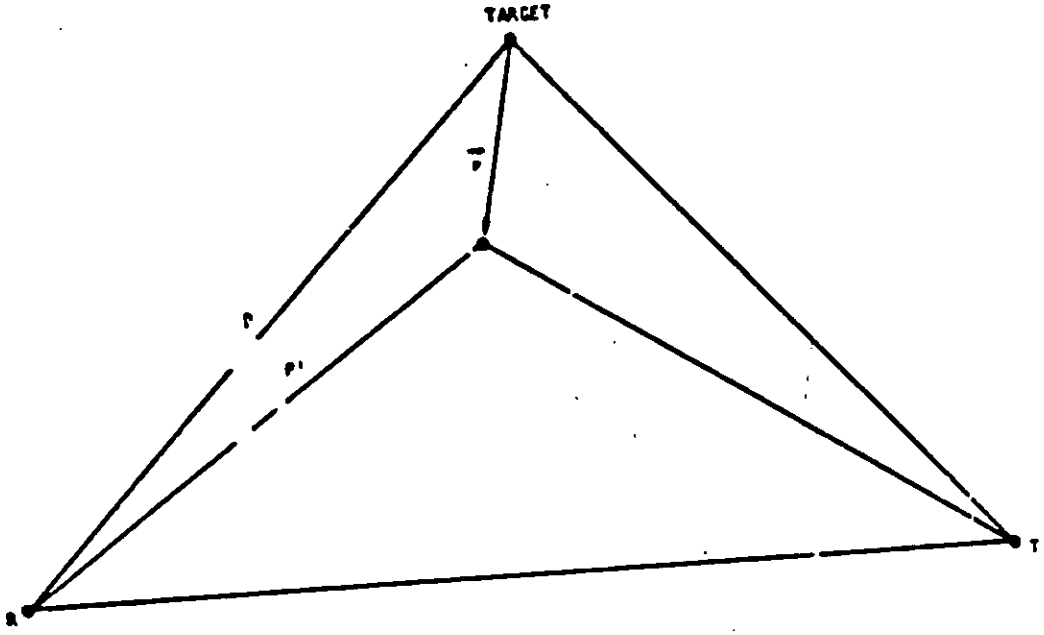

Figure 3-11. (U) Single Baseline Model. (U)

[redacted]

UNCLASSIFIED

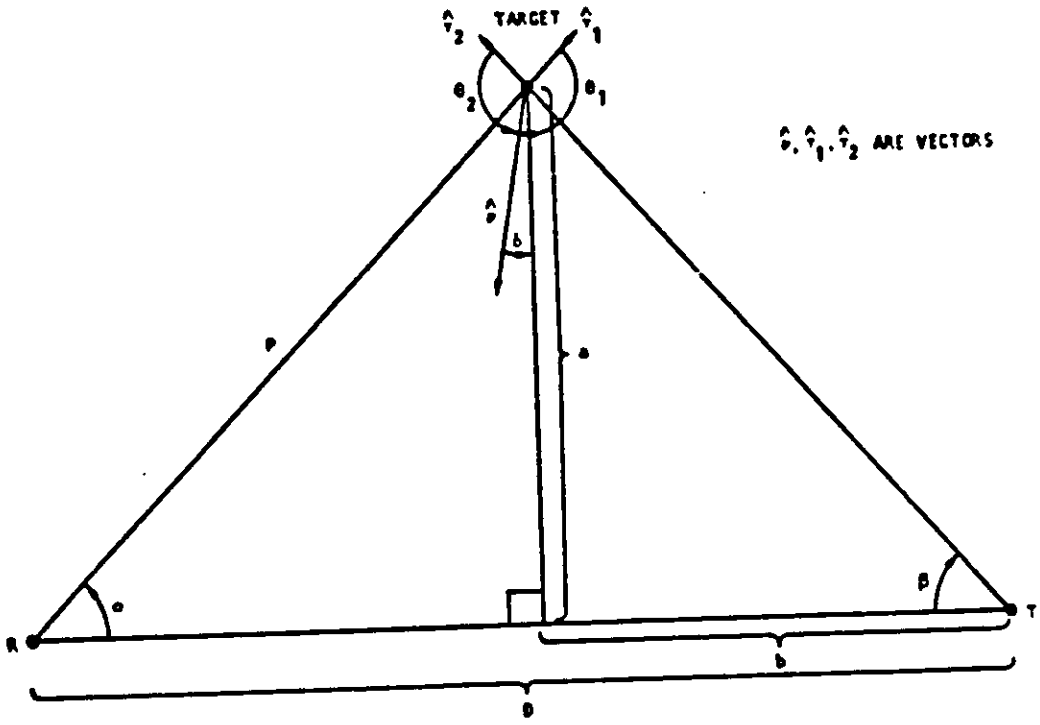

Figure 3-12. (U) Variables for Double-Baseline, Two-Measurements Model. (U)

3.2.1 (U) -- Continued.

Also,

$$\beta = \tan^{-1}\left(\frac{a}{b}\right)$$

$$= \tan^{-1}\left[\frac{a}{D - \frac{a}{\tan \alpha}}\right] = \tan^{-1}\left[\frac{a \tan \alpha}{D \tan \alpha - a}\right]$$

If there are two transmitter geometries, which shall be distinguished using subscripts, then the following three equations can be written:

$$\Delta f_1 = \frac{v}{\lambda_1}\left\{\sin(\alpha_1 + \delta_1) + \sin\left[\tan^{-1}\left(\frac{a_1 \tan \alpha_1}{D_1 \tan \alpha_1 - a_1}\right) - \delta_1\right]\right\} \quad (3\text{-}1)$$

$$\Delta f_2 = \frac{v}{\lambda_2}\left\{\sin(\alpha_2 + \delta_2) + \sin\left[\tan^{-1}\left(\frac{a_2 \tan \alpha_2}{D_2 \tan \alpha_2 - a_2}\right) - \delta_2\right]\right\} \quad (3\text{-}2)$$

and

$$\delta_2 = \delta_1 + \varepsilon \quad (3\text{-}3)$$

where ε is the angle between the two baselines, as shown in Figure 3-9. The value of ε may be calculated because the coordinates of the two transmitters and the receivers are assumed known.

If additional azimuth and Doppler measurements are made for these same two geometries at some time Δt later, then four more equations can be written. This set of equations is distinguished by a superscript prime.

$$\Delta f_1' = \frac{v}{\lambda_1}\left\{\sin(\alpha_1' + \delta_1) + \sin\left[\tan^{-1}\left(\frac{a_1' \tan \alpha_1'}{D_1 \tan \alpha_1' - a_1'}\right) - \delta_1\right]\right\} \quad (3\text{-}4)$$

$$\Delta f_2' = \frac{v}{\lambda_2}\left\{\sin(\alpha_2' + \delta_2) + \sin\left[\tan^{-1}\left(\frac{a_2' \tan \alpha_2'}{D_2 \tan \alpha_2' - a_2'}\right) - \delta_2\right]\right\} \quad (3\text{-}5)$$

3.2.1 (U) -- Continued.

$$a_1' = a_1 - v\,\Delta t\,\cos\delta_1 \tag{3-6}$$

$$a_2' = a_2 - v\,\Delta t\,\cos\delta_2 \tag{3-7}$$

The last two equations are a result of the constant velocity and direction assumption. All seven equations can be combined into a system of four equations in four unknowns by eliminating δ_2 from the equations. The results are:

$$\Delta f_1 = F_1(v, a_1, \delta_1)$$

$$\Delta f_2 = F_2(v, a_2, \delta_1)$$

$$\Delta f_1' = F_3(v, a_1, \delta_1)$$

$$\Delta f_2' = F_4(v, a_2, \delta_1)$$

where the $F_i(\cdot)$ are different functions of the argument parameters. The unknowns are v, a_1, a_2 and δ_1. The measured quantities are α_1, α_2', α_1', α_2, Δf_1, $\Delta f_1'$, Δf_2, and $\Delta f_2'$. The quantities known a priori are D_1, D_2, λ_1, λ_2, Δt, and c. The above set of simultaneous equations may be solved for the unknowns and the ground range from the receiver to the target could be calculated by

$$P = \frac{a_1}{\sin\alpha_1}$$

Although this procedure yields four independent equations which may be solved for the target position, a slight reformulation of the problem can reduce the number of equations by two as described on the following page. Because this reformulation simplifies the double baseline, two measurement technique, this first target location technique will not be examined further.

3.2.2 (U) Double-Baseline, One-Measurement Range Estimator. (U)

The variables for the double-baseline, one-measurement model are defined in Figure 3-13. As in the previous case, the transmitter-receiver distances, D_1 and D_2, and the transmitter wavelengths, λ_1 and λ_2, are assumed known a priori. The azimuths, α_1, and α_2, and Doppler shifts, Δf_1 and Δf_2, are the only quantities requiring measurement.

From another form of the Doppler equation,

$$\Delta f_1 = \frac{-1}{\lambda_1} (\dot{p} + \dot{n}_1)$$

$$\Delta f_2 = \frac{-1}{\lambda_2} (\dot{p} + \dot{n}_2)$$

where $\dot{p} = dp/dt$ and $\dot{n}_i = dn/dt$.

From the law of cosines,

$$n_1 = (p^2 + D_1^2 - 2pD_1 \cos \alpha_1)^{1/2}$$

so

$$\dot{n}_1 = \frac{(p\dot{p} - \dot{p}D_1 \cos \alpha_1 + pD_1 \dot{\alpha}_1 \sin \alpha_1)}{(p^2 + D_1^2 - 2pD_1 \cos \alpha_1)^{1/2}} \quad (3\text{-}8)$$

where $\dot{\alpha}_1 = d\alpha_1/dt$.

Similarly

$$\dot{n}_2 = \frac{(p\dot{p} - \dot{p}D_2 \cos \alpha_2 + pD_2 \dot{\alpha}_2 \sin \alpha_2)}{(p^2 + D_2^2 - 2pD_2 \cos \alpha_2)^{1/2}} \quad (3\text{-}9)$$

Note that $\dot{\alpha}_1 = \dot{\alpha}_2 = \dot{\alpha}$. The quantity $\dot{\alpha}$ can be estimated using the previous azimuth measurements as follows:

$$\dot{\alpha} = \frac{[\alpha_1(t) - \alpha_1 (t-\Delta t)] + [\alpha_2(t) - \alpha_2 (t-\Delta t)]}{2\Delta t}$$

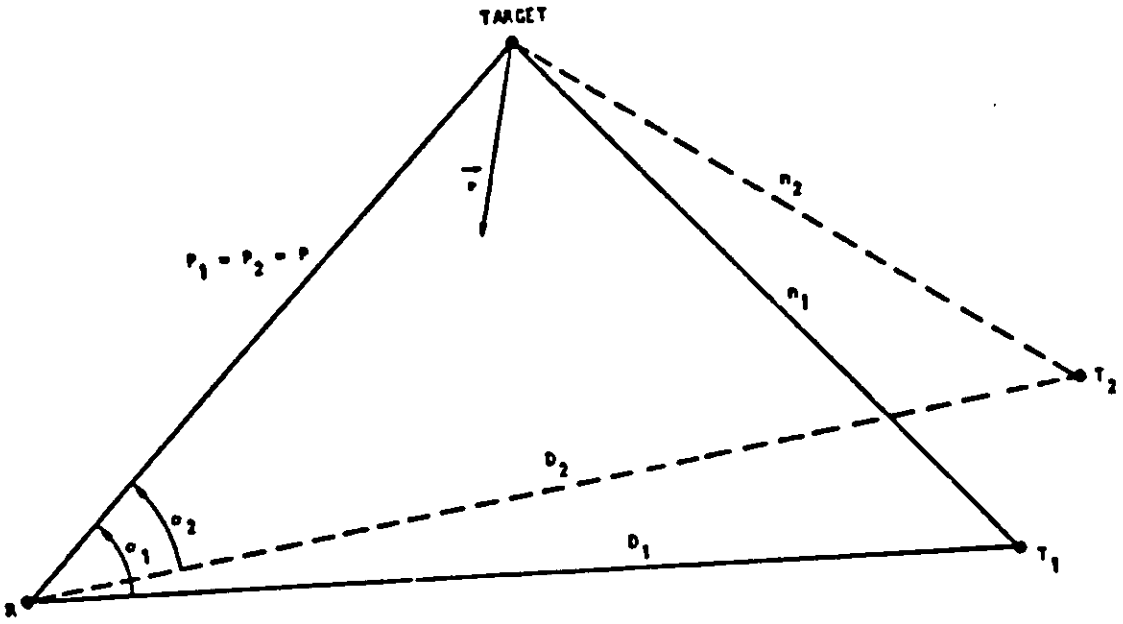

Figure 3-13. (U) Variables for Double-Baseline, One-Measurement Model. (U)

3.2.2 (U) -- Continued.

Now define h_1 , q_1 , r_1 , and s_1 as follows:

$$h_1 = (p^2 + D_1^2 - 2pD_1 \cos \alpha_1)^{1/2}$$

$$q_1 = \Delta f_1 \lambda_1$$

$$r_1 = D_1 \cos \alpha_1$$

$$s_1 = D_1 \dot{\alpha} \sin \alpha_1$$

The quantities h_2 , q_2 , r_2 , and s_2 are similarly defined. Equations 3-8 and 3-9 can then be written as

$$\dot{h}_1 = \frac{p\dot{p} - \dot{p} r_1 + p s_1}{h_1}$$

$$\dot{h}_2 = \frac{p\dot{p} - \dot{p} r_2 + p s_2}{h_2}$$

So Δf_1 can be written

$$\Delta f_1 = \frac{-1}{\lambda_1} \left[\dot{p} + \frac{\dot{p} (p - r_1) + p s_1}{h_1} \right]$$

Similarly

$$\Delta f_2 = \frac{-1}{\lambda_2} \left[\dot{p} + \frac{\dot{p} (p - r_2) + p s_2}{h_2} \right]$$

Solving for $\dot{p}$.

$$\dot{p} = - \frac{(q_2 h_2 + p s_2)}{(h_2 + p - r_2)} \qquad (3\text{-}10)$$

3.2.2 (U) -- Continued.

Also,

$$-q_1 h_1 = \dot{p}\, h_1 + \dot{p}\,(p - r_1) + p\, s_1$$

and so

$$p = \frac{-[q_1 h_1 + \dot{p}\,(h_1 - r_1)]}{s_1 + \dot{p}} \qquad (3\text{-}11)$$

Equations (3-10) and (3-11) form a system of two equations in two unknowns (p and $\dot{p}$) that may be solved using standard iterative techniques. Note also that, for this formulation, the assumption of constant velocity and directions are not necessary.

3.2.3 (U) Single Baseline Model. (U)

The third derivation to be considered is that involving the model using only one transmitter. The variables for the single baseline model are defined in Figure 3-14. As before, the transmitter-receiver distance, D, and the transmitter wavelength, λ, are assumed known. The azimuths, α and α', and Doppler shifts Δf and $\Delta f'$, are measured quantities where the primes signify measurement at some time Δt after the first (unprimed) measurements. The velocity $\hat{U}$, of the vehicle is not known.

From the Doppler equation

$$f = \frac{-1}{\lambda}\,(\dot{p} + \dot{n})$$

$$f' = \frac{-1}{\lambda}\,(\dot{p}' + \dot{n}')$$

From the law of cosines,

$$n = (p^2 + D^2 - 2pD\cos\alpha)^{1/2}$$

$$\dot{n} = \frac{(p\dot{p} - \dot{p}D\cos\alpha + pD\dot{\alpha}\sin\alpha)}{(p^2 + D^2 - 2pD\cos\alpha)^{1/2}}$$

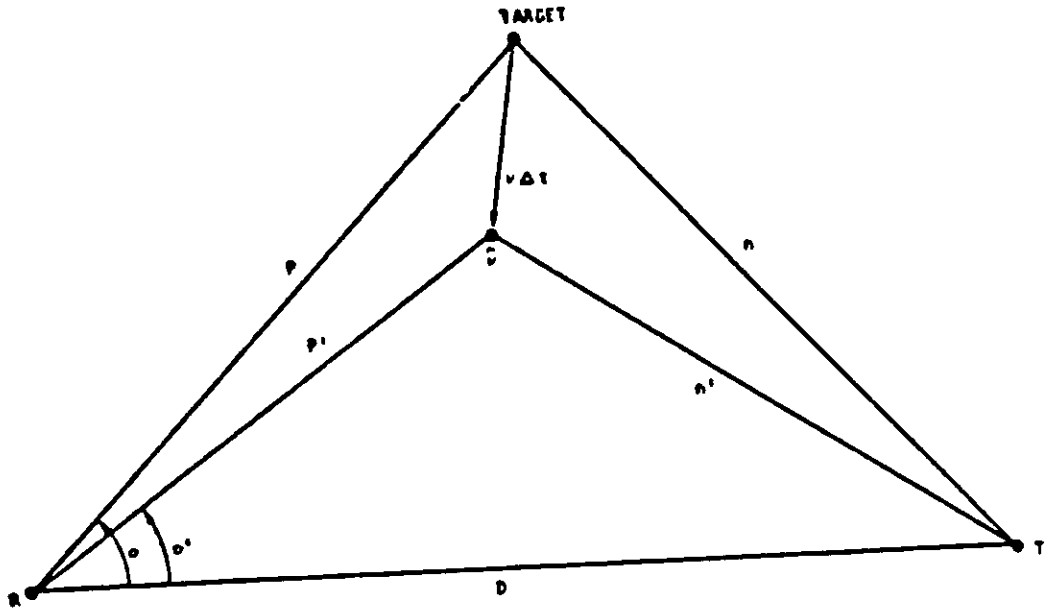

Figure 3-14. (U) Variables for Single Baseline Model. (U)

3.2.3 (U) -- Continued.

Similarly,

$$\dot{h}' = \frac{(p'\dot{p}' - \dot{p}' D \cos\alpha' + p' D \dot{\alpha}' \sin\alpha')}{(p'^2 + D^2 - 2p' D \cos\alpha')^{1/2}}$$

In order to find a solution using only one baseline, two approximations have to be made

(a) $\dot{p}$ is constant; i.e., $\dot{p}' = \dot{p}$ and, furthermore,

$$p \cdot p' - \dot{p}\,\Delta t$$

(b) $\dot{\alpha}$ is constant; i.e., $\dot{\alpha}' = \dot{\alpha}$

Over short time intervals (small Δt) these assumptions are reasonable. The angular velocity $\dot{\alpha}$ can be estimated as follows:

$$\dot{\alpha} = \frac{\alpha' - \alpha}{\Delta t}$$

These approximations are strictly true if the target is flying on a radial path, toward or away from the ship.

Combining the equations and approximations above gives

$$-\Delta f\lambda = -q = \dot{p} + \frac{\dot{p}\,(p-r) + ps}{h}$$

where

$$q = \Delta f\lambda$$

$$r = D\cos\alpha$$

$$s = D\dot{\alpha}\sin\alpha$$

$$h = (p^2 + D^2 - 2pD\cos\alpha)^{1/2}$$

3.2.3 (U) -- Continued.

Substituting $p = p' - \dot{p}\Delta t$, squaring to eliminate square roots and algebraic manipulation of the results yields the cubic equation

$$A\dot{p}^3 + B\dot{p}^2 - C\dot{p} + D = 0 \qquad (3\text{-}12)$$

where

$$A = 2\Delta t^2 (q-s)$$

$$B = \Delta t^2 (q^2-s^2) + \Delta t (4qr-4qp') + 2s\Delta t (2p'-r) + D^2 - r^2$$

$$C = \Delta t (2q^2 r-2q^2 p'+2p's^2) + 2p'^2 (q-s) + 2p'r (s-2q) + 2qD^2$$

$$D = p'^2 (q^2-s^2) + q^2 (D^2-2p'r)$$

This cubic equation can be solved for $\dot{p}$ and the correct root chosen. Also note that $\dot{p}$ is still a function of the single unknown p'.

In similar fashion,

$$\Delta f' = \frac{-1}{\lambda} (\dot{p}'+\dot{n}')$$

or

$$-\Delta f\lambda = -q' = \dot{p} + \frac{\dot{p}(p'-r') + p's'}{h'}$$

Where h', q', r' and s' are defined similarly to h, q, r and s. Now

$$-q'h' - \dot{p}(h'-r') = p'(\dot{p}+s')$$

or

$$p' = \frac{-q'h' - \dot{p}(h'-r')}{\dot{p}+s'} \qquad (3\text{-}13)$$

Equations (3-12) and (3-13) form a set of simultaneous equations in the two unknowns p' and $\dot{p}$ which may be solved for the target position.

3.2.4 (U) Doppler Location Finder (DLF). (U)

The range estimation techniques discussed in the previous sections all utilized measurements of target bearing and Doppler frequency. The Doppler Location Finder (DLF) described in this section uses only Doppler measurements and yields both range and bearing information.

The variables for the DLF are defined in Figure 3-15. The transmitter-receiver distances, D_1, D_2, D_3, and D_4, and the transmitter wavelengths, λ_1, λ_2, λ_3, and λ_4, are assumed known a priori. The angles, β_1, β_2, β_3, and β_4, formed by the reference baseline with the transmitter-receiver are also assumed known a priori. The only measured quantities are the Doppler shifts, Δf_1, Δf_2, Δf_3, and Δf_4. The variables estimated by the DLF technique are range p, bearing α, range velocity, $\dot{p}$, and bearing velocity $\dot{\alpha}$. The latter two variables described the change of target position with time and are of secondary importance. The range and bearing estimates describe the target location and have primary significance.

From the Doppler equation:

$$\Delta f_i = -\frac{1}{\lambda_i}(\dot{p} + \dot{n}_i) \tag{3-14}$$

where

$$\dot{n}_i = dn_i/dt \ , \quad i = 1, 2, 3, 4 \ .$$

From the law of cosines,

$$n_i = [p^2 + D_i^2 - 2pD_i \cos(\alpha + \beta_i)]^{1/2}$$

so

$$\dot{n}_i = \frac{[p\dot{p} - \dot{p}D_i \cos(\alpha + \beta_i) + pD_i\dot{\alpha}\sin(\alpha + \beta_i)]}{[p^2 + D_i^2 - 2pD_i \cos(\alpha + \beta_i)]^{1/2}} \ . \tag{3-15}$$

Thus, from (3-14) and (3-15) it can be seen that

$$\Delta f_i = h(p, \alpha, \dot{p}, \dot{\alpha}; D_i, \beta_i, \lambda_i) \tag{3-16}$$

where h is a function of the argument parameters.

3.2.4 (U) -- Continued.

The desired parameters (p, α, $\dot{p}$, and $\dot{\alpha}$) can therefore be estimated by the solution of the following system of equations.

$$\begin{aligned} \Delta f_1 &= h(p, \alpha, \dot{p}, \dot{\alpha}; D_1, \theta_1, \lambda_1) \\ \Delta f_2 &= h(p, \alpha, \dot{p}, \dot{\alpha}; D_2, \theta_2, \lambda_2) \\ \Delta f_3 &= h(p, \alpha, \dot{p}, \dot{\alpha}; D_3, \theta_3, \lambda_3) \\ \Delta f_4 &= h(p, \alpha, \dot{p}, \dot{\alpha}; D_4, \theta_4, \lambda_4) \ . \end{aligned} \tag{3-17}$$

This system of equations can be solved using standard iterative methods. Unlike the other techniques discussed, this method is truly instantaneous; the estimate at one point in time requires no previous measurements. Also, the equations are exact; they require no assumptions as to the constancy of p or $\dot{\alpha}$.

The Doppler Location Finder can thus estimate target range and bearing using only Doppler frequency measurements.

3.3 (U) ERROR ANALYSIS. (U)

The target location estimation techniques discussed in Section 3.2 result in two kinds of errors. One is a bias in the estimate that arises because of one or more approximations that are employed in the technique. This is a systematic error that can, in some cases, be minimized by processing. The second kind of error arises because the inputs needed for the estimate involve measurements that contain random errors. These two kinds of errors generally limit the accuracy of an estimation technique.

In Sections 3.3.1 through 3.3.3 the error expressions for both kinds of errors are derived for:

a. the double baseline, single measurement range estimator,

b. the single baseline, double measurement range estimator, and

c. the Doppler location finder.

Some assumptions on independence of error sources have been made. In Section 3.4 the several other possible sources of error that do not significantly alter the estimate are described.

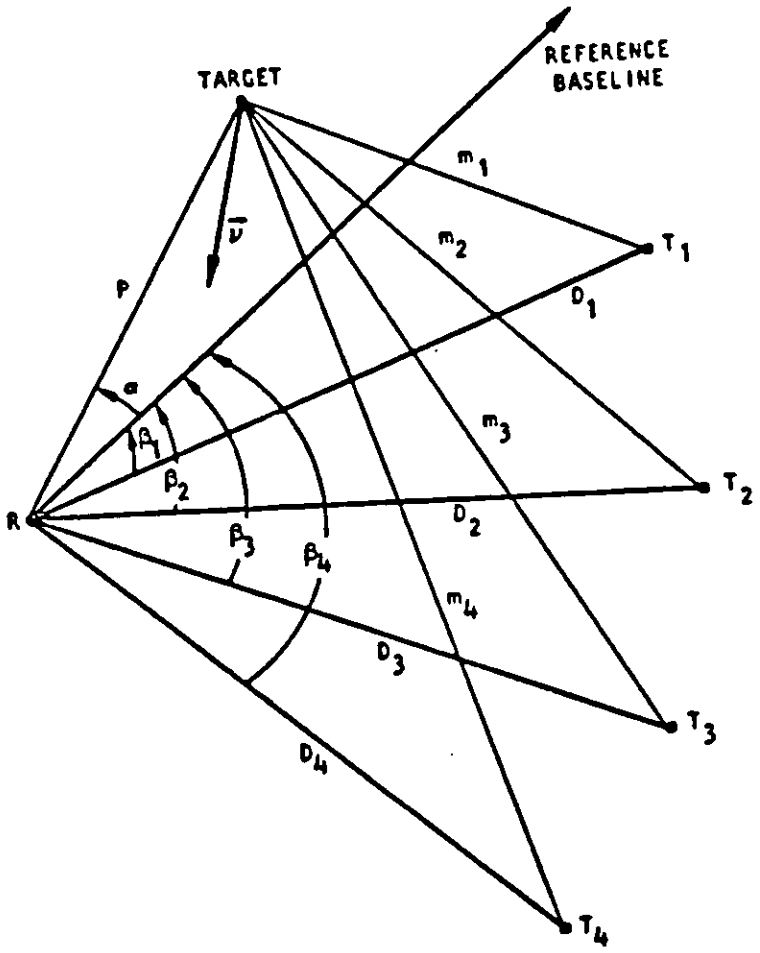

Figure 3-15. (U) Variables for Doppler Location Finder. (U)

3.3.1 (U) Error Analysis of Double-Baseline, Single-Measurement Range Estimator. (U)

The range estimate given by the Double-Baseline, Single-Measurement technique (Section 3.2.2) is dependent on the measured values of target bearing and Doppler frequency. An expression is derived below relating RMS measurement errors of azimuth and Doppler shift to RMS estimation errors of target range. This error expression is valid at specific target locations and has been evaluated for several configurations of target, shipboard receiver, and transmitters using reasonable values for RMS measurement errors. The bias of the range estimate is also computed. The results indicate that for certain system geometrics and parameters, total ranging errors of less than 15% can be achieved.

3.3.1.1 (U) Derivation of Error Expressions. (U)

As shown in Section 3.2.2, the true range p is the solution of the nonlinear system of equations:

$$p = \frac{-[q_1 h_1 + \dot{p}(h_1 - r_1)]}{S_1 + \dot{p}}$$

$$\dot{p} = \frac{-(q_2 h_2 + pS_2)}{(h_2 + p - r_2)}$$

where h_1, h_2, q_1, q_2, r_1, r_2, S_1, S_2 are functions of α_1, α_2, $\dot{\alpha}$, Δf_1, Δf_2. The expression for $\dot{p}$ can be substituted into the equation for p and it is seen that p is the solution of

$$G = (p ; \alpha_1, \alpha_2, \dot{\alpha}, \Delta f_1, \Delta f_2) = 0 \qquad (3\text{-}18)$$

where G is a nonlinear function of p and the coefficients involve α_1, α_2, $\dot{\alpha}$, Δf_1, Δf_2. The parameter $\dot{\alpha}$, however, is estimated by

$$\dot{\alpha} \sim \frac{1}{2\Delta t}(\alpha_1 + \alpha_2 - \alpha_3 - \alpha_4)$$

where

$$\alpha_3 = \alpha_1(t - \Delta t)^*$$

*Although the technique is described as a single measurement technique, it does require α_1 and α_3 vales at time $t - \Delta t$.

3.3.1.1 (U) -- Continued.

and

$$\alpha_4 = \alpha_2 (t - \Delta t) .$$

Thus, instead of (3-18) an equation of the following form is solved:

$$H (\hat{p} ; \alpha_1, \alpha_2, \alpha_3, \alpha_4, \Delta f_1, \Delta f_2) = 0 \qquad (3\text{-}19)$$

where $\hat{p}$ is the estimated range. Since the estimated value of $\hat{\alpha}$ may be in error, the solution $\hat{p}$ of (3-19) may be slightly biased away from the true p. Let P_{bias} be this bias in the range estimate. Thus,

$$P_{bias} = \hat{p} - p .$$

As mentioned previously, this bias from the use of an estimated value of $\hat{\alpha}$ is one of the two important types of errors in this range estimation technique. The other (random) error arises from using measured values of bearing and Doppler. The true α_i and Δf_i are not available; the measured values $\hat{\alpha}_i$ and $\Delta\hat{f}_i$ must be used instead. Thus, the estimate of range is taken to be the solution of

$$H (\hat{p} ; \hat{\alpha}_1, \hat{\alpha}_2, \hat{\alpha}_3, \hat{\alpha}_4, \Delta\hat{f}_1, \Delta\hat{f}_2) = 0 .$$

The measurements $\hat{\alpha}_i$ and $\Delta\hat{f}_i$ will generally have mean values of α_i and Δf_i, and standard deviations $\Delta(\alpha)_{RMS}$ and $\Delta(\Delta f)_{RMS}$, respectively.

Note that $\hat{p}$ is implicitly a function of the $\hat{\alpha}_i$ and $\Delta\hat{f}_i$; as these measured values change so does $\hat{p}$ in order to keep H = 0. Thus,

$$\hat{p} = \hat{p} (\hat{\alpha}_1, \hat{\alpha}_2, \hat{\alpha}_3, \hat{\alpha}_4, \Delta\hat{f}_1, \Delta\hat{f}_2).$$

The change in $\hat{p}$ due to changes in the $\hat{\alpha}_i$ and $\Delta\hat{f}_i$ is given by

$$\Delta(\hat{p}) = \frac{\partial\hat{p}}{\partial\hat{\alpha}_1}\Delta(\hat{\alpha}_1) + \frac{\partial\hat{p}}{\partial\hat{\alpha}_2}\Delta(\hat{\alpha}_2) + \frac{\partial\hat{p}}{\partial\hat{\alpha}_3}\Delta(\hat{\alpha}_3) + \frac{\partial\hat{p}}{\partial\hat{\alpha}_4}\Delta(\hat{\alpha}_4)$$

$$+ \frac{\partial\hat{p}}{\partial\Delta\hat{f}_1}\Delta(\Delta\hat{f}_1) + \frac{\partial\hat{p}}{\partial\Delta\hat{f}_2}\Delta(\Delta\hat{f}_2) \quad . \qquad (3\text{-}20)$$

3.3.1.1 (U) -- Continued.

The preceding equation is the deterministic form of the error equation. Because the measurement errors are random, we must employ a modified version. At each target location the partial derivatives $\partial\hat{p}/\partial\alpha_i$ and $\partial\hat{p}/\partial\Delta f_i$ are constant. Using two relations from probability theory*,

a. The RMS value of a zero-mean random variable is the standard deviation (σ).

b. If $\chi = \sum_i A_i Y_i$, then

$$\sigma = \left(\sum_i A_i^2 \sigma^2_{y_i}\right)^{1/2}$$

we can derive from (3-20)

$$\Delta(\hat{p})_{RMS} = \left\{\left(\frac{\partial\hat{p}}{\partial\hat{\alpha}_1}\Delta(\hat{\alpha}_1)_{RMS}\right)^2 + \left(\frac{\partial\hat{p}}{\partial\hat{\alpha}_2}\Delta(\hat{\alpha}_2)_{RMS}\right)^2 + \left(\frac{\partial\hat{p}}{\partial\hat{\alpha}_3}\Delta(\hat{\alpha}_3)_{RMS}\right)^2 + \left(\frac{\partial\hat{p}}{\partial\hat{\alpha}_4}\Delta(\hat{\alpha}_4)_{RMS}\right)^2 + \left(\frac{\partial\hat{p}}{\partial\Delta\hat{f}_1}\Delta(\Delta\hat{f}_1)_{RMS}\right)^2 + \left(\frac{\partial\hat{p}}{\partial\Delta\hat{f}_2}\Delta(\Delta\hat{f}_2)_{RMS}\right)^2\right\}^{1/2} \quad (3\text{-}21)$$

Equation (3-21) simplifies when $\Delta(\hat{\alpha}_i)_{RMS} = \Delta(\hat{\alpha})_{RMS}$ and $\Delta(\Delta\hat{f}_i)_{RMS} = \Delta(\Delta\hat{f})_{RMS}$ for all i:

$$\Delta(\hat{p})_{RMS} = \left\{\left[\left(\frac{\partial\hat{p}}{\partial\hat{\alpha}_1}\right)^2 + \left(\frac{\partial\hat{p}}{\partial\hat{\alpha}_1}\right)^2 + \left(\frac{\partial\hat{p}}{\partial\hat{\alpha}_3}\right)^2 + \left(\frac{\partial\hat{p}}{\partial\hat{\alpha}_4}\right)^2\right]\left[\Delta(\hat{\alpha})_{RMS}\right]^2 + \left[\left(\frac{\partial\hat{p}}{\partial\Delta\hat{f}_1}\right)^2 + \left(\frac{\partial\hat{p}}{\partial\Delta\hat{f}_2}\right)^2\right]\left[\Delta(\Delta\hat{f})_{RMS}\right]^2\right\}^{1/2}$$

*Pfeiffer, P. E., Concepts of Probability Theory, McGraw-Hill, N.Y., 1965, pp. 230-2.

3.3.1.1 (U) -- Continued.

The only remaining step is the evaluation of $\frac{\partial \hat{p}}{\partial \hat{\alpha}_i}$ and $\frac{\partial \hat{p}}{\partial \Delta \hat{f}_i}$. If the function $\hat{p}(\hat{\alpha}_1, \hat{\alpha}_2, \hat{\alpha}_3, \hat{\alpha}_4, \Delta \hat{f}_1, \Delta \hat{f}_2)$ were known explicitly, this calculation would be direct. However, the $\hat{p}$-function is only known implicitly and therefore the Implicit Function Theorem[2] must be invoked. By this theorem from calculus:

$$\frac{\partial \hat{p}}{\partial \hat{\alpha}_i} = \frac{-\frac{\partial H}{\partial \hat{\alpha}_i}}{\frac{\partial H}{\partial \hat{p}}}$$

and

$$\frac{\partial \hat{p}}{\partial \Delta \hat{f}_i} = \frac{-\frac{\partial H}{\partial \Delta \hat{f}_i}}{\frac{\partial H}{\partial \hat{p}}}$$

where the function $H(\hat{p}\,;\hat{\alpha}_1, \hat{\alpha}_2, \hat{\alpha}_3, \hat{\alpha}_4, \Delta \hat{f}_1, \Delta \hat{f}_2)$ is known explicitly:

$$H(p;\alpha_1, \alpha_2, \alpha_3, \alpha_4, \Delta f_1, \Delta f_2)$$

$$= p + \left[q_1 h_1 + \frac{(r_1 - h_1)(q_2 h_2 + (p)(D_2)(\sin \alpha_2)(\frac{1}{2\Delta t})(\alpha_1 + \alpha_2 - \alpha_3 - \alpha_4)}{h_2 - p - r_2} \right] \Bigg/$$

$$\left[\left((D_1)(\sin \alpha_1)(\frac{1}{2\Delta t})(\alpha_1 + \alpha_2 - \alpha_3 - \alpha_4) \right) \right.$$

$$\left. - \left(\frac{q_2 h_2 + (p)(D_2)(\sin \alpha_2)(\frac{1}{2\Delta t})(\alpha_1 + \alpha_2 - \alpha_3 - \alpha_4)}{h_2 - p - r_2} \right) \right]$$

where r_i, h_i, q_i are functions of α_1, α_2, Δf_1, Δf_2 and Δt is the time between measurements. Finally, the above equations can be evaluated for $\Delta(\hat{p})_{RMS}$:

[2] Protter, M. H. and Morrey, E. B., Modern Mathematical Analysis, Addison-Wesley, Reading, Mass., 1964, p. 492.

3.3.1.1 (U) -- Continued.

$$\Delta(\hat{P})_{RMS} = \left| \frac{1}{\frac{\partial H}{\partial \hat{P}}} \right| \left[\left[\left(\frac{\partial H}{\partial \hat{\alpha}_1} \right)^2 + \left(\frac{\partial H}{\partial \hat{\alpha}_2} \right)^2 + \left(\frac{\partial H}{\partial \hat{\alpha}_3} \right)^2 + \left(\frac{\partial H}{\partial \hat{\alpha}_4} \right)^2 \right] \cdot \right.$$

$$\left. \left| \Delta(\hat{\alpha})_{RMS} \right|^2 + \left[\left(\frac{\partial H}{\partial \Delta \hat{f}_1} \right)^2 + \left(\frac{\partial H}{\partial \Delta \hat{f}_2} \right)^2 \right] \left[\Delta(\Delta \hat{f})_{RMS} \right]^2 \right]^{1/2} . \quad (3\text{-}22)$$

In the next section, both the bias (P_{bias}) and the RMS error of range estimate for the double-baseline, single-measurement technique are evaluated for typical cases.

3.3.1.2 (U) Results of Error Analysis. (U)

In this section the bias and RMS error of the range estimate of the double-baseline, single-measurement technique are presented for several different system geometries (locations of radar transmitters and receiver and trajectory of target) and system parameters (operating frequency and time between measurements). It is shown that although the technique is not completely satisfactory under all circumstances, it is fairly successful for certain geometries and parameters.

All numerical calculations for the error analyses were performed on an IBM 360 general purpose digital computer. For any given case, P_{bias} (the range bias caused by using an approximation for $\hat{\alpha}$) was found by solving for $\hat{P}$ and subtracting the actual range P. $\Delta(\hat{P})_{RMS}$, the RMS error of the range estimate, was calculated using equation (3-22); the partial derivatives of

$$H\left(\frac{\partial H}{\partial \hat{P}} , \frac{\partial H}{\partial \alpha_i} , \frac{\partial H}{\partial \Delta \hat{f}_i} \right)$$

were determined by use of standard numerical differentiation algorithms*.

*Southworth, R. W. and Deleeuw, S. L., Digital Computation and Numerical Methods, McGraw-Hill, N.Y., 1965, pp. 352-363.

3.3.1.2 (U) -- Continued.

The computed range estimation errors for the double baseline, single measurement technique are displayed in Figures 3-16. The labeled dots indicate the location of the transmitters (T_1 and T_2) and the shipboard receiver (S). The various trajectories of the target are represented by dashed lines. The errors are represented by solid-line segments at various points along the trajectory. The lengths of these segments are scaled to twice the RMS error, while the offset of the center of the segment from the trajectory represents P_{bias}.

The various system parameters, such as operating frequency of the radar (f), time between measurements (Δt), and standard deviations or RMS errors of the measurements ($\sigma_\alpha, \sigma_{\Delta f}$) are listed on the figures, along with the scale of the drawing and the velocity of the target. Δt is not necessarily equal to the spacing of the displayed error segments.

For all the figures of displayed errors, the measurement uncertainties, $\Delta(\alpha)_{RMS}$ and $\Delta(\Delta f)_{RMS}$ were assumed to be 1 degree and .1 Hz, respectively. If these measurements errors in a particular case are larger, then the RMS error in the range estimate would be proportionately greater.

Several conclusions can be drawn from the figures. First, a particular configuration of transmitters and shipboard receiver may be fairly effective against certain target trajectories while much less successful against other trajectories. Also, performance may be acceptable at certain points in a given trajectory but not at others.

An interesting observation can be made from Figures 3-16. The geometries and parameters for the two configurations in Figures 3-16e and f are the same as for those in Figures 3-16g and h, respectively, except that Δt, the time between measurements, is 20 seconds for the former and 120 seconds for the latter. The interval Δt enters into the estimation of range in only one place: the estimation of $\dot{\alpha}$ from the formula

$$\dot{\alpha} \doteq \frac{1}{2\Delta t}(\alpha_1 + \alpha_2 - \alpha_3 - \alpha_4).$$

As Δt is increased, the RMS errors of the α_i are divided by a larger constant and thus the RMS range error should be less. On the other hand, for larger Δt, the first order approximation becomes weaker for those trajectories were $\dot{\alpha}$ is not constant, implying an increased P_{bias} for those cases.

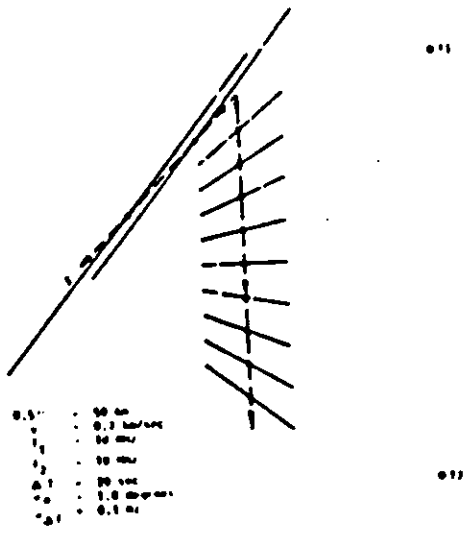

Figure 3-16a (U). Range Estimation Errors for Double Baseline, Single Measurement Technique--Geometry No. 1 (U)

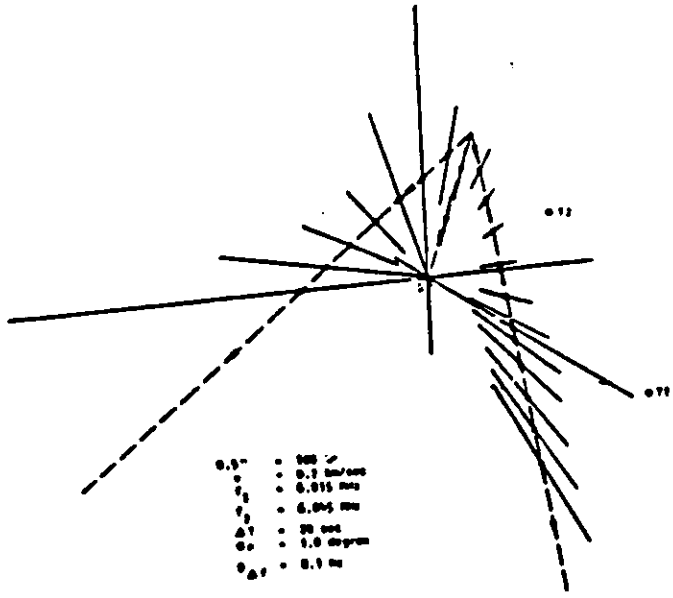

Figure 3-16b (U). Range Estimation Errors for Double Baseline, Single Measurement Technique--Geometry No. 2 (U)

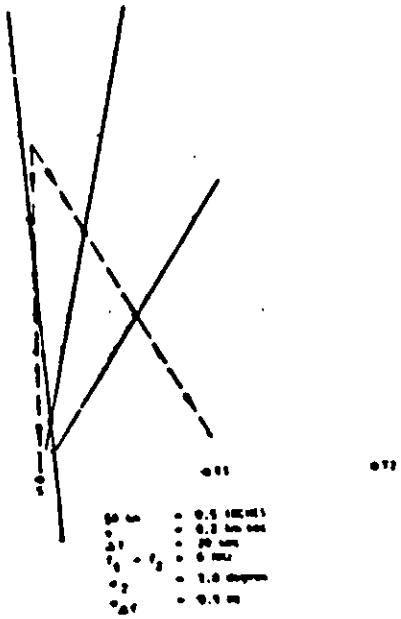

Figure 3-16c (U). Range Estimation Errors for Double Baseline, Single Measurement Technique--Geometry No. 3 (U)

Figure 3-16d (U). Range Estimation Errors for Double Baseline, Single Measurement Technique--Geometry No. 4 (U)

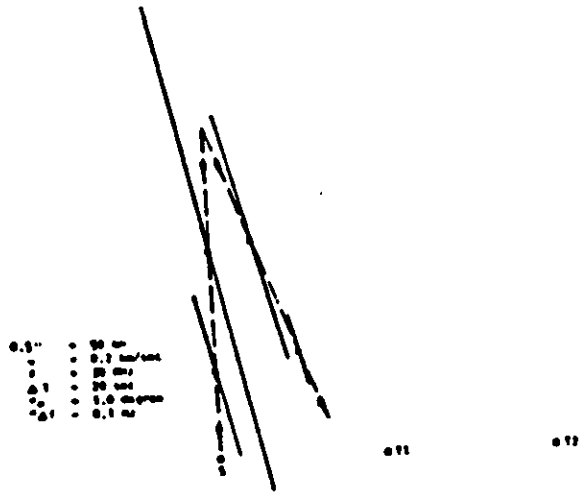

Figure 3-16e (U). Range Estimation Errors for Double Baseline, Single Measurement Technique--Geometry No. 5 (U)

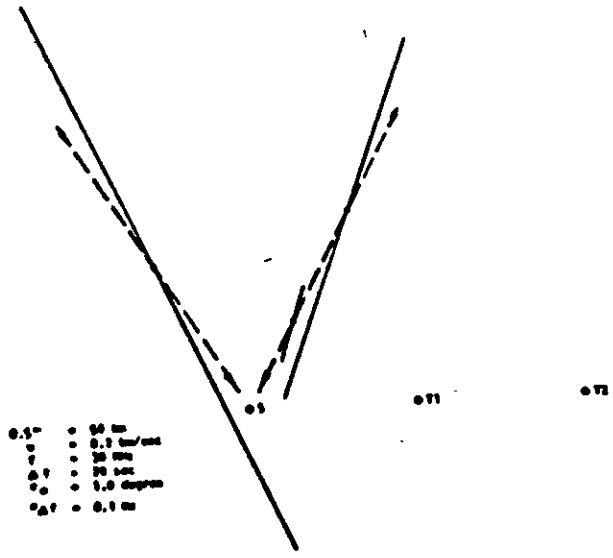

Figure 3-16f (U). Range Estimation Errors for Double Baseline, Single Measurement Technique--Geometry No. 6 (U)

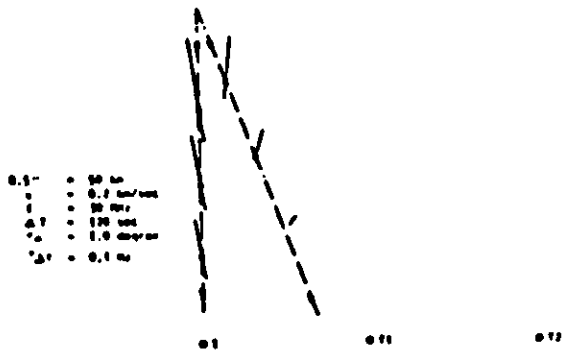

Figure 3-16g (U). Range Estimation Errors for Double Baseline, Single Measurement Technique--Geometry No. 7 (U)

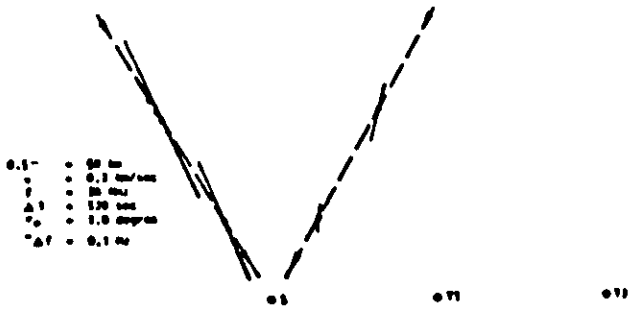

Figure 3-16h (U). Range Estimation Errors for Double Baseline, Single Measurement Technique--Geometry No. 8 (U)

3.3.1.2 (U) -- Continued.

Both these effects are observed in Figures 3-16. The RMS errors in Figures 3-16g and h (Δt = 120 sec.) are generally much less than in Figures 3-16 e and f (Δt = 20 sec.). Yet, also as predicted, in the one trajectory in each pair of figures where the target is not heading at the ship and hence $\dot{\alpha}$ is not constant, there is a significant range bias for Δt = 120 sec., but not for Δt = 20 sec. However, the total range estimate error is still much smaller for Δt = 120 sec.; for several target trajectories, range estimate errors of less than 15 percent are achieved.

3.3.2 (U) Error Analysis of Single-Baseline, Double-Measurement Range Estimator. (U)

The accuracy of the Single-Baseline, Double-Measurement range estimating technique (Section 3.2.3) is also a function of the accuracies of the measurements of target bearing and Doppler frequency. Expressions relating RMS measurement errors to RMS ranging errors are derived and evaluated for several target trajectories. The biases in the estimate are also computed, and it is shown that for several trajectories, the total range estimate errors are less than 15 percent.

3.3.2.1 (U) Derivation of Error Expressions. (U)

As shown in Section 3.2.3, the true range can be estimated by the solution of the set of equations (3-12 and 3-13).

The following approximations are also used to evaluate the RMS range error for this range estimation technique:

$$\hat{\alpha}' = \hat{\alpha} + \dot{\alpha}\Delta t \tag{3-23}$$

and

$$\hat{p}' = \hat{p} + \dot{p}\Delta t \quad . \tag{3-24}$$

Equation (3-12) is used to find an expression for $\dot{p}$ which is then inserted into (3-13) to yield:

$$F(\hat{p}'; \alpha', \alpha, \Delta f', \Delta f) = 0 \tag{3-25}$$

a single equation for $\hat{p}'$ which depends on the present and past measured values of target bearing and Doppler frequency.

3.3.2.1 (U) -- Continued.

The estimate $\hat{p}'$ has, in general, both a bias error and RMS error. The bias arises from the fact that for linear trajectories, $\hat{\alpha}'$ and $\hat{p}'$ are exactly true only when that trajectory is radial with respect to the shipboard receiver. Thus, in most cases, even if the exact values α', α, $\Delta f'$, Δf are known, the solution $\hat{p}'$ will be in error by a p_{bias}. Thus:

$$p'_{bias} = \hat{p}' - p' \ .$$

An expression for RMS range estimation error in terms of the RMS errors in target bearing and Doppler shift measurements can be obtained by noting the similarity of equations for the double-baseline, single measurement technique and (3-25). Thus, analogous to (3-22), it follows directly that

$$\Delta(\hat{p}')_{RMS} = \left\{\left(\frac{1}{\left|\frac{\partial F}{\partial \hat{p}'}\right|}\right)\left[\left(\frac{\partial F}{\Delta \hat{\alpha}'}\right)^2 + \left(\frac{\partial F}{\partial \hat{\alpha}}\right)^2\right]\left[\left(\Delta(\hat{\alpha})_{RMS}\right)^2\right]\right.$$
$$\left. + \left[\left(\frac{\partial F}{\partial \hat{\Delta} f'}\right)^2 + \left(\frac{\partial F}{\partial \hat{\Delta} f}\right)^2\right]\left[\left(\Delta(\hat{\Delta} f)_{RMS}\right)^2\right]\right\}^{1/2} \ .$$

The next section presents the results of evaluating the bias and RMS errors of range estimate for the single-baseline, double-measurement technique.

3.3.2.2 (U) Results of Error Analysis. (U)

The expected errors are presented for two typical cases using the single-baseline, double-measurement range estimator. From Figures 3-17 and 3-18 it can be seen that for two target trajectories (one for each case), the range estimation errors are less than 15 percent. The detection system parameters are the same in all cases. As in the previous section the trajectories are shown by dashed lines and the errors by solid line segments; the length of a segment equals twice the RMS range error, while the displacement of the segment center from the trajectory represents the range estimation bias.

Several observations can be made from the figures. First, of all the trajectories shown, only one shows any bias; this is the trajectory on Figure 3-17 that is not aimed at the ship. This result was predicted in

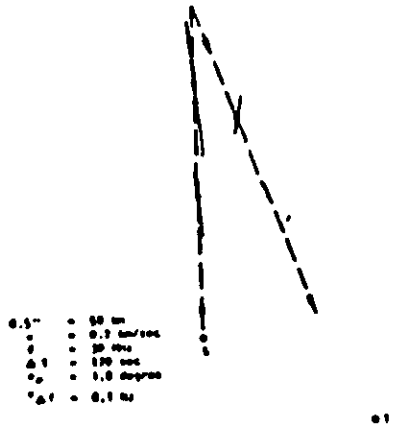

Figure 3-17 (U). Range Estimation Errors for Single Baseline, Double Measurement Technique. (U)

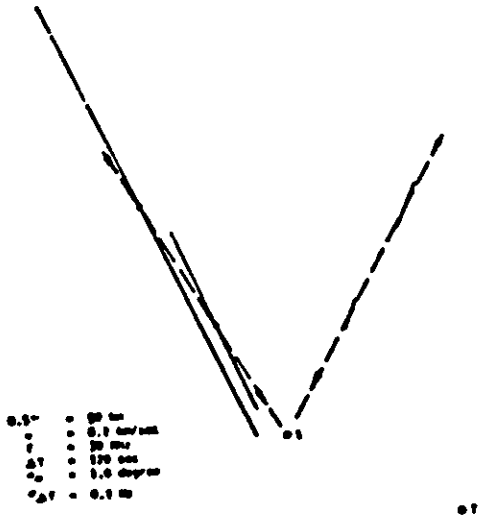

Figure 3-18 (U). Range Estimation Errors for Single Baseline, Double Measurement Technique. (U)

3.3.2.2 (U) -- Continued.

the last section, because bias errors are caused by the variation of $\dot{a}$ and $\dot{p}$ between measurements. These variations occur only for off-ship trajectories. As shown in Figure 3-17, the bias is about the same magnitude as the RMS error. The bias could be reduced by decreasing the time interval between observations, but at the expense of greater RMS errors. Another observation from the figures is that the estimator's performance depends on the location of the target with respect to the transmitter and shipboard receiver. For example, Figure 3-18 shows a trajectory in which the ship is between the target and transmitter and the target is headed directly at the ship. For this trajectory the range errors are greater than 80 percent. In contrast the two trajectories of Figures 3-17 and 3-18, in which the target is on a fly by trajectory or headed toward the ship in a different geometry resulted in errors of less than 15 percent.

3.3.3 (U) Error Analysis of the Doppler Location Finder. (U)

The range and location estimates given by the Doppler Location Finder (DLF) depend on the measured values of Doppler frequency. An expression is derived below relating measurement uncertainties to estimation errors. Results are presented that demonstrate for a wide class of system geometries range errors of less than 15 percent and bearing errors of less than 6° can be achieved. In addition, for one particular system geometry the range errors are shown to be less than 5 percent.

3.3.3.1 (U) Derivation of Error Expressions. (U)

As described in Section 3.2.4 target location and time derivative variables, p, α, $\dot{p}$, and $\dot{\alpha}$, are the solution of:

$$\Delta f_i = h(p, \alpha, \dot{p}, \dot{\alpha}; D_i, \beta_i, \lambda_i) \qquad i = 1, 2, 3, 4.$$

Because Δf_i will always be measured with some error, it is denoted as $\Delta \hat{f}_i$; the estimates of p, α, $\dot{p}$, and $\dot{\alpha}$ are similarly denoted by $\hat{p}$, $\hat{\alpha}$, $\hat{\dot{p}}$, and $\hat{\dot{\alpha}}$ so that

$$\Delta \hat{f}_i = h(\hat{p}, \hat{\alpha}, \hat{\dot{p}}, \hat{\dot{\alpha}}; D_i, \beta_i, \lambda_i) \qquad i = 1, 2, 3, 4.$$

As done in the previous sections define

3.3.3.1 (U) -- Continued.

$$\Delta(\Delta\hat{f}_i) = \left(\frac{\partial h}{\partial \hat{p}}\right)_i \Delta\hat{p} + \left(\frac{\partial h}{\partial \hat{\alpha}}\right)_i \Delta\hat{\alpha} + \left(\frac{\partial h}{\partial \dot{\hat{p}}}\right)_i \Delta\dot{\hat{p}} + \left(\frac{\partial h}{\partial \dot{\hat{\alpha}}}\right)_i \Delta\dot{\hat{\alpha}} .$$

Letting the vectors $\underset{\sim}{m}$ and $\underset{\sim}{v}$ be defined as

$$\underset{\sim}{m} = \begin{pmatrix} \Delta f_1 \\ \Delta f_2 \\ \Delta f_3 \\ \Delta f_4 \end{pmatrix} , \qquad \underset{\sim}{v} = \begin{pmatrix} \Delta\hat{p} \\ \Delta\hat{\alpha} \\ \Delta\dot{\hat{p}} \\ \Delta\dot{\hat{\alpha}} \end{pmatrix}$$

and the matrix A defined as

$$A = \begin{Bmatrix} \left(\frac{\partial h}{\partial \hat{p}}\right)_1 & \left(\frac{\partial h}{\partial \hat{\alpha}}\right)_1 & \left(\frac{\partial h}{\partial \dot{\hat{p}}}\right)_1 & \left(\frac{\partial h}{\partial \dot{\hat{\alpha}}}\right)_1 \\ \left(\frac{\partial h}{\partial \hat{p}}\right)_2 & \left(\frac{\partial h}{\partial \hat{\alpha}}\right)_2 & \left(\frac{\partial h}{\partial \dot{\hat{p}}}\right)_2 & \left(\frac{\partial h}{\partial \dot{\hat{\alpha}}}\right)_2 \\ \left(\frac{\partial h}{\partial \hat{p}}\right)_3 & \left(\frac{\partial h}{\partial \hat{\alpha}}\right)_3 & \left(\frac{\partial h}{\partial \dot{\hat{p}}}\right)_3 & \left(\frac{\partial h}{\partial \dot{\hat{\alpha}}}\right)_3 \\ \left(\frac{\partial h}{\partial \hat{p}}\right)_4 & \left(\frac{\partial h}{\partial \hat{\alpha}}\right)_4 & \left(\frac{\partial h}{\partial \dot{\hat{p}}}\right)_4 & \left(\frac{\partial h}{\partial \dot{\hat{\alpha}}}\right)_4 \end{Bmatrix}$$

then $\underset{\sim}{m} = A\,\underset{\sim}{v}$; assuming A is invertible, $\underset{\sim}{v} = A^{-1}\,\underset{\sim}{m}$.

Evaluating just the first two components of $\underset{\sim}{v}$ and expressing them in RMS form yields

$$(\Delta\hat{p})_{RMS} = \left(\sum_{i=1}^{4} \left(A^{-1}\right)_{1,i}^2 \cdot \left(\Delta(\Delta\hat{f}_i)\right)^2_{RMS} \right)^{1/2} .$$

$$(\Delta\hat{\alpha})_{RMS} = \left(\sum_{i=1}^{4} \left(A^{-1}\right)_{2,i}^2 \cdot \left(\Delta(\Delta f_i)\right)^2_{RMS} \right)^{1/2} .$$

3.3.3.1 (U) -- Continued.

Assuming $(\Delta(\hat{\Delta f}_i))_{RMS}$ is the same for all i,

$$(\Delta\hat{p})_{RMS} = (\Delta(\Delta\hat{f}))_{RMS} \cdot \left(\sum_{i=1}^{4} \left[\left((A^{-1})_{1,i} \right)^2 \right] \right)^{1/2}$$

$$(\Delta\hat{\alpha})_{RMS} = (\Delta(\Delta\hat{f}))_{RMS} \cdot \left(\sum_{i=1}^{4} \left[\left((A^{-1})_{2,i} \right)^2 \right] \right)^{1/2} .$$

These last two equations relate the RMS errors in Doppler frequency measurement to the RMS errors in target range and bearing estimation. The other type of estimation error is a possible bias. For the Doppler Location Finder there are no biases since the equations are exact and use measurements from only one time point. Thus, the RMS error describes the total range and estimation errors of the DLF techniques.

3.3.3.2 (U) Results of Error Analysis. (U)

The expressions for range and bearing uncertainties derived in Section 3.3.3.1 for the Doppler Location Finder were evaluated for a number of configurations. It is shown that with reasonable Doppler measurement errors (i.e., 0.1 Hz) the range error is less than 15 percent and the bearing error is less than 6° in many cases. The error results are presented in Figures 3-19 to 3-28. As with the error analyses for the other techniques, the target trajectories are represented by dashed lines, the transmitters and shipboard receivers are represented by labeled dots, and the assumed system parameters for each case are included. The Doppler measurement RMS error for all cases is assumed to be 0.1 Hz; no value is given for time between measurements because the DLF is an "instantaneous" estimator. For this location estimation technique the errors in both range and azimuth are presented. The RMS range errors are represented by line segments scaled to twice the RMS range error along a radial line from the target to the receiver. The RMS bearing errors are similarly scaled with a line segment perpendicular to the radial line. Note that no biases are shown. The one major observation that can be made is the good performance of the DLF for a variety of receiver-transmitter configurations and against a number of target trajectories. In most cases the range errors were less than 15 percent and the bearing errors less than 6°. Of particular interest is the system geometry shown in Figure 3-28 for which the range errors

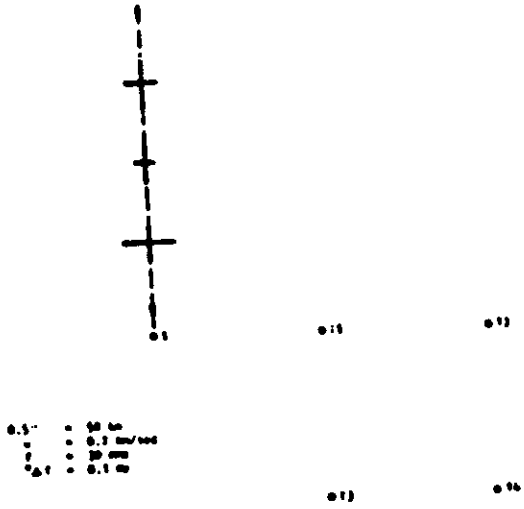

Figure 3-19 (U). Location Error for Doppler Location Finder--Geometry No. 1 (U)

Figure 3-20 (U). Location Error for Doppler Location Finder--Geometry No. 2 (U)

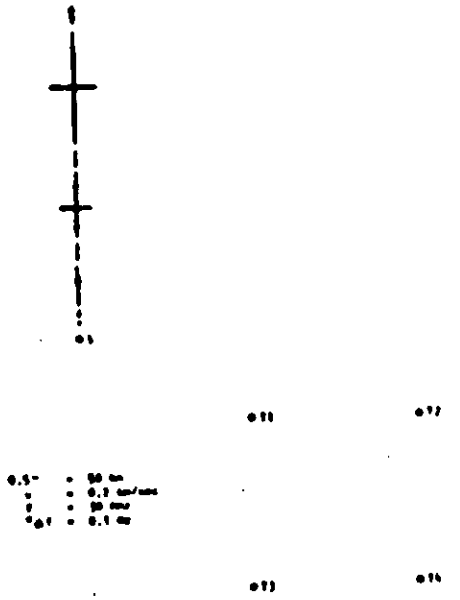

Figure 3-21 (U). Location Error for Doppler Location Finder--Geometry No. 3 (U)

Figure 3-22 (U). Location Error for Doppler Location Finder--Geometry No. 4 (U)

Figure 3-23 (U) Location Error for Doppler Location Finder-- Geometry No. 5 (U)

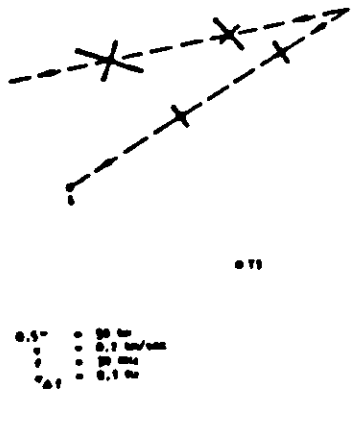

Figure 3-24 (U). Location Error for Doppler Location Finder-- Geometry No. 6 (U)

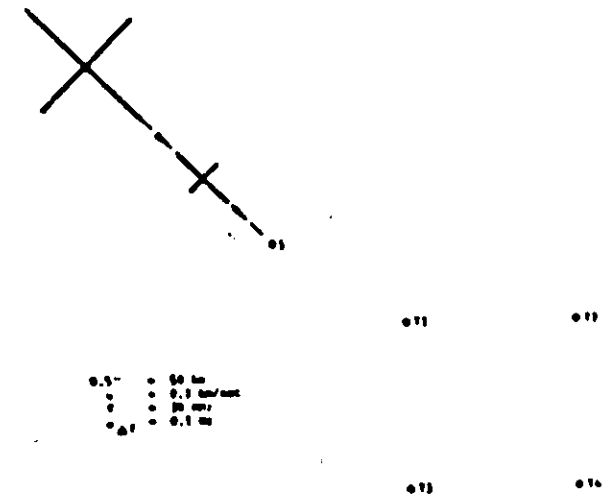

Figure 3-25 (U). Location Error for Doppler Location Finder--Geometry No. 7 (U)

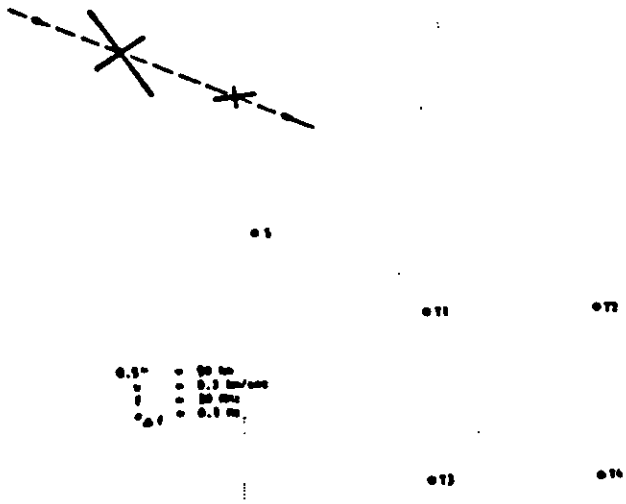

Figure 3-26 (U). Location Error for Doppler Location Finder--Geometry No. 8 (U)

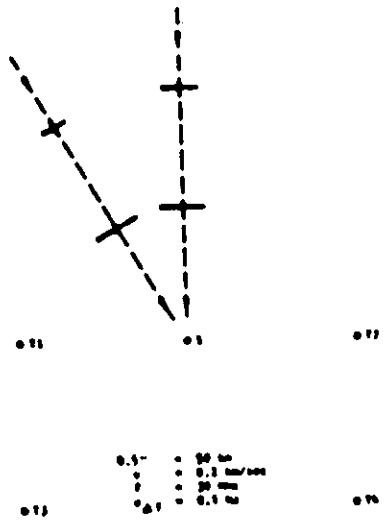

Figure 3-27 (U). Location Error for Doppler Location Finder-- Geometry No. 9 (U)

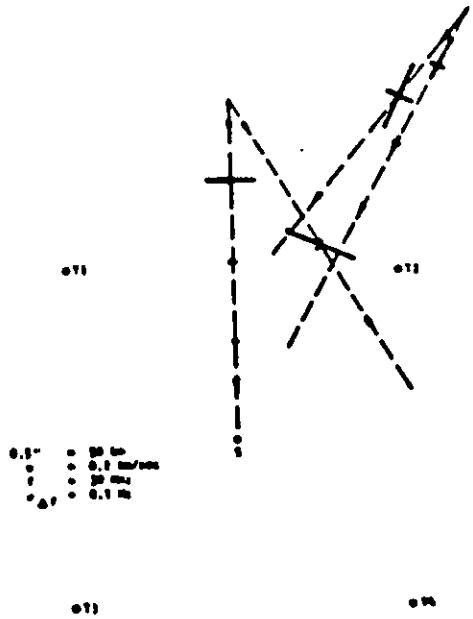

Figure 3-28 (U). Location Error for Doppler Location Finder--Geometry No. 10 (U)

3.3.3.2 (U) -- Continued.

are less than 5 percent. This configuration can represent the use of transmitters on picket ships to protect a fleet aircraft carrier.

3.3.4 (U) Other Possible Sources of Error. (U)

The previous sections have discussed the RMS errors caused by measurement uncertainties and the bias errors due to equation approximations for the various estimation techniques. In this section several other possible sources of error are discussed; it is shown that errors from these sources are not significant compared to those described previously.

One of these sources of error is due to the period over which the bearings in the double and single baseline techniques are measured in practice. These are taken over a time duration of about ten seconds. The average value calculated is assigned as the bearing at the middle of the interval; in reality, due to non-linearities, the actual bearing at that middle time-point may be different. Yet, in all cases considered in this study, this bearing error was less than 0.1°, significantly smaller than the one degree uncertainty that was assumed for bearing measurements.

A second source of error comes from the use of a two-dimensional model for system geometries. In practice, targets may fly at higher altitudes above the ocean surface although the principal threats are expected to employ low altitudes to avoid line-of-sight radar detection. For these situations the actual Dopplers and bearing angles will not be the same as those used in a planar model. In most cases, however, the differences are masked by the measurement uncertainty. For example, a target 10 km high and 100 km from the ship is at a 6° elevation angle. According to the Doppler equation, the actual Doppler would be cos 6° times the Doppler if the target were indeed flying in the plane of the transmitter and receiver. Because cos 6° is greater than 0.99, the Doppler would be in error by less than 1 percent, which is about the accuracy of Doppler measurement. In a similar manner the slant range would differ from the planar range by less than 1 percent.

Another source of error is the determination of distance between the i^{th} transmitter and the ship (D_i). The accuracy of this measurement depends on the accuracy of the shipborne navigation system. Because the typical accuracies for the LORAN C and D systems are less than 1 km and this represents less than 1 percent at a target range of 100 km (compared to approximately 15 percent range accuracy for the location estimation techniques), the associated errors can be neglected.

3.3.4 (U) -- Continued.

The measurement of transmitter frequencies (f_i) can also give rise to errors in the estimation techniques. However, with an RMS measurement accuracy of 0.1 Hz, the errors are less than one part in 10^7 in the HF band and is dominated by the limitations in computational accuracy.

Thus, the errors that arise from these other sources can be neglected compared to those examined in the previous sections.

3.3.5 (U) Conclusions of Error Analysis. (U)

The principal conclusion to be drawn from the error analysis is that all three techniques analyzed, the double-baseline, single-measurement technique, the single-baseline, double-measurement estimator, and the Doppler Location Finder, performs to within 15 percent range error for classes of target trajectories. The DLF, in particular, performs well over a wide range of trajectories and attains 5 percent accuracy for one of the geometries examined. In addition, it estimates bearing to an accuracy of 6°.

For all the estimation methods, however, expected errors strongly depend on both system geometry and system parameters. Because the three techniques perform reasonably well under different specific conditions, it appears that a hybrid location technique that employs the basic methods contained in the three techniques investigated can be developed that will perform satisfactorily (better than 15 percent accuracy) over a wider range of fleet operating geometries. This hybrid technique may rely on the DLF method as a basis, but include measurements of target bearing. Alternately, the hybrid technique may employ all three methods for estimating target range, but incorporate tests to discard estimates having large RMS values. Those estimates within an acceptable accuracy may then be weighted to provide the "hybrid" estimate of target range. Based on the potential of deriving a practical target location estimator for a wide range of transmitter, fleet, and target geometries it is recommended that a hybrid target location technique be investigated.

[redacted]

Section 4

EXPERIMENTAL TESTING OF FAD POLYSTATIC TECHNIQUES

[redacted] (U) In the previous sections the investigation of a polystatic radar technique that can be employed for FAD was presented. This investigation included an examination of detection regions, target location methods and a detailed error analysis. Because the results have been derived analytically there is a need to verify them experimentally and to demonstrate that a FAD early warning system using transmitters of opportunity is feasible. Experimental tests are therefore recommended for the FAD polystatic techniques.

[redacted] (U) This section describes the experimental design considerations and a system designed particularly for these tests. The specific objectives of the experiments are first discussed. Then the factors that impact on the test design and the system design are described. Based on a tradeoff analysis of these factors a specific set of experiments and hardware are recommended.

4.1 (U) [redacted] OBJECTIVES. (U)

The objectives of the FAD polystatic techniques experiments are to:

a. demonstrate the detection range of the polystatic technique, and

b. verify the predicted accuracies of the target location estimation methods.

The first objective is to show that the target detection ranges derived analytically using surface wave attenuation values and nominal radar cross sections agree with experimental values. This objective has been met partially when experiments were conducted for the early warning portion of the Aquarius study. (In these experiments a P3B aircraft was detected with a bistatic radar system using propagation modes comparable to those expected for FAD.) Also, target detection is necessary before the other experimental objectives can be met. Therefore, tests to satisfy this objective can be included with those to meet the other objectives.

The second objective is to verify that the target location accuracies of the estimation techniques agree with the analytic results. The majority of the experiments will be devoted to satisfying this objective because it includes

[redacted]

4.1 (U) [redacted] -- Continued.

the most tenuous area and contains numerous random variables (e.g., transmitter-target-receiver geometry, measurement accuracies, etc.)

4.2 (U) EXPERIMENTAL CONSIDERATIONS. (U)

In the design of experiments care must be taken to include all those system parameters that are crucial to the satisfaction of the test objectives. In addition, the experiments should be structured for performance at a nominal cost utilizing existing equipment and systems where possible. In the experimental design there are a number of factors that need to be considered. A list of the primary ones are included in Table 4-1. The majority of the factors (e.g., transmitters, targets, receivers) deal with the equipment/systems needed for the experiment. The use of existing equipment for the tests reduces the cost of the experiment. For some test elements (e.g., simulated targets, shipborne antenna arrays) it is not economically feasible to build or buy the system solely for the experiment and hence the time and location of the experiment is restricted to the availability of these systems.

4.2.1 (U) [redacted] Transmitter Sources. (U)

To conduct the tests, sources of opportunity (i.e., broadcast transmitters) or cooperative transmitters (e.g., Carter Cay transmitters) can be employed. A partial list of candidate transmitters for the experiment are included in Table 4-2. A substantial number of HF sources are available with established transmitter powers and operational schedules. Lists of these sources can be found in the World Radio and TV Handbook.

Experimental HF transmitters and other radars may be employed to track the target during the tests and for calibration purposes, and ionospheric soundings and propagation measurements are desirable during the test to verify the use of 1F propagation modes.

4.2.2 (U) [redacted] Targets. (U)

For Fleet Air Defense the primary targets are enemy aircraft and missiles. The P3B aircraft has a radar cross section which is typical for enemy aircraft. Air-to-surface and surface-to-surface missiles generally have a smaller cross section and should be tested separately. Table 4-3 summarizes the estimates of operating characteristics for some of the Soviet aircraft and missiles that are threats to the U.S. Fleet.

TABLE 4-1. (U) EXPERIMENTAL FACTORS. (U)

1. Transmitter Sources
   - a. Location
   - b. Operating Frequency
   - c. Schedule of Operation
   - d. Effective Radiated Power

2. Simulated Targets
   - a. Type and Size
   - b. Availability
   - c. Number

3. Receiving System
   - a. Platform: Shipborne/Landbased
   - b. Antenna Arrays
   - c. Receivers
   - d. Processing and Data Storage Equipment
   - e. Test Equipment

4. Test Location/Conditions
   - a. Sources Availability
   - b. Target(s) Availability
   - c. Receiver Ability
   - d. Similarity to Operational Environment
   - e. False Alarm/Noise Levels

[redacted] (U)

TABLE 4-2. CANDIDATE SOURCES FOR FAD POLYSTATIC EXPERIMENT. (U)

1. Atlantic Coast

   a. Broadcast Transmitters

      CBC - Sackville, New Brunswick
      WNYW - New York, New York
      VOA - Greenville, North Carolina

   b. Experimental HF Transmitters

      MADRE Radar - Virginia
      Carter Cay - Bahamas

2. Pacific Coast

   a. Broadcast Transmitters

      VOA - Dixon, California
      VOA - Delano, California
      KGEI - Belmont, California

   b. Experimental HF Transmitters

      Stanford University - Palo Alto, California

[redacted]

TABLE 4-3. TYPICAL AIRCRAFT AND MISSILE THREATS. (U)

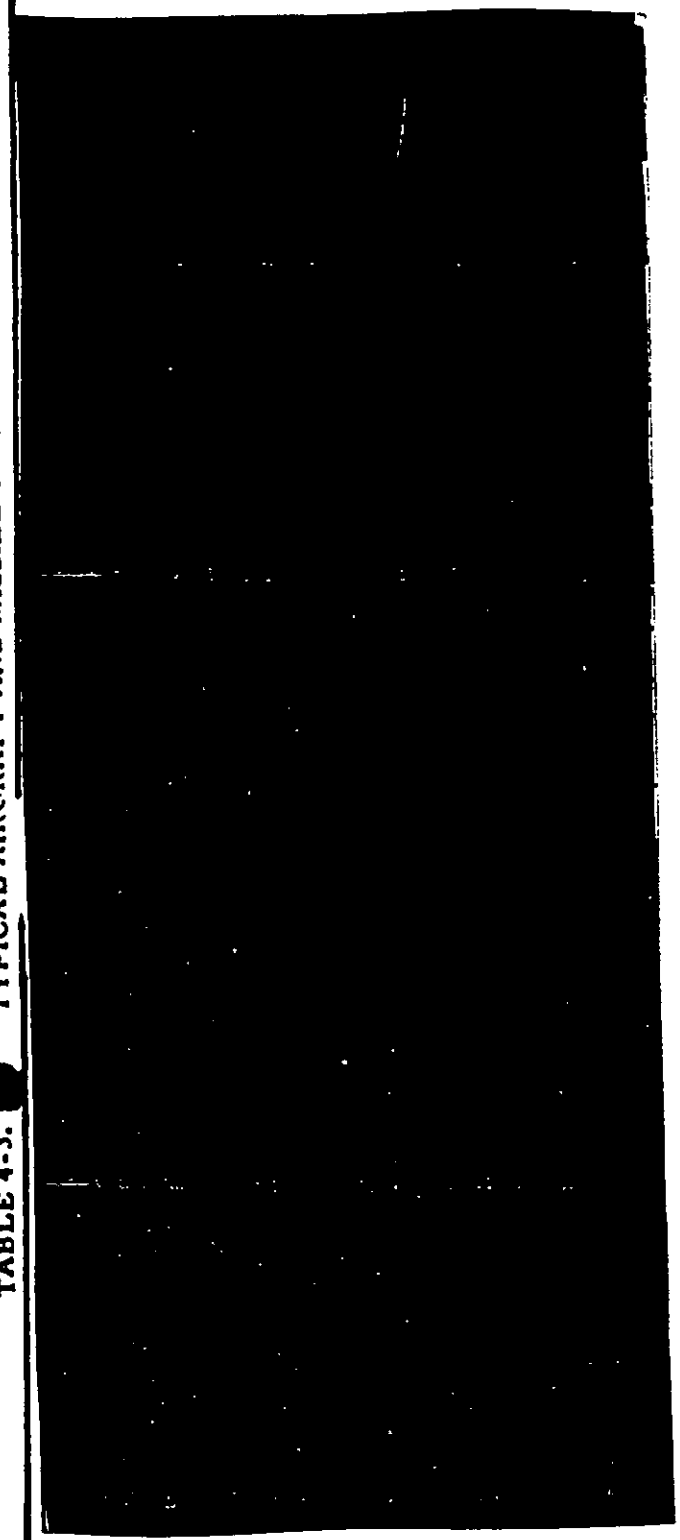

4.2.2 [redacted] (U) -- Continued.

In the experiments the aircraft and missiles need to be evaluated for a variety of operational profiles, including a number of scattering geometries and target altitudes. Soviet air-to-surface missiles, for example, are known to be capable of being launched at a range of altitudes but follow a low altitude profile for minimum detection. The typical aircraft approach is to fly close to the ocean surface to avoid line-of-sight radar detection. The targets used in the experiment should consist of two sizes (aircraft and missile) and be operated at velocities comparable to those of the expected threats. Turns and other aircraft maneuvers should be tested. Should the tests be constrained to a threat target, then the use of a P3 aircraft flying at 300 feet above the ocean surface for a variety of transmitters-target-receiver geometries is recommended. Should a number of test aircraft and missiles be available, single and multiple aircraft/missile signatures should be obtained for multiple signature and location evaluation.

Besides the intended targets, there may be commercial and military aircraft that are operating in the vicinity of the transmitters and receiver sites during tests. These aircraft will provide false alarms during the experiments. Schedules of such flights need to be obtained where possible for the evaluation of the experimentally collected data.

4.2.3 (U) Receiving Site. (U)

In the FAD polystatic radar system concept the receiving system is located on one or more of the ships of the fleet being protected. However, for experimental testing the receiving system can be located on a ship or at a landbased site. The use of a shipborne platform necessitates a ship having an accurate HF direction finding antenna system. It also would entail the assignment of a ship for the calibration and collection of experimental data and possibly the processing of ship navigational data to evaluate location estimation accuracies. In contrast, the use of a landbased receiving site simplifies the conduct of the experiments because the normal operational problems are circumvented and attention can be focused on the key facets of the FAD polystatic experiment. The destroyer DD714 (USS Gilbert Roan) contains an HF DF array and appears suitable as shipborne receiving platform. The potential landbased sites include the following:

a. Vint Hill Farm Station
b. Madre
c. White House

} East Coast

d. Eastern Test Range

[redacted]

UNCLASSIFIED

4.2.3 (U) -- Continued.

e. Stanford Antenna Array
f. Los Banos Antenna Array
} West Coast

Of the two types of sites the landbased site is recommended because of operational simplicity in conducting the tests. For this alternative there is greater access to test equipment and the scheduling of data collection is not as severe as for shipborne operation. In addition, the collection and processing of ship navigational data is not required for experiments using a landbased site.

4.2.4 (U) Test Location/Conditions/Evaluation. (U)

The specific test location, conditions and evaluation depend on a combination of the factors described above. The availability of sources, targets, and receiving sites dictate the feasibility and cost of conducting tests on the Atlantic and Pacific coasts. When all three factors are considered, the principle test locations for consideration are the Pacific coast, Northern Atlantic area, and Southern Atlantic region. Of these regions the one that appears most suitable is the southern Atlantic region.

4.2.4.1 [redacted] (U) Test Location. (U)

The southern Atlantic region is recommended for the FAD polystatic tests for a number of reasons. First there are a number of broadcast stations available. Second, forward-scatter geometry that is most representative for FAD can be achieved by using transmitters from Costa Rica, San Jose, Cuba, Paraguay and a receiving site at Vint Hill Farms Station, the Madre radar site, the White House site and/or the Eastern Test Range site. This allows a landbased site to be employed instead of a ship for the receiving system. The test region contains a sufficient amount of non-hostile aircraft so that false alarm signatures can be examined in conjunction with target signatures. In addition, most of the necessary receiving equipment is available and demonstrations can readily be made to Government personnel from the Washington, D.C. area. These reasons, plus others such as the availability of HF calibration equipment (e.g., ionospheric sounders), make the southern Atlantic region preferable to the others.

4.2.4.2 [redacted] (U) Test Conditions. (U)

Once the test location is selected the test conditions that need to be delineated include primarily the transmitter frequencies to be used, target test trajectories, the equipment to be utilized, and the data to be collected.

[redacted]

UNCLASSIFIED

4.2.4.2 [redacted] (U) -- Continued.

As mentioned previously, the targets must include both aircraft and missiles. The aircraft should be flown at various ranges, azimuths, and altitudes from the receiving site. Various aircraft maneuvers such as turns and dives should be included. A head-on approach to the receiver site as well as a fly-by-trajectory should be conducted. The time and location for each aircraft maneuver should be noted for correlation and with the collected experimental data. Missiles comparable to the Soviet AS-2 through AS-5 series should be fired, if possible, to obtain missile signatures at various ranges, altitudes and operating conditions. At least three signatures of missile trajectories should be obtained at different frequencies for the extrapolation of experimental data from aircraft targets and to demonstrate the system's ability to differentiate between aircraft and missile signatures. Table 4-4 summarizes the recommended transmitter source and target test parameters.

The receiving equipment system required to perform the experiment include an antenna system, receivers, a data processor, and associated peripheral equipment. If one of the landbased sites (e.g., Vint Hill Farms Station) is employed, then most of the antenna system equipment necessary for the experiments exist. Only the commitment of the equipment for the tests is required by the responsible agency to conduct the experiments.

The experimental data that needs to be collected include signal and noise measurements, Doppler signatures, and the DF information associated with the signatures for aircraft and missiles under various conditions. This data can be processed to:

a. demonstrate the detection range of the polystatic technique, and

b. verify the accuracies of the target location estimation method.

4.3 [redacted] (U) SYSTEM DESIGN. (U)

In order to demonstrate the FAD target detection range capability and the accuracy of the location techniques described in previous sections of this report, a system as shown in the functional block diagram in Figure 4-1 may be used. By using both cooperative and noncooperative HF CW transmitters, this receiving system will be able to determine target Doppler and azimuth for test targets at beyond line-of-sight distances. This system would be capable of being operated in any of the three following modes:

[redacted]

UNCLASSIFIED

TABLE 4-4. (U) TEST PARAMETERS FOR EXPERIMENT. (U)

Transmitters:	Cooperative HF, and Noncooperative HF Broadcast
Target Types:	Aircraft, Missiles
Transmitter-Target Ranges:	50, 100, 200 N.M.
Target-Receiver Ranges:	50, 100, 200 N.M.
Aircraft Altitudes:	200, 500, 1000 feet above ocean level
Approaches:	Head-on, Flyby
Maneuvers:	Turn, Climb, Dive
Target Velocities:	250-400 ft/sec. (Aircraft)
	700-7,000 ft/sec. (Missile)*

* At least three missile signatures at 100 NM range, 200 ft altitude with a head-on approach.

[redacted]

UNCLASSIFIED

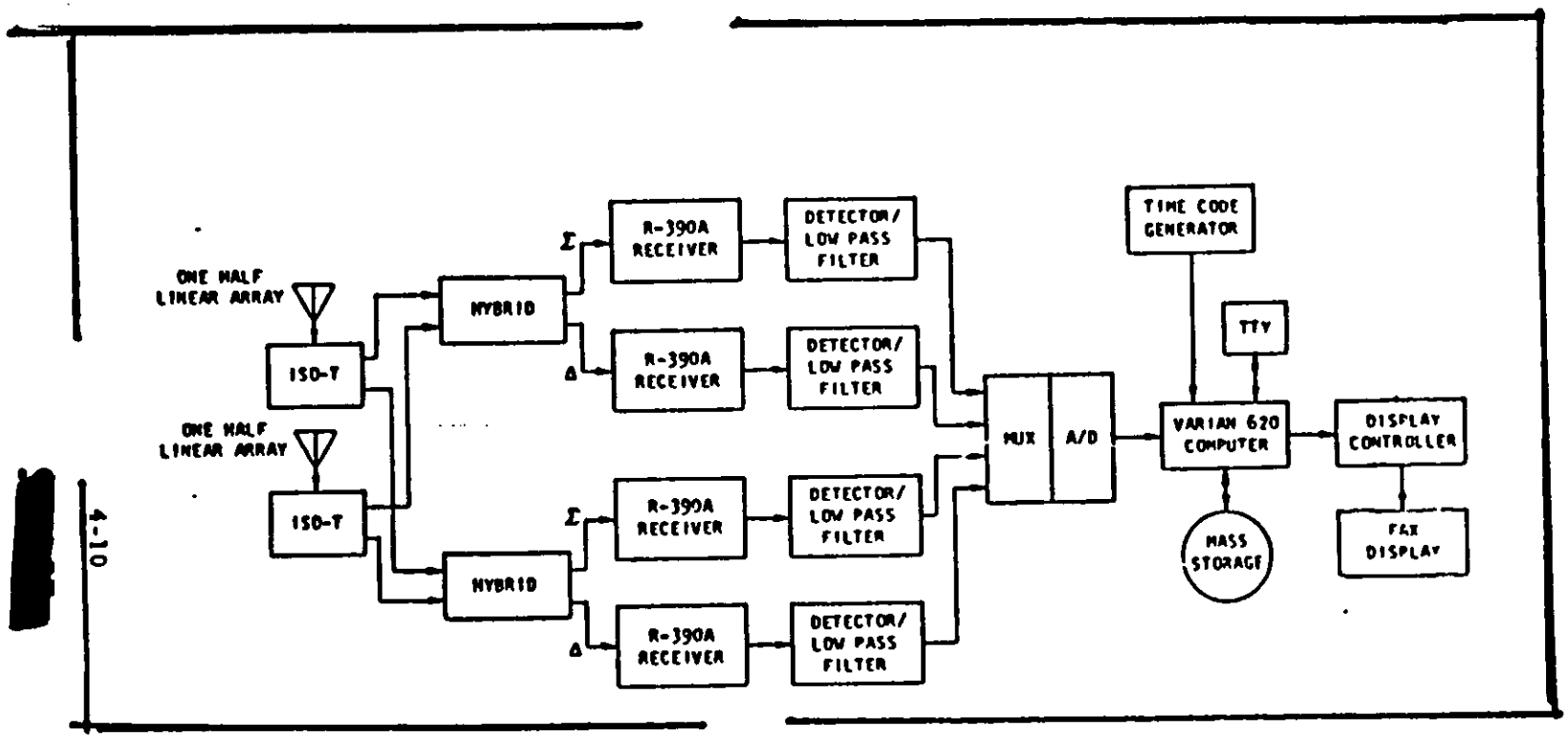

Figure 4-1 [redacted]. (U) System Block Diagram. (U)

UNCLASSIFIED
UNCLASSIFIED

[redacted] (U)

4.3 -- Continued.

a. the double baseline, single measurement mode;

b. the single baseline, double measurement mode; and

c. the four Doppler location mode.

Target tracking using the double-baseline technique would be accomplished by measuring the Doppler shift on two paths and the apparent angle-of-arrival to the target for each transmitter frequency. Both real-time Doppler and real-time azimuth would be displayed on a fax display. Similarly, the single baseline, two-measurement technique may also be used for target location by making two successive Doppler and two successive azimuth measurements separated by at least 10 and no more than 100 seconds. Finally, the four Doppler target location technique may also be tested with this system by using each of the four receivers to measure and display Doppler only.

The design goals of this system are to--

a. measure azimuth to 1° and Doppler to 0.1 Hertz;

b. be easy to operate by an untrained operator;

c. be ultimately suitable for shipboard shock and vibration environment; and

d. be principally composed of off-the-shelf hardware.

The one degree azimuth and 0.1 Hertz Doppler measurement accuracy are based upon the location technique and error analysis results. The required operator skill to use this system for target tracking is quite simple. The operator simply tunes each pair of receivers to the appropriate transmitter frequency of interest. During an event he observes and records the displayed Doppler and displayed azimuth signature for the target. Finally, the operator scales the Doppler and azimuth data, and inputs this information back into the computer to solve for range. The basic hardware items for this system are off-the-shelf and generally rugged enough for a shipboard environment. All of the electronics is solid state, except for the R390 receiver, which is used for shipboard HF communications.

4.4 (U) DESIGN CONCEPT. (U)

The following subsections discuss in detail the block diagram, techniques for Doppler and azimuth measurement, the required data displays and general operational procedures.

[redacted]

4.4.1 (U) System Description. (U)

As shown in Figure 4-1 the antenna array consists of a linear disposed antenna with one-half of the array connected to one of the two data channels. ISO-T's are used to divide the signal power between the two channels. In each data channel the signals are combined in a hybrid which produces sum (Σ) and difference (Δ) output signals. The particular transmitter to be spectrum analyzed is tuned up using standard R390A receivers. The paired receivers are gain matched to provide necessary monopole DF technique accuracy. The IF output of each receiver is envelope detected using high dynamic range AM detector, is low-pass filtered to approximately a 20 Hertz bandwidth to prevent aliasing during the sampling process in the A/D converter. Following sampling and A/D conversion the data is input in a recirculating buffer in the Varian 620/f computer. A total of four input buffers are used to store each 10-second duration signal to provide the 0.1 Hertz resolution required. One channel at a time is spectrum analyzed using the FFT algorithm and the voltage spectral density is calculated. The sum data signal is logrithmically compressed and matched to the dynamic range of the display and finally output to the display. The display matching process is used to automatically adjust the average level of a spectral data to the most sensitive range of the grey scale on the fax display. Each Doppler channel appears in the conventional time-frequency-intensity format on the display.

4.4.2 (U) Azimuth Angle-of-Arrival Calculations. (U)

The magnitude of the spectrum from the delta channel is combined with the previous spectrum from the sum channel to compute the angle-of-arrival of each time frequency cell for that spectrum. The angle-of-arrival from boresight for each time frequency cell may be expressed as:

$$\alpha_i = \sin^{-1}\left[\frac{\lambda \tan^{-1}(\Delta_i/\Sigma_i)}{\pi\, d \cos E}\right]$$

where

λ is the operating wavelength,

d is the physical separation between phase centers of the LDAA antenna,

E is the elevation angle-of-arrival,

4.4.2 (U) -- Continued.

Δ_i is the i^{th} frequency in the delta spectral array,

Σ_i is the i^{th} member of the sum spectral array, and

α_i is the azimuth angle-of-arrival of the i^{th} frequency time component.

Thus, we compute for each spectrum and each frequency, the angle-of-arrival of that bit of data. The α_i data is then formed into an alpha array, is amplitude compressed, display matched and displayed on the fax in a time-angle-intensity format.

The function $\alpha(t_i, f_i)$ is also stored in a mass-storage disk for later operator recall. This data is stored also in a recirculating buffer format so that the most recent 10 minutes of data is available to the operator. This same time-angle-amplitude data is computed for both channels and is displayed on a fax paper as well as being stored on the disk.

4.4.3 (U) Data Extraction. (U)

When a target detection is made as noted by observing the Doppler on the Doppler channel displays, the operator then manually measures the target Doppler frequency and target angle-of-arrival. If the double baseline, single-measurement technique is under test, measurements are made for both data channels. If the single baseline, double-measurement technique is under test, the operator first enters the time, frequency and target azimuth data at time T_o, then on the order 10 to 60 seconds later the operator again measures the time, Doppler and target azimuth data on that same channel. Or, if the four Doppler target location technique is being employed, one frequency measurement is made for each of the four Dopplers. The appropriate data is then entered by the operator into the computer system via the teletype. For each set of data entered by the operator, the computer will solve the target range-azimuth algorithm and print out the results for the operator to review.

Although the operator has displayed for his viewing the computed target azimuth on the fax display, the operator scaling of the angle data will probably not be used in the actual range calculation. The appropriate angle information for each time-frequency cell entered by the operator will be retrieved from the disk storage device. This is because greater angular precision is stored on the disk and can be displayed on the fax display.

4.4.3 (U) -- Continued.

An artist's concept of what this system might look like is shown in Figure 4-2. The rack at the left shows the four R390A receivers. The next rack contains the computer core memory, power supply, disk, A/D converter and other associated electronics. The operator is shown seated in front of the electrographic display with the teletype shown to the right.

4.5 (U) DETAILED DESIGN SPECIFICATIONS. (U)

4.5.1 (U) Spectrum Analysis Specifications. (U)

The specifications for the spectrum analysis portion of the system are given in Table 4-5.

Table 4-5 (U). Spectrum Analysis Specifications. (U)

INPUT	Sample rate (per channel)	51.2 samples per second
	Number of channels	4
	Fast Fourier Transform size	512 points
	Number of seconds of data per transform	10
OUTPUT	Frequency resolution	0.1 Hz
	Bandwidth (folded)	0-25.6 Hz
	Displayed bandwidth	0-20 Hz
	Approximate time required for FFT and angle calculations (per channel)	500 msec
DUTY FACTOR		500 percent

The requirement for a displayed bandwidth of 0-20 Hz is set by the back-scatter radar. Thus, the Doppler frequency shift equals--

$$\frac{2vf}{c}$$

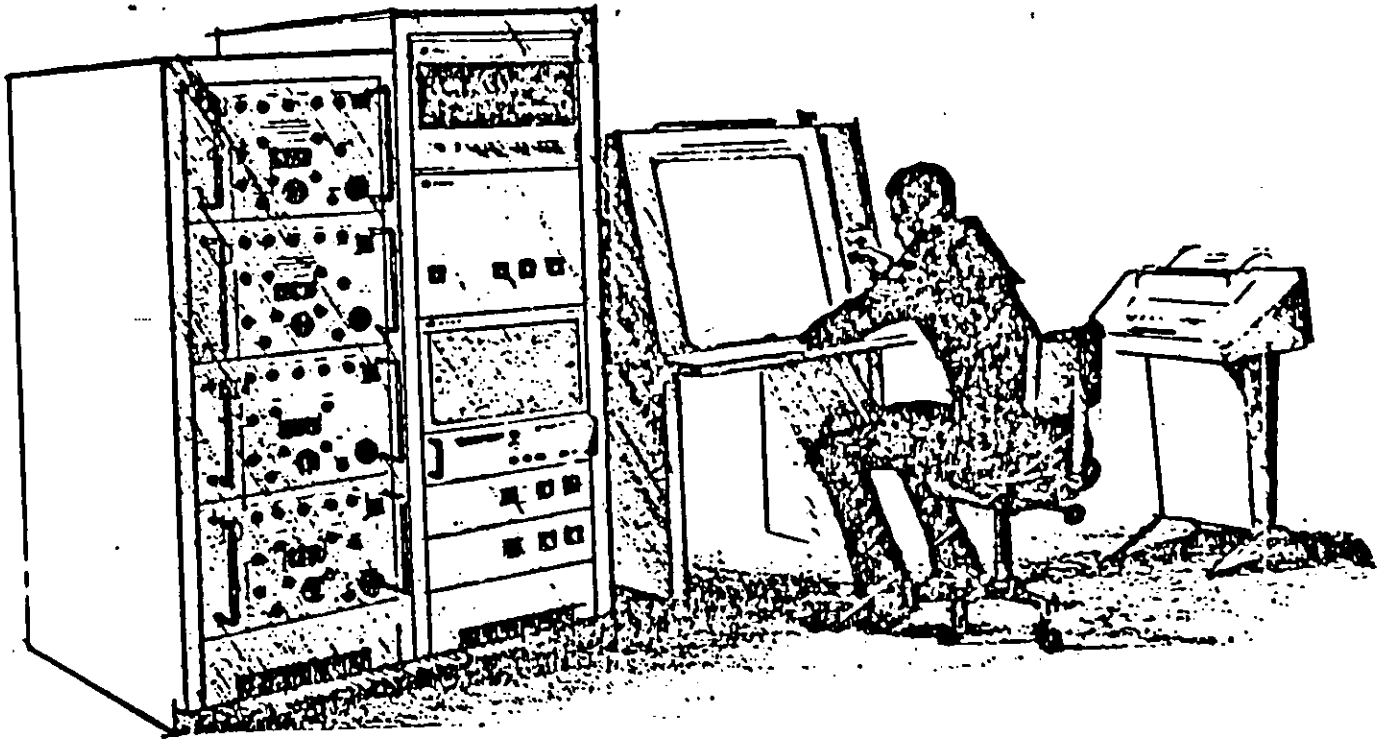

Figure 4-2 (U). Artist's Concept of Data Collection System (U).

UNCLASSIFIED

4.5.1 (U) -- Continued.

where $c = 3 \times 10^8$ meters per second. If we assume v = 600 MPH, the maximum airspeed for the P3 aircraft recommended for the experiment and f = 10 mHz which will be a typical transmitter frequency used in the experiment, we get a frequency shift of 18 Hz. The backscatter case produces the largest frequency shift and shifts of 10 Hz or less are expected in most cases. Thus a displayed bandwidth of 0-20 Hz should adequately display all data collected in the experiment. The receiver output will be diode detected and the sidebands will be folded about zero Hertz in the 0-20 Hz displayed bandwidth, thus sideband sense will not be available from the display. However since the system will be used as part of an experiment, the sideband sense of the target Doppler will be known a priori to the operator. The chief advantage to the folded spectrum is that the time required for the Fast Fourier Transform and the disk and core storage are all halved by using the folded spectrum.

The requirement for 0.1 Hz resolution is set by the nature of the range estimation techniques.

Using the requirements for resolution and bandwidth, the A/D sample rate is 51.2 samples per second. The time samples are stored for 10 seconds and a Fast Fourier Transform (FFT) is performed on the 512 samples. The output of this transform is 256 frequency domain points which represent a bandwidth of 0-25.6 Hz with a resolution of 0.1 Hz. Since the low-pass filter used after the detector in the receiver is not an ideal low-pass filter, there will be some attenuation on the skirt of the filter and several frequency points will be affected. The displayed bandwidth has been set at 0-20 Hz for this reason.

The time required to perform the 512 point FFT and associated data manipulations is estimated to be 350 milliseconds. The time required for the azimuth angle calculations and associated data manipulations is estimated to be 300 milliseconds. The FFT estimate was obtained from a relative computational power and speed comparison between the SEL 810B computer and the computer proposed for this system, the Varian 620/f. Programs written for the 810B require 250 milliseconds to do the transform and the slightly slower 620/f should require 350 milliseconds or less. The estimate for the azimuth calculations was determined by coding a sample loop which computes the azimuth, and calculating the time to perform this operation on the 200 frequency domain points from each of the two channels used. A factor is then added to cover the overhead involved in the data manipulations.

4.5.1 (U) -- Continued.

This total of 700 milliseconds for the two FFTs and the 300 milliseconds for the azimuth angle calculations for each of the two receiver pair gives an average of 500 milliseconds per data channel. Thus, the system is able to process each sample of data with a duty factor of 500 percent. Duty factor is defined as the time duration of the transformed data divided by the time required to process that data for all the channels. Thus for 4 channels of data at 500 milliseconds per channel the duty factor is:

$$\frac{10.0}{(0.50)(4)} = \frac{10.0}{2.0} = 500 \text{ percent.}$$

Simply stated, each time sample of data is processed 5 times. Storing the time samples in a recirculating buffer permits the processing of the most recent 10 seconds of data. The higher the duty factor, the more smoothing and averaging of the data results, and the longer the Doppler-related data is displayed.

The two-tone dynamic range of the system will be 90 db which is the limit available with a 16-bit computer. This 90 db two-tone dynamic range is also approximately the dynamic range of the R390A receiver that is to be used in the experiment. In addition, atmospheric conditions are generally such that signals which necessitate a two-tone dynamic range of greater than 90 db are very rare.

4.5.2 (U) Azimuthal Specifications. (U)

The azimuth angle calculations will be done using the algorithm explained in Section 4.4. The azimuth calculated will have a range of -30° to +30° and will have a calculation resolution of 0.25°. The calculated azimuth can therefore be expressed as an 8-bit number which can represent up to 256 values, although only 240 values are required.

4.5.3 (U) Storage and Display Specifications. (U)

The computer core storage requirements for the programming and buffers required for the software implementation of the system are shown in Table 4-6. The total of 7,150 words will fit into the 8 K of core which is available on the Varian 620/f. If other features are added to the system or if the estimates given in Table 4-6 prove to be low, additional 4 K increments of memory are available.

TABLE 4-6. (U) COMPUTER CORE REQUIREMENTS. (U)

	Words
Programs	
Signal Processing Programs	1500
Disc Handling	400
Teletype Handling	400
Range Algorithm	2000
	3900
Buffers	
Input Buffer	2048
Time-Weight Table	256
Sin/Cos Table	128
Work Area	512
Display Buffer	275
	3219 ≈ 3250
Total	7150

4.5.3 (U) -- Continued.

The azimuth calculations will result in an 8-bit number (or byte). Each of two receiver pairs will compute 200 azimuthal points every 2.0 seconds. These azimuthal points will be stored 2 bytes to a 16-bit word on the disk. The disk to be used in the system has a storage capacity of 64,000 words; approximately 4,000 words will be used for program storage. At 200 words every 2 seconds, 600 seconds of data will be stored on the disk. The disk will always contain the most recent 10 minutes of data.

The spectral and azimuthal data will be displayed on an electrographic facsimile display. The display, shown in Figure 4-3, contains data from each of the two receiver pairs; these pairs are referred to as Channel A and Channel B in the figure. Each channel contains a spectral display of frequency, amplitude and time and an azimuthal display of angle, amplitude and time. The specification for the display are also given in the figure. At a sweep rate of one line per second and a resolution of 99 lines per inch, the most recent 30 minutes of data will be displayed on the fax at one time. In addition to the spectral and azimuthal display on the fax, the time code will be put on the fax. On the edges of the fax the time of day and the Julian day of the year will be encoded; this code will be put on once an hour. In the area between the spectrum and azimuth displays, marks will appear at every one and ten minute transition of the time code generator.

4.6 (U) COMPUTER HARDWARE DESCRIPTION. (U)

4.6.1 (U) Computer. (U)

The computer selected to perform the signal processing and related functions is the Varian 620/f. The Varian 620/f computer is a high-speed, general purpose, digital computer for scientific and industrial applications. Its features include--

Fast operation:	750-nanosecond memory cycle
Large instruction repertoire:	148 instructions
Word length:	16 bits
Modular core memory:	Expandable to 32,768 words in 4,096 increments
Automatic data transfer:	Direct memory access facility provides automatic data transfers with rates to 276,000 words per second

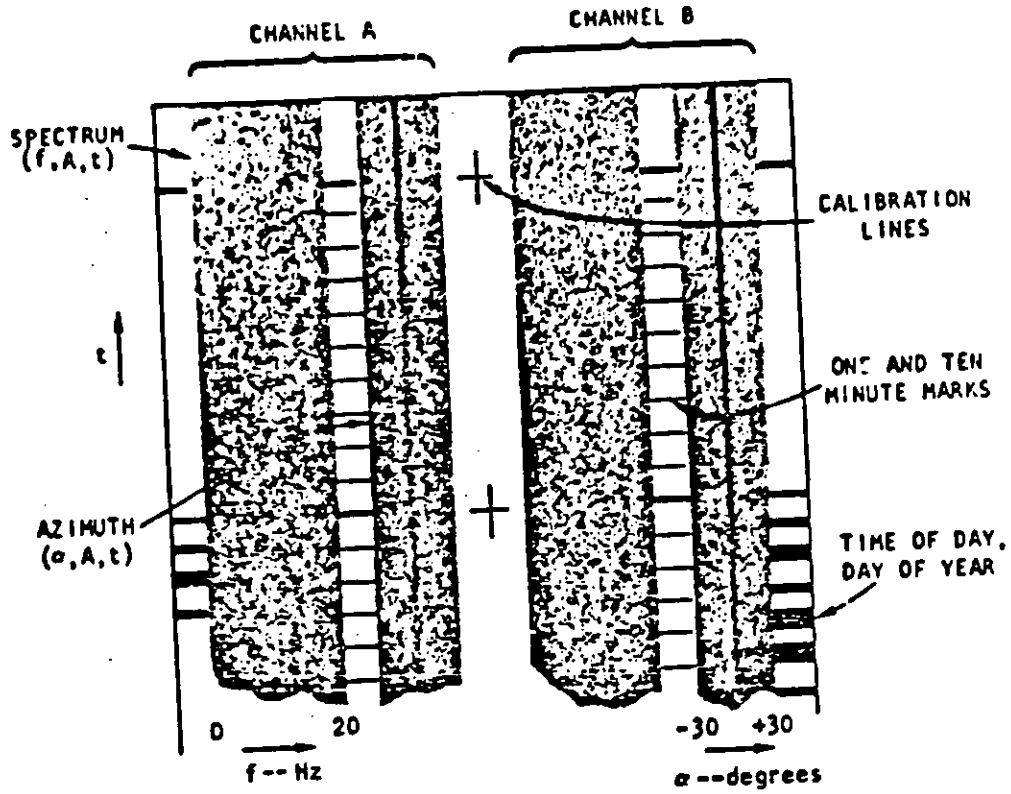

SPECTRAL CHANNEL	0-20 Hz 0.1 Hz RESOLUTION 4 IN. WIDE 5 Hz PER INCH
AZIMUTHAL CHANNEL	-30° TO $+30^{\circ}$ 0.25° RESOLUTION 2.4 IN. WIDE 25° PER INCH
AMPLITUDE	32 LEVELS OF GREY SCALE
HORIZONTAL RESOLUTION	50 LINES PER INCH
VERTICAL (TIME) RESOLUTION	99 LINES (SECONDS) PER INCH
SWEEP RATE	1 LINE PER SECOND

Figure 4-3 (U). Fathometer Display. (U)

4.6.1 (U) -- Continued.

Multiple addressing:	Direct, indirect, relative, index (pre and post), immediate, and extended
Flexible I/O:	Ten devices may be placed on the I/O bus. The I/O system can easily be expanded to include features such as automatic block transfer, priority interrupt, and cycle-stealing data transfers
Extensive software:	Complete package includes a symbolic assembler, subroutine library, A/D diagnostics, and an ASA FORTRAN compiler

The mechanical specifications for the 620/f are--

Dimensions:	The mainframe and expansion frames are 10-1/2 inches high, 19 inches wide, and 21 inches deep.
Input voltage:	105 to 125V ac or 210 to 250V ac, 60 Hz
Input current:	The mainframe power supply requires approximately 15 amperes ac; each expansion frame power supply requires approximately 4 amperes ac.
Temperature:	
Operating	0 to 50 degrees C
Storage	20 to 70 degrees C
Humidity:	
Operating	To 90 percent without condensation
Storage	To 95 percent without condensation
Vibration:	3 to 10 Hz at 1g force or 0.25 double amplitude, whichever is less. Exponentially-raised frequency from 3 to 10 Hz and back to 3 Hz over a 10 minute period, three complete cycles. This specifications applies for all three principal axes.
Shock:	4g for 11 milliseconds (all three principal axes)

4.6.1 (U) -- Continued.

The 620/f was chosen on the basis of four factors--

a. speed,

b. capability,

c. mechanical specifications, and

d. cost.

The 750 nanosecond cycle time of the 620/f makes it one of the fastest 16-bit computers commercially available. This speed is combined with a powerful instruction set which permits fast execution of the FFT and azimuth angle calculation algorithms and thus gives a duty factor of over 500 percent in the processing. The temperature, vibration and shock specifications exceed most computers in the 620/f's price/performance field. The basic cost of the 620/f is below or comparable to most of the 16-bit computers in its performance field.

4.6.2 (U) Analog-to-Digital Converter. (U)

The analog to digital converter (A/D) selected for the system is the Raytheon Miniverter. The model of the Miniverter selected is a 12-bit A/D which has a throughput rate of 45 KHz, an aperture time of 50 nanoseconds and a resolution of 5 millivolts. The Miniverter is packaged in a very compact unit and has proven to be very reliable as a system component.

4.6.3 (U) Disk. (U)

The disk selected for the system is the Singer-Librascope, Model L107. The Singer-Librascope disk is a small, inexpensive and very rugged disk system which meets all the system requirements.

The specifications for the Model L107 are--

Maximum capacity bits:	1,080,000
Maximum capacity words:	67,000
Data heads:	45
Timing heads:	1

4.6.3 (U) -- Continued.

Maximum bits/track:	24,000
Rotation speed, RPM:	3,600
Clock frequency, MHz Max.:	1.4

The mechanical specifications are--

Dimensions:	6 inches high x 9 inches diameter
Weight:	12 pounds (approximately)
Operating environment:	
Temperature	0°C to 55°C
Humidity	90 percent R.H. without condensation
Shock	10-Gs 11-msec rise time (no shock isolators required)
Vibration	2-Gs acceleration max., 5 Hz to 50 Hz (no shock isolators required)
Nonoperating environment:	
Temperature	-50°C to +75° C
Humidity	95 percent relative humidity, no condensation.
Shock	15-Gs 11-msec rise time (with no shock isolators)
Vibration	Mil-Std-810B, Method 514, Category (G) equipment specification used as a guideline. This equipment category is for shipment by common carrier, land or air.
Power requirements:	
Disk	115V ac, 50/60 Hz, single phase 1.5A
Electronics	+5V dc at 1.4A -5V dc at 0.25A +25V dc at 0.2A

This Page Intentionally Blank

[redacted]

UNCLASSIFIED

APPENDIX A

PROPAGATION PREDICTION PROGRAM. (U)

(U) [redacted] The propagation prediction program used to estimate the system performance basically combines a modified version of the ITSA/ESSA HF propagation prediction program for mode and mode amplitude prediction; the bistatic radar range equation to predict the received scatter path power; and an ITSA/ESSA noise prediction program to estimate atmospheric, man made, and galactic noise at the receiver site.

(U) [redacted] The prediction program package consists of individual computer programs that (a) compute a target trajectory; (b) predict propagation mode structure and mode amplitude; and (c) predict the doppler and missile cross-section.

(U) [redacted] The trajectory simulation program estimates the missile or aircraft trajectory based upon fitting the flight profile to a functional form using a least-squares fit technique. The required inputs to generate the model profile are liftoff and burnout times, launch azimuth, apogee, and range. The program then computes altitude, range, latitude, longitude, velocity, the speed of sound, Mach number, Mach angle, local target bearings, local target elevation angles, and acceleration. The computed parameters serve as inputs to the propagation prediction program to determine mode structures with a time varying terminal point on the trajectory.

(U) [redacted] The ITSA/ESSA propagation prediction program has been modified to allow for non-congruent hop structures and for propagation to and reflection from a point above the earth. The program predicts the mode structures that meet ionospheric propagation conditions on each of the three paths: the direct (transmitter-receiver) path, the transmitter-target half path, and target-receiver half path. In addition, the propagation losses and antenna gains for each mode are determined. For each mode predicted on the transmitter-missile half path, an "incident" (at the target) elevation angle, measured from the local horizon, is found. For each mode predicted on the target-receiver half path, the "scattered" elevation angle is also found. These parameters are then used with a modeled profile to predict doppler frequencies.

(U) [redacted] Propagation predictions are based on empirically derived world-wide numerical maps of vertical ionosonde data. The results are monthly ionospheric coefficients which can be used with the parabolic layer assumption (parabolic electron density variations in the E and F layers) to predict monthly average ionospheric conditions affecting a specific ray path at any hour of the day.

[redacted]

UNCLASSIFIED

App. A (U) [redacted] --Continued.

(U) [redacted] In the prediction model, all line of sight, E and F propagating modes are determined between the transmitter and the target, between the receiver and the target, and between the transmitter and the receiver. The determination of these "half paths" is a generalization of the ground-to-ground prediction technique to include the case of ground-to-elevation-point predictions.

(U) [redacted] After the mode structures that meet the ionospheric conditions are identified, (those between horizontal screening and ionospheric penetration) propagation losses and antenna gains are determined. The losses calculated are free space loss (inverse square law), D-layer absorption loss, and ground reflection loss. The NBS empirical adjustment factor is included on the direct-path predictions to account for non-calculated losses. This factor is statistical and varies with season, path length, and earth location of the path. No similar adjustment factor is used or known for the half paths. The antenna types are specified for the system and the appropriate gain routines or gain tables are used.

(U) [redacted] The target scattering model for missile targets above 100 km is a hyperboloid compressed-ambient ionization in the exhaust-plume bow shock wave. The shock-wave scattering surface is considered hyperboloidal from photographic observations which have shown that the shock-wave surface could be described by a second order function and that the shock-wave surface should be asymptotic to the Mach cone.

(U) [redacted] The direction of the rays for the transmitter-missile and receiver-missile propagation paths uniquely define a plane tangent to the hyperboloidal surface which has the proper orientation for a reflection, provided the incident ray encounters a high enough electron density for reflection.

(U) [redacted] Since little definitive work has been done to accurately model missile cross sections below 100 km or aircraft cross sections at HF, a constant (adjustable) cross section is used for aircraft and missile targets below 100 km.

(U) [redacted] The antenna gain patterns for both the monopole transmitter antennas and the LDAA receiving antenna are part of the program. The gain pattern for the LDAA was obtained from data supplied by ITT by using azimuth patterns predicted by the array factor technique for 16 monopole elements and the elevation patterns from scaled model measurements.

END

DATE

FILMED

6-71